

Durham E-Theses

*Synthesis and applications of Palladium complexes
Part I. The synthesis, single crystal structures and
liquid crystalline phase behavior of Alkoxy substituted
Tolans. Part II. Palladium-Complexes of Thioureas
and phosphine sulfides*

Wongkhan, Kittiya

How to cite:

Wongkhan, Kittiya (2008) *Synthesis and applications of Palladium complexes Part I. The synthesis, single crystal structures and liquid crystalline phase behavior of Alkoxy substituted Tolans. Part II. Palladium-Complexes of Thioureas and phosphine sulfides*, Durham theses, Durham University.
Available at Durham E-Theses Online: <http://etheses.dur.ac.uk/2139/>

Use policy

The full-text may be used and/or reproduced, and given to third parties in any format or medium, without prior permission or charge, for personal research or study, educational, or not-for-profit purposes provided that:

- a full bibliographic reference is made to the original source
- a [link](#) is made to the metadata record in Durham E-Theses
- the full-text is not changed in any way

The full-text must not be sold in any format or medium without the formal permission of the copyright holders.

Please consult the [full Durham E-Theses policy](#) for further details.

Academic Support Office, The Palatine Centre, Durham University, Stockton Road, Durham, DH1 3LE
e-mail: e-theses.admin@durham.ac.uk Tel: +44 0191 334 6107
<http://etheses.dur.ac.uk>



Synthesis and Applications of Palladium Complexes

**Part I. The Synthesis, Single Crystal Structures and Liquid
Crystalline Phase Behavior of Alkoxy Substituted Tolans**

**Part II. Palladium-Complexes of Thioureas and Phosphine
Sulfides**

The copyright of this thesis rests with the author or the university to which it was submitted. No quotation from it, or information derived from it may be published without the prior written consent of the author or university, and any information derived from it should be acknowledged.

Kittiya Wongkhan

**A thesis presented to Durham University in fulfillment of the thesis
requirement for the degree of Doctor of Philosophy in Chemistry**

Durham 2008



VOLUME 1

Declaration

The work described in this thesis was carried out in the Department of Chemistry at Durham University between October 2004 and December 2008, under the supervision of Prof. Todd B. Marder. All the work is my own, unless otherwise stated, and has not been submitted previously for a degree at this or any other university.

Kittiya Wongkhan

Statement of Copyright

The copyright of this thesis rests with the author. No quotation from it should be published without their prior consent and information derived from it should be acknowledged.

To my parents for their continual love and support

Acknowledgements

I would like to express my sincere gratitude and deep appreciation to my supervisor, Prof. Todd B. Marder, for his excellent supervision, inspiring guidance and encouragement throughout the course of this study. Thank you for supporting and backing me up no matter what decision I have made and provide plenty of advice and make me feel at home. I know you train me to be a good scientist and I am very grateful to have had you as my supervisor.

I would like to give a special thanks to Dr. Jonathan C. Collings who helped me to get started in the lab and prove read almost all documents I wrote including this thesis. Thanks for providing advice for the past four years. Thank to Andrew Crawford for encouragement, prove read some part of this thesis, and look after GC-MS.

I wish to thank Dr. Andrei Batsanov for running all of the single-crystal X-ray diffraction experiments I have submitted over four years and spending time on the structures reported in my thesis.

I thank Prof. Zhen Yang and his research group for supplying me all the thiourea ligands and for hosting me at Peking University, both in Beijing and Shenzhen. Thank to his students (Bo, Jing and Yingxiang) for synthesized the thiourea ligands.

I also thank to Prof. Aiwen Lei for supplying P-olefin ligand and very warm welcome to Wuhan University, Prof. Hiroto Nakano (Tohoku Pharmaceutical University) for supplying the POT and POZ ligands and Prof. Zhenfeng Xi (Peking University) for the supplying semibullvalene compounds, although none of the results on these systems are included in this thesis.

I wish to express my profound gratitude and sincere appreciation to the Royal Thai Government for the opportunity and financial support given in undertaking this study. My gratitude goes to Department of Chemistry, Ubon Rajathanee University, Thailand, for providing leave to allow me to come here.

Many thanks to all of the Chemistry department services at Durham University for all of the help I received. Dr. Alan Kenwrite, Catherine Hefferman and Ian Mckeag for all highfield solution NMR results, Jaroslava Dostal and Judith Magee for the elemental analysis sample, Dr. Micheal Jones and Lara Turner for mass spectrometry, Douglas Carswell for obtaining the DSC data, Professor Duncan W.

Bruce (York, UK) for assistance with polarised light microscopy (tplm) and discussions, Donocadh P. Lydon for preliminary training on how to use tplm, Dr. David Apperly for solid state NMR data, Dr. Jason Lynam (York, UK) for NMR simulation, Dr. Andrew Beeby for allowing me to use the Raman spectrometer and Lucas for training me on its case. I would like to thank Brian Hall for his work for the group and always having time to help me.

To my sweet parent, for all your support and allow me to choose what I want to do in my life and never complain while waiting for me to come home.

I would like to thank all Thai students: Pi Fai, Pi May, Nim, Bank, Nong Fai and Bath for making me so happy during my stay in Durham. Thank to the Cartner family: David, Pore and Christopher, for having me a place to stay, otherwise I would be a homeless by now.

Thank you to all of the Marder group and group visitors, past and present, for making the lab a nice place to work and me so welcome: Dr. Dave Coventry, Dr. Tolu Fasina, Nathan Bell, Dr. Ibraheem Mkhaliid, Maha Al-Haddad, Dr. Richard Ward, Michael Green, Mark Sinkinson, Tom Turner, Dr. Marco Gianni Grestani, Dr. Marie-Halen, Dr. Nicole, Dr. Andreas Steffen, Dr. Christain Kleeburg, Dr. Manolo Romero, Dr. Bianca Bitterlich, Jonathan Barnard, Meng Guan Tay, Peter Harrison, Laura M, Laura S, Zher Qiang Liu, Li Qiang, Lui Chao and Nim. I also thank the Bryce group for lending chemical and support: Chang Zhen, Kate, Jamie, Katy, Haying, Kiran and Kara.

To my best friend, PKN, thank you so much for your support, plenty of help, suggestions in chemistry, encouragement and proof reading the whole thesis. Thanks for coming here and being with me.

Finally, I give my heart and soul to thank Almighty Creator from up above for giving me so power, patient and inspired.

Kittiya Wongkhan

Publications

Synthesis of Thiourea-Oxazolines, a New Class of Chiral S₂N-Heterobidentate Ligands: Application in Pd-catalyzed Asymmetric Bis-methoxycarbonylation of Terminal Olefins.

B. Liang, J. Liu, Y.-X. Gao, K. Wongkhan, D.-X. Shu, Y. Lan, A. Li, A. S. Batsanov, J. A. K. Howard, T. B. Marder, J.-H. Chen, and Z. Yang. *Organometallics* **2007**, *26*, 4756-4762

Acceleration of Reductive Elimination of Csp³-Pd-Ar *via* a Phosphine/Electron-Deficient Olefin Ligand: A Kinetic Investigation.

H. Zhang, X. Luo, K. Wongkhan, H. Duan, Q. Li, L. Zhu, J. Wang, A. S. Batsanov, J. A. K. Howard, T. B. Marder, and A. Lei, *Chem. Eur. J.*, accepted November 2008.

Synthesis, Single Crystal Structures and Liquid Crystal Phase Behavior of Three Homologous Series of para-Alkoxy Substituted Tolans.

K. Wongkhan, A. S. Batsanov, M. D. Green, J. C. Collings, J. A. K. Howard, D. W. Bruce and T. B. Marder. In preparation.

A Novel Self-Promoted Morita-Baylis-Hillman Dimerization Reaction and Preliminary Experimental and DFT Studies of its Mechanism.

Q. Li, K. Wongkhan, A. S. Batsanov, Y. Lan, Y. Wu, A. Lei, and T. B. Marder. In preparation.

The Dynamic Study of Palladium-C₂-Symmetric Thiourea Complexes: VT-NMR Experimental and Simulations.

K. Wongkhan, J. Liu, T. P.W. Turner, A. S. Batsanov, J. A. K. Howard, J. M. Lynam, J.-H. Chen, Z. Yang and T. B. Marder. In preparation.

Abstract

Three series of alkoxy substituted tolans $p\text{-X-C}_6\text{H}_4\text{-C}\equiv\text{C-C}_6\text{H}_4\text{-p-OC}_n\text{H}_{2n+1}$ [$X = \text{H}$ (series 1), CH_3 (series 2), OCH_3 (series 3)] with varying chain length were synthesized by Pd/Cu-catalysed Sonogashira cross-coupling reactions of terminal alkynes and iodoarenes, crystal structures and phase behavior of three series of tolans. Twenty-eight of the tolans were structurally characterised by single-crystal X-ray diffraction. Their phase behavior was characterised by tplm; only the tolans in series 3 show liquid crystalline phases. The melting points of the tolans decrease with increasing chain length due to a higher degree of flexibility of the terminal chain. An odd-even effect is clearly observed for the clearing point of the nematic phase upon both heating and cooling, with the higher temperature for even and low temperature for odd number carbon chains for series 3.

Monomeric and dimeric palladium dichloride complexes containing the monodentate thioureas, tetramethyl thiourea (tmtu) and a chiral C_2 symmetric thiourea were synthesized. Their structures were obtained from single-crystal X-ray diffraction. The structures of the mono-palladium complexes are the *trans*-isomers, whereas the dimer complexes present *cis*-configurations, and are also the first examples of palladium complexes with sulfur-bridging thiourea ligands. NMR studies of the monomeric and dimeric complexes with tmtu reveal that, in solution, the dimeric complexes are interconverting with mono-palladium complexes, which suggests that the systems are labile. A dynamic equilibrium in solution was also observed between the *rac*- and *meso*-dipalladium complexes with the C_2 -symmetric ligand. The energy barrier to exchange was obtained from a variable temperature NMR study. It is proposed that this equilibrium results from the monomer-dimer interconversion.

S,N -bidentate β -dimethyl and β -monomethyl oxazoline thiourea ligands and α -isoquinoline thiourea ligands and their palladium complexes have been obtained. Single-crystal X-ray diffraction analyses allow us to distinguish between some of their atropoisomers and diastereomers. Most of the Pd complexes were shown to be monomers in the solid state, although one ligand with a cyclohexyl group formed exclusively dimers, and one formed a trimer, as well as a monomer, depending on the solvent mixture that the crystals were grown from. The ligands were found to coordinate through their S and N atoms. All of the mono-palladium

complexes and most of the dimers have *cis*-configurations at the Pd centers; however, we also found a *trans*-configuration in the trimer and the dimer of one of the palladium complex of the β -monomethyl ligands. The structures show that the β -monomethyl oxazoline and α -isoquinoline thiourea complexes appear to be more weakly coordinated than the β -dimethyl oxazoline ones which may be responsible for their lower stabilities in solution. The structure of the ligands (in particular the 'up' or 'down' conformation of the atropoisomers) is intimately related to their enantioselectivities in bis(methoxycarbonylation) reactions of styrene using palladium complexes. The β -dimethyl ligands were, in general, found to be more selective in this reaction than the β -monomethyl oxazoline ones, with palladium complexes of the latter generally found to be less stable in NMR studies.

Several bis(phosphine) monosulfide and disulfide ligands and their palladium complexes have been synthesized and analyzed by single-crystal X-ray diffraction. The reaction with 1:1 molar ratios of Pd source to monosulfide ligands were found to produce monomeric palladium complexes with chelating ligands, apart from the reaction with bis(diphenylphosphino)butane monosulfide, which was found to result in a dimer being formed. The reactions with 1:2 molar ratios of Pd source to monosulfide ligand gave complexes which were coordinated only through the phosphine groups, except for that with bis(diphenylphosphino)methane monosulfides which formed cationic palladium complexes with two chelating ligands. Analogous reactions with the disulfide ligands and the Pd source $[\text{Pd}(\text{CH}_3\text{CN})_4](\text{BF}_4)_2$ also resulted in cationic Pd complexes incorporating two chelating ligands. In some cases, in solution, the complexes showed dynamic equilibria between *cis*- and *trans*- isomers which suggests that the phosphine sulfide ligands are labile. The Pd-S-P angles in the complexes were found to be variable but, since there are none less than 90° , it is unlikely that there is any η^2 - π bonding involving the P=S bond. Preliminary results show that the activities of phosphine sulfide palladium complexes in the oxidative homo-coupling of phenylacetylene are comparable to that of the commonly used pre-catalyst, $\text{PdCl}_2(\text{PPh}_3)_2$.

Volume I

Table content

Declaration.....	ii
Statement of Copyright.....	ii
Acknowledgements.....	iv
Publications.....	vi
Abstract.....	vii
Chapter 1 Introduction.....	1
I. Pd-catalysed cross-coupling reactions.....	2
I.1 General concepts.....	2
I.2 Ligands effects.....	8
II. Organization of the thesis.....	13
III. References.....	13
Part I The Synthesis, Single Crystal Structures and Liquid Crystalline Phase Behavior of Alkoxy Substituted Tolans.....	18
Chapter 2 The Synthesis, Single Crystal Structures and Liquid Crystalline Phase Behavior of Alkoxy Substituted Tolans.....	19
I. Introduction.....	20
II. Results and Discussion.....	21
II.1 Synthesis.....	21
II.2 Phase characterisation by differential scanning calorimetry and thermal optical microscopy.....	22
II.3 Mesomorphism.....	25
II.4 Crystal and molecular structures.....	27
III. Conclusions.....	55
IV. Experimental.....	56
IV.1 Synthesis and characterization.....	56
IV.2 X-ray crystallography.....	74
V. References.....	75
Part II Palladium-Complexes of Thioureas and Phosphine Sulfides.....	77
Chapter 3 Monodentate Thioureas and Their Palladium Complexes.....	78
Abbreviations.....	79
I. Literature Review.....	80
I.1 Introduction.....	80
I.2 Thiourea ligands.....	81
I.2.1 Synthesis of thioureas.....	81
I.2.2 Properties and DFT calculations of thiourea.....	83
I.2 Synthesis of thiourea palladium complexes.....	85
I.3 Solid state studies of thiourea palladium complexes.....	90
I.4 Applications of palladium-thiourea complexes in catalysis.....	95
II. Results and Discussion.....	115

II.1 Tetramethyl thiourea (tmtu)	115
II.1.1 Synthesis of tetramethyl thiourea palladium complexes.....	115
II.1.2 Characterization of the palladium complexes	115
II.2 C ₂ -symmetric chiral thiourea	121
II.2.1 Ligand characterizations	121
II.2.2 Synthesis of chiral thiourea palladium complexes.....	126
II.2.3 Characterization of palladium complexes.....	127
II.2.3.A) Crystal structures of palladium complexes	128
II.2.3.B) NMR Characterization of palladium complexes.....	135
II.2.4 NMR spectroscopic studies of chiral thiourea palladium complexes.	145
II.2.4.A) The variable temperature (VT) ¹ H NMR study of dimeric palladium complexes	145
II.2.4.B) Monitoring of the reaction of PdCl ₂ with L(S,S) at 1:1 molar ratio	152
II.2.4.C) Monitoring of the reaction of PdCl ₂ with L(<i>rac</i>) at 1:1 molar ratio	154
II.2.4.D) Monitoring of the conversion of <i>rac</i> -Pd / <i>meso</i> -Pd	158
II.2.4.E) Monitoring of the conversion of <i>rac</i> -Pd ₂ / <i>meso</i> -Pd ₂	161
II.2.4.F) Monitoring of the conversion pure enantiomer palladium complexes to mixed diastereoisomers.....	163
II.2.3 Testing of chiral-thiourea ligand in bis(methoxycarbonylation) of styrenes	167
III. Conclusion	169
IV. Experimental.....	170
V. References	176
Chapter 4 S,N-Bidentate Thioureas and Their Palladium Complexes	181
I. Introduction	182
II. Results and Discussion.....	193
II.1 Ligand characterization.....	193
II.1.1 The crystal structures of oxazoline thiourea free ligands.....	193
II.1.2 The NMR characterization of the oxazoline thiourea ligands.....	199
II.2 Synthesis of S,N-bidentate thiourea palladium complexes.....	216
II.3 Characterization of S,N-bidentate thiourea palladium complexes.....	217
II.3.1 The crystal structures of S,N-bidentate thiourea palladium complexes...	217
II.3.2 NMR characterization of S,N-bidentate thiourea complexes.....	255
II.4 NMR study of S,N-bidentate thiourea palladium complexes	269
II.5 Testing of the S,N-bidentate thioureas as ligands for Pd/Cu catalysed bis(methoxycarbonylation) of styrene	281
III. Conclusions	285
IV. Experimental.....	286
V. References.....	307
Chapter 5 Phosphine Sulfides and Their Palladium Complexes	309
Abbreviations.....	310
I. Literature Review	311
I.1 Introduction	311
I.2 Synthesis of phosphine sulfides ligands	311
I.3 Synthesis of metal-phosphine sulfide complexes.....	313
I.4 Properties of phosphine sulfides and their metal complexes.....	318
I.4.1 Bond properties.....	318
I.4.2 Spectroscopic studies: IR and ³¹ P{ ¹ H} NMR spectroscopy.....	319

I.4.3 Crystal structure studies.....	321
I.5 Applications of phosphine sulfide complexes.....	335
II. Results and Discussion.....	341
II.1 Synthesis and characterization of ligands	341
II.2 Synthesis and characterization of palladium complexes.....	351
II.2.1 Palladium complexes obtained from reaction of Pd with L in a 1:1 molar ratio	351
II.2.2 Palladium complexes obtained from reactions of Pd with L in a 1:2 molar ratio	364
II.3 Discussion of the crystal structures of the palladium complexes.....	378
II.4 Activity of palladium complexes in homo-coupling reaction.....	390
III. Conclusions.....	392
IV. Experimental.....	393
V. References.....	406
Chapter 6 Summary and Suggestions for Future Work	412
I. Summary.....	413
II. Suggestion for future work.....	415
II.1 Mono- and S,N-bidentate thioureas and their palladium complexes	415
II.2 Phosphine Sulfides and Their Palladium Complexes	417

Volume II

Appendix A Monodentate Thioureas and Their Palladium Complexes.....	1
Appendix B S,N-Bidentate Thioureas and Their Palladium Complexes.....	23
Appendix C Phosphine Sulfides and Their Palladium Complexes.....	64

Volume 1

List of Figures

Chapter 1

Figure 1. Buchwald's biaryl phosphine ligands.....	9
Figure 2. Chiral monophosphine ligands A, ⁶⁹ B ⁷⁰ and C. ⁷¹	9
Figure 3. Chiral bis(phosphine) ligands.....	10
Figure 4. Phosphine oxazoline ligand. ⁷²	10
Figure 5. Bis(phosphine) mono-oxides. ⁷³	10
Figure 6. (A) (IMes)VOCl ₃ and (B) I'Bu.	12

Chapter 2

Figure 1. The melting point for each homologous series plotted against the number of carbon atoms (n) in the terminal alkyl chain of series 1, 2 and 3.	26
Figure 2. Plot of the clearing point (N→I) for homologous series 3 vs. number of carbon atoms (n) in the terminal alkyl chain.	26
Figure 3. The molecular structures of tolans.	28
Figure 4. The molecular packing of H(n)	41
Figure 5. The molecular packing of Me(n)	45
Figure 6. The molecular packing of MeO(n)	49

Chapter 3

Figure 1. Molecular orbital diagram for tu (energies in eV). ⁵⁵	84
Figure 2. <i>Cis</i> - and <i>trans</i> -isomers PdCl ₂ (DMT) ₂ . ¹⁸	86
Figure 3. The structure of [Pd(η^2 -AMTTO-N,S)Cl ₂]. ⁶²	88
Figure 4. <i>Trans</i> -bis(N-benzoyl-N'-propylthiourea)dibromo palladium(II). ⁷⁹	88
Figure 5. <i>Cis</i> - and <i>trans</i> -isomers of PdX(npt)(tbp). ⁶⁵	89
Figure 6. The influence of nitrogen atoms in thiocarbonyl (left), ⁸² thioamide (middle) ⁸³ and thiourea (left) ⁸⁴ on Pd-S bond lengths.	91
Figure 7. Palladium imidoyl derivatives; thiourea (left) and thiocarbonyl (right). ⁶⁴	91
Figure 8. The structure of four-membered ring thiouracil-di-palladium(II) complex.	92
Figure 9. [Pd(tu) ₄]Cl ₂ . ⁸⁷	93
Figure 10. Salicylidene thiosemicarbazone and its palladium complex.	94
Figure 11. PdCl ₂ (Bimt) ₂ . ⁸⁶	94
Figure 12. PdBr ₂ (AMTTO) (left) and [PdBr(PPh ₃)(AMTTO)]Br (right). ⁶⁶	94
Figure 13. Pyridine-morpholine carbothiamide palladium complex. ⁴⁵	95
Figure 14. PdCl ₂ (PPh ₃)(tu) (hydrogen bonds are shown as a dash line). ⁹⁰	95
Figure 15. Salicylaldehyde N-4-hexamethyleneiminylthiosemicarbazone palladium complex. ¹⁶	100
Figure 16. Chiral thiourea (L1). ¹⁷	102
Figure 17. The preparation of the Pd-tmtu complexes.	115
Figure 18. The molecular structure of Pd(tmtu)	116
Figure 19. The molecular structure of Pd₂(tmtu) (CH ₃ CN solvate molecules omitted for clarity). ⁵²	116

Figure 20. The molecular structure of tmtu.	117
Figure 21. The interconversion of Pd₂(tmtu) and Pd(tmtu) in solution.	120
Figure 22. The structures of chiral thiourea ligands.	121
Figure 23. The COSY (500 MHz) spectrum of the aliphatic region of L(rac)	122
Figure 24. The NOESY (500 MHz) spectrum of L(rac)	123
Figure 25. The molecular structure of L(S,S)	125
Figure 26. The MALDI TOF mass spectrum of rac-Pd₂ / meso-Pd₂	128
Figure 27. The MALDI TOF mass spectrum of rac-Pd / meso-Pd	128
Figure 28. The molecular structure of trans-meso-Pd (solvent molecules omitted for clarity).	129
Figure 29. The molecular structure of trans-meso-Pd showing one CD ₂ Cl ₂ solvate molecule.	129
Figure 30. The molecular structure of meso-Pd₂ ; (solvate molecules and minor disordered positions omitted for clarity).	134
Figure 31. The molecular structure of meso-Pd₂ with the toluene solvate molecule and minor disordered positions shown with open bonds.	134
Figure 32. The molecular structure of R,R-Pd₂	134
Figure 33. The ¹ H NMR (500 MHz, CD ₂ Cl ₂ , -60 °C) spectrum of rac-Pd / meso-Pd	135
Figure 34. The ¹³ C{ ¹ H} NMR (125 MHz, CD ₂ Cl ₂ , -60 °C) spectrum of rac-Pd / meso-Pd	136
Figure 35. The ¹³ C{ ¹ H} NMR (125 MHz) spectrum of rac-Pd / meso-Pd in CD ₂ Cl ₂	137
Figure 36. The structure of S,S-Pd₂	137
Figure 37. The ¹ H NMR spectrum (500 MHz, CD ₂ Cl ₂ , -60 °C) of S,S-Pd₂	138
Figure 38. The ¹³ C{ ¹ H} NMR (500 MHz, CD ₂ Cl ₂ , -60 °C) spectrum of S,S-Pd₂	138
Figure 39. The COSY spectrum (CD ₂ Cl ₂ , -60 °C) of the aromatic region of S,S-Pd₂	139
Figure 40. The ¹ H NMR (500 MHz, CD ₂ Cl ₂ , -60 °C) spectra of S,S-Pd₂ (bottom) and rac-Pd₂ / meso-Pd₂ (top); * = meso-Pd₂ signals.	140
Figure 41. The ¹³ C{ ¹ H} NMR (125 MHz, CD ₂ Cl ₂ , -60 °C) spectra of the aromatic region of S,S-Pd₂ (bottom) and rac-Pd₂ / meso-Pd₂ (top); * = meso-Pd₂ signals.	140
Figure 42. The ¹³ C{ ¹ H} NMR (125 MHz, CD ₂ Cl ₂ , -60 °C) spectra showing the C=S and C3 signals of S,S-Pd₂ (bottom) and rac-Pd₂ / meso-Pd₂ (top); ^a = rac-Pd₂ ; ^b = meso-Pd₂ signals.	141
Figure 43. The ¹³ C{ ¹ H} NMR (125 MHz, CD ₂ Cl ₂ , -60 °C) spectra of the aliphatic region of S,S-Pd₂ (bottom) and rac-Pd₂ / meso-Pd₂ (top); ^a = rac-Pd₂ ; ^b = meso-Pd₂ signals.	142
Figure 44. The ¹ H NMR (500 MHz) of the aliphatic region of rac-Pd₂ / meso-Pd₂ in CD ₂ Cl ₂ at various temperatures.	146
Figure 45. The ¹ H NMR (500 MHz) of the aliphatic region of rac-Pd₂ / meso-Pd₂ in TCE-d ₂ at various temperatures.	147
Figure 46. The ¹ H NMR (500 MHz) spectrum in the aliphatic region of rac-Pd₂ / meso-Pd₂ in TCE-d ₂ at no exchanging process 20 °C (scale in Hz).	148
Figure 47. The ¹ H NMR (500 MHz) spectra in the aromatic region of rac-Pd₂ / meso-Pd₂ in TCE-d ₂ at various temperatures; * = unknown complex.	149
Figure 48. The ¹ H NMR (500 MHz) monitoring of rac-Pd₂ / meso-Pd₂ in TCE-d ₂ at various temperatures; L= ligand.	150
Figure 49. The ¹ H NMR (500 MHz) spectra of L(rac) (bottom) and rac-Pd₂ / meso-Pd₂ (top) in TCE-d ₂ at 100 °C.	151

Figure 50. The ^1H NMR (500 MHz) spectra on the aromatic of <i>rac</i> -Pd ₂ / <i>meso</i> -Pd ₂ in TCE-d ₂ at room temperature before (top) and after (bottom) heating to 100 °C.....	152
Figure 51. The $^{13}\text{C}\{^1\text{H}\}$ NMR (100 MHz) spectrum of the reaction of PdCl ₂ with L(S,S) at 1:1 molar ratio in CD ₂ Cl ₂ at room temperature after 6 h (bottom); the expanded C=S (top left) and C3 (top right) regions.	153
Figure 52. The <i>in situ</i> $^{13}\text{C}\{^1\text{H}\}$ NMR (100 MHz) spectrum in CD ₂ Cl ₂ of the reaction of PdCl ₂ with L(<i>rac</i>) at 1:1 molar ratio at room temperature after 3 h (bottom), the expanded C=S (top left) and C3 region (top right); L = L(<i>rac</i>); * = <i>trans-rac</i> -Pd and <i>cis-rac</i> -Pd.	155
Figure 53. The <i>in situ</i> $^{13}\text{C}\{^1\text{H}\}$ (125 MHz) NMR spectrum of the reaction of PdCl ₂ with L(<i>rac</i>) at 1:1 molar ratio in CD ₂ Cl ₂ at -60 °C after a considerable amount of time at room temperature (bottom); the expanded C=S (top left) and C3 region (top right); L = L(<i>rac</i>); * = <i>trans-rac</i> -Pd and <i>cis-rac</i> -Pd.	156
Figure 54. The $^{13}\text{C}\{^1\text{H}\}$ NMR (125 MHz) spectrum of <i>rac</i> -Pd / <i>meso</i> -Pd in CD ₂ Cl ₂ at room temperature after 24 h (bottom); the expanded C=S (top left) and C3 region (top right); L = ligand; ^a = <i>trans-rac</i> -Pd; ^b = <i>cis-rac</i> -Pd; ^{a'} = <i>trans-meso</i> -Pd; ^{b'} = <i>cis-meso</i> -Pd; * = unknown Pd complex.....	159
Figure 55. The aromatic region of the ^1H NMR (500 MHz) spectra in CD ₂ Cl ₂ at -60 °C of <i>rac</i> -Pd / <i>meso</i> -Pd (top) and <i>rac</i> -Pd ₂ / <i>meso</i> -Pd ₂ (bottom).	160
Figure 56. The $^{13}\text{C}\{^1\text{H}\}$ NMR (125 MHz) spectrum of S,S-Pd ₂ in CD ₂ Cl ₂ at -60 °C (bottom); the expanded C=S (top left) and C3 region (top right); * = intermediate..	161
Figure 57. The $^{13}\text{C}\{^1\text{H}\}$ NMR (125 MHz) spectrum of <i>rac</i> -Pd ₂ / <i>meso</i> -Pd ₂ in CD ₂ Cl ₂ at -60 °C (bottom); the expanded C=S (top left) and C3 regions (top right); ^a <i>rac</i> -Pd ₂ ; ^b <i>meso</i> -Pd ₂ ; * intermediate.	163
Figure 58. The ^1H NMR (500 MHz) spectra at -60 °C of a mixture of S,S-Pd ₂ and R,R-Pd ₂ in CD ₂ Cl ₂ after 0, 24, 48 and 72 h at room temperature.....	165

Chapter 4

Figure 1. Chiral thiourea (L1). ⁶	182
Figure 2. Mono- and di-palladium complexes of L1.....	182
Figure 3. (A) β -dimethyl oxazoline thioureas, (B) β -monomethyl oxazoline thioureas and (C) α -isoquinoline thiourea.....	184
Figure 4. The structures of the β -dimethyl oxazoline thiourea ligands.	187
Figure 5. The synthesis of L13 by the group of Prof. Z. Yang.....	188
Figure 6. The TLC of compounds B, C and L9.....	190
Figure 7. The structure of the α -isoquinoline thiourea L12.	191
Figure 8. The structures of the 'up' (left) and 'down' (right) atropoisomers of L2. .	193
Figure 9. The molecular structure of L2up with two independent molecules (I, I') in the asymmetric unit.....	194
Figure 10. The molecular structure of L2down.....	194
Figure 11. The molecular structure of L7.	195
Figure 12. The molecular structure of R-L10.....	196
Figure 13. The structure of L7 with carbons positions numbered for NMR assignment.	199
Figure 14. The ^1H NMR (500 MHz, CDCl ₃) spectrum of L7.	199
Figure 15. The $^{13}\text{C}\{^1\text{H}\}$ NMR (125 MHz, CDCl ₃) spectrum of L7.	199
Figure 16. The COSY spectrum in the aliphatic region of L7.....	201
Figure 17. The HSQC spectrum in the aliphatic region of L7.....	201
Figure 18. The NOESY spectrum of L7.	202

Figure 19. The COSY spectrum in the aromatic region of L7 .	202
Figure 20. The HMBC spectrum of L7 .	203
Figure 21. The ^1H NMR (500 MHz, CD_2Cl_2) spectra of L2up (top) and L2down (bottom).	215
Figure 22. The $^{13}\text{C}\{^1\text{H}\}$ (125 MHz, CD_2Cl_2) spectra of L2up (top) and L2down (bottom).	215
Figure 23. The molecular structures of the β -dimethyl oxazoline thiourea mono-palladium complexes.	218
Figure 24. The crystal packing of PdL2up showing the close intermolecular contacts.	228
Figure 25. The crystal packing of PdL2down showing the close intermolecular contacts.	228
Figure 26. The crystal packing of PdL3 showing the close intermolecular contacts.	229
Figure 27. The crystal packing of PdL4 showing the close intermolecular contacts.	229
Figure 28. The crystal packing of PdL4 \cdot 0.5 CH_2Cl_2 showing the close intermolecular contacts.	229
Figure 29. The crystal packing of PdL4 \cdot CH_3OH showing the close intermolecular contacts.	230
Figure 30. The crystal packing of PdL6 showing the close intermolecular contacts.	230
Figure 31. The crystal packing of PdL7 showing the close intermolecular contacts.	230
Figure 32. The crystal packing of PdL11up showing the close intermolecular contacts.	231
Figure 33. The molecular structures of five different solvates of Pd₂L5 .	232
Figure 34. The molecular structure of the palladacycle of Pd₂L5 \cdot 0.5 CH_2Cl_2 (most of atoms are omitted for clarity).	234
Figure 35. Definition of the plane in palladium complex of L5 (plane ν is Pd-S-N-Cl).	234
Figure 36. The crystal packing of Pd₂L5 \cdot CH_2Cl_2 showing the close intermolecular contacts.	239
Figure 37. The crystal packing of Pd₂L5 \cdot 2 CH_2Cl_2 showing the close intermolecular contacts.	239
Figure 38. The crystal packing of Pd₂L5 \cdot 4 CH_2Cl_2 showing the close intermolecular contacts.	240
Figure 39. The crystal packing of Pd₂L5 \cdot CHCl_3 \cdot 3 CH_3COCH_3 showing the close intermolecular contacts.	240
Figure 40. The crystal packing of Pd₂L5 \cdot H_2O showing the close intermolecular contacts.	240
Figure 41. The molecular structure of Pd₃L7 (disordered is shown in open bond, hydrogen atoms and solvent molecules are omitted for clarity).	242
Figure 42. The molecular structure of Pd-R-L9up .	244
Figure 43. The molecular structure of Pd-R-L10 .	244
Figure 44. The molecular structure of Pd₂-S-L9down (hydrogen atoms and solvent molecules omitted for clarity).	248
Figure 45. The cross-section of the Pd₂-S-L9down structure (half of the atoms omitted for clarity).	249

Figure 46. The molecular cross-section shows close intermolecular Cl.....H contact of Pd₂-S-L9down (most of the atoms are omitted for clarity).	250
Figure 47. The crystal packing of Pd₂-S-L9down	250
Figure 48. The molecular structure of PdL12	252
Figure 49. The crystal packing of PdL12 showing the close intermolecular contacts.	253
Figure 50. The ¹ H NMR (500 MHz, CDCl ₃) spectra of the <i>in situ</i> reaction of 1:1 PdCl ₂ (PhCN) ₂ and L5 (bottom) and Pd₂L5 crystals (top).....	270
Figure 51. The ¹ H NMR (700 MHz, CDCl ₃) spectra of the aliphatic region of PdL7 (bottom) and the Pd₃L7 crystals after 24 h at room temperature (top); * = PdL7 ...	272
Figure 52. The ¹ H NMR (CDCl ₃) spectra of the aliphatic region of the Pd₃L7 crystals at various times; bottom (400 MHz immediately after the solution was prepared), middle (700 MHz, after 24 h at room temperature) and top (700 MHz, after 48 h at room temperature); M = monomer; * = intermediates.	272
Figure 53. The ¹ H NMR (200 MHz, CDCl ₃) spectrum of a solution of the Pd₂-S-L9down crystals shortly after preparation.	274
Figure 54. The ¹ H NMR (700 MHz, CDCl ₃) of the aliphatic region of Pd₂-S-L9down (D) after standing overnight (Pd-S-L9down signals marked with *).	274
Figure 55. ¹ H NMR (400 MHz, CDCl ₃) spectra of the aliphatic region of Pd-R-L10 at various times.	276
Figure 56. ¹ H NMR (400 MHz, CDCl ₃) spectra of the aliphatic region of R-L10 (bottom), the <i>in situ</i> reaction of PdCl ₂ (PhCN) ₂ with R-L10 at 1:1 molar ratio soon after preparation (middle) and the <i>in situ</i> reaction of PdCl ₂ (PhCN) ₂ with R-L10 at 1:2 molar ratio after 3 days (top).	276
Figure 57. ¹ H NMR (400 MHz, CDCl ₃) spectra of the aliphatic region of the <i>in situ</i> reaction of 1:1 PdCl ₂ (PhCN) ₂ : S-L10 at various times.	277
Figure 58. ¹ H NMR (400 MHz, CDCl ₃) spectra of the aliphatic region of S-L10 (bottom) and the <i>in situ</i> reaction soon after preparation of PdCl ₂ (PhCN) ₂ with S-L10 at 1:1 (middle) and 1:2 (top) molar ratios.	278
Figure 59. ¹ H NMR (400 MHz, CDCl ₃) spectra of L6 (bottom) and the <i>in situ</i> reaction of [(η ³ -allyl)Pd(μ-Cl)] ₂ with L6 in different molar ratios.	279
Figure 60. ¹ H NMR (400 MHz, CDCl ₃) spectra of L7 (bottom) and the <i>in situ</i> reaction of [(η ³ -allyl)Pd(μ-Cl)] ₂ with L7 in different molar ratios.	280
Figure 61. The general structure of the β-dimethyl oxazoline thioureas.	282
Figure 62. The atropisomer oxazoline thioureas.....	282
Figure 63. The structures of L3 , L6 , L11up and L13	283
Figure 64. The general structures of the β-monomethyl oxazoline thioureas.	284

Chapter 5

Figure 1. <i>Cis</i> - and <i>trans</i> - [Pd{Ph ₂ P(E)NPPH ₂ }]Cl ₂ . ¹⁷	317
Figure 2. The resonance structures of phosphine oxide.....	318
Figure 3. A phosphine sulfide monocarbonyl palladium complex. ⁵¹	330
Figure 4. Bis(thiophosphinoyl)methylene ruthenium (left), ¹⁴² and [RhCl(Cp*)(<i>o</i> -Ph ₂ PNHC ₆ H ₄ P(S)Ph ₂ -P,S]ClO ₄ (right). ⁸⁵	331
Figure 5. Tris(1-methyl-3,5-diphenyl-2,6-bis(diphenylphosphine sulfide)-14-.....	331
Figure 6. 1,3-Diphosphapropene sulfide iodine adduct. ⁴⁶	332
Figure 7. [Mo(CO) ₄ (SPPH(py)-κ ³ -N,S,N)]. ¹³⁶	332

Figure 8. 4,5-Bis(diphenylthiophosphinoyl)-1,2,3-triazole(κ^3 -methallyl)-palladium (left) ⁷¹ and bis(4,5-bis(diphenylthiophosphinoyl)-1,2,3-triazole)-palladium (right). ⁷¹	333
Figure 9. (3,4-Dimethyl-1-phenylphosphole)palladium dichloride. ⁸⁶	333
Figure 10. CuCl(dppmS ₂) ¹¹⁹ (left) and CuI(dppmS ₂) (right). ¹²¹	334
Figure 11. Phosphinine (left), bis(diphenylphosphinine sulfide) (middle) and resonance structure (right).	334
Figure 12. Bis(diphenylphosphinine sulfide) palladium ¹²⁵ and copper complexes. ⁶⁹	335
Figure 13. Palladacyclic pincer complexes of phosphine sulfides used in the Suzuki-Miyaura reactions. ⁵	338
Figure 14. Polymer supported with phosphine sulfide side chain. ¹⁵¹	339
Figure 15. Fluorescent molecular sensor for Hg ²⁺ . ¹⁵²	340
Figure 16. The ³¹ P{ ¹ H} NMR chemical shifts of the bis(phosphine) monosulfides.	342
Figure 17. The ³¹ P{ ¹ H} NMR chemical shifts of the bis(phosphine) disulfides.	343
Figure 18. The molecular structure of dppmS (minor disordered position shown with open bonds).	344
Figure 19. The molecular structure of dppeS (minor disordered position shown with open bonds).	344
Figure 20. The molecular structure of dppfS (one disordered position shown with open bonds).	345
Figure 21. The molecular structure of dppbS₂ .	345
Figure 22. The molecular structure of dcpeS₂ .	345
Figure 23. Close intermolecular contacts in dppmS .	349
Figure 24. Close intermolecular contacts in dppfS (both disordered position of S atom are shown).	349
Figure 25. Close intermolecular contacts in dppbS₂ .	349
Figure 26. Close intermolecular contacts in dcpeS₂ .	350
Figure 27. Close intermolecular contacts in molecule I of dppeS .	350
Figure 28. Close intermolecular contacts in molecule I' of dppeS .	350
Figure 29. The molecular structures of dppbS:dppbSO (0.33:0.67) (left) dppbS:dppbSO (0.75:0.25) (right) (dppbSO is shown with dashed bonds).	351
Figure 30. The bis(phosphine) monosulfide palladium complex products.	352
Figure 31. The molecular structures of the bis(phosphine) monosulfide palladium complexes.	353
Figure 32. The bis(phosphine) disulfide palladium complexes.	359
Figure 33. The molecular structure of Pd(dppmS₂) .	360
Figure 34. The molecular structure of Pd(dcpeS₂) .	360
Figure 35. The molecular structure of Pd(dppeS₂) . ¹¹⁵	360
Figure 36. Close intermolecular contacts in the structure of Pd(dppmS₂) .	363
Figure 37. Close intermolecular contacts in the structure of Pd(dcpeS₂) .	363
Figure 38. The molecular structure of Pd(dppfS)₂ ; selected bond lengths (Å) and angles (deg); Pd–Cl(1) 2.2980(7), Pd–Cl(2) 2.2993(7), Pd–P(1) 2.3383(8), Pd–P(2) 2.3462(8), P(3)–S(1) 1.953(11), P(4)–S(2) 1.9527(11), P(1)–CH 1.808(3), P(2)–CH 1.793(3), P(1)–Pd–P(2) 179.02(3) ^o , Cl(1)–Pd–Cl(2) 179.22(3) ^o .	364
Figure 39. The ³¹ P{ ¹ H} NMR spectrum (202 MHz) in CD ₂ Cl ₂ of the products of the 1:2 molar ratio reaction of PdCl ₂ (PhCN) ₂ with dppeS .	365
Figure 40. The molecular structure of Pd(dppeS)₂ (solvate molecules are omitted for clarity); Pd–Cl 2.3079(5), Pd–P(2) 2.3182(4), P(1)–S 1.9605(6), P(1)–C(1) 1.8188(14), P(1)–C(11) 1.8124(15), P(1)–C(21) 1.8133(15), P(2)–C(2) 1.8383(14),	

P(2)–C(31) 1.8166 (15), P(2)–C(41) 1.8165(14). P(2A)-Pd-P(2) 180.000(1)°, Cl(1)-Pd-Cl(1A) 179.998(13)°, P(2A)-Pd-Cl(1) 86.068(18)°.....	366
Figure 41. The molecular structure of Pd(dppmS)₂ ·2CD ₂ Cl ₂ (Cl counter anions and solvate molecules omitted for clarity).....	367
Figure 42. The molecular structure of Pd(dppmS)₂ ·4CHCl ₃ (solvate molecules and Cl counter anions omitted for clarity).....	367
Figure 43. Close intermolecular contacts in the structure of Pd(dppmS)₂ ·2CD ₂ Cl ₂	370
Figure 44. The ³¹ P{ ¹ H} NMR spectrum (202 MHz) of Pd(dppmS)₂ in CD ₂ Cl ₂	371
Figure 45. The ³¹ P{ ¹ H} NMR spectrum (161 MHz) of Pd(dppmS)₂ in dmsO-d ₆ at t = 15 min and 18 h.....	371
Figure 46. The palladium complex products from the 1:2 molar ratio reaction of [Pd(CH ₃ CN) ₄](BF ₄) ₂ :L (L = bis(phosphine) disulfides).....	373
Figure 47. The molecular structure of Pd(dppmS₂)₂ (BF ₄ ⁻ counter anions omitted for clarity).....	373
Figure 48. The molecular structure of Pd(dppeS₂)₂ (BF ₄ ⁻ counter anions omitted for clarity).....	374
Figure 49. The molecular structure of Pd(dppfS₂)₂ (BF ₄ ⁻ counter anions omitted for clarity).....	374
Figure 50. Close intermolecular contacts in the structure of Pd(dppeS₂)₂	377
Figure 51. Close intermolecular contacts in the structure of Pd(dppfS₂)₂	377
Figure 52. Comparison of the geometries about the Pd atoms in the related palladium complexes.	379
Figure 53. Comparison of the geometries of the Pd(dppmS) and Pd(dppmS)₂ structures.	382
Figure 54. Comparison of the geometries of the Pd(dppm) , Pd(dppmS) and Pd(dppmS₂) structures.	382
Figure 55. Comparison of the geometries of the Pd(dppe) , Pd(dppeS) and Pd(dppeS₂) structures.....	383
Figure 56. Comparison of the geometries of the Pd(dcpe) and Pd(dcpeS₂) structures.	383
Figure 57. Comparison of the geometries of the Pd(dppf) ·CHCl ₃ , Pd(dppfS) ·CH ₂ Cl ₂ and Pd(dppfS) structures.....	383
Figure 58. Views along the central bonds in the torsion angles in the palladium complexes (the atoms at the rare are shown with open bonds).....	389
Figure 59. Views perpendicular to the Cp rings in Pd(dppf) (left) and Pd(dppfS) (right).	390

Chapter 6

Figure 1. The structures of carbene, phosphine, thiourea and phosphine sulfide ligands.....	413
Figure 2. The structures of urea, phosphine oxide, thiourea and phosphine sulfide.....	413
Figure 3. The structure of monomethyl thioureas.....	416
Figure 4. Crystal structure of the PdL11up.....	416

List of Tables

Chapter 2

Table 1. Transition temperatures (°C) observed by tpm Me(9) , MeO(2)-MeO(14) . 24	
Table 2. Crystallographic data for compounds in the homologous series 1.	32
Table 3. Crystallographic data for the compounds in the homologous series 2.	33
Table 4. Crystallographic data for the compounds in the homologous series 3.	34
Table 5. Dihedral angles between benzene rings (deg).	35
Table 6. Torsion angle C(2)-C(1)-O(1)-C(15) (deg).	35
Table 7. Torsion angle C(1)-O(1)-C(15)-C(16) (deg).	36
Table 8. Torsion angle O-C(15)-C(16)-C(17) (deg).	36

Chapter 3

Table 1. Bond lengths and angles in free thiourea ligands.	83
Table 2. Bond lengths, angles and dihedral angles for palladium-thiourea complexes.	103
Table 3. Crystallographic data for tmtu and its palladium complexes.	118
Table 4. Selected bond lengths and angles for tmtu and its palladium complexes.	119
Table 5. The ¹ H (500 MHz) and ¹³ C{ ¹ H} (125 MHz) NMR resonances for tmtu, Pd(tmtu) and Pd₂(tmtu) in CD ₂ Cl ₂ (ppm); ¹³ C{ ¹ H} (100 MHz) resonances in the solid state are given in parentheses.	120
Table 6. ¹ H (500 MHz) and ¹³ C{ ¹ H} (125 MHz) NMR shifts for L(rac) . ^a	124
Table 7. Crystallographic data for C ₂ chiral thioureas and its palladium complexes.	130
Table 8. Selected bond lengths and angles of C ₂ chiral thioureas and their palladium complexes.	131
Table 9. The torsion angles and the angles between planes in L(S,S) , L(rac) , <i>trans-meso-Pd</i> and <i>meso-Pd₂</i>	132
Table 10. The ¹ H NMR (500MHz) and ¹³ C{ ¹ H} NMR (125 MHz) signals in CD ₂ Cl ₂ at -60 °C of <i>rac-Pd₂</i> and <i>meso-Pd₂</i>	143
Table 11. The ¹³ C{ ¹ H} NMR (125 MHz) signals in CD ₂ Cl ₂ at room temperature and -60 °C of the C3 and C=S carbon atoms of <i>rac-Pd</i> and <i>meso-Pd</i> and the <i>in situ</i> NMR reactions of PdCl ₂ with L(S,S) and L(rac) at 1:1 molar ratio.	157
Table 12. The solution ¹³ C{ ¹ H} NMR signals of C3 and C=S of the <i>rac-Pd</i> / <i>meso-Pd</i> after 24 h in CD ₂ Cl ₂ and the <i>in situ</i> reaction of PdCl ₂ and L(rac) after 6 h. ^a	159
Table 13. Bis(methoxycarbonylations) of terminal olefins using chiral-thiourea L1 and its palladium complexes. ¹⁴	168

Chapter 4

Table 1. Names and codes of the oxazoline thiourea ligands.	185
Table 2. Crystallographic data of L2up , L2down , L7 and R-L10	197
Table 3. Selected bond lengths and angles for the β-mono- and dimethyl oxazoline thioureas.	198
Table 4. ¹ H NMR assignment of the β-dimethyl oxazoline thioureas (positions 1 – 12) with coupling constants given in Hz in parentheses.	204
Table 5. ¹ H NMR assignment for the R-substituent of the β-dimethyl oxazoline thioureas (positions 14 – 16).	207

Table 6. ^1H NMR assignment of R'-substituent for the β -dimethyl oxazoline thiourea (positions 17 - 24).	209
Table 7. ^1H NMR assignment for the β -monomethyl oxazoline thioureas (positions 1 - 12).	214
Table 8. ^1H NMR assignment for R and R'-substituent of the β -monomethyl oxazoline thioureas (positions 14 - 23).	213
Table 9. Crystallographic data for PdL2up , PdL2down , PdL3 and PdL6	220
Table 10. Selected bond lengths and angles of the mono-palladium β -dimethyl oxazoline thiourea complexes.	222
Table 11. The angles between planes in the mono-palladium β -dimethyl oxazoline thiourea complexes. ^a	226
Table 12. Intermolecular Cl...H(D) contact distances in the mono-palladium complexes of the β -dimethyl oxazoline thioureas. ^a	227
Table 13. Crystal structure of palladium complexes of L5	235
Table 14. Selected bond lengths, angles and dihedral angles of di-palladium β -dimethyl oxazoline thiourea complexes. ^a	236
Table 15. Close intermolecular contact distances and angles in Pd₂L5 . ^a	238
Table 16. Crystallographic data of Pd₃L7	242
Table 17. Selected bond lengths, angles and dihedral angles of Pd₃L7	243
Table 18. Crystallographic data for Pd-R-L9up and Pd-R-L10	245
Table 19. Selected bond lengths and angles of Pd-R-L9up and Pd-R-L10	247
Table 20. Crystallographic data for Pd₂-S-L9down	251
Table 21. Selected bond lengths and angles of Pd₂-S-L9down	251
Table 22. Crystallographic data for PdL12	254
Table 23. Selected bond lengths and angles of PdL12	254
Table 24. ^1H NMR assignments for the β -dimethyl oxazoline thiourea monopalladium complexes (positions 1-12).	256
Table 25. ^1H NMR assignments for R-substituents of the β -dimethyl oxazoline thiourea monopalladium complexes.	259
Table 26. ^1H NMR assignment for R'-substituents of the β -dimethyl oxazoline thiourea monopalladium complexes.	261
Table 27. ^1H NMR assignment for Pd₂L5	265
Table 28. ^1H NMR assignment for the β -monomethyl oxazoline thiourea monopalladium complexes (positions 1 - 16).	266
Table 29. ^1H NMR assignment for the R'-substituent of the β -monomethyl oxazoline thiourea mono-palladium complexes.	267
Table 30. ^1H NMR assignment for Pd₂-S-L9down	268
Table 31. The $^{13}\text{C}\{^1\text{H}\}$ NMR shifts (ppm) for the C=S and C=N carbons of the β -dimethyl oxazoline thiourea palladium complexes in CD_2Cl_2 unless other noted. ...	269
Table 32. The C=S and C=N $^{13}\text{C}\{^1\text{H}\}$ signals of the β -monomethyl oxazoline thiourea palladium complexes in CDCl_3 (ppm).	275
Table 33. Pd-catalyzed bis(methoxycarbonylation) of styrene using oxazoline thioureas. ^a	281

Chapter 5

Table 1. P=S stretching of phosphine sulfides.....	319
Table 2. The $^{13}\text{C}\{^1\text{H}\}$ and $^{31}\text{P}\{^1\text{H}\}$ NMR shifts and $^{13}\text{C}-^{31}\text{P}$ coupling constants of EPR_3 (E = O, S; R = Ph, $^n\text{Bu}_3$).....	320
Table 3. P=S bond lengths of phosphine sulfides.....	321
Table 4. Bond lengths and angles of monodentate metal-phosphine sulfide complexes.....	322
Table 5. Bond lengths and angles of $\kappa^2\text{-C,S}$ bidentate metal-phosphine sulfide complexes.....	323
Table 6. Bond lengths and angles of $\kappa^2\text{-N,S}$ bidentate metal-phosphine sulfide complexes. ^a	323
Table 7. Bond lengths and angles of $\kappa^2\text{-P,S}$ bidentate metal-phosphine sulfide complexes.....	324
Table 8. Bond lengths and angles of $\kappa^2\text{-S,S}$ bidentate metal-phosphine sulfide complexes.....	325
Table 9. Bond lengths and angles of $\kappa^3\text{-S,P,S}$ tridentate metal-phosphine sulfide complexes.....	327
Table 10. Bond lengths and angles of $\kappa^3\text{-S,C,S}$ tridentate metal-phosphine sulfide complexes.....	328
Table 11. Bond lengths and angles of other tridentate metal-phosphine sulfide complexes.....	329
Table 12. Pd-S bond lengths and Pd-S-P bond angles in phosphine sulfide palladium complexes.....	329
Table 13. Crystallographic data for dppmS , dppeS , dppfS , dcpeS₂ and dppbS₂	346
Table 14. Selected bond lengths and angles of dppmS , dppeS and dppfS	347
Table 15. Selected bond lengths and angles of the bis(phosphine) disulfides.....	347
Table 16. Intermolecular contact distances in the monosulfides and disulfides.....	348
Table 17. Crystallographic data for Pd(dppmS) , Pd(dppeS) , Pd(dppfS) and Pd(dppbS)	354
Table 18. Selected bond lengths and angles of the bis(phosphine) monosulfide palladium complexes.....	355
Table 19. Intermolecular contact distances in monosulfide complexes.....	357
Table 20. The $^{31}\text{P}\{^1\text{H}\}$ (202 MHz) NMR chemical shifts and $J_{\text{P-C}}$ couplings of bis(phosphine) monosulfide palladium complexes and the free ligands. ^a	358
Table 21. The $^{31}\text{P}\{^1\text{H}\}$ chemical shifts of the bis(phosphine) disulfide palladium complexes. ^a	359
Table 22. Crystallographic data for Pd(dppmS₂) and Pd(dcpeS₂)	361
Table 23. Bond lengths and angles of Pd(dppmS₂) , Pd(dppeS₂) and Pd(dcpeS₂)	362
Table 24. Crystallographic data for Pd(dppmS)₂ and Pd(dppeS)₂	368
Table 25. Selected bond lengths and angles of Pd(dppmS)₂·2CD₂Cl₂ and Pd(dppmS)₂·4CHCl₃	369
Table 26. Crystallographic data for Pd(dppmS₂)₂ , Pd(dppeS₂)₂ and Pd(dppfS₂)₂	375
Table 27. Bond lengths and angles of Pd(dppmS₂)₂ , Pd(dppeS₂)₂ and Pd(dppfS₂)₂	376
Table 28. Bond lengths and angles of the structures of Pd(dppm) , Pd(dppe) , Pd(dppp) , Pd(dcpe) , Pd(dppf)·CHCl₃ , Pd(dppf)·CH₂Cl₂ and Pd(dppe)₂	380
Table 29. Isolated yields for the homo-coupling of phenylacetylene using palladium complexes of bis(phosphine) monosulfides and disulfides.....	391

List of Schemes

Chapter 1

Scheme 1. Generic catalytic cycle of palladium catalysed cross-coupling reactions.	3
Scheme 2. The Heck-Mizoroki reaction.	4
Scheme 3. Mechanism of the Heck-Mizoroki reaction.	4
Scheme 4. The Stille reaction.	5
Scheme 5. The Suzuki-Miyaura reaction.	5
Scheme 6. The Sonogashira reaction.	6
Scheme 7. The Negishi reaction.	6
Scheme 8. General scheme for hydroxy- and alkoxyacylation. ⁴⁵	7
Scheme 9. General scheme for the bis(alkoxyacylation) of alkenes. ⁵⁴	8
Scheme 10. Resonance structures of imidazolyl-2-ylidenes.	11
Scheme 11. The conversion between NHC carbene and thiourea. ^{113, 114}	13

Chapter 2

Scheme 1. Synthesis of tolans.	21
-------------------------------------	----

Chapter 3

Scheme 1. Synthesis of symmetric thioureas from amine and thiophosgene. ¹²	81
Scheme 2. Preparation of symmetrical thioureas. ⁴¹	81
Scheme 3. Synthesis of chiral thiourea. ¹⁷	82
Scheme 4. Synthesis of an unsymmetric thiourea from amines.	82
Scheme 5. Synthesis of an unsymmetric thiourea from the reaction of molybdenum dithiocarbamate with amines. ^{49, 50}	82
Scheme 6. The preparation of chiral thiourea-oxazoline S,N heterobidentate ligands. ¹³	83
Scheme 7. Delocalization of the C=S bond (A) and (B) and a model of the π -system in thioureas (C).	84
Scheme 8. Preparation of palladium-monodentate thiourea complexes.	86
Scheme 9. Preparation of chelated palladium thiourea complexes.	87
Scheme 10. The preparation of a [5,6] bicyclic palladium thiourea complex. ⁷⁸	87
Scheme 11. The reaction of palladium acetate with thiosemicarbazide derivatives. ⁶³	87
Scheme 12. Tmtu ligand exchange to afford a cyclometallated palladium thiourea complex. ⁸⁰	89
Scheme 13. Synthesis of an ortho-cyclometalated N,N-dimethyl pyrrole-1-carbothioamide complex. ⁶⁵	89
Scheme 14. Synthesis of cyclometallated palladium-thiourea complexes from iminoacyl palladium complexes. ⁶⁴	90
Scheme 15. Rearrangements of a thiourea palladium complex. ⁸¹	90
Scheme 16. Diyne ring closure <i>via</i> Pd-catalyzed carbonylation. ⁹¹	96
Scheme 17. Oxidative carbonylation of a vinyl alcohol. ⁹²	96
Scheme 18. Combined oxidative and reductive carbonylation of terminal alkynes with palladium iodide-thiourea catalysts. ⁹³	96
Scheme 19. The application of bis(thiourea) ligand in Heck-Mizoroki and Suzuki-Miyaura reaction. ¹⁵	97

Scheme 20. Reaction condition used in Heck-Mizoroki and Suzuki-Miyaura reactions of arenediazonium salt. ¹⁷	97
Scheme 21. Reaction condition in Heck-Mizoroki and Suzuki-Miyaura reactions of aryl halide. ¹⁹	97
Scheme 22. Reaction condition in Suzuki-Miyaura carbonylation reactions of aryl halide. ¹⁹	98
Scheme 23. Reaction condition used in Heck-Mizoroki reaction of a sterically hindered. ¹⁸	98
Scheme 24. Bis(methoxycarbonylation) of terminal olefins and ligands used in the reaction. ¹²	98
Scheme 25. Asymmetric bis(methoxycarbonylation) of styrenes. ¹³	99
Scheme 26. Heck-Mizoroki reactions of styrene with aryl bromides. ¹⁴	99
Scheme 27. The synthesis of a resin-bound palladium thiourea complex. ⁹⁴	100
Scheme 28. The Pauson-Khand reaction of allylpropargylamine. ²⁰	101
Scheme 29. Thiourea-palladium-catalyzed carbonylative annulation of iodophenol acetates. ⁹⁶	101
Scheme 30. Synthetic route to Crisamicin A. ⁹⁷	101
Scheme 31. The synthetic routes for the mono- and di-palladium chiral thiourea complexes.	127
Scheme 32. The reaction of PdCl ₂ with L(S,S).	154
Scheme 33. The reaction of PdCl ₂ and L(rac).	157
Scheme 34. Postulated summary of the <i>trans-rac-Pd</i> / <i>trans-meso-Pd</i> conversion.	160
Scheme 35. Postulated summary of S,S-Pd ₂ conversion.	162
Scheme 36. The conversion of <i>rac-Pd</i> ₂ / <i>meso-Pd</i> ₂ .	163
Scheme 37. Formation of an equilibrium mixture of <i>rac-Pd</i> ₂ and <i>meso-Pd</i> ₂ from reaction of S,S-Pd ₂ and R,R-Pd ₂ .	165

Chapter 4

Scheme 1. Bis(methoxycarbonylation) of terminal olefins. ¹²	184
Scheme 2. Synthesis of β -dimethyl oxazoline thioureas developed by the group of Prof. Z. Yang.	186
Scheme 3. The synthesis of the β -monomethyl oxazoline thiourea L9 developed by the group of Prof. Z. Yang.	189
Scheme 4. The synthesis of the β -monomethyl oxazoline thiourea L10 reported by the group of Prof. Z. Yang.	191
Scheme 5. The preparation of oxazoline thiourea palladium complexes.	216
Scheme 6. The conversion of PdL5 to Pd ₂ L5.	271
Scheme 7. The interconversion of PdL7 and Pd ₃ L7 in solution at room temperature.	273
Scheme 8. The interconversion between dimeric Pd ₂ -S-L9down and monomeric Pd-S-L9down.	275

Chapter 5

Scheme 1. The synthesis of phosphine sulfides from the reaction of phosphines with sulfur.	311
Scheme 2. The synthesis of phosphine sulfides using the Lawesson reagent.	312
Scheme 3. Synthesis of acyclic phosphine sulfides. ⁶	312
Scheme 4. Interconversion of SPR ₃ and SePR ₃ . ⁷	313

Scheme 5. The synthesis of unsymmetric phosphine sulfides developed by Seyferth. ^{8,9}	313
Scheme 6. Preparation of phosphine sulfide complexes.	314
Scheme 7. A bis(diphenyl phosphino)zirconium(IV) carbene disulfide complex and its molecular structure. ¹¹	314
Scheme 8. The synthesis of a κ^3 -S, P ⁻ , S-(diphenylphosphine)phosphinine disulfide manganese tricarbonyl complex. ¹²	315
Scheme 9. Synthesis of cyclometallation rhodium phosphine sulfide. ¹³	315
Scheme 10. A cyclometalated phosphine sulfide ruthenium complex. ¹⁴	315
Scheme 11. The synthesis of a zirconaindene phosphine sulfide complex.	316
Scheme 12. The synthesis of a tetracarbonyl chromium phosphine sulfide complex. ¹⁶	316
Scheme 13. The dynamic equilibrium of $[\text{PdCl}(\kappa^4\text{-pp}_3\text{E}_2)]\text{Cl}$ (E = S, Se) with $[\text{PdCl}_2(\kappa^2\text{-pp}_3\text{E}_2)]$.	317
Scheme 14. The resonance structures of phosphine sulfide.	319
Scheme 15. Applications of phosphine sulfide metal complexes.	335
Scheme 16. Bis(methoxycarbonylation) reaction using SPPH ₃ ligand as ligand. ¹⁴⁴	336
Scheme 17. Cobalt-catalyzed Pauson-Khand reaction using phosphine sulfide as ligand. ¹⁴⁵	336
Scheme 18. The methanol carbonylation with a dppeS rhodium complex. ⁹¹	336
Scheme 19. The hydroformylation of 1-octene with platinum phosphine sulfide complexes. ¹⁴⁶	337
Scheme 20. The Suzuki-Miyaura reaction with a palladium tris(phosphine) disulfide complex as catalyst.	337
Scheme 21. The Heck-Mizoroki reaction with palladium catalysts and dppeS ₂ as ligand.	338
Scheme 22. Allylic alkylations using a chiral P,S ligand. ¹⁴⁸	338
Scheme 23. The asymmetric lithiation-silylation of a phosphine sulfide. ¹⁵⁰	339
Scheme 24. The synthesis of the bis(phosphine) monosulfides and disulfides.	341
Scheme 25. The synthesis of the bis(phosphine) disulfides.	342
Scheme 26. The equilibria of Pd(dppmS) ₂ in CD ₂ Cl ₂ solution.	372

Chapter 6

Scheme 1. The mechanism for the Sonogashira cross-coupling reaction.	414
--	-----

Chapter 1

Introduction



I. Pd-catalyzed cross-coupling reactions

I.1 General concepts

In recent decades, palladium-catalyzed coupling reactions have proven to be among the most powerful and versatile metal-mediated transformations in organic chemistry. Due to the excellent performance of these reactions, they have been used extensively, for example, in total synthesis and in the synthesis of conjugated materials with great success.

Palladium is a member of Group 10 of the periodic table. Its complexes exist in three oxidation states, Pd(0), Pd(II), and Pd(IV). The facile interconversion between these oxidation states is responsible for the role of palladium in catalysis, as each oxidation state exhibits different chemistries. Palladium(0) complexes are fairly nucleophilic, rather labile and are also easily oxidized, usually to the Pd(II) state. The most synthetically useful reaction is based on the oxidative addition of aryl, vinylic, or allylic halides or triflates to Pd(0) to form Pd(II) species. Palladium(II) complexes are extremely important in organopalladium chemistry. They are typically electrophilic, soluble in most common organic solvents, and stable to air in which they can be easily stored and handled. The most common organic substrates for Pd(II) are electron-rich species, such as olefins, alkynes, and arenes. Some of the most useful Pd(II) chemistry is based on the fast and reversible formation of Pd(II) complexes with olefins and alkynes, which undergo subsequent attack by nucleophiles. Numerous Pd(II) complexes of the type L_2PdCl_2 are easily formed from $PdCl_2$ and the appropriate ligand L.

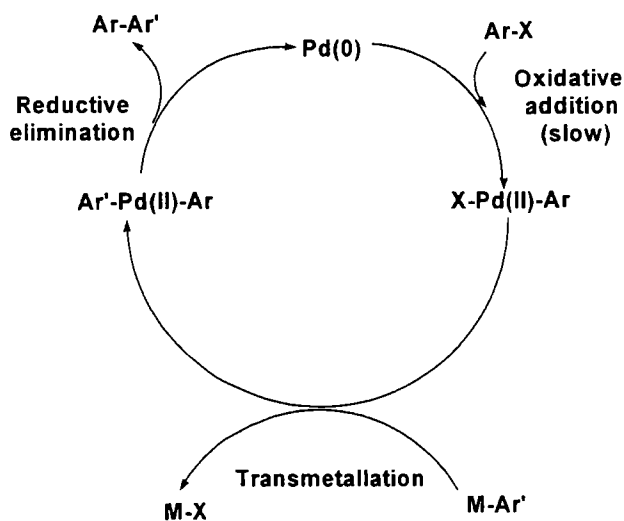
Some useful examples of Pd(II) complexes are $PdCl_2(PPh_3)_2$, $Pd(OAc)_2$, and $PdCl_2(RCN)_2$. Palladium(II) complexes are often added to reactions as precatalysts and are then reduced to Pd(0), typically stabilised in solution by appropriate ligands which also raise the electron density at the metal to facilitate oxidative addition and provide enough bulkiness to accelerate reductive elimination.

It is in the synthesis of compounds containing C–C, C–N, C–O bonds, that palladium catalyzed cross-coupling methods have the greatest impact. The Suzuki-Miyaura, Stille, Sonogashira, Kumada-Tamuo-Corriu, and Negishi couplings are among the most powerful and versatile tools for the synthesis of these compounds, exhibiting high functional group compatibility and broad reaction scope. Although reaction conditions and the nature of the organometallic component vary from one

type of cross-coupling reaction to another, all of these reactions are mechanistically related (Scheme 1).

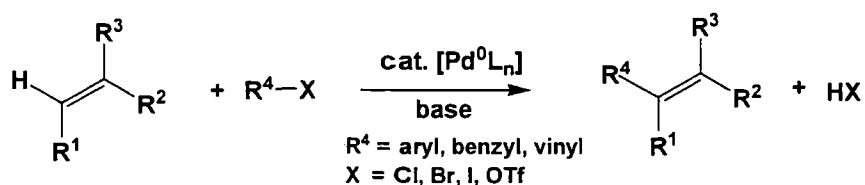
The first step of the catalytic cycle involves the oxidative addition of a carbon-halide bond (or equivalent) to a Pd(0) catalyst to generate an electrophilic aryl- or vinyl- palladium(II) intermediate. Reaction of this species with a nucleophilic organometallic reagent *via* transmetallation provides a diorganyl-palladium(II) species which undergoes reductive elimination to form the C–C bond and regenerate the Pd(0) catalyst. Important progress has been made over the last decade in catalyst development leading to mild, high yielding processes that can be performed with low catalyst loadings.

The majority of catalyst development efforts have been directed at enhancing the rate of the first step of the catalytic cycle, *i.e.*, oxidative addition, which in most cases is the rate determining step of the catalytic cycle. Notably, this work has enabled extension of these reactions to include very challenging aryl halides such as deactivated aryl chlorides and very sterically hindered bis ortho-substituted aryl halides. In contrast, the transmetallation step has been less extensively studied and optimized. Since transmetallation is typically not rate-determining or problematic, this reduced attention compared to oxidative addition seemed reasonable until the first step was optimized.

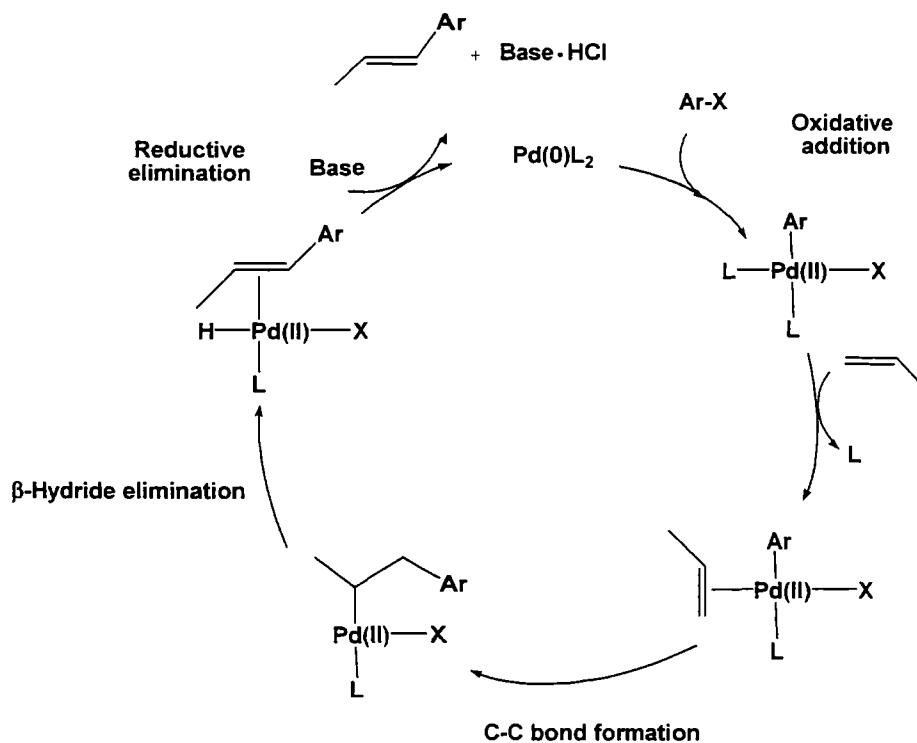


Scheme 1. Generic catalytic cycle of palladium catalyzed cross-coupling reactions.

The Heck-Mizoroki reaction is a palladium catalyzed coupling of alkenyl or aryl (sp^2) halides or triflates with alkenes to yield diene or vinyl arene products (Scheme 2). The first examples of this reaction were reported independently by Mizoroki (1971)¹ and, in an improved form, by Heck (1972).² The development of catalytic asymmetric Heck reactions in the late 1980s led to a further resurgence of interest in this field.³⁻⁵ Mechanistically, it is similar to most other cross-coupling reactions, except that it also involves alkene insertion and β -hydride elimination (Scheme 3).



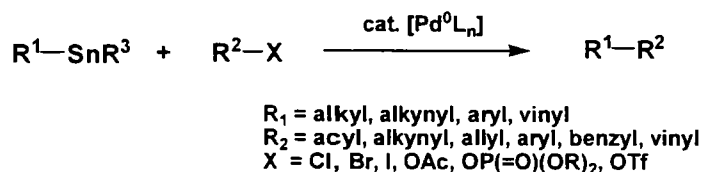
Scheme 2. The Heck-Mizoroki reaction.



Scheme 3. Mechanism of the Heck-Mizoroki reaction.

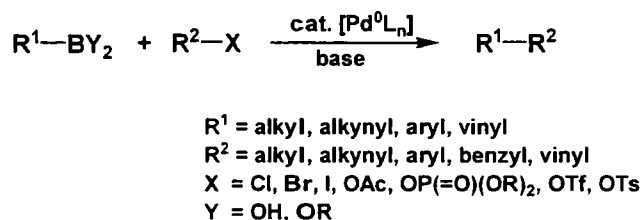
The Stille reaction is a palladium catalyzed cross-coupling reaction of organic electrophiles with vinyl organotin compounds⁶⁻¹⁰ (Scheme 4). The Stille reaction is

one of the most widely applied palladium-catalyzed C–C bond forming reactions, due to typically mild reaction conditions and the tolerance to a wide variety of sensitive functionalities in this transformation.



Scheme 4. The Stille reaction.

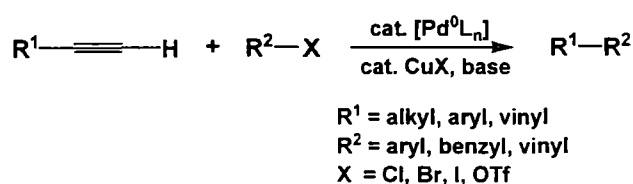
Another extraordinary C–C bond forming reaction involves the palladium-catalyzed coupling of organic electrophiles, such as aryl or alkenyl halides and triflates, with organoboron compounds in the presence of a base (Scheme 5),¹¹ a process known as the Suzuki-Miyaura reaction, the first examples of which were reported in 1979.¹²⁻¹⁴ The Suzuki-Miyaura reaction is particularly useful as a method for the construction of conjugated dienes and higher polyene systems of high stereoisomeric purity, as well as of biaryl and related systems. Progress has been made in the development of Suzuki-Miyaura coupling reactions of unactivated alkyl halides, enabling C(sp²)–C(sp³) and even C(sp³)–C(sp³) bond-forming processes.¹⁵⁻¹⁷ The ease of preparation of organoboronates (*e.g.* aryl, vinyl, alkyl) and their relative stability to air and water, combined with the relatively mild conditions for the reaction as well as the formation of nontoxic by-products, makes the Suzuki-Miyaura reaction a valuable synthetic method for organic chemists.



Scheme 5. The Suzuki-Miyaura reaction.

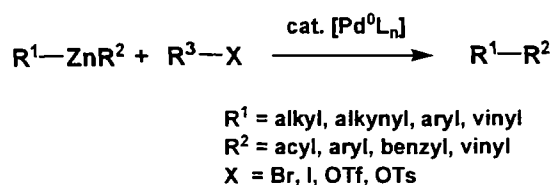
The palladium-catalyzed coupling of terminal alkynes with vinyl or aryl halides was first reported independently and simultaneously by the groups of Cassar¹⁸

and Heck¹⁹ in 1975. A few months later, Sonogashira *et al.* demonstrated that, in many cases, this cross-coupling reaction could be accelerated by the addition of co-catalytic Cu(I) salts to the reaction mixture.^{20, 21} The Sonogashira reaction (Scheme 6) can be viewed as an application of palladium catalysis to the venerable Stephens-Castro reaction (the coupling of vinyl or aryl halides with stoichiometric amounts of copper(I) acetylides).²² The Sonogashira reaction provides a method for the synthesis of conjugated acetylenic systems, which are used in a diverse array of important applications from natural products and pharmaceuticals to designer molecules of interest in biotechnology and nanotechnology.



Scheme 6. The Sonogashira reaction.

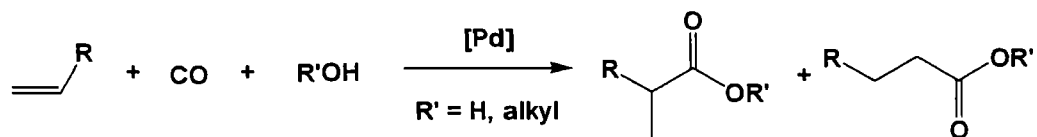
The use of organozinc reagents as the nucleophilic component in palladium-catalyzed cross-coupling reactions is known as the Negishi coupling (Scheme 7). Organozinc reagents exhibit a very high intrinsic reactivity in palladium-catalyzed cross-coupling reactions which, combined with the availability of a number of procedures for their preparation and their relatively low toxicity, makes the Negishi coupling an exceedingly useful alternative to other cross-coupling procedures, as well as constituting an important method for C–C bond formation.^{23, 24}



Scheme 7. The Negishi reaction.

There are many recent reviews of the Heck-Miyaura,^{25, 26} Stille,^{27, 28} Suzuki-Miyaura^{29, 30} and Sonogashira reactions³¹⁻³³ and general Pd-catalyzed cross-coupling reactions.^{10, 34-44}

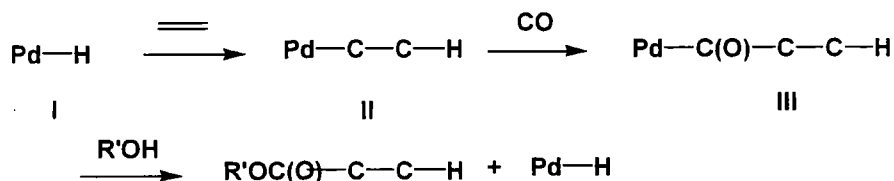
Another palladium catalyzed reaction worth including in this introduction is the hydroxy- and alkoxy-carbonylation of olefins (Scheme 8). This reaction is used to transform cheap feedstocks (e.g. CO, olefins and alcohols) into esters.



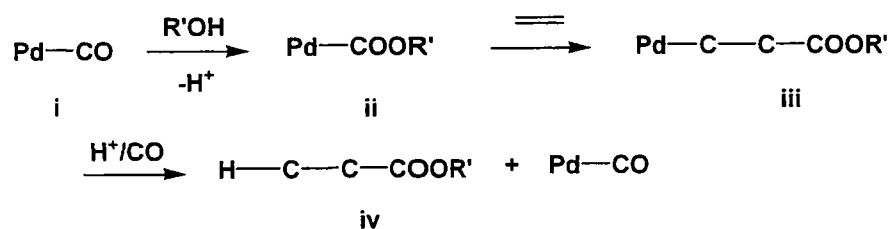
Scheme 8. General scheme for hydroxy- and alkoxy-carbonylation.⁴⁵

Two mechanistic pathways, *vide infra*, proposed for the alkoxy-carbonylation of olefins catalyzed by palladium complexes are (A) a hydride mechanism⁴⁶⁻⁵⁰ and (B) an alkoxy mechanism.^{2, 47, 51, 52}

Mechanism I:



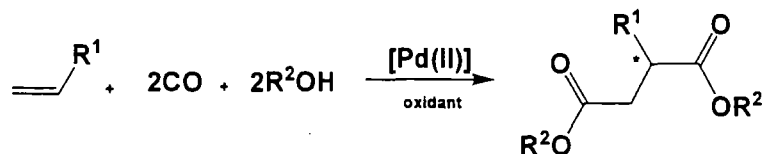
Mechanism II:



In the hydride mechanism (A), the first step is the insertion of the alkene into the Pd-H bond to form an alkyl complex, followed by coordination and migratory insertion of CO to produce a Pd-acyl species. Alcoholysis of the Pd-acyl regenerates the Pd-H complex and yield the ester. For alkoxy-carbonyl mechanism (B), alkene inserts into the M-C σ bond of the alkoxy-carbonyl-palladium complex ii, followed by alcoholysis to yield an alkoxy-palladium complex and the ester.

The bis(alkoxy-carbonylation) of alkenes is shown in Scheme 9. The reactions are usually performed using styrene as a substrate for the palladium catalysts, in the

presence of an oxidant (e.g. O₂, benzoquinone). The role of the oxidant is to reoxidise the Pd(0) formed during the process. No complete mechanistic studies have been reported.



Scheme 9. General scheme for the bis(alkoxycarbonylation) of alkenes.⁵³

I.2 Ligands effects

Initially, the substrates which were used in cross-coupling reactions were only reactive aryl bromides and iodides. However, aryl chlorides are more widely available and generally less expensive than the bromides and iodides. So the search for the suitable ligands showing higher reactivity and selectivity has been a field of enormous activity. Palladium complexes which contain electron-rich and bulky ligands (*i.e.* phosphines and carbenes) have been found to improve the catalytic activity in coupling reactions. There are several groups who have established the combination of bulky and electron-rich phosphines with different sources of palladium to generate species that show high catalytic activity in cross-coupling reactions, for example, mixtures of P^tBu₃ and either Pd(OAc)₂ or [Pd₂(dba)₃] have unusually high activities in amination reactions,⁵⁴ and Suzuki-Miyaura coupling reactions of a broad spectrum of aryl halides.⁵⁵ Fu *et al.* studied the catalytic properties of palladium complexes with different phosphines as ligands, compared by using different aryl halides as substrates.⁵⁶ In these studies, it was shown that a mixture of [Pd₂(dba)₃] and P^tBu₃ catalyzed the Suzuki-Miyaura cross-coupling of vinyl and aryl halides (including chlorides) with arylboronic acids. With Pd(OAc)₂ in the presence of PCy₃, a good catalyst for the cross-coupling reaction of vinyl and aryl triflates with arylboronic acids is generated. The system with P^tBu₃ showed high selectivity with the order of reactivity I>Br>Cl>>OTf. Littke and Fu also demonstrated that a mixture of [Pd₂(dba)₃] and P^tBu₃ yields a general catalyst system for Stille cross-coupling⁵⁷ and Heck-Mizoroki reactions.⁵⁷ Hartwig *et al.* reported that this palladium/phosphine combination produces an excellent catalyst for the arylation of ketones and malonates.^{58, 59} They also studied in detail the formation of C–N bonds catalyzed by palladium in the presence of bulky and electron-rich phosphines.⁶⁰⁻⁶² Beller *et al.*

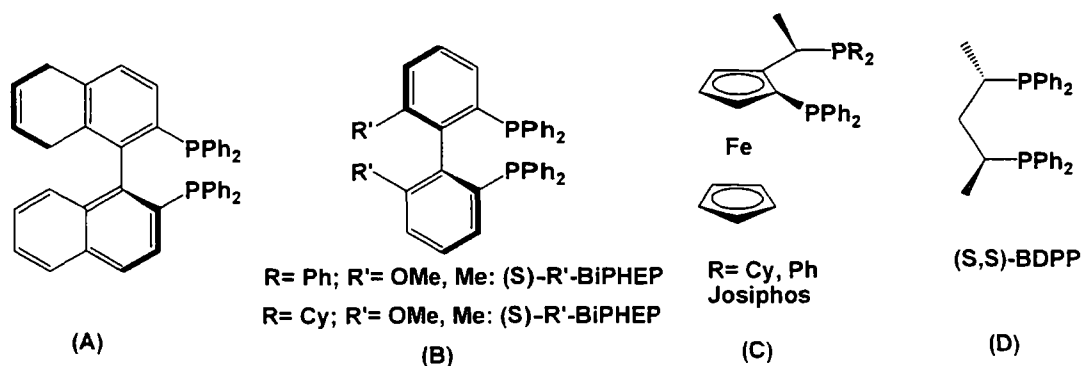
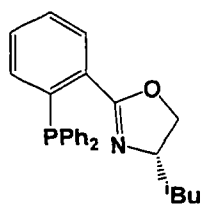
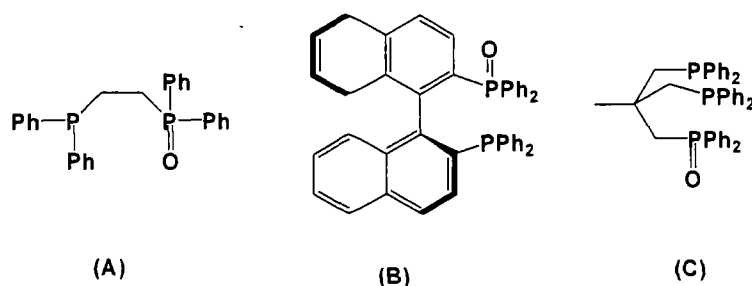


Figure 3. Chiral bis(phosphine) ligands.

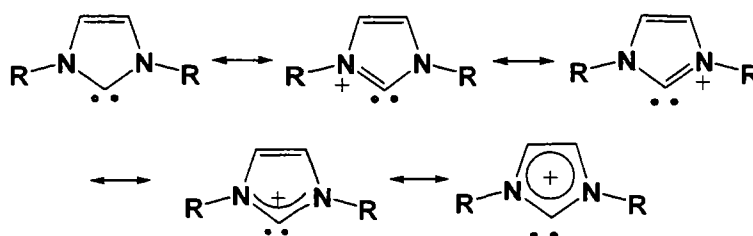
Figure 4. Phosphine oxazoline ligand.⁷¹

From the applications point of view, phosphine ligands are affected by one problem: they are subject to oxidation. Therefore, reactions need to be carried out in an inert atmosphere. To overcome this problem, several phosphine oxides including chiral ones have been reported (Figure 5).

Figure 5. Bis(phosphine) mono-oxides.⁷²

Tertiary phosphine ligands are useful in controlling reactivity and selectivity in organometallic chemistry and homogeneous catalysis.^{73, 74} However, their sensitivity to air has limited their use in certain types of (*e.g.* oxidation) catalysis. They can also suffer from P–C bond cleavage at elevated temperatures. In some catalytic processes, these result in deactivation of the catalyst and higher phosphine concentrations are required.

N-heterocyclic carbenes (NHC) are considered as neutral, two electron donor ligands with negligible π -back bonding tendency (Scheme 10).⁷⁵ As such, they have attracted considerable attention as alternatives to phosphines.⁷⁶⁻⁸⁰ Complexes of NHC ligands with main-group and transition metals in both high and low oxidation states have been synthesized.^{81, 82} In the palladium complexes, as with most other transition metals, the NHCs act as powerful, neutral, two electron donors to the metal atom.^{83, 84}



Scheme 10. Resonance structures of imidazolyl-2-ylidenes.

While the π -acceptor properties of phosphines are well established,^{85, 86} in carbenes, the π -back donation from Pd to the NHC π^* orbital is negligible.^{87, 88} But, some recent computational and experimental studies challenge such views⁸⁹ –the NHCs can use different orbitals for bonding to match the complementary metal orbitals. This bonding is illustrated by the following two examples: Abernethy *et al.* found significant π -back bonding from the chloro ligands in the *cis* position to the NHC in the isolated [(IMes)VOC₃] complex (Figure 6).⁹⁰ The stability of this compound to air makes it an excellent entry point into vanadium-oxo chemistry and demonstrates the utility of N-heterocyclic carbenes to stabilize high-oxidation-state transition metal complexes. This is supported by crystal structure and DFT calculations which suggest that these interligand bonding interactions involve significant vanadium d-orbital contributions. There can be considered to be a form of back-bonding to the carbene with the electron density originating from the chloride ligand lone pairs rather than the metal.

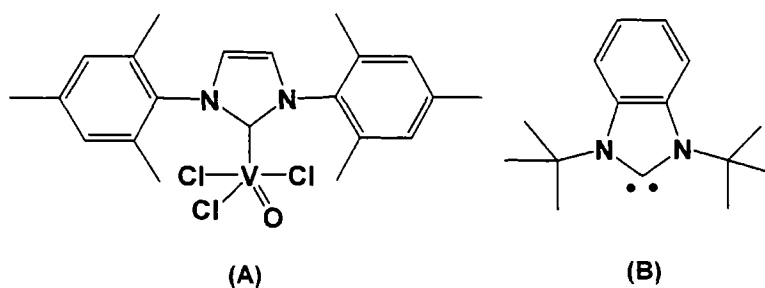
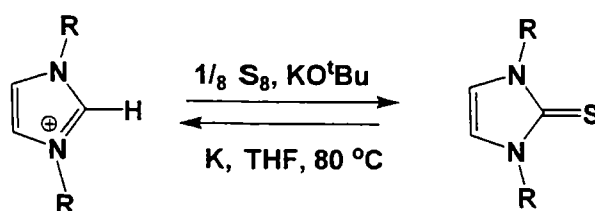


Figure 6. (A) (IMes)VOCl₃ and (B) I'Bu.

Nolan *et al.* observed π -donation from I'Bu in a low coordinate, 14-electron iridium complex.⁸³ Thermochemical and computational studies on NHC complexes of ruthenium⁹¹ and nickel⁹² have shown that NHCs form considerably stronger bonds to the metal atom than do phosphines. It was observed that the carbenes appear to give a greater degree of thermal stability with regard to dissociation of the ligand from the metal center. As a consequence, the number of catalytic reactions making use of nucleophilic carbenes as catalyst modifiers is increasing. There are some examples of the use of metal-carbene complexes in hydrosilylation,⁹³ Ru-catalyzed furan synthesis⁹⁴ and olefin metathesis.⁹⁵⁻⁹⁸ The concept of NHCs as “phosphine mimics” proved to be extremely fruitful for catalysis. There are several reviews dealing with separate aspects of the field; chiral NHCs,^{99, 100} structure, bonding, and the reactivity of free NHCs,^{101, 102} as well as NHC complexes with transition metals.^{83, 84, 103-106} The early Pd–NHC chemistry specifically directed towards C–C cross-coupling reactions was summarized by Herrmann *et al.* in 2003.¹⁰⁷ There are various other reviews on phosphines and carbenes in the literature.¹⁰⁸⁻¹¹⁰

Like phosphine ligand, almost all NHCs are air and moisture unstable. Therefore, another type of the related ligand can be introduced, *i.e.* thiourea ligands. Thioureas are an oxidized version of NHCs (Scheme 11). They are air and moisture stable. Several thiourea ligands have been reported to be useful in palladium catalyzed reactions (more details are provided in Chapter 3).



Scheme 11. The interconversion between NHC carbene and thiourea.^{111, 112}

Thioureas can be considered to be sulfur adducts of NHCs, analogous to the relationship between phosphine sulfides and phosphines (see Chapter 5)

Since their discovery, Pd catalysts have been developed and have proved to be useful tools in organic synthesis. Many different substrates can be coupled as discussed above. Variation of the ligand on the Pd metal center can allow chemists to improve catalysis and allow for many different catalytic processes to be conducted with various substrates. In particular, ligands that are easy to prepare and air stable are of great interest.

Several such air stable ligands, were investigated including their palladium complexes, and the results are discussed in Chapters 3, 4 and 5.

II. Organization of the thesis

This thesis is composed of two parts. The first part examines Pd-catalyzed cross-coupling reactions, focusing on the synthesis of diarylacetylenes using the Sonogashira reaction. The single crystal structures and liquid crystal phases of these diarylacetylenes have been explored, although little correlation of the solid state packing and liquid crystal mesophase can be made. The second part is devoted to an investigation of palladium complexes of chiral thiourea, chiral thiourea-oxazoline, and bis(phosphine) mono- and disulfide ligands. The chiral thioureas and chiral thiourea-oxazolines are part of an ongoing collaboration with Prof. Zhen Yang, Peking University, China. All synthesis of the chiral thiourea and thiourea-oxazoline ligands was performed at Peking University and the Pd-complexes were prepared and characterized in Durham.

Chapter 1 explains the organization and aims of the thesis. It includes an overview and an introduction to the research with a literature review on palladium-catalyzed cross-coupling reactions and the ligands employed (*e.g.* phosphine and carbene).

Chapter 2 introduces the synthesis, single crystal structures and liquid crystal phase behavior of alkoxy substituted tolans, synthesized using the Sonogashira cross-coupling reaction. Both the phase-behavior and single-crystal structures of three homologous series of tolans were examined. The objective was to study the single-crystal structures of compounds which can attain liquid crystalline phases in order to provide possible insight into the forces which direct the organisation of the mesophases.

The next section is devoted to the studies of two types of thiourea ligands, monodentate thiourea and S,N-bidentate thiourea oxazolines. Chapter 3 presents the syntheses and dynamic NMR studies of palladium complexes of a C₂-symmetric thiourea and tetramethyl thiourea. Chapter 4, on the bidentate S,N-thiourea oxazolines, is devoted to the synthesis and full characterization of their palladium complexes and their application in the Pd-catalyzed asymmetric bis(methoxycarbonylation) of terminal olefins. The thiourea ligands and their palladium complexes are investigated in order to better understand their catalytic properties.

Chapter 5 explores two types of ligands and their palladium complexes. The synthesis of bis(phosphine) mono- and di-sulfides and their application as catalyst precursors for the oxidative homo-coupling of phenylacetylene are described. Our premise was that phosphine sulfides have the same relationship to phosphines that thioureas have to N-heterocyclic carbenes.

Final chapter, Chapter 6, is the summary and suggestion for future work.

III. References

1. Mizoroki, T.; Mori, K.; Ozaki, A., *Bull. Chem. Soc. Jpn.* **1971**, *44*, 581.
2. Heck, R. F., *Palladium reagents in organic syntheses*, London, 1990; p 461.
3. Dounay, A. B.; Overman, L. E., *Chem. Rev.* **2003**, *103*, 2945.
4. Shibasaki, M.; Christopher, D. J. B.; Kojima, A., *Tetrahedron* **1997**, *53*, 7371.
5. Shibasaki, M.; Vogl, E. M., *J. Organomet. Chem.* **1999**, *576*, 1.
6. Milstein, D.; Stille, J. K., *J. Am. Chem. Soc.* **1978**, *100*, 3636.
7. Milstein, D.; Stille, J. K., *J. Am. Chem. Soc.* **1979**, *101*, 4992.
8. Stille, J. K., *Angew. Chem.* **1986**, *98*, 504.
9. Kosugi, M.; Sasazawa, K.; Shimizu, Y.; Migita, T., *Chem. Lett.* **1977**, 301.
10. Negishi, E., *J. Organomet. Chem.* **2002**, *653*, 34.
11. Suzuki, A., *Acc. Chem. Res.* **1982**, *15*, 178.
12. Miyaura, N.; Yamada, K.; Suzuki, A., *Tetrahedron Lett.* **1979**, *20*, 3437.
13. Miyaura, N.; Suzuki, A., *J. Chem. Soc., Chem. Commun.* **1979**, 866.
14. Miyaura, N.; Suzuki, A., *Chem. Rev.* **1995**, *95*, 2457.

15. Ishiyama, T.; Abe, S.; Miyaura, N.; Suzuki, A., *Chem. Lett.* **1992**, 691.
16. Zhou, J.; Fu, G. C., *J. Am. Chem. Soc.* **2004**, *126*, 1340.
17. Frisch, A. C.; Beller, M., *Angew. Chem.* **2005**, *117*, 680.
18. Cassar, L., *J. Organomet. Chem.* **1975**, *93*, 253.
19. Dieck, H. A.; Heck, F. R., *J. Organomet. Chem.* **1975**, *93*, 259.
20. Sonogashira, K.; Tohda, Y.; Hagihara, N., *Tetrahedron Lett.* **1975**, *16*, 4467.
21. Sonogashira, K., *J. Organomet. Chem.* **2002**, *653*, 46.
22. Stephens, R. D.; Castro, C. E., *J. Org. Chem.* **1963**, *28*, 3313.
23. Erdik, E., *Tetrahedron* **1992**, *48*, 9577.
24. Negishi, E.; Takahashi, T.; Babu, S.; Horn, D. E. v.; Okukado, N., *J. Am. Chem. Soc.* **1987**, *109*, 2393.
25. Djakovitch, L.; Wagner, M.; Hartung, C. G.; Beller, M.; Koehler, K., *J. Mol. Cat. A, Chemical* **2004**, *219*, 121.
26. Trzeciak, A. M.; Ziólkowski, J. J., *Coord. Chem. Rev.* **2005**, *249*, 2308.
27. Kosugi, M.; Fugami, K., *J. Organomet. Chem.* **2002**, *653*, 50.
28. Shirakawa, E.; Hiyama, T., *J. Organomet. Chem.* **2002**, *653*, 114.
29. Baudoin, O., *Angew. Chem. Int. Ed.* **2007**, *46*, 1373.
30. Suzuki, A., *J. Organomet. Chem.* **1999**, *576*, 147.
31. Tykwinski, R. R., *Angew. Chem. Int. Ed.* **2003**, *142*, 1566.
32. Doucet, H.; Hierso, J.-C., *Angew. Chem. Int. Ed.* **2007**, *6*, 834.
33. Chinchilla, R.; Nájera, C., *Chem. Rev.* **2007**, *107*, 874.
34. Wolfe, J. P.; Wagaw, S.; Marcoux, J.-F.; Buchwald, S. L., *Acc. Chem. Res.* **1998**, *31*, 805.
35. Hartwig, J. F., *Acc. Chem. Res.* **1998**, *31*, 852.
36. Littke, A. F.; Fu, G. C., *Angew. Chem. Int. Ed.* **2002**, *41*, 4176.
37. Cárdenas, D. J., *Angew. Chem. Int. Ed.* **2003**, *42*, 384.
38. Zapf, A., *Angew. Chem. Int. Ed.* **2003**, *42*, 5394.
39. Schlummer, B.; Scholz, U., *Adv. Synth. Catal.* **2004**, *346*, 1599.
40. Tietze, L. F.; Ila, H.; Bell, H. P., *Chem. Rev.* **2004**, *104*, 3453.
41. Nicolaou, K. C.; Bulger, P. G.; Sarlah, D., *Angew. Chem. Int. Ed.* **2005**, *44*, 4442.
42. Zeni, G.; Larock, R. C., *Chem. Rev.* **2006**, *106*, 4644.
43. Batsanov, A. S.; Collings, J. C.; Fairlamb, I. J. S.; Holland, J. P.; Howard, J. A. K.; Lin, Z.; Marder, T. B.; Parsons, A. C.; Ward, R. M.; Zhu, J., *J. Org. Chem.* **2005**, *70*, 703.
44. Liégault, B.; Renaud, J.-L.; Bruneau, C., *Chem. Soc. Rev.* **2008**, *37*, 290.
45. Bianchini, C.; Lee, H. M.; Mantovani, G.; Meli, A.; Oberhauser, W., *New J. Chem.* **2002**, *26*, 387.
46. Knifton, J. F., *J. Org. Chem.* **1976**, *41*, 793.
47. Milstein, D., *Acc. Chem. Res.* **1988**, *21*, 428.
48. Cavinato, G.; Toniolo, L., *J. Organomet. Chem.* **1990**, *398*, 187.
49. Kanawa, M.; S.Nakamura; Watanabe, E.; Urata, H., *J. Organomet. Chem.* **1997**, *542*, 185.
50. Sperrle, M.; Consiglio, G., *Chem. Ber.* **1997**, *130*, 1557.
51. Fenton, D. M., *J. Org. Chem.* **1973**, *38*, 3192.
52. Schoenberg, A.; Bartoletti, I.; Heck, R. F., *J. Org. Chem.* **1974**, *39*, 3318.
53. Godard, C.; Muñoz, B. K.; Ruiz, A.; Claver, C., *Dalton Trans.* **2008**, 853.
54. Hayashi, M.; Takezaki, H.; Hashimoto, Y.; Yamamoto, Y.; Takaoki, K.; Saigo, K., *Tetrahedron Lett.* **1998**, *39*, 7529.
55. Littke, A. F.; Fu, G. C., *Angew. Chem.* **1998**, *110*, 3586.

56. Littke, A. F.; Dai, C.; Fu, G. C., *J. Am. Chem. Soc.* **2000**, *122*, 4020.
57. Littke, A. F.; Fu, G. C., *Angew. Chem.* **1999**, *111*, 2568.
58. Kawatsura, M.; Hartwig, J. F., *J. Am. Chem. Soc.* **1999**, *121*, 1473.
59. Beare, N. A.; Hartwig, J. F., *J. Org. Chem.* **2002**, *67*, 541.
60. Kuwano, R.; Utsunomiya, M.; Hartwig, J. F., *J. Org. Chem.* **2002**, *67*, 6479.
61. Hooper, M. W.; Hartwig, J. F., *Organometallics* **2003**, *22*, 3394.
62. Hooper, M. W.; Utsunomiya, M.; Hartwig, J. F., *J. Org. Chem.* **2003**, *68*, 2861.
63. Zapf, A.; Ehrentraut, A.; Beller, M., *Angew. Chem.* **2000**, *112*, 4315.
64. Aranyos, A.; Old, D. W.; Kiyomori, A.; Wolfe, J. P.; Sadighi, J. P.; Buchwald, S. L., *J. Am. Chem. Soc.* **1999**, *121*, 4369.
65. Wolfe, J. P.; Singer, R. A.; Yang, B. H.; Buchwald, S. L., *J. Am. Chem. Soc.* **1999**, *121*, 9550.
66. Wolfe, J. P.; Buchwald, S. L., *Angew. Chem.* **1999**, *111*, 2570.
67. Wolfe, J. P.; Buchwald, S. L., *Angew. Chem. Int. Ed. Engl.* **1999**, *38*, 2413.
68. Cometti, G.; Chiusoli, G. P., *J. Organomet. Chem.* **1982**, *236*, C31.
69. Alper, H.; Hamel, N., *J. Am. Chem. Soc.* **1990**, *112*, 2803.
70. Nozaki, K.; Kantam, M. L.; Horiuchi, T.; Takaya, H., *J. Mol. Cat. A, Chemical* **1997**, *118*, 247.
71. Sperrle, M.; Consiglio, G., *Inorg. Chim. Acta* **2000**, *300-302*, 264.
72. Grushin, V. V., *Chem. Rev.* **2004**, *104*, 1629.
73. Parshall, G. W.; Ittel, S. D., *Homogeneous Catalysis*, 2nd ed.; Wiley Interscience: 1992; p 106.
74. Pignolet, L. H., *Homogenous Catalysis with Metal Phosphine Complexes*, Plenum Press: New York, 1983.
75. Arduengo, A. J.; Dias, H. V. R.; Harlow, R. L.; Kline, M., *J. Am. Chem. Soc.* **1992**, *114*, 5530.
76. Wanzlick, H.-W., *Angew. Chem. Int. Ed.* **1962**, *1*, 75.
77. Lappert, M. F., *J. Organomet. Chem.* **1988**, *358*, 185.
78. Arduengo, A. J.; Krafczyk, R., *Chem. Z.* **1988**, *32*, 6.
79. Huang, J.; Schanz, H.-J.; Stevens, E. D.; Nolan, S. P., *Organometallics* **1999**, *18*, 2370.
80. Huang, J.; Stevens, E. D.; Petersen, J. L.; Nolan, S. P., *J. Am. Chem. Soc.* **1999**, *121*, 2674.
81. Herrmann, W. A., *Angew. Chem.* **2002**, *114*, 1342.
82. Herrmann, W. A., *Angew. Chem. Int. Ed.* **2002**, *41*, 1290.
83. Graves, C. R.; Schelter, E. J.; Cantat, T.; Scott, B. L.; Kiplinger, J. L., *Organometallics* **2008**, *27*, 5371.
84. Crabtree, R. H., *J. Organomet. Chem.* **2005**, *690*, 5451.
85. Casares, J. A.; Espinet, P.; Hernando, R.; Iturbe, G.; Villafane, F.; Ellis, D. D.; Orpen, A. G., *Inorg. Chem.* **1997**, *36*, 44.
86. Marynick, D. S., *J. Am. Chem. Soc.* **1984**, *106*, 4064.
87. Green, J. C.; Scurr, R. G.; Arnold, P. L.; Geoffrey, F.; Cloke, N., *Chem. Commun.* **1997**, 1963.
88. Green, J. C.; Herbert, B. J., *Dalton Trans.* **2005**, *1214*.
89. Chutia, P.; Kumari, N.; Sharma, M.; Woollins, J. D.; Slawin, A. M. Z.; Dutta, D. K., *Polyhedron* **2004**, *23*, 1657.
90. Abernethy, C. D.; Codd, G. M.; Spicer, M. D.; Taylor, M. K., *J. Am. Chem. Soc.* **2003**, *125*, 1128.

91. Hillier, A. C.; Sommer, W. J.; Yong, B. S.; Petersen, J. L.; Cavallo, L.; Nolan, S. P., *Organometallics* **2003**, *22*, 4322.
92. Dorta, R.; Stevens, E. D.; Hoff, C. D.; Nolan, S. P., *J. Am. Chem. Soc.* **2003**, *125*, 10490.
93. Herrmann, W. A.; Goosen, L. T.; Köcher, C.; Artus, G. R. J., *Angew. Chem. Int. Ed.* **1996**, *35*, 2805.
94. Kücübay, H.; Çetinkaya, B.; Salaheddine, G.; Dixneuf, P. H., *Organometallics* **1996**, *15*, 2434.
95. Weskamp, T.; Schattenmann, W. C.; Spiegler, M.; Herrmann, W. A., *Angew. Chem. Int. Ed.* **1998**, *37*, 2490.
96. Scholl, M.; Trnka, T. M.; Morgan, J. P.; Grubbs, R. H., *Tetrahedron Lett.* **1999**, *40*, 2674.
97. Trnka, T. M.; Grubbs, R. H., *Acc. Chem. Res.* **2001**, *34*, 18.
98. Jafarpour, L.; Nolan, S. P., *Adv. Organomet. Chem.* **2001**, *46*, 181.
99. César, V.; Bellemin-Laponnaz, S.; Gade, L. H., *Chem. Soc. Rev.* **2004**, *33*, 619.
100. Perry, M. C.; Burgess, K., *Tetrahedron: Asymmetry* **2003**, *14*, 951.
101. Nair, V.; Bindu, S.; Sreekumar, V., *Angew. Chem.* **2004**, *116*, 5240.
102. Nair, V.; Bindu, S.; Sreekumar, V., *Angew. Chem. Int. Ed.* **2004**, *43*, 5130.
103. Cavallo, L.; Correa, A.; Costabile, C.; Jacobsen, H., *J. Organomet. Chem.* **2005**, *690*, 5407.
104. Youngs, W. J.; Garrison, J. C., *Chem. Rev.* **2005**, *105*, 3978.
105. Crudden, C. M.; Allen, D. P., *Coord. Chem. Rev.* **2004**, *248*, 2247.
106. Peris, E.; Crabtree, R. H., *Coord. Chem. Rev.* **2004**, *248*, 2239.
107. Herrmann, W. A.; Öfele, K.; Preysing, D. v.; Schneider, K. S., *J. Organomet. Chem.* **2003**, *687*, 229.
108. Hillier, A. C.; Grasa, G. A.; Viciu, M. S.; Lee, H. M.; Yang, C.; Nolan, S. P., *J. Organomet. Chem.* **2002**, *653*, 69.
109. Herrmann, W. A.; Öfele, K.; Preysing, D. V.; Schneider, S. K., *J. Organomet. Chem.* **2003**, *687*, 229.
110. Kantchev, E. A. B.; Brien, C. J. O.-.; Organ, M. G., *Angew. Chem. Int. Ed.* **2007**, *46*, 2768.
111. Bildstein, B.; Malaun, M.; Kopacka, H.; Ongania, K.-H.; Wurst, K., *J. Organomet. Chem.* **1999**, *572*, 177.
112. Kuhn, N.; Kratz, T., *Synthesis* **1993**, 561.

Part I

The Synthesis, Single Crystal Structures and Liquid Crystalline Phase Behavior of Alkoxy Substituted Tolans

Chapter 2

I. Introduction

There are numerous studies of the mesogenic behavior of liquid crystals; however, less attention has been paid to their solid-state crystalline structures. Sheikh-Ali *et al.* studied the molecular conformations and crystal packing of *trans*-1-*n*-alkyl-4-(4-cyanophenyl)piperidines,¹ and *trans*-1-*n*-alkyl-4-(4-cyanophenyl)cyclohexanes were examined by Eidenschink *et al.*² Sheikh-Ali *et al.*¹ have come to the conclusion that dipole-dipole interactions are important, but do not completely control the packing arrangement on the crystals. They noted that the most important factor is the angle of twist between the aromatic and nonaromatic rings which leads the alkyl chain to project along very different axes to the aromatic planes. The aromatic and nonaromatic rings of the mesogenic compound are twisted; however, there is almost untwisted in the case of related nonmesogenic compounds.

Cotrait *et al.* studied the relationship between lengthening of aliphatic alkyl chains and mesomorphic properties of *p*-methoxy-*p'*-alkyltolans.^{3, 4} The authors came to the conclusion that a unidirectional three dimensional arrangement of molecules is one of the main requirements for the formation of the mesophases. The group of Prasad *et al.* found that the results from Cotrait did not conform with the detailed structures of a homologueous series of a mesogenic 4-(4'-ethoxyphenylazo)phenyl alkanoates. Prasad *et al.* thus found that the packing coefficient is a meaningful parameter to describe the changes in physical properties such as clearing point and orientation order parameter.⁵ The more precise estimated packing coefficient value is correlated well with clearing point which showed that the packing coefficient is decreased for the nonmesogenic compound but increased for the compounds showing mesogenic behavior.⁶⁻¹⁰

The effect of the carbon number in the alkyl chain is often related to various physical properties (*i.e.*, an odd - even effect), for example, thermal properties of [n]-polyurethanes,¹¹ molecular alignment in monolayers of *n*-alkyloxy-cyanobiphenyls,¹² fusion temperatures and fusion enthalpies of *n*-alkanes,¹³ and thermotropic properties of liquid crystalline epoxy compounds.¹⁴ It has also been found that varying both the chain length and *trans* - *cis* conformation of double bonds influences the clearing point of the nematic phase,¹⁵ which shows an odd - even effect.

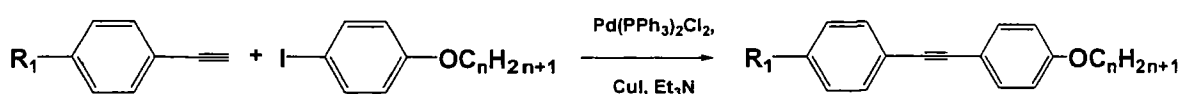
There are, as yet, few reports on the mesomorphism of tolans discussed in relation to their single-crystal structures. We felt that it would be of interest to study

both the phase-behavior and single-crystal structures of several homologous series of tolans in order to examine them in both solid and fluid phases to explore (i) the odd-even effect; (ii) effect of terminal groups; (iii) short-range interactions involved in molecular packing and molecular orientation; and (iv) the effect of the chain length on the crystal packing, in order to develop a better understanding of the intra- and intermolecular interactions in rod-like structures. Single-crystal structures of compounds which can attain liquid crystalline phases may provide insight into the forces which direct the organisation of the mesophases. Herein we report the synthesis, crystal structures and phase behavior of three series of tolans with varying chain length, with the general formulae $p\text{-X-C}_6\text{H}_4\text{-C}\equiv\text{C-C}_6\text{H}_4\text{-p-OC}_n\text{H}_{2n+1}$ [$\text{X} = \text{H}$ (series 1), CH_3 (series 2), OCH_3 (series 3)].

II. Results and Discussion

II.1 Synthesis

The cross-coupling reactions were carried out under standard Sonogashira conditions, using a catalyst system composed of 1 mol% of each of $\text{PdCl}_2(\text{PPh}_3)_3$ and CuI with respect to the starting materials. Triethylamine was used as both a solvent and a base for the reactions. As the reactions occurred, the ammonium halide salt which was formed slowly precipitated. All of the reactions were initially stirred at room temperature and were then heated to reflux at $80\text{ }^\circ\text{C}$ until complete. In this study, *in situ* GC-MS was used to monitor the reactions which not only detected the completion of the reaction but also the formation of any side-product (*e.g.* alkyne homo-coupling). A dry, N_2 atmosphere and de-oxygenated amine solvents were used for all reactions. The tolans were prepared (Scheme 1) by the coupling of 4-*n*-alkoxy-4'-iodobenzenes with the appropriate phenylethynyl reagent. Purification of the product required either re-crystallisation or column chromatography.



Series 1 $\text{R}_1 = \text{-H}$, **H(n)** where $n = \text{no. of carbons in the alkyl chain}$ (*i.e.*, $n = 1 - 10, 12, 14, 16$)

Series 2 $\text{R}_1 = \text{-CH}_3$, **Me(n)** where $n = \text{no. of carbons in the alkyl chain}$ (*i.e.*, $n = 1 - 6, 9, 12$)

Series 3 $\text{R}_1 = \text{-OCH}_3$, **MeO(n)** where $n = \text{no. of carbons in the alkyl chain}$ (*i.e.*, $n = 1 - 10, 12, 14$)

* Iodotoluene and 4-ethoxyphenylacetylene were used to prepare **Me(2)**

Scheme 1. Synthesis of tolans.

It should be noted that; **Me(1)** was synthesized by K. Roscoe;¹⁶ **MeO(1)** was received from J. Collings; **MeO(3)**, **MeO(4)**, **MeO(12)** and **MeO(14)** were synthesized by M. Green.¹⁷ Compounds **H(1)**,¹⁸⁻²⁰ **H(4)**,²¹ **Me(1)**,^{3, 4, 6, 22, 23}, **Me(2)**,^{3, 4, 6, 24}, **Me(3)**,^{3, 4, 6} **Me(4)**,^{3, 4, 6} **Me(5)**,^{3, 4, 6, 25} **Me(9)**,²⁶⁻³⁰ **MeO(1)**,³¹⁻³³ **MeO(2)**,³⁴ **MeO(4)**³⁵ and **MeO(9)**²⁸ are known in the literature.

The UV-vis spectra of representative compounds **H(1)**, **H(8)**, **H(14)**, **Me(3)**, **Me(6)**, **Me(12)**, **MeO(1)**, **MeO(7)** and **MeO(14)** at 10 μM concentration in cyclohexane showed two nearly identical absorptions for each compound with maxima at 290 and 310 nm and extinction coefficients of *ca.* 5.00×10^4 and $4.00 \times 10^4 \text{ mol}^{-1} \cdot \text{cm}^{-1} \cdot \text{L}$, respectively. Compounds **H(1)**, **H(8)**, **H(14)**, **Me(3)**, **Me(6)**, **Me(12)**, **MeO(1)**, **MeO(7)** and **MeO(14)** were examined by IR spectroscopy as Nujol mulls between NaCl plates. Peaks appeared at 2217-2221 cm^{-1} attributed to the $\text{C}\equiv\text{C}$ stretch which is weak due to the limited change in dipole moment caused by the vibrations in the nearly centrosymmetric systems. Representative compounds were examined by Raman spectroscopy, displaying strong absorptions at 2215-2224 cm^{-1} attributed to the $\text{C}\equiv\text{C}$ stretch which causes a large change in polarisability.

II.2 Phase characterisation by differential scanning calorimetry and thermal optical microscopy

The values for the phase transition temperatures of all compounds were obtained by differential scanning calorimetry (DSC). Good agreement ($\sim 1\text{-}2 \text{ }^\circ\text{C}$) with values determined by hot-stage, transmitted polarised light microscopy (tplm) was found. A degree of supercooling below the melting point is observed on cooling leading to hysteresis. The clearing point of the tolans decreases with increasing chain length due to the higher degree of flexibility of the terminal chain.

Only 4-n-nonyloxy-4'-methyltolan (**Me(9)**) and the 4-n-alkoxy-4'-methoxytolans (**MeO(2)**-**MeO(14)**) displayed liquid crystalline phases. Most of these compounds displayed schlieren textures, with two and four-point brushes when examined by tplm, which is characteristic of a nematic phase. The birefringent areas flashed brightly on mechanical disturbance confirming that the mesophase observed is indeed nematic. The liquid crystal phase transitions of the mesomorphic tolans are listed in Table 1.

Compounds **Me(9)**, **MeO(2)**, **MeO(3)**, **MeO(9)**, **MeO(12)** and **MeO(14)** melted directly from solid to isotropic liquid, and no LC phase was observed on heating. On cooling, monotropic nematic phases were observed at 62.7, 122.7, 101.3, 88.5, 87.2 and 86.7 °C respectively, followed by hardening of the material. Transition temperatures upon cooling are given in parentheses in Table 1. The nematic phase transition for **MeO(9)** was observed to be 1.7 °C higher than that previously reported at 86.8 °C by Malthête *et al.*²⁶

Table 1. Transition temperatures (°C) observed by DSC and/or tplm **Me(9)**, **MeO(2)** - **MeO(14)**.

Compound	Cr	T/°C ($\Delta H/\text{kJ}\cdot\text{mol}^{-1}$, $\Delta S/\text{kJ}\cdot\text{mol}^{-1}\cdot\text{K}^{-1}$)	N	T/°C ($\Delta H/\text{kJ}\cdot\text{mol}^{-1}$, $\Delta S/\text{kJ}\cdot\text{mol}^{-1}\cdot\text{K}^{-1}$)	I
Me(9)	•	75.9 (44.2, 127)		62.7 ^{a, b}	•
MeO(2)	•	140 (32.4, 78)		122.7 ^a (1.4, 4)	•
MeO(3)	•	115.9 (34.5, 89)		101.3 ^{a, b}	•
MeO(4)	•	108.4 (32.1, 84)	•	109.5 (1.4, 4)	•
MeO(5)	•	84.6 (29.1, 81)	•	89.9 ^b	•
MeO(6)	•	82.4 (26.0, 73)	•	99.4 (1.3, 3)	•
MeO(7)	•	84.0 (43.2, 121)	•	89.8 ^b	•
MeO(8)	•	83.5 (46.2, 129)	•	93.0 ^b	•
MeO(9)	•	90.4 (54.0, 149)		88.5 ^{a, b}	•
MeO(10)	•	88.2 (52.4, 145)	•	89.3 ^b	•
MeO(12)	•	92.8 (56.7, 155)		87.2 ^{a, b}	•
MeO(14)	•	97.0 (66.2, 179.0)		86.7 ^{a, b}	•

^a monotropic transition temperature on cooling, ^b observed by tplm

Compounds **MeO(4)**, **MeO(5)**, **MeO(6)**, **MeO(7)**, **MeO(8)** and **MeO(10)** displayed enantiotropic liquid crystal phases. On heating compound **MeO(4)**, a nematic phase with a schlieren texture was observed at 108.4 °C and the clearing point was reached at 109.5 °C. On cooling from the isotropic liquid, a nematic phase with a schlieren texture formed at 109.6 °C. Compound **MeO(5)** softened on heating into a nematic phase at 84.6 °C, and then cleared to an isotropic liquid at 89.9 °C. On cooling from the isotropic liquid, a nematic phase with a marble texture formed at 91.2 °C, which persisted until crystallisation.

On heating compound **MeO(6)**, a nematic phase with a schlieren texture was observed at 82.4 °C, and the clearing point was reached at 99.4 °C. On cooling, the schlieren texture of the nematic phase was again observed at 99.4 °C. Compound **MeO(7)** shows a nematic phase at 84.0 °C and then clears at 89.8 °C. On cooling, a nematic phase was observed at 89.7 °C. For compound **MeO(10)**, a nematic phase was observed at 88.2 °C and the clearing point is 89.3 °C. On cooling, a nematic phase with a schlieren texture was observed at 89.3 °C.

II.3 Mesomorphism

Figure 1 shows the melting point for each homologous series plotted against the number of carbon atoms (n) in the terminal alkyl chain of series 1 (**H(n)**), 2 (**Me(n)**) and 3 (**MeO(n)**). The melting points shown in Figure 1 are the transition temperatures K to I for series 1 and 2, and K to N for some of series 3. In all three series, the temperature initially decreases with increasing chain length but then begins to increase again when the chain length is increased further. In series 1, the melting point of compound **H(1)** ($n = 1$ of series 1 in Figure 1) was lower than expected and it is not clear for whether this is an odd-even effect. However, **H(1)** has three molecules in the asymmetric unit as evidenced from single crystal studies. The low melting point may result from the packing which is discussed later. Figure 2 shows the transition temperatures N to I and I to N for series 3 on heating and cooling respectively, plotted against the number of carbon atoms (n) in the terminal alkyl chain. [The melting points exhibited the odd-even effect when the length of the alkoxy chain less than five for series 1 and 3 but it was not clear for series 2.] An odd-even effect is observed for the clearing point of the nematic phase obtained from both heating and cooling runs, with the higher temperature for even and low temperature for an odd number for

series 3. As a chain becomes longer, its flexibility makes the odd-even effect smaller until it becomes unnoticeable for the longer chains.

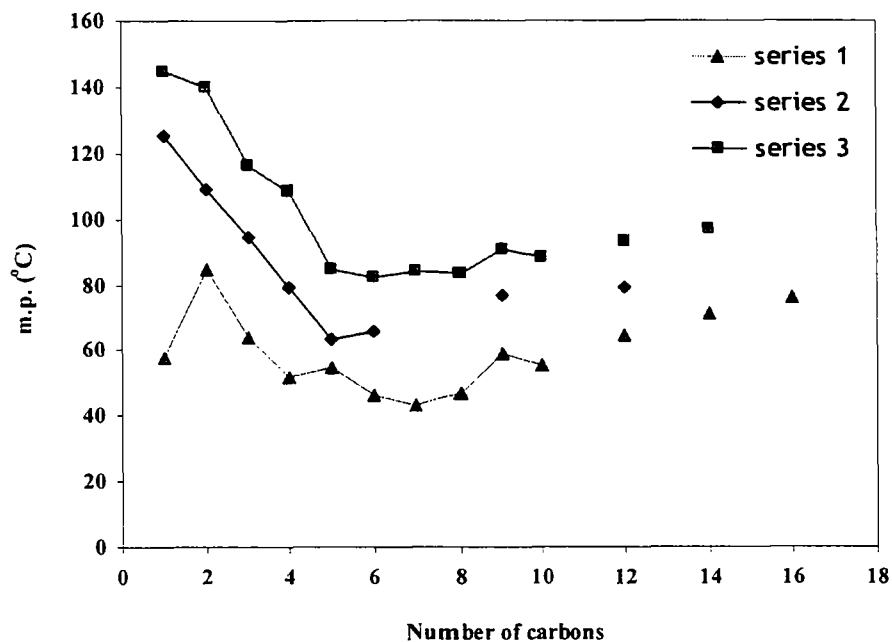


Figure 1. The melting point for each homologous series plotted against the number of carbon atoms (n) in the terminal alkyl chain of series 1, 2 and 3.

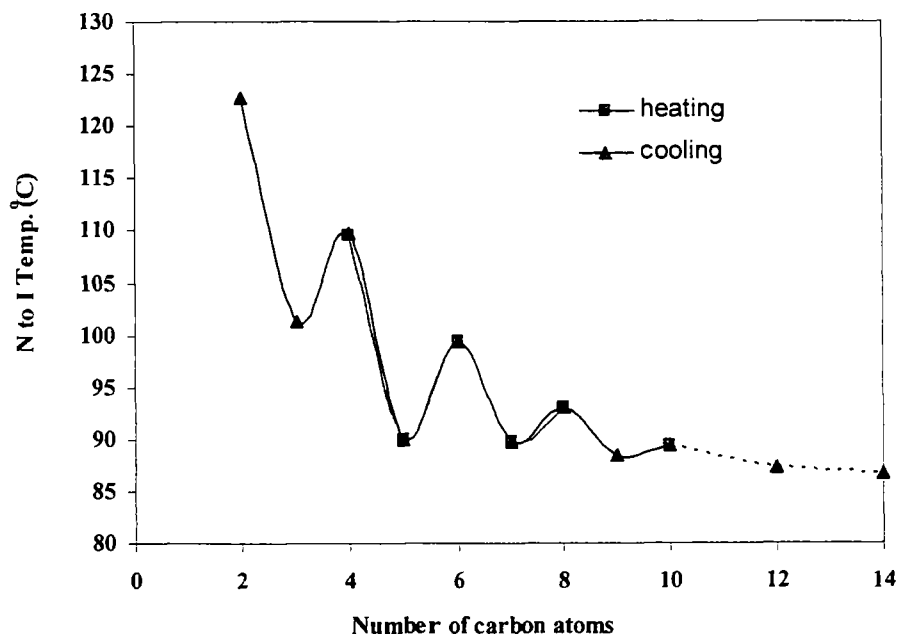


Figure 2. Plot of the clearing point ($N \leftrightarrow I$) for homologous series 3 vs. number of carbon atoms (n) in the terminal alkyl chain.

II.4 Crystal and molecular structures

Compounds **H(1)**, **H(2)**, **H(3)**, **H(4)**, **H(5)**, **H(6)**, **H(8)**, **H(9)**, **Me(1)**, **Me(2)**, **Me(3)**, **Me(4)**, **Me(5)**, **Me(6)**, **Me(9)**, **Me(12)**, **MeO(1)**, **MeO(2)**, **MeO(3)**, **MeO(4)**, **MeO(5)**, **MeO(6)**, **MeO(7)**, **MeO(8)**, **MeO(9)** and **MeO(10)** have been characterised by single-crystal X-ray diffraction. It should be noted that single crystal of **H(2)** and **Me(1)** were grown by M. Green¹⁷ and K. Roscoe,¹⁶ respectively. The crystal structure of **MeO(1)** was solved at Newcastle University by Prof. William Clegg. The molecular structures are shown in Figure 3 (disorder is shown with dashed lines). Summaries of dihedral and torsion angles are given in Tables 5 – 8. Crystallographic data for compounds in series 1, 2 and 3 are listed in Tables 2, 3 and 4, respectively. Bond distances are unexceptional,³⁶ as are the conformations of the tolan moieties.

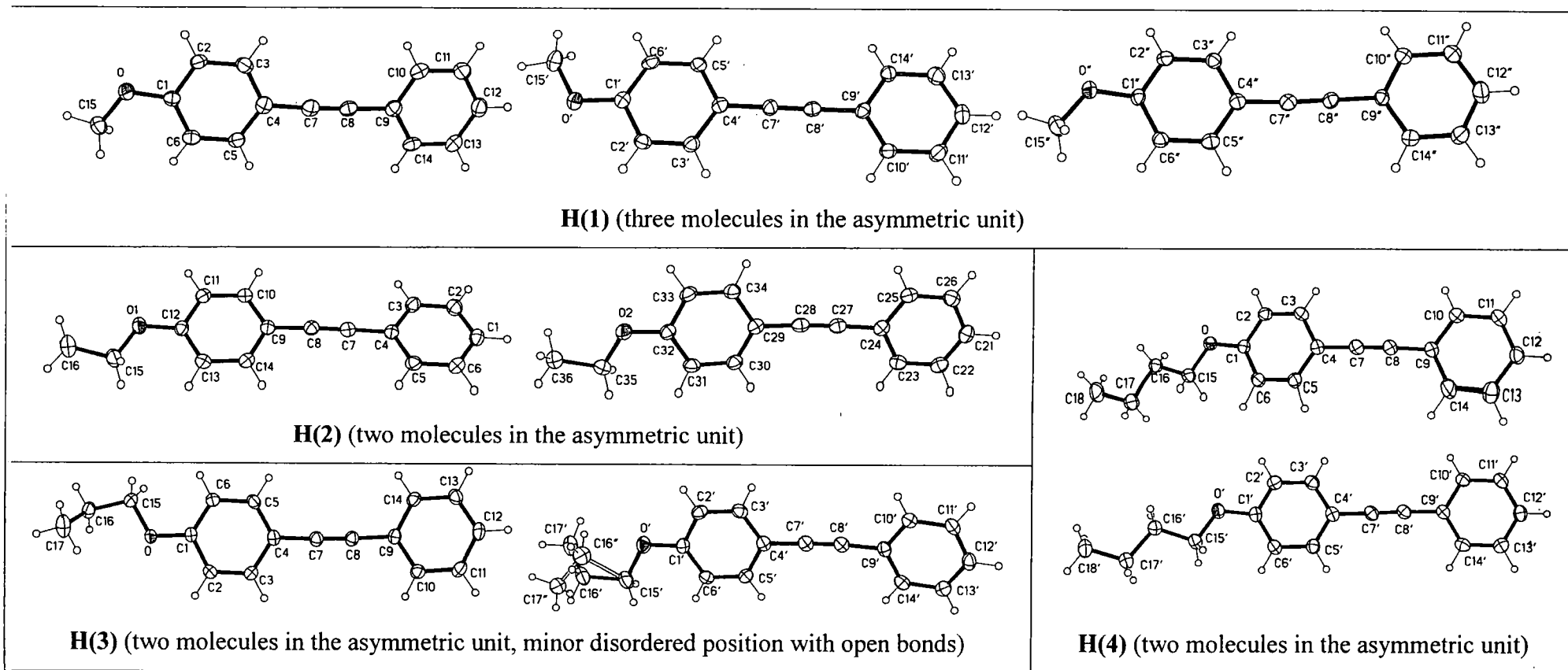


Figure 3. The molecular structures of tolans.

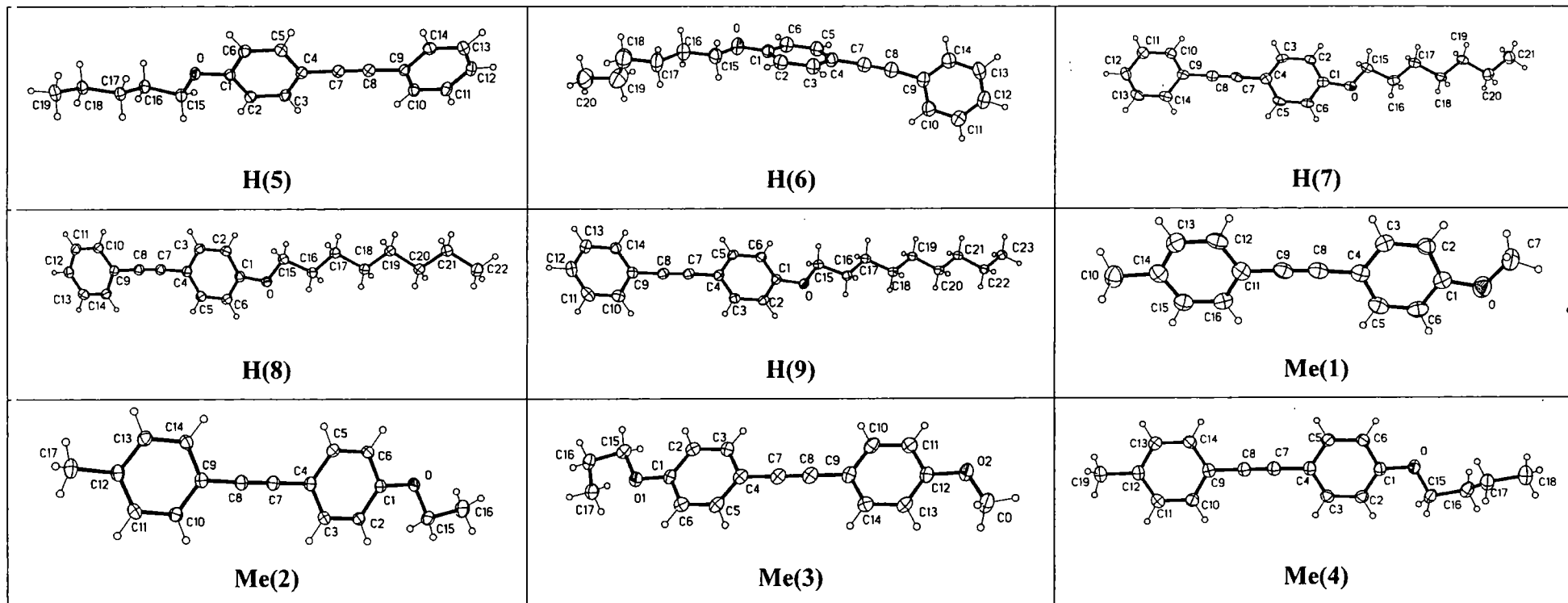


Figure 3 (continued)

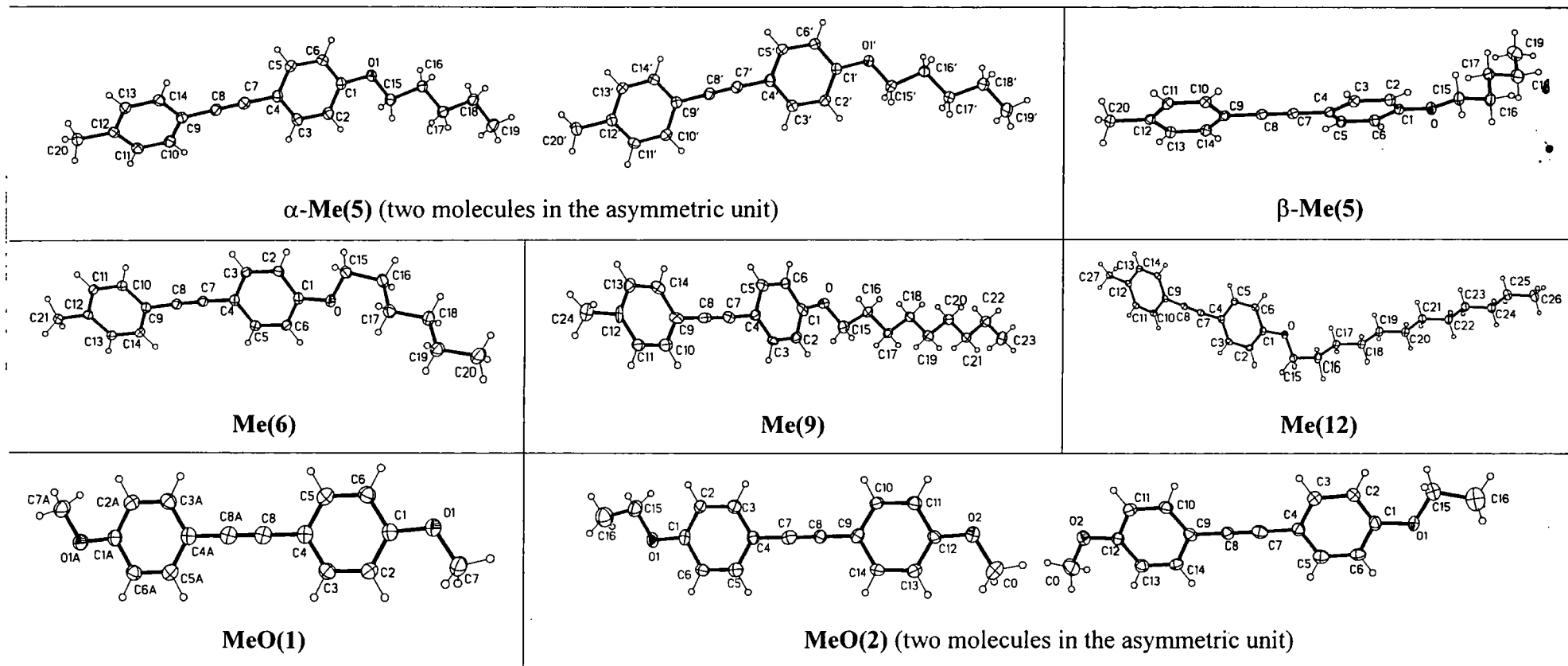


Figure 3 (continued)

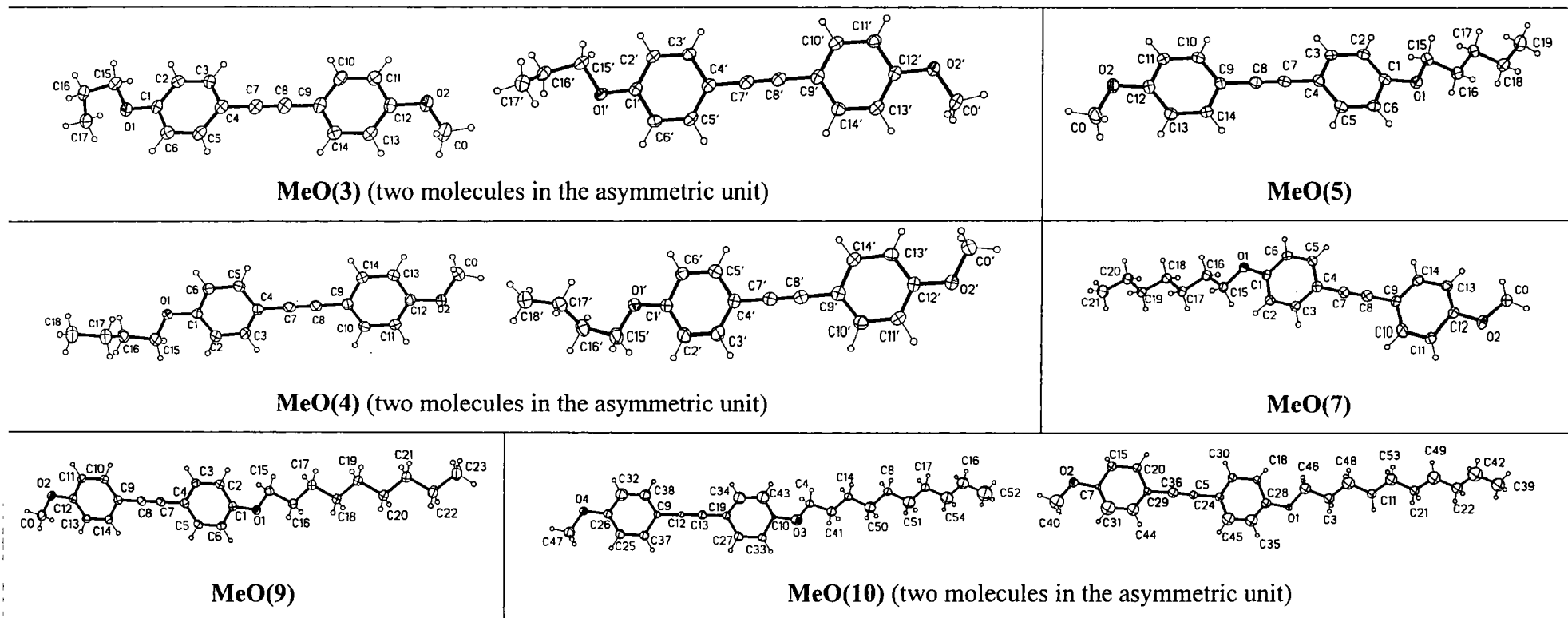
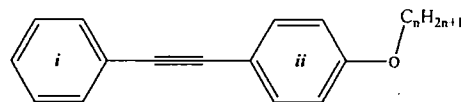


Figure 3 (continued)

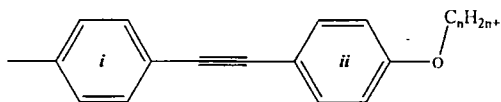
Table 2. Crystallographic data for compounds in the homologous series 1.



Compound	H(1)	H(2)	H(3)	H(4)	H(5)	H(6)	H(7)	H(8)	H(9)
Formula	$C_{15}H_{12}O$	$C_{16}H_{14}O$	$C_{17}H_{16}O$	$C_{18}H_{18}O$	$C_{19}H_{20}O$	$C_{20}H_{22}O$	$C_{21}H_{24}O$	$C_{22}H_{26}O$	$C_{23}H_{28}O$
Formula weight	208.25	222.27	236.30	250.32	264.35	278.38	292.40	306.43	320.45
T /K	120(2)	120(2)	120(2)	120(2)	120(2)	120(2)	120(2)	120(2)	120(2)
Crystal system	Monoclinic	Monoclinic	Triclinic	Triclinic	Monoclinic	Orthorhombic	Monoclinic	Triclinic	Monoclinic
Space group	$P2_1$ (#4)	$P2_1/c$ (#14)	$P-1$ (#2)	$P-1$ (#2)	$P2_1$ (#4)	$P2_12_1$ (#19)	$P2_1/c$ (#14)	$P-1$ (#2)	$P2_1/c$ (#14)
a /Å	7.3322(5)	9.6850(10)	9.749(1)	9.828(1)	9.4354(12)	7.935(1)	39.128(7)	5.6048(5)	5.5989(5)
b /Å	17.846(1)	10.3190(11)	10.274(1)	10.123(1)	7.5845(10)	9.625(1)	7.1683(13)	7.8211(8)	9.2377(7)
c /Å	13.287(1)	25.0714(19)	14.540(2)	15.928(2)	10.8850(14)	21.141(2)	6.1275(11)	21.525(2)	36.294(3)
α /°	90	90	83.95(1)	104.51(1)	90	90	90	87.80(1)	90
β /°	90.03(1)	102.08(3)	84.03(1)	90.39(1)	106.82(1)	90	91.20(2)	89.68(1)	91.02(1)
γ /°	90	90	67.71(1)	111.52(1)	90	90	90	71.33(1)	90
V /Å ³	1738.6(2)	2450.1(4)	1336.8(3)	1418.6(3)	745.64(17)	1614.6(3)	1718.3(5)	893.22(15)	1876.9(3)
Z (z')	6 (3)	8 (2)	4 (2)	4 (2)	2 (1)	4 (1)	4 (1)	2 (1)	4 (1)
ρ_{calcd} /mg m ⁻³	1.193	1.205	1.174	1.172	1.177	1.145	1.130	1.139	1.134
Total reflections	17816	28479	13575	19739	8831	18643	13531	12292	17886
Unique reflections	4720*	7452	6120	8269	2128*	2146*	3384	5175	4219
Refined parameters	440	391	336	348	261	192	202	211	329
R_{int}	0.111	0.051	0.088	0.033	0.023	0.121	0.080	0.054	0.032
R [F , $I > 2\sigma(I)$]	0.046	0.054	0.047	0.052	0.034	0.054	0.138	0.049	0.038
wR (F^2 , all data)	0.115	0.131	0.137	0.157	0.091	0.161	0.289	0.137	0.104

* Friedel equivalents merged

Table 3. Crystallographic data for the compounds in the homologous series 2.



Compound	Me(1)	Me(2)	Me(3)	Me(4)	α -Me(5)	β -Me(5)	Me(6)	Me(9)	Me(12)
Formula	C ₁₆ H ₁₄ O	C ₁₇ H ₁₆ O	C ₁₈ H ₁₈ O	C ₁₉ H ₂₀ O	C ₂₀ H ₂₂ O	C ₂₀ H ₂₂ O	C ₂₁ H ₂₄ O	C ₂₄ H ₃₀ O	C ₂₇ H ₃₆ O
Formula weight	222.27	236.30	250.32	264.35	278.38	278.38	292.40	334.48	376.56
T /K	150(2)	120(2)	120(2)	120(2)	120(2)	120(2)	120(2)	120(2)	120(2)
Crystal system	Orthorhombic	Monoclinic	Monoclinic	Monoclinic	Orthorhombic	Monoclinic	Monoclinic	Orthorhombic	Monoclinic
Space group (no.)	<i>Pna</i> 2 ₁ (#33)	<i>P</i> 2 ₁ / <i>n</i> (#14)	<i>P</i> 2 ₁ / <i>n</i> (#14)	<i>P</i> 2 ₁ / <i>n</i> (#14)	<i>Pna</i> 2 ₁ (#33)	<i>P</i> 2 ₁ / <i>c</i> (#14)	<i>P</i> 2 ₁ / <i>c</i> (#14)	<i>Pca</i> 2 ₁ (#29)	<i>P</i> 2 ₁ / <i>c</i> (#14)
a /Å	11.791(2)	8.5263(3)	9.063(1)	9.948(1)	11.511(1)	28.366(4)	29.896(3)	5.9918(17)	40.610(9)
b /Å	13.976(3)	7.3143(3)	7.384(1)	7.512(1)	20.087(2)	4.8899(6)	4.8874(4)	7.1784(18)	4.7965(12)
c /Å	7.448(2)	22.010(1)	21.757(2)	21.183(2)	13.818(1)	11.3406(15)	11.3492(11)	45.654(13)	11.331(3)
α /°	90	90	90	90	90	90	90	90	90
β /°	90	100.84(1)	99.46(1)	103.58(1)	90	95.43(1)	91.939(3)	90	91.19(1)
γ /°	90	90	90	90	90	90	90	90	90
V /Å ³	1227.4(5)	1348.1(1)	1436.2 (3)	1538.7 (3)	3195.0(5)	1566.0(4)	1657.3(3)	1963.6(9)	2206.6(9)
Z (z')	4 (1)	4(1)	4 (1)	4 (1)	8 (2)	4 (1)	4 (1)	4 (1)	4 (1)
$\rho_{\text{calcd}} / \text{mg m}^{-3}$	1.203	1.164	1.158	1.141	1.157	1.181	1.172	1.131	1.134
Total reflections	1542	17894	12878	15837	36963	19631	14454	22768	17542
Unique reflections	1115*	3925	2529	3202	4836*	4525	3802	2265*	4897
Refined parameters	159	166	172	200	387	194	203	230	257
R _{int}	0.022	0.032	0.092	0.079	0.043	0.036	0.071	0.061	0.030
R [<i>F</i> , >2 σ (<i>I</i>)]	0.047	0.047	0.048	0.048	0.042	0.049	0.066	0.082	0.058
wR (<i>F</i> ² , all data)	0.131	0.147	0.152	0.151	0.108	0.140	0.188	0.188	0.141

* Friedel equivalents merged

Table 4. Crystallographic data for the compounds in the homologous series 3.



Compound	MeO(1)	MeO(2)	MeO(3)	MeO(4)	MeO(5)	MeO(6)*	MeO(7)	MeO(8)*	MeO(9)	MeO(10)*
Formula	C ₁₆ H ₁₄ O ₂	C ₁₇ H ₁₆ O ₂	C ₁₈ H ₁₈ O ₂	C ₁₉ H ₂₀ O ₂	C ₂₀ H ₂₂ O ₂	C ₂₁ H ₂₄ O ₂	C ₂₂ H ₂₆ O ₂	C ₂₃ H ₂₈ O ₂	C ₂₄ H ₃₀ O ₂	C ₂₄ H ₃₂ O ₂
Formula weight	238.27	252.30	266.32	280.35	294.38		322.43		350.48	
T /K	160(2)	120(2)	120(2)	120(2)	120(2)	120(2)	120(2)	120(2)	120(2)	120(2)
Crystal system	Monoclinic	Monoclinic	Triclinic	Triclinic	Orthorhombic	Orthorhombic	Orthorhombic	Orthorhombic	Orthorhombic	Orthorhombic
Space group	<i>P</i> 2 ₁ / <i>c</i> (#14)	<i>P</i> 2 ₁ / <i>c</i> (#14)	<i>P</i> -1 (#2)	<i>P</i> -1 (#2)	<i>Pbca</i> (#61)		<i>Pbca</i> (#61)		<i>Pbca</i> (#61)	
a /Å	8.4401(13)	8.556(1)	7.7287(13)	7.931(1)	7.1597(5)	7.1633(11)	7.1529(12)	7.1598(3)	7.1545(7)	7.1591(17)
b /Å	5.7031(9)	7.364(1)	8.1030(14)	8.368(1)	6.2416(4)	6.2096(8)	6.1995(8)	6.1567(3)	6.1542(7)	6.1063(13)
c /Å	13.243(2)	21.701(2)	23.375(3)	24.403(2)	74.394(5)	80.111(11)	83.222(12)	89.425(4)	92.234(10)	98.51(2)
α /°	90	90	89.36(1)	93.27(1)	90	90	90	90	90	90
β /°	91.805(4)	97.04(1)	84.54(1)	96.94(1)	90	90	90	90	90	90
γ /°	90	90	89.40(1)	101.41(1)	90	90	90	90	90	90
V /Å ³	637.2(2)	1357.0(3)	1457.1(4)	1570.4(3)	3324.5(4)	3563.4(13)	3690.4(9)	3941.9(4)	4061.1(8)	4307(2)
Z (z')	2 (1)	4 (1)	4 (2)	4 (2)	8 (1)	8(?)	8 (1)	8 (?)	8 (1)	8 (?)
ρ _{calc} /mg m ⁻³	1.242	1.235	1.214	1.186	1.176		1.161		1.146	
Total reflections	2576	18010	14060	18253	25061		27989		30885	
Unique reflections	1077	3943	5128	7222	4171		3831		4585	
Refined parameters	83	184	369	387	203		221		239	
R _{int}	0.037	0.026	0.096	0.060	0.063		0.038		0.056	
R _[F_o > 2σ(I)]	0.034	0.052	0.063	0.048	0.074		0.067		0.068	
w R _[F_o > 2σ(I)]	0.095	0.161	0.158	0.127	0.224		0.172		0.164	

* The diffraction data of MeO(6), MeO(8) and MeO(8) are insufficient to solve and/or refine their atomic structures.

Table 5. Dihedral angles between benzene rings (deg).

	H	Me	MeO
1	1.9, 6.3, 8.4	6.6	0
2	7.7, 10.1	2.3	3.8, 3.1
3	6.8, 9.9	1.6	2.2, 2.3
4	4.4, 7.2	11.8	3.3
5	12.0	α 23.0, 16.3 β 8.1	0.7
6	88.3	7.6	-
7	3.4	-	0.5
8	2.4	-	-
9	9.7	5.5	0.5
12		8.5	-

Table 6. Torsion angle C(2)-C(1)-O(1)-C(15) (deg).

	H	Me	MeO
1	8.2(4), 2.5(4), 10.6(4)	4.4(6)	3.7
2	3.9(2), 6.9(2)	3.5(1)	1.3(6), 1.3(6)
3	5.54(15), 5.30(15)	4.2(4)	1.9(3), 2.4(3)
4	2.7(1), 7.6(1)	1.5(2), -16(1)	0.7(2), 6.3(2)
5	2.6(2)	α 3.1(3), 5.2(3) β 3.0(2)	6.3(4)
6	6.2(4)	3.0(2)	-
7	6.6(8)	-	6.0(3)
8	1.6(2)	-	-
9	1.0(1)	5(1)	6.1(3)
12		3.6(2)	

Table 7. Torsion angle C(1)-O(1)-C(15)-C(16) (deg).

	H	Me	MeO
2	175.8(1), 177.(1)	178.7(1)	174.9(4) 164.9(4), 175.4(4)
3	175.8(1), 170.3(1)	174.9(3), -162.6(4)	173.7(2), 173.5(2)
4	178.8(1), 176.7(1)	177.3(1), -158(1)	176.2(1), 178.6(1)
5	171.2(1)	α 179.0(2), 174.2(2) β 179.5(1)	165.7(2)
6	173.4(3)	179.2(1)	-
7	165.7(5)	-	165.5(2)
8	179.4(1)	-	-
9	179.5(1)	164.6(4)	165.2(2)
12	-	179.8(1)	-

Table 8. Torsion angle O-C(15)-C(16)-C(17) (deg).

	H	Me	MeO
3	65.0(1), 66.2(2)	73.4(5), -68.6(6)	-67.1(3), -67.3(3)
4	178.8(1), 176.7(1)	63.2(2), -56(2)	-64.8(2), -60.4(2)
5	64.3(2)	α 176.2(2), 179.9(2) β 66.1(1)	171.7(2)
6	178.9(4)	65.9(2)	-
7	172.5(4)	-	172.0(2)
8	177.85(9)	-	-
9	179.6(1)	171.7(4)	171.6(2)
12	-	66.7(2)	-

The two benzene rings of the unsubstituted tolan are practically coplanar in the crystals of both its polymorphs (monoclinic³⁷⁻³⁹ and orthorhombic³⁹ and its various molecular complexes, although the rotation barrier is quite small and the rotation in the gas phase is quasi-free.^{37, 40} The same nearly planar conformation (the interring angle ranging from 0 to 12°) is observed here (Table 5), except for **H(6)** and α -**Me(5)**. The conformations around the C(benzene)-O bonds are eclipsed; the largest C(2)-C(1)-O-C(15) torsion angle is 10.6(4)° [in **H(1)**]. This, again, could be expected.⁴¹ Thus, we need to consider only two parts: the molecular core (including oxygen atoms), which is usually planar within <0.1 Å, and the conformationally flexible n-alkyl chain.

Compound **H(1)** crystallises in a chiral monoclinic space group with three molecules per the asymmetric unit. Notwithstanding the pseudo-orthorhombic ($\beta \approx 90^\circ$) lattice, there is no approximate higher symmetry in the structure. The structures of **H(2)**, **H(3)** and **H(4)** have two molecules per the asymmetric unit, and all the higher homologues have one. The conformation around the C(1)-O(1) bond is always eclipsed (see above) and that around O(1)-C(15) is staggered, *i.e.* *trans* (Table 3); the rest of the chain adopts various conformations. In **H(3)**, one molecule has a *gauche* conformation around the C(15)-C(16) bond, and the other is disordered between *gauche* (92%) and *trans* (8%) conformations. In **H(4)**, the chain has a planar all-*trans* conformation and is almost coplanar with the core. Note that in each case the conformations of symmetrically independent molecules are essentially the same. **H(5)** is similar to **H(3)** in adopting a *gauche* conformation around the C(15)-C(16) bond; the C(5) chain is planar and inclined by 60° to the core. The conformation of **H(6)** is highly unusual, with perpendicular benzene rings and the alkyl chain adopting a *gauche* conformation around the C(17)-C(18) bond but *trans* around all other bonds. The alkyl chains are *trans*-planar in **H(7)**, **H(8)** and **H(9)**, and coplanar with the core in the latter two molecules, in **H(7)** the conformation about O(1)-C(15) deviating from being exactly *trans*, the alkyl C(7) plane being inclined by 16° to the core plane.

All compounds of series 2 have one molecule per asymmetric unit, except α -**Me(5)** which has two. The structure of **Me(1)** is practically identical with that determined earlier at room temperature.⁴¹ Molecular conformations of **Me(1)**, **Me(2)** and **Me(3)** are essentially the same as those of the corresponding members of series 1. The alkyl chains in **Me(3)** and **Me(4)** are disordered between two different, but similar, conformations, with a

gauche conformation around the C(15)-C(16) bond. Crystallisation of **Me(5)** yielded two concomitant polymorphs, orthorhombic (α) and monoclinic (β). The asymmetric unit of the former comprises two molecules related by a local inversion center ($0.358 \frac{1}{2} \frac{1}{2}$), with and both structures adopting an all-*trans* conformation of the alkyl chain, which is practically coplanar with the adjacent benzene ring (although the θ angles are relatively large, 23.0 and 16.3°). The only independent molecule in the structure of the β -polymorph, however, has a *gauche* conformation around the C(15)-C(16) bond (and *trans* around other C-C bonds), thus the alkyl C(5) plane is inclined by 72° to the mean plane of the core. Similar conformations are adopted by **Me(6)** and **Me(12)**, where the corresponding angles are 70 and 71°, whilst **Me(9)** has an all-*trans*-planar conformation.

In series 3, the molecule of **MeO(1)** has a crystallographic inversion center.* The molecule of **MeO(2)** (its long axis practically parallel to the glide plane *c*) is disordered between two orientations of opposite polarity, so that all non-hydrogen atoms coincide except one terminal carbon, which is distributed between positions C(16) and C(16') with the occupancies of 0.67 and 0.33, respectively. This molecule and its symmetrical equivalents *via* the glide plane (symmetry transformations $x+2, -y, z+1/2$ or $x-2, -y, z-1/2$) comprise an infinite chain with impossibly short C(16)...C(16') 'contacts' of 2.34 Å between adjacent molecules. To avoid such crowding, all molecules within one chain must have the same polarity, although the relative polarities of different chains are random, the diffraction pattern giving no evidence of a superlattice). The asymmetric units of **MeO(3)** and **MeO(4)** comprise two molecules each, and those of the higher homologues, one molecule.

The conformations of the first three compounds of series 3 are essentially the same as in both series 1 and 2; that of **MeO(4)** is similar to **Me(4)** but not **H(4)**. **MeO(5)**, **MeO(7)** and **MeO(9)** are similar to **H(7)** and **Me(9)** in having an imperfect *trans* conformation around the O(1)-C(15) bond, so that the planar (all-*trans*) C(5), C(7) or C(9) chain is inclined by 14-15° to the core plane.

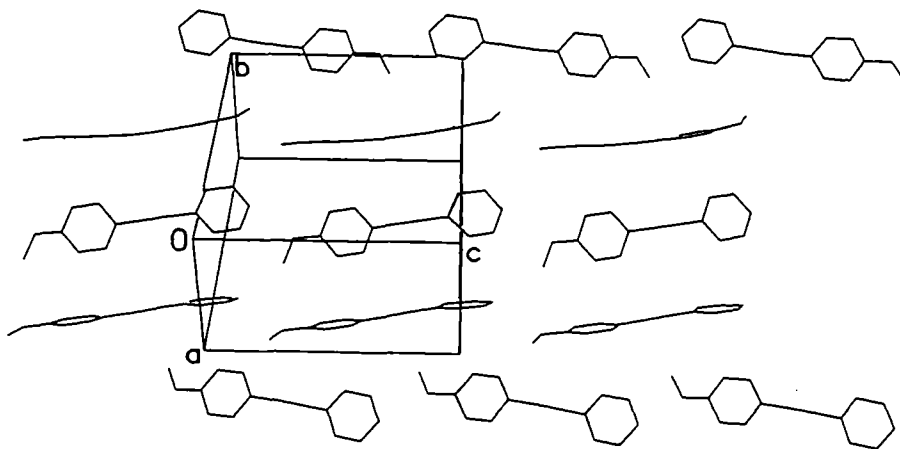
* Chawdhury and Shibby have reported this compound to crystallise in orthorhombic space group *Pbca* with $a = 24.41(6)$, $b = 15.72(5)$, $c = 7.94(4)$, but the atomic coordinates are not available. Probably they have studied some solvate, since the volume per molecule (assuming $Z = 8$) of 381 Å³ is much bigger than our result (318.6 Å³).

Molecules of **H(3)**, **H(4)**, **H(5)**, **H(7)**, **Me(2)**, **Me(3)**, **Me(4)**, **MeO(2)**, **MeO(3)** and **MeO(4)** pack in a herring-bone motif (Figures 4, 5 and 6 for the molecular packing of **H(n)**, **Me(n)** and **MeO(n)**, respectively). The planar tolan moieties contact one another edge-to-face at dihedral angles (θ) of 59 to 71°, while the long axes L of these molecules [C(1).....C(12) vectors] are practically parallel throughout the structure, the maximum misalignment angle (φ) being ca. 4° for **H(3)** and **H(5)** and $\leq 1^\circ$ for the rest. The first homologue of each series show a distorted version of the same motif, with φ increased to 30° for **H(1)** and **Me(1)**, and 9° for **MeO(1)**. There is particular similarity between structures (and lattices) of **H(3)** and **H(4)**, and **Me(2)** and **Me(3)**.

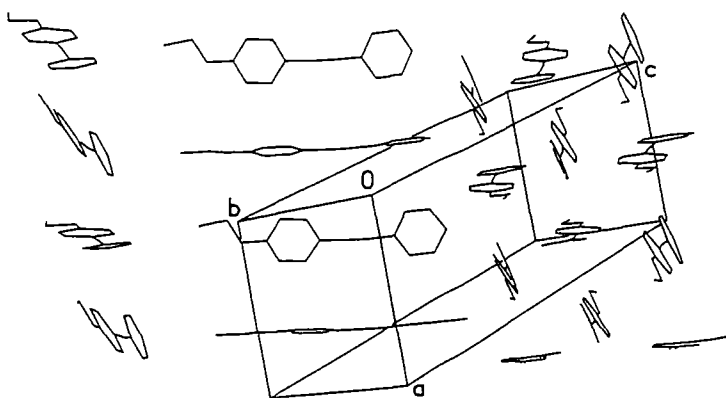
Compounds **MeO(5)** to **MeO(10)** (Figure 6) all crystallise in similar orthorhombic unit cells, with two short parameters remaining practically constant ($a \approx 7.16$ and $b \approx 6.2$ Å) while the very long c parameter steadily increases with the length of the alkyl chain. In the fully determined structures of **MeO(5)**, **MeO(7)** and **MeO(9)**, molecules pack in a herringbone manner (Figure 5) to form a succession of double-layers, parallel to the (0 0 1) plane. Within each double-layer all molecular axes are parallel ($\varphi < 1^\circ$), but those of adjacent layers are inclined by 47 – 48°. The diffraction data of **MeO(6)**, **MeO(8)** and **MeO(10)** were insufficient to solve and/or refine their atomic structures, but the similarity of their packing can be inferred from the similarity of their crystal lattices.

Thus, series 3 presents only two distinct, and closely related, packing motifs. Note also that all of these molecules, except **MeO(2)** [and of course the symmetric **MeO(1)**], are arrayed in a head-to-head fashion. Hence, the structures contain successive layers of segregated (i) alkyl chains, (ii) tolan moieties and (iii) methoxy groups. Series 1 and 2, apart from the early homologues (see above), show no such uniformity. The structure of **H(2)** (Figure 4) comprises herringbone monomolecular layers. The long axes of molecules (transverse to the layer) are nearly parallel within each layer ($\varphi = 4^\circ$) but nearly perpendicular to such axes of the adjacent layers ($\varphi = 82 - 86^\circ$), related *via* 2_1 transformations. The packing of **H(6)** (Figure 4) is characterised by edge-to-face contacts between individual benzene rings rather than entire tolan moieties; φ is rather high (23°). The packing of **Me(9)** (Figure 4) resembles those of series 3 higher homologues, but with single (rather than double) layers and a head-to-tail arrangement of molecules. Hence, the structure is polar (rather than centrosymmetric) with two (rather than four) molecules per

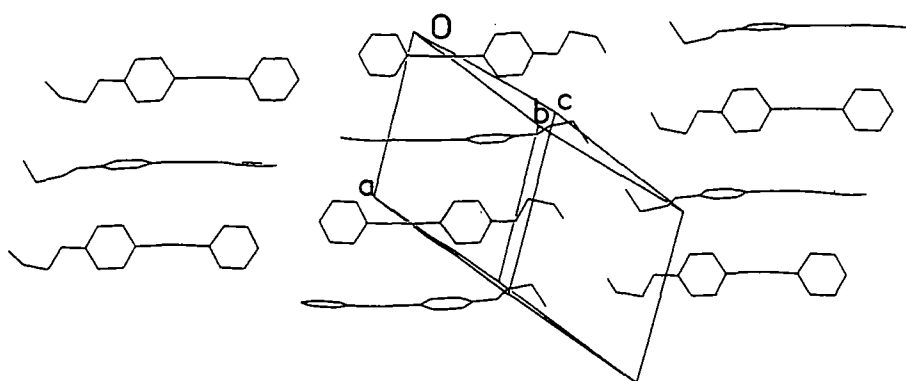
one c translation, while the a and b parameters are nearly the same as in series 3. The remaining structures, *i.e.* **H(8)**, **H(9)**, both polymorphs of **Me(5)**, **Me(6)** and **Me(12)**, depart entirely from edge-to-face packing and show various stacking motifs instead. Near-planar and near-linear molecules of **H(8)** or **H(9)** are stacked head-to-tail (Figure 4), so that the alkyl chain of one molecule overlaps with the tolan moiety of the next; the packing of **H(8)** is laminar with all molecular axes essentially parallel, whereas in **H(9)**, the stacks form a herringbone pattern with $\phi = 66^\circ$. In β -**Me(5)**, **Me(6)** and **Me(12)** (Figure 5) only the tolan moieties are stacked (in a head-to-head fashion). The tolan planes (as well as the long axes) in adjacent stacks are mutually perpendicular, while the alkyl tails, which are neither colinear nor co-planar with the tolan groups, aggregate together in a parallel manner. α -**Me(5)**, however, has a laminar packing, comprising slightly puckered, parallel layers with rather inefficient overlap between individual molecules. It is noteworthy that the density of the β -polymorph is 2% higher.



H(1)



H(2)



H(3)

Figure 4. The molecular packing of the H(n).

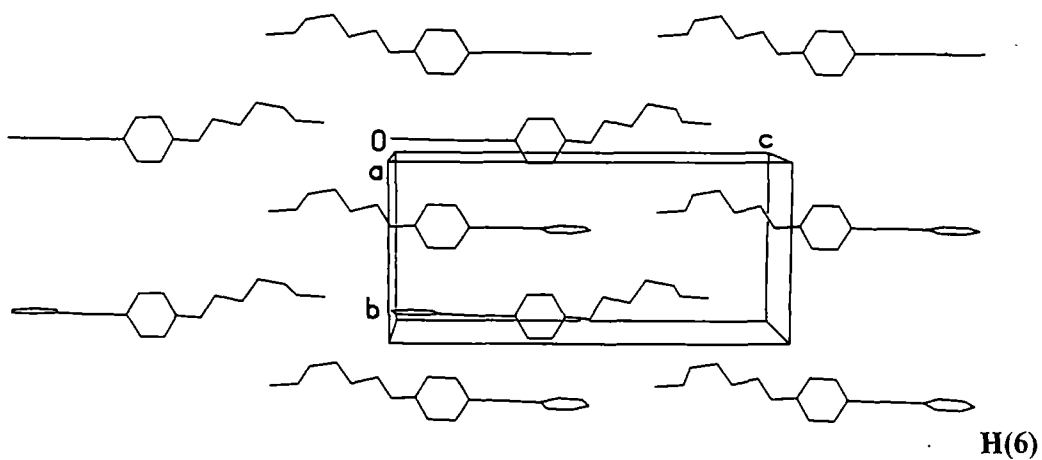
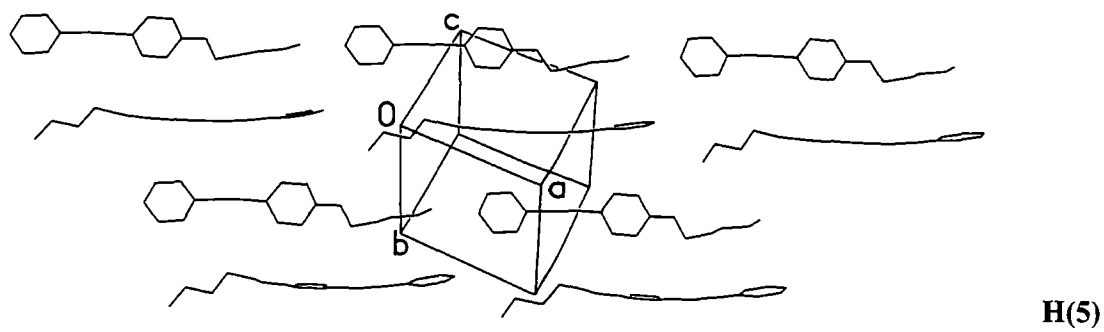
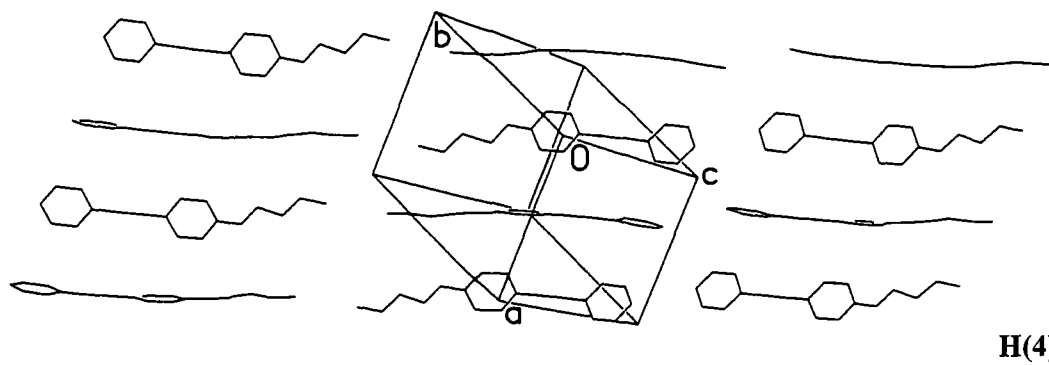


Figure 4 (continued)

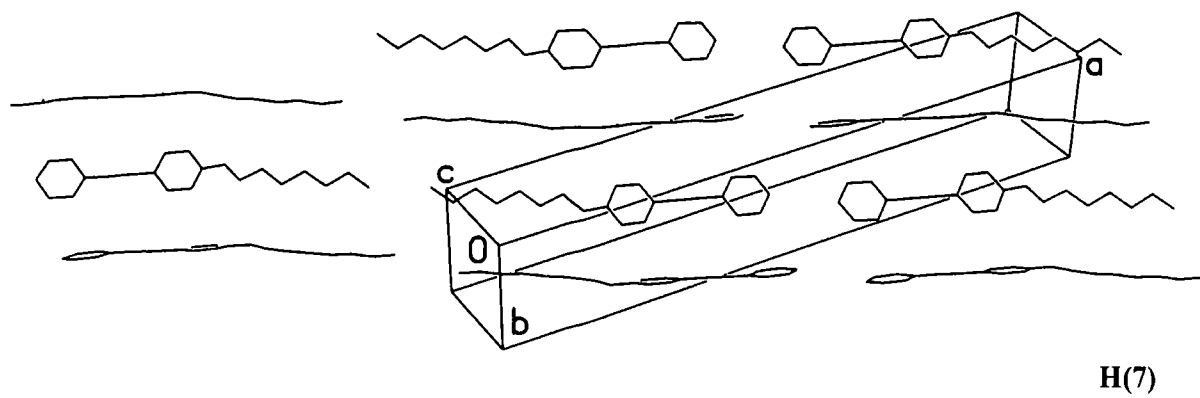
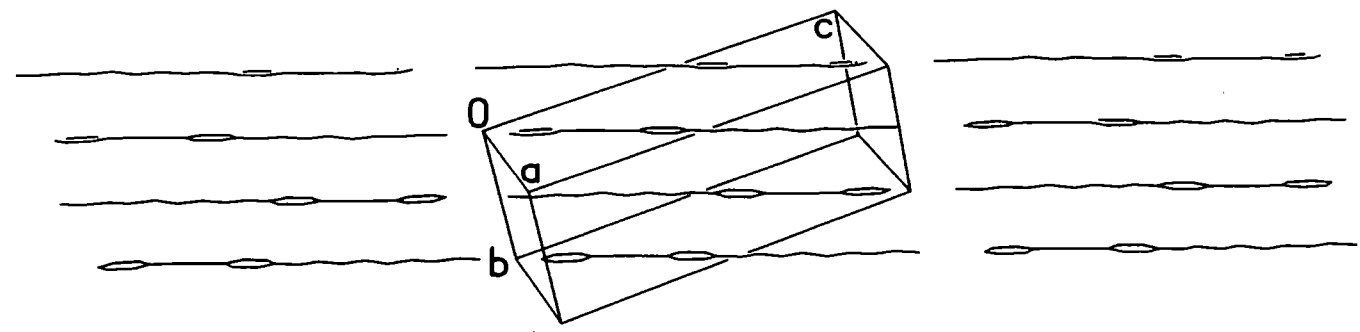
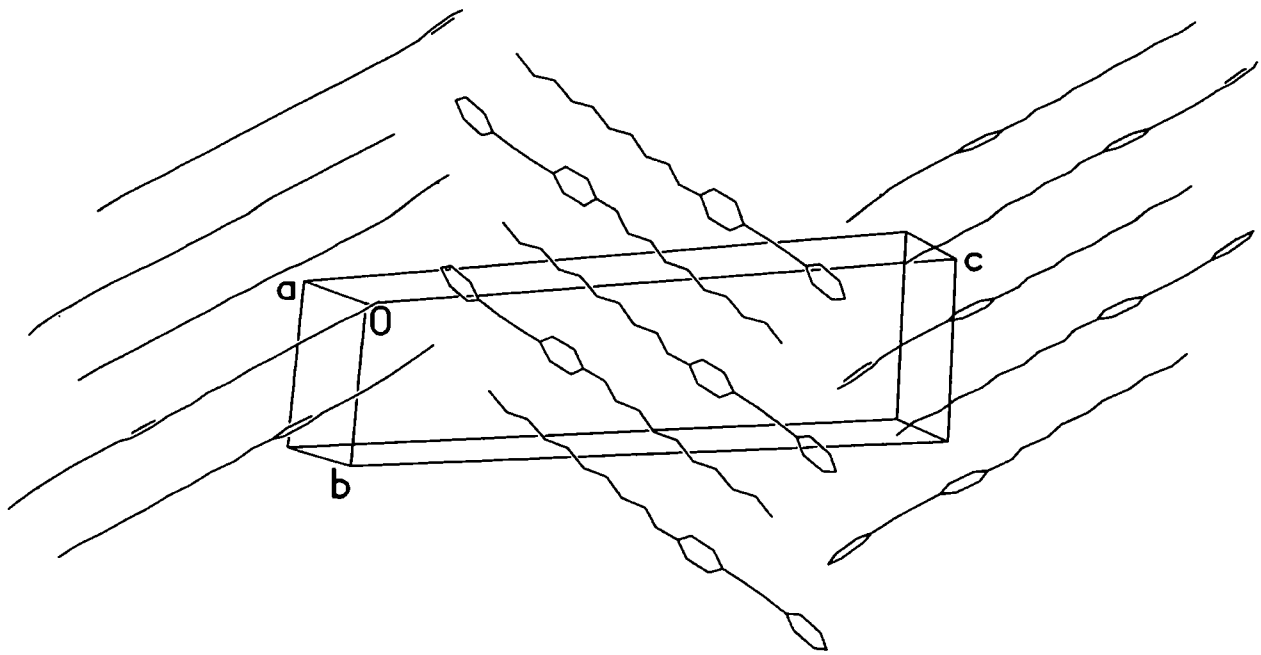


Figure 4 (continued)

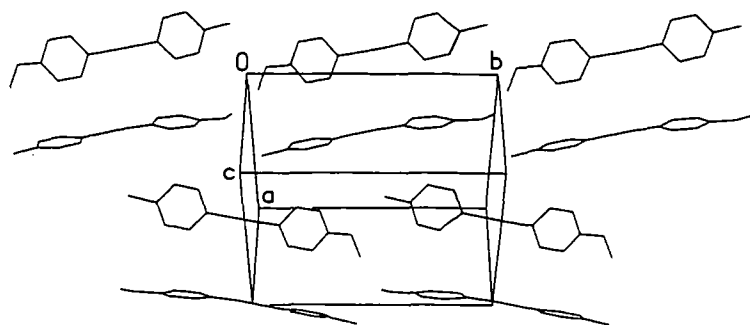
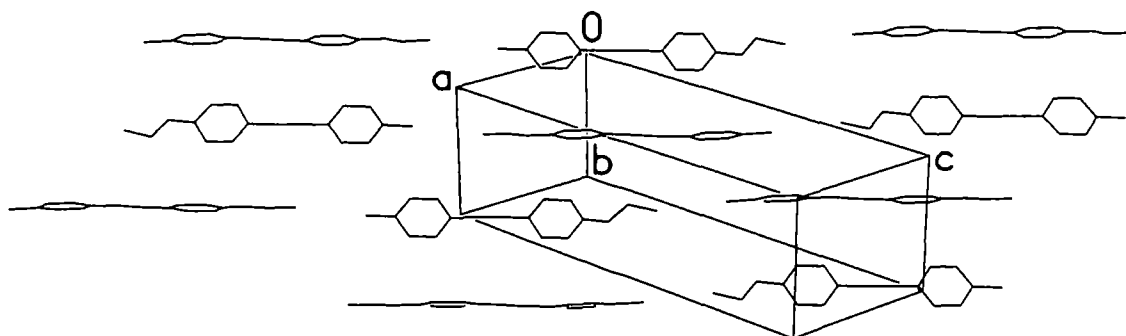
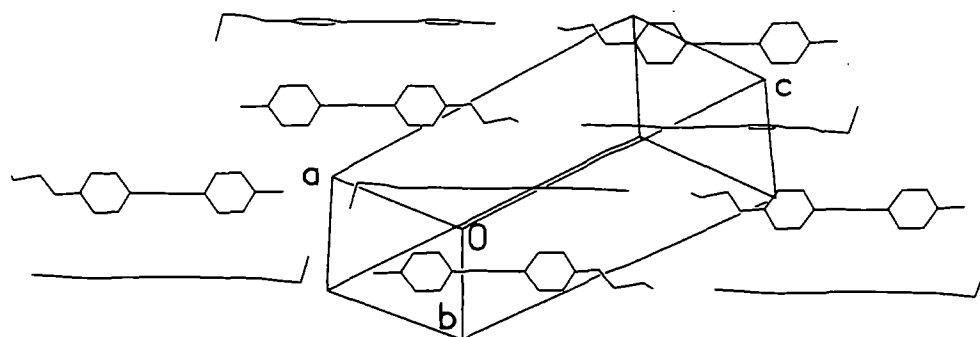
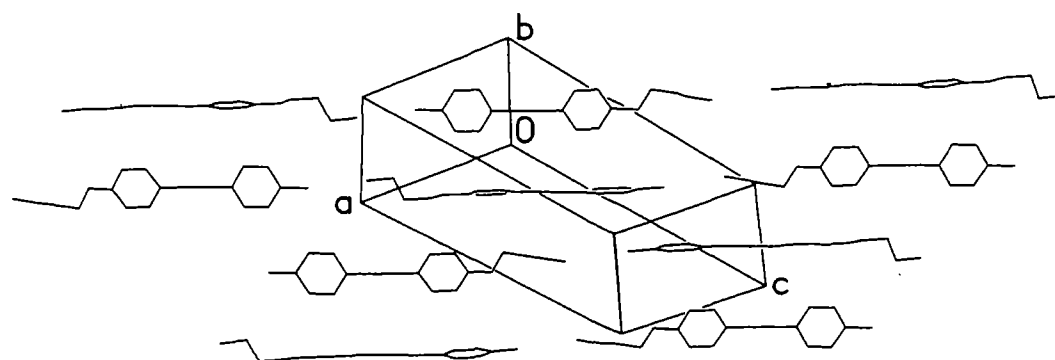


H(8)



H(9)

Figure 4 (continued)

**Me(1)****Me(2)****Me(3)****Me(4)**Figure 5. The molecular packing of **Me(n)**.

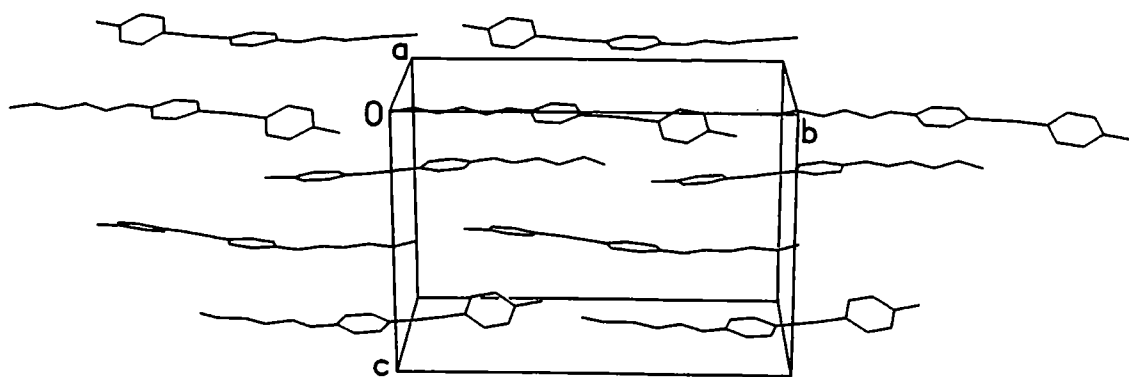
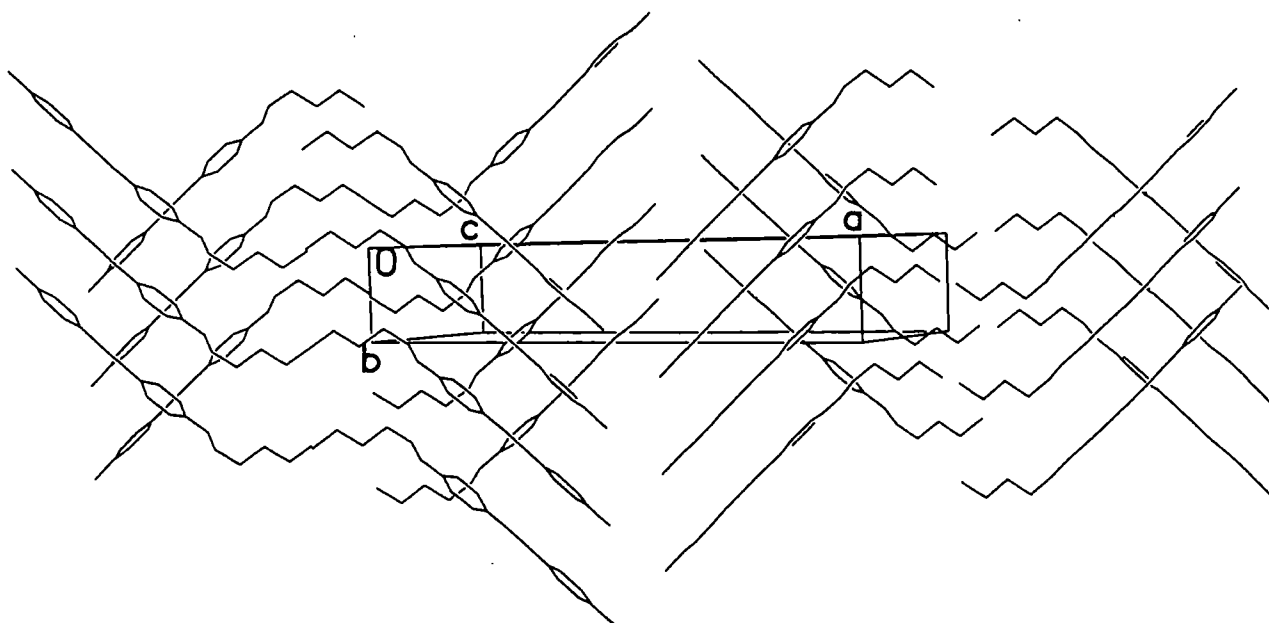
 α -Me(5) β -Me(5)

Figure 5 (continued)

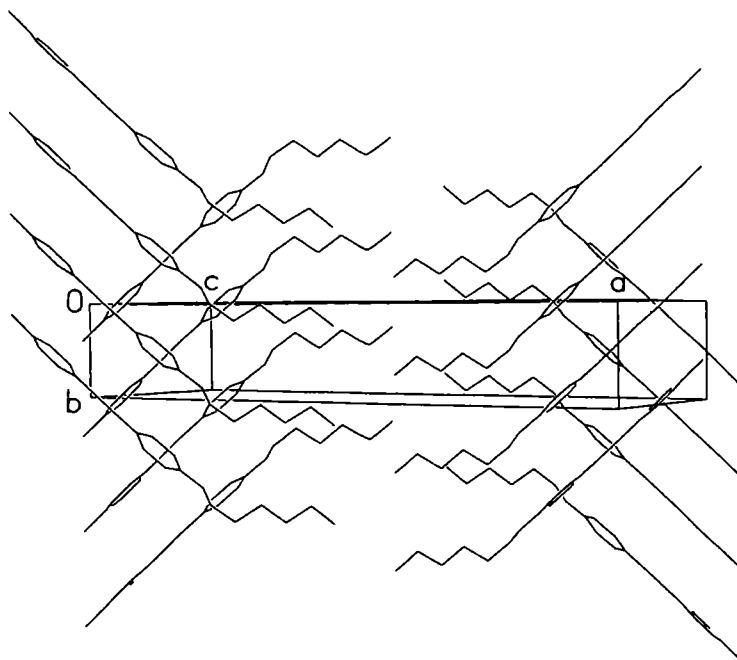
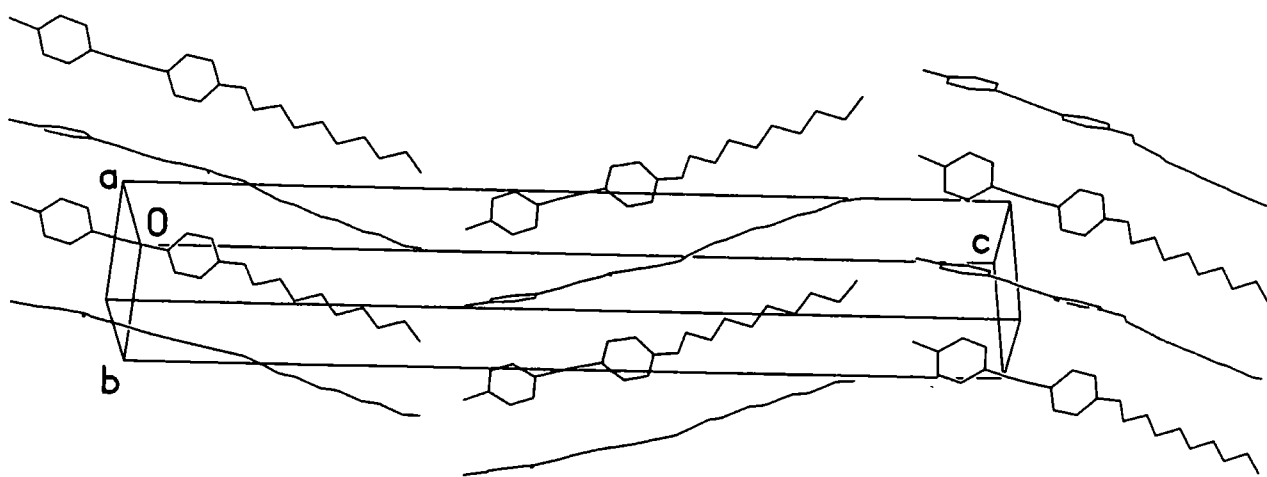
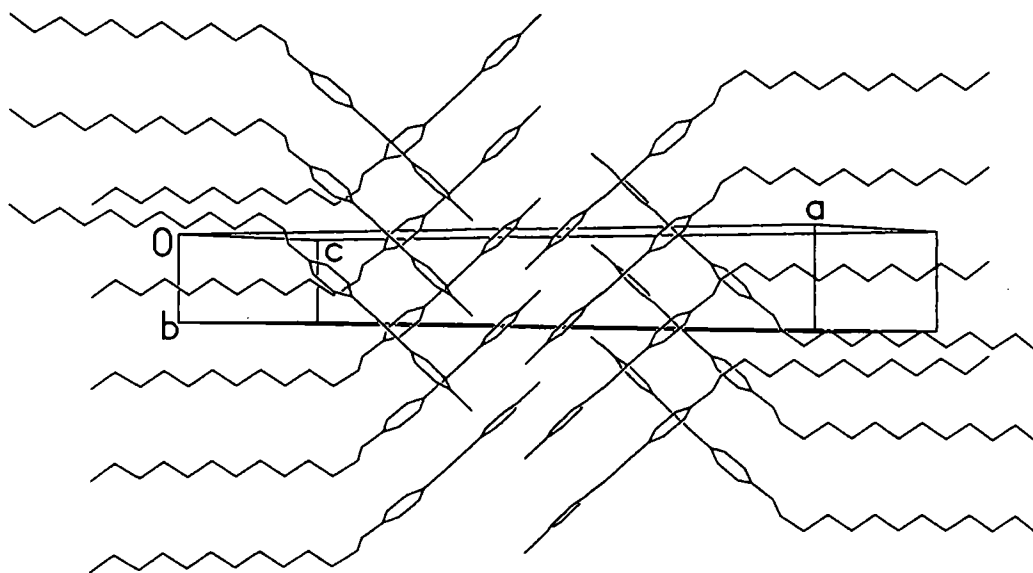
**Me(6)****Me(9)**

Figure 5 (continued)



Me(12)

Figure 5 (continued)

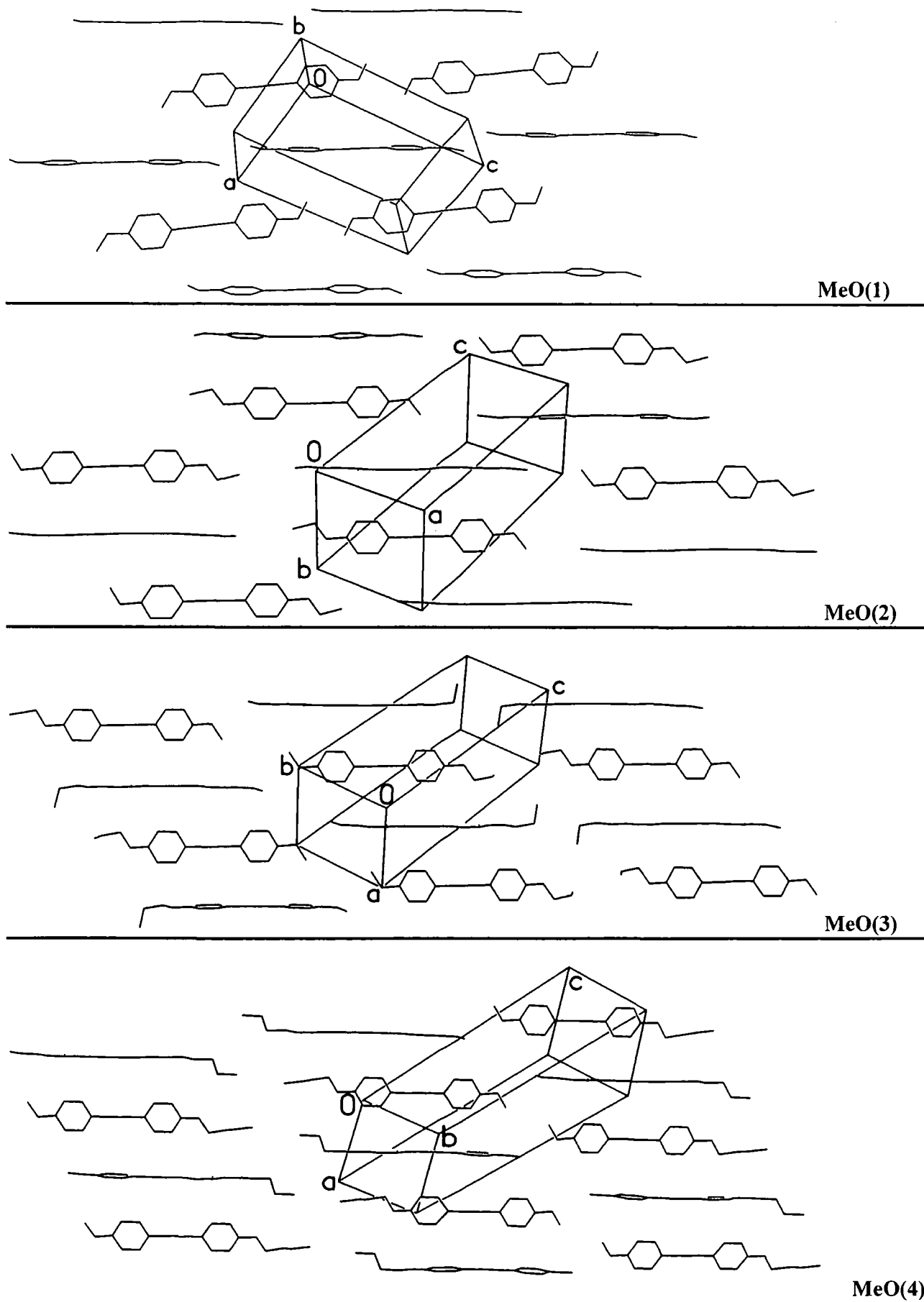
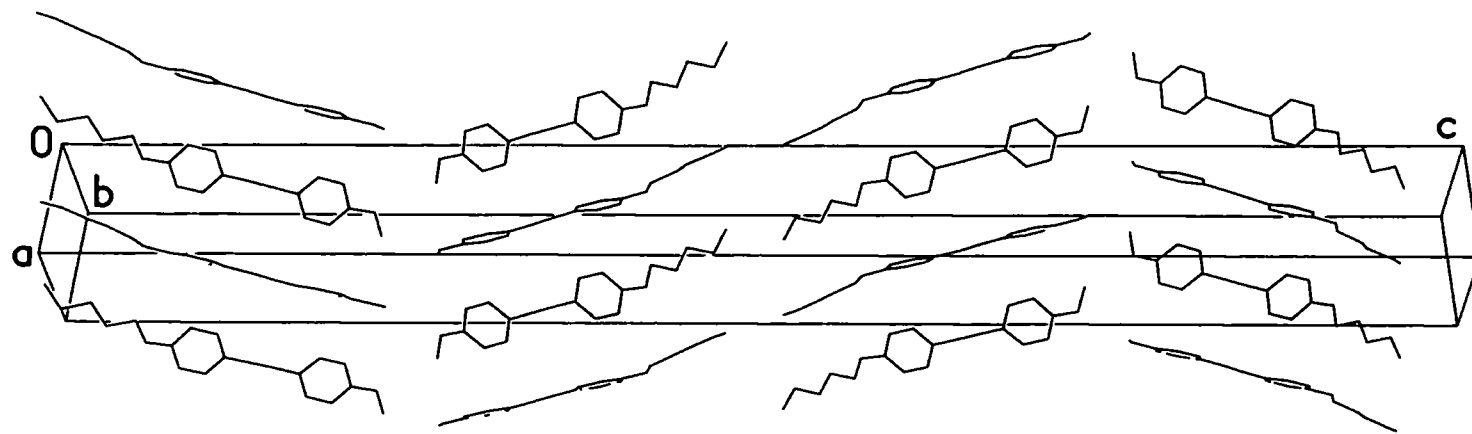
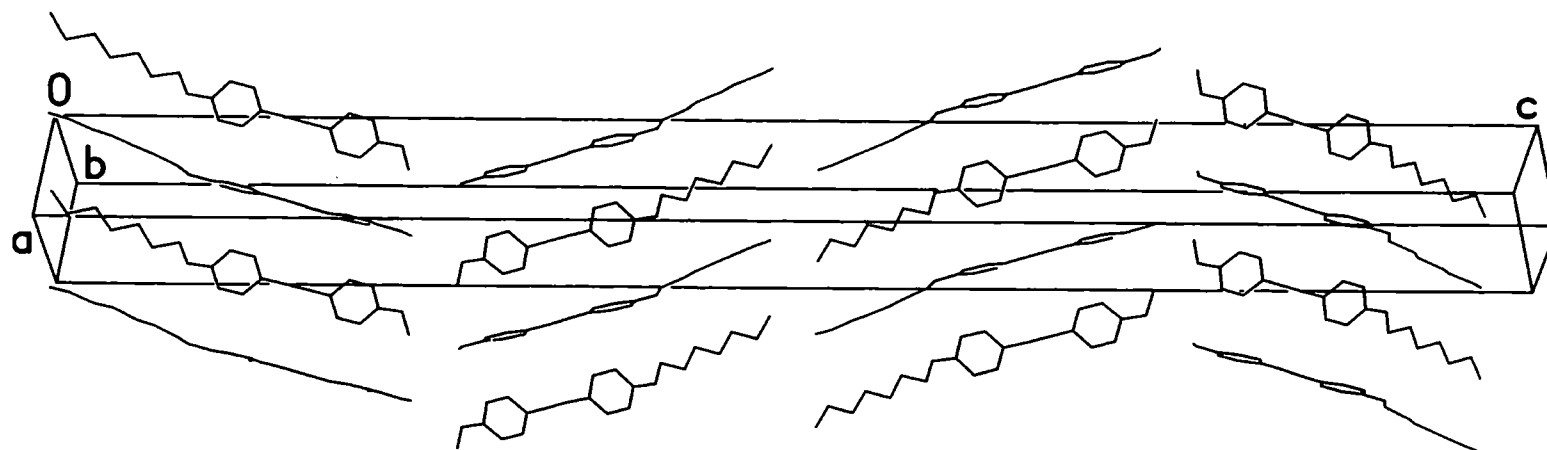


Figure 6. The molecular packing of MeO(n).



MeO(5)



MeO(7)

Figure 6 (continued)

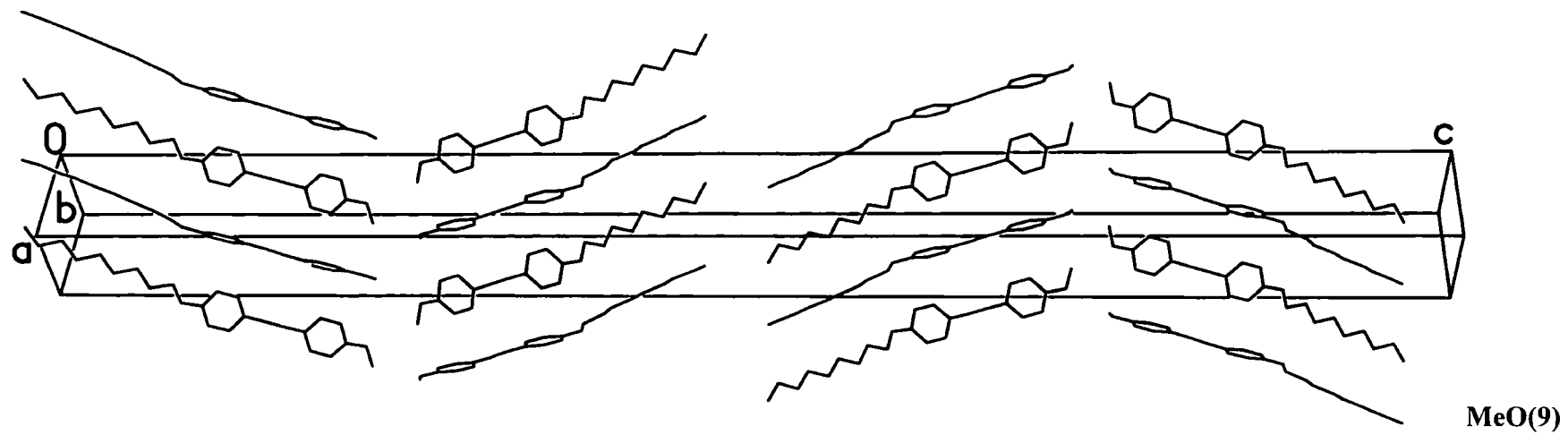


Figure 6 (continued)

The volume occupied by each molecule and the packing coefficients of the tolans are given in Table 9. The volume occupied by each molecule is increased when the length of the alkyl chain is lengthened. Furthermore, with the same alkyl chain length, the molecules in series 3 occupy the largest volumes whereas those of series 1 occupy the smallest volumes. Packing coefficients of tolans in these three series are very similar. No trends between the packing coefficients and the alkyl chain length were observed:

Table 9. The volume occupied by each molecule and packing coefficients of the tolans.^a

	Volume			Packing coefficients		
	H	Me	MeO	H	Me	MeO
1	290	306	319	67.5	68.9	68.9
2	306	337	339	68.9	68.5	69.2
3	334	359	364	67.9	67.7	68.9
4	355	384	393	68.4	67.3	67.9
5	373	α 399 β 391	416	69.3	α 68.7 β 70.1	68.2
6	404	414	-	67.5	70.2	68.2
7	430	-	461	67.5	-	
8	447	-	-	68.5	-	
9	469	491	508	69.0	68.7	68.2
12	-	552	-	-	69.8	-

^a Packing coefficients were calculated using PLATON with atomic radii as followed C 1.70 Å, H 1.20 Å and O 1.52 Å by Dr. Andrei Batsanov.

From the mesophases, crystal structures and molecular packing of the tolans we can make following observations:

i) The packing of early homologous ($n \leq 4$) are similar and defined by edge-to-face arrays of tolan groups. At $n = 5$ and 6 , the series 1 and 2 show some "uncertainty". At $n \geq 7$, the packing switch to stacking motifs with the exception of **Me(9)** which is similar to series 3. The latter ($n \geq 5$) adopts uniform packing with edge-to-face arrangements of tolans. For the long alkyl chains, it is possible that the similarity in molecular packing will continue as the length of the alkyl chain is further increased.

ii) In general, the melting points decrease when chains are lengthened. However, an unusual trend of the melting point of the compounds in series 1 is observed when the alkyl chain is short. The melting point of **H(2)** is 20°C higher than **H(1)** which is very close to the melting point of **H(3)** ($\text{H(2)} > \text{H(1)} \approx \text{H(3)}$, ca. $80 > 61 \approx 58^\circ\text{C}$, respectively (see Figure 1). Close inspection of the structure of **H(2)** reveals closer packing than in **H(1)** and **H(3)** (see packing coefficient of **H(1)**, **H(2)** and **H(3)** in Table 9). This may be the reason for the low melting point of **H(1)**. The low melting points of **H(1)** and **H(3)** may also be explained by the similarity of the packing coefficients of these two compounds.

iii) We do not observe any relationship between the transition temperatures and the molecular packing; *i.e.* the odd-even effect on the N to I and I to N transition temperatures (on heating and cooling, respectively) was observed in series 3 when the alkyl chain are long ($n = 5 - 12$) but the molecular packing of **MeO(5)**, **MeO(6)**, **MeO(7)**, **MeO(8)**, **MeO(9)** and **MeO(10)** are similar. It should be noted that poor diffraction intensities do not permit full structure determination of **MeO(6)**, **MeO(8)** and **MeO(10)**; however, similarity of the lattices and preliminary structure solution leave little doubt that the packing of all six compounds is similar. Nevertheless, the c parameter, the unit cell volume and the (calculated) density all show an odd-even alternation.

iv) Prasad *et al.* suggested that the packing coefficient is a meaningful parameter to describe the changes in physical properties such as clearing point and orientation order parameter.⁵ The authors concluded that the packing coefficient is lower for the nonmesogenic compounds than the mesogenic ones.⁶⁻¹⁰ In our case (see Table 9), we

do not observe any obvious correlation between the packing coefficient and the formation of mesophases.

v) Since molecules in series 3 generally form mesophases while those of series 1 and 2 do not, it is interesting to note how they differ in their crystalline phases. The most important difference seems to be the dipole moment due to the difference of the substituents at the para-position of the tolanes. For the **MeO(n)** (series 3), it is reasonable to expect that the dipole moments are smaller than in series 1 and series 2. However, dipole moments alone are not sufficient for mesophase formation as we do not observe a mesophase in **MeO(1)**. However, for some reason **Me(9)** gives a nematic phase on cooling. Close inspection of the crystal packing reveals that it is very similar to those of the molecules in series 3 (**MeO(5)** – **Me(10)**). Further investigation of the crystal packing of **Me(12)** reveals no similarity to **Me(9)**. For this reason, we hypothesise that the crystal packing may be at least loosely related to mesophase formation. Our observations agree very well with the studies of Sheikh-Ali *et al.*,¹ who also concluded that dipole-dipole interactions are important, but do not completely control the packing arrangements of such crystals. However, they noted that the most important factor is the angle of twist between the aromatic and nonaromatic rings which leads the alkyl chain to project along very different axes to the aromatic planes. The aromatic and nonaromatic rings of the mesogenic compounds are twisted but there is almost no twist in the case of related nonmesogenic compounds. From our results, interestingly, there is no relationship between the dihedral angles between benzene rings (see Table 5) or torsion angles (see Tables 6 – 8) in the solid state and the occurrence of mesophases in these three tolan series.

III. Conclusions

We report the synthesis by Pd/Cu-catalyzed Sonogashira cross-coupling reactions of terminal alkynes and iodoarenes, crystal structures and phase behavior of three series of tolans with varying chain length. Twenty-eight of the tolans were structurally characterised by single-crystal X-ray diffraction. Their phase behavior was characterised by tplm; only the tolans in series 3 show liquid crystalline phases. The melting points of the tolans decrease with increasing chain length due to a higher degree of flexibility of the terminal chain. An odd-even effect is clearly observed for the clearing point of the nematic phase upon both heating and cooling, with the higher temperature for even and low temperature for odd number carbon chains for series 3. We found that the dipole moment in the tolan molecules is an important factor to yield mesophases; however, the crystal packing also may be related to mesophases formation indicating the types of intermolecular interactions responsible for this. We do not observe any relationship between the packing coefficients, dihedral or torsion angles and the information of mesophases.

IV. Experimental

IV.1 Synthesis and characterization

All reactions were carried out under a dry N₂ atmosphere using standard Schlenk techniques. After the reactions were complete, further procedures were carried out without precautions against air. Et₃N was distilled over CaH₂ under N₂. All other solvents were AR grade and were used without further purification or drying. The catalyst, PdCl₂(PPh₃)₂, were synthesized using a literature procedure.⁴² The starting material for compounds **H(1)** to **H(16)**, ethynylbenzene, was obtained from commercial suppliers and used without further purification. The starting materials for compounds **Me(1)**-**Me(12)**, ethynyltoluene, and for **Me(1)**-**Me(14)**, 4-ethynylanisole, were prepared by Sonogashira cross-coupling of p-iodotoluene and p-iodoanisole respectively with ethynyltrimethylsilane (TMSA) followed by deprotection using Na₂CO₃ in H₂O/MeOH.⁴³ The 1-iodo-4-n-alkoxybenzenes were prepared *via* Williamson ether alkylation⁴⁴ of 4-iodophenol with the commercially available 1-bromoalkanes.

Proton and ¹³C{¹H} NMR spectra were obtained using Bruker Avance 400 and Inova 500 spectrometers at the following frequencies: ¹H - 400, 500 MHz, ¹³C{¹H} - 100, 125 MHz in CDCl₃. Chemical shifts are reported in ppm and are referenced to the internal standard SiMe₄.

GC-MS analyses were performed using both a Hewlett-Packard 5890 Series II gas chromatograph equipped with a 5971 mass selective detector and an Agilent 6890 gas chromatograph equipped with a 5973N mass selective detector with a 10 m fused silica capillary column (5% cross linked phenylmethylsilicone), under the following operating conditions: injector temperature 300 °C, the oven temperature was ramped from 50 °C to 280 °C at 20 °C/min. UHP helium was used as the carrier gas.

Elemental analyses were performed using an Exeter Analytical CE-440 analyzer. Melting points of **H(n)** and **Me(n)** were obtained using a Laboratory Devices Mel-Temp II and are uncorrected.

A Perkin Elmer Pyris 1 DSC equipped with a Cryofill cooling system, operated at a heating rate of 10 °C min⁻¹, was used to record the thermal behavior of the samples. An Olympus BX51 microscope fitted with Linkam THMS 600 hot-stage and a Linkam TMS 94 temperature controller was used to examine the phase behavior of

the materials by transmitted polarised light microscopy. The melting point (crystal to isotropic) reported for **MeO(n)** are the recorded on the this hot-stage.

UV-vis spectra were recorded on a Hewlett-Packard 8453 spectrophotometer using standard 1 cm width quartz cells and cyclohexane as the solvent. A Perkin Elmer 1600 series FTIR spectrophotometer was used to record the IR spectra. IR samples were prepared as Nujol mulls between NaCl plates. A Horiba Jobin-Yvon LabRam-HR Raman microscope with excitation at 632.8 nm (HeNe laser) was used to record the Raman spectra.

4-Methoxytolan (**H(1)**)¹⁸⁻²⁰

Ethynylbenzene (1.02 g, 10 mmol) was added to a mixture of 4-iodoanisole (2.34 g, 10 mmol), PdCl₂(PPh₃)₂ (0.07 g, 0.1 mmol) and CuI (0.02 g, 0.1 mmol) in Et₃N (300 ml). The mixture was stirred at r.t. overnight and then refluxed at 80 °C for 3 h. After the reaction was complete as shown by GC-MS, the solvent was removed under reduced pressure. The residue was re-dissolved in hexane and then filtered through a 5 cm silica pad with additional hexane. Purification by column chromatography on silica using hexane:EtOAc (9:1) as eluent gave the product as pale yellow crystals. Yield: 2.00 g (96 %), m.p. 56.5-58.5°C. ¹H NMR (500 MHz): δ 7.51 (d, *J*_{H-H} = 8 Hz, 2H, H_{arom}), 7.47 (d, *J*_{H-H} = 9 Hz, 2H, H_{arom}), 7.33 (m, 3H, H_{arom}), 6.88 (d, *J*_{H-H} = 9 Hz, 2H, H_{arom}), 3.83 (s, 3H, OCH₃). ¹³C{¹H} NMR (125 MHz): δ 159.6 (C), 133.4 (CH), 133.0 (CH), 131.4 (CH), 128.2 (CH), 127.9 (CH), 123.6 (C), 115.4 (C), 89.0 (C≡C), 88.0 (C≡C), 55.2 (CH₃). MS (EI) *m/z* (rel): 208 (m⁺, 100), 194 (60), 165 (84), 139 (25). Anal. Calcd. for C₁₅H₁₂O: C 86.51, H 5.81; Found C 86.28, H 5.78 %.

4-Ethoxytolan (**H(2)**)

Compound **H(2)** was synthesized by a similar procedure as for **H(1)** using ethynylbenzene (1.02 g, 10 mmol), 1-iodo-4-ethoxybenzene (2.48 g, 10 mmol), PdCl₂(PPh₃)₂ (0.07 g, 0.1 mmol) and CuI (0.02 g, 0.1 mmol) in Et₃N (300 ml). The mixture was stirred at r.t. overnight and then refluxed at 80 °C for 1 h. The solvent was removed under reduced pressure and the residue was re-dissolved in hexane and then filtered through a 3 cm silica pad with additional hexane. Purification by re-crystallisation from hexane gave the product as pale yellow crystals. Yield: 1.40 g (63

%), m.p. 78-80 °C. ^1H NMR (500 MHz): δ 7.52 (d, $J_{\text{H-H}} = 8$ Hz, 2H, H_{arom}), 7.45 (d, $J_{\text{H-H}} = 9$ Hz, 2H, H_{arom}), 7.33 (m, 3H, H_{arom}), 6.87 (d, $J_{\text{H-H}} = 9$ Hz, 2H, H_{arom}), 4.05 (q, $J_{\text{H-H}} = 7$ Hz, 2H, OCH_2), 1.43 (t, $J_{\text{H-H}} = 7$ Hz, 3H, CH_3). $^{13}\text{C}\{^1\text{H}\}$ NMR (125 MHz): δ 159.1 (C), 133.1 (CH), 131.5 (CH), 128.3 (CH), 127.9 (CH), 123.7 (C), 115.2 (C), 114.5 (CH), 88.5 (C \equiv C), 88.0 (C \equiv C), 63.5 (OCH_2), 14.8 (CH_3). MS (EI) m/z (rel): 222 (m^+ , 42), 194 (100), 165 (59), 139 (25). Anal. Calcd. for $\text{C}_{16}\text{H}_{14}\text{O}$: C 86.45, H 6.35; Found C 86.65, H 6.35 %.

4-n-Propoxytolan (**H(3)**)

Compound **H(3)** was synthesized by a similar procedure as for **H(1)** using ethynylbenzene (0.204 g, 2 mmol), 1-iodo-4-n-propoxybenzene (0.524 g, 2 mmol), $\text{PdCl}_2(\text{PPh}_3)_2$ (0.014 g, 0.02 mmol) and CuI (0.0085 g, 0.02 mmol) in Et_3N (150 ml). The mixture was stirred at r.t. over night and then refluxed at 80 °C for 4 h. The solvent was removed under reduced pressure and the residue was re-dissolved in hexane and then filtered through a 5 cm silica pad with additional hexane. Purification by re-crystallisation from hexane gave the product as pale yellow crystals. Yield: 0.415 g (88 %), m.p. 60-61 °C. ^1H NMR (500 MHz): δ 7.52 (d, $J_{\text{H-H}} = 8$ Hz, 2H, H_{arom}), 7.47 (d, $J_{\text{H-H}} = 9$ Hz, 2H, H_{arom}), 7.33 (m, 3H, H_{arom}), 6.87 (d, $J_{\text{H-H}} = 9$ Hz, 2H, H_{arom}), 3.94 (t, $J_{\text{H-H}} = 6$ Hz, 2H, OCH_2), 1.82 (m, 2H, CH_2), 1.05 (t, $J_{\text{H-H}} = 7$ Hz, 3H, CH_3). $^{13}\text{C}\{^1\text{H}\}$ NMR (125 MHz): δ 159.3 (C), 133.0 (CH), 131.5 (CH), 128.3 (CH), 127.9 (CH), 123.7 (CH), 115.2 (C), 114.6 (C), 89.5 (C \equiv C), 88.0 (C \equiv C), 69.6 (OCH_2), 22.5 (CH_2), 10.5 (CH_3). MS (EI) m/z (rel): 236 (m^+ , 32), 194 (100), 165 (32). Anal. Calcd. for $\text{C}_{17}\text{H}_{16}\text{O}$: C 86.40, H 6.82; Found C 86.37, H 6.81 %.

4-n-Butoxytolan (**H(4)**)²¹

Compound **H(4)** was synthesized by a similar procedure as for **H(1)** using ethynylbenzene (0.204 g, 2 mmol), 1-iodo-4-n-butoxybenzene (0.552 g, 2 mmol), $\text{PdCl}_2(\text{PPh}_3)_2$ (0.014 g, 0.02 mmol) and CuI (0.0085 g, 0.02 mmol) in Et_3N (150 ml). The mixture was stirred at r.t. over night and then refluxed at 80 °C for 3 h. The solvent was removed under reduced pressure and the residue was re-dissolved in hexane and filtered through a 5 cm silica pad with additional hexane. Purification by re-crystallisation from hexane gave the product as pale yellow crystals. Yield: 0.457 g (90 %), m.p. 50-51 °C. ^1H NMR (500 MHz): δ 7.52 (d, $J_{\text{H-H}} = 8$ Hz, 2H, H_{arom}), 7.46

(d, $J_{H-H} = 9$ Hz, 2H, H_{arom}), 7.33 (m, 3H, H_{arom}), 6.87 (d, $J_{H-H} = 9$ Hz, 2H, H_{arom}), 3.98 (t, $J_{H-H} = 6$ Hz, 2H, OCH_2), 1.78 (m, 2H, CH_2), 1.50 (m, 2H, CH_2), 0.99 (t, $J_{H-H} = 7$ Hz, 3H, CH_3). $^{13}\text{C}\{^1\text{H}\}$ NMR (125 MHz): δ 159.3 (C), 133.0 (CH), 131.5 (CH), 128.3 (CH), 127.9 (CH), 123.7 (CH), 115.2 (C), 114.6 (C), 89.5 ($\text{C}\equiv\text{C}$), 89.0 ($\text{C}\equiv\text{C}$), 67.8 (OCH_2), 31.3 (CH_2), 19.2 (CH_2), 13.8 (CH_3). MS (EI) m/z (rel): 250 (m^+ , 20), 194 (100), 165 (31). Anal. Calcd. for $\text{C}_{18}\text{H}_{18}\text{O}$: C 86.36, H 7.25; Found C 86.43, H 7.30 %.

4-n-Pentoxytolan (H(5))

Compound **H(5)** was synthesized by a similar procedure as for **H(1)** using ethynylbenzene (1.02 g, 10 mmol), 1-iodo-4-n-pentoxybenzene (2.90 g, 10 mmol), $\text{PdCl}_2(\text{PPh}_3)_2$ (0.07 g, 0.1 mmol) and CuI (0.02 g, 0.1 mmol) in Et_3N (300 ml). The mixture was stirred at r.t. for 0.5 h and then refluxed at 80 °C for 2 h. The solvent was removed under reduced pressure and the residue was re-dissolved in hexane and then filtered through a 5 cm silica pad with additional hexane. Purification by recrystallisation from hexane gave the product as a white solid. Yield: 2.04 g (77 %), m.p. 53-54 °C. ^1H NMR (500 MHz): δ 7.51 (d, $J_{H-H} = 8$ Hz, 2H, H_{arom}), 7.46 (d, $J_{H-H} = 9$ Hz, 2H, H_{arom}), 7.32 (m, 3H, H_{arom}), 6.86 (d, $J_{H-H} = 9$ Hz, 2H, H_{arom}), 3.97 (t, $J_{H-H} = 7$ Hz, 2H, OCH_2), 1.80 (quint, $J_{H-H} = 7$ Hz, 2H, CH_2), 1.41 (m, 4H, CH_2), 0.94 (t, $J_{H-H} = 7$ Hz, 3H, CH_3). $^{13}\text{C}\{^1\text{H}\}$ NMR (125 MHz): δ 159.3 (C), 133.0 (CH), 131.4 (CH), 128.3 (CH), 127.9 (CH), 123.7 (CH), 115.1 (C), 114.6 (C), 89.5 ($\text{C}\equiv\text{C}$), 88.0 ($\text{C}\equiv\text{C}$), 68.1 (OCH_2), 28.9 (CH_2), 28.2 (CH_2), 22.4 (CH_2), 14.0 (CH_3). MS (EI) m/z (rel): 264 (m^+ , 10), 194 (100), 176 (7), 165 (33), 139 (14). Anal. Calcd. for $\text{C}_{19}\text{H}_{20}\text{O}$: C 86.32, H 7.63; Found C 86.19, H 7.61 %.

4-n-Hexyloxytolan (H(6))

Compound **H(6)** was synthesized by a similar procedure as for **H(1)** using ethynylbenzene (1.02 g, 10 mmol), 1-iodo-4-n-hexyloxybenzene (3.04 g, 10 mmol), $\text{PdCl}_2(\text{PPh}_3)_2$ (0.07 g, 0.1 mmol) and CuI (0.02 g, 0.1 mmol) in Et_3N (300 ml). The mixture was stirred at r.t. for 3 h and then refluxed at 80 °C for 3 h. The solvent was removed under reduced pressure and the residue was re-dissolved in hexane and then filtered through a 5 cm silica pad with additional hexane. Purification by recrystallisation from hexane gave the product as a white solid. Yield: 1.28 g (46 %),

m.p. 43-44 °C. ^1H NMR (500 MHz): δ 7.52 (d, $J_{\text{H-H}} = 8$ Hz, 2H, H_{arom}), 7.48 (d, $J_{\text{H-H}} = 9$ Hz, 2H, H_{arom}), 7.34 (m, 3H, H_{arom}), 6.88 (d, $J_{\text{H-H}} = 9$ Hz, 2H, H_{arom}), 3.97 (t, $J_{\text{H-H}} = 7$ Hz, 2H, OCH_2), 1.80 (quint, $J_{\text{H-H}} = 7$ Hz, 2H, CH_2), 1.48 (m, 2H, CH_2), 1.37 (m, 4H, CH_2), 0.91 (t, $J_{\text{H-H}} = 7$ Hz, 3H, CH_3). $^{13}\text{C}\{^1\text{H}\}$ NMR (125 MHz): δ 159.3 (C), 133.2 (CH), 131.4 (CH), 128.3 (CH), 127.9 (CH), 127.3 (CH), 115.1 (C), 114.6 (C), 89.5 ($\text{C}\equiv\text{C}$), 88.0 ($\text{C}\equiv\text{C}$), 68.1 (OCH_2), 31.6 (CH_2), 29.2 (CH_2), 25.7 (CH_2), 22.6 (CH_2), 14.0 (CH_3). MS (EI) m/z (rel): 278 (m^+ , 8), 194 (100), 165 (34), 139 (8). Anal. Calcd. for $\text{C}_{20}\text{H}_{22}\text{O}$: C 86.29, H 7.97; Found C 86.23, H 7.91 %.

4-n-Heptyloxytolan (H(7))

Compound **H(7)** was synthesized by a similar procedure as for **H(1)** using ethynylbenzene (0.36 g, 3 mmol), 1-iodo-4-n-heptyloxybenzene (1.12 g, 3 mmol), $\text{PdCl}_2(\text{PPh}_3)_2$ (0.07 g, 0.1 mmol) and CuI (0.02 g, 0.1 mmol) in Et_3N (150 ml). The mixture was stirred at r.t. over night and then refluxed at 80 °C for 2.5 h. The solvent was removed under reduced pressure and the residue was re-dissolved in hexane and then filtered through a 5 cm silica pad with additional hexane. Purification by column chromatography on silica gel using hexane: CH_2Cl_2 (95:5) as eluent gave the product as a white solid. Yield: 0.59 g (67 %), m.p. 42-43 °C. ^1H NMR (500 MHz): δ 7.52 (d, $J_{\text{H-H}} = 8$ Hz, 2H, H_{arom}), 7.47 (d, $J_{\text{H-H}} = 9$ Hz, 2H, H_{arom}), 7.33 (m, 3H, H_{arom}), 6.87 (d, $J_{\text{H-H}} = 9$ Hz, 2H, H_{arom}), 3.97 (t, $J_{\text{H-H}} = 7$ Hz, 2H, OCH_2), 1.80 (quint, $J_{\text{H-H}} = 7$ Hz, 2H, CH_2), 1.47 (m, 2H, CH_2), 1.33 (m, 6H, CH_2), 0.92 (t, $J_{\text{H-H}} = 7$ Hz, 3H, CH_3). $^{13}\text{C}\{^1\text{H}\}$ NMR (125 MHz): δ 159.5 (C), 133.0 (CH), 131.4 (CH), 128.3 (CH), 127.9 (CH), 123.7 (CH), 115.1 (C), 114.6 (C), 89.5 ($\text{C}\equiv\text{C}$), 88.0 ($\text{C}\equiv\text{C}$), 68.1 (OCH_2), 31.8 (CH_2), 29.1 (CH_2), 29.0 (CH_2), 26.0 (CH_2), 22.6 (CH_2), 14.1 (CH_3). MS (EI) m/z (rel): 292 (m^+ , 5), 194 (100), 165 (19). Anal. Calcd. for $\text{C}_{21}\text{H}_{24}\text{O}$: C 86.26, H 8.27; Found C 85.99, H 8.35 %.

4-n-Octyloxytolan (H(8))

Compound **H(8)** was synthesized by a similar procedure as for **H(1)** using ethynylbenzene (1.02 g, 10 mmol), 1-iodo-4-n-octyloxybenzene (3.322 g, 10 mmol), $\text{PdCl}_2(\text{PPh}_3)_2$ (0.07 g, 0.1 mmol) and CuI (0.02 g, 0.1 mmol) in Et_3N (150 ml). The mixture was stirred at r.t. for 4 h and then refluxed at 80 °C for 3 h. The solvent was removed under reduced pressure and the residue was re-dissolved in hexane and then

filtered through a 5 cm silica pad with additional hexane. Purification by column chromatography on silica gel using a petroleum ether:CH₂Cl₂ (95:5) as eluent gave the product as a white solid. Yield: 2.68 g (88 %), m.p. 45-46 °C. ¹H NMR (500 MHz): δ 7.51 (d, *J*_{H-H} = 8 Hz, 2H, H_{arom}), 7.45 (d, *J*_{H-H} = 9 Hz, 2H, H_{arom}), 7.32 (m, 3H, H_{arom}), 6.86 (d, *J*_{H-H} = 9 Hz, 2H, H_{arom}), 3.97 (t, *J*_{H-H} = 7 Hz, 2H, OCH₂), 1.79 (quint, *J*_{H-H} = 7 Hz, 2H, CH₂), 1.46 (m, 2H, CH₂), 1.30 (m, 8H, CH₂), 0.89 (t, *J*_{H-H} = 7 Hz, 3H, CH₃). ¹³C{¹H} NMR (125 MHz): δ 159.5 (C), 133.3 (CH), 131.7 (CH), 128.5 (CH), 128.1 (CH), 123.9 (CH), 115.3 (C), 114.8 (C), 89.7 (C≡C), 88.2 (C≡C), 68.3 (OCH₂), 32.1 (CH₂), 29.6 (CH₂), 29.5 (CH₂), 29.4 (CH₂), 26.3 (CH₂), 22.9 (CH₂), 14.4 (CH₃). MS (EI) *m/z* (rel): 306 (m⁺, 2), 194 (100), 165 (35). Anal. Calcd. for C₂₂H₂₆O: C 86.23, H 8.55; Found C 85.86, H 8.56 %.

4-n-Nonyloxytolan (H(9))

Compound **H(9)** was synthesized by a similar procedure as for **H(1)** using ethynylbenzene (1.02 g, 10 mmol), 1-iodo-4-n-nonyloxybenzene (3.46 g, 10 mmol), PdCl₂(PPh₃)₂ (0.07 g, 0.1 mmol) and CuI (0.02 g, 0.1 mmol) in Et₃N (300 ml). The mixture was stirred at r.t. for 2 h and then refluxed at 80 °C for 3 h. The solvent was removed under reduced pressure and the residue was re-dissolved in hexane and then filtered through a 5 cm silica pad with additional hexane. Purification by column chromatography on silica gel using hexane:CH₂Cl₂ (9:1) as eluent gave the product as a white solid. Yield: 3.12 g (97 %), m.p. 60-61 °C. ¹H NMR (500 MHz): δ 7.52 (d, *J*_{H-H} = 8 Hz, 2H, H_{arom}), 7.46 (d, *J*_{H-H} = 9 Hz, 2H, H_{arom}), 7.33 (m, 3H, H_{arom}), 6.87 (d, *J*_{H-H} = 9 Hz, 2H, H_{arom}), 3.97 (t, *J*_{H-H} = 7 Hz, 2H, OCH₂), 1.79 (quint, *J*_{H-H} = 7 Hz, 2H, CH₂), 1.46 (m, 2H, CH₂), 1.31 (m, 10H, CH₂), 0.90 (t, *J*_{H-H} = 7 Hz, 3H, CH₃). ¹³C{¹H} NMR (125 MHz): δ 159.3 (C), 133.0 (CH), 131.4 (CH), 128.3 (CH), 127.9 (CH), 123.7 (CH), 115.3 (C), 114.8 (C), 89.7 (C≡C), 88.0 (C≡C), 68.1 (OCH₂), 31.9 (CH₂), 29.5 (CH₂), 29.4 (CH₂), 29.24 (CH₂), 29.22 (CH₂), 26.0 (CH₂), 22.7 (CH₂), 14.1 (CH₃). MS (EI) *m/z* (rel): 320 (m⁺, 5), 194 (100), 165 (16). Anal. Calcd. for C₂₃H₂₈O: C 86.20, H 8.81; Found C 86.20, H 8.81 %.

4-n-Decyloxytolan (H(10))

Compound **H(10)** was synthesized by a similar procedure as for **H(1)** using ethynylbenzene (0.204 g, 2 mmol), 1-iodo-4-n-decyloxybenzene (0.720 g, 2 mmol),

$\text{PdCl}_2(\text{PPh}_3)_2$ (0.014 g, 0.02 mmol) and CuI (0.0085 g, 0.1 mmol) in Et_3N (150 ml). The mixture was stirred at r.t. for 2 h and then refluxed at 80 °C for 4 h. The solvent was removed under reduced pressure and the residue was re-dissolved in hexane and then filtered through a 5 cm silica pad with additional hexane. Purification by column chromatography on silica gel using hexane: CH_2Cl_2 (9:1) as eluent gave the product as a white solid. Yield: 3.03 g (90 %), m.p. 52-53 °C. ^1H NMR (500 MHz): δ 7.51 (d, $J_{\text{H-H}} = 8$ Hz, 2H, H_{arom}), 7.46 (d, $J_{\text{H-H}} = 9$ Hz, 2H, H_{arom}), 7.33 (m, 3H, H_{arom}), 6.87 (d, $J_{\text{H-H}} = 9$ Hz, 2H, H_{arom}), 3.97 (t, $J_{\text{H-H}} = 7$ Hz, 2H, OCH_2), 1.79 (quint, $J_{\text{H-H}} = 7$ Hz, 2H, CH_2), 1.46 (m, 2H, CH_2), 1.31 (m, 12H, CH_2), 0.97 (t, $J_{\text{H-H}} = 7$ Hz, 3H, CH_3). $^{13}\text{C}\{^1\text{H}\}$ NMR (125 MHz): δ 159.5 (C), 133.3 (CH), 131.7 (CH), 128.5 (CH), 128.1 (CH), 123.9 (CH), 115.3 (C), 114.8 (C), 89.7 ($\text{C}\equiv\text{C}$), 88.2 ($\text{C}\equiv\text{C}$), 68.3 (OCH_2), 32.2 (CH_2), 29.83 (CH_2), 29.81 (CH_2), 29.64 (CH_2), 29.58 (CH_2), 29.4 (CH_2), 26.3 (CH_2), 22.9 (CH_2), 14.4 (CH_3). MS (EI) m/z (rel): 334 (m^+ , 41), 194 (100), 165 (10). Anal. Calcd. for $\text{C}_{24}\text{H}_{30}\text{O}$: C 86.18, H 9.04; Found C 86.12, H 9.11 %.

4-n-Dodecyloxytolan (**H(12)**)

Compound **H(12)** was synthesized by a similar procedure as for **H(1)** using ethynylbenzene (1.02 g, 10 mmol), 1-iodo-4-n-dodecyloxybenzene (3.88 g, 10 mmol), $\text{PdCl}_2(\text{PPh}_3)_2$ (0.07 g, 0.1 mmol) and CuI (0.02 g, 0.1 mmol) in Et_3N (150 ml). The mixture was stirred at r.t. for 2 h and then refluxed at 80 °C for 4 h. The solvent was removed under reduced pressure and the residue was re-dissolved in hexane and then filtered through a 5 cm silica pad with additional hexane. Purification by column chromatography on silica gel using hexane: CH_2Cl_2 (95:5) as eluent gave the product as a white solid. Yield: 3.43 g (95 %), m.p. 61-62 °C. ^1H NMR (500 MHz): δ 7.51 (d, $J_{\text{H-H}} = 8$ Hz, 2H, H_{arom}), 7.46 (d, $J_{\text{H-H}} = 9$ Hz, 2H, H_{arom}), 7.32 (m, 3H, H_{arom}), 6.86 (d, $J_{\text{H-H}} = 9$ Hz, 2H, H_{arom}), 3.97 (t, $J_{\text{H-H}} = 7$ Hz, 2H, OCH_2), 1.79 (quint, $J_{\text{H-H}} = 7$ Hz, 2H, CH_2), 1.45 (m, 2H, CH_2), 1.30 (m, 16H, CH_2), 0.88 (t, $J_{\text{H-H}} = 7$ Hz, 3H, CH_3). $^{13}\text{C}\{^1\text{H}\}$ NMR (125 MHz): δ 159.5 (C), 133.3 (CH), 131.7 (CH), 128.5 (CH), 128.1 (CH), 123.9 (CH), 115.3 (C), 114.8 (C), 89.7 ($\text{C}\equiv\text{C}$), 88.2 ($\text{C}\equiv\text{C}$), 68.3 (OCH_2), 32.2 (CH_2), 29.91 (2CH_2), 29.89 (CH_2), 29.84 (CH_2), 29.82 (CH_2), 29.64 (CH_2), 29.61 (CH_2), 29.4 (CH_2), 26.3 (CH_2), 23.0 (CH_2), 14.4 (CH_3). MS (EI) m/z (rel): 362 (m^+ , 14), 194 (100), 165 (16). Anal. Calcd. for $\text{C}_{26}\text{H}_{34}\text{O}$: C 86.13, H 9.45; Found C 86.12, H 9.48 %.

4-n-Tetradecyloxytolan (H(14))

Compound **H(14)** was synthesized by a similar procedure as for **H(1)** using ethynylbenzene (0.213 g, 2.1 mmol), 1-iodo-4-n-tetradecyloxybenzene (0.87 g, 2.1 mmol), PdCl₂(PPh₃)₂ (0.07 g, 0.1 mmol) and CuI (0.02 g, 0.1 mmol) in Et₃N (200 ml). The mixture was stirred at r.t. for 2 h and then refluxed at 80 °C for 4 h. The solvent was removed under reduced pressure. The residue was re-dissolved in hexane and then filtered through a 5 cm silica pad with additional hexane. Purification by re-crystallisation from hexane gave the product as a white solid. Yield: 0.54 g (65 %), m.p. 68-69 °C. ¹H NMR (500 MHz): δ 7.51 (d, *J*_{H-H} = 8 Hz, 2H, H_{arom}), 7.45 (d, *J*_{H-H} = 9 Hz, 2H, H_{arom}), 7.31 (m, 3H, H_{arom}), 6.86 (d, *J*_{H-H} = 9 Hz, 2H, H_{arom}), 3.97 (t, *J*_{H-H} = 7 Hz, 2H, OCH₂), 1.79 (quint, *J*_{H-H} = 7 Hz, 2H, CH₂), 1.45 (m, 2H, CH₂), 1.30 (m, 20H, CH₂), 0.88 (t, *J*_{H-H} = 7 Hz, 3H, CH₃). ¹³C{¹H} NMR (125 MHz): δ 159.5 (C), 133.3 (CH), 131.7 (CH), 128.5 (CH), 128.1 (CH), 123.9 (CH), 115.3 (C), 114.8 (C), 89.7 (C≡C), 88.2 (C≡C), 68.3 (OCH₂), 32.2 (CH₂), 29.95 (CH₂), 29.93 (CH₂), 29.91 (2CH₂), 29.85 (CH₂), 29.82 (CH₂), 29.64 (CH₂), 29.62 (CH₂), 29.4 (CH₂), 26.3 (CH₂), 23.0 (CH₂), 14.4 (CH₃). MS (EI) *m/z* (rel): 390 (m⁺, 6), 194 (100), 165 (41), 69 (34), 55 (77). Anal. Calcd. for C₂₈H₃₈O: C 86.10, H 9.81; Found C 85.86, H 9.80 %.

4-n-Hexadecyloxytolan (H(16))

Compound **H(16)** was synthesized by a similar procedure as for **H(1)** using ethynylbenzene (1.02 g, 2 mmol), 1-iodo-4-n-hexadecyloxybenzene (4.44 g, 2 mmol), PdCl₂(PPh₃)₂ (0.07 g, 0.1 mmol) and CuI (0.02 g, 0.1 mmol) in Et₃N (200 ml). The mixture was stirred at r.t. over night and then refluxed at 80 °C for 3 h. The solvent was removed under reduced pressure and the residue was re-dissolved in hexane and then filtered through a 5 cm silica gel column with additional hexane. Purification by re-crystallisation from hexane gave the product as a white solid. Yield: 4.07 g (97 %), m.p. 73-74 °C. ¹H NMR (500 MHz): δ 7.51 (d, *J*_{H-H} = 8 Hz, 2H, H_{arom}), 7.45 (d, *J*_{H-H} = 9 Hz, 2H, H_{arom}), 7.33 (m, 3H, H_{arom}), 6.86 (d, *J*_{H-H} = 9 Hz, 2H, H_{arom}), 3.97 (t, *J*_{H-H} = 7 Hz, 2H, OCH₂), 1.79 (quint, *J*_{H-H} = 7 Hz, 2H, CH₂), 1.45 (m, 2H, CH₂), 1.30 (m, 24H, CH₂), 0.88 (t, *J*_{H-H} = 7 Hz, 3H, CH₃). ¹³C{¹H} NMR (125 MHz): δ 159.5 (C), 133.3 (CH), 131.7 (CH), 128.6 (CH), 128.1 (CH), 123.9 (CH), 115.3 (C), 114.8 (C), 89.7 (C≡C), 88.2 (C≡C), 68.3 (OCH₂), 32.2 (CH₂), 29.95 (2CH₂), 29.93 (2CH₂), 29.92 (2CH₂), 29.85 (CH₂), 29.82 (CH₂), 29.64 (CH₂), 29.62 (CH₂), 29.4 (CH₂), 26.2 (CH₂),

23.0 (CH₂), 14.4 (CH₃). Anal. Calcd. for C₃₀H₄₂O: C 86.07, H 10.11; Found C 85.81, H 10.16 %.

4-n-Methoxy-4'-methyltolan (Me(1))^{3, 4, 6, 22, 23}

Compound **Me(1)** was synthesized by a similar procedure as for **H(1)** using 1-iodo-4-methylbenzene (1.091 g, 5 mmol), 4-methoxyphenylacetylene (0.800 g, 6 mmol), PdCl₂(PPh₃)₂ (0.0349 g, 0.05 mmol) and CuI (0.0095 g, 0.05 mmol) in *i*-Pr₂NH (50 ml). The mixture was stirred at r.t. for 2 h. The solvent was removed under reduced pressure to yield white crystals. The crude product was re-dissolved in toluene and purified *via* column chromatography. One fraction remains impure, from which the solvent was removed *in vacuo*. This sample was dissolved in hexane:EtOAc (9:1) and purified *via* column chromatography. The product was re-crystallised from hot toluene to yield white needle-shaped crystals upon cooling. Yield: 0.75 g (68 %), m.p. 125.1-125.6 °C. ¹H NMR (200 MHz): δ 7.47 (d, *J*_{H-H} = 9 Hz, 2H, H_{arom}), 7.42 (d, *J*_{H-H} = 8 Hz, 2H, H_{arom}), 7.15 (d, *J*_{H-H} = 8 Hz, 2H, H_{arom}), 6.88 (d, *J*_{H-H} = 9 Hz, 2H, H_{arom}), 3.83 (s, 3H, OCH₃), 2.37 (s, 3H, CH₃). ¹³C{¹H} NMR (100 MHz): δ 159.7 (C), 138.3 (C), 133.2 (CH), 131.6 (CH), 129.3 (CH), 120.7 (C), 155.8 (C), 114.2 (CH), 88.9 (C≡C), 88.4 (C≡C), 55.5 (OCH₃), 21.7 (CH₃). MS (EI) *m/z* (rel): 222 (m⁺, 100), 207 (63), 178 (20), 176 (4). Anal. Calcd. for C₁₆H₁₄O: C 86.45, H 6.35; Found C 86.30, H 6.38 %.

4-n-Ethoxy-4'-methyltolan (Me(2))^{3, 4, 6, 24}

Compound **Me(2)** was synthesized by a related procedure as for **H(1)** but using 4-iodotoluene (0.232 g, 2 mmol), 4-ethoxyphenylacetylene (0.496 g, 2 mmol), PdCl₂(PPh₃)₂ (0.014 g, 0.02 mmol) and CuI (0.0085 g, 0.02 mmol) in Et₃N (200 ml). The mixture was stirred at r.t. over night and then refluxed at 80 °C for 3 h. The solvent was removed under reduced pressure and the residue was re-dissolved in hexane and then filtered through a 5 cm silica gel column with additional hexane:CH₂Cl₂ (8:2). Purification by re-crystallisation from hexane gave the product as a white solid. Yield: 0.329 g (70 %), m.p. 108.5-109.5 °C. ¹H NMR (400 MHz): δ 7.45 (d, *J*_{H-H} = 9 Hz, 2H, H_{arom}), 7.40 (d, *J*_{H-H} = 8 Hz, 2H, H_{arom}), 7.14 (d, *J*_{H-H} = 8 Hz, 2H, H_{arom}), 6.86 (d, *J*_{H-H} = 9 Hz, 2H, H_{arom}), 4.05 (q, *J*_{H-H} = 7 Hz, 2H, OCH₂), 2.36 (s, 3H, CH₃), 1.42 (t, *J*_{H-H} = 7 Hz, 3H, CH₃). ¹³C{¹H} NMR (100 MHz): δ 158.9 (C),

138.0 (C), 133.0 (CH), 131.3 (CH), 129.1 (CH), 120.6 (C), 115.5 (C), 114.5 (CH), 88.7 (C≡C), 88.1 (C≡C), 63.5 (OCH₂), 21.5 (CH₃), 14.8 (CH₃). MS (EI) *m/z* (rel): 236 (*m*⁺, 100), 208 (97), 178 (26), 152 (9). Anal. Calcd. for C₁₇H₁₆O: C 86.40, H 6.82; Found C 86.45, H 6.83 %.

4-*n*-Propoxy-4'-methyltolan (Me(3))^{3,4,6}

Compound **Me(3)** was synthesized by a similar procedure as for **H(1)** using 4-ethynyltoluene (0.232 g, 2 mmol), 1-iodo-4-*n*-propoxybenzene (0.524 g, 2 mmol), PdCl₂(PPh₃)₂ (0.07 g, 0.1 mmol) and CuI (0.02 g, 0.1 mmol) in Et₃N (150 ml). The mixture was stirred at r.t. for 0.5 h and then refluxed at 80 °C for 4 h. The solvent was removed under reduced pressure and the residue was re-dissolved in hexane and then filtered through a 5 cm silica pad with additional of hexane:CH₂Cl₂ (9:1). Purification by re-crystallisation from hexane gave the product as white crystals. Yield: 0.406 g (81 %), m.p. 90.5-91.5 °C. ¹H NMR (500 MHz): δ 7.44 (d, *J*_{H-H} = 9 Hz, 2H, H_{arom}), 7.40 (d, *J*_{H-H} = 8 Hz, 2H, H_{arom}), 7.14 (d, *J*_{H-H} = 8 Hz, 2H, H_{arom}), 6.86 (d, *J*_{H-H} = 9 Hz, 2H, H_{arom}), 3.93 (t, *J*_{H-H} = 7 Hz, 2H, OCH₂), 2.36 (s, 3H, CH₃), 1.81 (m, 2H, CH₂), 1.03 (t, *J*_{H-H} = 7 Hz, 3H, CH₃). ¹³C{¹H} NMR (125 MHz): δ 159.0 (C), 137.9 (C), 132.9 (CH), 131.3 (CH), 129.0 (CH), 120.5 (C), 115.2 (C), 114.4 (CH), 88.7 (C≡C), 88.0 (C≡C), 69.5 (OCH₂), 22.5 (CH₃), 21.4 (CH₂), 10.5 (CH₃). MS (EI) *m/z* (rel): 250 (*m*⁺, 13), 208 (100), 178 (65), 152 (26). Anal. Calcd. for C₁₈H₁₈O: C 86.36, H 7.25; Found C 86.61, H 7.14 %.

4-*n*-Butoxy- 4'-methyltolan (Me(4))^{3,4,6}

Compound **Me(4)** was synthesized by a similar procedure as for **H(1)** using 4-ethynyltoluene (0.232 g, 2 mmol), 1-iodo-4-*n*-butoxybenzene (0.552 g, 2 mmol), PdCl₂(PPh₃)₂ (0.07 g, 0.1 mmol) and CuI (0.02 g, 0.1 mmol) in Et₃N (150 ml). The mixture was stirred at r.t. for 1 h and then refluxed at 80 °C for 4 h. The solvent was removed under reduced pressure and the residue was re-dissolved in hexane and then filtered through a 5 cm silica pad with additional hexane. Purification by re-crystallisation from hexane gave the product as white crystals. Yield: 0.33 g (62 %), m.p. 71-73 °C. ¹H NMR (500 MHz): δ 7.44 (d, *J*_{H-H} = 9 Hz, 2H, H_{arom}), 7.40 (d, *J*_{H-H} = 8 Hz, 2H, H_{arom}), 7.14 (d, *J*_{H-H} = 8 Hz, 2H, H_{arom}), 6.87 (d, *J*_{H-H} = 9 Hz, 2H, H_{arom}), 3.97 (t, *J*_{H-H} = 6 Hz, 2H, OCH₂), 2.36 (s, 3H, CH₃), 1.78 (quint, *J*_{H-H} = 7 Hz, 2H,

CH₂), 1.48 (m, 2H, CH₂), 0.98 (t, $J_{H-H} = 7$ Hz, 3H, CH₃). ¹³C{¹H} NMR (125 MHz): δ 159.1 (C), 137.9 (CH), 132.9 (CH), 131.3 (CH), 129.1 (CH), 120.6 (C), 115.4 (C), 114.5 (CH), 88.8 (C \equiv C), 88.1 (C \equiv C), 67.8 (OCH₂), 31.3 (CH₃), 21.5 (CH₂), 19.2 (CH₂), 13.8 (CH₃). MS (EI) m/z (rel): 264 (m^+ , 40), 208 (100), 178 (67), 152 (29). Anal. Calcd. for C₁₉H₂₀O: C 86.32, H 7.63; Found C 86.36, H 7.58 %.

4-n-Pentoxy-4'-methyltolan (Me(5))^{3, 4, 6, 25}

Compound **Me(5)** was synthesized by a similar procedure as for **H(1)** using 4-ethynyltoluene (0.232 g, 2 mmol), 1-iodo-4-n-pentoxybenzene (0.524 g, 2 mmol), PdCl₂(PPh₃)₂ (0.07 g, 0.1 mmol) and CuI (0.02 g, 0.1 mmol) in Et₃N (150 ml). The mixture was stirred at r.t. for 1 h and then refluxed at 80 °C for 4 h. The solvent was removed under reduced pressure and the residue was re-dissolved in hexane and then filtered through a 5 cm silica pad with additional hexane. Purification by re-crystallisation from hexane gave the product as white crystals. Yield: 0.392 g (82 %), m.p. 61.5-62.5 °C. ¹H NMR (500 MHz): δ 7.44 (d, $J_{H-H} = 9$ Hz, 2H, H_{arom}), 7.40 (d, $J_{H-H} = 8$ Hz, 2H, H_{arom}), 7.14 (d, $J_{H-H} = 8$ Hz, 2H, H_{arom}), 6.85 (d, $J_{H-H} = 9$ Hz, 2H, H_{arom}), 3.96 (t, $J_{H-H} = 7$ Hz, 2H, OCH₂), 2.36 (s, 3H, CH₃), 1.79 (quint, $J_{H-H} = 7$ Hz, 2H, CH₂), 1.40 (m, 4H, CH₂), 0.93 (t, $J_{H-H} = 7$ Hz, 3H, CH₃). ¹³C{¹H} NMR (125 MHz): δ 159.0 (C), 137.9 (C), 132.9 (CH), 131.3 (CH), 129.0 (CH), 120.5 (C), 115.2 (C), 114.4 (CH), 88.7 (C \equiv C), 88.0 (C \equiv C), 68.0 (OCH₂), 28.8 (CH₃), 28.1 (CH₂), 22.4 (CH₂), 21.4 (CH₂), 14.0 (CH₃). MS (EI) m/z (rel): 278 (m^+ , 29), 208 (100), 178 (94), 152 (36). Anal. Calcd. for C₂₀H₂₂O: C 86.29, H 7.97; Found C 86.43, H 7.92 %.

4-n-Hexyloxy-4'-methyltolan (Me(6))

Compound **Me(6)** was synthesized by a similar procedure as for **H(1)** using 4-ethynyltoluene (0.232 g, 2 mmol), 1-iodo-4-n-hexyloxytolan (0.553 g, 2 mmol), PdCl₂(PPh₃)₂ (0.07 g, 0.1 mmol) and CuI (0.02 g, 0.1 mmol) in Et₃N (150 ml). The mixture was stirred at r.t. for 1 h and then refluxed at 80 °C for 4 h. The amine solvent was removed under reduced and the residue was re-dissolved in hexane and then filtered through a 5 cm silica pad with additional hexane. Purification by re-crystallisation from hexane gave the product as a white solid. Yield: 0.384 g (66 %), m.p. 70-71.5 °C. ¹H NMR (400 MHz): δ 7.44 (d, $J_{H-H} = 9$ Hz, 2H, H_{arom}), 7.39 (d, $J_{H-H} = 8$ Hz, 2H, H_{arom}), 7.13 (d, $J_{H-H} = 8$ Hz, 2H, H_{arom}), 6.84 (d, $J_{H-H} = 9$ Hz, 2H, H_{arom}),

3.96 (t, $J_{H-H} = 7$ Hz, 2H, OCH₂), 2.36 (s, 3H, CH₃), 1.78 (quint, $J_{H-H} = 7$ Hz, 2H, CH₂), 1.46 (m, 2H, CH₂), 1.34 (m, 4H, CH₂), 0.91 (t, $J_{H-H} = 7$ Hz, 3H, CH₃). ¹³C{¹H} NMR (100 MHz): δ 159.1 (C), 137.9 (C), 132.9 (CH), 131.3 (CH), 129.1 (CH), 120.6 (C), 115.4 (C), 114.5 (CH), 88.8 (C \equiv C), 88.1 (C \equiv C), 68.1 (OCH₂), 31.6 (CH₃), 29.2 (CH₂), 25.7 (CH₂), 22.6 (CH₂), 21.5 (CH₂), 14.0 (CH₃). MS (EI) m/z (rel): 292 (m^+ , 8), 208 (100), 178 (42), 152 (14). Anal. Calcd. for C₂₁H₂₄O: C 86.26, H 8.27; Found C 86.29, H 8.25 %.

4-n-Nonyloxy-4'-methyltolan (Me(9))²⁶⁻³⁰

Compound **Me(9)** was synthesized by a similar procedure as for **H(1)** using 4-ethynyltoluene (0.232 g, 2 mmol), 1-iodo-4-n-nonyloxybenzene (0.629 g, 2 mmol), PdCl₂(PPh₃)₂ (0.014 g, 0.02 mmol) and CuI (0.0085 g, 0.02 mmol) in Et₃N (150 ml). The mixture was stirred at r.t. for 2 d and then refluxed at 80 °C for 5 h. The solvent was removed under reduced and the residue was re-dissolved in hexane and then filtered through a 5 cm silica pad with additional hexane. Purification by recrystallisation from hexane gave the product as a white solid. Yield: 0.540 g (81 %), m.p. 72.5-75.9 °C. ¹H NMR (400 MHz): δ 7.44 (d, $J_{H-H} = 9$ Hz, 2H, H_{arom}), 7.39 (d, $J_{H-H} = 8$ Hz, 2H, H_{arom}), 7.13 (d, $J_{H-H} = 8$ Hz, 2H, H_{arom}), 6.85 (d, $J_{H-H} = 9$ Hz, 2H, H_{arom}), 3.97 (t, $J_{H-H} = 7$ Hz, 2H, OCH₂), 2.36 (s, 3H, CH₃), 1.76 (quint, $J_{H-H} = 7$ Hz, 2H, CH₂), 1.45 (m, 2H, CH₂), 1.31 (m, 10H, CH₂), 0.89 (t, $J_{H-H} = 7$ Hz, 3H, CH₃). ¹³C{¹H} NMR (100 MHz): δ 159.1 (C), 137.9 (C), 132.9 (CH), 131.3 (CH), 129.1 (CH), 120.6 (C), 115.0 (C), 114.5 (CH), 88.8 (C \equiv C), 88.1 (C \equiv C), 68.1 (OCH₂), 31.9 (CH₃), 29.5 (CH₂), 29.4 (CH₂), 29.24 (CH₂), 29.21 (CH₂), 26.0 (CH₂), 22.7 (CH₂), 21.5 (CH₂), 14.1 (CH₃), MS (EI) m/z (rel): 334 (m^+ , 41), 208 (100), 178 (12). Anal. Calcd. for C₂₄H₃₀O: C 86.18, H 9.04; Found C 86.06, H 9.04 %.

4-n-Dodecyloxy-4'-methyltolan (Me(12))

Compound **Me(12)** was synthesized by a similar procedure as for **H(1)** using 4-ethynyltoluene (0.232 g, 2 mmol), 1-iodo-4-n-dodecyloxybenzene (0.776 g, 2 mmol), PdCl₂(PPh₃)₂ (0.07 g, 0.1 mmol) and CuI (0.02 g, 0.1 mmol) in Et₃N (150 ml). The mixture was stirred at r.t. for 2 d and then refluxed at 80 °C for 3 h. The solvent was removed under reduced and the residue was re-dissolved in hexane and then filtered through a 5 cm silica pad with additional hexane:CH₂Cl₂ (9:1). Purification by re-

crystallisation from hexane gave the product as a white solid. Yield: 0.702 g (93 %), m.p. 76-77 °C. ^1H NMR (500 MHz): δ 7.45 (d, $J_{\text{H-H}} = 9$ Hz, 2H, H_{arom}), 7.40 (d, $J_{\text{H-H}} = 8$ Hz, 2H, H_{arom}), 7.14 (d, $J_{\text{H-H}} = 8$ Hz, 2H, H_{arom}), 6.85 (d, $J_{\text{H-H}} = 9$ Hz, 2H, H_{arom}), 3.96 (t, $J_{\text{H-H}} = 7$ Hz, 2H, OCH_2), 2.36 (s, 3H, CH_3), 1.78 (quint, $J_{\text{H-H}} = 7$ Hz, 2H, CH_2), 1.45 (m, 2H, CH_2), 1.30 (m, 16H, CH_2), 0.81 (t, $J_{\text{H-H}} = 7$ Hz, 3H, CH_3). $^{13}\text{C}\{^1\text{H}\}$ NMR (125 MHz): δ 159.1 (C), 137.9 (C), 132.9 (CH), 131.3 (CH), 129.1 (CH), 120.6 (C), 115.4 (C), 114.5 (CH), 88.9 (C \equiv C), 88.1 (C \equiv C), 68.1 (OCH_2), 31.9 (CH_3), 29.7 (CH_2), 29.6 (CH_2), 29.58 (CH_2), 29.56 (CH_2), 29.38 (CH_2), 29.34 (CH_2), 29.21 (CH_2), 26.0 (CH_2), 22.7 (CH_2), 21.5 (CH_2), 14.1 (CH_3). MS (EI) m/z (rel): 376 (m^+ , 31), 208 (100), 178 (18), 55 (22). Anal. Calcd. for $\text{C}_{27}\text{H}_{36}\text{O}$: C 86.12, H 9.64; Found C 86.04, H 9.62 %.

4,4'-Dimethoxytolan (MeO(1))³¹⁻³³

Sample of MeO(1) were prepared using modifications of literature procedure.²² m.p. 149.1 °C. ^1H NMR (500 MHz): δ 7.46 (d, $J_{\text{H-H}} = 9$ Hz, 4H, H_{arom}), 6.88 (d, $J_{\text{H-H}} = 9$ Hz, 4H, H_{arom}), 3.83 (s, 6H, OCH_3), $^{13}\text{C}\{^1\text{H}\}$ NMR (125 MHz): δ 159.4 (C), 132.9 (CH), 115.7 (CH), 113.9 (C), 87.9 (C \equiv C), 55.3 (OCH_3). MS (EI) m/z (rel): 238 (m^+ , 100), 223 (72), 152 (15). Anal. Calcd. for $\text{C}_{16}\text{H}_{14}\text{O}_2$: C 80.65, H 5.92; Found C 80.60, H 6.01 %.

4-Ethoxy-4'-methoxytolan (MeO(2))³⁴

Compound MeO(2) was synthesized by a similar procedure as for H(1) using 4-ethynylanisole (0.264 g, 2 mmol), 4-iodo-4'-ethoxybenzene (0.50 g, 2 mmol), $\text{PdCl}_2(\text{PPh}_3)_2$ (0.014 g, 0.02 mmol) and CuI (0.004 g, 0.02 mmol) in Et_3N (50 ml). The mixture was stirred at r.t. overnight and then refluxed at 80 °C for 2 h. After the reaction was complete as evidenced by GC-MS, the amine solvent was removed under reduced pressure. The residue was eluted through a 3 cm silica pad with hexane: CH_2Cl_2 (5:1). Purification by re-crystallisation from hexane gave the product as a white solid. Yield: 0.38 g (76%). m.p. 136.0-140.0 °C. ^1H NMR (500 MHz): δ 7.46 (d, $J_{\text{H-H}} = 9$ Hz, 2H, H_{arom}), 7.42 (d, $J_{\text{H-H}} = 9$ Hz, 2H, H_{arom}), 6.88 (d, $J_{\text{H-H}} = 9$ Hz, 2H, H_{arom}), 6.84 (d, $J_{\text{H-H}} = 9$ Hz, 2H, H_{arom}), 4.05 (q, $J_{\text{H-H}} = 7$ Hz, 2H, CH_2), 3.82 (s, 3H, OCH_3), 1.42 (t, $J_{\text{H-H}} = 7$ Hz, 3H, CH_3). $^{13}\text{C}\{^1\text{H}\}$ NMR (125 MHz): δ 159.4 (C),

158.8 (C), 132.9 (2CH), 115.8 (C), 115.6 (C), 114.5 (CH), 114.0 (CH), 88.0 (C≡C), 87.9 (C≡C), 63.5 (OCH₂), 55.3 (OCH₃), 14.8 (CH₃). MS (EI) *m/z* (rel): 252 (*m*⁺, 29), 223 (76), 209 (100). Anal. Calcd. for C₁₇H₁₆O₂: C 80.93, H 6.39 %. Found C 80.85, H 6.35%.

4-n-Propoxy-4'-methoxytolan (MeO(3))

Compound **MeO(3)** was synthesized by a similar procedure as for **H(1)** using 4-ethynylanisole (0.264 g, 2 mmol), 4-iodo-4'-n-propoxybenzene (0.55 g, 2 mmol), PdCl₂(PPh₃)₂ (0.014 g, 0.02 mmol) and CuI (0.004 g, 0.02 mmol) in Et₃N (50 ml). The mixture was stirred at r.t. overnight and then refluxed at 80 °C for 1 h. The solvent was removed under reduced pressure and the residue was eluted through a 3 cm silica pad with hexane:CH₂Cl₂ (5:1). Purification by re-crystallisation from hexane gave the product as a white solid. Yield: 0.38 g (71%). m.p. 110.0-115.9 °C. ¹H NMR (500 MHz): δ 7.44 (d, *J*_{H-H} = 9 Hz, 2H, H_{arom}), 7.43 (d, *J*_{H-H} = 9 Hz, 2H, H_{arom}), 6.86 (d, *J*_{H-H} = 9 Hz, 2H, H_{arom}), 6.85 (d, *J*_{H-H} = 9 Hz, 2H, H_{arom}), 3.93 (t, *J*_{H-H} = 7 Hz, 2H, OCH₂), 3.82 (s, 3H, OCH₃), 1.81 (m, 2H, CH₂), 1.04 (t, *J*_{H-H} = 7 Hz, 3H, CH₃). ¹³C{¹H} NMR (125 MHz): δ 159.4 (C), 159.0 (C), 132.9 (2CH), 115.8 (C), 115.5 (C), 114.5 (CH), 114.0 (CH), 88.1 (C≡C), 87.8 (C≡C), 69.6 (OCH₂), 55.3 (OCH₃), 22.5 (CH₂), 10.5 (CH₃). MS (EI) *m/z* (rel): 280 (*m*⁺, 100), 224 (95). Anal. Calcd. for C₁₈H₁₈O₂: C 81.17, H 6.81%. Found C 81.18, H 6.80%.

4-n-Butoxy-4'-methoxytolan (MeO(4))³⁵

Compound **MeO(4)** was synthesized by a similar procedure as for **H(1)** using 4-ethynylanisole (0.26 g, 2 mmol), 4-iodo-4'-n-butoxybenzene (0.55 g, 2 mmol), PdCl₂(PPh₃)₂ (0.014 g, 0.02 mmol) and CuI (0.004 g, 0.02 mmol) in Et₃N (50 ml). The mixture was stirred at r.t. overnight and then refluxed at 80 °C for 1 h. The solvent was removed under reduced pressure and the residue was eluted through a 3 cm silica pad with hexane:CH₂Cl₂ (5:1). Purification by re-crystallisation from hexane gave the product as a white solid. Yield: 0.28 g (50%). m.p. 108.4-109.5 °C. ¹H NMR (500 MHz): δ 7.44 (d, *J*_{H-H} = 9 Hz, 2H, H_{arom}), 7.43 (d, *J*_{H-H} = 9 Hz, 2H, H_{arom}), 6.86 (d, *J*_{H-H} = 9 Hz, 2H, H_{arom}), 6.85 (d, *J*_{H-H} = 9 Hz, 2H, H_{arom}), 3.97 (t, *J*_{H-H} = 6 Hz, 2H, OCH₂), 3.82 (s, 3H, OCH₃), 1.77 (m, 2H, CH₂), 1.47 (m, 2H, CH₂), 0.98 (t, *J*_{H-H} = 7 Hz, 3H, CH₃). ¹³C{¹H} NMR (125 MHz): δ 159.4 (C), 159.0 (C), 132.85 (CH),

132.84 (CH), 115.8 (C), 115.5 (C), 114.5 (CH), 114.0 (CH), 88.1 (C≡C), 87.8 (C≡C), 67.8 (OCH₂), 55.3 (OCH₃), 31.3 (CH₂), 19.2 (CH₂), 13.8 (CH₃). MS (EI) *m/z* (rel): 280 (*m*⁺, 100), 224 (95). Anal. Calcd. for C₁₉H₂₀O₂: C 81.40, H 7.19 %. Found C 81.32, H 7.18%.

4-n-Pentoxy-4'-methoxytolan (MeO(5))

Compound **MeO(5)** was synthesized by a similar procedure as for **H(1)** using 4-ethynylanisole (0.264 g, 2 mmol), 1-iodo-4-n-pentoxybenzene (0.580 g, 2 mmol), PdCl₂(PPh₃)₂ (0.07 g, 0.1 mmol) and CuI (0.02 g, 0.1 mmol) in Et₃N (300 ml). The mixture was stirred at r.t. for 1 h and then refluxed at 80 °C for 2.5 h. The solvent was removed under reduced pressure and the residue was re-dissolved in hexane and then filtered through a 5 cm silica pad with additional hexane:CH₂Cl₂ (9:1). Purification by re-crystallisation from hexane gave the product as white solid. Yield: 0.55 g (93 %), m.p. 84.6-89.9°C. ¹H NMR (400 MHz): δ 7.45 (d, *J*_{H-H} = 9 Hz, 2H, H_{arom}), 7.43 (d, *J*_{H-H} = 9 Hz, 2H, H_{arom}), 6.87 (d, *J*_{H-H} = 9 Hz, 2H, H_{arom}), 6.85 (d, *J*_{H-H} = 9 Hz, 2H, H_{arom}), 3.89 (t, *J*_{H-H} = 7 Hz, 2H, OCH₂), 3.76 (s, 3H, OCH₃), 1.72 (m, 2H, CH₂), 1.34 (m, 4H, CH₂), 0.87 (t, *J*_{H-H} = 7 Hz, 3H, CH₃). ¹³C{¹H} NMR (100 MHz): δ 159.4 (C), 159.0 (C), 132.9 (CH), 132.8 (CH), 115.8 (C), 115.5 (C), 114.5 (CH), 114.0 (CH), 88.1 (C≡C), 87.8 (C≡C), 68.1 (OCH₂), 55.3 (OCH₃), 28.9 (CH₂), 28.2 (CH₂), 22.4 (CH₂), 14.0 (CH₃). MS (EI) *m/z* (rel): 294 (*m*⁺, 8), 224 (90), 209 (57), 181 (30), 152 (100). Anal. Calcd. for C₂₀H₂₂O: C 81.60, H 7.53; Found C 81.39, H 7.53 %.

4-n-Hexyloxy-4'-methoxytolan (MeO(6))

Compound **MeO(6)** was synthesized by a similar procedure as for **H(1)** using 4-ethynylanisole (0.26 g, 2 mmol), 1-iodo-4-hexyloxybenzene (0.61 g, 2 mmol), PdCl₂(PPh₃)₂ (0.014 g, 0.02 mmol) and CuI (0.004 g, 0.02 mmol) in Et₃N (50 ml). The mixture was stirred at r.t. overnight and then refluxed at 80 °C for 1 h. The amine solvent was removed under reduced pressure and the residue was eluted through a 3 cm silica pad with hexane:CH₂Cl₂ (5:1). Purification by re-crystallised from hexane gave the product as a white solid. Yield: 0.30 g (49%). m.p. 82.4-99.4 °C. ¹H NMR (400 MHz): δ 7.37 (d, *J*_{H-H} = 9 Hz, 2H, H_{arom}), 7.35 (d, *J*_{H-H} = 9 Hz, 2H, H_{arom}), 6.79 (d, *J*_{H-H} = 9 Hz, 2H, H_{arom}), 6.78 (d, *J*_{H-H} = 9 Hz, 2H, H_{arom}), 3.89 (t, *J*_{H-H} = 7 Hz, 2H,

OCH₂), 3.75 (s, 3H, OCH₃), 1.71 (m, 2H, CH₂), 1.39 (m, 2H, CH₂), 1.27 (m, 4H, CH₂), 0.84 (t, $J_{H-H} = 7$ Hz, 3H, CH₃). ¹³C{¹H} NMR (100 MHz): δ 159.4 (C), 159.0 (C), 132.85 (CH), 132.84 (CH), 115.8 (C), 115.5 (C), 114.5 (CH), 114.0 (CH), 88.1 (C \equiv C), 87.8 (C \equiv C), 68.1 (OCH₂), 55.3 (OCH₃), 31.6 (CH₂), 29.2 (CH₂), 25.7 (CH₂), 22.6 (CH₂), 14.0 (CH₃). MS (EI) m/z (rel): 308 (m^+ , 51), 224 (100), 209 (56). Anal. Calcd. for C₂₁H₂₄O₂: C 81.78, H 7.84 %. Found C 81.79, H 7.61%.

4-n-Heptyloxy-4'-methoxytolan (MeO(7))

Compound **MeO(7)** was synthesized by a similar procedure as for **H(1)** using 4-ethynylanisole (0.264 g, 2 mmol), 1-iodo-4-n-heptoxybenzene (0.636 g, 2 mmol), PdCl₂(PPh₃)₂ (0.07 g, 0.1 mmol) and CuI (0.02 g, 0.1 mmol) in Et₃N (300 ml). The mixture was stirred at r.t. for 1 h and then refluxed at 80 °C for 2.5 h. The solvent was removed under reduced pressure and the residue was re-dissolved in hexane and then filtered through a 5 cm silica pad with additional hexane:CH₂Cl₂ (9:1). Purification by re-crystallisation from hexane gave the product as a white solid. Yield: 0.309 g (48 %), m.p. 84.0-89.8 °C. ¹H NMR (500 MHz): δ 7.44 (d, $J_{H-H} = 9$ Hz, 2H, H_{arom}), 7.42 (d, $J_{H-H} = 9$ Hz, 2H, H_{arom}), 6.86 (d, $J_{H-H} = 9$ Hz, 2H, H_{arom}), 6.85 (d, $J_{H-H} = 9$ Hz, 2H, H_{arom}), 3.96 (t, $J_{H-H} = 7$ Hz, 2H, OCH₂), 3.82 (s, 3H, OCH₃), 1.78 (quint, $J_{H-H} = 7$ Hz, 2H, CH₂), 1.46 (m, 2H, CH₂), 1.33 (m, 6H, CH₂), 0.89 (t, $J_{H-H} = 7$ Hz, 3H, CH₃). ¹³C{¹H} NMR (125 MHz): δ 159.3 (C), 159.0 (C), 132.9 (CH), 132.8 (CH), 115.8 (C), 115.5 (C), 114.5 (CH), 114.0 (CH), 88.1 (C \equiv C), 87.8 (C \equiv C), 68.1 (OCH₂), 55.3 (OCH₃), 31.8 (CH₂), 29.2 (CH₂), 29.0 (CH₂), 26.0 (CH₂), 22.6 (CH₂), 14.1 (CH₃). MS (EI) m/z (rel): 322 (m^+ , 60), 224 (100), 209 (43), 152 (22). Anal. Calcd. for C₂₂H₂₆O₂: C 81.95, H 8.13; Found C 82.04, H 8.08 %

4-n-Octyloxy-4'-methoxytolan (MeO(8))

Compound **MeO(8)** was synthesized by a similar procedure as for **H(1)** using 4-ethynylanisole (0.264 g, 2 mmol), 1-iodo-4-n-octyloxybenzene (0.664 g, 2 mmol), PdCl₂(PPh₃)₂ (0.07 g, 0.1 mmol) and CuI (0.02 g, 0.1 mmol) in Et₃N (300 ml). The mixture was stirred at r.t. for 2 d and then refluxed at 80 °C for 2.5 h. The solvent was removed under reduced pressure and the residue was re-dissolved in hexane and then filtered through a 5 cm silica pad with additional hexane:CH₂Cl₂ (9:1). Purification by re-crystallisation from hexane gave the product as a white solid. Yield:

0.368 g (55 %), m.p. 83.5-93.0 °C. ^1H NMR (500 MHz): δ 7.46 (d, $J_{\text{H-H}} = 9$ Hz, 2H, H_{arom}), 7.44 (d, $J_{\text{H-H}} = 9$ Hz, 2H, H_{arom}), 6.89 (d, $J_{\text{H-H}} = 9$ Hz, 2H, H_{arom}), 6.86 (d, $J_{\text{H-H}} = 9$ Hz, 2H, H_{arom}), 3.97 (t, $J_{\text{H-H}} = 7$ Hz, 2H, OCH_2), 3.84 (s, 3H, OCH_3), 1.80 (quint, $J_{\text{H-H}} = 7$ Hz, 2H, CH_2), 1.46 (m, 2H, CH_2), 1.30 (m, 8H, CH_2), 0.90 (t, $J_{\text{H-H}} = 7$ Hz, 3H, CH_3). $^{13}\text{C}\{^1\text{H}\}$ NMR (125 MHz): δ 159.3 (C), 158.9 (C), 132.8 (CH), 132.79 (CH), 115.7 (C), 115.4 (C), 114.4 (CH), 113.9 (CH), 88.0 ($\text{C}\equiv\text{C}$), 87.9 ($\text{C}\equiv\text{C}$), 68.0 (OCH_2), 55.2 (OCH_3), 31.8 (CH_2), 29.3 (CH_2), 29.2 (CH_2), 29.81 (CH_2), 26.0 (CH_2), 22.6 (CH_2), 14.1 (CH_3). MS (EI) m/z (rel): 336 (m^+ , 59), 224 (100), 209 (41), 152 (21). Anal. Calcd. for $\text{C}_{23}\text{H}_{28}\text{O}_2$: C 82.10, H 8.39; Found C 82.27, H 8.46 %

4-n-Nonyloxy-4'-methoxytolan (MeO(9))²⁸

Compound **MeO(9)** was synthesized by a similar procedure as for **H(1)** using 4-ethynylanisole (0.264 g, 2 mmol), 1-iodo-4-n-nonyloxybenzene (0.692 g, 2 mmol), $\text{PdCl}_2(\text{PPh}_3)_2$ (0.07 g, 0.1 mmol) and CuI (0.02 g, 0.1 mmol) in Et_3N (300 ml). The mixture was stirred at r.t. for 45 min and then refluxed at 80 °C for 2 h. The solvent was removed under reduced pressure and the residue was re-dissolved in hexane and then filtered through a 5 cm silica pad with additional hexane: CH_2Cl_2 (9:1). Purification by re-crystallisation from hexane gave the product as a white solid. Yield: 0.372 g (53 %), m.p. 88.0-90.4 °C. ^1H NMR (500 MHz): δ 7.44 (d, $J_{\text{H-H}} = 9$ Hz, 2H, H_{arom}), 7.43 (d, $J_{\text{H-H}} = 9$ Hz, 2H, H_{arom}), 6.86 (d, $J_{\text{H-H}} = 9$ Hz, 2H, H_{arom}), 6.85 (d, $J_{\text{H-H}} = 9$ Hz, 2H, H_{arom}), 3.96 (t, $J_{\text{H-H}} = 7$ Hz, 2H, OCH_2), 3.82 (s, 3H, OCH_3), 1.78 (quint, $J_{\text{H-H}} = 7$ Hz, 2H, CH_2), 1.45 (m, 2H, CH_2), 1.29 (m, 10H, CH_2), 0.89 (t, $J_{\text{H-H}} = 7$ Hz, 3H, CH_3). $^{13}\text{C}\{^1\text{H}\}$ NMR (125 MHz): δ 159.4 (C), 159.0 (C), 132.9 (CH), 132.8 (CH), 115.8 (C), 115.5 (C), 114.5 (CH), 114.0 (CH), 88.1 ($\text{C}\equiv\text{C}$), 87.8 ($\text{C}\equiv\text{C}$), 68.1 (OCH_2), 55.3 (OCH_3), 31.9 (CH_2), 29.5 (CH_2), 29.4 (CH_2), 29.24 (CH_2), 29.21 (CH_2), 26.0 (CH_2), 22.7 (CH_2), 14.4 (CH_3). MS (EI) m/z (rel): 350 (m^+ , 64), 224 (100), 209 (38), 152 (16). Anal. Calcd. for $\text{C}_{24}\text{H}_{30}\text{O}_2$: C 82.24, H 8.63; Found C 82.27, H 8.70 %.

4-n-Decyloxy-4'-methoxytolan (MeO(10))

Compound **MeO(10)** was synthesized by a similar procedure as for **H(1)** using 4-ethynylanisole (0.264 g, 2 mmol), 1-iodo-4-n-decyloxybenzene (0.721 g, 2 mmol), $\text{PdCl}_2(\text{PPh}_3)_2$ (0.07 g, 0.1 mmol), CuI (0.02 g, 0.1 mmol) in Et_3N (300 ml). The mixture was stirred at r.t. for 45 min and then refluxed at 80 °C for 2 h. The solvent

was removed under reduced pressure and the residue was re-dissolved in hexane and then filtered through a 5 cm silica pad with additional hexane:CH₂Cl₂ (85:15). Purification by re-crystallisation from hexane gave the product as a white solid. Yield: 0.367 g (50 %), m.p. 82.0-89.3 °C. ¹H NMR (500 MHz): δ 7.45 (d, *J*_{H-H} = 9 Hz, 2H, H_{arom}), 7.42 (d, *J*_{H-H} = 9 Hz, 2H, H_{arom}), 6.86 (d, *J*_{H-H} = 9 Hz, 2H, H_{arom}), 6.85 (d, *J*_{H-H} = 9 Hz, 2H, H_{arom}), 3.96 (t, *J*_{H-H} = 7 Hz, 2H, OCH₂), 3.82 (s, 3H, OCH₃), 1.77 (quint, *J*_{H-H} = 7 Hz, 2H, CH₂), 1.45 (m, 2H, CH₂), 1.29 (m, 12H, CH₂), 0.88 (t, *J*_{H-H} = 7 Hz, 3H, CH₃). ¹³C{¹H} NMR (125 MHz): δ 159.4 (C), 159.0 (C), 132.9 (CH), 132.8 (CH), 115.8 (C), 115.5 (C), 114.5 (CH), 114.0 (CH), 88.1 (C≡C), 87.8 (C≡C), 68.1 (OCH₂), 55.3 (OCH₃), 31.9 (CH₂), 29.6 (CH₂), 29.5 (CH₂), 29.4 (CH₂), 29.3 (CH₂), 29.2 (CH₂), 26.0 (CH₂), 22.7 (CH₂), 14.1 (CH₃). MS (EI) *m/z* (rel): 364 (m⁺, 62), 224 (100), 209 (37), 159 (18). Anal. Calcd. for C₂₅H₃₂O₂: C 82.37, H 8.85; Found C 82.29, H 8.93 %

4-n-Dodecyloxy-4'-methoxytolan (MeO(12))

Compound MeO(12) was synthesized by a similar procedure as for H(1) using 4-ethynylanisole (0.26 g, 2 mmol), 4-iodo-4'-n-dedecyloxybenzene (0.78 g, 2 mmol), PdCl₂(PPh₃)₂ (0.014 g, 0.02 mmol) and CuI (0.004 g, 0.02 mmol) in Et₃N (50 ml). The mixture was stirred at r.t. overnight and then refluxed at 80 °C for 1 h. The solvent was removed under reduced pressure and the residue was eluted through a 3 cm silica pad with hexane:CH₂Cl₂ (5:1). Purification by re-crystallisation from hexane gave the product as a white solid. Yield: 0.61 g (78 %). m.p. 89.0-92.8 °C. ¹H NMR (500 MHz): δ 7.44 (d, *J*_{H-H} = 9 Hz, 2H, H_{arom}), 7.42 (d, *J*_{H-H} = 9 Hz, 2H, H_{arom}), 6.86 (d, *J*_{H-H} = 9 Hz, 2H, H_{arom}), 6.85 (d, *J*_{H-H} = 9 Hz, 2H, H_{arom}), 3.96 (t, *J*_{H-H} = 7 Hz, 2H, OCH₂), 3.82 (s, 3H, OCH₃), 1.78 (quint, *J*_{H-H} = 7 Hz, 2H, CH₂), 1.45 (m, 2H, CH₂), 1.30 (m, 16H, CH₂), 0.88 (t, *J*_{H-H} = 7 Hz, 3H, CH₃). ¹³C{¹H} NMR (125 MHz): δ 159.4 (C), 159.0 (C), 132.85 (CH), 132.84 (CH), 115.8 (C), 115.5 (C), 114.5 (CH), 114.0 (CH), 88.1 (C≡C), 87.8 (C≡C), 68.1 (OCH₂), 55.3 (OCH₃), 31.9 (CH₂), 29.66 (CH₂), 29.63 (CH₂), 29.59 (CH₂), 29.57 (CH₂), 29.39 (CH₂), 29.34 (CH₂), 29.2 (CH₂), 26.0 (CH₂), 22.7 (CH₂), 14.1 (CH₃). MS (EI) *m/z* (rel): 392 (m⁺, 79), 224 (100). Anal. Calcd. For C₂₇H₃₆O₂: C 82.61, H 9.24 %. Found C 82.34, H 9.31%.

4-n-Tetradecyloxy-4'-methoxytolan (MeO(14))

Compound **MeO(14)** was synthesized by a similar procedure as for **H(1)** using 4-ethynylanisole (0.26 g, 2 mmol), 1-iodo-4-tetradecoxybenzene (0.83 g, 2 mmol), PdCl₂(PPh₃)₂ (0.014 g, 0.02 mmol) and CuI (0.004 g, 0.02 mmol) in Et₃N (50 ml). The mixture was stirred at r.t. overnight and then refluxed at 80 °C for 1 h. The solvent was removed under reduced pressure and the residue was eluted through a 3 cm silica pad with hexane:CH₂Cl₂ (5:1). Purification by re-crystallised from hexane gave the product as a white solid. Yield: 0.45 g (53%). m.p. 93-97.0 °C. ¹H NMR (500 MHz): δ 7.44 (d, *J*_{H-H} = 9 Hz, 2H, H_{arom}), 7.41 (d, *J*_{H-H} = 9 Hz, 2H, H_{arom}), 6.86 (d, *J*_{H-H} = 9 Hz, 2H, H_{arom}), 6.85 (d, *J*_{H-H} = 9 Hz, 2H, H_{arom}), 3.96 (t, *J*_{H-H} = 7 Hz, 2H, OCH₂), 3.82 (s, 3H, OCH₃), 1.78 (quint, *J*_{H-H} = 7 Hz, 2H, CH₂), 1.45 (m, 2H, CH₂), 1.30 (m, 20H, CH₂), 0.88 (t, *J*_{H-H} = 7 Hz, 3H, CH₃). ¹³C{¹H} NMR (125 MHz): δ 159.4 (C), 159.0 (C), 132.85 (CH), 132.84 (CH), 115.8 (C), 115.5 (C), 114.5 (CH), 114.0 (CH), 88.1 (C≡C), 87.8 (C≡C), 68.1 (OCH₂), 55.3 (OCH₃), 31.9 (CH₂), 29.68 (CH₂), 29.67 (CH₂), 29.65 (CH₂), 29.59 (CH₂), 29.56 (2CH₂), 29.38 (CH₂), 29.35 (CH₂), 29.22 (CH₂), 26.0 (CH₂), 22.7 (CH₂), 14.1 (CH₃). MS (EI) *m/z* (rel): 420 (m⁺, 26), 224 (100), 209 (69). Anal. Calcd. For C₂₉H₄₀O₂: C 82.81, H 9.59 %. Found C 83.07, H 9.67%.

IV.2 X-ray crystallography

Single crystal of compounds **H(1)** - **H(6)**, **H(8)**, **Me(9)**, **MeO(1)** - **MeO(5)**, **MeO(7)**, **MeO(9)** and **MeO(10)** were obtained from the slow evaporation of hexane solutions. Crystals of compound **Me(1)** were obtained from the slow evaporation of a toluene solution and **H(9)** and **Me(12)** were obtained from the slow evaporation of a mixture of ethanol and hexane.

All X-ray diffraction experiments were carried out on SMART 3-circle diffractometers at 120 K. The structures were solved by direct methods, and refined by full matrix least squares on F² of all the data, using SHELXTL software.⁴⁵ All carbon and oxygen atoms were refined anisotropically.

V. References

1. Sheikh-Ali, B. M.; Papta, M.; Jameson, G. B.; Weiss, R. G., *Acta Crystallogr.* **1995**, *B51*, 823.
2. Eidschink, R.; Edman, D.; Krause, J.; Pohl, L., *Angew. Chem. Int. Ed. Engl.* **1977**, *16*, 100.
3. Destrade, D.; Guillon, F.; Gasparoux, H., *Mol. Cryst. Liq. Cryst.* **1976**, *36*, 115.
4. Destrade, D.; Guillon, F.; Gasparoux, H., *Mol. Cryst. Liq. Cryst.* **1977**, *36*, 159.
5. Prasad, J. S., *Liq. Cryst. Ord. Flu.* **1984**, *4*, 673.
6. Prasad, J. S., *Mol. Cryst. Liq. Cryst.* **1978**, *47*, 115.
7. Prasad, J. S., *Acta Cryst.* **1979**, *B35*, 1404.
8. Prasad, J. S.; Rajalakshmi, P. K., *Journal de Physique IV* **1979**, 309.
9. Prasad, J. S., *Mol. Cryst. Liq. Cryst.* **1980**, *60*, 1.
10. Prasad, J. S., *Mol. Cryst. Liq. Cryst.* **1981**, *74*, 215.
11. Neffgen, S.; Kusan, J.; Fay, T.; Keul, H.; Hôcker, H., *Macromol. Chem. Phys.* **2000**, *201*, 2108.
12. Taki, S.; Kai, S., *Jpn. J. Appl. Phys.* **2001**, *40*, 4187.
13. Balaban, A. T.; Klein, D. J.; March, N. H.; Tosi, M. P.; Ausloos, M., *Chem. Phys. Chem.* **2005**, *6*, 1741.
14. Zheng, Y. Q.; Ren, S. P.; Ling, Y. D.; Lu, M. G., *Mol. Cryst. Liq. Cryst.* **2006**, *452*, 3.
15. Skelton, G. W.; Dong, D.; Tuffin, R. P.; Kelly, S. M., *J. Mater. Chem.* **2003**, *13*, 450.
16. Roscoe, K. Forth year report: Conjugated Rigid-Rods as Multifunctional Materials and Studies of Weak Intermolecular Interactions. Durham University, Durham, M. Sc. (Chemistry) 1999.
17. Green, M. D. Forth year report: Transition Metal Catalysts for Organic Reactions. Durham University, Durham, M. Sc. (Chemistry) 2005.
18. Hargis, J. H.; Alley, W. D., *J. Chem. Soc., Chem. Commun.* **1975**, 612.
19. Martin, S.; Sauvêtre, R.; Normant, J.-F., *Tetrahedron Lett.* **1982**, *23*, 4329.
20. Kakusawa, N.; Kurita, J., *Chem. Pharm. Bull.* **2005**, *53*, 1369.
21. Tachimori, H.; Masuda, T.; Kouzai, H.; Higashimura, *Polym. Bull.* **1994**, *32*, 133.
22. Wan, Z.; Jones, C. D.; Mitchell, D.; Pu, J. Y.; Zhang, T. Y., *J. Org. Chem.* **2006**, *71*, 826.
23. Faller, J. W.; Kultyshev, R. G., *Organometallics* **2002**, *21*, 5911.
24. Tasros, W.; Sakla, A. B.; Moheb, S., *J. Chem. Soc.* **1958**, 4210.
25. Gauza, S.; Wen, C.-H.; Tan, B.; Wu, S.-T., *Jpn. J. Appl. Phys.* **2004**, *43*, 7176.
26. Malthête, J.; Canceill, J.; Gabard, J.; Jacques, J., *Tetrahedron* **1981**, *37*, 2815.
27. Malthête, J.; Leclercq, M.; Gabard, J.; Billard, J.; Jacques, J., *Sciences Chimiques* **1971**, *273*, 265.
28. Malthête, J.; Leclercq, M.; Dvolaitzky, M.; Gabard, J.; Billard, J.; Pontikis, V.; Jacques, J., *Mol. Cryst. Liq. Cryst.* **1973**, *23*, 233.
29. Malthête, J.; Billard, J.; Canceill, J.; Gabard, J.; Jacques, J., *Journal de Physique, Colloque* **1976**, *3*, 1.
30. Liebert, L.; Daniels, W. B.; Billard, J., *Mol. Cryst. Liq. Cryst.* **1977**, *41*, 57.
31. Pugh, C.; Percec, V., **1990**, *31*, 512.

32. Krone-Schmidt, W.; Sieber, W. J.; Boag, N. M.; Knobler, C. B.; Kaesz, H. D., *J. Organomet. Chem.* **1990**, *394*, 433.
33. Wan, S.; Wang, R. S.; Lu, W., *J. Org. Chem.* **2006**, *7*, 4349.
34. Tadros, W.; Alfy, B.; Ishak, M. S., *J. Chem. Soc.* **1958**, 4210.
35. Miyazowa, K.; Koga, K.; Matsui, S.; Hachiya, N.; Nakagawa, E., *PCT Int. Appl.* **1988**, p. 98
36. Allen, F. H.; Kennard, O.; Watson, D. G.; Brammer, L.; Orpen, A. G.; Taylor, R., *J. Chem. Soc., Perkin Trans.* **1987**, *2*, Supplement p.1.
37. Abramenkov, A. V.; Almenningen, A.; Cyvin, B. N.; Cyvin, S. J.; Jonvik, T.; Khaikin, L. L. S.; Romming, C.; Vilkov, L. V., *Acta Chem. Scand. Ser. A* **1988**, *42*, 674.
38. Zanin, I. E.; Antipin, M. Y.; Struchkov, Y. T., *Kristallografiya* **1991**, *36*, 411.
39. Thomas, R.; Lakshmi, S.; Pati, S. K.; Kulkarni, G. U., *J. Phys. Chem. B* **2006**, *110*, 24674.
40. Okuyama, K.; Hasegawa, T.; Ito, T.; Mikami, N., *J. Phys. Chem. B* **1984**, *88*, 1711.
41. Cotrait, M.; Destrade, C.; Gasparoux, H., *Mol. Cryst. Liq. Cryst.* **1977**, *39*, 159.
42. Heck, R. F., *Palladium reagents in organic syntheses*, London, 1990; p 461.
43. Takahashi, S.; Kurayama, K.; Sonogashira, K.; Hagihara, H., *Synthesis* **1980**, 627.
44. Williamson, A., *Justus Liebigs Ann. Chem.* **1851**, *77*, 37.
45. SHELXTL; ver. 6.12, B. A., Madison, Wisconsin, USA, 2001.

Part II

Palladium-Complexes of Thioureas and Phosphine Sulfides

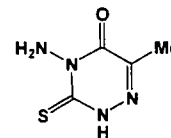
Chapter 3

**Monodentate Thioureas and Their
Palladium Complexes**

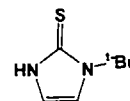
Abbreviations

Ac Acetyl

Anth Anthracene

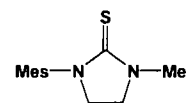
AMTTO 4-Amino-6-methyl-1,2,4-triazine-3(2*H*)-thione-5-one

Ar Aryl

Bimt 1-^tButyl-1*H*-imidazole-2(3*H*)-thione^tBu *tert*-Butyl

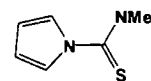
DMF Dimethylformamide

DMT N,N'-Dimesitylimidazolidine-2-thione



Et Ethyl

Hnpt N,N'-Dimethyl pyrole-1-carbothioamide



Me Methyl

NEt₃ Triethylamine

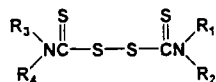
Ph Phenyl

ⁱPr *iso*-Propyl

tu Thiourea

tmtu Tetramethyl thiourea

thiourea disulfides



TFAA Trifluoroacetic anhydride

I. Literature Review

I.1 Introduction

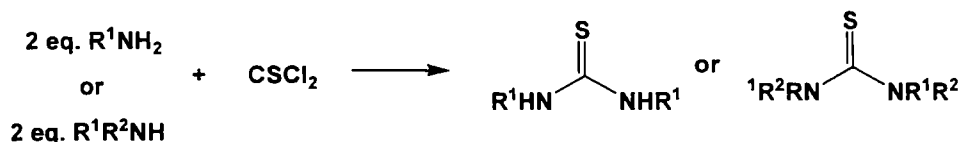
Thioureas are important in medicinal chemistry¹ due to their biological activities,²⁻⁴ for example, against bacteria and microbial infection,⁵ and as fungicides, herbicides and rodenticides.^{6, 7} Thioureas are air and moisture stable, furthermore, their physical and chemical properties can be changed by modifying their nitrogen substituents.⁸⁻¹⁰ They also can coordinate to metals, and nearly 4000 examples of such complexes are found in the CSD (2007).¹¹ Due to their air and moisture stability, they were found to be of use in oxidative reactions including those employing O₂ as an oxidant *viz.* alkene bis(methoxycarbonylation),^{12, 13} and in Suzuki-Miyaura reactions under aerobic conditions.¹⁴⁻¹⁶ Thioureas has been used as ligands in metal catalyzed reactions such as in Pd-catalyzed in Heck-Mizoroki^{15, 17-19} Suzuki-Miyaura carbonylations¹⁹ and Pauson-Khand reactions.²⁰ Recently, rhodium complexes of thioureas proved to be better catalysts in the hydroformylation of 1-hexene than carbene ligands.²¹ Free NH-thioureas display hydrogen-bonding, and for this reason they are used in organocatalysis²²⁻²⁵ and sensor applications.²⁶⁻²⁹

To the best of our knowledge, there is no review concerning the investigation of the coordination properties of thioureas. This review will concentrate on the coordination of thioureas to Pd. Although examples of coordination to other metals are known, these will not be discussed here. The structural parameters from X-ray crystallographic studies of a large number of palladium thiourea complexes will be reported in order to understand the bonding properties of thiourea ligands. The synthesis of thioureas, thiourea palladium complexes and the applications in the Pd-catalyzed reactions will also be discussed.

I.2 Thiourea ligands

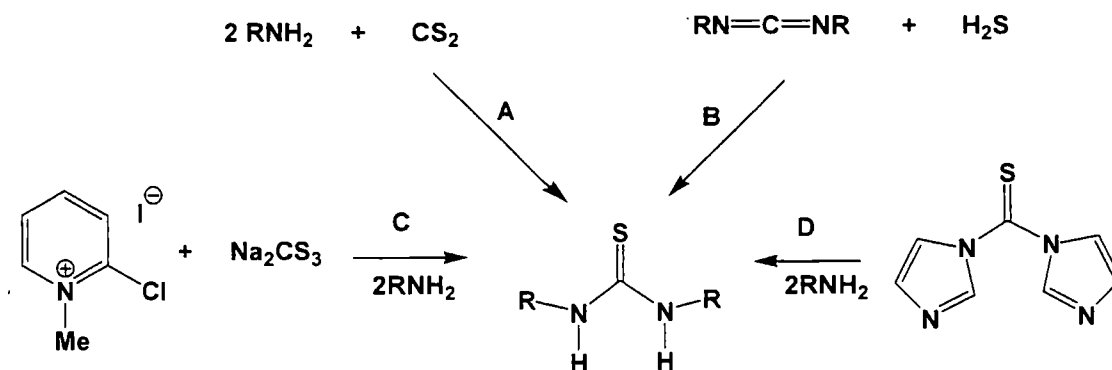
I.2.1 Synthesis of thioureas

Thioureas can be divided into two categories; symmetric and unsymmetric thioureas. Symmetric thioureas can be synthesized by reaction of two equivalents of a primary or secondary amine with thiophosgene (Scheme 1).^{30, 31}



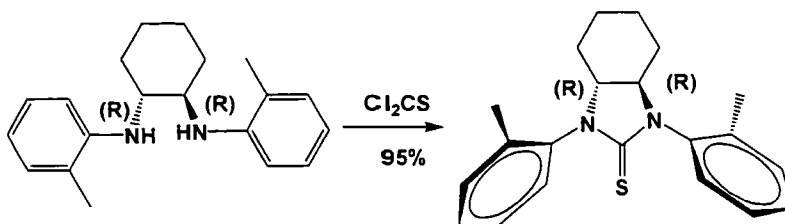
Scheme 1. Synthesis of symmetric thioureas from amine and thiophosgene.¹²

However, toxic thiophosgene can be avoided (Scheme 2) by using CS₂ (route A),^{32, 33} carbodiimides (route B), sodium trithiocarbonate (route C),³⁴ or thiocarbonyldiimidazole (route D).³⁰ It is reported that heterogeneous catalysis using a ZnO/Al₂O₃ composite in the reaction of carbon disulfide and anilines is another route to prepare thioureas³⁵ and isocyanates or thiocyanates.³⁶⁻⁴⁰



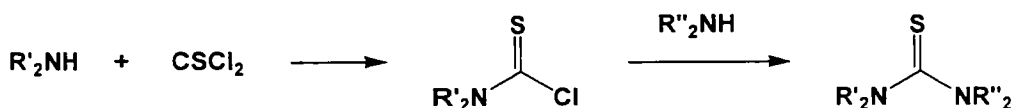
Scheme 2. Preparation of symmetrical thioureas.⁴¹

Recently, an optically-active thiourea was synthesized from a homo-chiral secondary amine with thiophosgene by Z. Yang and co-workers (Scheme 3).¹⁷

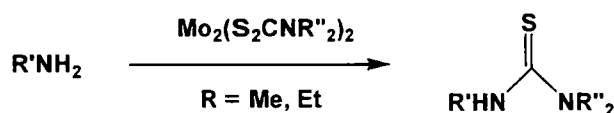


Scheme 3. Synthesis of chiral thiourea.¹⁷

Unsymmetric thioureas can be obtained by controlling ratio of the amine. The reaction of symmetric thioureas with one equivalent of amine can afford unsymmetric thioureas (Scheme 4).^{41, 42} Other starting materials have been also reported in the synthesis of unsymmetric thioureas; *viz.*, nitrosothiourea,⁴³ dithiocarbamate,^{44, 45} thiourea,⁴⁶ 1-(methyldithiocarbonyl)imidazole⁴⁷ and thiuram disulfide.⁴⁸ Molybdenum dithiocarbamate complexes can be reacted with amines (Scheme 5) to give quantitatively unsymmetrical thioureas.^{49, 50}

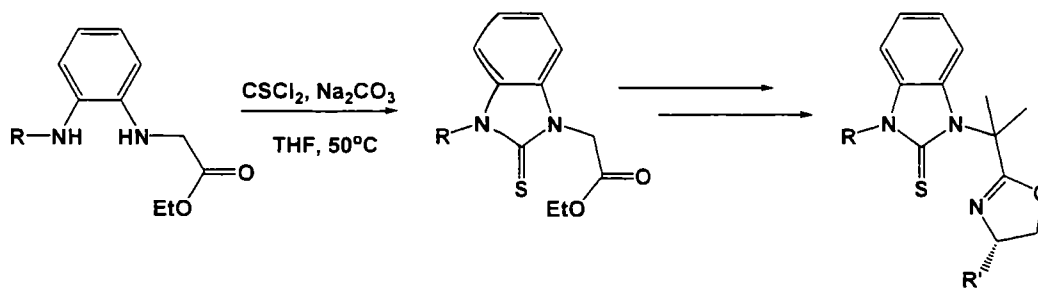


Scheme 4. Synthesis of an unsymmetric thiourea from amines.



Scheme 5. Synthesis of an unsymmetric thiourea from the reaction of molybdenum dithiocarbamate with amines.^{49, 50}

Recently, Z. Yang and co-workers showed that an unsymmetrical ortho phenylene diamine reacted with thiophosgene to obtain an unsymmetric cyclic thiourea which can be further converted to a new class of chiral thiourea-oxazoline S₂N heterobidentate ligands (Scheme 6).¹³ These ligands have shown potential in the asymmetric bis(methoxycarbonylation) reactions of styrenes.



Scheme 6. The preparation of chiral thiourea-oxazoline S,N heterobidentate ligands.¹³

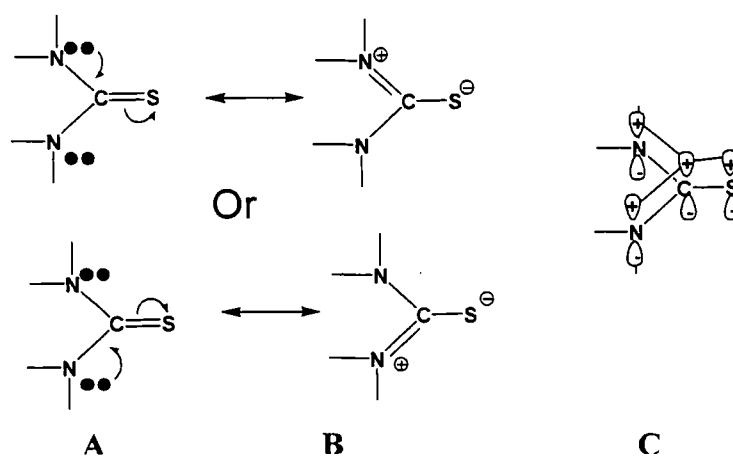
1.2.2 Properties and DFT calculations of thiourea

Before understanding the coordination of thiourea palladium complexes, it is useful to discuss the properties of the thiourea free ligand. The C=S, C–N bond lengths and S–C–N bond angles of representative thioureas: tu, tmtu and tetrahydropyrimidine-2(1*H*)-thione are given in Table 1.

Table 1. Bond lengths and angles in free thiourea ligands.

Compounds	S=C (Å)	C–N (Å)	S–C–N (°)	Ref
	1.720(9)	1.340(6)	120.5(5)	51
	1.6876(15)	1.3613(11)	122.32(6)	52
	1.722(7)	1.334(6)	119.8(4)	53

The thiourea structures suggest mainly sp^2 hybridization for the C atom in the C=S bond. The C=S bond lengths are 1.68 – 1.72 Å, longer than a standard C=S double bond (1.60 Å) but shorter than a C–S single bond (1.82 Å). This can be explained by delocalization of the C=S bond over the adjacent N atoms (A and B Scheme 7); the C–N bond lengths are about 1.33 – 1.36 Å, which are shorter than a normal C–N bond (1.47 Å).⁵⁴ A simple model of the π -bonding in thioureas is shown in C.



Scheme 7. Delocalization of the C=S bond (A) and (B) and a model of the π -system in thioureas (C).

The molecular orbital diagram for tu shown in Figure 1 is based on DFT M.O. calculations carried out by Yu *et al.*⁵⁵ The HOMO is the in-plane nonbonding lone pair on the S atom (n_2) and the LUMO is the C=S (and C-N) π anti-bonding (π_4) orbital. HOMO-1 (π_3) is C=S π bonding. The remaining S-lone pair (n_1) is sp-hybridized and lies well below the frontier orbitals.

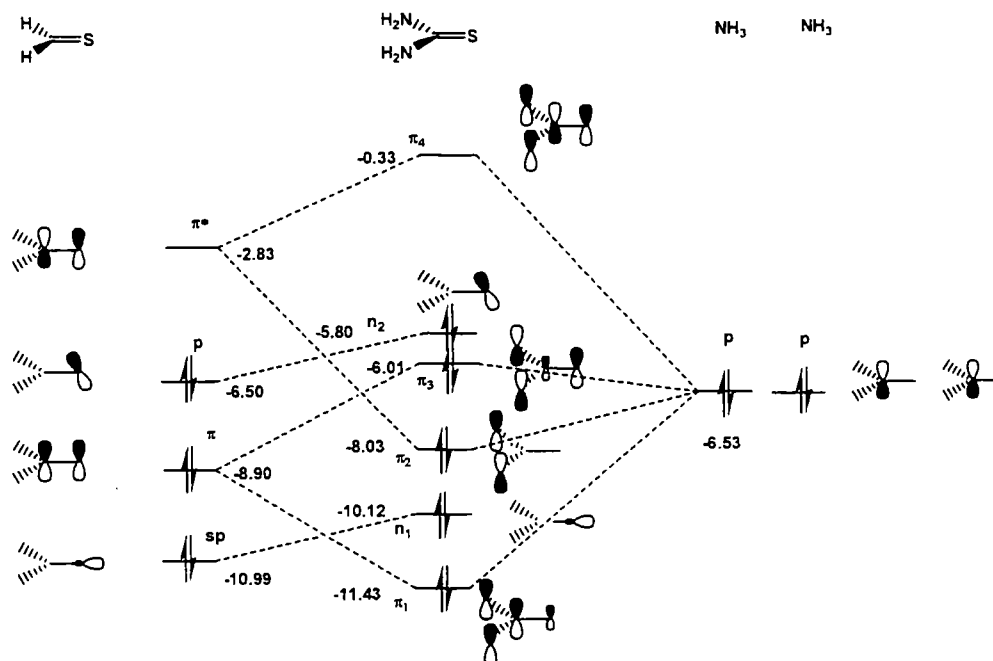
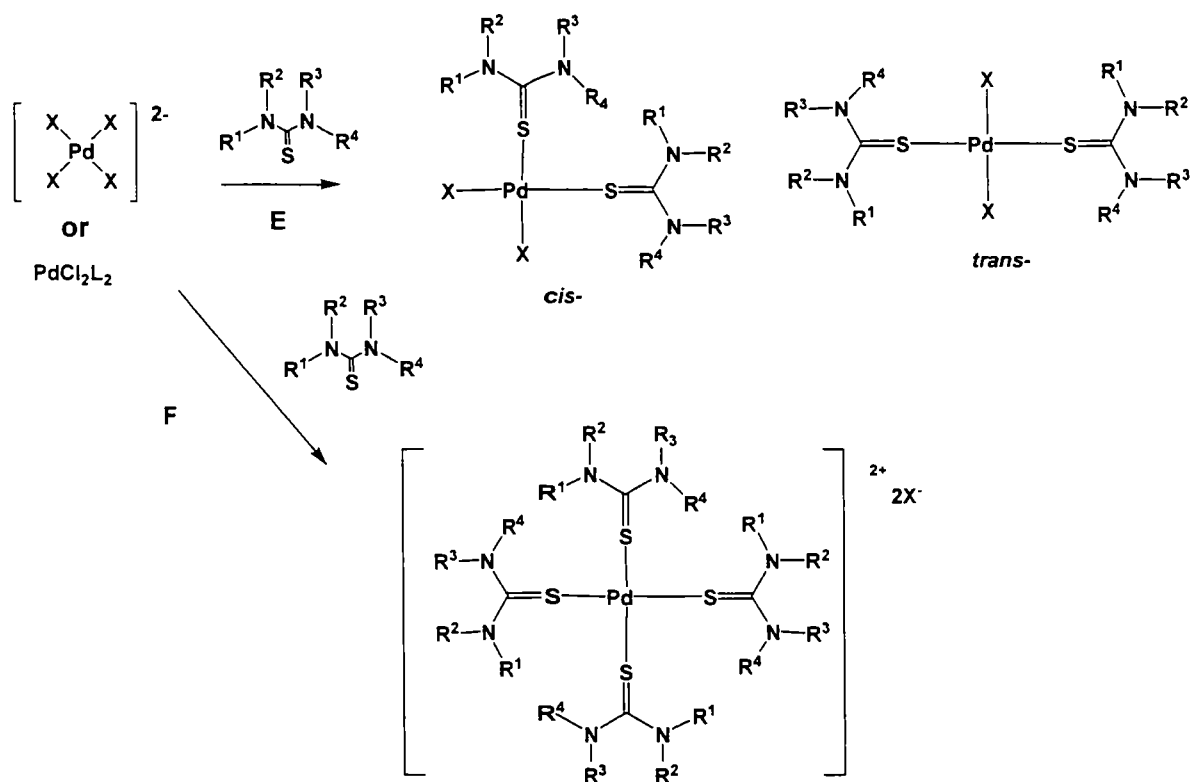


Figure 1. Molecular orbital diagram for tu (energies in eV).⁵⁵

From the molecular orbital diagram, thioureas can use the in-plane nonbonding lone pair on the S atom (n_2) and the π bonding orbital (π_3) to coordinate to metals. The remaining S- lone pair (n_1) is too low in energy to be used in coordination. If the lone pair on the S atom was used to form a ligand metal bond, a tetrahedral geometry around the S atom should be expected. However, if the π electrons was used for bonding, a lengthening of the C=S bond with the subsequent shortening of the C-N bonds should be observed. This observation is very important and will be discussed in relation to their palladium complexes.

I.2 Synthesis of thiourea palladium complexes

Most of the palladium complexes containing thioureas and their derivatives were prepared by using ligand substitution processes, which are summarized in Schemes 8 and 9. The reactions of palladium chlorides (*e.g.* PdCl_2 , $\text{PdCl}_2(\text{PhCN})_2$, Li_2PdCl_4 *etc.*) with thioureas are described in Scheme 8. In route **E**, addition of two equivalents of thiourea affords the *cis*- and/or *trans*- PdX_2L_2 complexes. There is a general preference for the *trans*- isomer. The mixture of isomers are normally distinguishable by solution NMR or melting point analysis and, in some cases, they can be separated by fractional crystallization.^{56, 57} However, D. Yang *et al.* have reported *cis*- and *trans*- $\text{PdCl}_2(\text{DMT})_2$ (Figure 2) which co-crystallized in the same unit cell.¹⁸ When the reactions employ four equivalents of a thiourea ligand, the ionic palladium(II)-tetrakis(thiourea) complexes are formed with halides as counter anions as shown in route **F**.⁵⁸⁻⁶⁰



Scheme 8. Preparation of palladium-monodentate thiourea complexes.

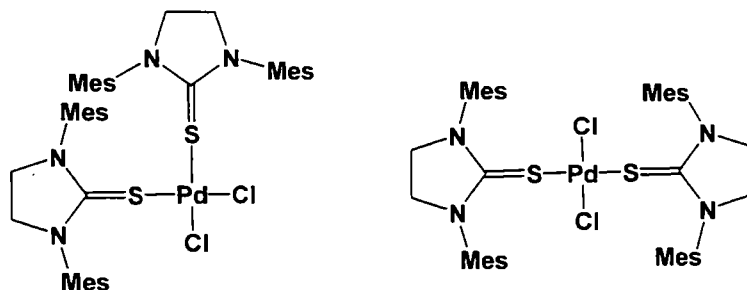
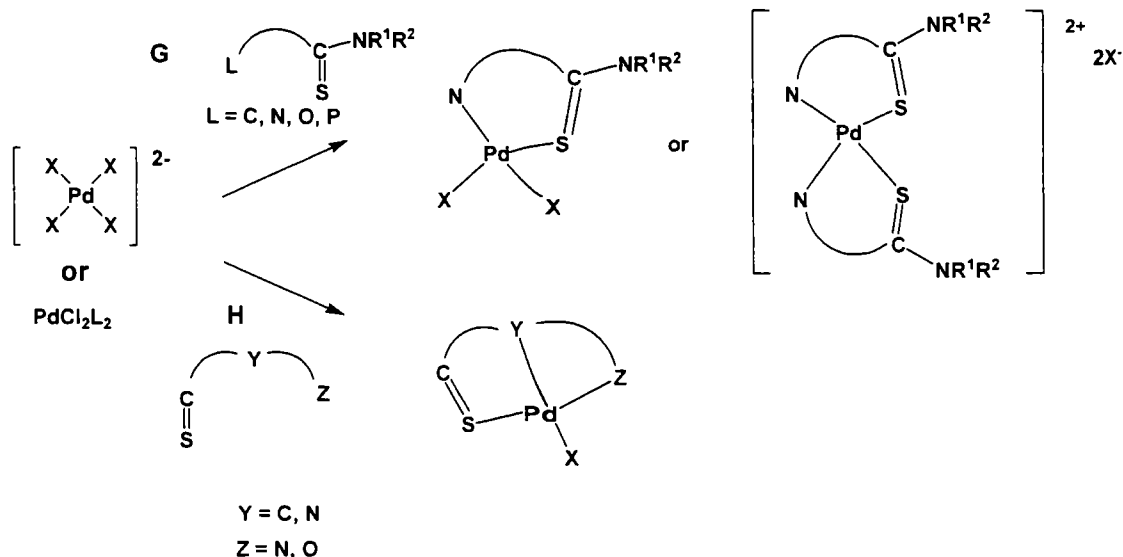
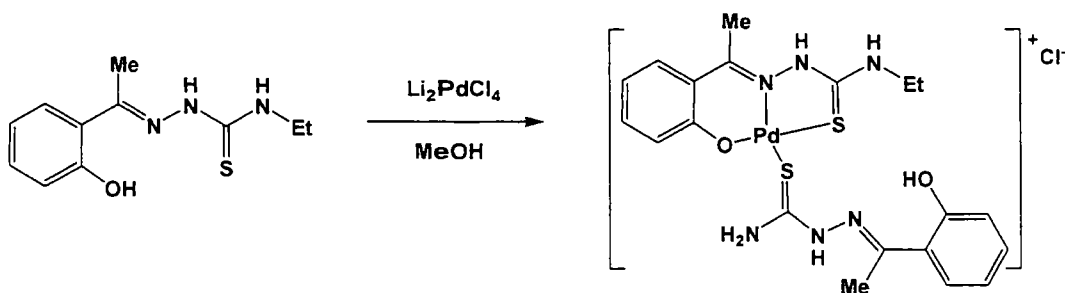


Figure 2. *Cis-* and *trans-* isomers $PdCl_2(DMT)_2$.¹⁸

Furthermore, palladium complexes with bidentate and tridentate thiourea ligands can be prepared as described in routes **G** and **H** (Scheme 9). The ring size of the bidentate products varies from very strained four-membered rings,⁶¹ five-,^{16, 62-70} six-,^{45, 71-73} seven-⁷⁴ to macrocyclic nine-membered rings.⁷⁵ Tridentate ligands gave [5,5]^{70, 76, 77} or [5,6]^{14, 78} bicyclic products. An example of the preparation of a [5,6] bicyclic product is described in Scheme 10.⁷⁸

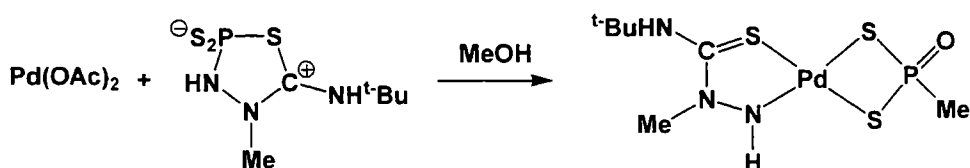


Scheme 9. Preparation of chelated palladium thiourea complexes.



Scheme 10. The preparation of a [5,6] bicyclic palladium thiourea complex.⁷⁸

An unexpected bidentate palladium–thiourea complex was obtained by the decomposition of a cyclic thiourea (Scheme 11)⁶³ with methanol and then subsequent reaction with palladium diacetate.



Scheme 11. The reaction of palladium acetate with thiosemicarbazide derivatives.⁶³

Mitra and co-workers reported that the reaction of 4-amino-6-methyl-1,2,4-triazine-3(2*H*)-thione-5-one (AMTTO) with a palladium(II) source leads to the mono-

palladium, $[\text{Pd}(\eta^2\text{-AMTTO-N,S})\text{Cl}_2]\cdot\text{CH}_3\text{OH}$,⁶² di-palladium, $[(\text{AMTTO})\text{PdBr}_2]_2\cdot 3.5\text{THF}$ ⁶⁶ and tri-palladium $[(\text{AMTTO})\text{PdX}_2]_3\cdot 8\text{CH}_3\text{OH}$ ⁶⁹ ($\text{X} = \text{Cl}$ (Figure 3) and $\text{X} = \text{Br}$) N,S coordinated complexes, which have been characterized by single crystal X-ray diffraction.

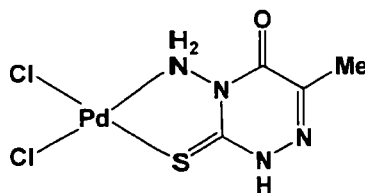


Figure 3. The structure of $[\text{Pd}(\eta^2\text{-AMTTO-N,S})\text{Cl}_2]$.⁶²

Interestingly, S,O N-benzoyl-N'-propylthiourea ligands have been found to coordinate to Pd(II) only through the sulfur atom. This can be explained by the fact that the carbonyl oxygen atoms are effectively blocked by an intramolecular hydrogen bond with NH to form *cis*-bis(N-benzoyl-N'-propylthiourea)dichloropalladium(II) (Figure 4).⁷⁹ In contrast, for the analogous PdBr₂ complex, in CDCl₃ solution, the *trans*- isomer predominates with an equilibrium constant $K = 2.33$ at 25 °C.⁷⁹

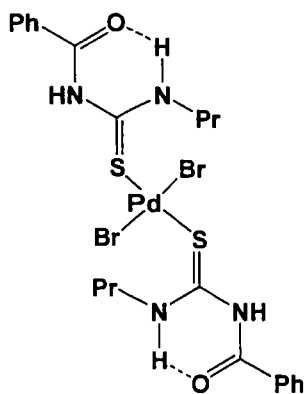
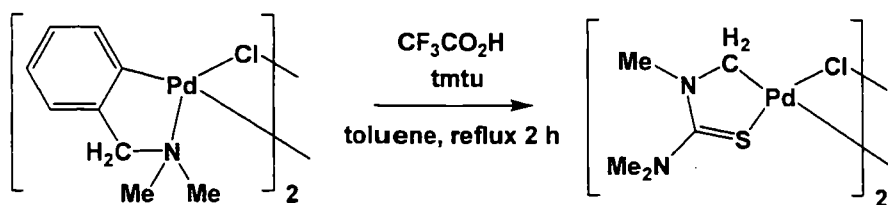


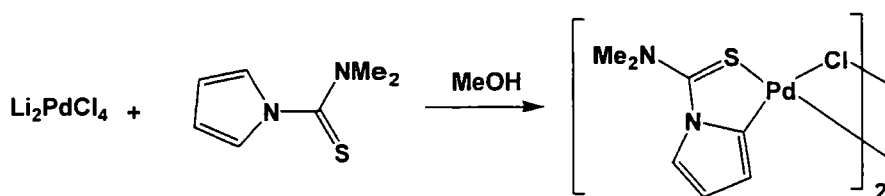
Figure 4. *Trans*-bis(N-benzoyl-N'-propylthiourea)dibromo palladium(II).⁷⁹

Cyclometallated palladium-thiourea complexes are also known in the literature. Treatment of a palladacycle complex (Scheme 12)⁸⁰ with tmtu and CF₃CO₂H in refluxing toluene gave a dimeric carba-palladacycle in high yield.



Scheme 12. Tmtu ligand exchange to afford a cyclometallated palladium thiourea complex.⁸⁰

Another example of cyclometallated thiourea palladium complex, ortho-cyclometalated *N,N*-dimethyl pyrrole-1-carbothioamide (Hnpt) (Scheme 13),⁶⁵ was formed in the reaction of Hnpt with Li_2PdCl_4 in methanol. Furthermore, the cyclometallated palladium complex of Hnpt, $\text{PdX}(\text{npt})(\text{tbp})$ (tbp = tri-butylphosphine, X = Cl, I), was found to exist as both a *cis*- and a *trans*-isomer in solution (Figure 5). The *cis/trans* ratio is 44:56 (X = Cl), or 60:40 (X = I). Both isomers were successfully characterized by single-crystal X-ray diffraction.



Scheme 13. Synthesis of an ortho-cyclometalated *N,N*-dimethyl pyrrole-1-carbothioamide complex.⁶⁵

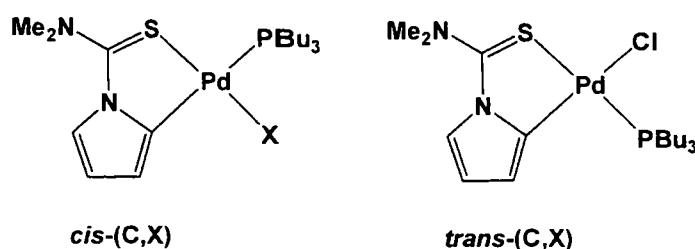
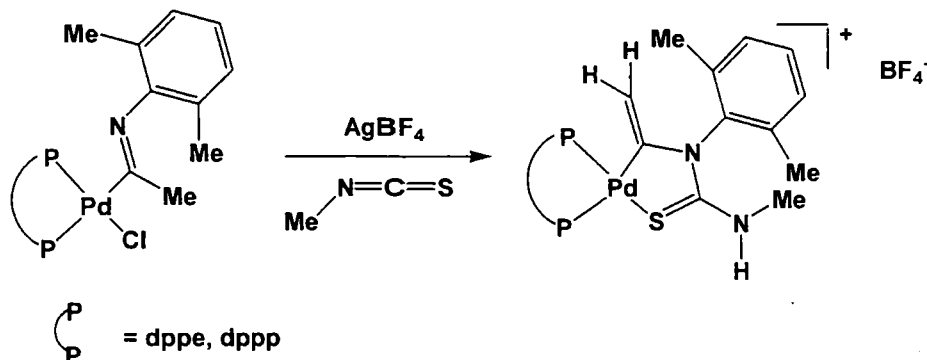


Figure 5. *Cis*- and *trans*-isomers of $\text{PdX}(\text{npt})(\text{tbp})$.⁶⁵

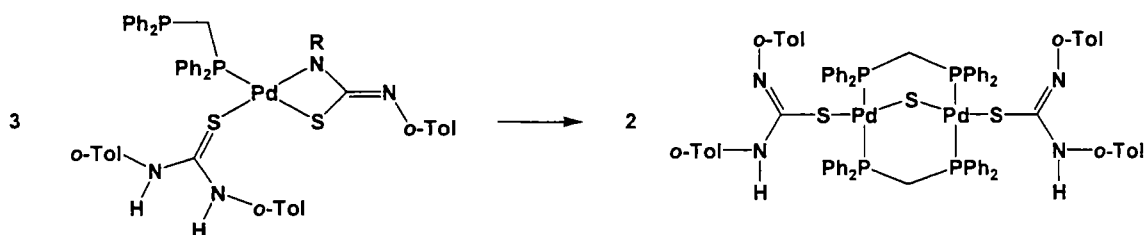
Owen *et al.* have shown (Scheme 14) the reaction of cyclometallated palladium complexes with methyl isothiocyanate to give the rearranged thiourea palladium product. The authors suggested that the reaction proceeds *via* attack by the nitrogen of the iminoacyl on the carbon of the isothiocyanate moiety followed by a

1,5 proton migration from the imino methyl group to the nitrogen of the isothiocyanate to afford cyclometallated palladium–thiourea complexes.⁶⁴



Scheme 14. Synthesis of cyclometallated palladium–thiourea complexes from iminoacyl palladium complexes.⁶⁴

A Pd(II)–thiourea complex (Scheme 15), which is unstable, can undergo a rearrangement to give a dinuclear Pd(II) complex with a sulfide-bridge. However, the mechanism of the reaction was not reported.⁸¹



Scheme 15. Rearrangements of a thiourea palladium complex.⁸¹

I.3 Solid state studies of thiourea palladium complexes

As mentioned previously, thiourea structures suggest mainly sp^2 hybridization which can be explained by delocalization of the C=S bond over the adjacent N atoms (Scheme 7). The influence of the nitrogen in thioureas also affects the Pd–S bond length in the complexes. This can be observed in the three analogous compounds: thiocarbonyl, thioamide and thiourea, shown in Figure 6. Interestingly, the thiourea shows similar Pd–S bond lengths to the thioamide; however, the thiocarbonyl shows significantly longer Pd–S bonds (Figure 6). This indicates that the nitrogen atoms have affected the strength of the Pd–S bond in thiocarbonyls.

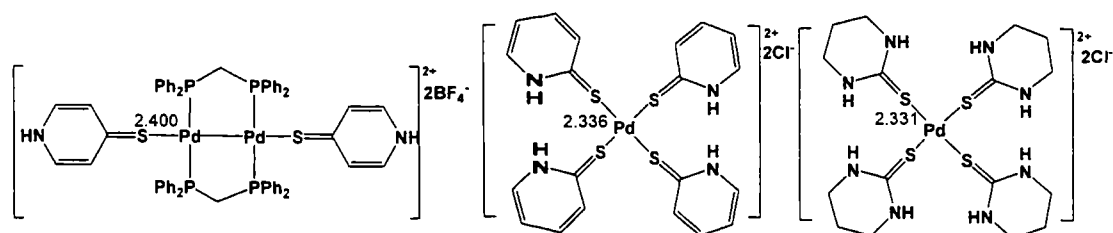


Figure 6. The influence of nitrogen atoms in thiocarbonyl (left),⁸² thioamide (middle)⁸³ and thiourea (right)⁸⁴ on Pd-S bond lengths.

The *trans*-influence of thioureas is stronger than ureas, for example, in palladium-immidoyl complexes (Figure 7). The thiocarbonyl demonstrated a stronger *trans*- influence than the carbonyl as the Pd-P1 bond lengths are markedly longer (2.2807(16) or 2.2908(16) Å in the thiourea complexes) than in the urea complex (2.2266(14) Å). Furthermore, within the thiourea moiety, the C1-N2 bond distance in the thiourea is slightly shorter than that in the urea.⁶⁴ This is consistent with the S atom in thiourea being a better donor to Pd than the O atom of urea.

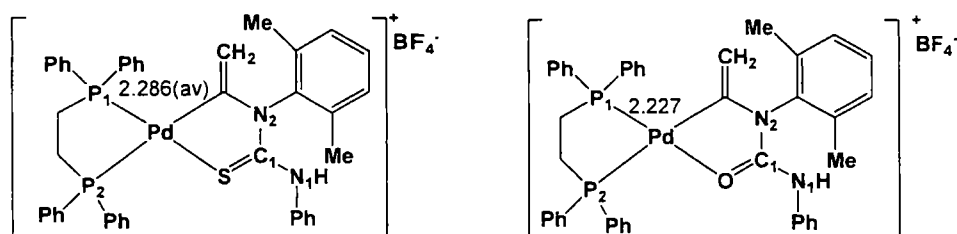


Figure 7. Palladium imidoyl derivatives; thiourea (left) and thiocarbonyl (right).⁶⁴

In order to understand the bonding of thioureas with palladium, the inspection of the Pd-S and C=S bond lengths, Pd-S-C bond angles and Pd-S-C-N torsion angles will be investigated. The Pd-S bond lengths will reveal the strength of the Pd-S bond compared to the sum of the covalent radii (2.37 Å).⁸⁵ The C=S bond lengths and the Pd-S-C bond angles can give information on the types of orbitals used in coordination. The Pd-S-C-N torsion angles can be used to explain which orbital is used for bonding to Pd, *i.e.*, the nonbonding lone pair on the S atom or the π electrons. The Pd-S-C-N torsion angles should be zero or almost planar if bonding is

due to the in-plane nonbonding lone pair, whereas it should be almost 90° in the case of the π electrons.

With this information in mind, a comparison of the X-ray crystallographic studies of palladium thiourea complexes reported in CSD (2007)¹¹ is investigated. The Pd–S and C=S bond lengths, Pd–S–C bond angles and Pd–S–C–N torsion angles are listed in Table 2 at the end of this review.

From Table 2, we can make the following observations with the exception of some complexes which will be discussed later:

1. The palladium(II) thiourea complexes show square planar geometries and the Pd–S bond lengths in thiourea complexes are in the range 2.21 – 2.36 Å, which are shorter than the sum of the covalent radii (2.37 Å).⁸⁵
2. All of the thiourea complexes show longer C=S bonds than found in free thioureas. This indicates a decreased C=S double bond character upon coordination to palladium. This is accompanied by a shortening of the C–N bond lengths in the complexes compared with those in the free ligands by at least 0.07 Å. This suggests that the electrons in the π orbital are used to form the coordination bond.
3. Most of the Pd–S–C bond angles are in the range $100\text{--}110^\circ$; however, the angle in a strained, four-membered ring thiouracil-di-palladium(II) complex was found to be 79° (Figure 8).⁶¹ The angles in seven-membered ring complexes have been reported to be $116\text{--}118^\circ$.⁷⁴ This suggests that the geometries of the S atoms are flexible.

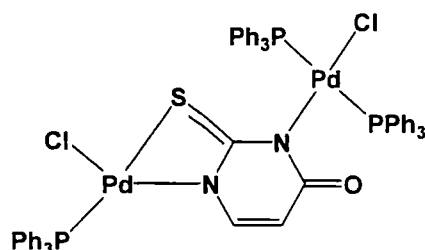


Figure 8. The structure of four-membered ring thiouracil-di-palladium(II) complex.

4. The dihedral angles, Pd–S–C–N range from $0\text{--}92.30^\circ$ with no obvious correlation with the structure of the thiourea ligands. For example, dihedral angles in sterically hindered *trans*-PdCl₂(DMT)₂¹⁸ are 19.82, 20.95, -16.10 and -19.82° whereas in the less hindered thiourea palladium complex *trans*-PdCl₂(tmtu)₂, the angles are 58

and -58° .⁵² In another example, the dihedral angles in the sterically hindered $[\text{Pd}(\text{Bimt})_4]\text{Cl}_2$ (Figure 11, *vide infra*)⁸⁶ are 59, -59 , 0.1 and -0.1° whereas in $[\text{Pd}(\text{tu})_4]\text{Cl}_2$, they are in the range of $15 - 30^\circ$ (see Table 2). Due to the hydrogen-bonding in thioureas which makes them of use in organocatalysis,²²⁻²⁵ it is possible that hydrogen bonding in the crystal packing in the solid state of the complexes may play a role in the variation of Pd–S–C–N dihedral angles.

5. Some of the known thiourea palladium complexes show polymorphism. For example, $\text{Pd}(\text{tu})_4\text{Cl}_2$ was shown to crystallize in both monoclinic⁸⁷ and orthorhombic^{88, 89} space groups which may be related to hydrogen bonding in thioureas.

As mentioned above, the C–N bonds in the complexes are shorter than in the free ligand; however, one C–N bond in $[\text{Pd}(\text{tu})_4]\text{Cl}_2$ ⁸⁷ is remarkably longer; 1.482 Å (Figure 9), compared to the other three bonds, 1.31 – 1.37 Å, suggesting a single bond character.

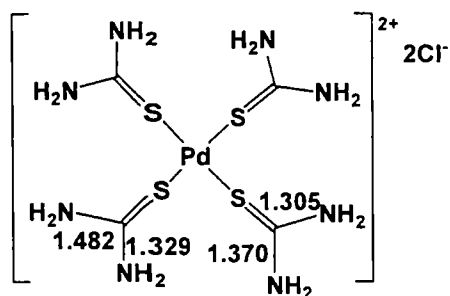


Figure 9. $[\text{Pd}(\text{tu})_4]\text{Cl}_2$.⁸⁷

The Pd–S–C angles in thiourea palladium complexes are in the range $79 - 118^\circ$ (values include the smallest and largest Pd–S–C angles). However, in the palladium complex of salicylidene thiosemicarbazone (Figure 10), where one ligand behaves as η^1 and the other as η^3 to palladium, significantly different Pd–S and C=S bond lengths and also Pd–S–C angles are observed as indicated in Figure 10. Furthermore, the Pd–S–C angles are likely to depend on the steric bulk of the ligand.⁸⁶ This was observed in $\text{PdCl}_2(\text{Bimt})_2$, where the angles are 95.70° and 102.76° (Figure 11). The Pd–S–C angles can also be changed by substitution of the other ligands as was found in palladium complexes of AMTTO, as the angle was reported to be wider when one Br was replaced by PPh_3 (Figure 12).⁶⁶ The rigidity of the

molecules may affect the Pd–S–C angle, for example, in the rigid palladium complex of pyridine-morpholine carbothiamide where the Pd–S–C angle of 92.97° (Figure 13)⁴⁵ is significantly smaller than in other six-membered rings ($100 - 110^\circ$).

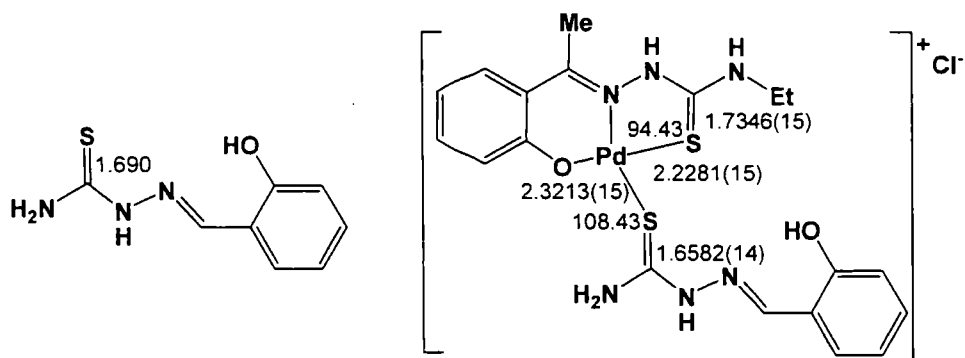


Figure 10. Salicylidene thiosemicarbazone and its palladium complex.

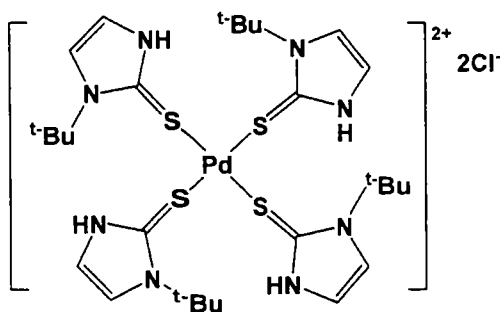


Figure 11. $\text{PdCl}_2(\text{Bimt})_2$.⁸⁶

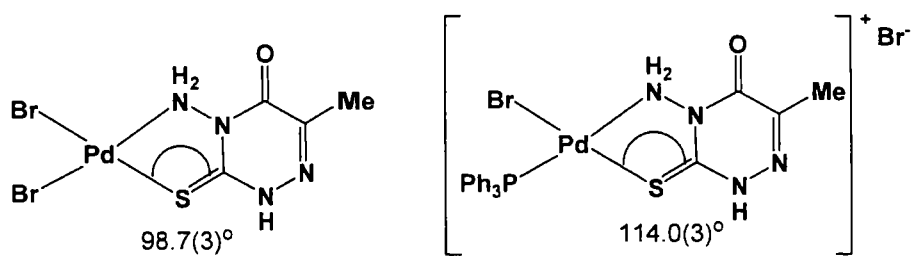


Figure 12. $\text{PdBr}_2(\text{AMTTO})$ (left) and $[\text{PdBr}(\text{PPh}_3)(\text{AMTTO})]\text{Br}$ (right).⁶⁶

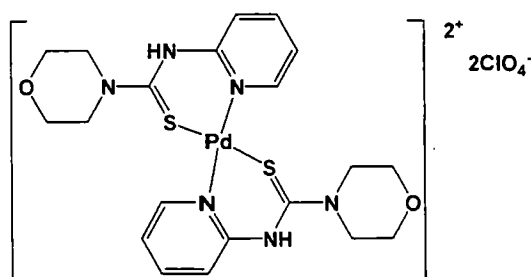


Figure 13. Pyridine-morpholine carbothiamide palladium complex.⁴⁵

Most of the monodentate thiourea palladium complexes which have been reported are *trans*- isomers. Interestingly, the crystal structure of $\text{PdCl}_2(\text{PPh}_3)(\text{tu})$ shows that it forms the *cis*- isomer. This can be explained by the *cis*-complex being stabilized through $\text{N-H}\cdots\text{Cl-Pd}$ hydrogen bonds, which are also responsible for the formation of a dimeric structure (Figure 14).⁹⁰ The sulfur atoms in thioureas show a stronger *trans* influence than nitrogen^{13, 62, 66} and oxygen-containing ligands⁶⁴ as longer Pd-X (X = Cl, I) bonds *trans*- to sulfur are observed. However, the *trans*-influence is weaker than that of phosphorus.⁹⁰

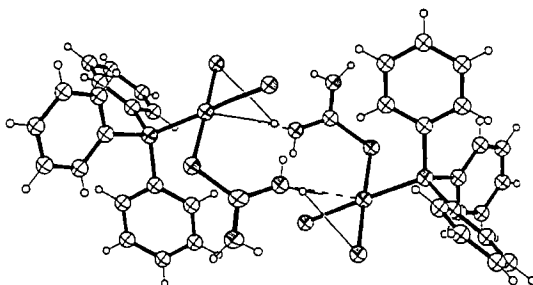
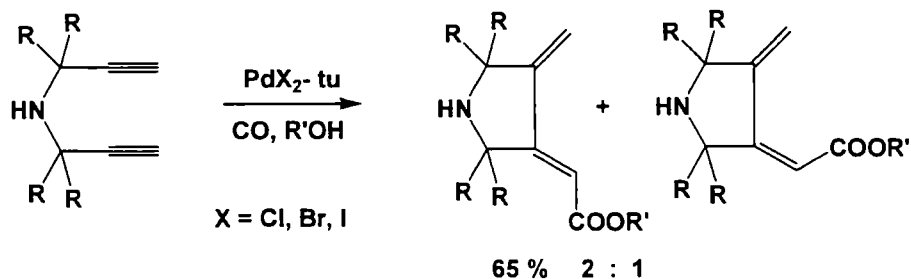


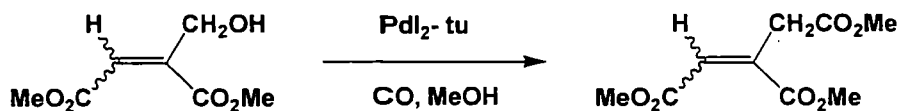
Figure 14. $\text{PdCl}_2(\text{PPh}_3)(\text{tu})$ (hydrogen bonds are shown as a dash line).⁹⁰

I.4 Applications of palladium-thiourea complexes in catalysis

An early application palladium-thiourea complexes in organic synthesis was reported in palladium-catalyzed ring closure of a 1,6-diyne induced by hydrocarboxylation with carbon monoxide, which take places under mild conditions, *i.e.*, room temperature and atmospheric pressure (Scheme 16).⁹¹ The same catalyst, $\text{PdX}_2\text{-tu}$, also works well at 40 °C and 6.0 MPa of CO, leading to oxidative carbonylation of vinyl alcohols to form methyl esters (Scheme 17).⁹² However, there was no characterization reported on the active catalytic species in these reactions.

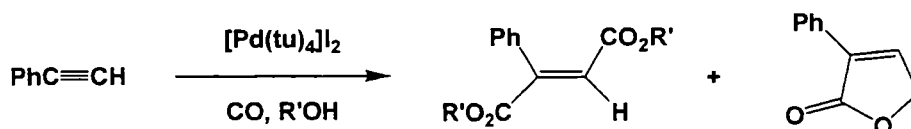


Scheme 16. Diyne ring closure *via* Pd-catalyzed carbonylation.⁹¹



Scheme 17. Oxidative carbonylation of a vinyl alcohol.⁹²

The same research group also reported $\text{PdI}_2\text{-tu}$ to be more effective than $\text{PdCl}_2\text{-tu}$ to obtain bis(alkoxycarbonylation) and carbonyl lactonization products of phenylacetylene (Scheme 18). The Pd source was reported to be $[\text{Pd}(\text{tu})_4]\text{I}_2$ based on an examination of its molecular weight in methanol by vapour pressure osmometry and conductivity in methanol.⁹³ The complex $[\text{Pd}(\text{tu})_4]\text{I}_2$ is an 16 electron compound and it is possible that dissociation from the Pd center occurs to give an active species.

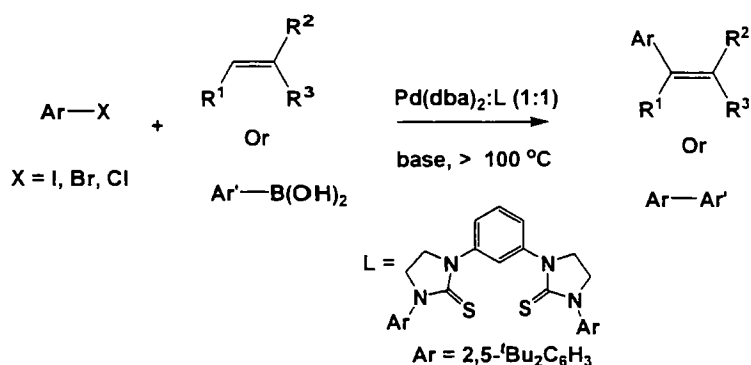


Scheme 18. Combined oxidative and reductive carbonylation of terminal alkynes with palladium iodide-thiourea catalysts.⁹³

The thioureas can be effectively utilized in organic synthesis in Suzuki-Miyaura,¹⁵ Suzuki-Miyaura carbonylation¹⁹ and Heck-Mizoroki reactions,^{15, 17-19} all of which are performed in aerobic conditions.

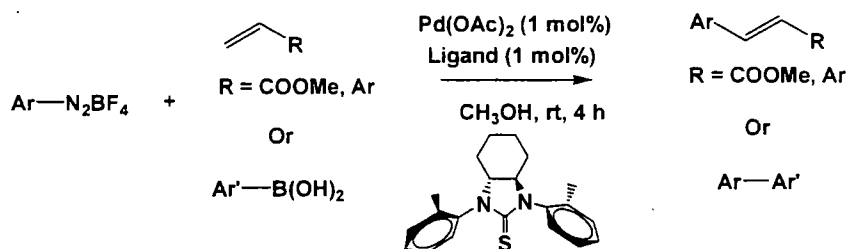
Scheme 19 shows the bis(thiourea) ligand used under aerobic conditions which it was found to give an excellent catalyst for Heck-Mizoroki and Suzuki-Miyaura cross-coupling reaction of aryl iodides and bromides to obtain a quantitative yield (moderate yield for aryl chlorides). TONs were as high as 10000000 and TOFs

as high as 200000 for aryl iodides. Catalysis is observed at very low loadings as low as 0.001 mol%.

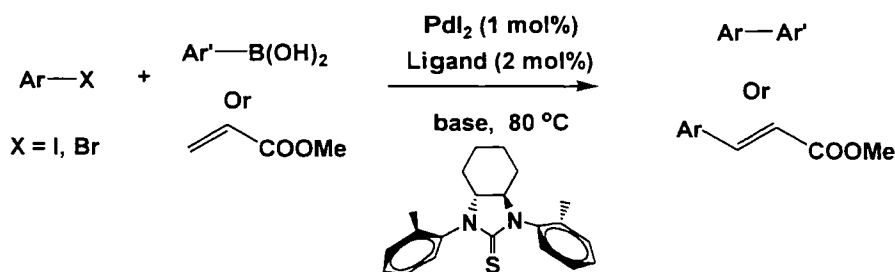


Scheme 19. The application of a bis(thiourea) ligand in Heck-Mizoroki and Suzuki-Miyaura reaction.¹⁵

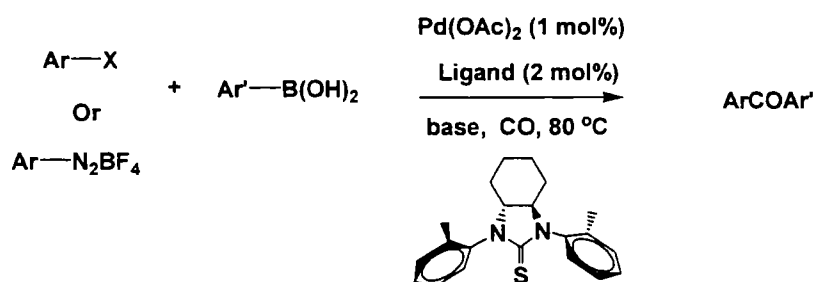
A chiral C₂-symmetric thiourea was used in Heck-Mizoroki and Suzuki-Miyaura reactions of the arenediazonium salt (Scheme 20).¹⁷ The reaction was performed at room temperature under aerobic conditions; no base was added, and the product was obtained in a good yield. This ligand is also efficient in the Heck-Mizoroki and Suzuki-Miyaura reaction of aryl halides (Scheme 21) and the Suzuki-Miyaura carbonylation reaction (Scheme 22).¹⁹



Scheme 20. Reaction conditions used in Heck-Mizoroki and Suzuki-Miyaura reactions of an arenediazonium salt.¹⁷

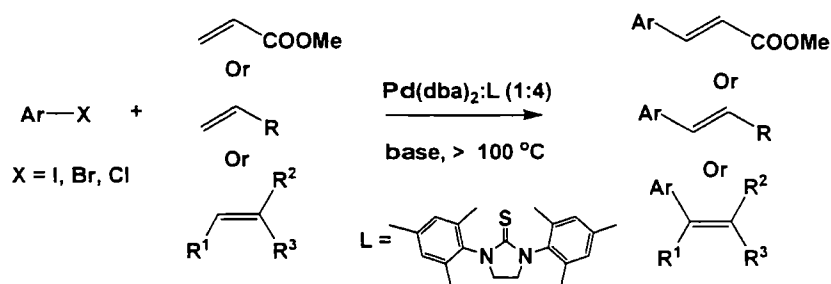


Scheme 21. Reaction conditions used in Heck-Mizoroki and Suzuki-Miyaura reactions of aryl halides.¹⁹



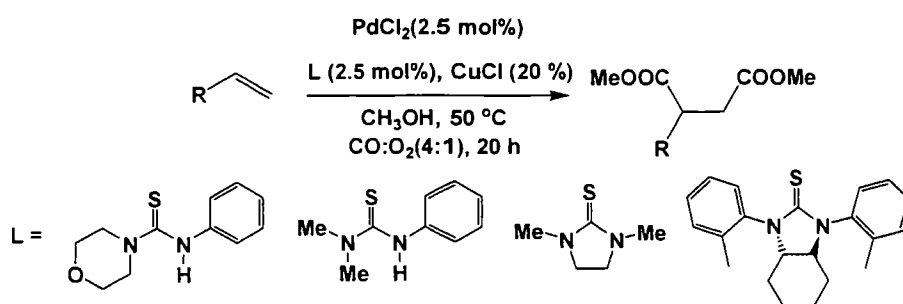
Scheme 22. Reaction conditions used in Suzuki-Miyaura carbonylation reactions of aryl halides or diazonium salts.¹⁹

A sterically hindered thiourea (Scheme 23) was used in the Heck-Mizoroki reaction of aryl halides. It was found to give a highly active catalyst with TONs up to 500000 for the reaction of aryl iodides in the presence of 1 mol% Pd catalyst.



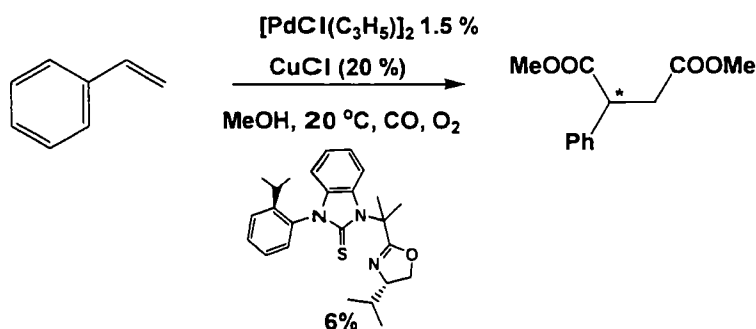
Scheme 23. Reaction conditions used in the Heck-Mizoroki reaction.¹⁸

Recently, the asymmetric bis(methoxycarbonylation) of alkenes (Scheme 24) was studied using an *in situ* prepared catalyst derived from thioureas including a chiral thiourea derivative and palladium chloride.¹² The ligand structures shown in Scheme 24 are those which gave a good yield (up to 90 %).



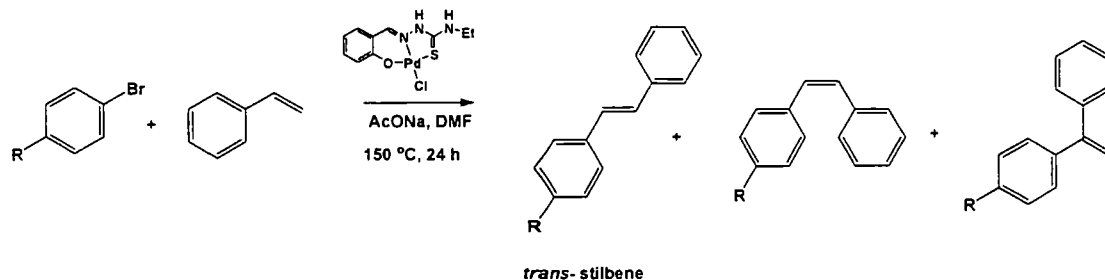
Scheme 24. Bis(methoxycarbonylation) of terminal olefins and ligands used in the reaction.¹²

Other S,N-bidentate chiral thiourea-oxazoline ligands were applied in the Pd-catalyzed alkoxy-carbonylation of aryl iodides to obtain yields of up to 99 % with *ee*'s as high as 68 % (Scheme 25).¹³



Scheme 25. Asymmetric bis(methoxycarbonylation) of styrenes.¹³

Palladium complexes of thiosemicarbazone were applied in Heck–Mizoroki reactions of styrene with aryl bromides and gave good selectivity for formation of *trans*-stilbene of up to 96%. The reaction works well in both an inert atmosphere and in air (Scheme 26).¹⁴



Scheme 26. Heck–Mizoroki reactions of styrene with aryl bromides.¹⁴

Another air- and moisture-stable zwitterionic, salicylaldehyde N-4-hexamethyleneiminylthiosemicarbazone palladium complex (Figure 15), has been used in microwave-promoted Suzuki–Miyaura reactions of aryl bromides and chlorides in $\text{DMF}/\text{H}_2\text{O}$ under aerobic conditions with turnover numbers up to 37,000 at 100 °C in 24 h.¹⁶

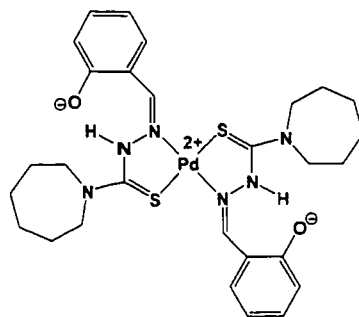
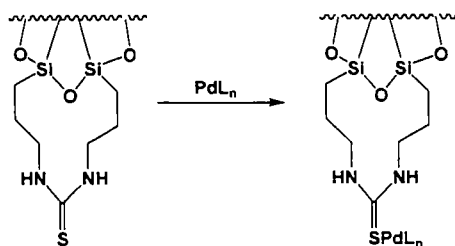


Figure 15. Salicylaldehyde N-4-hexamethyleneiminylthiosemicarbazone palladium complex.¹⁶

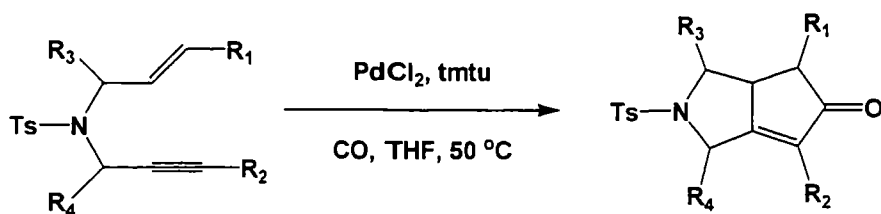
Zhang *et al.* reported the use of polymer-supported palladium complexes of thioureas at 80 °C in wet *t*-PrOH for 3 h in Suzuki-Miyaura reactions of aryl iodides and aryl bromide with phenylboronic acid to obtain quantitative yields of cross-coupled products.⁹⁴ The preparation of the catalyst is shown in Scheme 27.



Scheme 27. The synthesis of a resin-bound palladium thiourea complex.⁹⁴

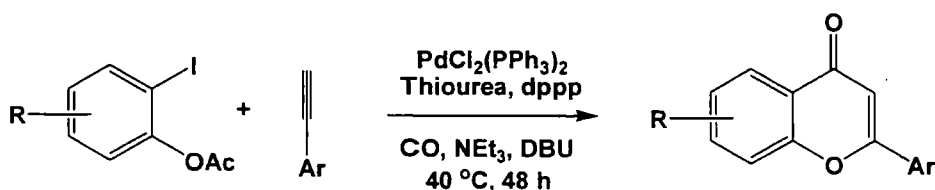
Preliminary results suggest that palladium-thioureas $[\text{Pd}(\text{Ptu})_2][\text{CoCl}_4]^-$; $\text{Ptu} = (\text{PPh}_2)\text{CH}_2\text{CH}_2\text{NHC}(\text{S})\text{NHPh}$, can be used in the homogenous hydrogenation of styrene to give good yields.⁷⁴ Moreover, a palladium-thiourea xerogel was also used for the reduction of phenylacetylene at 25 °C in CH_3OH at atmospheric pressure. The products can be controlled by reaction time to give either alkane or alkene in better yield than using the Lindlar catalyst (88 vs 82%).⁹⁵

Thiourea-palladium complexes were established as novel catalysts for the Pauson-Khand reaction of allylpropargylamine (Scheme 28).²⁰



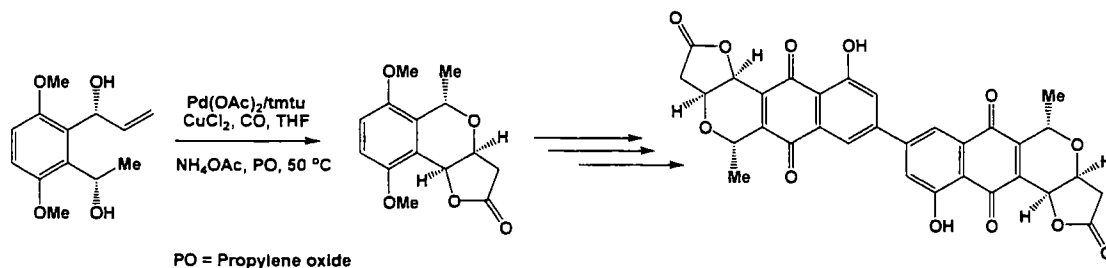
Scheme 28. The Pauson–Khand reaction of allylpropargylamine.²⁰

The highly effective catalyst system of PdI_2 -thiourea was developed for carbonylation of *o*-hydroxyarylacetylenes to afford methyl benzo[*b*]furan-3-carboxylate scaffolds.⁹⁶ Recent advances have been made in thiourea-palladium-catalyzed carbonylative annulation of iodophenol acetates and acetylenes to obtain flavones as shown in Scheme 29.



Scheme 29. Thiourea-palladium-catalyzed carbonylative annulation of iodophenol acetates.⁹⁶

Very recently, the natural product, Crisamicin A, has been synthesized *via* a key intermediate lactone, which can be constructed from palladium-catalyzed alkoxy-carbonylation–lactonization using $\text{Pd}(\text{OAc})_2/\text{tmtu}$ as the catalyst (Scheme 30).⁹⁷



Scheme 30. Synthetic route to Crisamicin A.⁹⁷

Clearly, thiourea ligands are potentially good ligands in palladium catalysis and they are air and moisture stable. They represent a new type of ligand which is effective and also easy to handle.



Previously, we have shown the synthesis of the chiral thiourea **L1** (Figure 16) which was first reported by the group of Prof. Z. Yang at Peking University.¹⁷ **L1** was found to be efficient for Heck-Mizoroki^{17, 19} and Suzuki-Miyaura cross-coupling reactions,¹⁹ Suzuki-Miyaura carbonylations,¹⁹ bis(methoxycarbonylation)¹² reactions and alkoxy carbonylations of aryl iodides, *vide supra*.⁹⁸ In collaboration with the group of Prof. Z. Yang, who synthesized the ligands, we focused on detailed characterization of the mono- and di-palladium complexes of **L1**.

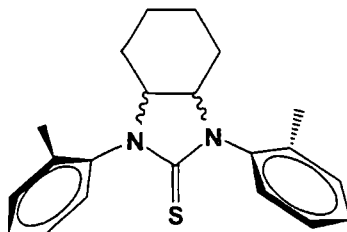


Figure 16. Chiral thiourea (**L1**).¹⁷

The objectives of this study are:

1. the synthesis of the palladium complexes of monodentate thioureas (tmtu) and chiral thiourea **L1**; and
2. full characterization and investigation of their palladium complexes.

Table 2. Bond lengths, angles and dihedral angles for palladium-thiourea complexes.

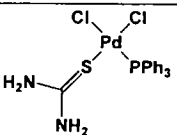
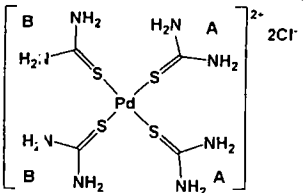
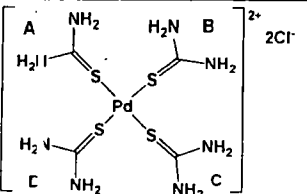
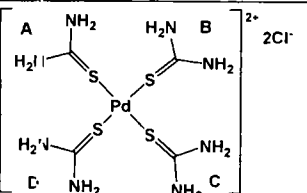
Compound	Pd-S (Å) ^a	S-C (Å) ^a	C-N (Å) ^a	Pd-S-C (°)	Pd-S-C-N (°)	Ref ^c
	2.319(1)	1.723 [1.720(9)] ^b	1.302 1.318 [1.340(6)] ^b	107.14	25.22	90 [51]
	A 2.333 B 2.364	A 1.734 B 1.718	A 1.305 1.370 B 1.329 1.482	A 107.99 B 107.35	A 25.44 B 6.80	87
	A 2.316 B 2.341 C 2.331 D 2.346	A 1.714 B 1.729 C 1.742 D 1.726	A 1.314 1.329 B 1.311 1.330 C 1.316 1.325 D 1.322 1.335	A 110.46 B 109.52 C 109.74 D 110.62	A 25.87 B -27.12 C -27.46 D 17.21	88
	A 2.313 B 2.336 C 2.320 D 2.345	A 1.721 B 1.730 C 1.729 D 1.746	A 1.322 1.334 B 1.307 1.315 C 1.313 1.316 D 1.295 1.326	A 110.51 B 111.33 C 109.64 D 108.01	A -24.82 B -17.94 C 27.87 D 29.61	89

Table 2 (continued)

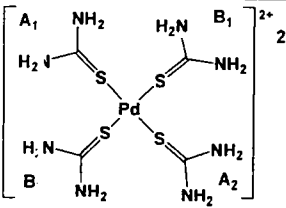
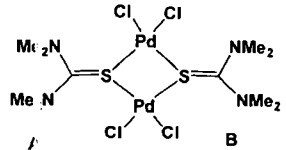
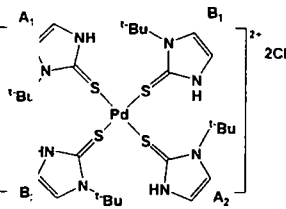
Compound	Pd-S (Å) ^a	S-C (Å) ^a	C-N (Å) ^a	Pd-S-C (°)	Pd-S-C-N (°)	Ref ^c
	A 2.336(1) B 2.338(1)	A 1.712(4) B 1.716(2)	A 1.311 1.321 B 1.293 1.326	A 109.0(1) B 110.(2)	A ₁ 15.21 A ₂ -15.21 B ₁ 16.36 B ₂ -16.36	99
	A 2.3135(5) 2.2814(7) B 2.3052(5) 2.2906(6)	A 1.7876(19) B 1.7908(18) [1.6876(15)] ^b	A 1.331(2) 1.322(2) B 1.326(2) 1.326(2) [1.3613(11)] ^b	A 113.63(6) 112.93(6) B 113.80(6) 105.60(6)	A -45.59 135.09 B 73.32 -106.91	52 [52]
	A 2.3191(11) B 2.3263(9)	A 1.723(4) B 1.709(3) [1.700] ^b	CN(H) CN(C) A 1.336 1.349 B 1.328 1.362 [1.348 1.363] ^b	A 95.70 B 102.76(12)	A ₁ 59.83 A ₂ -59.83 B ₁ 0.10 B ₂ -0.10	86 [100]

Table 2 (continued)

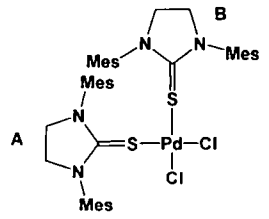
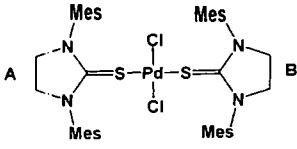
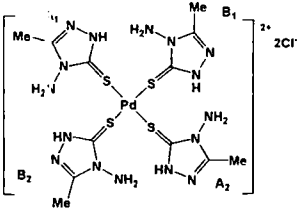
Compound	Pd-S (Å) ^a	S-C (Å) ^a	C-N (Å) ^a	Pd-S-C (°)	Pd-S-C-N (°)	Ref ^c
	1A 2.297 1B 2.282 2A 2.279 2B 2.310	1A 1.695 1B 1.707 2A 1.662 2B 1.702 [1.666(2)] ^b	1A 1.310 1.384 1B 1.354 1.325 2A 1.342 1.352 2B 1.355 1.370 [1.355(2)] ^b	1A 110.01 1B 111.12 2A 111.06 2B 110.35	1A 31.03 1B 28.15 2A 25.16 2B 31.17	18 [101]
	1A 2.317 1B 2.325 2A 2.311 2B 2.310	1A 1.663 1B 1.685 2A 1.675 2B 1.726	1A 1.310 1.407 1B 1.330 1.352 2A 1.343 1.361 2B 1.269 1.376	1A 110.70 1B 110.62 2A 111.54 2B 111.80	1A 19.66 1B -16.10 2A 20.95 2B -19.82	18
	A 2.323 B 2.325	A 1.718 B 1.707	CN(H) CN(C) A 1.320 1.351 B 1.320 1.356	A 106.25 B 107.20	A ₁ 74.87 A ₂ -74.87 B ₁ 3.86 B ₂ -3.66	102

Table 2 (continued)

Compound	Pd-S (Å) ^a	S-C (Å) ^a	C-N (Å) ^a	Pd-S-C (°)	Pd-S-C-N (°)	Ref
	A 2.327(1) B 2.336(2)	A 1.701(4) B 1.704(6)	C-N(H) C-N(C) A 1.352 1.365 B 1.357 1.327	A 109.3(2) B 105.6(2)	A ₁ 43.29 A ₂ -43.29 B ₁ 26.95 B ₂ -26.95	58
	A 2.284 B 2.307 C 2.307 D 2.303	A 1.701 B 1.713 C 1.700 D 1.683	C-N(C) C-N(Pd) A 1.262 1.589 B 1.343 1.341 C 1.291 1.518 D 1.377 1.344	A 102.58 B 101.74 C 102.55 D 102.30	A -3.25 B -10.09 C -30.55 D -7.09	59
	A 2.332 B 2.336	A 1.701 B 1.711	C-N(H) C-N(C) A 1.340 1.336 B 1.329 1.342	A 106.24 B 106.18	A ₁ 4.14 A ₂ -4.14 B ₁ -13.13 B ₂ 13.13	59

Table 2 (continued)

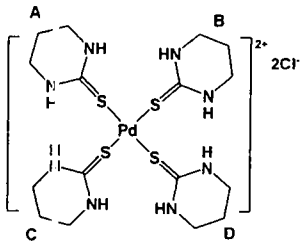
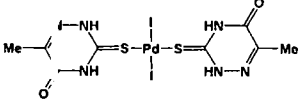
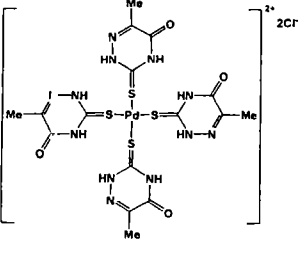
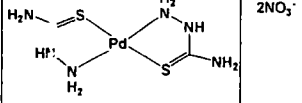
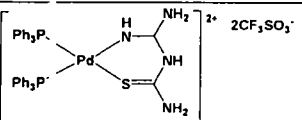
Compound	Pd-S (Å) ^a	S-C (Å) ^a	C-N (Å) ^a	Pd-S-C (°)	Pd-S-C-N (°)	Ref ^c
	A 2.338 B 2.334 C 2.337 D 2.316	A 1.730 B 1.737 C 1.726 D 1.726 [1.722(7)] ^b	A 1.318 1.329 B 1.299 1.334 C 1.302 1.313 D 1.307 1.323 [1.334(6)] ^b	A 105.33 B 109.20 C 110.89 D 106.89	A -46.50 B -61.67 C -0.73 D -19.03	84 [53]
	2.321	1.685	C-N(CO) C-N(N) 1.360 1.322	107.15	5.44 -5.44	69
	A 2.310 B 2.330	A 1.703 B 1.701	C-N(CO) C-N(N) A 1.349 1.349 B 1.327 1.348	A 111.37 B 107.51	A ₁ -13.16 A ₂ 13.16 B ₁ -13.46 B ₂ 13.46	69
	2.264 2.265	1.724 1.734	1.311 1.319	97.82 98.09	< 2.0	67
	2.3148(14)	1.707	1.315 - 1.351	106.27	18.87	68

Table 2 (continued)

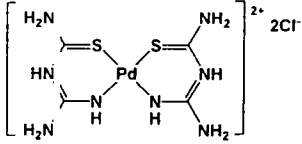
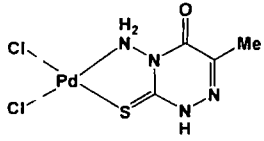
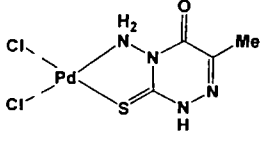
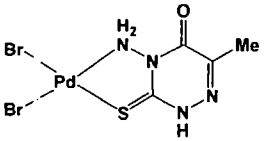
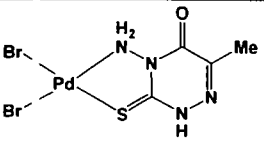
Compound	Pd-S (Å) ^a	S-C (Å) ^a	C-N (Å) ^a	Pd-S-C (°)	Pd-S-C-N (°)	Ref
	2.253(2) 2.261(3)	1.648(11) 1.729(10)	1.257(12) 1.337(11) 1.343(18) 1.372(15)	110.5(3) 110.6(4)	1.11 4.53	71
	2.264(1)	1.695(4)	1.332(6) 1.345(6)	97.2(2)	2.73	62
	2.240 2.242	1.692 1.702	1.314 – 1.343	96.98 97.26	< 1	69
 (disordered structure)	2.246 – 2.251	1.694 – 1.700	1.323 – 1.352	97.88 – 97.35	0.5 – 2	69
	2.252(2) 2.259(2)	1.694(7) 1.685(8)	1.313(8) – 1.373(8)	97.6(3) 97.9(3)	0 – 3.13	66

Table 2 (continued)

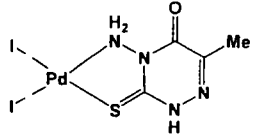
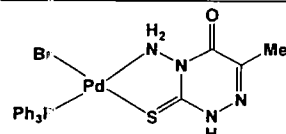
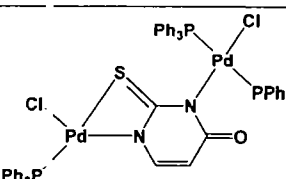
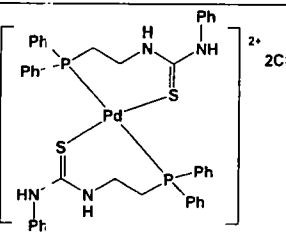
Compound	Pd-S (Å) ^a	S-C (Å) ^a	C-N (Å) ^a	Pd-S-C (°)	Pd-S-C-N (°)	Ref
	2.274(2)	1.692(6)	1.328 1.353	97.9(2)	10.53	66
	2.275(2)	1.711(5)	1.322 1.350	114.0(3)	14.02	66
	2.289	1.728	1.325 1.351	79.63	18.0	61
 (disordered structure)	2.327(5) – 2.355(2)	1.711(10) – 1.745(7)	1.312(8) – 1.338(9)	114.5(3) – 116.8(3)	40.85 – 40.85	74

Table 2 (continued)

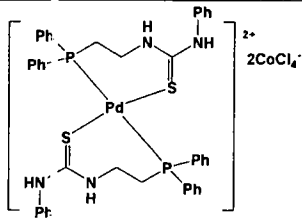
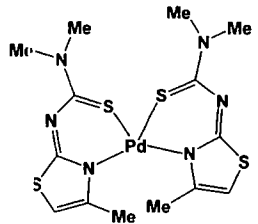
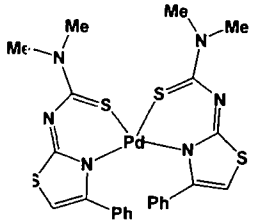
Compound	Pd-S (Å) ^a	S-C (Å) ^a	C-N (Å) ^a	Pd-S-C (°)	Pd-S-C-N (°)	Ref
	2.314(6) 2.337(6)	1.67(2) 1.73(2)	1.29(2) – 1.36(2)	117(1)	59.98 60.55	74
	2.282	1.770	1.304 – 1.377	101.36	-39.95 -39.95	72
	2.274 2.287	1.758 1.761	1.318 – 1.355	100.13 101.45	-31.71 -37.39	72

Table 2 (continued)

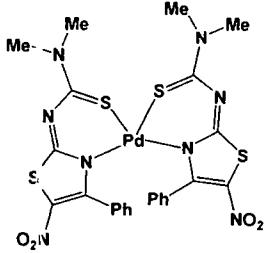
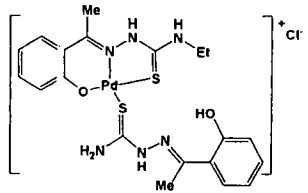
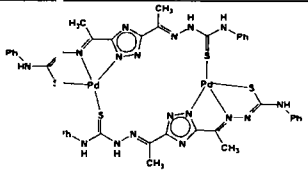
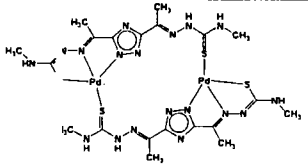
Compound	Pd-S (Å) ^a	S-C (Å) ^a	C-N (Å) ^a	Pd-S-C (°)	Pd-S-C-N (°)	Ref ^c
	2.276	1.752	1.333 – 1.337	98.10	49.97 49.997	72
	2.2281(15) (chelate) 2.3213(14)	1.7346(15) (chelate) 1.6582(14) [1.690] ^b	C-N(H ₂) C-N(H) 1.328 1.340 1.340 1.350 [1.333 1.349] ^b	94.43 (chelate) 108.43	-0.27 (chelate) 3.68	78 [103]
	2.303 2.305	1.729 1.723	1.326 1.326 1.336 1.337	107.57 107.21	2.51 35.97	76
	2.263(3) 2.306(3)	1.727(10) 1.774(10)	1.307 1.334	95.19 107.61	2.46 24.76	77

Table 2 (continued)

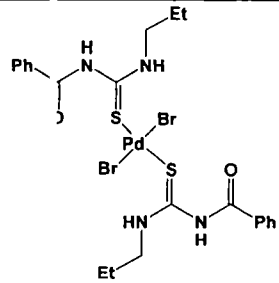
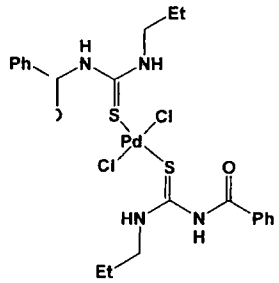
Compound	Pd-S (Å) ^a	S-C (Å) ^a	C-N (Å) ^a	Pd-S-C (°)	Pd-S-C-N (°)	Ref ^c
	2.3164(10)	1.689(4) [1.623(4)] ^b	C-N(CO) C-N(C) 1.315(5) 1.379(5) [1.367(5) 1.312(4)] ^b	114.81	-10.24 14.18	79 [104]
	2.322	1.690	C-N(CO) C-N(C) 1.377 1.327	113.54	11.84 -11.84	105

Table 2 (continued)

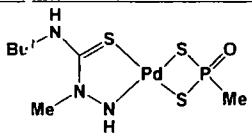
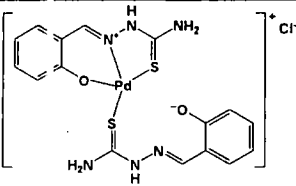
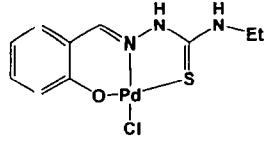
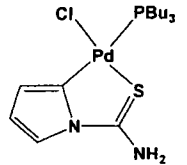
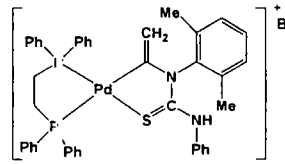
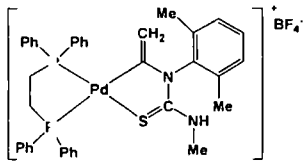
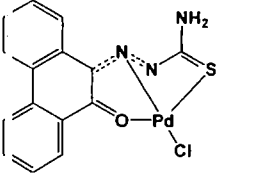
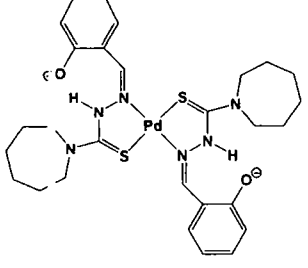
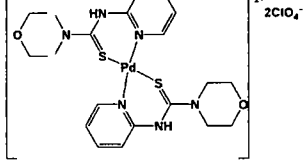
Compound	Pd-S (Å) ^a	S-C (Å) ^a	C-N (Å) ^a	Pd-S-C (°)	Pd-S-C-N (°)	Ref
	2.2762(17)	1.714(6)	1.341(8) 1.345(8)	98.8(2)	3.93	63
	2.253 2.298	1.712 1.714	1.309 – 1.325	97.57 115.59	0 – 4	75
	2.246	1.712	1.332 1.336	97.23	1.53	14
	2.318(3)	1.72(1)	1.32(2) 1.36(2)	98.5(4)	7.92	65
	A 2.2760(17) B 2.2894(15)	A 1.706(6) B 1.718(6)	C-N(H) C-N(Ph) A 1.349 1.327 B 1.345 1.325	A 99.29 B 99.02	7.77 -5.44	64

Table 2 (continued)

Compound	Pd-S (Å) ^a	S-C (Å) ^a	C-N (Å) ^a	Pd-S-C (°)	Pd-S-C-N (°)	Ref
	2.302(2)	1.719(7)	1.333 1.346	99.40	5.10	64
	2.227	1.723	1.284 1.347	94.99	9.23	70
	2.282	1.741(15)	1.324(19) 1.34(2)	99.10	1.95	16
	2.315	1.731	1.315 1.349	92.97	56.94	45

^a Values from CSD, ^b Value in thiourea free ligands, ^c References in brackets are for free ligands.

II. Results and discussion

II.1 Tetramethyl thiourea (tmtu)

II.1.1 Synthesis of tetramethyl thiourea palladium complexes

The reactions of the tmtu ligand and $\text{PdCl}_2(\text{PhCN})_2$ gave the mono-palladium complex $\text{PdCl}_2(\text{tmtu})_2$ **Pd(tmtu)** and the di-palladium complex $[\mu-(\text{tmtu})\text{PdCl}_2]_2$ **Pd₂(tmtu)**⁵² when two and one equivalents, respectively, of tmtu were employed relative to one equivalent of $\text{PdCl}_2(\text{PhCN})_2$ in CH_2Cl_2 at room temperature as shown in Figure 17. **Pd₂(tmtu)** was prepared in our group by Mr. T. Turner.⁵²

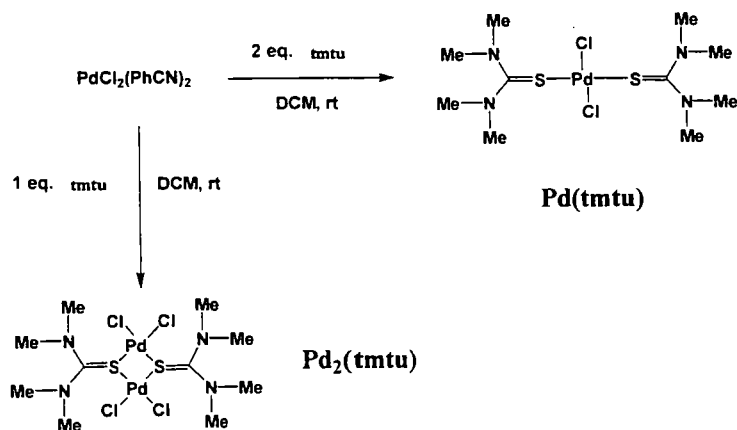


Figure 17. The preparation of the Pd-tmtu complexes.

II.1.2 Characterization of the palladium complexes

The complexes were characterized by NMR spectroscopy, including $^{13}\text{C}\{^1\text{H}\}$ solid state NMR spectroscopy, elemental analysis and single-crystal X-ray diffraction. Analogous characterization was carried out on the free ligand tmtu for comparison.

Single crystal structure of palladium complexes

Single crystals of **Pd(tmtu)** suitable for X-ray diffraction were grown *via* slow evaporation of a solution in $\text{CH}_2\text{Cl}_2:\text{Et}_2\text{O}$. It crystallizes in the triclinic space group $P\bar{1}$ with $Z = 1$ and 0.5 molecules in the asymmetric unit. The molecular structure of **Pd(tmtu)** is shown in Figure 18. The Pd center is coincident with a crystallographic center of inversion and the complex has a *trans* square-planar geometry.

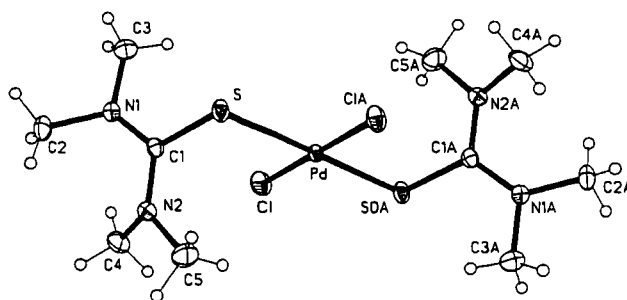


Figure 18. The molecular structure of **Pd(tmtu)**.

The molecular structure of **Pd₂(tmtu)** was confirmed *via* single-crystal X-ray diffraction. A good quality single crystal of **Pd₂(tmtu)** was obtained from slow evaporation of a solution in CH₃CN in our group by Mr. T. Turner.⁵² It was found to crystallize in the monoclinic space group $P2_1/n$ with $Z = 4$, with one molecule of **Pd₂(tmtu)** and two molecules of CH₃CN solvate in the asymmetric unit. The molecular structure of **Pd₂(tmtu)** is shown in Figure 19 (solvate molecules omitted). Interestingly, the chloride ligands are terminal whereas the sulfur atoms are bridging. The two Pd centers have *cis*- configurations but exhibit small tetrahedral distortions: the dihedral angles between the S(1)Pd(1)S(2) and Cl(1)Pd(1)Cl(2) planes and between the S(1)Pd(2)S(2) and Cl(3)Pd(2)Cl(4) planes are both 4°. The two tmtu ligands show an *endo* configuration with respect to the puckered Pd₂S₂ core. This sulfur bridged structure is the first example found for a palladium thiourea complex, but this coordination mode is known for other metals, for example, Cu¹⁰⁶ and Ag.¹⁰⁷

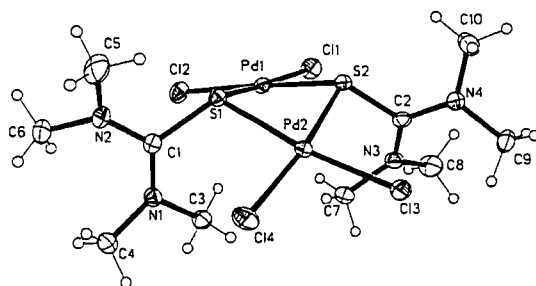


Figure 19. The molecular structure of **Pd₂(tmtu)** (CH₃CN solvate molecules omitted for clarity).⁵²

The single crystal structure of the tmtu ligand is depicted in Figure 20 for comparison; the crystal was obtained from H₂O in our group by Mr. T. Turner.⁵² The ligand crystallizes in the monoclinic space group $C2/c$ with $Z = 4$.

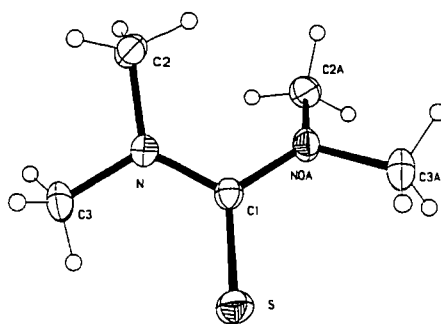


Figure 20. The molecular structure of tmtu.

The crystallographic data and refinement parameters for tmtu, **Pd(tmtu)** and **Pd₂(tmtu)** are given in Table 3, and selected bond lengths and angles are listed in Table 4.

The Pd–S–C angle in **Pd(tmtu)** is smaller than in **Pd₂(tmtu)** ($108.60(5)^\circ$ vs $113.33(6)^\circ$ (av), respectively). The C–N bonds are slightly shortened compared to tmtu by 0.02 \AA (**Pd(tmtu)**) and 0.04 \AA (**Pd₂(tmtu)**). The C=S bonds in **Pd₂(tmtu)** are significantly longer ($1.7892(19) \text{ \AA}$ (av)) than in the **Pd(tmtu)** ($1.7337(15) \text{ \AA}$) and in the free ligand ($1.687(6) \text{ \AA}$). This suggests a weakening of the C=S bond with concomitant strengthening of the C–N bonds on complexation to Pd, an effect which is even larger in the dimer, where the sulfur is bonded to two Pd centers. Interestingly, the Pd–S distances in the S-bridged dimer are slightly shorter (by *ca.* 0.03 \AA) than in the monomer, whereas the Pd–Cl distances are nearly identical in both complexes. Whilst the S–C–N angles in tmtu are equivalent, this is not the case for the complexes (*ca.* 3° and 9° differences in **Pd(tmtu)** and **Pd₂(tmtu)**, respectively).

Table 3. Crystallographic data for tmtu and its palladium complexes.

Compound	tmtu	Pd(tmtu)	Pd ₂ (tmtu)
Formula	C ₅ H ₁₂ N ₂ S	C ₁₀ H ₂₅ Cl ₂ N ₄ PdS ₂	C ₁₀ H ₂₅ Cl ₄ N ₄ -Pd ₂ S ₂ ·2CH ₃ CN
FW	132.23	442.80	660.11
<i>T</i> (K)	120(2)	120	120(2)
Crystal system	Monoclinic	Triclinic	Monoclinic
Space group (no.)	<i>C2/c</i>	<i>P</i> -1	<i>P2₁/n</i>
<i>a</i> (Å)	5.4685(6)	7.3045(7)	12.2740(14)
<i>b</i> (Å)	12.0328(13)	7.8020(8)	13.4802(16)
<i>c</i> (Å)	10.9346(10)	8.3679(8)	14.2629(17)
α (°)	90.00	110.92(1)	90.00
β (°)	95.62(2)	95.59(1)	102.07(2)
γ (°)	90.00	100.81(1)	90.00
<i>U</i> (Å ³)	716.05(13)	430.46(7)	2307.7(5)
<i>Z</i>	4	1	4
<i>D</i> (Mg cm ⁻³)	1.227	1.708	1.900
μ (mm ⁻¹)	0.36	1.62	2.21
Refls measured	4946	5238	26458
unique, <i>R</i> _{int} , %	1049, 2.3	2473, 2.8	6534, 3.0
Refls with <i>I</i> ≥ 2σ(<i>I</i>)	1049	2327	5414
<i>R</i> ₁ , w <i>R</i> ₂ , %	3.1, 8.2	1.9, 4.6	2.0, 4.7

Table 4. Selected bond lengths and angles for tmtu and its palladium complexes.

Bond lengths (Å)	tmtu	Pd(tmtu)	Pd ₂ (tmtu)
Pd-S		2.3268(4)	2.2814(7), 2.2906(9)
Pd-S'		2.3268(4)	2.3052(5), 2.3135(5)
Pd-Cl(1)		2.3103(5)	2.3075(5), 2.3201(5)
Pd-Cl(2)		2.3103(5)	2.3227(7), 2.3292(6)
C(2)-S	1.687(6)	1.7337(15)	1.7876(19), 1.7908(18)
C(2)-N(1)	1.361(3)	1.341(2)	1.322(2), 1.326(2)
C(2)-N(3)	1.361(3)	1.341(2)	1.326(2), 1.331(2)
N(1)-C(11)	1.458(7)	1.462(2)	1.467 (av)
N(3)-C(21)	1.463(9)	1.458(2)	1.473(av)
Bond angles (deg)			
Pd-S-C(2)		108.60(5)	112.93(6), 113.63(6)
S-C-N(1)	122.32(6)	119.35(11)	114.22(14), 123.82(14)
S-C-N(2)	122.32(6)	121.80(11)	115.20(13), 123.85(14)
Cl-Pd-Cl		179.998(1)	94.260(19), 94.14(2)
Cl-Pd-S		86.706(17)	92.507(18), 94.531(18)
		93.294(17)	94.50(2), 93.262(2)
S-Pd-S		179.999(2)	78.798(17), 79.15(2)

The ¹H and ¹³C{¹H} NMR resonances in CD₂Cl₂ and the ¹³C{¹H} resonances in the solid state are listed in Table 5. In solution, the ¹³C{¹H} resonance for the C=S carbon in the free tmtu ligand (δ 195.05 ppm) exhibits a lower field chemical shift than that for the complexes (*ca.* δ 188 – 189 ppm). On the other hand, the CH₃ (δ 43.79 ppm) signal for the free ligand is observed at a higher field than in the complexes (*ca.* δ 45 ppm). The same results were observed in the ¹H NMR spectra; the CH₃ groups in the complexes exhibit resonances at slightly lower fields than those for the free ligand. Interestingly, the solution NMR spectrum of **Pd(tmtu)** displays two C=S signals (δ 188.38 and 189.29 ppm) and two CH₃ signals (δ 45.07 and 45.23 ppm) suggesting that two complexes are present in solution. These two complexes are postulated to be *cis*- and *trans*-**Pd(tmtu)**, as the *cis*- and *trans*- isomers of analogous complexes with other thiourea ligands have been reported previously.^{18, 65} Interestingly, these signals are essentially identical to those observed in the NMR spectrum of **Pd₂(tmtu)** (C=S at δ 188.42, 189.31 ppm and CH₃ at δ 45.08, 45.24 ppm,

respectively (see Table 5)). For this reason, we believe that, in solution, both monomeric and dimeric complexes give rise to the same species (*i.e.*, *cis*- and *trans*-monomeric complexes). In the solid state, the $^{13}\text{C}\{^1\text{H}\}$ NMR spectrum of $\text{Pd}_2(\text{tmtu})$ shows two C=S signals at δ 171.33 and 173.00 ppm, consistent with the two environments in the single crystal structure, which are significantly shifted with respect to the C=S signals observed in solution. Five signals for the CH_3 groups are observed. Eight independent CH_3 groups are found in the crystal structure of $\text{Pd}_2(\text{tmtu})$, which suggests that some of the $^{13}\text{C}\{^1\text{H}\}$ signals are overlapped in the solid state NMR spectrum.

Table 5. The ^1H (500 MHz) and $^{13}\text{C}\{^1\text{H}\}$ (125 MHz) NMR resonances for tmtu, $\text{Pd}(\text{tmtu})$ and $\text{Pd}_2(\text{tmtu})$ in CD_2Cl_2 (ppm); $^{13}\text{C}\{^1\text{H}\}$ (100 MHz) resonances in the solid state are given in parentheses.

Compounds	^1H	$^{13}\text{C}\{^1\text{H}\}$	
		CH_3	C=S
tmtu	3.00 (s, 12H)	43.79 (42.38, 44.53)	195.05 (192.96)
$\text{Pd}(\text{tmtu})$	3.23, 3.21 (s, 24H)	45.07, 45.23 (46.79)	188.38, 189.29 (188.45)
$\text{Pd}_2(\text{tmtu})$	3.23, 3.21 (s, 24H)	45.08, 45.24 (44.94, 46.51, 47.45, 48.66, 51.30)	188.42, 189.31 (171.33, 173.00)

Because of the low solubility of $\text{Pd}_2(\text{tmtu})$, no dynamic NMR studies have been carried out. However, from the solution and solid state NMR spectra, we can speculate on the interconversion of $\text{Pd}_2(\text{tmtu})$ and $\text{Pd}(\text{tmtu})$ as summarized in Figure 21.

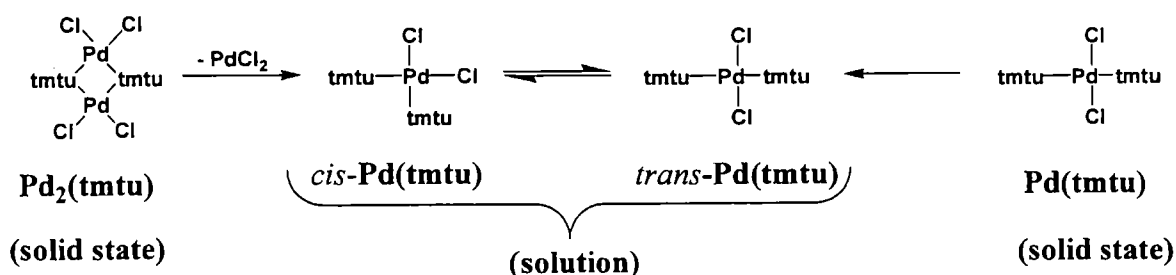


Figure 21. The interconversion of $\text{Pd}_2(\text{tmtu})$ and $\text{Pd}(\text{tmtu})$ in solution.

Thus, the dimer appears to be relatively unstable in solution, with respect to the monomeric complex and PdCl_2 . Presumably, the *trans*- isomer of the monomer crystallized more readily than the *cis*- isomer. Clearly, the Pd–S bonds are fairly weak and the system is labile.

II.2 C_2 -symmetric chiral thiourea

II.2.1 Ligand characterizations

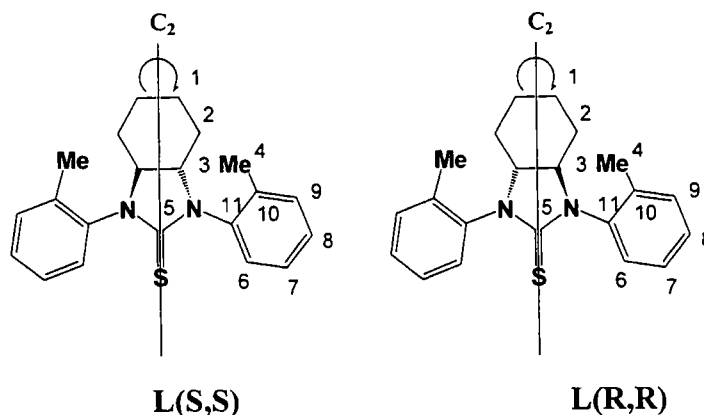


Figure 22. The structures of chiral thiourea ligands.

The chiral thioureas, (S,S)-1,3-di-*o*-tolyl-hexahydro-1*H*-benzo[*d*]imidazole-2(3*H*)-thione **L(S,S)** (Figure 22) and (R,R)-1,3-di-*o*-tolyl-hexahydro-1*H*-benzo[*d*]imidazole-2(3*H*)-thione **L(R,R)** (Figure 22) and a racemic mixture of the two **L(rac)** were synthesized by the group of Prof. Z. Yang at Peking University. The ligands were characterized by NMR (^1H , $^{13}\text{C}\{^1\text{H}\}$, COSY, NOESY, HSQC and HMBC), IR, mass spectrometry, HMRS, elemental analysis and single-crystal X-ray diffraction. Their $^{13}\text{C}\{^1\text{H}\}$ NMR spectra show only 11 signals which implies that they are C_2 symmetric molecules. Their proton and carbon resonances were assigned using two-dimensional NMR techniques. A COSY experiment (Figure 23) was performed to assign the protons in the six-membered cyclohexane ring. The proton at position 3 (δ ca. 3.7 ppm) correlates with the resonances at δ 1.44 and 1.80 ppm which can thus be assigned to the axial and equatorial protons at position 2. The protons at position 2 also couple with the axial and equatorial protons at position 1. The assignment of protons in the aromatic ring was aided by a NOESY spectrum (Figure 24). The doublet at position 6 (δ 7.19 ppm) correlates with the resonance at position 3 (if the N–C11 single bond rotates by 180° from the orientation shown in Figure 22, C6 and

C3 are in proximity to one another). Finally, HSQC and HMBC spectra (Appendix A, Figures A14 and A15) can be used to identify all carbons. The ^1H and $^{13}\text{C}\{^1\text{H}\}$ resonances of **L(rac)** at -60, 20 and 100 °C (^1H only) are summarized in Table 6.

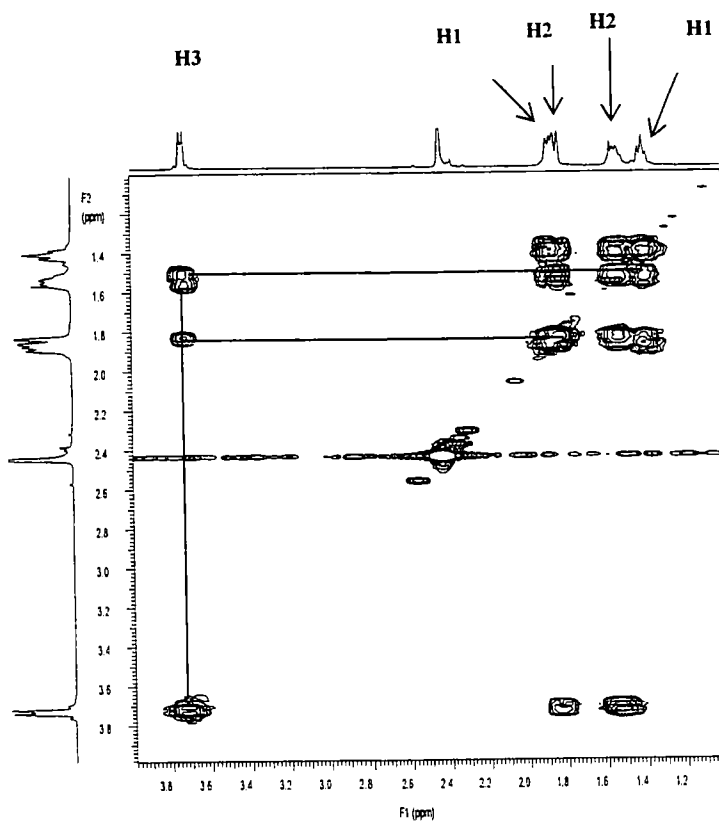


Figure 23. The COSY (500 MHz) spectrum of the aliphatic region of **L(rac)**.

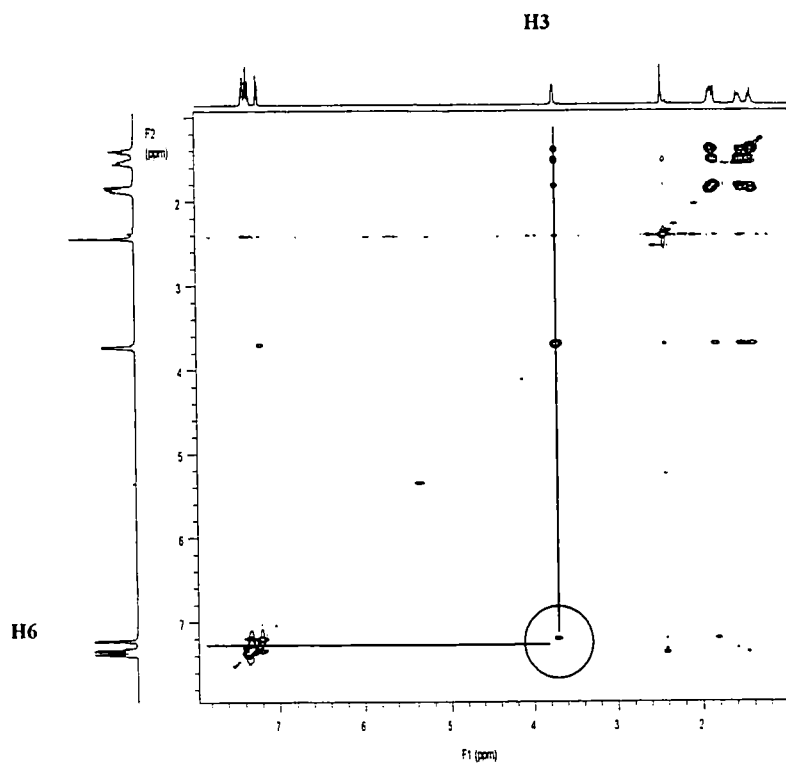


Figure 24. The NOESY (500 MHz) spectrum of **L(rac)**.

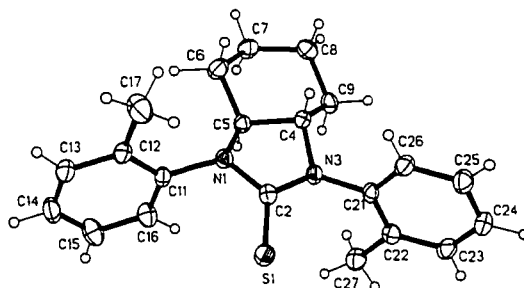


Figure 25. The molecular structure of **L(S,S)**.

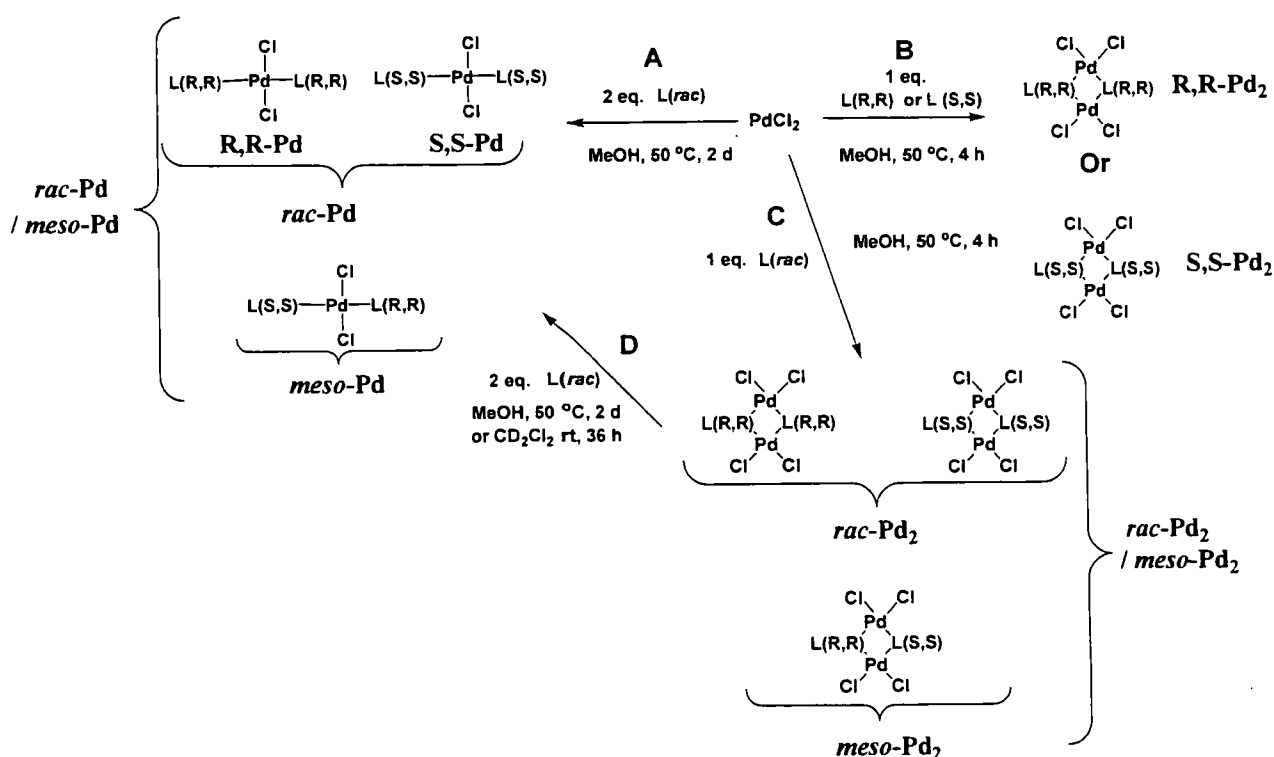
The molecular structure of **L(S,S)** is depicted in Figure 25. The single crystal structure of **L(rac)** was solved previously at 293 K on crystals obtained by Ms. J. Liu at Peking University, and was found to crystallize the monoclinic space group $P2_1/n$. The ligand **L(S,S)** crystallizes in the monoclinic, chiral space group $P2_1$. The crystallographic data and selected bond lengths and angles are given in Tables 7 and 8, respectively. Both structures show very similar bond lengths and angles. The C=S bond length in **L(S,S)** is 1.661(2) Å which is 0.02 and 0.06 Å shorter than the corresponding distances in tmtu⁵² and thiourea (tu),⁵¹ respectively. Furthermore, the C–N bond lengths (1.40 (av) Å) are 0.04 and 0.06 Å longer than those in tmtu and tu, respectively. Clearly, the C=S bond has more double bond character in **L(S,S)** whereas the C–N bonds have more single bond character than in tmtu and tu, respectively. This effect can be explained by the increased localization of lone pair electrons on the nitrogen atoms rather than on the C=S bond in **L(S,S)**.

The S–C–N angles (125.85° (av)) are significantly wider than those in tu and tmtu (120.5(5)° and 122.32(6)°, respectively). The influence of the cyclohexyl ring may be responsible for this. The structure shows the *trans* fused junction, the cyclohexyl ring in a chair conformation and the five-membered heterocycle to adopt an asymmetrically twisted conformation (the C(4) and C(5) atoms are displaced from the SC(2)N(1)N(3) plane by 0.26 and –0.35 Å, respectively).

Interestingly, the main difference between the structure of **L(S,S)** and **L(rac)** is the dihedral angle between one of the tolyl groups and the five-membered heterocycle which is 66.6° in **L(rac)** compared to 82.7° in **L(S,S)**. The dihedral angles between the heterocycle and the other tolyl group are identical in both structures (82.6°).

II.2.2 Synthesis of chiral thiourea palladium complexes

The chiral thiourea ligands can be converted to mono- and di-palladium complexes (Scheme 31). In route **A**, two equivalents of **L(rac)** and PdCl₂ in refluxing methanol for 2 days gave a racemic mixture of the mono-palladium complexes [Pd{L(R,R)}₂Cl₂] and [Pd{L(S,S)}₂Cl₂] collectively referred to as **rac-Pd**, as well as the *meso* mono-palladium complex [Pd{L(S,S)}{L(R,R)}Cl₂] **meso-Pd**. This mixture will be referred to as **rac-Pd / meso-Pd**. The dimeric-palladium complexes were synthesized as shown in routes **B**, **C** and **D**. One equivalent of homochiral **L(R,R)** or **L(S,S)** was reacted with one equivalent of PdCl₂ in refluxing methanol for 4 h to give the optically pure palladium dimer complexes [Pd-μ-L(R,R)Cl₂]₂ **R,R-Pd₂** or [Pd-μ-L(S,S)Cl₂]₂ **S,S-Pd₂** respectively. Route **C** was used with **L(rac)** to afford a racemic mixture of **R,R-Pd₂** and **S,S-Pd₂** collectively referred to as **rac-Pd₂**, and the *meso* di-palladium complex [Cl₂Pd-μ-L(S,S)-μ-L(R,R)Cl₂] **meso-Pd₂**. This mixture is referred to as **rac-Pd₂ / meso-Pd₂**. Finally, route **D** shows the conversion of the palladium dimer complexes **rac-Pd₂** and **meso-Pd₂** to the mono-palladium complexes **rac-Pd** and **meso-Pd** by adding two equivalents of **L(rac)** to one of the palladium dimers in refluxing methanol for two days. The reaction was repeated in CD₂Cl₂ at room temperature and was monitored by ¹H NMR. The reaction was found to be complete at room temperature in 36 h (See Figure A21 in Appendix A). There are two mechanisms which can explain the conversion of the palladium dimer to monomer: (i) the cleavage of the dimer followed by attack of thiourea nucleophile (S_N1); or (ii) attack of the ligand with concomitant ring opening of the dimer (S_N2). The conversion of the dimer to the monomer is very important and is related to the dynamic behavior in this system which will be discussed in detail in due course.



Scheme 31. The synthetic routes for the mono- and di-palladium chiral thiourea complexes.

II.2.3 Characterization of palladium complexes

The complexes were characterized by NMR spectroscopy (^1H , $^{13}\text{C}\{^1\text{H}\}$, COSY, NOESY, HSQC and HMBC), IR, elemental analysis and single-crystal X-ray diffraction.

The IR spectra of $L(\text{rac})$, $\text{rac-Pd} / \text{meso-Pd}$ and $\text{rac-Pd}_2 / \text{meso-Pd}_2$ are given in Appendix A, Figures A16, A17 and A18, respectively. The MALDI-TOF mass spectra of $\text{rac-Pd}_2 / \text{meso-Pd}_2$ and $\text{rac-Pd} / \text{meso-Pd}$ are shown in Figures 26 and 27, respectively. Both mixtures show complex, albeit similar, fragmentation, displaying major peaks at m/z 778 and 815 which were identified as PdL_2 and PdL_2Cl , respectively. The relative intensity of the peak at $m/z = 921$, attributed to $\text{Pd}_2\text{L}_2\text{Cl}$, was 50 % in $\text{rac-Pd}_2 / \text{meso-Pd}_2$ whereas in $\text{rac-Pd} / \text{meso-Pd}$ it was *ca.* 10%. Another significant peak in $\text{rac-Pd}_2 / \text{meso-Pd}_2$ is $m/z = 1506$ which was attributed to $\text{Pd}_4\text{L}_3\text{Cl}_2$. Interestingly, this signal is not observed in $\text{rac-Pd} / \text{meso-Pd}$.

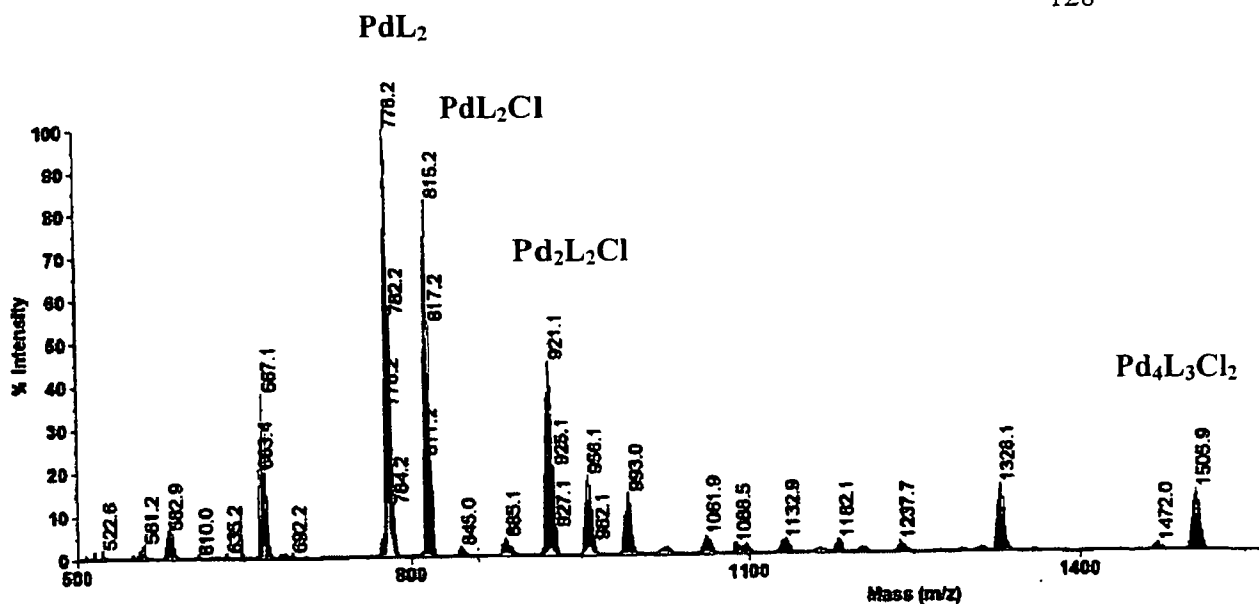


Figure 26. The MALDI TOF mass spectrum of *rac*-Pd₂ / *meso*-Pd₂.

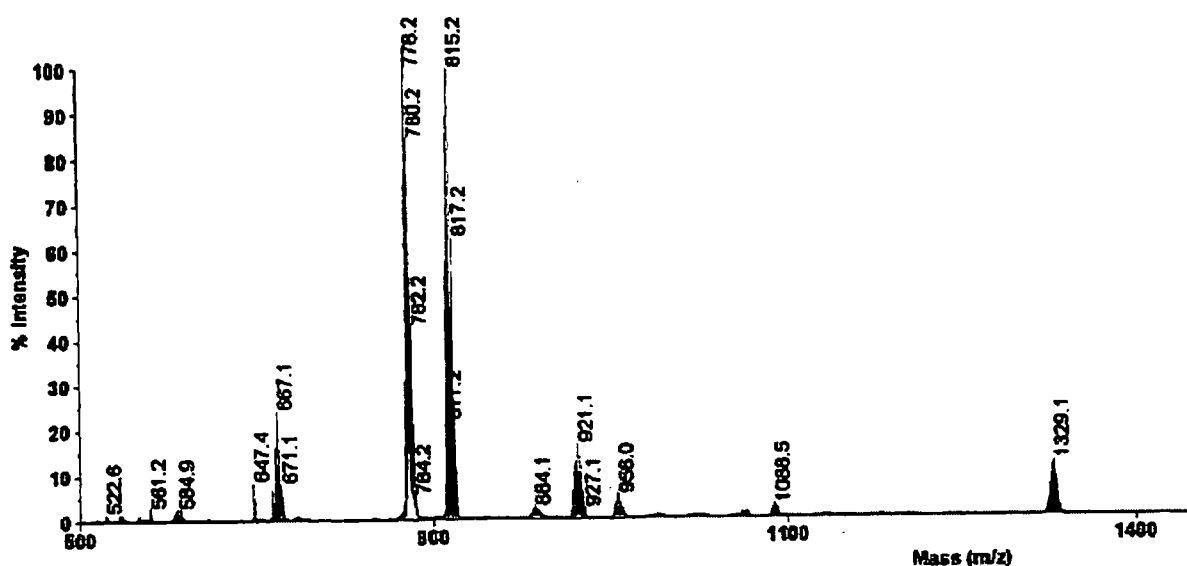


Figure 27. The MALDI TOF mass spectrum of *rac*-Pd / *meso*-Pd.

II.2.3.A) Crystal structures of palladium complexes

Monomeric palladium complex

The structure of the *meso*-Pd was confirmed by single-crystal X-ray diffraction on a crystal grown *via* the slow evaporation of a solution of *rac*-Pd / *meso*-Pd in CD₂Cl₂:Et₂O. The complex crystallizes in the monoclinic space group *P*2₁/*n* with *Z* = 4. There is one molecule in the asymmetric unit with two molecules of CD₂Cl₂ (solvate). The *meso*-Pd structure (Figure 28) has been solved previously on two occasions from X-ray diffraction data on crystals grown from CH₂Cl₂ (data collection at 293 K) and CHCl₃ by the group of Prof. Z. Yang at Peking University and Ms. J. Liu of our group, respectively. The CHCl₃ solvate has the same space

group ($P2_1/n$) and very similar cell parameters to the structure reported in this work but contain CHCl_3 solvate molecules in place of the CD_2Cl_2 ones. However, the crystal obtained from CH_2Cl_2 is crystallized in the triclinic space group $P-1$ and contains no CH_2Cl_2 solvate molecule in the lattice (Figure 29). In all of the structures, the Pd atom lies on an inversion center and has a *trans* square-planar coordination similar to that observed in **Pd(tmtu)** but with two (symmetrically related) solvent molecules.

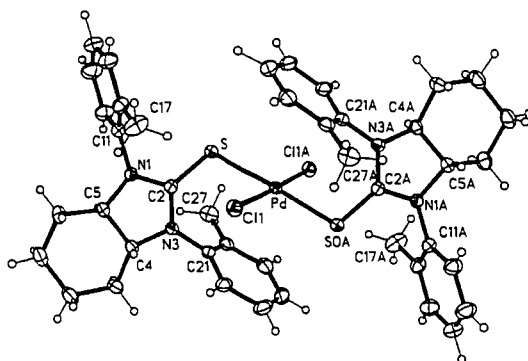


Figure 28. The molecular structure of *trans-meso*-Pd (solvent molecules omitted for clarity).

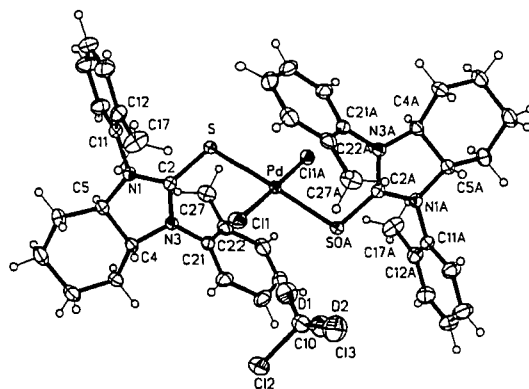


Figure 29. The molecular structure of *trans-meso*-Pd showing one CD_2Cl_2 solvate molecule.

The crystallographic data and selected bond lengths and bond angles are given in Tables 7 and 8, respectively. Table 9 provides a summary of the torsion angles and the angles between planes.

Table 7 Crystallographic data for the C₂ chiral thiourea and its palladium complexes.

Compound	L(rac)	L(S,S)	<i>trans-meso-Pd</i>	<i>meso-Pd</i> ₂
Formula	C ₂₁ H ₂₄ N ₂ S	C ₂₁ H ₂₄ N ₂ S	C ₄₂ H ₄₈ Cl ₂ N ₄ - PdS ₂ ·2CD ₂ Cl ₂	C ₄₂ H ₄₈ Cl ₄ N ₄ - Pd ₂ S ₂ ·C ₇ H ₈
FW	336.5	336.5	1024.1	1119.7
<i>T</i> (K)	293	120	120	120
Crystal system	Monoclinic	Monoclinic	Monoclinic	Triclinic
Space group (no.)	<i>P</i> 2 ₁ / <i>n</i>	<i>P</i> 2 ₁	<i>P</i> 2 ₁ / <i>n</i>	<i>P</i> -1
<i>a</i> (Å)	11.9354(5)	10.5371(10)	14.566(1)	9.8917(8)
<i>b</i> (Å)	12.8695(5)	8.5080(8)	10.364(1)	10.813(1)
<i>c</i> (Å)	12.7849(5)	11.2311(11)	16.089(1)	12.575(1)
α (°)	90.00	90.00	90.00	96.18(1)
β (°)	104.46(2)	113.17(1)	98.69(1)	95.34(1)
γ (°)	90.00	90.00	90.00	113.42(1)
<i>U</i> (Å ³)	1901.6(1)	925.65(15)	2400.9(3)	1213.3(2)
<i>Z</i>	4	2	2	1
<i>D</i> _x (Mg cm ⁻³)	1.175	1.207	1.417	1.532
μ (mm ⁻¹)	0.17	0.18	0.84	1.09
Refls measured	7603	8582	32449	13934
unique, <i>R</i> _{int} , %	4331, 1.7	4479, 2.9	6999, 4.1	5556, 8.7
Refls with <i>I</i> ≥ 2σ(<i>I</i>)	2486	6120	5988	2963
<i>R</i> ₁ , w <i>R</i> ₂ , %	3.8, 10.4	3.8, 8.1	2.9, 7.8	4.9, 9.9

Table 8. Selected bond lengths and angles of the C₂ chiral thioureas and its palladium complexes.

Bond distances (Å)	L(<i>rac</i>)	L(S,S)	<i>trans-meso</i>-Pd	<i>meso</i>-Pd₂
Pd-S			2.3160(4)	2.3055(14)
Pd-S'			2.3160(4)	2.2956(13)
Pd-Cl(1)			2.3184(4)	2.3104(14)
Pd-Cl(2)			2.3184(4)	2.3132(15)
C(2)-S	1.6570(15)	1.661(2)	1.6944(16)	1.748(5)
C(2)-N(1)	1.367(2)	1.375(2)	1.351(2)	1.334(6)
C(2)-N(3)	1.382(2)	1.364(2)	1.355(2)	1.338(6)
N(1)-C(11)	1.434(2)	1.442(2)	1.439(2)	1.449(6)
N(3)-C(21)	1.430(2)	1.440(2)	1.428(2)	1.442(7) ^a 1.448(8) ^b
Angles (deg)				
Cl(1)-Pd-S			89.93(2)	91.47(5)
Cl(2)-Pd-S'			89.93(2)	90.98(5)
Cl(2)-Pd-S			90.07(2)	172.60(6)
Cl(1)-Pd-S'			90.07(2)	170.84(5)
Cl(1)-Pd-Cl(2)			180	93.71(5)
S-Pd-S'			180	84.64(5)
Pd-S-Pd'			-	95.36(5)
Pd-S-C(2)			105.05(5)	104.2(2)
Pd'-S-C(2)			-	108.6(2)
C-N(1)-C, mean	118.3	114.7	118.4	119.4
C-N(3)-C, mean	117.4	116.75	119.5	118.7 ^a , 120 ^b

^a major, ^b minor positions of disordered moieties.

Table 9. The torsion angles and the angles between planes in **L(S,S)**, **L(rac)**, *trans-meso-Pd* and *meso-Pd*₂.

Torsion angles (deg)	L(rac)	L(S,S)	<i>trans-meso-Pd</i>	<i>meso-Pd</i> ₂
Cl(1)-Pd-S-C(2)			-51.19(5)	-61.0(2)
Pd-S-C(2)-N(1)			143.8(1)	131.0(4)
Pd-S-C(2)-N(3)			-37.7(2)	-46.5(4)
S-C(2)-N(1)-C(11)	15.8(2)	-22.0(2)	10.5(2)	-3.5(7)
S-C(2)-N(3)-C(21)	13.7(2)	-15.6(0)	0.8(2)	-19.2(9), ^a 5(1) ^b
C(2)-N(1)-C(11)-C(12)	-92.7(2)	114.7(2)	-88.1(2)	110.4(6)
C(2)-N(3)-C(21)-C(22)	-76.1(2)	94.2(2)	-67.0(2)	111.7(9), ^a -99(4) ^b
N(3)-C(4)-C(5)-N(1)	-37.7(1)	35.59(16)	-36.8(1)	23.6(6)
Distance from plane <i>i</i> , (Å)				
C(4)	-0.40	0.26	-0.32	0.11
C(5)	0.23	0.35	0.31	-0.27
C(11)	0.31	0.40	0.24	-0.11
C(21)	-0.31	0.31	0.01	0.33, ^a -0.15 ^b
Interplanar angles (deg): <i>i/ii</i>	82.6	82.63	82.4	72.1
<i>i/iii</i>	66.6	82.69	65.2	79.2, ^a 88.1 ^b
<i>i/Pd</i>	-	-	67.9	85.6
<i>iii/Pd</i>	-	-	17.4	12.0, ^a 11.3 ^b
Interplanar gap (Å), <i>iii/iii'</i>	-	-	6.33	6.13, ^a 6.05 ^b

Planes: *i* through S, C(2), N(1), N(2); *ii* through C(11) to C(16); *iii* through C(21) to C(26); *iii'* through C(21') to C(26'); *Pd* – coordination plane of Pd (for monomers) or Pd₂S₂ plane (for dimers), ^a major, ^b minor positions of disordered moieties.

In comparison to the crystal structure of **L(S,S)**, the ligands show a more symmetric conformation of the imidazole ring (the C(4) and C(5) atoms are displaced from the SC(2)N(1)N(3) plane by -0.32 and 0.31 Å in **meso-Pd** and 0.26 and -0.35 Å in **L(S,S)**). The dihedral angles of both tolyl groups to the imidazole of the ligand in **trans-meso-Pd** are very similar to those observed in the structure of **L(rac)** (82.4° and 65.2° in **trans-meso-Pd**, 82.6° and 66.6° in **L(rac)**). However, whilst one of these angles is similar to that observed in **L(S,S)** the other is significantly different (65.2° in **trans-meso-Pd** vs 82.7° in **L(S,S)**).

The C=S bond length in **trans-meso-Pd** is 1.6944(16) Å which is *ca.* 0.03 Å longer than those in the free ligands (1.6570(15) and 1.661(2) Å for **L(rac)** and **L(S,S)**, respectively). The Pd center is sandwiched between tolyl rings. The interplanar separation between these tolyl rings (6.33 – 6.40 Å) is shorter than twice the thickness of an aromatic molecule (3.4 Å).

Dimeric palladium complex

The molecular structure of **meso-Pd₂** was confirmed by single-crystal X-ray diffraction on crystals obtained from the slow evaporation of a solution of **rac-Pd₂** / **meso-Pd₂** in toluene. It crystallizes in the triclinic space group *P*-1 with 0.5 molecules of **meso-Pd₂** and 0.5 molecules of toluene solvate in the asymmetric unit. One of the tolyl groups is disordered over two positions, with a 3:1 occupancy ratio, which differ by a *ca.* 19° tilt of the C–N bond and a rotation about this bond of *ca.* 167°. The disorder is purely conformational and does not involve any of the asymmetric atoms. The molecular structure of **meso-Pd₂** is shown with minor disordered positions and solvate molecules omitted in Figure 30, and with solvate molecules included and the minor disordered positions shown with open bonds in Figure 31. The structure of **R,R-Pd₂** has also been solved previously from X-ray diffraction by Dr. Albesa Jové on a crystal grown by Ms. J. Liu in our group. It crystallizes in the monoclinic space group *P*2₁ with 0.5 molecules in the asymmetric unit. The molecular structure of **R,R-Pd₂** is shown in Figure 32 for comparison.

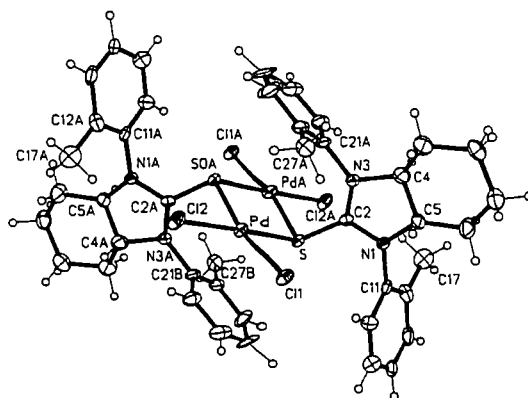


Figure 30. The molecular structure of *meso*-Pd₂ with solvate molecules and minor disordered positions omitted for clarity.

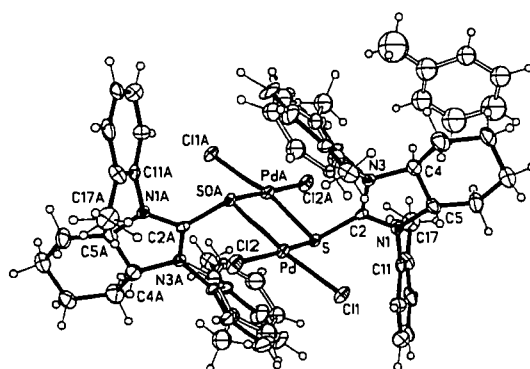


Figure 31. The molecular structure of *meso*-Pd₂ with the toluene solvate molecule and minor disordered positions shown with open bonds.

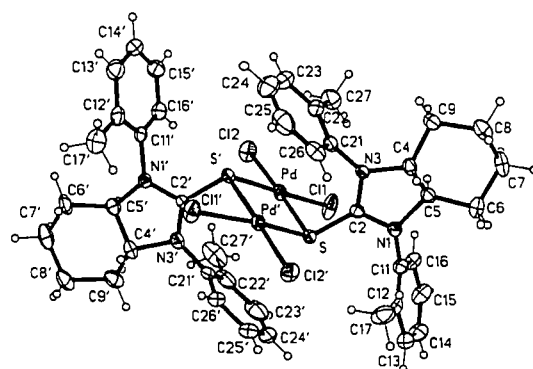


Figure 32. The molecular structure of *R,R*-Pd₂.

The center of the *meso*-Pd₂ molecules lie on a crystallographic inversion center. The chloride ligands are terminal, whereas the sulfur atoms are bridging in an almost symmetrical fashion, and have a substantially pyramidalised geometry. In contrast with *trans-meso*-Pd, the square planar coordination about the Pd centers is *cis* and there are significant tetrahedral distortions (the dihedral angle between the

SPdS(0A) and Cl(1)PdCl(2) planes is 10°). The thioureas have an *exo* conformation in contrast to **Pd₂(tmtu)**. The Pd centers are sandwiched between two tolyl moieties, similar to *trans-meso-Pd*, but at even shorter distances, *viz.* Pd...C(26A) = 3.02 Å or Pd...C(26B) = 3.00 Å. The C=S bond length is 1.748(5) Å which is *ca.* 0.1 Å longer than that in the ligand (1.661(2) and 1.6570(15) Å for **L(S,S)** and **L(rac)**, respectively). The lengthening of this bond is accompanied by a shortening of the adjacent C(2)–N bonds (*ca.* 1.33 Å in *trans-meso-Pd₂* vs 1.37 – 1.38 Å in **L(S,S)** and **L(rac)**).

II.2.3.B) NMR Characterization of palladium complexes

Monomeric palladium complex

The ^1H and $^{13}\text{C}\{^1\text{H}\}$ NMR spectra in CD_2Cl_2 at room temperature and -60°C of *rac-Pd* / *meso-Pd* (obtained shortly after the solution was prepared) show very complicated signals even at -60°C (Figures 33 and 34 show ^1H and $^{13}\text{C}\{^1\text{H}\}$ NMR spectra at -60°C and Figures A19 and A20 in Appendix A show the ^1H and $^{13}\text{C}\{^1\text{H}\}$ NMR spectra at room temperature).

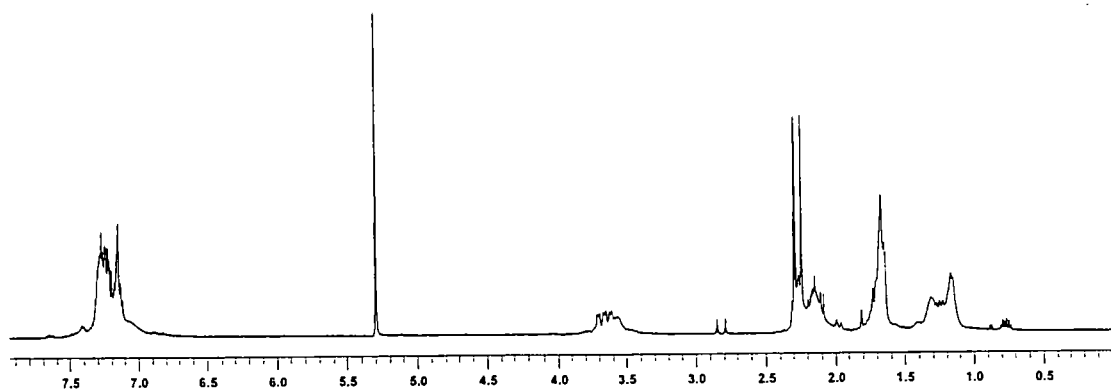


Figure 33. The ^1H NMR (500 MHz, CD_2Cl_2 , -60°C) spectrum of *rac-Pd* / *meso-Pd*.

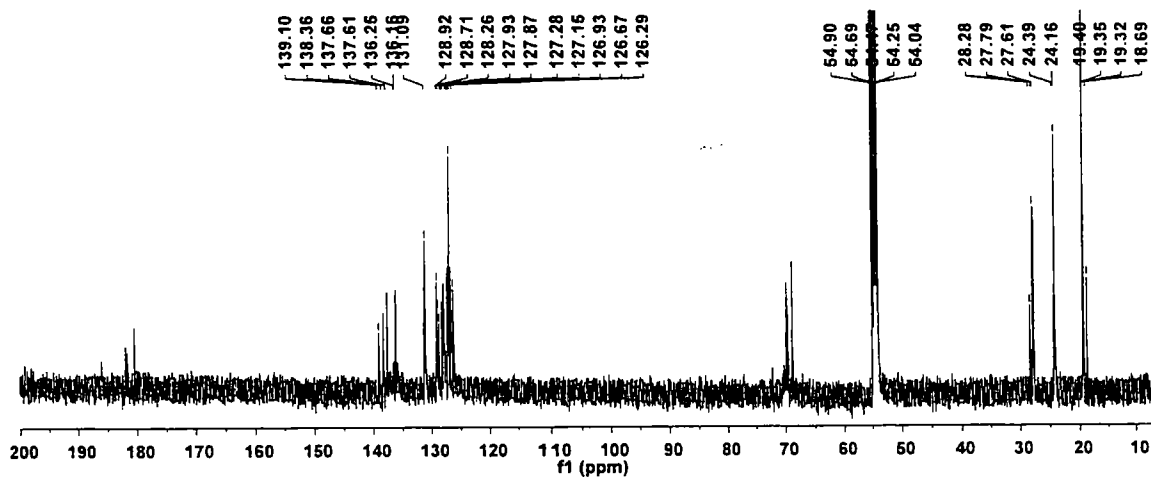


Figure 34. The $^{13}\text{C}\{^1\text{H}\}$ NMR (125 MHz, CD_2Cl_2 , $-60\text{ }^\circ\text{C}$) spectrum of *rac*-Pd/*meso*-Pd.

Although the $^{13}\text{C}\{^1\text{H}\}$ spectra are very complicated, resonances for C3 can be readily identified. The $^{13}\text{C}\{^1\text{H}\}$ resonance of C=S at room temperature is very weak even in concentrated solutions which were run for 3 h, but the C3 signal can be assigned (δ 70 – 71 ppm). Interestingly, the $^{13}\text{C}\{^1\text{H}\}$ spectrum at $-60\text{ }^\circ\text{C}$ of *rac*-Pd / *meso*-Pd shows four signals for the C=S carbons (Figure 34 and the expanded spectrum in Figure 35) and three for the ones at C3. As the *cis*- and *trans*- isomers of other thiourea palladium complexes are known in the literature,^{65, 79} the four C=S signals (182.01, 181.89, 181.72 and 180.49 ppm) can be attributed to the *cis*- and *trans*- isomers of *rac*-Pd and *meso*-Pd. The fact that only three signals at 69.83, 69.68 and 68.91 ppm were observed for C3 suggests that two are overlapping. Clearly, in solution, the Pd–S bonds in this chiral thiourea palladium monomeric complex are weak as we observed both *cis*- and *trans*-isomers. Interconversion between the two is slow at $-60\text{ }^\circ\text{C}$. Presumably, the *trans*-isomers of the monomeric complex crystallizes more readily than the *cis*-isomer.

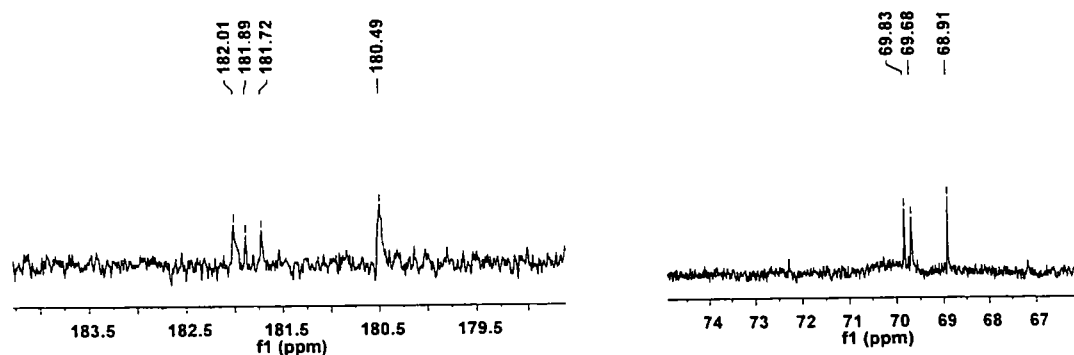


Figure 35. The $^{13}\text{C}\{^1\text{H}\}$ NMR (125 MHz) spectrum of *rac*-Pd / *meso*-Pd in CD_2Cl_2 at $-60\text{ }^\circ\text{C}$ in the C=S (left) and C3 (right) region.

Dimeric palladium complex

The NMR spectra of the dimeric palladium complexes reveal a distinct dependence on the solvent and temperature as illustrated in Figures A22 – A24 in Appendix A. CD_2Cl_2 was chosen for the low temperature spectra, as the resolution is much higher at low temperatures, and the higher boiling point TCE- d_2 for the high temperature solution NMR studies.

The optically pure **S,S-Pd₂** (Figure 36) and **R,R-Pd₂** were characterized by ^1H and $^{13}\text{C}\{^1\text{H}\}$ NMR spectroscopy at $-60\text{ }^\circ\text{C}$ in CD_2Cl_2 . Both, of course, display identical NMR spectra. The proton and carbon signals of **S,S-Pd₂** in Figure 37, indicate that the complexes are C_2 symmetric molecules and, as there are two signals for the methyl groups in the ^1H and $^{13}\text{C}\{^1\text{H}\}$ spectra, that the two tolyl rings in each ligand are nonequivalent (see Figures 37 and 38 for ^1H and $^{13}\text{C}\{^1\text{H}\}$ spectra of **S,S-Pd₂**, respectively). The C=S signals at $-60\text{ }^\circ\text{C}$ for the dimers (δ 172 ppm) are shifted to higher field compared to the ligand (δ 187 ppm) and the monomer (δ ca. 180 ppm).

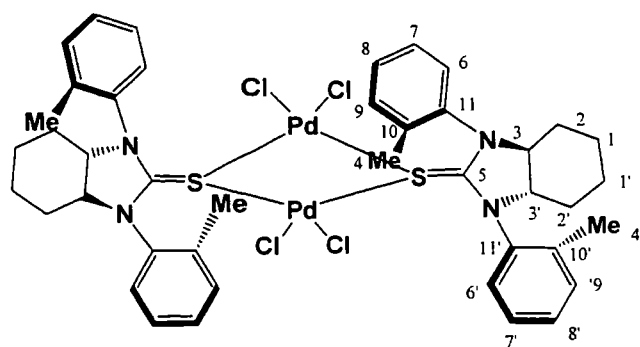


Figure 36. The structure of **S,S-Pd₂**.

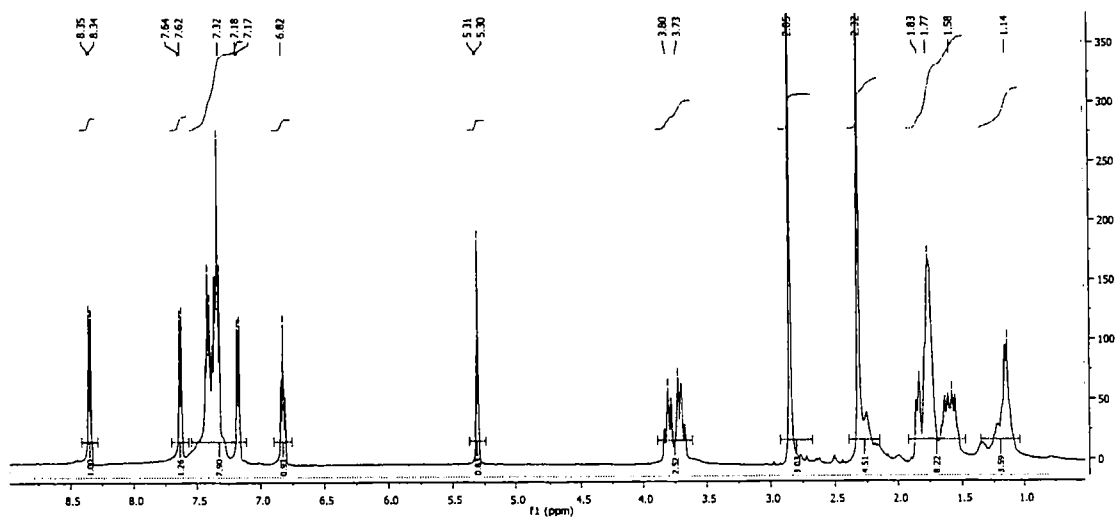


Figure 37. The ^1H NMR spectrum (500 MHz, CD_2Cl_2 , -60°C) of S,S-Pd_2 .

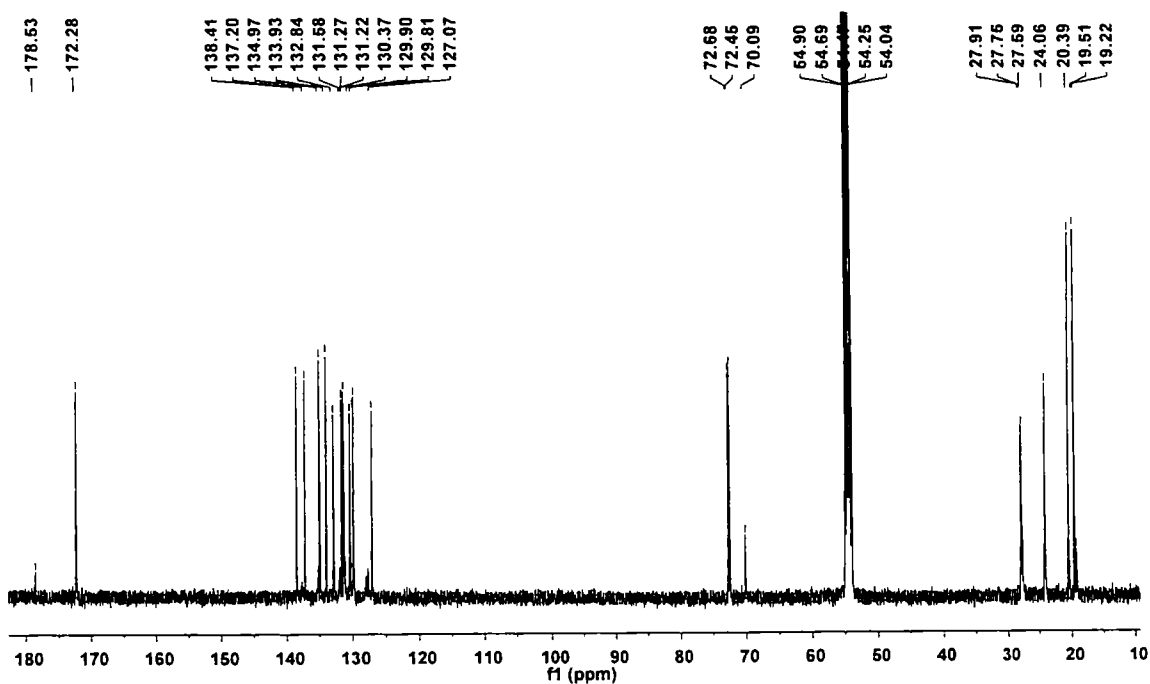


Figure 38. The $^{13}\text{C}\{^1\text{H}\}$ NMR (500 MHz, CD_2Cl_2 , -60°C) spectrum of S,S-Pd_2 .

2D NMR spectroscopy was used to assign the other ^1H and $^{13}\text{C}\{^1\text{H}\}$ resonances of **S,S-Pd₂** and **R,R-Pd₂**. One Me (H4) signal shows NOESY correlation with one proton in the aromatic region identified as H9. COSY was then used to assign H6, H7 and H8 from H9 (Figure 39). HSQC and HMBC correlations were used to assign the carbons (see Figures A28 – A30 in Appendix A for more details).

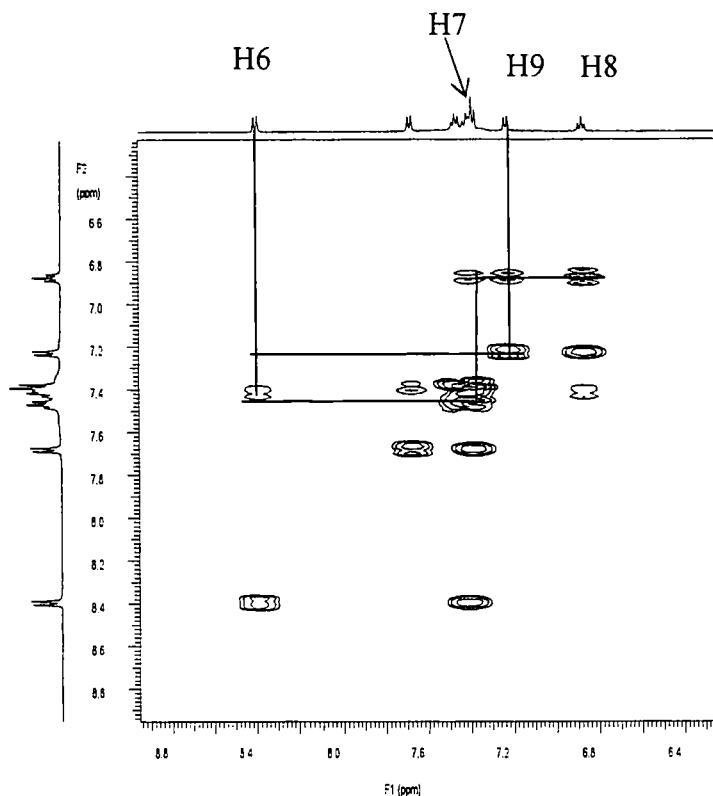


Figure 39. The COSY spectrum (CD_2Cl_2 , $-60\text{ }^\circ\text{C}$) of the aromatic region of **S,S-Pd₂**.

With the NMR signals of **S,S-Pd₂** and **R,R-Pd₂** assigned, peaks for *meso*-**Pd₂** in the NMR spectrum of *rac*-**Pd₂** / *meso*-**Pd₂** can be identified, and are marked with asterisks in Figure 40 for ^1H and Figures 41 – 43 for $^{13}\text{C}\{^1\text{H}\}$, respectively. The ^1H and $^{13}\text{C}\{^1\text{H}\}$ resonances of *rac*-**Pd₂** and *meso*-**Pd₂** are listed in Table 10.

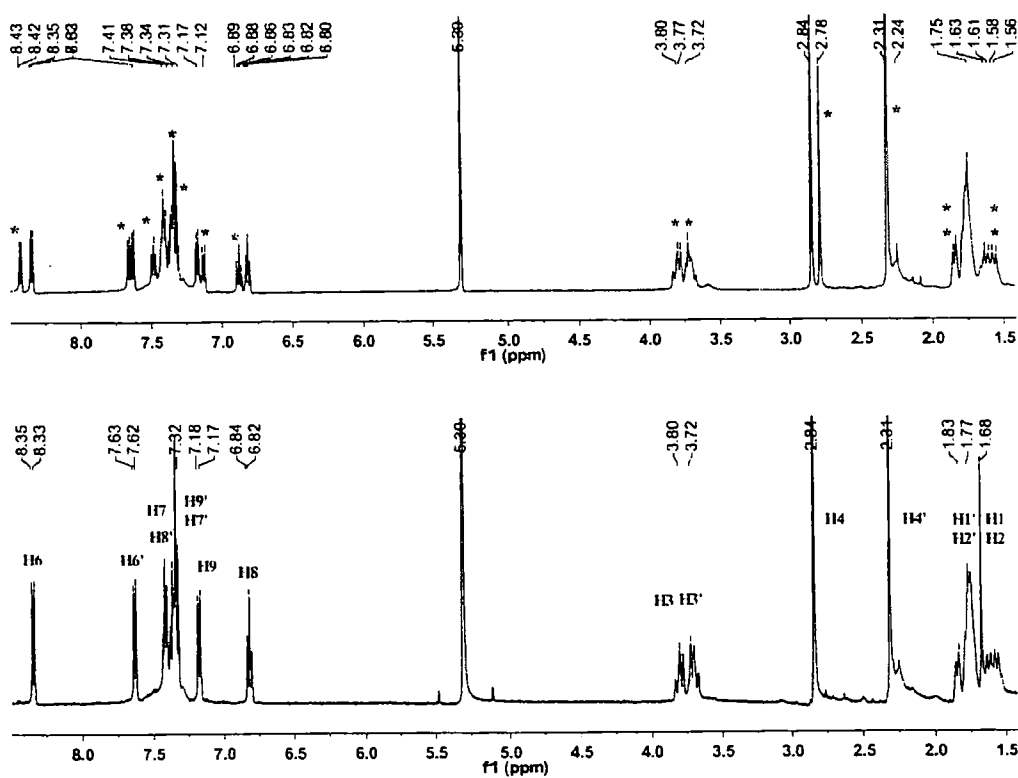


Figure 40. The ^1H NMR (500 MHz, CD_2Cl_2 , -60°C) spectra of S,S-Pd_2 (bottom) and $\text{rac-Pd}_2 / \text{meso-Pd}_2$ (top); * = meso-Pd_2 signals.

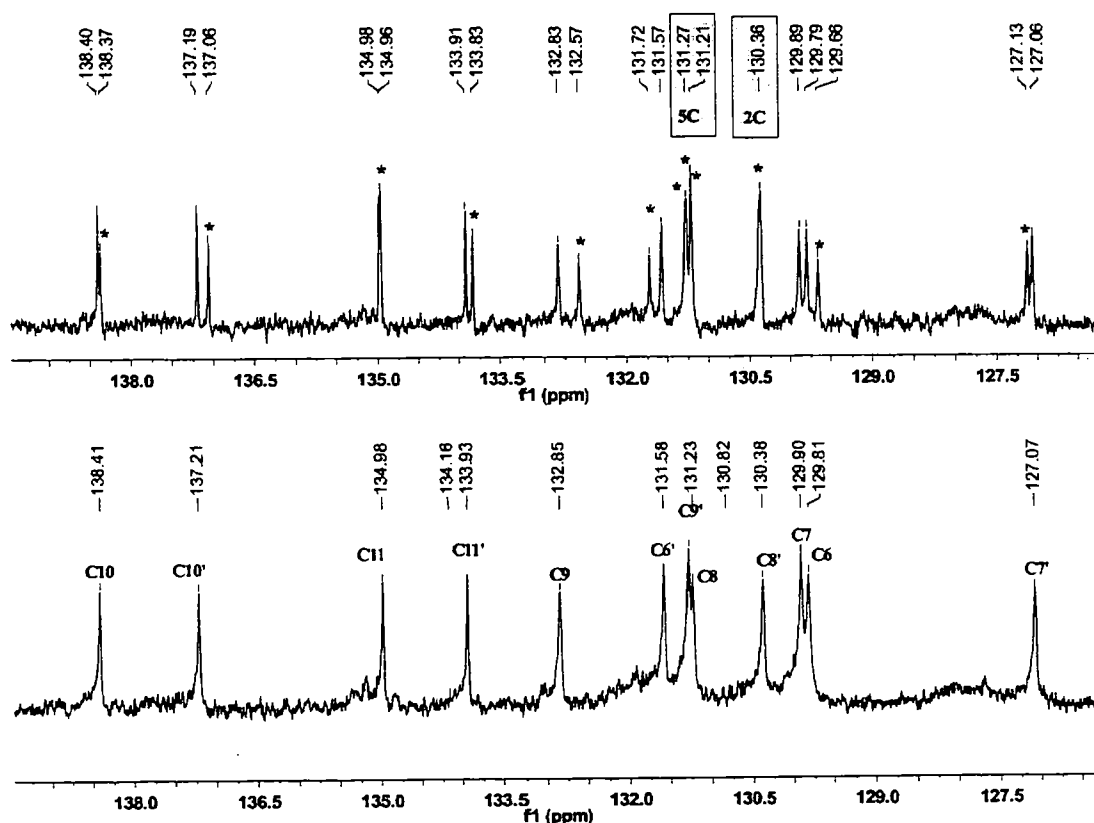


Figure 41. The $^{13}\text{C}\{^1\text{H}\}$ NMR (125 MHz, CD_2Cl_2 , -60°C) spectra of the aromatic region of S,S-Pd_2 (bottom) and $\text{rac-Pd}_2 / \text{meso-Pd}_2$ (top); * = meso-Pd_2 signals.

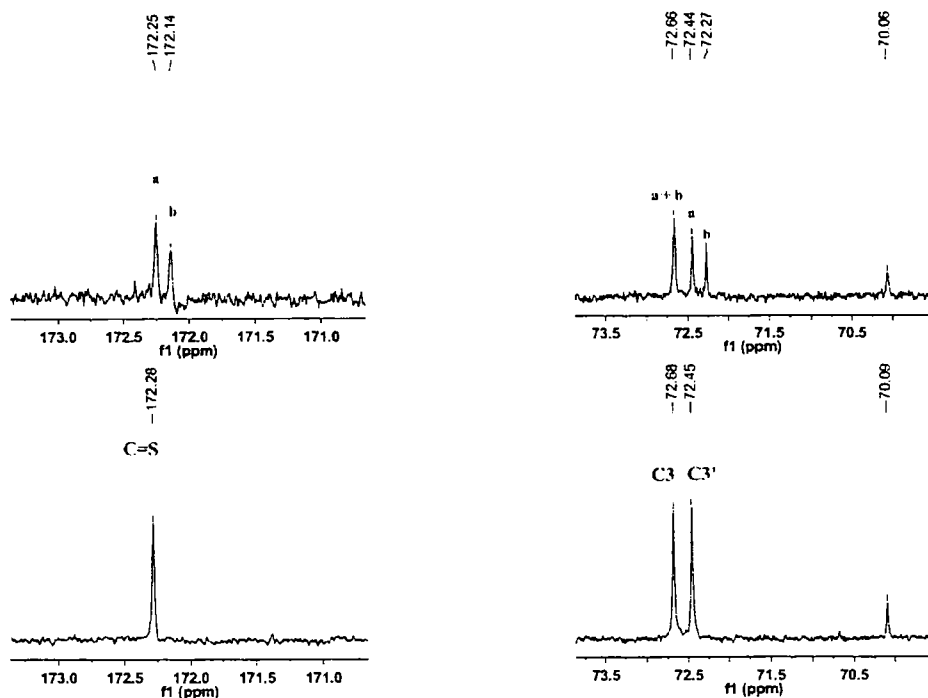


Figure 42. The $^{13}\text{C}\{^1\text{H}\}$ NMR (125 MHz, CD_2Cl_2 , -60°C) spectra showing the C=S and C3 signals of $S,S\text{-Pd}_2$ (bottom) and $rac\text{-Pd}_2 / meso\text{-Pd}_2$ (top); $a = rac\text{-Pd}_2$; $b = meso\text{-Pd}_2$ signals.

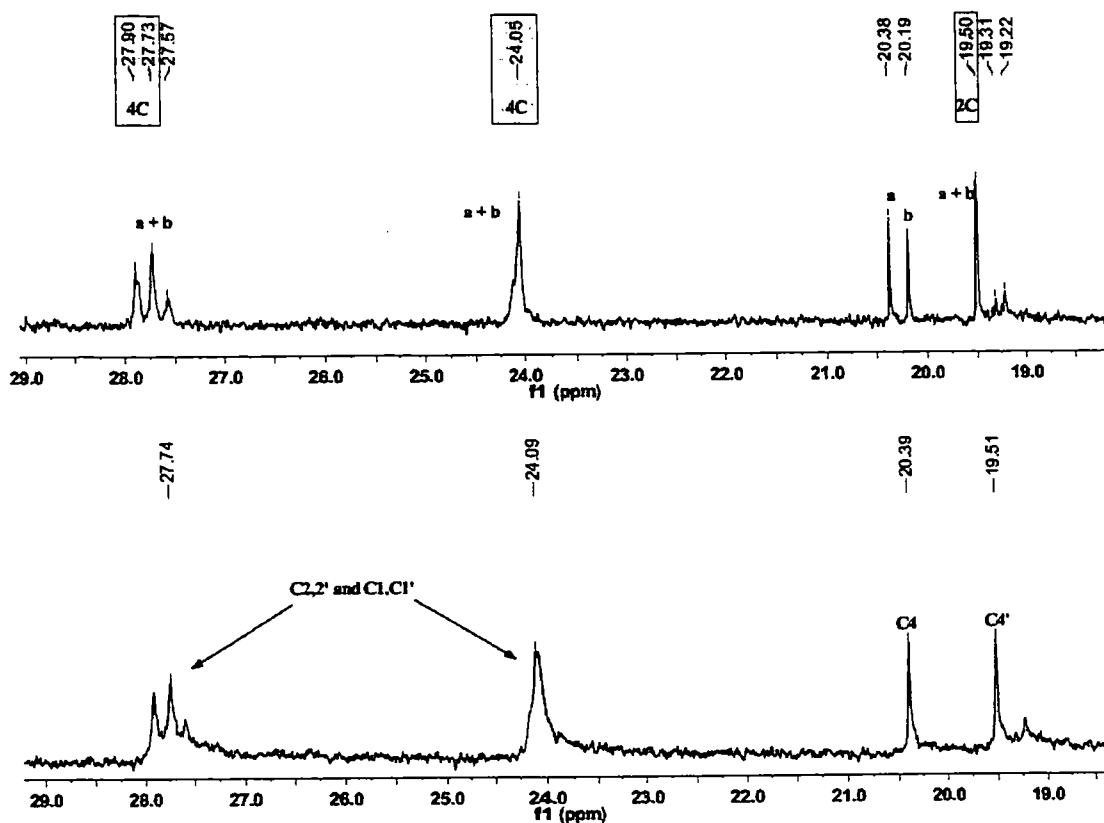


Figure 43. The $^{13}\text{C}\{^1\text{H}\}$ NMR (125 MHz, CD_2Cl_2 , -60°C) spectra of the aliphatic region of S,S-Pd_2 (bottom) and rac-Pd_2 / meso-Pd_2 (top); $a = \text{rac-Pd}_2$; $b = \text{meso-Pd}_2$ signals.

Additional, C=S signal at 178.53 ppm and C3 signal at 70.09 ppm (see Figures 38 and 42) which appear in the $^{13}\text{C}\{^1\text{H}\}$ NMR spectrum of S,S-Pd_2 cannot be identified. These signals will be discussed later.

Table 10 (continued)

^1H	<i>rac</i> -Pd ₂	<i>meso</i> -Pd ₂	$^{13}\text{C}\{^1\text{H}\}$	<i>rac</i> -Pd ₂	<i>meso</i> -Pd ₂
H3'	3.70 (t, J = 4, 2H)	3.67 – 3.74 ^a (m, 2H)	C8	131.22	131.21 ^a
H4'	2.32 (s, 6H)	2.31 ^a (s, 6H)	C9	132.84	132.57
H6'	7.63 (d, J = 8, 2H)	7.66 (d, J = 8, 2H)	C10	138.41	138.37
H7'	7.32 – 7.38 (m, 2H)	7.31 – 7.50 ^a (m, 2H)	C11	134.98	134.96
H8'	7.42 (t, J = 8, 2H)	7.54 (t, J = 8, 2H)	C3'	72.45	72.27
H9'	7.32 – 7.38 (m, 2H)	7.31 – 7.50 ^a (m, 2H)	C4'	19.51	19.50 ^a
			C6'	131.58	131.72
			C7'	127.07	127.13
			C8'	130.38	130.36 ^a
			C9'	131.28	131.27 ^a
			C10'	137.20	137.06
			C11'	133.93	133.83

* m = multiplet; d = doublet; t = triplet; the numbers in parentheses are coupling constants (Hz); xH = number of protons; ^a overlapped *rac*-Pd₂ and *meso*-Pd₂ signals.

II.2.4 NMR spectroscopic studies of chiral thiourea palladium complexes.

II.2.4.A) The variable temperature (VT) ^1H NMR study of dimeric palladium complexes

The temperature and solvent dependence of the ^1H and $^{13}\text{C}\{^1\text{H}\}$ NMR spectra of the palladium thiourea complexes suggested the presence of dynamic behavior. For this reason, ^1H NMR measurements of *rac*-**Pd**₂ / *meso*-**Pd**₂ in TCE-d₂ at 0, 10, 20, 30, 40, 50, 60, 70, 80, 90 and 100 °C were carried out. Similarly, ^1H NMR spectra of *rac*-**Pd**₂ / *meso*-**Pd**₂ in CD₂Cl₂ at -80, -70, -60, -50, -40, -30 and 25 °C were also obtained. CD₂Cl₂ were used as the solvent because it allows low-temperature measurements to be made above -85 °C and TCE-d₂ was used for high-temperature measurements. The expanded spectra in the CH₃ region (H4 and H4') at low and high temperature are displayed in Figures 44 and 45, respectively (The full spectra are shown in Figures A41 and A42 in Appendix A, respectively).

At -80 °C (Figure 44), the two CH₃ (H4 and H4') signals of *meso*-**Pd**₂ appear at 2.75 and 2.29 ppm and the two CH₃ signals of *rac*-**Pd**₂ at 2.82 and 2.29 ppm are clearly distinguishable although two of the CH₃ signals are coincident at 2.29 ppm. Upon increasing the temperature, the signals are broad.

^1H NMR spectra in TCE-d₂ at various temperatures (Figure 45) reveal the best separation of the diastereomer signals at 20 °C which suggests that the exchange is slow at this temperature. Upon increasing the temperature, the two CH₃ signals of both *meso*-**Pd**₂ and *rac*-**Pd**₂ coalesce at 70 °C.

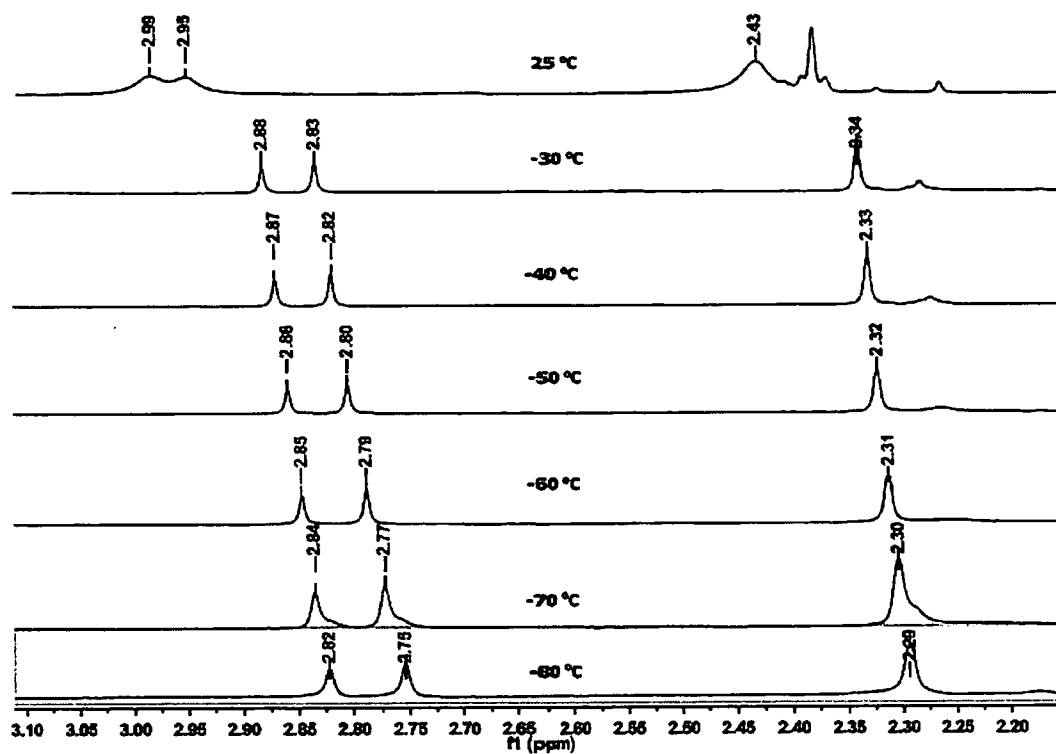


Figure 44. The ^1H NMR (500 MHz) of the aliphatic region of $\text{rac-Pd}_2 / \text{meso-Pd}_2$ in CD_2Cl_2 at various temperatures.

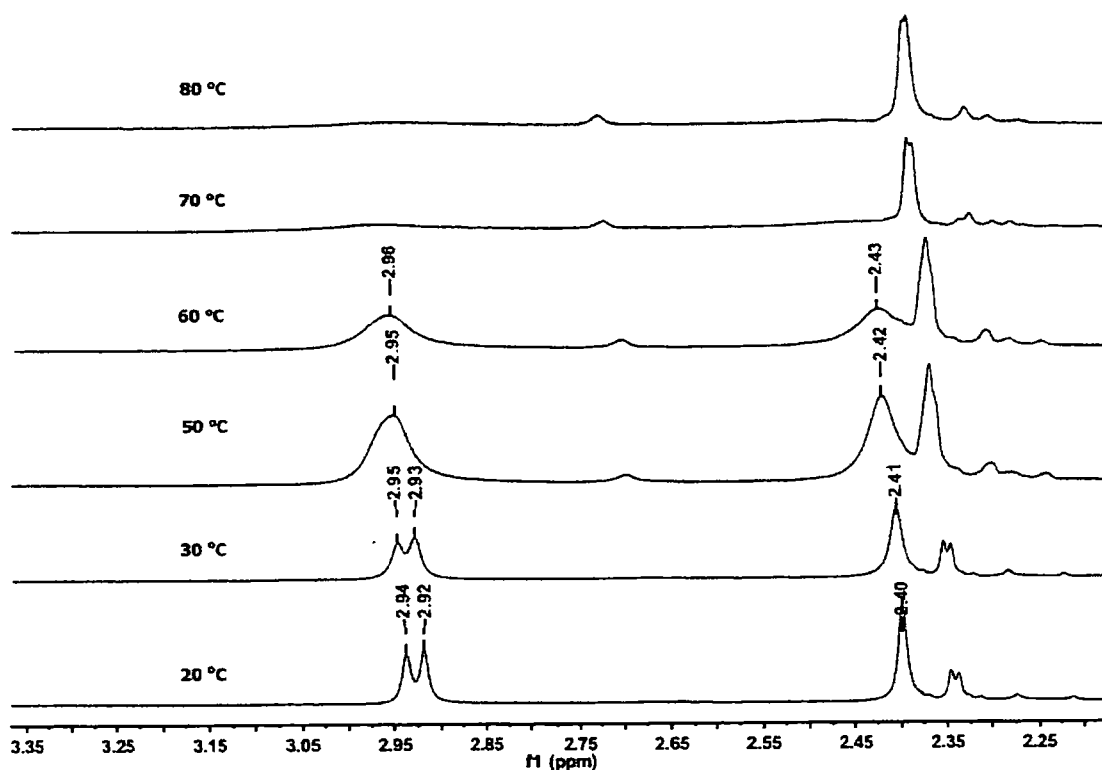


Figure 45. The ^1H NMR (500 MHz) of the aliphatic region of *rac*- Pd_2 / *meso*- Pd_2 in TCE-d_2 at various temperatures.

The energy barrier, ΔG^\ddagger of the exchange process in TCE-d_2 of *rac*- Pd_2 / *meso*- Pd_2 from the signal of H4 (see Figure 46, scale in Hz) was calculated from the Eyring–Polanyi (eq. 1) equation^{108, 109} to be $66.25 \text{ kJ}\cdot\text{mol}^{-1}$ ($15.8 \text{ kcal}\cdot\text{mol}^{-1}$) and $66.15 \text{ kJ}\cdot\text{mol}^{-1}$ ($15.8 \text{ kcal}\cdot\text{mol}^{-1}$) for *meso*- Pd_2 and *rac*- Pd_2 , respectively (see below).

$$\Delta G^\ddagger = -RT \ln \left[\frac{kh}{k_B T} \right] \quad (\text{eq. 1})$$

$$k = \frac{\pi \Delta \nu}{\sqrt{2}} \quad (\text{eq. 2})$$

- | | |
|--|---|
| R = Gas constant | $= 8.314 \text{ J}\cdot\text{K}^{-1}\cdot\text{mol}^{-1}$ |
| k_B = Boltzmann constant | $= 1.380 \times 10^{-23} \text{ J}\cdot\text{K}^{-1}$ |
| h = Planck constant | $= 6.626 \times 10^{-34} \text{ J}\cdot\text{s}$ |
| T = Temperature at coalescence (K) ($70 \text{ }^\circ\text{C} = 343 \text{ K}$) | |

k = rate constant at the temperature of coalescence (s^{-1})

$\pi = 3.141$

$\delta\nu$ = chemical shift difference at no exchange (20 °C in TCE- d_2) (Hz) (271 Hz and 262 Hz for *rac*- Pd_2 and *meso*- Pd_2 , respectively)

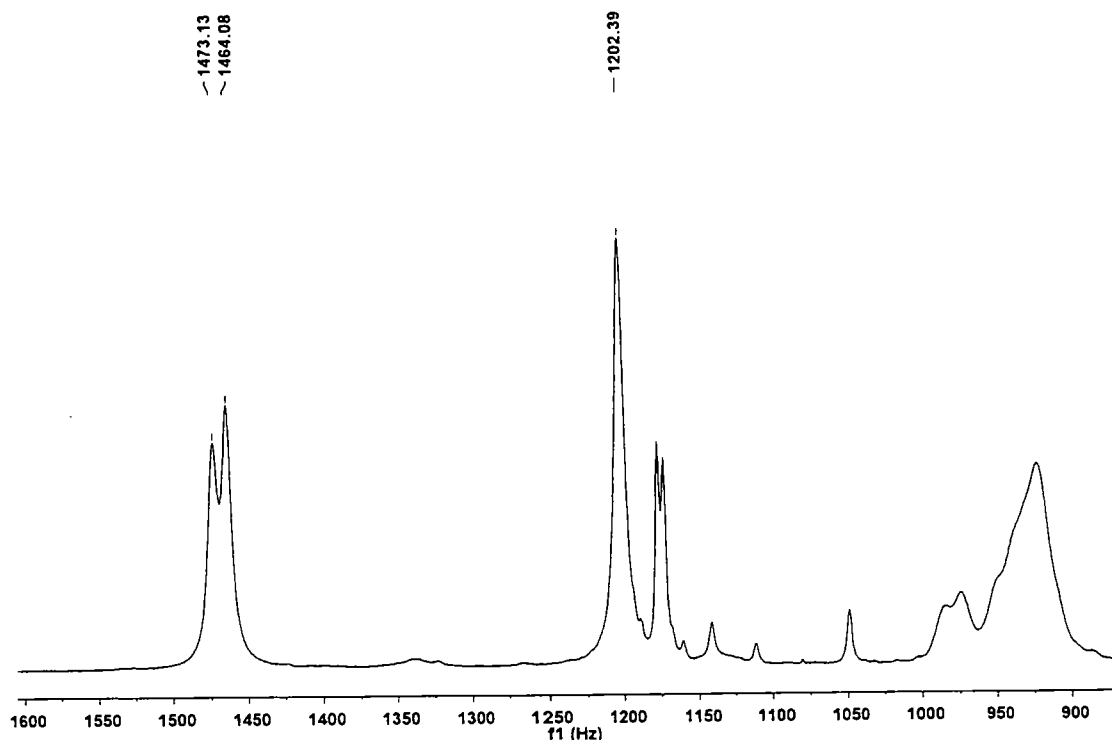


Figure 46. The 1H NMR (500 MHz) spectra in the aliphatic region of *rac*- Pd_2 / *meso*- Pd_2 in TCE- d_2 at no exchanging process 20 °C (scale in Hz).

The energies barrier of the exchanging process of both *rac*- Pd_2 and *meso*- Pd_2 are quite similar. To confirm the energies barrier in this system, the simulation of NMR spectra was carried out by Dr. Jason Lynam (York, UK). The thermodynamic values for the exchange process were calculated to be $\Delta H^\ddagger = 52.8 \pm 8.9 \text{ kJ}\cdot\text{mol}^{-1}$, $\Delta S^\ddagger = -48.8 \pm 29.9 \text{ kJ}\cdot\text{mol}^{-1}\cdot\text{K}^{-1}$ for *rac*- Pd_2 and $\Delta H^\ddagger = 51.5 \pm 9.6 \text{ kJ}\cdot\text{mol}^{-1}$, $\Delta S^\ddagger = -54.9 \pm 32.0 \text{ kJ}\cdot\text{mol}^{-1}\cdot\text{K}^{-1}$ for *meso*- Pd_2 . The energy barrier ΔG^\ddagger at 20 °C of the exchange process is $15.4 \text{ kcal}\cdot\text{mol}^{-1}$, in good agreement with our previous calculations.

Interestingly, the VT NMR spectra of *rac*-Pd₂ / *meso*-Pd₂ in TCE-d₂, show new signals appearing at *ca.* 7.7 ppm and 8.2 ppm above 60 °C and also a substantial increase in signal intensity at δ 7.55 ppm (Figure 47). We postulate that new species are formed at these temperatures. Furthermore, at high temperatures (60, 70, 80, 90 and 100 °C), free ligand signals were detected as shown in Figure 48. A comparison between the NMR spectra in TCE-d₂ of *rac*-Pd₂ / *meso*-Pd₂ and L(*rac*) at 100 °C is displayed in Figure 49.

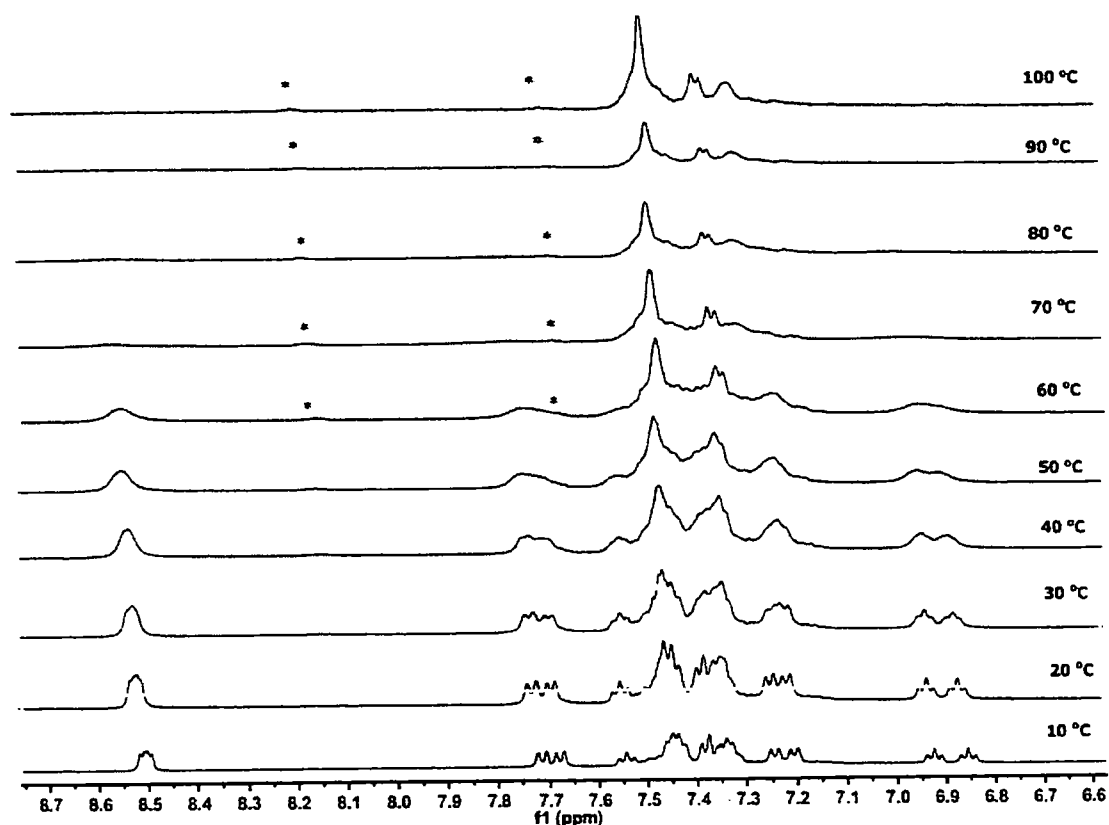


Figure 47. The ¹H NMR (500 MHz) spectra in the aromatic region of *rac*-Pd₂ / *meso*-Pd₂ in TCE-d₂ at various temperatures; * = unknown complex.

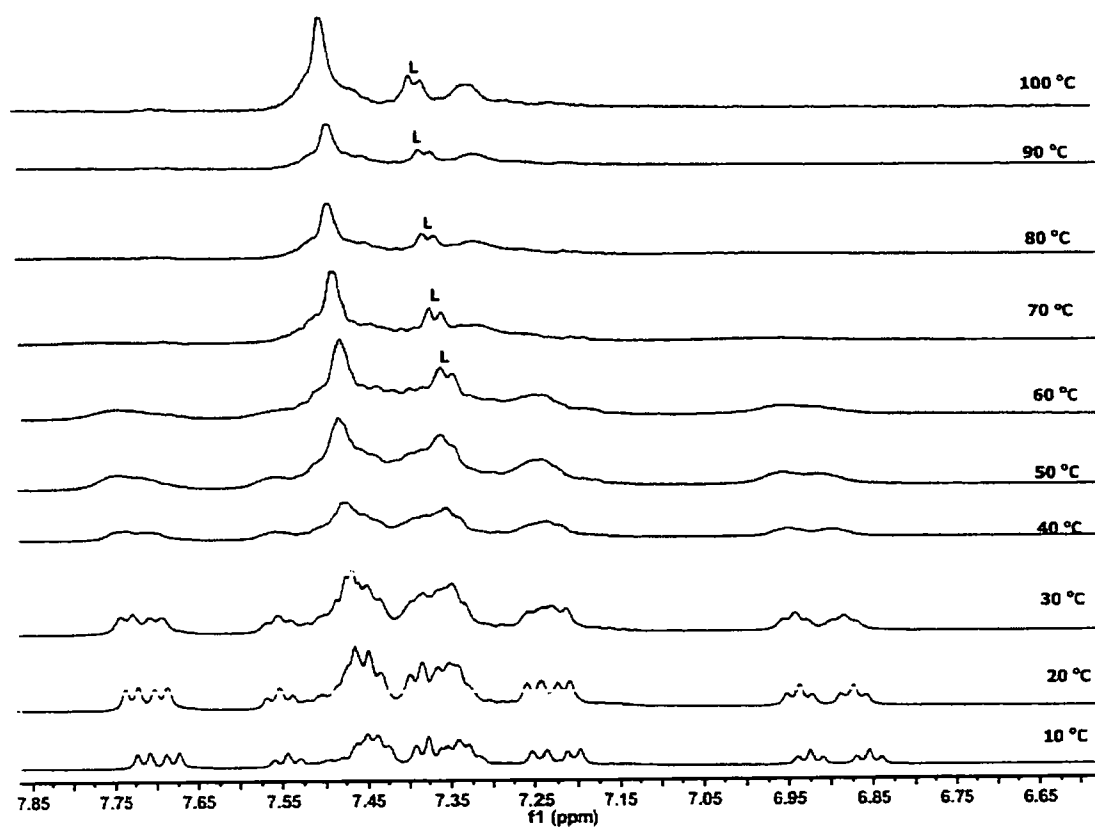


Figure 48. The ^1H NMR (500 MHz) spectra of *rac*- Pd_2 / *meso*- Pd_2 in TCE-d_2 at various temperatures; L= ligand.

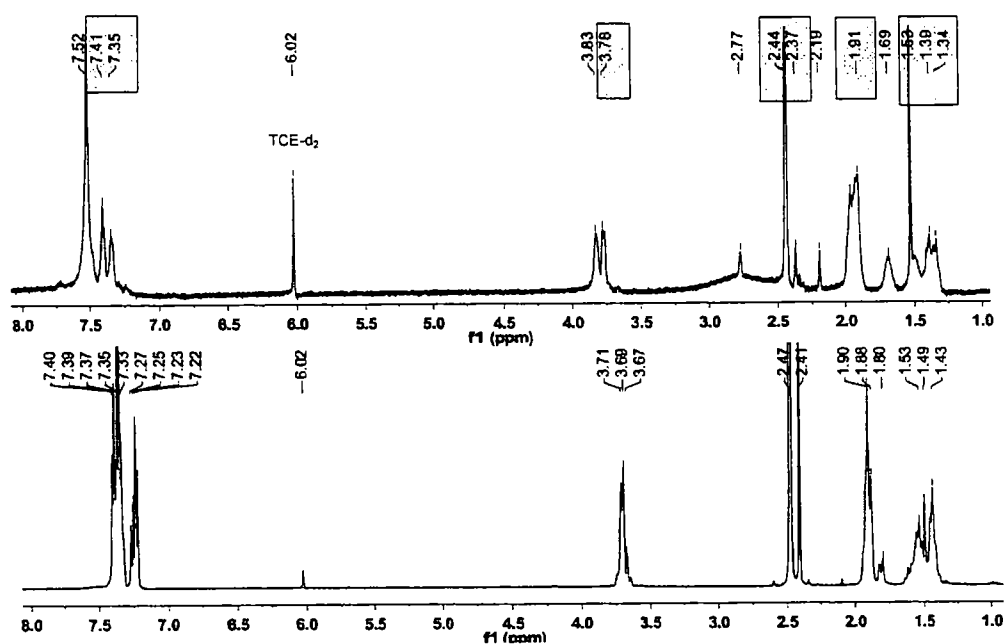


Figure 49. The ¹H NMR (500 MHz) spectra of *L(rac)* (bottom) and *rac-Pd*₂ / *meso-Pd*₂ (top) in TCE-d₂ at 100 °C.

The ¹H NMR spectra before and after the variable temperature measurement are shown in Figure 50. This shows an increase in the integral in the aromatic region (*ca.* 7.1 – 7.6 ppm) from *ca.* 8 prior to VT measurement to *ca.* 13 afterwards. This result suggests that some of the new species are formed irreversibly.

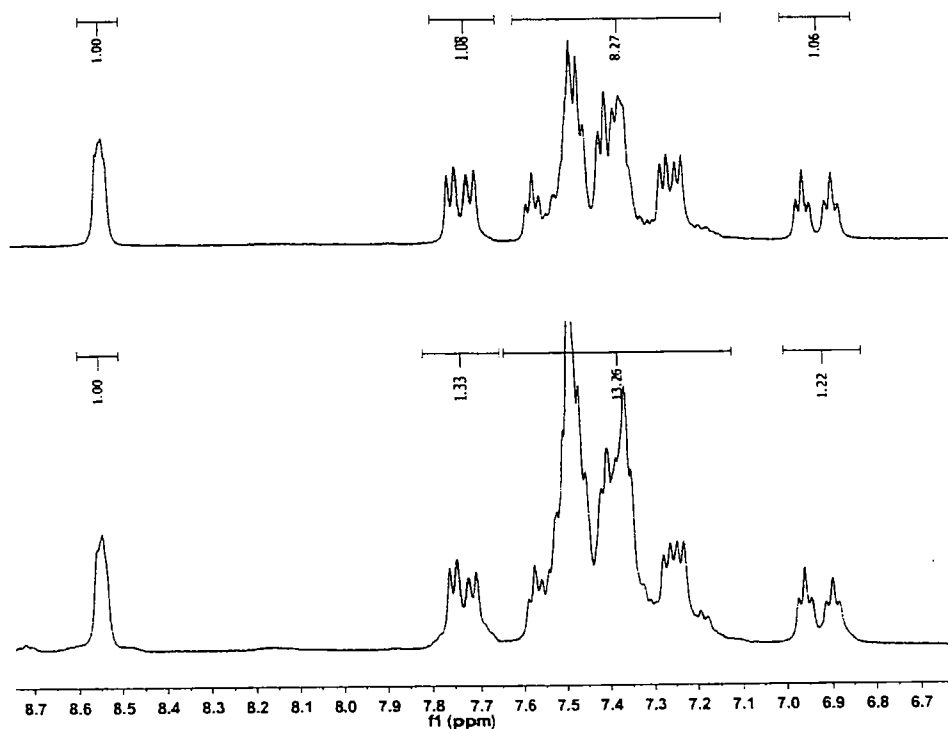


Figure 50. The ^1H NMR (500 MHz) spectra on the aromatic of *rac*- Pd_2 / *meso*- Pd_2 in TCE-d_2 at room temperature before (top) and after (bottom) heating to 100 $^\circ\text{C}$.

In our VT solution NMR studies, we found that other palladium species appear to be formed as discussed above. This observation made us investigate the original monomeric and dimeric complexes in considerably more detail (*vide infra*).

II.2.4.B) Monitoring of the reaction of PdCl_2 with $L(S,S)$ at 1:1 molar ratio

The reaction of $L(S,S)$ with PdCl_2 in a 1:1 ratio in CD_2Cl_2 was monitored by *in situ* $^{13}\text{C}\{^1\text{H}\}$ NMR spectroscopy at room temperature. The aim of this experiment was to detect an intermediate before the formation of the dimeric palladium complex. The $^{13}\text{C}\{^1\text{H}\}$ NMR spectrum after 6 h is shown in Figure 51. Two signals are observed at δ 70.79 and 70.59 ppm with a *ca.* 3.5:1 ratio of integrals, respectively, which can be attributed to the C3 carbon of *cis*- $\text{PdCl}_2(L(S,S)_2)$ *cis*-**S,S-Pd** and *trans*- $\text{PdCl}_2(L(S,S)_2)$ *trans*-**S,S-Pd**. The small shifts of the signal can be postulated to be caused by the concentration dependence of chemical shifts. Related *cis*- and *trans*- complexes of Pd are known with other thiourea ligands.^{18, 65} The C=S signals of both *cis*-**S,S-Pd** and *trans*-

S,S-Pd are overlapped at δ 182.44 ppm. The signals assigned to C=S carbons of *trans-rac*-Pd and *cis-rac*-Pd were at 182.01 and 181.89 ppm at -60 °C. The difference is probably due to temperature and concentration dependence of the chemical shifts. From this 1:1 PdCl₂ and L(*S,S*) *in situ* reaction experiment, clearly, the intermediates before the dimer was formed are the monomeric *cis*- and *trans*-isomers. A summary of the *in situ* NMR reaction of L(*S,S*) and PdCl₂ in CD₂Cl₂ is shown in Scheme 32.

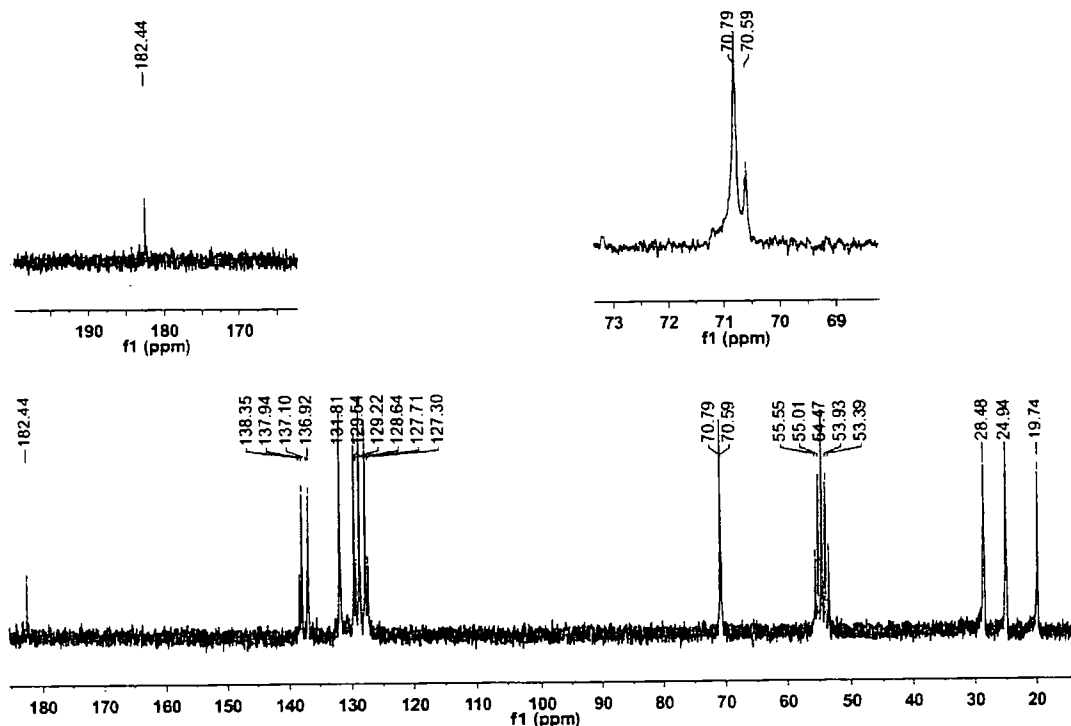
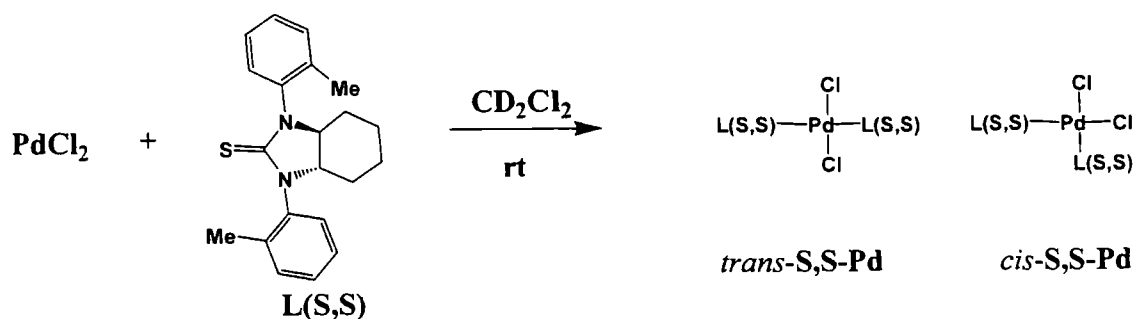


Figure 51. The ¹³C{¹H} NMR (100 MHz) spectrum of the reaction of PdCl₂ with L(*S,S*) in a 1:1 molar ratio in CD₂Cl₂ at room temperature after 6 h (bottom); the expanded C=S (top left) and C3 (top right) regions.



Scheme 32. The reaction of PdCl_2 with $\text{L}(\text{S,S})$.

II.2.4.C) Monitoring of the reaction of PdCl_2 with $\text{L}(\text{rac})$ at 1:1 molar ratio

An analogous *in situ* NMR reaction of $\text{L}(\text{rac})$ and PdCl_2 was carried out at room temperature and monitored by $^{13}\text{C}\{^1\text{H}\}$ NMR at room temperature (Figure 52). The aim of this experiment was the same as the previous experiment (*in situ* 1:1 reaction of PdCl_2 and $\text{L}(\text{S,S})$). From this experiment, we should be able to detect intermediate monomeric *cis*- and *trans*-isomer species, both from *rac*- and *meso*-monomer. The spectrum after 3 h shows four C=S and five C3 signals. The signals at δ 187.32 and 69.78 ppm were assigned to C=S and C3 carbons of the free ligand by comparison with the spectrum of $\text{L}(\text{rac})$. It is interesting that no free ligand signals were observed in the analogous reaction with $\text{L}(\text{S,S})$. The two signals at δ 70.84 and 70.65 ppm can be assigned to the C3 carbons, of course *trans*- and *cis-rac-Pd*, and that occurring at δ 182.50 ppm to the C=S carbons of these complexes. New peaks of the remaining C3 signals at δ 71.20 and 70.72 ppm and the C=S resonances at δ 183.61 and 183.25 ppm are postulated to belong to *trans*-[$\text{L}(\text{R,R})\text{L}(\text{S,S})\text{PdCl}_2$] *trans-meso-Pd* and *cis*-[$\text{L}(\text{R,R})\text{L}(\text{S,S})\text{PdCl}_2$] *cis-meso-Pd*. The differences in C=S peaks from the *rac-Pd* and *meso-Pd* spectrum (see Figure 34) can be explained from the temperature dependence of the chemical shifts, as the $^{13}\text{C}\{^1\text{H}\}$ NMR was carried out at -60 °C, whereas the *in situ* reaction was examined at room temperature. The $^{13}\text{C}\{^1\text{H}\}$ NMR at -60 °C of the *in situ* reaction was measured a considerable amount of time later in CD_2Cl_2 (Figure 53) and confirmed the temperature dependence of the C=S signals as they appear at δ 181.99, 181.90, 181.73 and 180.53 ppm which are almost the same as those observed at -60 °C in the spectrum of the isolated *rac-Pd* / *meso-Pd* complex (δ 182.01, 181.89, 181.72 and 180.49 ppm). The

signals from C3 observed at δ 69.81, 69.66 and 68.89 ppm in the *in situ* reaction also compare very well to those in *rac*-Pd / *meso*-Pd spectrum [cf. δ 69.83, 69.68, 68.91 ppm]. From this experiment, clearly, we not only detected the intermediate, *cis*- and *trans*-monomeric species, but also detected the dimer product (δ 172.27 and 172.16 ppm). The C=S signals for the free ligand (186.10 ppm) were also observed. The C=S signals at -60 °C in the spectrum of *L(rac)* is 186.16 ppm (see Table 6) and at 172.28 and 172.14 ppm in the spectrum of *rac*-Pd₂ / *meso*-Pd₂ (see Figure 35). Interestingly, there is also a broad signal in the C3 region which was not observed in the spectrum obtained at room temperature. The reaction of *L(rac)* with PdCl₂ in CD₂Cl₂ is shown in Scheme 33, and NMR assignments are given in Table 11.

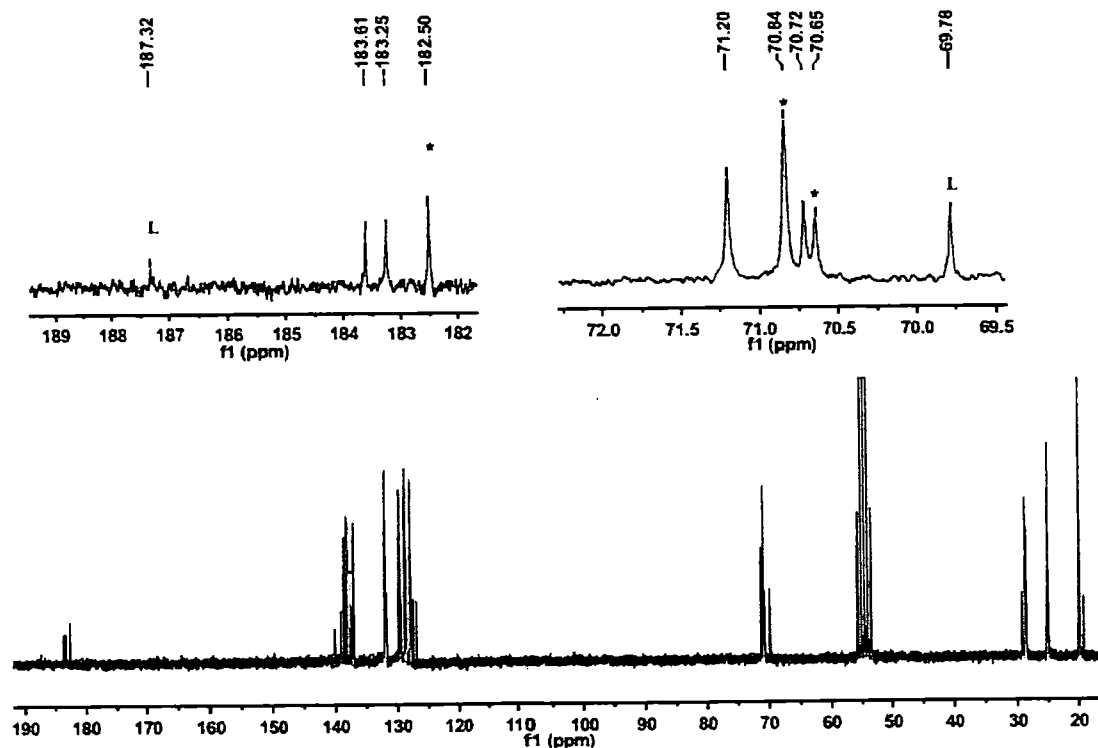


Figure 52. The *in situ* ¹³C{¹H} NMR (100 MHz) spectrum in CD₂Cl₂ of the reaction of PdCl₂ with *L(rac)* in a 1:1 molar ratio at room temperature after 3 h (bottom); and the expanded C=S (top left) and C3 region (top right); L = *L(rac)*; * = *trans-rac*-Pd and *cis-rac*-Pd.

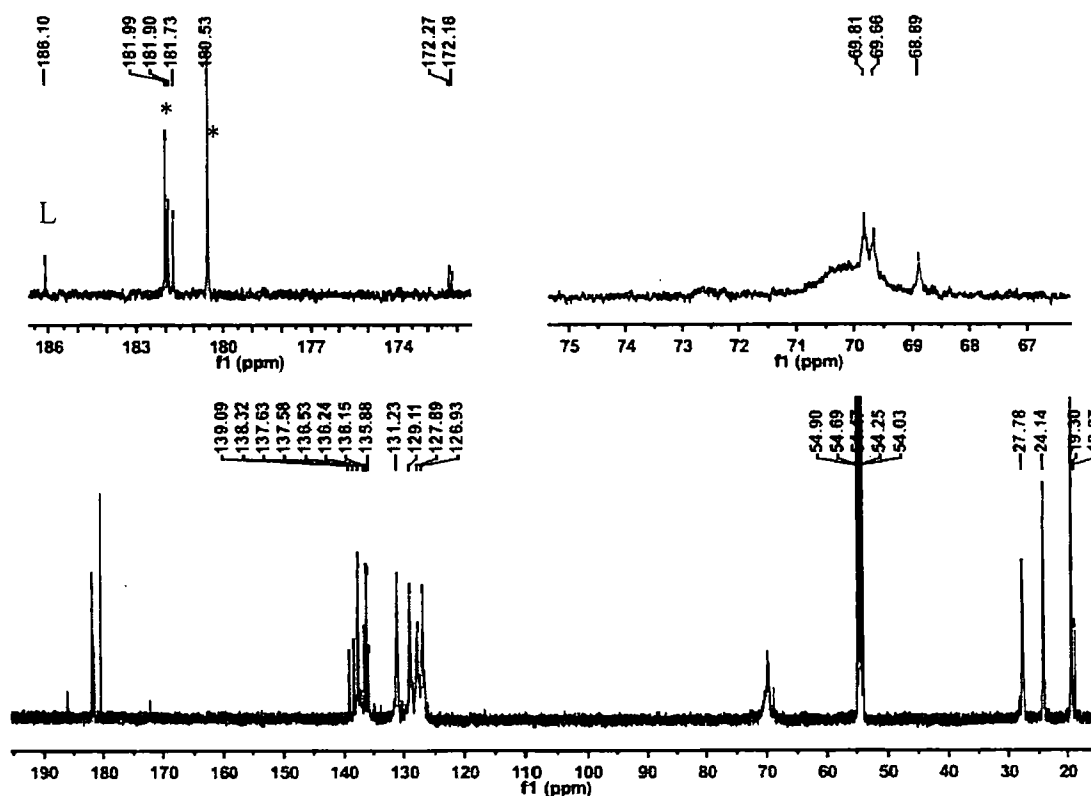
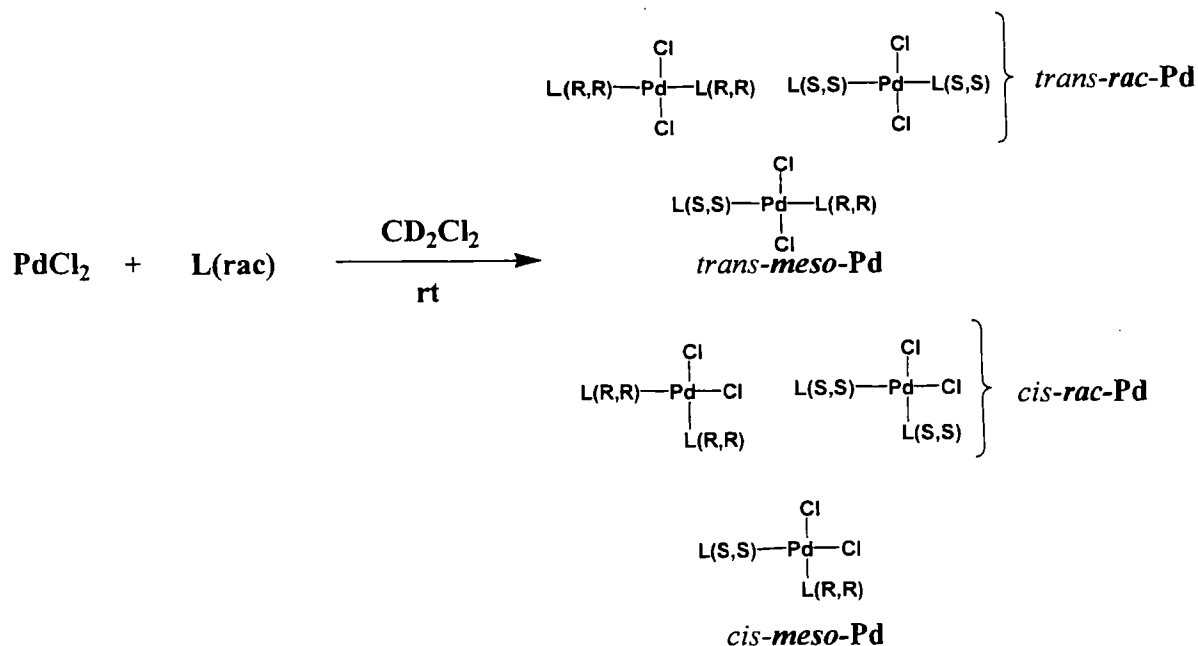


Figure 53. The *in situ* $^{13}\text{C}\{^1\text{H}\}$ (125 MHz) NMR spectrum of the reaction of PdCl_2 with $\text{L}(\text{rac})$ in a 1:1 molar ratio in CD_2Cl_2 at -60°C after a considerable amount of time at room temperature (bottom); and the expanded C=S (top left) and C3 region (top right); $\text{L} = \text{L}(\text{rac})$; * = *trans-rac-Pd* and *cis-rac-Pd*.

Scheme 33. The reaction of PdCl₂ and L(*rac*).Table 11. The ¹³C{¹H} NMR (125 MHz) signals in CD₂Cl₂ at room temperature and -60 °C of the C3 and C=S carbon atoms of *rac*-Pd and *meso*-Pd and the *in situ* NMR reactions of PdCl₂ with L(S,S) and L(*rac*) at 1:1 molar ratio.

Complex ^d		C3	C3 (-60 °C)	C=S	C=S (-60 °C)
Isolated complex	<i>trans-rac</i> -Pd	71.27, 70.90, 69.85 ^c	69.83, 69.68, 68.91	too weak to observe	182.01, 180.49, 181.89, 181.72
	<i>trans-meso</i> -Pd				
	<i>cis-rac</i> -Pd				
	<i>cis-meso</i> -Pd				
<i>in situ</i> reactions ^c	<i>trans</i> -S,S-Pd	70.79, 70.59 ^a	-	182.44, 182.44 ^a	-
	<i>cis</i> -S,S-Pd				
	<i>trans-rac</i> -Pd	70.84, 71.20, 70.65, 70.72 ^a	69.81, 69.66, 68.89	182.50, 183.61, 182.50, 183.25 ^a	181.99, 180.53, 181.90, 181.73
	<i>trans-meso</i> -Pd				
<i>cis-rac</i> -Pd					
<i>cis-meso</i> -Pd					

^a ¹³C{¹H} NMR at 100 MHz; ^b three peaks rather than four due to overlapped signals;^c extra broad peaks at *ca.* 70 ppm in the NMR spectrum at -60 °C.

II.2.4.D) Monitoring of the conversion of *rac*-Pd / *meso*-Pd

rac-Pd / *meso*-Pd was dissolved in CD₂Cl₂ and monitored by NMR after 24 h at room temperature. The ¹H and ¹³C{¹H} NMR spectra (Figure 54) are notably complicated, but many of the ¹³C{¹H} peaks can be identified by recourse to the ¹³C{¹H} signal of the free ligand and the *cis*- and *trans*-monomers. The complexes were identified by the C=S and C3 signals. The signals at 187.34 and 69.81 ppm can be assigned to the C=S and C3 of the free ligand **L**(*rac*). Signals at 182.48, 70.86 and 70.68 ppm can be assigned to the C=S and C3 of the *cis*- and *trans*-*rac*-Pd. Signals at 183.26, 183.57 and 70.75, 71.23 ppm can be assigned to the C=S and C3 respectively of the *cis*- and *trans*-*meso*-Pd. More information is obtained from the ¹H NMR spectrum at -60 °C (Figure 55) which shows traces of the Pd dimers *rac*-Pd₂ and *meso*-Pd₂. However, there are signals in the C=S region which cannot be assigned (δ 181.83, 182.95, 183.38 and 183.46 ppm). These signals are very close to those of the monomeric palladium complexes, which indicates that they are probably C=S signals from other palladium complexes. It can be postulated that the unassigned ¹³C{¹H} signals may originate from related *cis*-/*trans*-chloro-bridged dimer complexes as shown in Scheme 34. Another palladium complex which may possibly be presented is the 14 electron [PdLCl₂] Pd(L). However, examples of this types of unsaturated complex are rare, but they can be isolated when the ligands are bulky.¹¹⁰⁻¹¹³ It seems unlikely that such a species would be present at -60 °C, especially when free ligand is observed and several bridged dimeric structures are possible.

From this experiment, we can conclude that the monomer appears to be very unstable in solution. Furthermore, we detect *cis*- and *trans*- monomeric isomers as well as a mixture of other palladium complexes. Interconversion of *trans* and *cis* chloro-bridged dimers and the sulfur-bridge palladium dimers can be explained by a mechanism involving a monomeric species which has dissociated one ligand to form a 14 electron [PdLCl₂] Pd(L) intermediate. A summary of the proposed species is shown in Scheme 34.

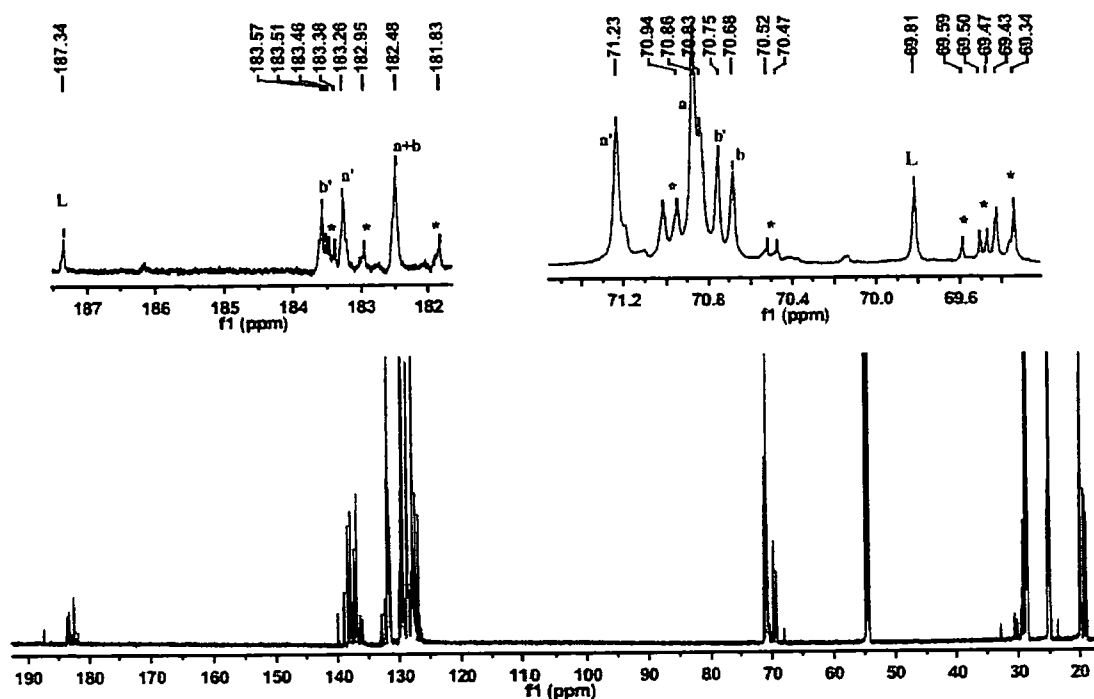


Figure 54. The $^{13}\text{C}\{^1\text{H}\}$ NMR (125 MHz) spectrum of *rac*-Pd / *meso*-Pd in CD_2Cl_2 at room temperature after 24 h (bottom), the expanded C=S (top left) and C3 region (top right); L = ligand; a = *trans-rac*-Pd; b = *cis-rac*-Pd; $^{a'}$ = *trans-meso*-Pd; $^{b'}$ = *cis-meso*-Pd; * = unknown Pd complex.

Table 12. The solution $^{13}\text{C}\{^1\text{H}\}$ NMR signals of C3 and C=S of the *rac*-Pd / *meso*-Pd after 24 h in CD_2Cl_2 and the *in situ* reaction of PdCl_2 and $\text{L}(\text{rac})$ after 6 h.^a

Complex	<i>in situ</i> reaction after 6 h at room temperature		<i>rac</i> -Pd / <i>meso</i> -Pd after 24 h at room temperature	
	C3	C=S	C3	C=S
<i>cis-rac</i> -Pd	70.65, 70.84, 70.72, 71.20	182.50, 182.50, 183.25, 183.61	70.68, 70.86, 70.75, 71.23	182.48, 182.48,
<i>trans-rac</i> -Pd				183.26, 183.57
<i>cis-meso</i> -Pd				
<i>trans-meso</i> -Pd				

^a *cis-meso*-Pd / *trans-meso*-Pd cannot be specified.

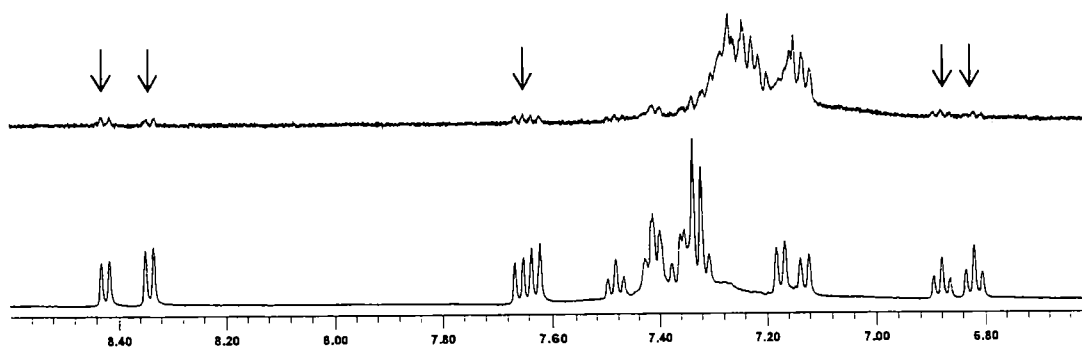
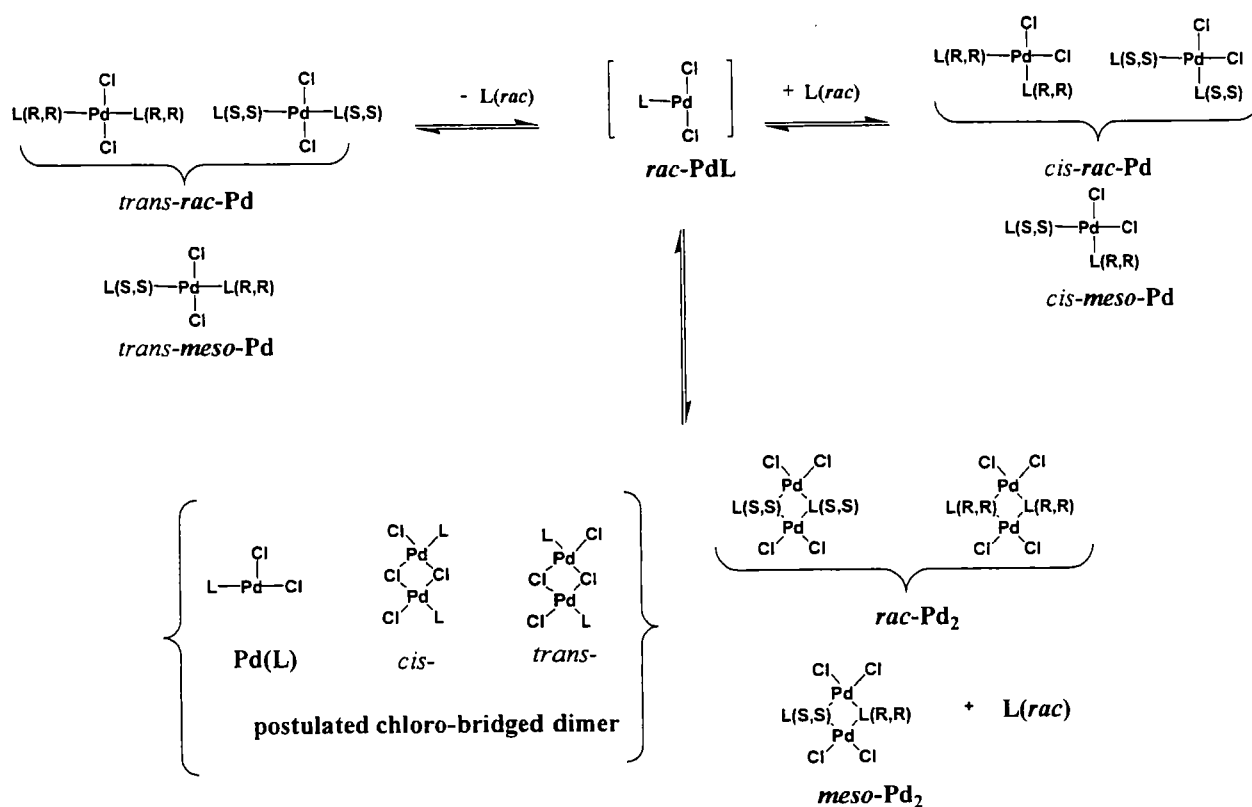


Figure 55. The aromatic region of the ^1H NMR (500 MHz) spectra in CD_2Cl_2 at -60°C of *rac*-Pd / *meso*-Pd (top) and *rac*-Pd₂ / *meso*-Pd₂ (bottom).



Scheme 34. Postulated summary of the *trans-rac*-Pd / *trans-meso*-Pd interconversion.

II.2.4.E) Monitoring of the conversion of *rac*-Pd₂ / *meso*-Pd₂

From the NMR spectroscopy studies on the monomer, we observed a mixture of palladium complexes including the dimer. This led us to investigate the dimer in more detail. Interestingly, the ¹³C{¹H} NMR of *S,S*-Pd₂ at -60 °C also shows other peaks at 178.53 and 70.09 ppm (Figure 56) as alluded to previously in the NMR characterization section. The first signal does not match the C=S signals of *cis-rac*-Pd, *trans-rac*-Pd, *cis-meso*-Pd or *trans-meso*-Pd. However, the signal at 70.09 ppm is consistent with that at 70.14 ppm observed in the spectrum of *rac*-Pd / *meso*-Pd after 24 h. We believe that the dimer may dissociate to give monomeric 14 electron [LPdCl₂] Pd(L) and then reassociate to give the *cis*- and *trans*- chloro-bridged dimers (Scheme 35) which were assigned to the signals at 178.53 and 70.09 ppm for C=S and C3 is observed, respectively. The fact that only one C=S and one C3 signal are observed suggests that they are overlapped. A summary of the interconversion is shown in Scheme 35.

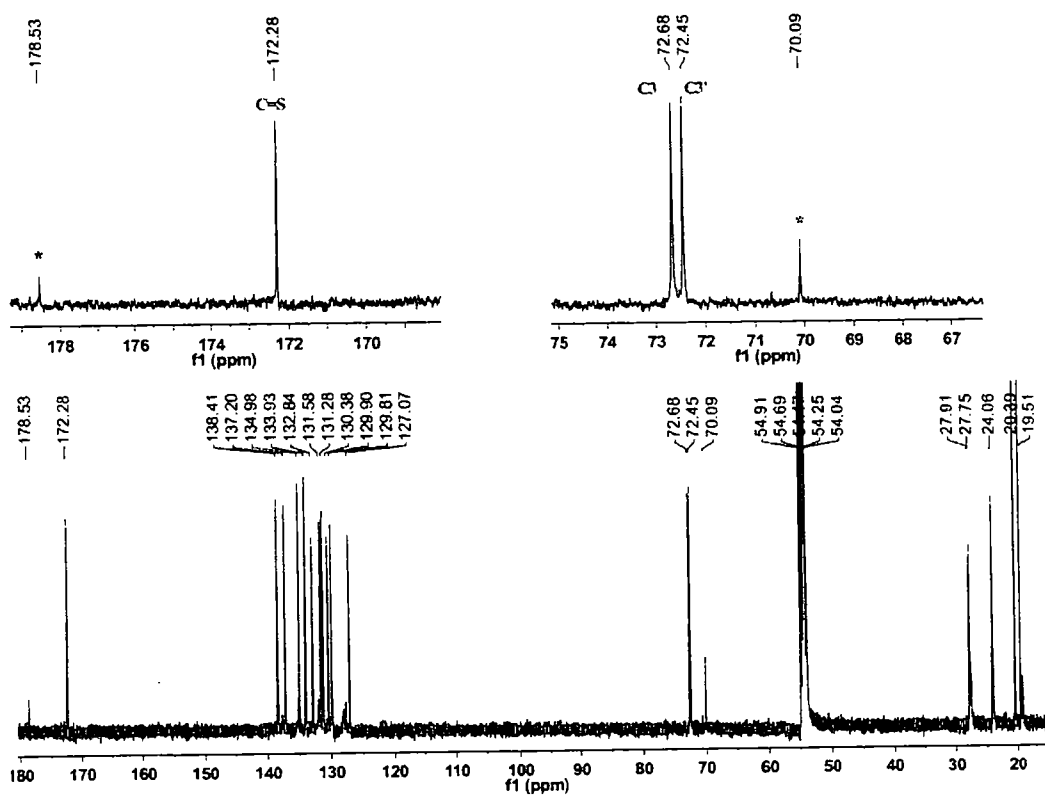
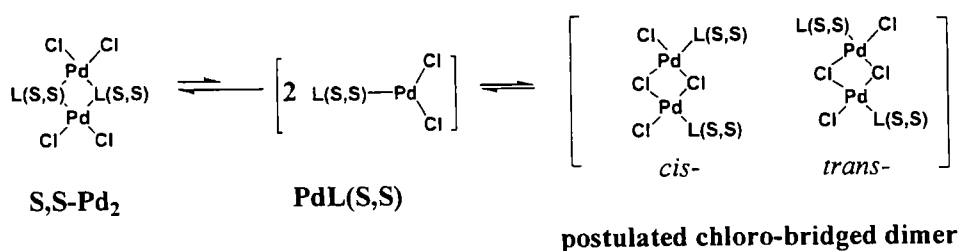


Figure 56. The ¹³C{¹H} NMR (125 MHz) spectrum of *S,S*-Pd₂ in CD₂Cl₂ at -60 °C (bottom), and the expanded C=S (top left) and C3 region (top right); * intermediate.



Scheme 35. Postulated **S,S-Pd₂** interconversions.

The analogous $^{13}\text{C}\{^1\text{H}\}$ NMR spectrum in CD_2Cl_2 of *rac*-Pd₂ / *meso*-Pd₂ was obtained after *ca.* 24 h and is shown in Figure 57. The peaks at 172.25, 72.44 and 72.66 ppm can be attributed to the respective C=S and C3 carbons of *rac*-Pd₂, whereas other peaks at 172.14, 72.27 and 72.66 ppm are attributed to *meso*-Pd₂. The *rac*-Pd₂ signals are, of course, identical to the **S,S-Pd₂** signals. We found another signal at 70.06 ppm which shows a similar chemical shift to that attributed to *cis-/trans-* chloro-bridged dimers of the **L(S,S)**, *vide supra*, and thus can be attributed to *cis-/trans-* chloro-bridged dimers of the *rac* and *meso* palladium complexes, as shown in Scheme 36. Due to the fact that the signals are weak, we did not observe the carbon signal for the C=S. The interconversion of *rac*-Pd₂ and *meso*-Pd₂ in solution is shown in Scheme 36.

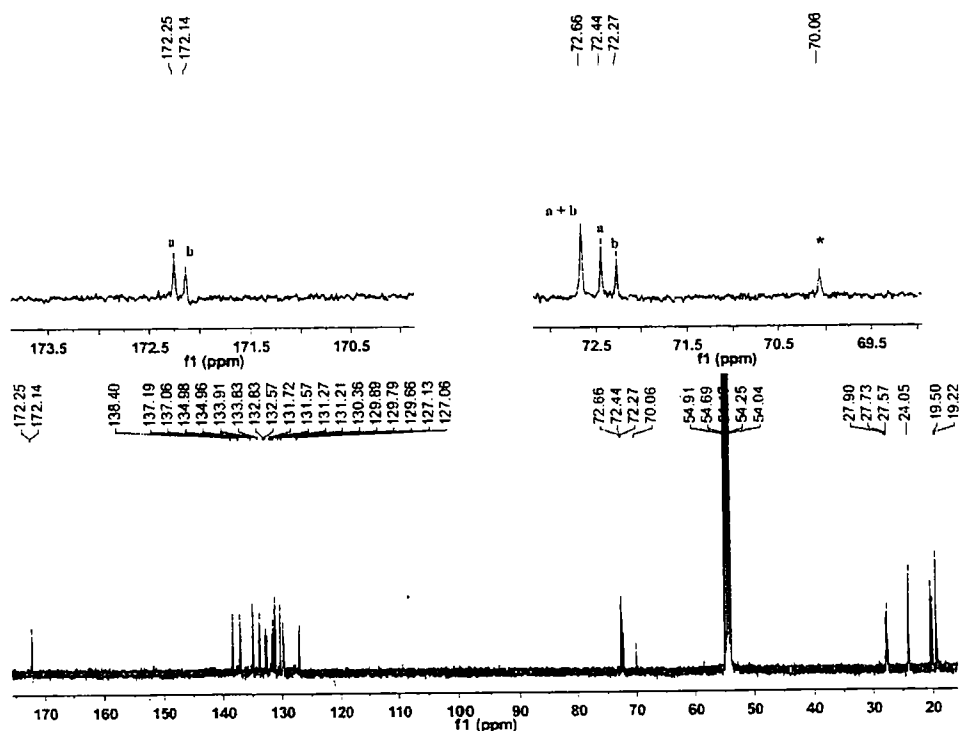
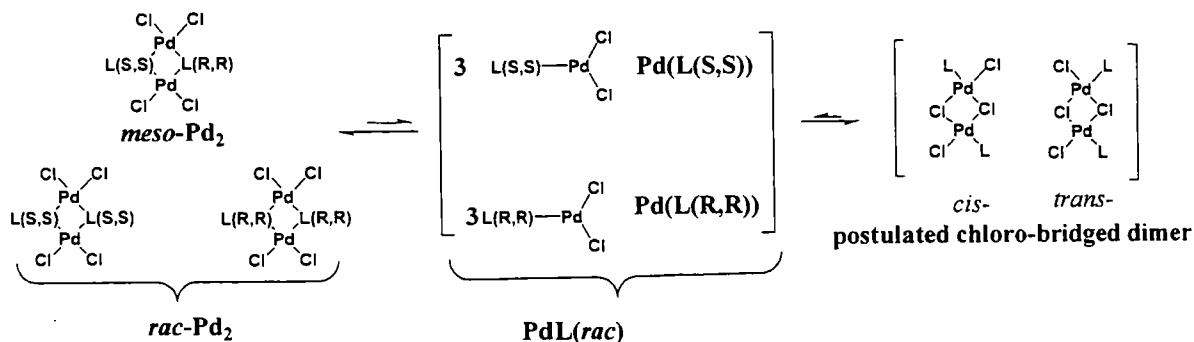


Figure 57. The $^{13}\text{C}\{^1\text{H}\}$ NMR (125 MHz) spectrum of *rac*- Pd_2 / *meso*- Pd_2 in CD_2Cl_2 at $-60\text{ }^\circ\text{C}$ (bottom); and the expanded C=S (top left) and C3 regions (top right); ^a *rac*- Pd_2 ; ^b *meso*- Pd_2 ; * intermediate.



Scheme 36. The interconversion of *rac*- Pd_2 / *meso*- Pd_2 .

II.2.4.F) Monitoring of the conversion pure enantiomer palladium complexes to mixed diastereoisomers

Our variable temperature NMR studies of *S,S*- Pd_2 and *rac*- Pd_2 / *meso*- Pd_2 showed that a dynamic process was occurring which served to exchange the two distinct

environments of, for example, the tolyl methyl groups, as well as appearing to exchange the *meso*- and *rac*- dimers. In order to establish whether cleavage of the dimers to monomeric $[\text{PdLCl}_2]$ species was occurring as an intermediate in the exchange process, equal amounts of S,S-Pd_2 and R,R-Pd_2 were mixed in CD_2Cl_2 at room temperature and the reaction was monitored by ^1H NMR spectroscopy at $-60\text{ }^\circ\text{C}$ after specific periods (0, 24, 48 and 72 hours) at room temperature. The aromatic regions of the ^1H spectra are shown in Figure 58.

At $t = 0\text{ h}$, ^1H NMR spectra shows only signals for S,S-Pd_2 and R,R-Pd_2 (*i.e.*, only one set of signals as the two species are enantiomeric). After 24 h at room temperature, new ^1H signals are observed which are identical to those of *meso-Pd*₂. After 48 h and 72 h, the ^1H NMR integrations are the same which suggests that the system has reached equilibrium. This observation can be explained through a mechanism involving the cleavage of S,S-Pd_2 and R,R-Pd_2 to give PdL(S,S) and PdL(R,R) respectively, and then recombination to form *meso-Pd*₂ as well as S,S-Pd_2 and R,R-Pd_2 (*rac-Pd*₂) as depicted in Scheme 37. We can conclude that the monomeric PdLCl_2 species, formed from the dimer dissociations, are the key intermediate involved in the dynamic behavior of this system. Furthermore, we can also refer back to the mechanism of the conversion of dimer to monomer, suggesting that the process most likely occurs through the ring opening of the dimer followed by the nucleophilic attack of the thiourea ligand ($\text{S}_{\text{N}}1$).

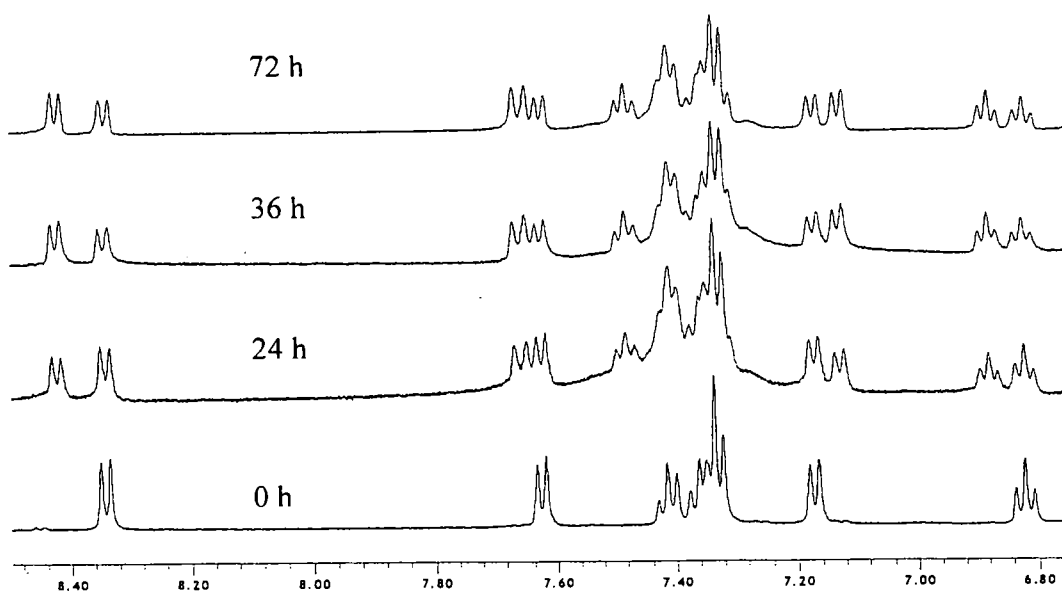
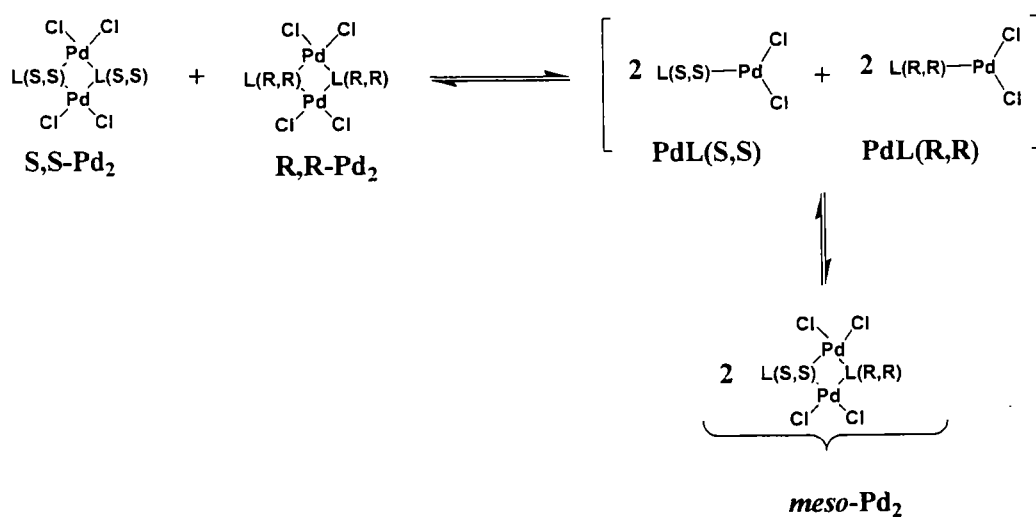


Figure 58. The ^1H NMR (500 MHz) spectra at $-60\text{ }^\circ\text{C}$ of a mixture of $S,S\text{-Pd}_2$ and $R,R\text{-Pd}_2$ in CD_2Cl_2 after 0, 24, 48 and 72 h at room temperature.



Scheme 37. Formation of an equilibrium mixture of $rac\text{-Pd}_2$ and $meso\text{-Pd}_2$ from reaction of $S,S\text{-Pd}_2$ and $R,R\text{-Pd}_2$.

We can summarize the NMR studies of the palladium complexes of the chiral thioureas as follows:

Monopalladium complexes

i. The ^1H NMR spectra, both at room temperature and $-60\text{ }^\circ\text{C}$, of the monomer (obtained shortly after the solution was prepared) show very complicated signals. However, the $^{13}\text{C}\{^1\text{H}\}$ NMR spectrum in CD_2Cl_2 at $-60\text{ }^\circ\text{C}$ reveals *cis*- and *trans*-monomeric species. From single crystal X-ray diffraction studies, we found only the *trans*- isomer. Presumably, this isomer crystallized more readily than the *cis*- isomer.

ii. The ^1H and $^{13}\text{C}\{^1\text{H}\}$ NMR spectra in CD_2Cl_2 both at room temperature and $-60\text{ }^\circ\text{C}$, of the monomer after 24 h shows *cis/trans*- monomeric and dimeric palladium species (from ^1H NMR) as well as other palladium complexes which could not be identified. These signals are very close to those of the monomeric palladium complexes. This observation suggested that the monomer is very unstable in solution and shows dynamic behavior, including dissociation of one thiourea ligand.

Dipalladium complexes

i. The NMR spectra of the dimeric palladium complexes reveal a distinctive dependence on the solvent and temperature suggesting dynamic equilibria in these systems.

ii. The NMR assignment of **S,S-Pd₂** was obtained from 2D NMR studies in CD_2Cl_2 at $-60\text{ }^\circ\text{C}$. The NMR assignment of *meso*-Pd₂ can be made by subtraction of the NMR spectrum of **S,S-Pd₂** from *rac*-Pd₂ / *meso*-Pd₂.

iii. The energy barrier, ΔG^\ddagger , of the exchange process in TCE-d₂ of *rac*-Pd₂ / *meso*-Pd₂ was calculated using the Eyring–Polanyi equation to be $66.25\text{ kJ}\cdot\text{mol}^{-1}$ ($15.8\text{ kcal}\cdot\text{mol}^{-1}$) and $66.15\text{ kJ}\cdot\text{mol}^{-1}$ ($15.8\text{ kcal}\cdot\text{mol}^{-1}$) for *meso*-Pd₂ and *rac*-Pd₂, respectively. From VT NMR studies, we observed new complexes formed irreversibly. Detailed line shape analysis gave ΔG^\ddagger $15.4\text{ kcal}\cdot\text{mol}^{-1}$, in good agreement with the simple analysis.

iv. From an *in situ* NMR reaction of PdCl₂ with L(S,S) and L(*rac*) in 1:1 molar ratios, *cis*- and *trans*-monomer complexes are observed as intermediates before the formation of the dimeric product. Furthermore, we also observed signals from other palladium species which are postulated to be *trans-rac-Pd* and *trans-meso-Pd*.

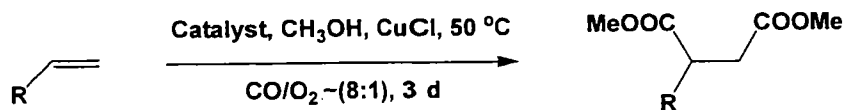
v. We believe that the monomer and dimer are in equilibrium and the conversion of *trans-rac-Pd* and *trans-meso-Pd* to their *cis*-isomers and the palladium dimers can be explained by a mechanism involving a monomer species which has dissociated one ligand to form a 14 electron [PdLCl₂] Pd(L) intermediate.

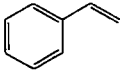
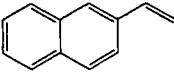
vi. Equal amounts of S,S-Pd₂ and R,R-Pd₂ were mixed in CD₂Cl₂ at room temperature and the reaction was monitored by ¹H NMR spectroscopy at -60 °C after specific periods (0, 24, 48 and 72 hours) at room temperature. After 24 h at room temperature, new ¹H signals are observed which are identical to those of *meso*-Pd₂. This observation confirms a mechanism involving the cleavage of S,S-Pd₂ and R,R-Pd₂ to give PdL(S,S) and PdL(R,R) respectively, and then recombination to form *meso*-Pd₂ as well as S,S-Pd₂ and R,R-Pd₂ (*rac*-Pd₂).

II.2.3 Testing of chiral-thiourea ligand in bis(methoxycarbonylation) of styrenes

Both the monomer and dimer were used as catalyst precursors in the bis(methoxycarbonylation) reaction of terminal olefins by Mr. B. Liang in the group of Prof. Z. Yang at Peking University. A summary of the results and reaction conditions is given in Table 13. Interestingly, the yields obtained were very similar (see Table 13). An *in situ* (1:1 Pd:L1) prepared catalyst system also gave a similar yield. These results lead to the question 'Why do they all give similar results?'

Table 13. Bis(methoxycarbonylations) of terminal olefins using chiral-thiourea **L1** and its palladium complexes.¹¹⁴



Olefin	Yields		
	<i>in situ</i> 1:1 Pd:L1	dimer	monomer
	90	93	90
	86	83	84

The results in Table 13, in combination with our extensive studies of the Pd-L1 system suggest that in all cases the active catalysts is likely to be an "LPdX₂" complex.

III. Conclusion

Monomeric and dimeric palladium dichloride complexes containing the monodentate thioureas, tetramethyl thiourea (tmtu) and the chiral 1,3-di-*o*-tolyl-hexahydro-1*H*-benzo[*d*]imidazole-2(3*H*)-thione **L**, were synthesized using two and one equivalents of ligand respectively. The complexes with **L** were obtained as optically pure compounds, and as mixtures of the racemate and the *meso*-complex. They have been fully characterized by solution NMR (including solid state $^{13}\text{C}\{^1\text{H}\}$ NMR in the case of the tmtu complexes), elemental analysis and single-crystal X-ray diffraction (for the tmtu complexes and *meso* **L** complexes). The structures of the mono-palladium complexes with tmtu and **L** are the *trans*-isomers, whereas the dimer complexes present a *cis*-configuration, and are also the first examples of palladium complexes with sulfur-bridging thiourea ligands. The solid state $^{13}\text{C}\{^1\text{H}\}$ NMR spectra of the 1:1 and 2:1 tmtu complexes are significantly different, whereas in solution, they are almost identical. This suggests that, in solution, the di-palladium tmtu complexes are converting to the mono-palladium complexes.

A dynamic equilibrium in solution was also observed between the *rac*- and *meso*-chiral thiourea dipalladium complexes. The energy barrier to exchange was obtained from a variable temperature NMR study. Monitoring of *in situ* reactions to form the monomeric complexes by NMR also revealed the presence of signals which were postulated to belong to *cis*-mono-palladium complexes. The NMR spectra of *trans*-monomer complexes after 24 h in solution show other peaks which may be from other palladium complexes. Traces of dimer are also observed. It is possible that the additional Pd complexes are chloride bridged dimers or higher order oligomers, such as trimers. Cleavage of the dimers to monomeric PdLX_2 species invoked to explain why the mixing of two optically pure dimers in solution results in signals from the *meso*- complex in the ^1H NMR spectra, can also account for the observed dynamic process observed by VT NMR spectroscopy.

IV. Experimental

Synthesis

^1H and $^{13}\text{C}\{^1\text{H}\}$ NMR spectra were obtained using Varian Inova- 500 spectrometer at the following frequencies: ^1H -400 or 500 MHz, $^{13}\text{C}\{^1\text{H}\}$ -125 MHz in CD_2Cl_2 and TCE-d_2 at room temperature unless otherwise stated. The chemical shifts are reported in ppm and referenced to the internal standard SiMe_4 . Assignments of the NMR spectroscopic data for the free ligands and their palladium complexes were based on a series of 2D NMR studies. Solid state ^{13}C NMR (100 MHz) was obtained using a Varian VNMRS spectrometer. Elemental analyses were performed using an Exeter Analytical CE-440 analyzer. MS analyses were performed using Thermo LTQFT (for ESI/HRMS-ESI) and Applied Biosystems Voyager-DE STR (for MALDI) instruments. Palladium dichloride (PdCl_2) and tetramethylthiourea (tmtu) were purchased from Precious Metals Online and Sigma-Aldrich, respectively, and were used without further purification. Bis(benzonitrile) palladium(II) dichloride [$\text{PdCl}_2(\text{PhCN})_2$] was prepared *via* the literature procedure.¹¹⁵ The chiral thiourea ligands were synthesized by the group of Prof. Z. Yang at Peking University.¹⁷

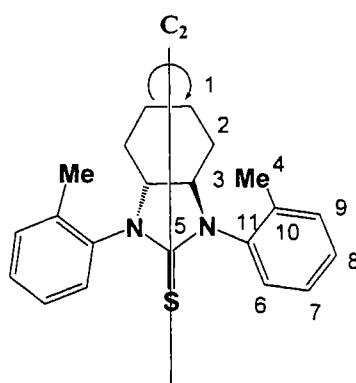
Synthesis of Pd(tmtu)

To a solution of $\text{PdCl}_2(\text{PhCN})_2$ (43.6 mg, 0.114 mmol) in CHCl_3 (4 ml) was added tmtu (30 mg, 0.227 mmol). The reaction mixture was stirred at room temperature for 30 min. The solvent was concentrated under reduced pressure and then Et_2O was added to the solution to give an orange precipitate. The precipitate was collected by filtration and washed with Et_2O (x3). Yield (40.1 mg, 80 %). Single crystals suitable for X-ray diffraction were grown *via* slow evaporation of a solution in CH_2Cl_2 :hexane (1:1 v/v). ^1H NMR (500 MHz, CD_2Cl_2) δ 3.23 (s, 12H, CH_3), 3.21 (s, 12H, CH_3). $^{13}\text{C}\{^1\text{H}\}$ NMR (125 MHz, CD_2Cl_2) δ 188.38 (C=S), 189.29 (C=S), 45.23 (CH_3), 45.07 (CH_3). Solid state $^{13}\text{C}\{^1\text{H}\}$. (100 MHz) δ 188.45 (C=S), 46.79 (CH_3). Anal. Calcd. for $\text{C}_{10}\text{H}_{24}\text{Cl}_2\text{N}_4\text{PdS}_2$: C 27.19, H 5.48, N 12.68; Found C 26.65, H 5.40, N: 12.34.

Synthesis of Pd₂(tmtu) (Preparation by Mr. T. Turner)⁵²

To a solution of PdCl₂(PhCN)₂ (0.87 g, 2.27 mmol) in CH₂Cl₂ (50 ml) was added tmtu (0.30 g, 2.27 mmol) which resulted in the immediately formation of an orange precipitate. The precipitate product was collected by filtration and washed with Et₂O (x3). Yield (0.64 g, 58 %). Re-crystallization from acetone gave pure orange product. A small sample of the product (~20 mg) was dissolved in the minimum volume of warm CH₃CN:CHCl₃ (1:1 v/v) and the solution cooled to yield crystals suitable for X-ray analysis. ¹H NMR (500 MHz, CD₂Cl₂) δ 3.23 (s, 12H, CH₃), 3.21 (s, 12H, CH₃). ¹³C{¹H} NMR (125 MHz, CD₂Cl₂) δ 188.42 (C=S), 189.31 (C=S), 45.24 (CH₃), 45.08 (CH₃). Solid state ¹³C{¹H} (100 MHz) δ 173.00 (C=S), 171.33 (C=S), 51.30 (CH₃), 48.66 (CH₃), 47.45 (CH₃), 46.51 (CH₃), 44.94 (CH₃). Anal. Calcd. for C₁₀H₂₄Cl₄N₄Pd₂S₂: C 19.40, H 3.91, N 9.05; Found C 19.71, H 3.95, N: 8.73.

(rac)-1,3-Di-*o*-tolyl-*trans*-hexahydro-1*H*-benzo[d]imidazole-2(3*H*)-thione: L(*rac*)



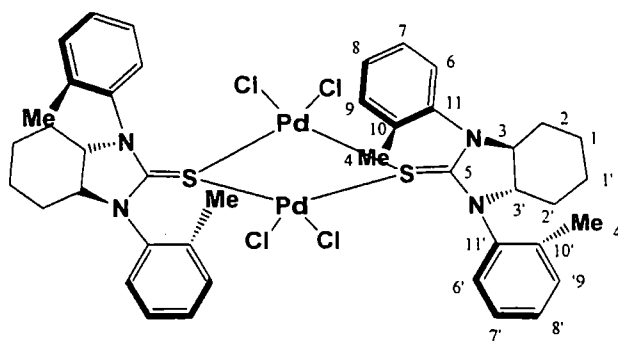
The ligand was synthesized following the reported procedure.¹⁷ ¹H NMR (500 MHz, CD₂Cl₂, 20 °C): δ 7.31 – 7.40 (m, 6H, H7,8,9), 7.19 (d, *J*_{H-H} = 8 Hz, 2H, H6), 3.69 – 3.76 (m, 2H, H3), 2.41 (s, 6H, H4), 1.80 – 1.86 (m, 4H, H1a,2a), 1.44 – 1.59 (m, 2H, H2b), 1.38 – 1.42 (m, 2H, H1b). ¹³C{¹H} NMR (125 MHz, CD₂Cl₂, 20 °C): δ 187.34 (C5), 140.11 (C11), 139.07 (C10), 131.71 (C8), 128.71 (C7), 127.81 (C9), 126.88 (C6), 69.80 (C3), 29.18 (C2),

25.21 (C1), 19.10 (C4). MS (ES+) *m/z*: 336; HRMS calcd. For C₂₁H₂₅N₂S (MH⁺) 337.1733; found: 337.1732. Anal. Calcd. for C₂₁H₂₄N₂S: C 74.96, H 7.19, N 8.33; Found C 75.04, H 7.21, N 8.48 %.

¹H NMR (500 MHz, CD₂Cl₂, -60 °C): δ 7.24 – 7.32 (m, 6H, H7,8,9), 7.16 (d, *J*_{H-H} = 8 Hz, 2H, H6), 3.60 – 3.68 (m, 2H, H3), 2.33 (s, 6H, H4), 1.71 – 1.77 (m, 4H, H1a,2a), 1.37 – 1.50 (m, 2H, H2b), 1.24 – 1.32 (m, 2H, H1b). ¹³C{¹H} NMR (125 MHz, CD₂Cl₂, -60 °C): δ 186.16 (C5), 139.14 (C11), 138.38 (C10), 131.12 (C8), 128.28 (C7), 127.31 (C9), 126.31 (C6), 68.94 (C3), 28.31 (C2), 24.43 (C1), 18.72 (C4).

^1H NMR (500 MHz, TCE- d_2 , 100 °C): δ 7.30 – 7.38 (m, 6H, H7,8,9), 7.20 – 7.24 (m, 2H, H6), 3.62 – 3.72 (m, 2H, H3), 2.45 (s, 6H, H4), 1.82 – 1.94, 1.34 – 1.47 (m, 8H, H1,2).

Synthesis of $[\mu\text{-L}(\text{S,S})\text{PdCl}_2]_2$: S,S-Pd₂



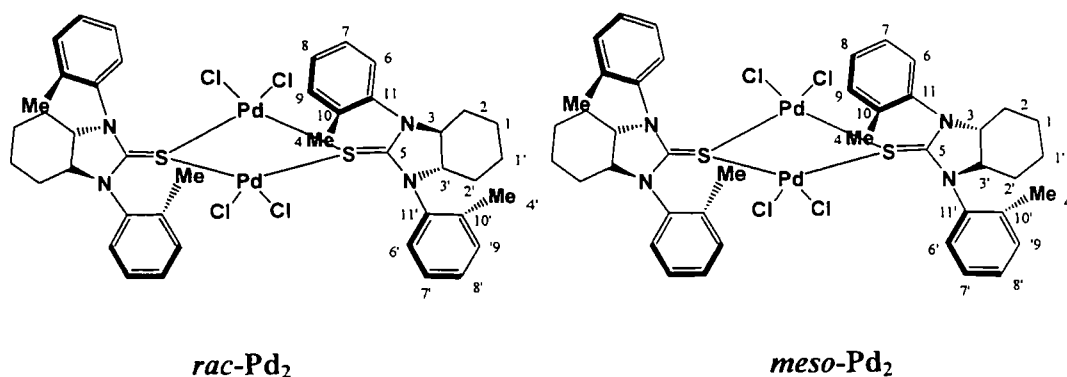
PdCl_2 (0.0225 g, 0.127 mmol) and $\text{L}(\text{S,S})$ (0.0420 g, 0.125 mmol) were added to methanol (8 ml). The reaction mixture was stirred at 50 °C for 4 h and then the hot solution was filtered. The filtrate was allowed to cool to room temperature and Et_2O was added to obtain an orange precipitate. The precipitate was collected by filtration and washed with Et_2O (x3). The solid was dried to obtain the product as an orange powder. Yield (0.0102 g, 80 %). ^1H NMR (500 MHz, CD_2Cl_2 , -60 °C): δ 8.34 (d, $J_{\text{H-H}} = 8$ Hz, 2H, H6), 7.63 (d, $J_{\text{H-H}} = 8$ Hz, 2H, H6'), 7.42 (t, $J_{\text{H-H}} = 8$ Hz, 2H, H8'), 7.32 – 7.38 (m, 6H, H7,H7',H9), 7.17 (d, $J_{\text{H-H}} = 8$ Hz, 2H, H9'), 6.82 (d, $J_{\text{H-H}} = 8$ Hz, 2H, H8), 3.80 (t, $J_{\text{H-H}} = 4$ Hz, 2H, H3), 3.70 (t, $J_{\text{H-H}} = 4$ Hz, 2H, H3'), 2.85 (s, 6H, H4), 2.32 (s, 6H, H4'), 1.54 – 1.86 (m, 16H, H1,H2,H1',H2'). $^{13}\text{C}\{^1\text{H}\}$ NMR (125 MHz, CD_2Cl_2 , -60 °C): δ 172.28 (C5), 138.41 (C10), 137.20 (C10'), 134.98 (C11), 133.93 (C11'), 132.84 (C9), 131.58 (C6'), 131.28 (C9'), 131.22 (C8), 130.38 (C8'), 129.90 (C7), 129.81 (C6), 127.07 (C7'), 72.68 (C3), 72.45 (C3'), 27.91, 27.75, 24.06 (C1,C1',C2, C2'), 20.39 (C4), 19.51 (C4'). Anal. Calcd. for $\text{C}_{42}\text{H}_{48}\text{Cl}_4\text{N}_4\text{Pd}_2\text{S}_2$: C 49.10, H 4.71, N 5.45; Found C 50.07, H 4.83, N 4.58 %.

Synthesis of $[\mu\text{-L}(\text{R,R})\text{PdCl}_2]_2$: R,R-Pd₂

R,R-Pd_2 was synthesized by a similar procedure as for S,S-Pd_2 using PdCl_2 (0.0216 g, 0.125 mmol) and $\text{L}(\text{R,R})$ (0.0409 g, 0.125 mmol). Yield (0.0102 g, 82 %).

NMR spectra were identical to those of **S,S-Pd₂**. Anal. Calcd. for C₄₂H₄₈Cl₄N₄Pd₂S₂: C 49.10, H 4.71, N 5.45; Found C 49.32, H 4.74, N 5.52 %.

**Synthesis of [Pd-μ-L(R,R)Cl₂]₂ / [Pd-μ-L(S,S)Cl₂]₂ and [Pd₂-μ-L(S,S)-μ-L(R,R)Cl₄]
rac-Pd₂ / *meso*-Pd₂**



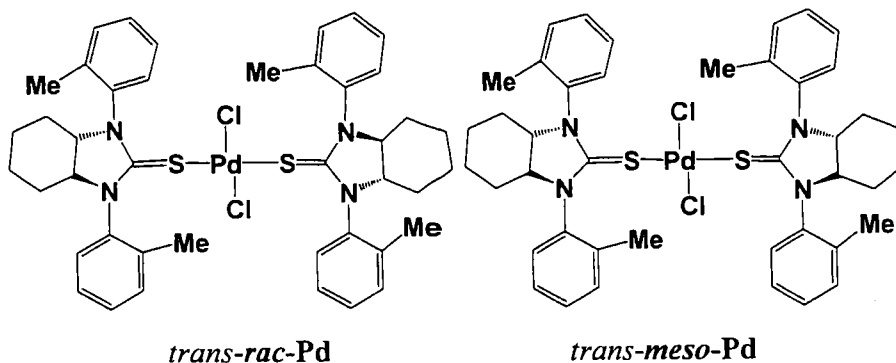
The mixture of *rac*-Pd₂ and *meso*-Pd₂ was synthesized by a similar procedure as for **S,S-Pd₂** using PdCl₂ (0.089 g, 0.5 mmol) and **L(rac)** (0.168 g, 0.5 mmol). Yield (0.220 g, 43 %). Single crystals of *meso*-Pd₂ suitable for single-crystal X-ray diffraction were obtained from slow evaporation of a solution in CH₂Cl₂:Et₂O. ¹H NMR (500 MHz, CD₂Cl₂, -60 °C):* δ 8.42 (d, *J*_{H-H} = 8 Hz, 2H, H6B), 8.34 (d, *J*_{H-H} = 8 Hz, 2H, H6A), 7.66 (d, *J*_{H-H} = 8 Hz, 2H, H6'B), 7.63 (d, *J*_{H-H} = 8 Hz, 2H, H6'A), 7.54 (t, *J*_{H-H} = 8 Hz, 2H, H8'B), 7.42 (t, *J*_{H-H} = 8 Hz, 2H, H8'A), 7.31 – 7.50 (m, 12H, H7A,H7B,H7'A,H7'B,H9'A,H9'B), 7.17 (d, *J*_{H-H} = 8 Hz, 2H, H9A), 7.13 (d, *J*_{H-H} = 8 Hz, 2H, H9B), 6.88 (d, *J*_{H-H} = 8 Hz, 2H, H8B), 6.82 (d, *J*_{H-H} = 8 Hz, 2H, H8A), 3.67 – 3.83 (m, 8H, H3A,H3'A,H3B, H3'B), 2.85 (s, 6H, H4A), 2.79 (s, 6H, H4B), 2.32 (s, 6H, H4'A), 2.31 (s, 6H, H4'B), 1.54 – 1.86 (m, 32H, H1A,H2A,H1'A,H2'A, H1B,H2B,H1'B,H2'B). ¹³C{¹H} NMR (125 MHz, CD₂Cl₂, -60 °C):* δ 172.28 (C=S(A)), 172.14 (C=S(B)), 138.41(C10A), 138.37 (C10B), 137.20 (C10'A), 137.06 (C10'B), 134.98 (C11A), 134.96 (C11B), 133.93 (C11'A), 133.83 (C11'B), 132.84 (C9A), 132.57 (C9B), 131.28 (C9'A), 131.72 (C6'B), 131.58 (C6'A), 131.27 (C8'B,C9'B), 131.22 (C8A), 131.21 (C8B), 130.21 (C7B), 130.38 (C8'A), 129.90 (C7A), 129.81 (C6A), 129.66 (C6B), 72.68 (C3A), 72.66 (C3B), 72.45 (C3'A), 72.27 (C3'B), 27.91, 27.90, 27.75, 27.73, 24.06, 24.05 (C1A, C1B, C1'A, C1'B,C2A, C2B, C2'A, C2'B), 20.39

(C4A), 20.19 (C4B), 19.51 (C4'A), 19.50 (C4'B). Anal. Calcd. for $C_{42}H_{48}Cl_4N_4Pd_2S_2$: C 49.10, H 4.71, N 5.45; Found C 48.83, H 4.72, N 5.35 %.

* A = *rac*-Pd₂ and B = *meso*-Pd₂.

Synthesis of [Pd(L(S,S)₂Cl₂)]/[Pd(L(R,R))Cl₂] and [PdL(S,S)L(R,R)Cl₂]

rac-Pd / *meso*-Pd



PdCl₂ (0.089 g, 0.5 mmol) and **L(rac)** (0.337 g, 1 mmol) were added to methanol (8 ml). The reaction mixture was stirred at 50 °C for 2 d and then the solvent was removed under reduced pressure. The residue was dissolved in CH₂Cl₂ and petroleum ether (40:60) was added to the solution to give the product as an orange solid. The solid was collected by filtration and dried *in vacuo*. Yield (0.349 g, 82 %). ¹H NMR (500 MHz, CD₂Cl₂, -60 °C): δ 7.25 (m, 16H, CH_{arom}), 3.70 (m, 4H, N-CH), 1.80 (m, 28H, CH₃/CH₂). ¹³C{¹H} NMR (125 MHz, CD₂Cl₂, 20 °C):* δ 139.11, 138.54, 138.53, 138.07, 137.01, 131.92, 129.43, 128.56, 127.79, 126.92, 110.78, 71.27 (C3), 70.90 (C3), 69.85 (C3), 31.64, 29.23, 28.75, 28.58, 24.89, 19.93, 19.83, 19.11. ¹³C{¹H} NMR (125 MHz, CD₂Cl₂, -60 °C):* δ 182.01 (C=S), 181.89 (C=S), 181.72 (C=S), 180.49 (C=S), 139.10, 138.36, 137.66, 137.61, 136.25, 136.16, 131.09, 128.92, 128.71, 128.26, 127.93, 127.87, 127.28, 127.15, 126.93, 126.67, 126.29, 69.83 (C3), 69.68 (C3), 68.91 (C3), 28.28, 27.79, 27.61, 24.39, 24.16, 19.40, 19.35, 19.32, 18.69. Anal. Calcd. for $C_{42}H_{48}Cl_2N_4PdS_2$: C 59.33, H 5.69, N 6.59; Found C 58.86, H 5.76, N 6.38 %.

* Not all ¹³C{¹H} signals were observed.

The conversion of *rac*-Pd₂ / *meso*-Pd₂ to *rac*-Pd / *trans-meso*-Pd at room temperature

The two equivalents of **L(rac)** (0.021 g, 0.062 mmol) were added to one equivalent of the mixture of *rac*-Pd₂ and *meso*-Pd₂ (0.032 g, 0.031 mmol) in CD₂Cl₂ (ca. 0.7 ml). The mixture was transferred to an NMR tube and examined by ¹H-NMR spectroscopy at various times. Only monomer was shown to be present.

The conversion of *rac*-Pd₂ / *meso*-Pd₂ to *rac*-Pd / *trans-meso*-Pd at 50 °C

The two equivalents of **L(rac)** (0.021 g, 0.062 mmol) were added to one equivalent of the mixture of *rac*-Pd₂ and *meso*-Pd₂ (0.032 g, 0.031 mmol) in CH₃OH (4 ml). The mixture was heated to reflux at 50 °C for 48 h and then the solvent was removed under reduced pressure. The residue was examined by ¹H-NMR spectroscopy in CD₂Cl₂. Only monomer was shown to be present.

In situ NMR reaction of PdCl₂ and **L(S,S)**

One equivalent of **L(S,S)** (0.0700 g, 0.208 mmol) and PdCl₂ (0.0370 g, 0.208 mmol) were transferred to an NMR tube and CD₂Cl₂ (ca. 0.7 ml) was added. The reaction mixture was monitored by ¹³C{¹H} NMR spectroscopy at t = 0 h and 6 h.

In situ NMR reaction of PdCl₂ with **L(rac)**

One equivalent of **L(rac)** (0.0700 g, 0.208 mmol) and PdCl₂ (0.0370 g, 0.208 mmol) were transferred to an NMR tube and CD₂Cl₂ (ca. 0.7 ml) was added. The reaction mixture was monitored by ¹³C{¹H} NMR spectroscopy at t = 0 h and 3 h.

VT-NMR studies of *rac*-Pd₂ / *meso*-Pd₂

rac-Pd₂ / *meso*-Pd₂ was dissolved in TCE-d₂ and then examined by ¹H NMR spectroscopy at 0, 20, 30, 40, 50, 60, 70, 80, 90, 100 °C and then at 20 °C again, which revealed that the compound had partially decomposed on heating.

rac-Pd₂ / *meso*-Pd₂ was dissolved in CD₂Cl₂ and then examined by ¹H-NMR spectroscopy at 25, 20, 0, -30, -40, -50, -60, -70 and -80 °C.

Reaction of R,R-Pd₂ with S,S-Pd₂

Single crystals of S,S-Pd₂ (1.57 mg) and R,R-Pd₂ (1.45 mg) were mixed in CD₂Cl₂ (ca. 0.7 ml) at room temperature and the reaction was monitored by ¹H NMR spectroscopy at -60 °C after various times (t = 0, 24, 48 and 72 h) at room temperature. The crystals were weighed on an analytical balance with an accuracy of +/- 0.01 mg.

V. References

1. Smith, J.; Liras, J. L.; Schneider, S. E.; Anslyn, E. V., *J. Org. Chem.* **1996**, *61*, 8811.
2. Chalina, E. G.; Chakarova, L., *Eur. J. Med. Chem.* **1998**, *33*, 975.
3. Stark, H.; Purand, K.; Ligneau, X.; Rouleau, A.; Arrang, J.-M.; Garbarg, M.; Schwartz, J.-C.; Schunack, W., *J. Med. Chem.* **1996**, *39*, 1157.
4. Walpole, C.; Ko, S. Y.; Brown, M.; Beattie, D.; Campbell, E.; Dickenson, F.; Ewan, S.; Hughes, G. A.; Lemaire, M.; Lerpiniere, J.; Patel, S.; Urban, L., *J. Med. Chem.* **1998**, *41*, 3159.
5. Mallams, A. K.; Morton, J. B.; Reichert, P. J., *J. Chem. Soc., Perkin Trans.* **1981**, 2186.
6. Schroeder, D. C., *Chem. Rev.* **1955**, 181.
7. Sarkis, G. Y.; Faisal, E. D., *J. Heterocycl. Chem.* **1985**, *22*, 137.
8. Boas, U.; Karlsson, A. J.; de Waal, B. F. M.; Meijer, E. W., *J. Org. Chem.* **2001**, *66*, 2136.
9. Henderson, W.; Nicholson, B. K.; Rickard, C. E. F., *Inorg. Chim. Acta* **2001**, *320*, 101.
10. Lo, K. K.-W.; Lau, J. S.-Y.; Fong, V. W.-Y.; Zhu, N. Y., *Organometallics* **2004**, *23*, 1098.
11. Allen, F., *Acta Crystallogr.* **1998**, *A54*, 758.
12. Dai, M.; Wang, C.; Dong, G.; Xiang, J.; Luo, T.; Liang, B.; Chen, J.; Yang, Z., *Eur. J. Org. Chem.* **2003**, 4346.
13. Liang, B.; Liu, J.; Gao, Y.-X.; Wongkhan, K.; Shu, D.-X.; Lan, Y.; Li, A.; Batsanov, A. S.; Howard, J. A. H.; Marder, T. B.; Chen, J.-H.; Yang, Z., *Organometallics* **2007**, *26*, 4756.
14. Kovala-Demertzi, D.; Yadav, P. N.; Demertzis, M. A.; Jasinski, J. P.; Andreadaki, F. J.; Kostas, I. D., *Tetrahedron Lett.* **2004**, *45*, 2923.
15. Chen, W.; Li, R.; Han, B.; Li, B.-J.; Chen, Y.-C.; Wu, Y.; Ding, L.-S.; Yang, D., *Eur. J. Org. Chem.* **2006**, 1177.
16. Kostas, I. D.; Heropoulos, G. A.; Kovala-Demertzi, D.; Yadav, P. N.; Jasinski, J. P.; Demertzis, M. A.; Andreadaki, F. J.; Vo-Thanh, G.; Petit, A.; Loupy, A., *Tetrahedron Lett.* **2006**, *47*, 4403.
17. Dai, M.; Wang, C.; Liang, B.; Chen, J.; Yang, Z., *Org. Lett.* **2004**, *6*, 221.
18. Yang, D.; Chen, Y.-C.; Zhu, N.-Y., *Org. Lett.* **2004**, *6*, 1577.
19. Dai, M.; Liang, B.; Wang, C.; You, Z.; Xiang, J.; Dong, G.; Chen, J.; Yang, Z., *Adv. Synth. Catal.* **2004**, 1669.

20. Tang, Y.; Deng, L.; Zhang, Y.; Dong, G.; Chen, J.; Yang, Z., *Org. Lett.* **2005**, *7*, 1657.
21. Neveling, A.; Julius, G. R.; Cronje, S.; Esterhuysen, C.; Raubenheimer, H. G., *Dalton Trans.* **2005**, 181.
22. Connon, S. J., *Chem. Commun.* **2008**, 2499
23. Doyle, A. G.; Jacobsen, E. N., *Chem. Rev.* **2007**, *107*, 5713
24. Akiyama, T.; Fuchibe, J. I. K., *Adv. Synth. Catal.* **2006**, *348*, 999
25. Taylor, M. S.; Jacobsen, E. N., *Angew. Chem. Int. Ed.* **2006**, *45*, 1520
26. Kim, Y.-J.; Kwak, H.; Lee, S. J.; Lee, J. S.; Kwon, H. J.; Nam, S. H.; Lee, K.; Kim, C., *Tetrahedron* **2006**, *62*, 9635.
27. Ghosh, K.; Adhikari, S., *Tetrahedron Lett.* **2006**, *47*, 8165.
28. Yen, Y.-P.; Ho, K.-W., *Tetrahedron Lett.* **2006**, *47*, 7357.
29. Choi, M. K.; Kim, H. N.; Choi, H. J.; Yoon, J.; Hyun, M. H., *Tetrahedron Lett.* **2008**, *49*, 4522.
30. Staab, H. A., *Angew. Chem. Int. Ed.* **1962**, *1*, 351.
31. Márquez, J. M.; López, Ó.; Maya, I.; Fuentes, J.; Fernández-Bolaños, J. G., *Tetrahedron Lett.* **2008**, *49*, 3912.
32. Bogatsky, A. V.; Lukyanenko, N. G.; Kirichenko, T. I., *Tetrahedron Lett.* **1980**, *21*, 313.
33. Yavari, I.; Hosseini, N.; Moradi, L.; Mirzaei, A., *Tetrahedron Lett.* **2008**, *49*, 4239.
34. Takikawa, Y.; Inoue, N.; Sato, R.; Takizawa, S., *Chem. Lett.* **1982**, 641.
35. Ballabeni, M.; Ballini, R.; Bigi, F.; Maggi, R.; Parrini, M.; Predieri, G.; Sartori, G., *J. Org. Chem.* **1999**, *64*, 1029.
36. Tamura, Y.; Adachi, M.; Kawasaki, T.; Kita, Y., *Tetrahedron Lett.* **1978**, 1753.
37. Köhna, U.; Günthera, W.; Görlsb, H.; Anders, E., *Tetrahedron: Asymmetry* **2004**, *15*, 1419.
38. Bowser, A. M.; Madalengoitia, J. S., *Tetrahedron Lett.* **2005**, *46*, 2869.
39. Aoyama, T.; Murata, S.; Nagata, Y.; Takido, T.; Kodomari, M., *Tetrahedron Lett.* **2005**, *46*, 4875.
40. Mascaraque, A.; Nieto, L.; Dardonville, C., *Tetrahedron Lett.* **2008**, *49*, 4571.
41. Katritzky, A. R.; Ledoux, S.; Witek, R. M.; Nair, S. K., *J. Org. Chem.* **2004**, *69*, 2976
42. Ramadas, K.; Srinivasan, N.; Janarthanan, N., *Tetrahedron Lett.* **1993**, *34*, 6447.
43. Xian, M.; Zhu, X.; Li, Q.; Cheng, J.-P., *Tetrahedron Lett.* **1999**, *40*, 1957.
44. Sugimoto, H.; Makino, I.; Hirai, K., *J. Org. Chem.* **1988**, *53*, 2263.
45. Bon, V. V.; Orysyk, S. I.; Pekhnyo, V. I.; Orysyk, V. V.; Volkov, S. V., *Polyhedron* **2007**, *26*, 2935.
46. Ciszewski, L.; Xu, D.; Repic, O.; Blacklock, T. J., *Tetrahedron Lett.* **2004**, *45*, 8091.
47. Mohanta, P. K.; Dhar, S.; Samal, S. K.; Ila, H.; Junjappa, H., *Tetrahedron Lett.* **2000**, *56*, 629.
48. Ramadas, K.; Srinivasan, N., *Synth. Commun.* **1995**, *25*, 3381.
49. Byrne, J. J.; Vallée, Y., *Tetrahedron Lett.* **1999**, *40*, 489.
50. Maddani, M.; Prabhu, K. R., *Tetrahedron Lett.* **2007**, *48*, 7151.
51. Truter, M., *Acta Crystallogr.* **1967**, *22*, 556.

52. Turner, T. P. W. *Fourth year report: The coordination chemistry of phosphine sulfides and thioureas and their applications*; Durham University: Durham, 2008.
53. Dias, H. W.; Truter, M. R., *Acta Crystallogr.* **1964**, *17*, 937.
54. Huheey, J. E.; Keiter, E. A.; Keiter, R. L., *Inorganic Chemistry: Principles of Structure and Reactivity*, Harper Collins College Publishers: New York, 1993.
55. Yu, L., *Private Communication* **2007**.
56. Minniti, D., *Inorg. Chem.* **1994**, *33*, 2631.
57. Brugat, N.; Duran, J.; Polo, A.; Real, J.; Alvarez-Larena, A.; Piniella, J. F., *Tetrahedron: Asymmetry* **2002**, *13*, 569.
58. Butler, L. M.; Creighton, J. R.; Oughtred, R. E.; Raper, E. S.; Nowell, I. W., *Inorg. Chim. Acta* **1983**, *75*, 149.
59. Wang, Y.-L.; Shi, Q.; Bi, W.-H.; Li, X.; Cao, R., *Z. Anorg. Allg. Chem.* **2006**, *632*, 167.
60. Aarrizabalaga, P.; Bernardinelli, G.; Geoffroy, M.; Castan, P.; Dahan, F., *Chem. Phys. Lett.* **1986**, *124*, 549.
61. Shaheen, F.; Badashah, A.; Gielen, M.; Marchio, L.; Vos, D. D.; Khosa, M. K., *Appl. Organomet. Chem.* **2007**, *21*, 626.
62. Ghassemzadeh, M.; Aghapoor, K.; Heravi, M. M.; Neumuller, B., *Z. Anorg. Allg. Chem.* **1998**, *624*, 1969.
63. Janca, M.; Taraba, J.; Prihoda, J., *Acta Crystallogr.* **2002**, *E58*, m245.
64. Owen, G. R.; Vilar, R.; White, A. J. P.; Williams, D. J., *Organometallics* **2003**, *22*, 4511.
65. Fukazawa, M.; Kita, M.; Nonoyama, M., *Polyhedron* **1994**, *13*, 1609.
66. Ghassemzadeh, M.; Bolourtchain, M.; Chitsaz, S.; Neumuller, B.; Heravi, M. M., *Eur. J. Inorg. Chem.* **2000**, 1877.
67. Dorazco-Gonzalez, A.; Hernandez-Ortega, S.; Valdes-Martinez, J., *Acta Crystallogr.* **2007**, *E63*, m1120.
68. Doxiadi, E.; Vilar, R.; White, A. J. P.; Williams, D. J., *Polyhedron* **2003**, *22*, 2991.
69. Ghassemzadeh, M.; Mirza-Aghayan, M.; Neumüller, B., *Inorg. Chim. Acta* **2005**, *358*, 2057.
70. Padhye, S.; Afrasiabi, Z.; Sinn, E.; Fok, J.; Mehta, K.; Rath, N., *Inorg. Chem.* **2005**, *44*, 1154.
71. Chakrabarty, K.; Kar, T.; Sen Gupta, S. P., *Acta Crystallogr.* **1990**, *C46*, 2065.
72. Yoda, R.; Yamamoto, Y.; Mutsushima, Y.; Fujie, T.; Iitaka, Y., *Chem. Pharm. Bull.* **1985**, *33*, 4935.
73. Bolte, M.; Fink, L., *Private Communication* **2003**, to the CSD: CCDC 214313.
74. Cauzzi, D.; Costa, M.; Cucci, N.; Graiff, C.; Grandi, F.; Predieri, G.; Tiripicchio, A.; Zanoni, R., *J. Organomet. Chem.* **2000**, *593-594*, 431.
75. Wu, W.-S.; Dai, J.-C.; Zheng, Y.-Y.; Huaug, T.-T.; Lan, X.-R.; Lin, Y.-X., *Acta Chim. Sinica* **2004**, *62*, 1801.
76. Matesanz, A. I.; Mosa, J.; Garcia, I.; Pastor, C.; Souza, P., *Inorg. Chem. Commun.* **2004**, *7*, 756.
77. Souza, P.; Matesanz, A. I.; Pastor, C., *Inorg. Chem. Commun.* **2002**, *5*, 344.
78. Papathanasis, L.; Demertzis, M. A.; Yadav, P. N.; Kovala-Demertzi, D.; Prentjas, C.; Castiñeiras, A.; Skoulika, S.; West, D. X., *Inorg. Chim. Acta* **2004**, *357*, 4113.

79. Koch, K. R.; Wang, Y.; Coetzee, A., *J. Chem. Soc., Dalton Trans.* **1999**, 1013.
80. Dupont, J.; Beydoun, N.; Pfeffer, M., *J. Chem. Soc., Dalton Trans.* **1989**, 1715.
81. Okeya, S.; Kameda, H.; Kawashima, H.; Shimomura, H.; Nishioka, T.; Isobe, K., *Chem. Lett.* **1995**, 501.
82. Maekawa, M.; Munakata, M.; Kuroda-Sowa, T.; Suenaga, Y., *Inorg. Chim. Acta* **1998**, *281*, 116.
83. Umakoshi, K.; Ichimura, A.; Kinoshita, I.; Ooi, S., *Inorg. Chem.* **1990**, *29*, 4005.
84. Aarrizabalaga, P.; Bernardinelli, G.; Geoffroy, M.; Castan, P.; Dahan, F., *Chem. Phys. Lett.* **1986**, *124*, 549.
85. Pauling, L., *The Nature of the Chemical Bond*, 3rd ed.; Cornell Univ. Press: Ithaca: 1960; p 246.
86. Wang, Y.-L.; Bi, W.-H.; Li, X.; Cao, R., *Acta Crystallogr.* **2004**, *E60*, m699.
87. Ooi, S.; Kawase, T.; Nakatsu, K.; Kuroya, H., *Bull. Chem. Soc. Jpn.* **1960**, *33*, 861.
88. Berta, D. A.; III, W. A. S.; Boldrini, P.; Amma, E. L., *Inorg. Chem.* **1970**, 136.
89. Fuks, L.; Sadlej-Sosnowska, N.; Samochocka, K.; Starosta, W., *J. Mol. Struct.* **2005**, *740*, 229.
90. Moro, A. C.; Watanabe, F. W.; Ananias, S. R.; Mauro, A. E.; Netto, A. V. G.; Lima, A. P. R.; Ferreira, J. G.; Santos, R. H. A., *Inorg. Chem. Commun.* **2006**, *9*, 493.
91. Chiusoli, G. P.; Costa, M.; Masarati, E.; Salerno, G., *J. Organomet. Chem.* **1983**, *255*, C35.
92. Gabriele, B.; Costa, M.; Salerno, G.; Chiusoli, G. P., *J. Chem. Soc., Chem. Commun.* **1992**, 1007.
93. Gabriele, B.; Salerno, G.; Costa, M.; Chiusoli, G. P., *J. Organomet. Chem.* **1995**, *503*, 21.
94. Zhang, T. Y.; Allen, M. J., *Tetrahedron Lett.* **1999**, *40*, 5813.
95. Ferrari, C.; Predier, G.; Tiripicchio, A., *Chem. Mater.* **1992**, *4*, 243.
96. Nan, Y.; Miao, H.; Yang, Z., *Org. Lett.* **2000**, *2*, 297.
97. Li, Z.; Gao, Y.; Tang, Y.; Dai, M.-j.; Wang, G.; Wang, Z.; Yang, Z., *Org. Lett.* **2008**, *10*, 3017.
98. Liu, J.; Liang, B.; Shu, D.; Hu, Y.; Yang, Z.; Lei, A., *Tetrahedron* **2008**, *64*, 9581.
99. Munno, G. D.; Gabriele, B.; Salerno, G., *Inorg. Chim. Acta* **1995**, *234*, 181.
100. White, J. L.; Tanski, J. M.; Churchill, D. G.; Rheingold, A. L.; Rabinovich, D., *J. Chem. Cryst.* **2003**, *33*, 437.
101. Paas, M.; Wibbeling, B.; Fröhlich, R.; Hahn, F. E., *Eur. J. Inorg. Chem.* **2006**, *2006*, 158.
102. Grap, S. R.; Kurbakova, A. P.; Kuz'mina, L. G.; I. A. Efimenko; Pontichelli, G., *Koord. Khim.* **1995**, *21*, 803.
103. Novakovic, S. B.; Fraise, B.; Bogdanovic, G. A.; Spasojevic-deBire, A., *Cryst. Growth Des.* **2007**, *7*, 191.
104. Dago, A.; Shepelev, Y.; Fajardo, F.; Alvarez, F.; Pomés, R., *Acta Crystallogr.* **1989**, *C45*, 1192.
105. Cauzzi, D.; Lanfranchi, M.; Marzolini, G.; Predieri, G.; Tiripicchio, A.; Camellini, M. T., *Gazz. Chim. Ital.* **1994**, *124*, 415.

106. Lobana, T. S.; Sharma, R.; Hundal, G.; Butcher, R. J., *Inorg. Chem.* **2006**, *45*, 9402.
107. Udupa, M. R.; Krebs, B., *Inorg. Chim. Acta* **1973**, *7*, 271.
108. Laidler, K. J.; King, M. C., *J. Phys. Chem.* **1983**, *87*, 2657.
109. Sandström, J., *Dynamic NMR Spectroscopy*, Academic Press Inc.: London, 1982; p 226.
110. Weng, Z.; Teo, S.; Koh, L. L.; Hor, T. S. A., *Organometallics* **2004**, *23*, 4342.
111. Kira, M.; Sekiguchi, Y.; Iwamoto, T.; Kabuto, C., *J. Am. Chem. Soc.* **2004**, *126*, 12778.
112. Burrows, A. D.; Mahon, M. F.; Varrone, M., *Dalton Trans.* **2004**, 3321.
113. Díaz-Requejo, M. M.; Nicasio, M. C.; Belderrain, Tomás R.; Pérez, Pedro J.; Puerta, M. C.; Valerga, P., *Eur. J. Inorg. Chem.* **2000**, *2000*, 1359.
114. Yang, Z., *Private Communication* **2004**.
115. Heck, R. F., *Palladium reagents in organic syntheses*, Academic Press: London, 1990; p 461.

Chapter 4

S,N-Bidentate Thioureas and Their Palladium Complexes

I. Introduction

Thiourea ligands have been found to be of use in metal catalyzed bis(methoxycarbonylations),^{1, 2} Suzuki-Miyaura cross-coupling reactions,³⁻⁵ Heck-Mizoroki cross-coupling reactions,^{4, 6-8} Suzuki-Miyaura carbonylations⁸ and Pauson-Khand reactions⁹ as well as other transformations,¹⁰ (see literature review in Chapter 3).

The synthesis of the chiral thiourea **L1** (Figure 1) was first reported by the group of Prof. Z. Yang at Peking University.⁶ **L1** was found to be efficient for Heck-Mizoroki^{6, 8} and Suzuki-Miyaura cross-coupling reactions,⁸ Suzuki-Miyaura carbonylations,⁸ bis(methoxycarbonylation)¹ reactions and alkoxy carbonylations of aryl iodides.¹¹

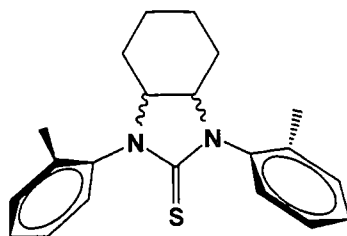


Figure 1. Chiral thiourea (**L1**).⁶

In collaboration with the group of Prof. Z. Yang, the mono- and dipalladium complexes of **L1** (A and B in Figure 2) were synthesized. Both complexes displayed complicated ¹H NMR spectra; however, the structures of both the monomer and dimer were confirmed by single-crystal X-ray diffraction studies.

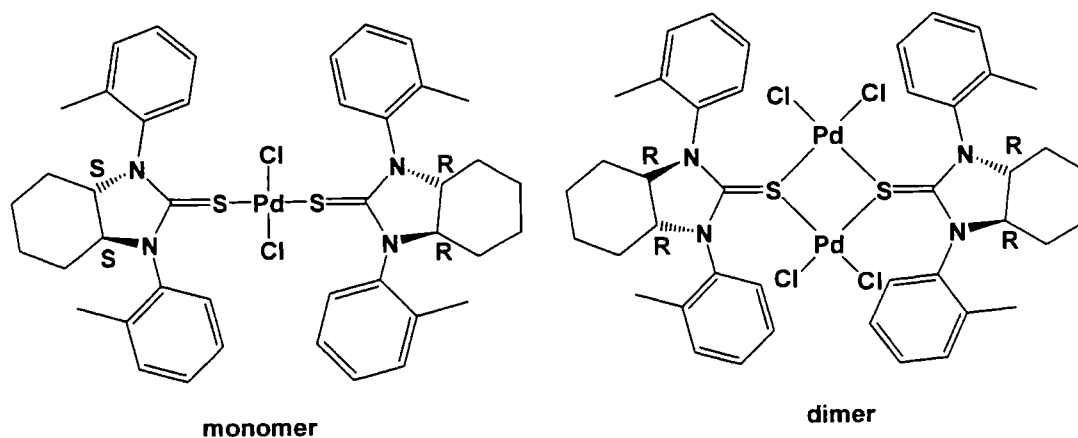


Figure 2. Mono- and di-palladium complexes of **L1**.

We have discussed that both the monomer and dimer and an *in situ* (1:1 Pd:L1) prepared catalyst system were used as catalyst precursors in the bis(methoxycarbonylations) reaction of terminal olefins (Table 13 in page 168). The yields obtained were very similar. These results combined with our extensive studies of the Pd–L1 system suggest that in all cases, the active catalyst is likely to be an “LPdX₂” complex. Clearly, these systems are extremely labile due to the nature of the S–Pd bond in the monodentate complex.

We therefore initiated a program focusing on the development of bidentate chiral S,N-oxazoline thiourea ligands for use in asymmetric bis(methoxycarbonylations) reactions. Their structures were designed on the basis of currently well-established heterobidentate ligands such as **A**¹²⁻¹⁵ and **B**¹⁶ (Figure 2) whose stereocontrol elements are derived from the oxazoline chirality.¹⁷⁻²¹ As the Pd-catalyzed bis(alkoxycarbonylation) was found to correspond to a *syn*-addition to the olefin double bond (Scheme 1),^{22, 23} we therefore envisaged that the *ee* values of the formed products would depend on the ability of the Pd-ligand complex to differentiate the two faces of the double bond, as well as on its orientation.

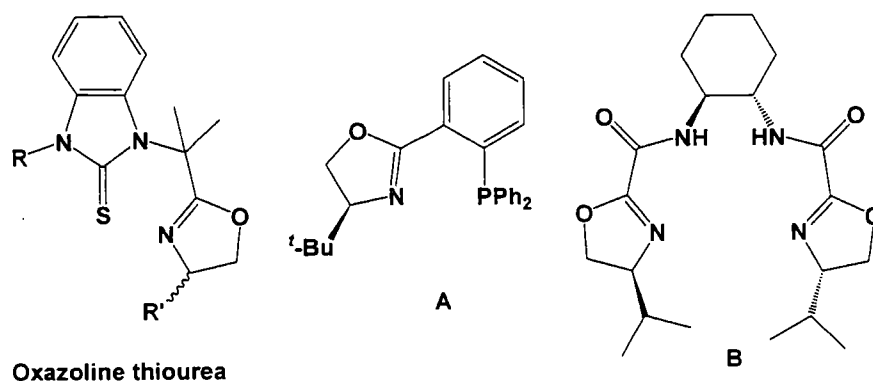
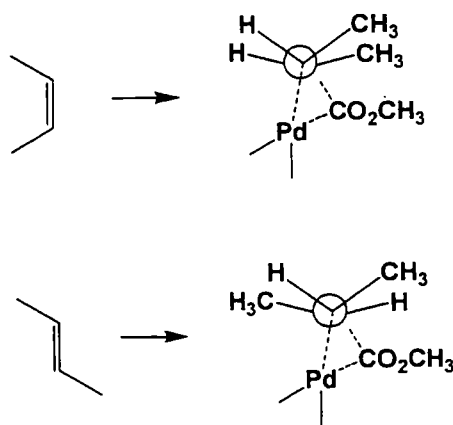


Figure 2. Heterobidentate ligands.



Scheme 1. Structures of *syn*-addition of carbomethoxy palladation transition states for *cis*- and *trans*-butene.²²

Several features of the oxazoline thiourea ligand are attractive. They have both S and N binding sites on the backbone which should afford rigid metal-ligand complexes with the bulky substituent on the oxazoline ring close to the metal center, which might enhance the facial differentiation ability of the complex toward its substrates and consequently lead to good *ee* values. Oxazoline thiourea ligands are anticipated to be bidentate, which is good for preventing Pd(0) aggregation.²⁴⁻²⁷ With the above in mind, the heterobidentate thiourea-oxazoline ligands with different types of -R and -R' groups were synthesized by the group of Prof. Z. Yang. The S₂N-thioureas can be classified into three types (Figure 3); (A) β -dimethyl oxazoline thioureas, (B) β -monomethyl oxazoline thioureas, and (C) the α -isoquinoline thiourea. The names and codes of the bidentate S₂N-thiourea ligands are given in Table 1.

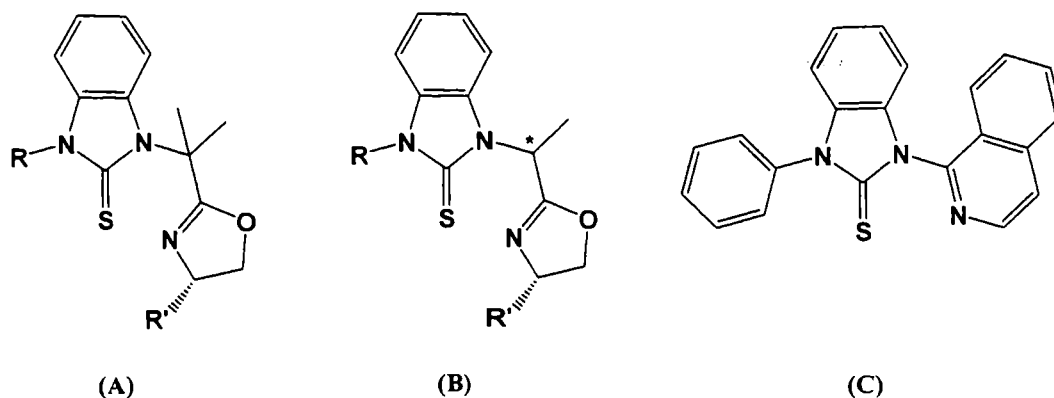


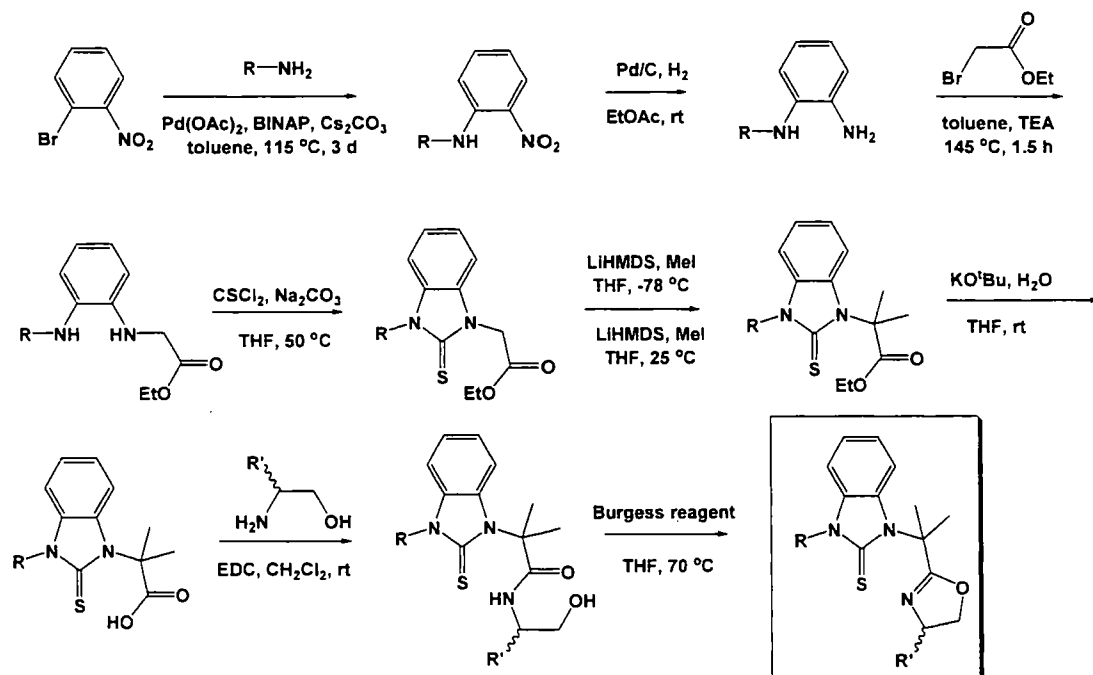
Figure 3. (A) β -dimethyl oxazoline thioureas, (B) β -monomethyl oxazoline thioureas and (C) α -isoquinoline thiourea.

Table 1. Names and codes of the bidentate S,N-thiourea ligands.

Codes	Names
L2	(S)-1-(2-(4-isopropyl-4,5-dihydrooxazol-2-yl)propan-2-yl)-3-(2-isopropylphenyl)-1 <i>H</i> -benzo[<i>d</i>]imidazole-2(3 <i>H</i>)-thione
L3	(R)-1-phenyl-3-(2-(4-phenyl-4,5-dihydrooxazol-2-yl)propan-2-yl)-1 <i>H</i> -benzo[<i>d</i>]imidazole-2(3 <i>H</i>)-thione
L4	(S)-1-(2-(4-isopropyl-4,5-dihydrooxazol-2-yl)propan-2-yl)-3-mesityl-1 <i>H</i> -benzo[<i>d</i>]imidazole-2(3 <i>H</i>)-thione
L5	(S)-1-cyclohexyl-3-(2-(4-isopropyl-4,5-dihydrooxazol-2-yl)propan-2-yl)-1 <i>H</i> -benzo[<i>d</i>]imidazole-2(3 <i>H</i>)-thione
L6	(S)-1-(2-(4-isopropyl-4,5-dihydrooxazol-2-yl)propan-2-yl)-3-phenyl-1 <i>H</i> -benzo[<i>d</i>]imidazole-2(3 <i>H</i>)-thione
L7	(S)-1-(2-(4-isopropyl-4,5-dihydrooxazol-2-yl)propan-2-yl)-3-p-tolyl-1 <i>H</i> -benzo[<i>d</i>]imidazole-2(3 <i>H</i>)-thione
L8	(S)-1-(4-(anthracen-9-yl)phenyl)-3-(2-(4-isopropyl-4,5-dihydrooxazol-2-yl)propan-2-yl)-1 <i>H</i> -benzo[<i>d</i>]imidazole-2(3 <i>H</i>)-thione
L9	1-(2-(anthracen-10-yl)phenyl)-3-(4-isopropyl-4,5-dihydrooxazol-2-yl)ethyl-1 <i>H</i> -benzo[<i>d</i>]imidazole-2(3 <i>H</i>)-thione
L10	1-(4-isopropyl-4,5-dihydrooxazol-2-yl)ethyl)-3-p-tolyl-1 <i>H</i> -benzo[<i>d</i>]imidazole-2(3 <i>H</i>)-thione
L11	(S)-1-(2-(anthracen-9-yl)phenyl)-3-(2-(4-isopropyl-4,5-dihydrooxazol-2-yl)propan-2-yl)-1 <i>H</i> -benzo[<i>d</i>]imidazole-2(3 <i>H</i>)-thione
L12	1-(isoquinolin-1-yl)-3-phenyl-1 <i>H</i> -benzo[<i>d</i>]imidazole-2(3 <i>H</i>)-thione
L13	1-(2-(anthracen-9-yl)phenyl)-3-(2-(4,5-dihydrooxazol-2-yl)propan-2-yl)-1 <i>H</i> -benzo[<i>d</i>]imidazole-2(3 <i>H</i>)-thione

A) β -Dimethyl oxazoline thioureas

The general approach to the synthesis of the β -dimethyl oxazoline thioureas is shown in Scheme 2 (see Figure 4 for R and R' substituents).



Scheme 2. Synthesis of β -dimethyl oxazoline thioureas developed by the group of Prof. Z. Yang.

Structures of the β -dimethyl oxazoline thioureas which were synthesized are depicted in Figure 4.

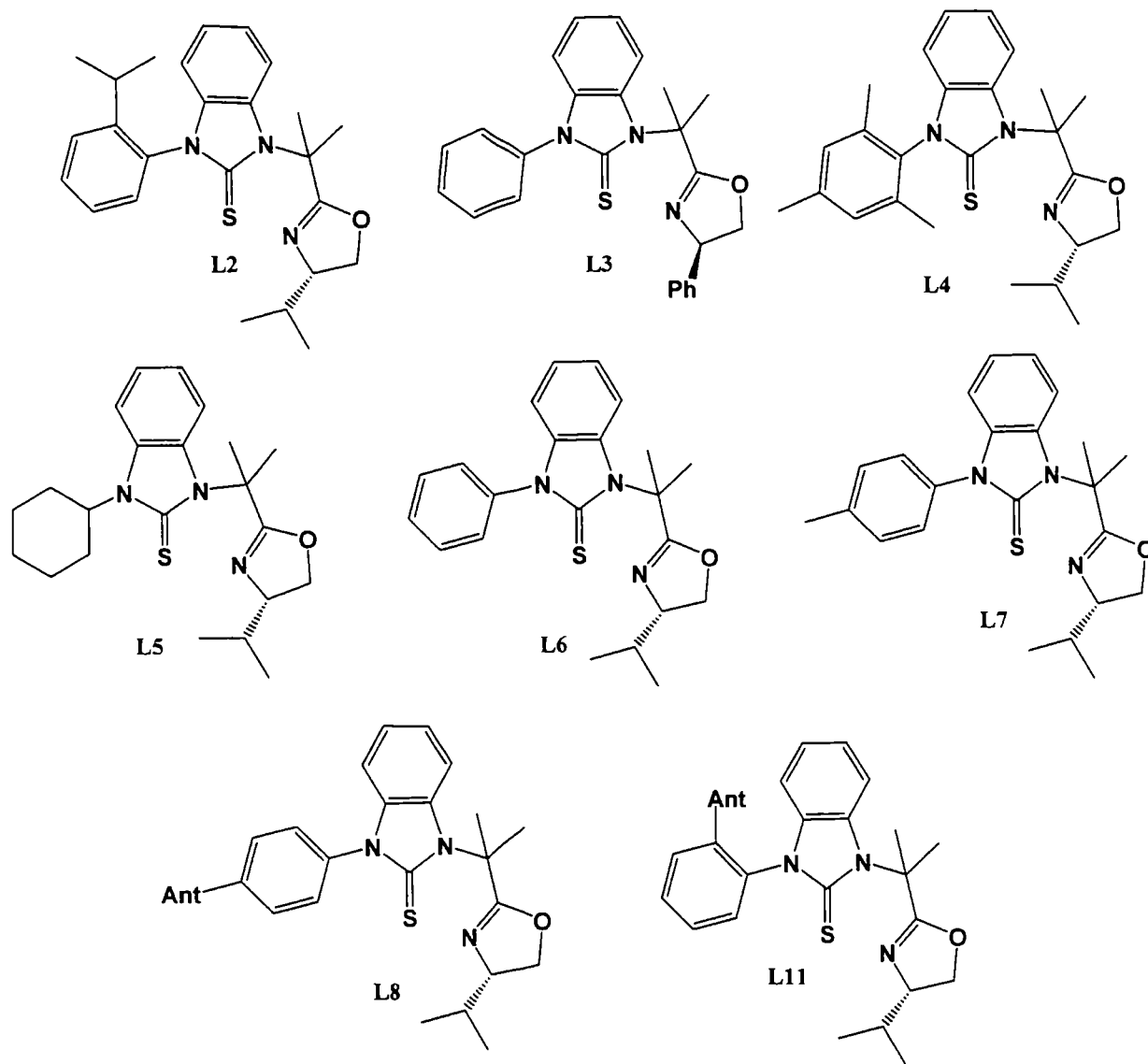


Figure 4. The structures of the β -dimethyl oxazoline thiourea ligands.

For **L2** and **L11**, two spots were observed on TLC plates, and silica column chromatography led to the isolation of two fractions. We postulated that these were atropisomers resulting from hindered rotation about the N–C bond of the phenyl ring caused by the respective bulky ^tPr and 9-anthryl groups. We have published the results on the use of palladium complexes of **L2** in the bis(methoxycarbonylation) of styrenes.²

The ^tPr group was cleaved from the **L11** fraction which eluted first to give **L13** (Figure 5).

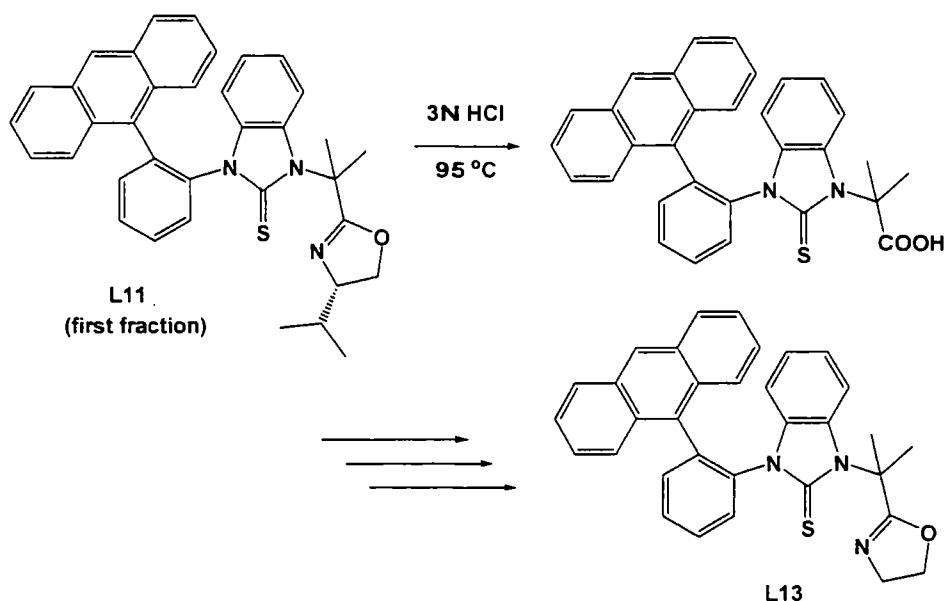


Figure 5. The synthesis of **L13** by the group of Prof. Z. Yang.

B) β -Monomethyl oxazoline thioureas

By using a similar procedure as was employed for the synthesis of the β -monomethyl oxazoline thioureas, **L9** and **L10** were obtained (Schemes 3 and 4, respectively). For **L9**, two spots were observed on TLC plates and silica column chromatography led to the isolation of two fractions (**B** and **C**) when the β -amino alcohol was introduced to **A**. We postulated that **B** and **C** were diastereomers differing in the configuration of H (or Me) at the β position of the oxazoline thiourea and atropoisomers due to restricted N-C_{Ar} rotation. They were separated by silica column chromatography. Furthermore, two spots on the TLC were obtained from both **B** (**B1** and **B2**) and **C** (**C1** and **C2**) after the cyclization of oxazoline arising from the presence of three chiral "centers" only one of which was of fixed geometry (*i.e.* the oxazoline). There were thus four final fractions from the synthesis of **L9**; however, due to the difficulty of the separations, only two fractions were obtained (**B1** and **C1**) (Scheme 3 and Figure 6 for the synthesis and the TLC of the **B** and **C** fractions, respectively). It should be noted that there are two diastereomers formed in the methylation reaction to obtain **A**; however, a good separation was achieved only after the β -amino alcohol was introduced to **A**. Furthermore, both **B** and **C** fraction contains two compounds, but they were separated only after the cyclization of the oxazoline ring.

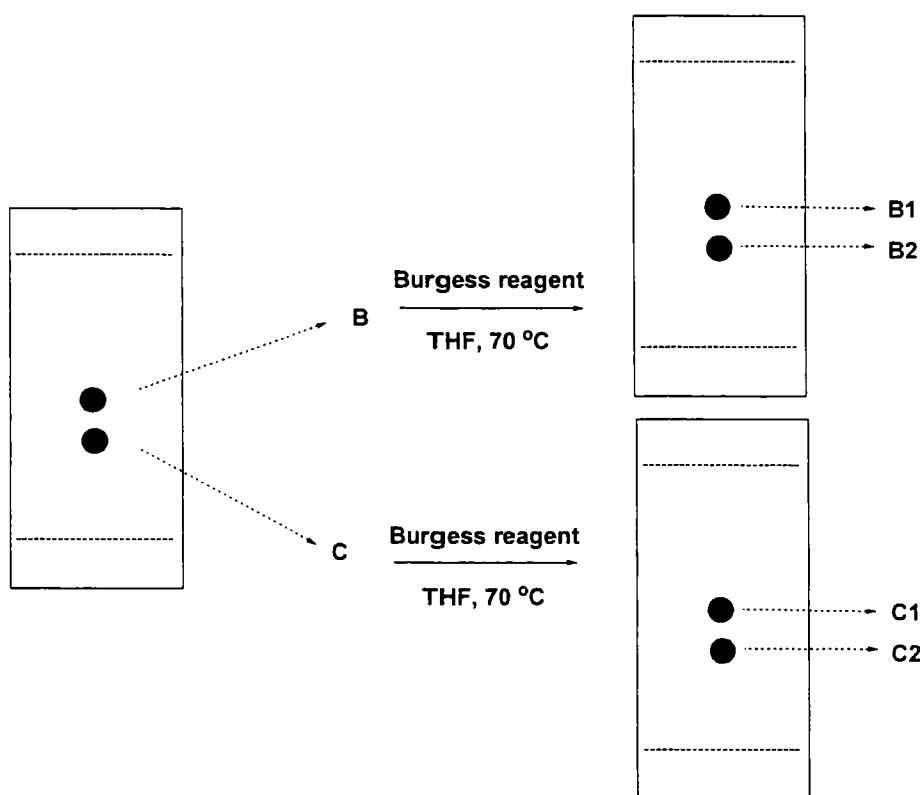
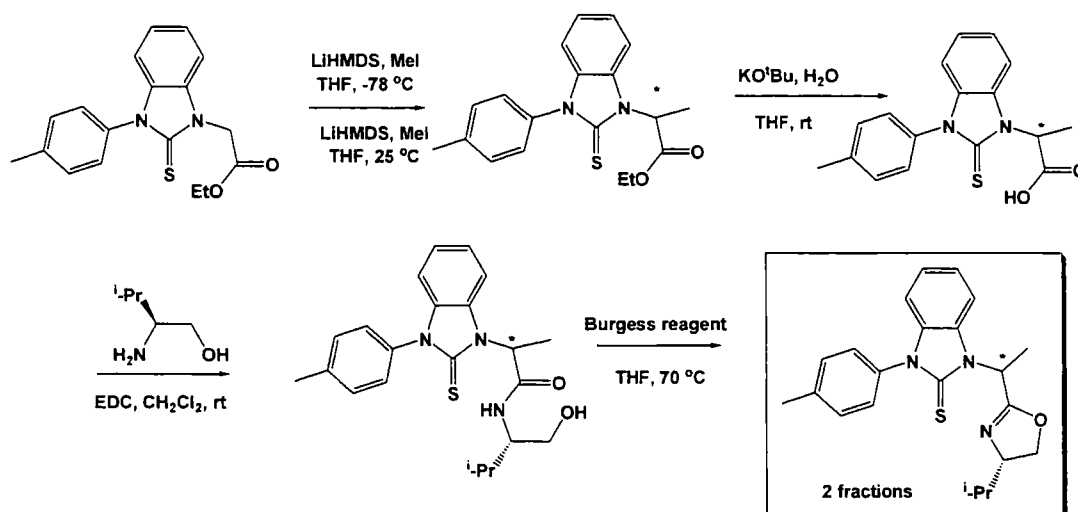


Figure 6. The TLC of compounds B, C and L9.

For **L10**, two spots were observed on TLC and silica column chromatography led to the isolation of two fractions as diastereomers. It should be noted that there are two diastereomers formed in the methylation reaction; however, a good separation was achieved only after the cyclization of the oxazoline ring (Scheme 4).



Scheme 4. The synthesis of the β -monomethyl oxazoline thiourea **L10** reported by the group of Prof. Z. Yang.

C) α -Isoquinoline thiourea **L12** (Figure 7)

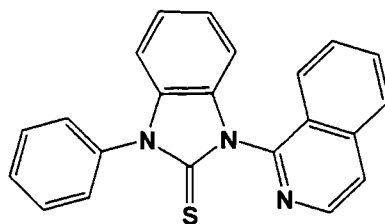


Figure 7. The structure of the α -isoquinoline thiourea **L12**.

In collaboration with the group of Prof. Z. Yang who synthesized the ligands and are testing their reactivity in Pd-catalyzed bis(methoxycarbonylation), we focused on detailed characterization of the ligands and on the synthesis and characterization of their palladium complexes. In some cases, these palladium complexes are also being tested for their catalytic activity.

The objectives of this study are:

1. the characterization of the bidentate S,N chiral thiourea ligands; and
2. the synthesis of the palladium complexes of bidentate S,N chiral thiourea ligands with full characterization and investigation into their properties.

II. Results and Discussion

II.1 Ligand characterization

The ligands were characterized by ^1H , $^{13}\text{C}\{^1\text{H}\}$, COSY, NOESY, HSQC and HMBC NMR spectroscopy, high resolution mass spectrometry and single-crystal X-ray diffraction (in some cases).

II.1.1 The crystal structures of oxazoline thiourea free ligands

Suitable single crystals for X-ray diffraction of both column fractions of **L2** were grown from slow evaporation of solutions in $\text{CH}_2\text{Cl}_2:\text{Et}_2\text{O}$ mixtures. Similarly, diffraction quality crystals of **L7** and the first fraction of **L10** were obtained from hexane. Crystallographic data of **L2**, **L7** and **L10** are summarized in Table 2 and selected bond lengths and angles for all of the structures are listed in Table 3.

A) The crystal structures of the β -dimethyl oxazoline thioureas

The two fractions of **L2**, which are indeed atropoisomers, are configurationally stable and were separated by silica column chromatography. We have termed the atropoisomers 'up' and 'down' based on the conformation of the 'Pr substituent on the phenyl ring (Figure 8).

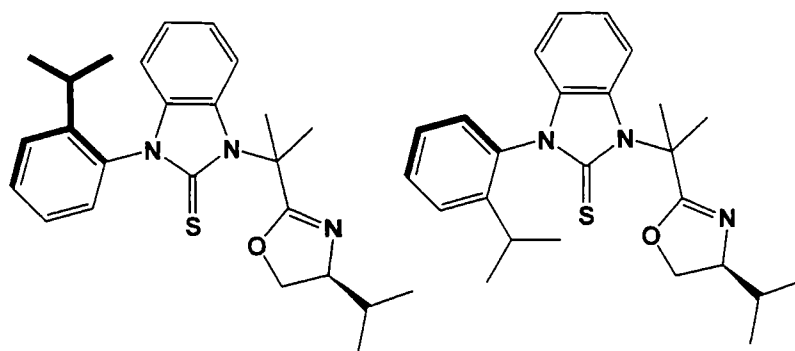


Figure 8. The structures of the 'up' (left) and 'down' (right) atropoisomers of **L2**.

The second fraction of **L2** was found to crystallize in the monoclinic space group $P2_1$ and contains two independent molecules in the asymmetric unit. The molecular structure of both is shown in Figure 9. Both show the 'up' conformation of the 'Pr substituent, so this isomer is referred to as **L2up**, and both show similar bond lengths and angles (Table 3).

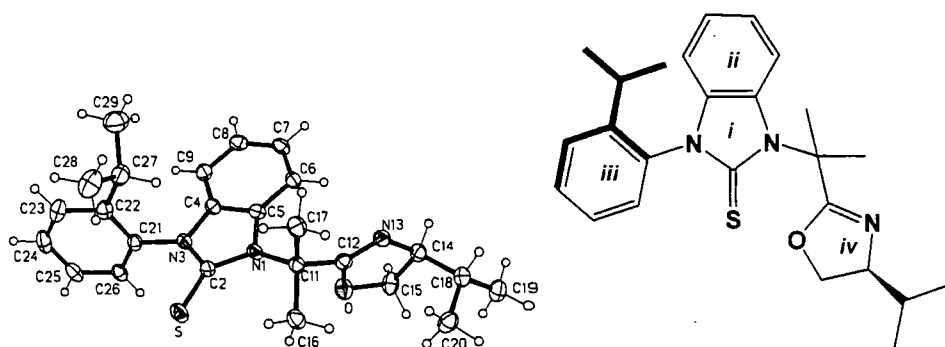


Figure 9. The molecular structure of **L2up** (two independent molecules in the asymmetric unit but only one molecule is shown).

The other **L2** fraction also crystallizes in space group $P2_1$, but with one molecule in the asymmetric unit. In this structure, the ⁱPr substituent on the phenyl ring is shown to be in the 'down' conformation, so it is referred to as **L2down**. The molecular structure of **L2down** is depicted in Figure 10.

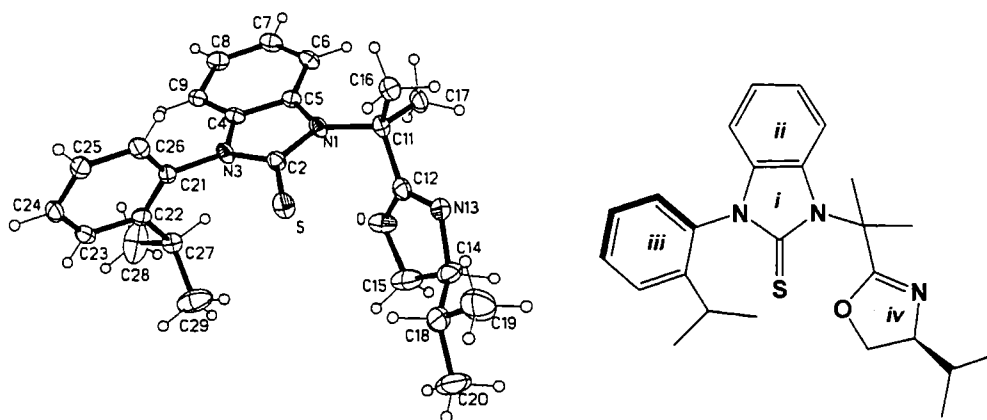


Figure 10. The molecular structure of **L2down**.

The structures of both **L2up** and **L2down** clearly show that the *ortho*-ⁱPr groups on the phenyl ring **iii** are on the opposite sides with respect to the bicyclic thiourea moiety. The bond lengths, angles and dihedral angles of the molecules are very similar (Table 3). The central N₂CS moiety (**i**) is slightly inclined to the fused benzene ring (**ii**) and almost normal to the phenyl ring (**iii**) and the mean plane of the oxazoline ring (**iv**). **L2up** shows a slight envelope-like distortion; in one molecule, C(14) deviates from the plane of the other four atoms on the oxazoline ring by 0.10 Å, whereas C(15) in the latter molecule deviates by 0.13 Å.

L7 crystallizes in the triclinic space group *P1* with two independent molecules in the asymmetric unit (**I** and **I'**), both showing similar bond lengths and angles. The molecular structure of **L7** is depicted in Figure 11. The dihedral angle C(2)–N(1)–C(11)–C(12) of molecule **I** (162.8°) is *ca.* 5° larger than its equivalent in molecule **I'**. Molecules **I** and **I'** differ because of the N(1)–C(11)–C(12)–N(13) torsion angles of 127.9° and -136.0° in molecules **I** and **I'**, respectively.

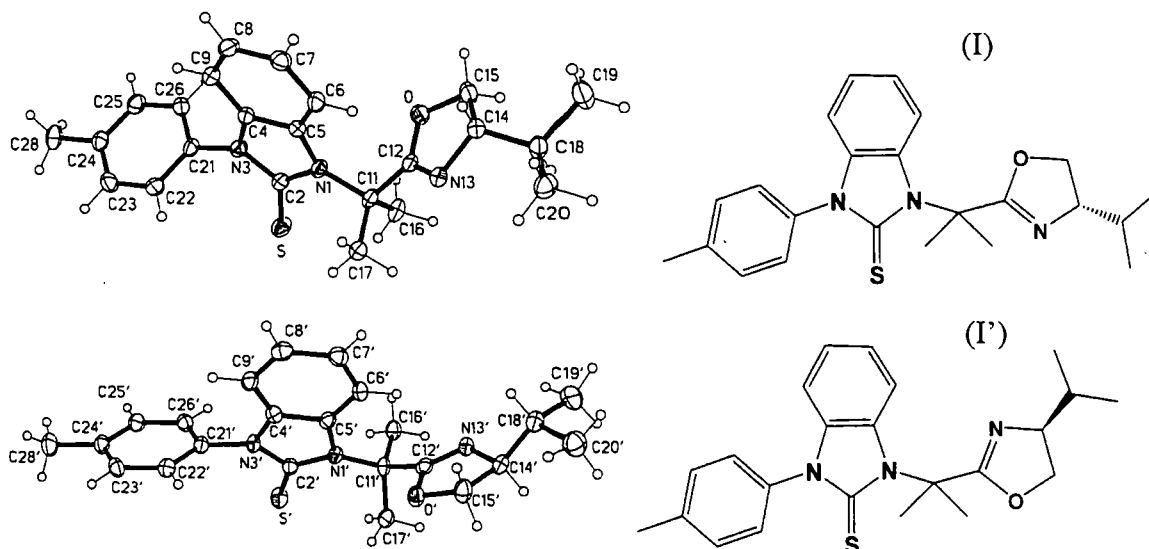


Figure 11. The molecular structure of **L7**.

The average C=S bond length in **L2up**, **L2down** and **L7** is 1.66 Å which is almost the same as those in the monodentate C_2 -chiral thiourea **L1(S,S)** and **L1(rac)**. The average C=S bond length is shorter than that in *tu* and *tmtu* by 0.02 and 0.06 Å, respectively. The C(2)–N(1) and C(2)–N(2) bond lengths are almost the same (C(2)–N(1) 1.384(3) – 1.388(3) Å, and C(2)–N(2) 1.367(3) – 1.384(3) Å), which are 0.02 and 0.04 Å longer than those in *tu* and *tmtu*. All three ligands show significant differences of the two S–C–N angles (S–C(2)–N(1); $129.07(19) - 131.4(2)^\circ$, and S–C(2)–N(3); $122.4(2) - 124.47(18)^\circ$). We believe that the steric bulk of the β -dimethyl oxazoline moiety may be responsible for S–C(2)–N(1) being wider than S–C(2)–N(3). The N(3)–C(2)–N(1) angles are $105.6 - 106.6^\circ$, significantly smaller than that of *tmtu* (115.4°), which can be explained by the fused five-membered thiourea ring *i* and the phenyl ring *ii*.

B) The crystal structure of the β -monomethyl oxazoline thiourea **L10**

The first fraction of **L10** crystallizes in the orthorhombic space group $P2_12_12_1$ with one molecule in the asymmetric unit. The molecular structure is shown in Figure 12. C(11) was found to have the **R** configuration with respect to the known **S** configuration of the CHⁱPr group on the oxazoline; therefore, this isomer is referred to as **R-L10** (Figure 13). The second fraction is therefore very likely to be its diastereomer with an **S** configuration at C(11) which is referred to as **S-L10**. Selected bond lengths and angles are displayed in Table 3. The bond lengths and angles are similar to those of the β -dimethyl oxazoline thiourea structures. Noteworthy differences are the S–C(2)–N bond angles and the angle between the mean planes of the thiourea ring *i* and the phenyl ring *ii*. The S–C(2)–N(1) ($127.22(17)^\circ$) and S–C(2)–N(3) ($126.53(15)^\circ$) angles in **R-L10** are fairly close, unlike the disparate values in the β -dimethyl oxazoline thioureas. We believe that this is because the monomethyl oxazoline moieties have less steric bulk and are thus more flexible than the β -dimethyl oxazoline ones. This is important to note and will be discussed later in the context of their complexes with palladium. Furthermore, the angle between rings *i* and *ii* of **R-L10** is very small (0.7°), whereas the equivalent angles in the β -dimethyl oxazoline thioureas are wider ($3.1 - 8.2^\circ$).

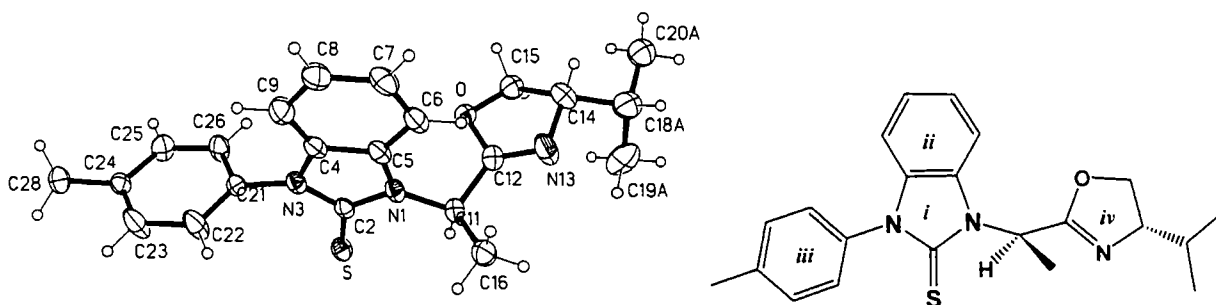


Figure 12. The molecular structure of **R-L10**.

We tried to grow diffraction-quality crystals of the other oxazoline thiourea ligands, in particular the fractions of **L11**, **L13** and **L9** to confirm their stereochemistry, but to no avail.

Table 2. Crystallographic data for **L2up**, **L2down**, **L7** and **R-L10**.

	L2up	L2down	L7	R-L10
Empirical formula	C ₂₅ H ₃₁ N ₃ OS	C ₂₅ H ₃₁ N ₃ OS	C ₂₃ H ₂₇ N ₃ OS	C ₂₂ H ₂₅ Cl ₂ N ₃ O
Formula weight	421.59	421.59	393.54	379.51
Temperature (K)	120(2)	120(2)	120(0)	120(2)
Crystal system	Monoclinic	Monoclinic	Triclinic	Orthorhombic
Space group	<i>P</i> 2 ₁	<i>P</i> 2 ₁	<i>P</i> 1	<i>P</i> 2 ₁ 2 ₁ 2 ₁
a (Å)	11.841(1)	8.9806(8)	9.2534(3)	6.2743(5)
b (Å)	15.138(1)	11.3367(12)	10.3115(4)	14.9802(12)
c (Å)	12.813(1)	11.9121(11)	12.7445(4)	21.4775(18)
α (°)	90.00	90.00	98.036(2)	90.00
β (°)	90.95(1)	104.65(1)	110.765(2)	90.00
γ (°)	90.00	90.00	109.899(2)	90.00
Volume (Å ³)	2296.4(3)	1173.3(2)	1021.16(6)	2018.7(3)
Z	4	2	2	4
Density (calculated) (Mg/m ³)	1.219	1.193	1.280	1.249
Absorption coefficient (mm ⁻¹)	0.162	0.159	0.177	0.177
Crystal size (mm ³)	0.28 x 0.20 x 0.17	0.14 x 0.12 x 0.10	0.30 x 0.12 x 0.07	^a
Theta range for data collection (°)	1.59 to 29.00	1.77 to 27.50	1.79 to 28.50	1.66 to 25.00
Reflections collected	29694	12256	19789	17940
Independent reflections	12198 [R(int)=0.0922]	5364 [R(int)=0.0514]	10223 [R(int)=0.0412]	3563 [R(int)=0.0444]
Data / restraints / parameters	12198 / 1 / 565	5364 / 1 / 283	10223 / 526 / 3	3563 / 7 / 256
Final R indices I > 2σ	R1=0.0496, wR2=0.0985	R1=0.0521, wR2=0.0952	R1=0.0389, wR2=0.0868	R1=0.0367, wR2=0.0819
R indices (all data)	R1=0.0758, wR2=0.1061	R1=0.0782, wR2=0.1035	R1=0.0521, wR2=0.0917	R1=0.0440, wR2=0.0852

^a not measured.

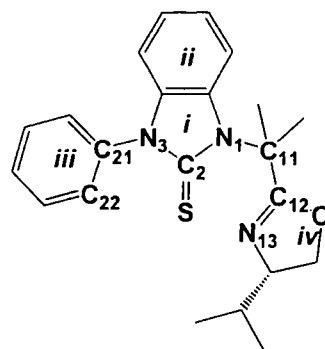


Table 3. Selected bond lengths and angles for the β -mono- and di-methyl oxazoline thioureas.

Selected bond lengths (Å)	L2up		L2down	L7		R-L10
S=C(2)	1.663(2)	1.656(2)	1.660(2)	1.673(2)	1.666(2)	1.658(2)
N(1)-C(2)	1.384(3)	1.387(3)	1.386(3)	1.388(3)	1.386(3)	1.381(3)
N(3)-C(2)	1.378(3)	1.384(3)	1.367(3)	1.374(3)	1.377(3)	1.374(3)
C(11)-C(12)	1.520(3)	1.520(3)	1.512(4)	1.513(3)	1.515(3)	1.512(3)
C(12)=N(13)	1.256(3)	1.254(3)	1.265(3)	1.266(3)	1.259(3)	1.254(3)
Selected bond angles (deg)						
S-C(2)-N(1)	131.4(2)	131.2(2)	129.07(19)	129.95(15)	130.43(15)	127.22(17)
S-C(2)-N(3)	122.4(2)	123.2(2)	124.47(18)	123.46(16)	123.35(15)	126.53(15)
N(3)-C(2)-N(1)	106.21(17)	105.58(18)	106.46(19)	106.57(17)	106.21(16)	106.25(18)
Selected dihedral angles (deg)						
S-C(2)-N(3)-C(21)	-171.1	-9.0	9.5	0.3	0.9	-4.6
C(2)-N(3)-C(21)-C(22)	90.6	90.4	-113.0	70.6	114.7	-82.4
C(2)-N(1)-C(11)-C(12)	149.7	144.9	48.7	162.8	-158.9	-3.1
N(1)-C(11)-C(12)-N(13)	129.3	129.9	-143.4	127.9	-136.0	122.0
Selected angles between planes (deg)						
<i>i/ii</i>	8.2	5.0	3.7	3.1	3.3	0.7
<i>i/iii</i>	86.4	79.2	72.7	73.0	70.2	84.1
<i>i/iv</i>	83.9	76.2	70.2	75.6	68.5	86.7

II.1.2 The NMR characterization of the oxazoline thiourea ligands

The characterization of oxazoline thioureas using NMR techniques is worth discussing in detail.

Figure 14 shows the structure of **L7** with all carbons positions numbered for NMR assignment. The ^1H and $^{13}\text{C}\{^1\text{H}\}$ NMR spectra of **L7** are depicted in Figures 15 and 16, respectively.

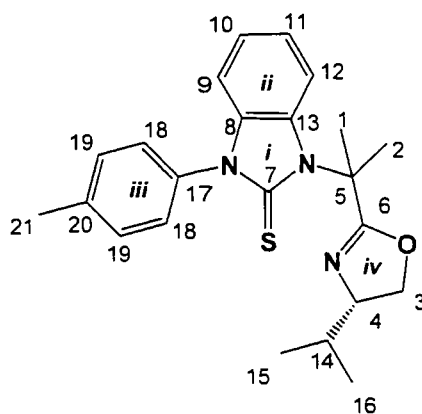


Figure 13. The structure of **L7** with carbons positions numbered for NMR assignment.

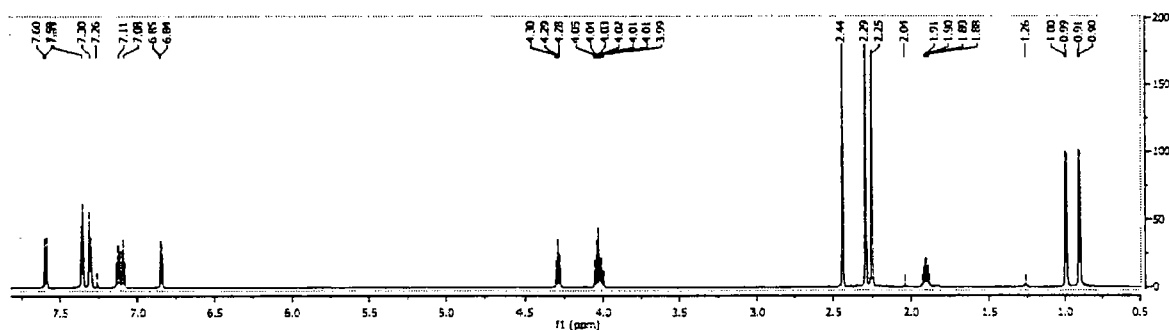


Figure 14. The ^1H NMR (500 MHz, CDCl_3) spectrum of **L7**.

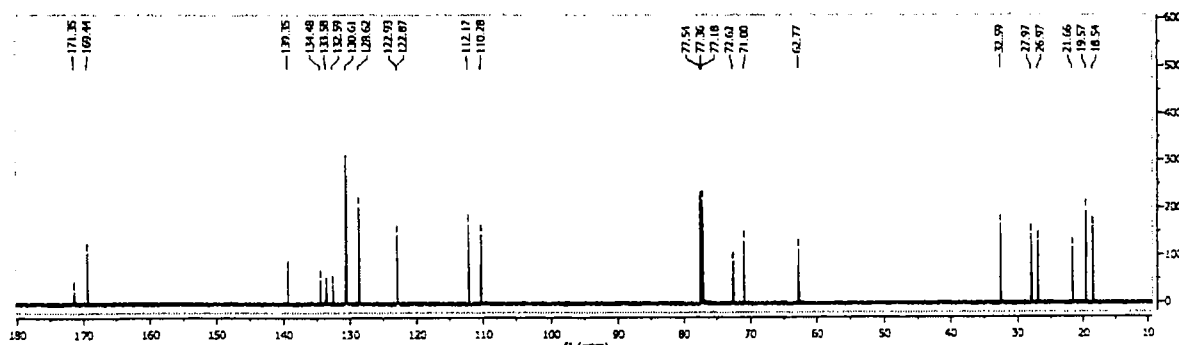


Figure 15. The $^{13}\text{C}\{^1\text{H}\}$ NMR (125 MHz, CDCl_3) spectrum of **L7**.

Initial inspection of the ^1H NMR spectrum of **L7** easily identifies the two doublet signals at δ 0.89 ($J_{\text{H-H}} = 7$ Hz) and 0.98 ($J_{\text{H-H}} = 7$ Hz) as belonging to the protons at positions 15 and 16, and the multiplet at δ 1.97 ppm as the proton at position 14 (Figure 15). Using COSY, the signal at position 14 can be used to assign the proton at position 4 in the oxazoline ring *iv* (the COSY spectrum is depicted in Figure 17). The proton at position 4 can then be used to assign the nonequivalent (axial and equatorial) protons at position 3. The assignment of the protons in positions 3 and 4 was confirmed by the HSQC spectrum (Figure 18).

Using NOESY, the singlets at δ 2.24 and 2.28 ppm can be assigned to the methyl protons at positions 1 and 2 which show NOESY correlation to the aromatic proton at position 12 (at δ 7.58 ppm) (Figure 19). The aromatic protons in phenyl ring *ii* can then be assigned by using the COSY spectrum. The COSY correlation of the proton at position 12 can be used to assign the protons at positions 11, 10 and 9 (Figure 20). Therefore, the other singlet at δ 2.43 ppm must belong to the methyl protons at position 21. This signal shows NOESY correlations to the aromatic protons at δ 7.34 ppm, (d, $J_{\text{H-H}} = 8$ Hz, 2H) (Figure 19). With this information, we assigned this signal to the protons at position 19 (in phenyl ring *iii* in Figure 14). Moreover, the COSY correlations of H19 can then be used to assign H18 protons in the phenyl ring *iii*.

All of the carbons except C6 and C7 were assigned using HSQC and then confirmed by HMBC. Finally, the quaternary carbons C6 and C7 were identified by HMBC, as C6 shows a correlation to the protons at positions 1, 2, 3 and 4 whereas C7 does not correlate with any proton (see Figure 21).

All of the oxazoline thiourea ligands can be characterized and their proton and carbon resonances assigned using the same 2D NMR techniques. The assignment of the ^1H NMR spectra of the oxazoline thiourea ligands is shown in Tables 4 – 8, whereas the $^{13}\text{C}\{^1\text{H}\}$ NMR assignments are given in the experimental section.

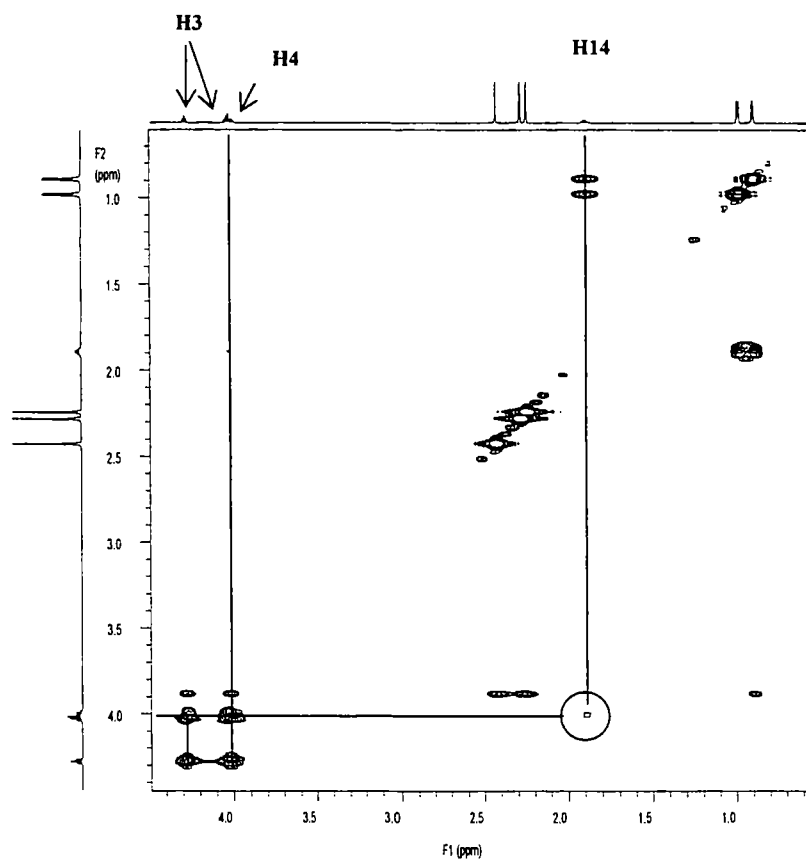


Figure 16. The COSY spectrum in the aliphatic region of L7.

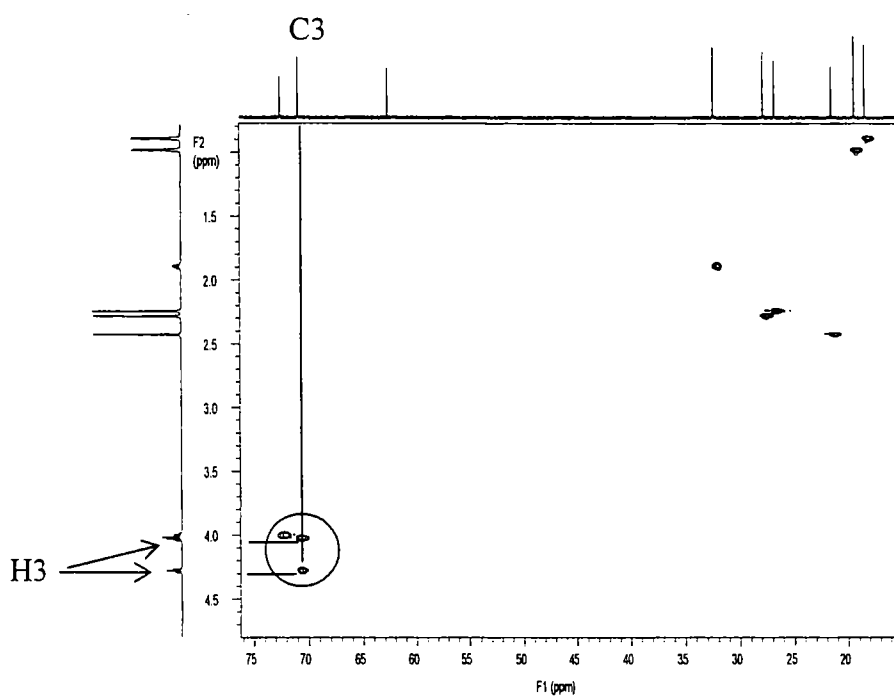


Figure 17. The HSQC spectrum in the aliphatic region of L7.

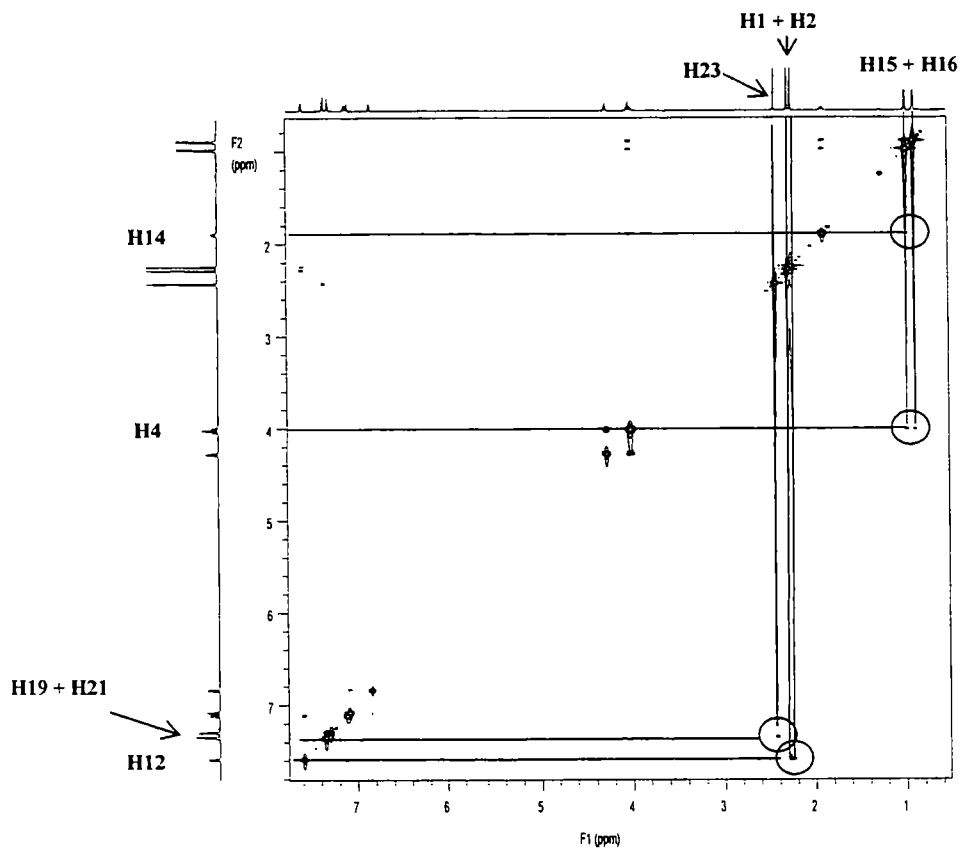


Figure 18. The NOESY spectrum of L7.

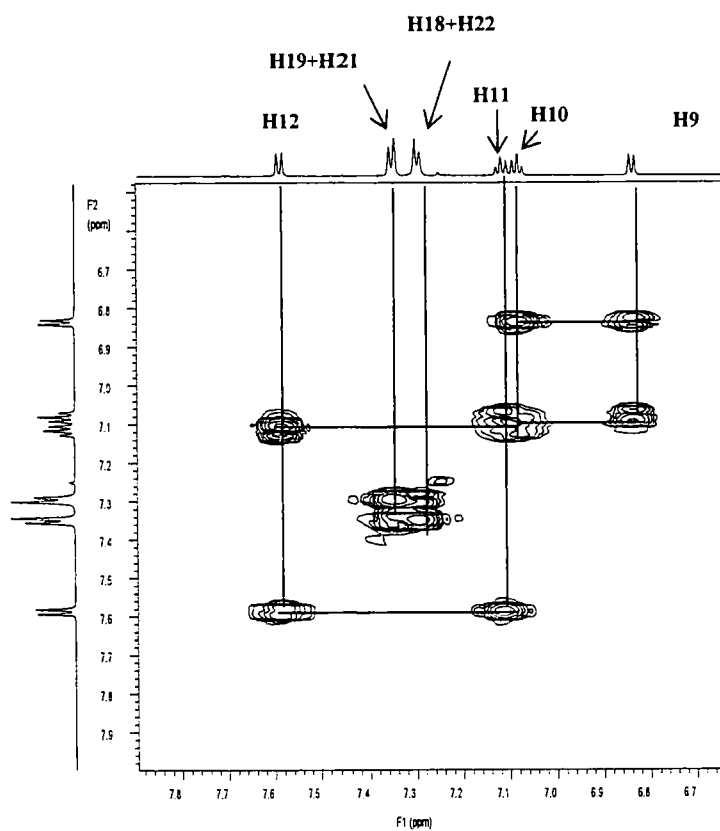


Figure 19. The COSY spectrum in the aromatic region of L7.

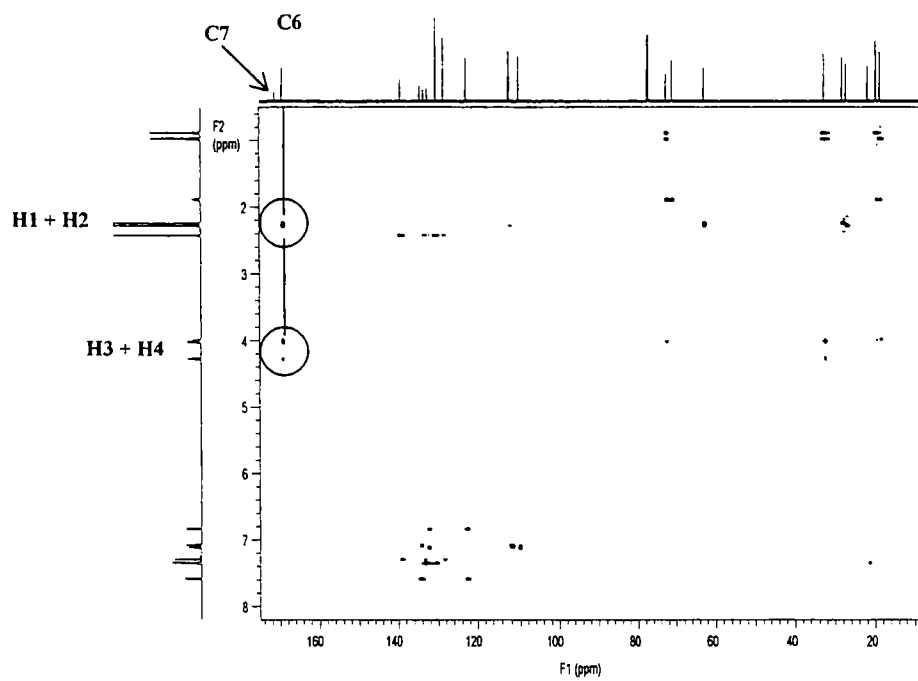
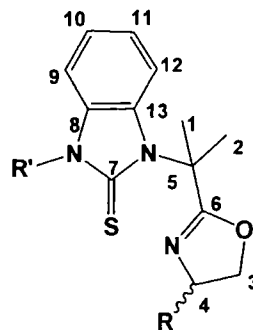
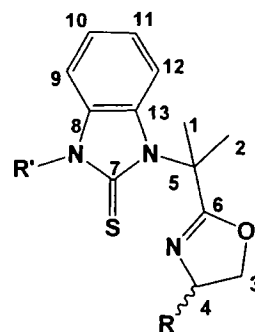


Figure 20. The HMBC spectrum of L7.

Table 4. ¹H NMR assignment of the β-dimethyl oxazoline thioureas (positions 1 – 12) with coupling constants given in Hz in parentheses.

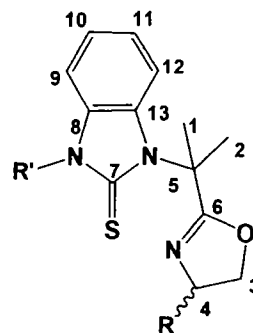
Compound	R	R'	H1, H2	H3	H4	H9	H10	H11	H12
L3			2.30, s, 3H 2.27, s, 3H	4.66, t (7), 1H 4.12, t (7), 1H	5.21 t (10) 1H	6.84 d (7) 1H	7.12 d (7) 1H	7.16 d (7) 1H	7.68 d (7) 1H
L2up			2.26, s, 3H 2.19, s, 3H	4.18 – 4.22, m, 1H 3.95 – 3.99, m, 1H	3.90 – 3.94 m 1H	6.62 d (8) 1H	7.08 t (8) 1H	7.18 – 7.21 m 1H	7.63 d (9) 1H
L2 down			2.24, s, 3H 2.20, s, 3H	4.23, t (9), 1H 3.89 – 3.95, m, 2H	6.62 d (7) 1H	7.08 t (7) 1H	7.12 – 7.14 m 1H	7.62 d (8) 1H	
L4			2.25, s, 3H 2.20, s, 3H	4.23, t (8), 1H 3.95, t (8), 1H	3.93 – 3.98 m 1H	6.58 d (7) 1H	7.08 d (8) 1H	7.14 d (8) 1H	7.64 d (8) 1H

Table 4 (continued)



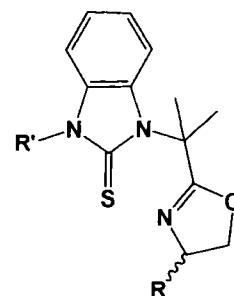
Compound	R	R'	H1, H2	H3	H4	H9	H10	H11	H12
L5			2.17, s, 3H 2.12, s, 3H	4.22, t (8), 1H 3.94, t (8), 1H	3.93 – 3.96 m 1H	7.49 d (8) 1H	7.08 d (8) 1H	7.14 d (8) 1H	7.57 d (8) 1H
L6			2.28, s, 3H 2.23, s, 3H	4.31, t (8), 1H 4.03, t (8), 1H	3.39 t (8) 1H	6.86 d (8) 1H	7.15 t (8) 1H	7.19 t (8) 1H	7.66 d (8) 1H
L7			2.28, s, 3H 2.24, s, 3H	4.28, t (8), 1H 4.00 – 4.05, m, 2H	6.83 d (8) 1H	7.08 t (8) 1H	7.12 t (8) 1H	7.58 d (8) 1H	
L8			2.36, s, 3H 2.34, s, 3H	4.39, t (8), 1H 4.08 – 4.15, m, 2H	7.14 d (8) 1H	7.26 t (7) 2H	7.65-7.77 m 1H		

Table 4 (continued)



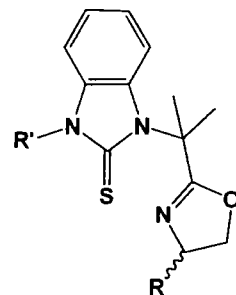
Compound	R	R'	H1, H2	H3	H4	H9	H10	H11	H12
L11 (2 nd fraction)		Ant 	1.89, s, 3H 1.76, s, 3H	3.90, t (8), 1H 3.76, t (8), 1H	3.82 – 3.86 m 1H	6.57 d (8) 1H	6.41 t (8) 1H	6.64 t (8) 1H	7.08 d (8) 1H
L11 (1 st fraction)		Ant 	1.94, s, 3H 1.68, s, 3H	4.06, t (8), 1H 3.70, t (8), 1H	3.87 t (8) 1H	6.57 d (7) 1H	6.41 t (7) 1H	6.64 t (7) 1H	7.08 d (7) 1H
L13	H	Ant 	1.93, s, 3H 1.68, s, 3H	4.09, q (9), 1H 3.98, q (9), 1H	3.76 – 3.84 m 2H ^a	6.59 d (8) 1H	6.42 t (8) 1H	6.65 t (8) 1H	7.09 d (8) 1H

^a Two protons with R = H.

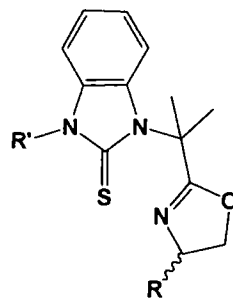
Table 5. ^1H NMR assignment for the R-substituent of the β -dimethyl oxazoline thioureas (positions 14 – 16).

Compound	R	R'	H14	H15, H16	Compound	R	R'	H14	H15, H16
L2up			1.74 – 1.81 m 1H	0.94, d (7), 3H 0.87, d (7), 3H	L5			1.82 – 1.87 m 1H	0.95, d (7), 3H 0.87, d (7), 3H
L2down			1.76 – 1.83 m 1H	0.96, d (7), 3H 0.86, d (7), 3H	L6			1.81 – 1.88 m 1H	1.02, d (7), 3H 0.93, d (7), H
L4			1.80 – 1.87 m 1H	0.95, d (7), 3H 0.86, d (7), 3H	L7			1.88 – 1.93 m 1H	0.98, d (7), 3H 0.89, d (7), 3H

Table 5 (continued)



Compound	R	R'	H14	H15, H16	Compound	R	R'	H15 – H19
L8			1.95 – 1.99 m 1H	1.02, d (7), 3H 0.92, d (7), 3H	L3			7.31 – 7.36, m, 4H 7.40 – 7.27, m, 1H
L11 (2 nd fraction)			1.78 – 1.83 m 1H	0.92, d (8), 3H 0.82, d (8), 3H				
L11 (1 st fraction)			1.76 – 1.81 m 1H	0.91, d (7), 3H 0.83, d (7), 3H				

Table 6. ¹H NMR assignment for R'-substituent for the β-dimethyl oxazoline thiourea (positions 17 - 24).

Compound	R	R'	H17 and H18	H19	H21	H22	H23	H24
L2up			1.19, d (7), 3H 0.98, d (7), 3H	2.46 – 2.51 m 1H	7.18 – 7.21 m 1H	7.39 – 7.42 m 1H	7.57 – 7.59 m 2H	
L2down			1.18, d (7), 3H 0.99, d (7), 3H	2.47 – 2.55 m 1H	7.12 – 7.14 m 1H	7.34 – 7.37 m 1H	7.50 – 7.52 m 2H	
L3			-	-	7.42 t (7) 2H	7.58 t (8) 2H	7.50 – 7.53 m 1H	-

Table 6 (continued)

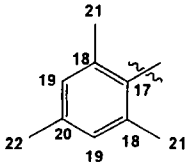
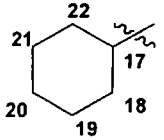
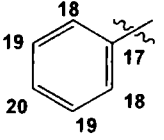
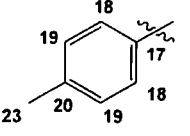
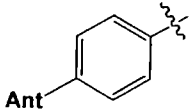
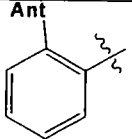
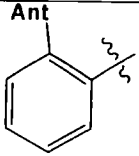
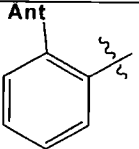
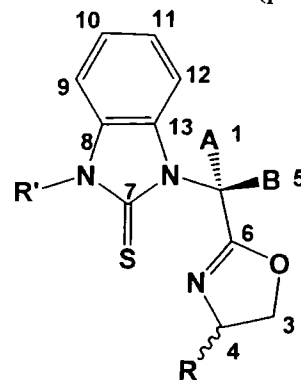
Compound	R	R'	H17	H18	H19	H20	H21	H22	H23
L4			-	-	7.03 s 2H	-	1.87 s 6H	2.35 s 3H	-
L5			2.08 – 2.02, m, 2H; 1.94 – 1.97, m, 2H; 1.82 – 1.87, m, 4H; 1.49 – 1.59, m, 2H; 1.29 – 1.38, m, 1H			-	-	-	-
L6			-	7.44 d (8) 2H	7.62 t (8) 2H	7.55 t (8) 1H	-	-	-
L7			-	7.29 d (8) 2H	7.34 d (8) 2H	-	-	-	2.43 s 3H

Table 6 (continued)

Compound	R	R'	Aromatic protons
L8 ^a			8.58, s, 1H; 8.11, t (9), 2H; 7.85, d (8), 1H; 7.65 – 7.77, m, 5H; 7.53, d (7), 2H; 7.41 – 7.47, m, 2H
L11 (2 nd fraction)			8.22, s, 1H; 8.15 – 8.16, m, 1H; 7.84, d (8), 1H; 7.78 – 7.82, m, 3H; 7.71 – 7.75, m, 2H; 7.67 – 7.69, m, 1H; 7.32 – 7.34, m, 3H; 7.27 – 7.29, m, 1H
L11 (1 st fraction)			8.21, s, 1H; 8.15 – 8.17, m, 1H; 7.84, d (8), 1H; 7.78 – 7.82, m, 3H; 7.72 – 7.74, m, 2H; 7.68 – 7.70, m, 1H; 7.31 – 7.32, m, 3H; 7.27, d (7), 1H
L13	H		8.21, s, 1H; 8.15 – 8.17, m, 1H; 7.81 – 7.84, m, 2H; 7.77 – 7.80, m, 2H; 7.72 – 7.75, m, 2H; 7.68 – 7.69, m, 1H; 7.31 – 7.33, m, 3H; 7.27, t (7), 1H

^a ¹H NMR spectrum in CDCl₃ at -30 °C.

Table 7. ^1H NMR assignment for the β -monomethyl oxazoline thioureas (positions 1 – 12).

Compound	R	R'	H1	H3	H4	H5	H9	H10	H11	H12
R-L10 A = CH ₃ , B = H			1.81 d (7) 3H	4.15 – 4.18, m, 1H 4.02 – 4.07, m, 2H		6.43 q (7) 1H	6.96 d (8) 1H	7.13 t (8) 1H	7.17 t (8) 1H	7.37 d (8) 1H
S-L10 A = H, B = CH ₃			1.83 d (8) 3H	4.31, t (9), 1H 3.87, t (9), 1H	3.98 q (9) 1H	6.44 q (8) 1H	6.95 d (8) 1H	7.13 t (8) 1H	7.17 t (8) 1H	7.41 d (8) 1H
L9 (B1 fraction)			1.14 d (7) 3H	4.04, t (8), 1H 3.97, t (8), 1H	3.88 – 3.91 m 1H	6.16 q (7) 1H	6.40 d (8) 1H	6.27 t (8) 1H	6.62 t (8) 1H	6.77 d (8) 1H
L9 (C1 fraction)			1.17 d (7) 3H	4.22, t (8), 1H 3.73, t (8), 1H	3.87 q (8) 1H	6.15 q (7) 1H	6.40 d (8) 1H	6.27 t (8) 1H	6.62 t (8) 1H	6.82 d (8) 1H

Table 8. ^1H NMR assignment for R and R'-substituent of the β -monomethyl oxazoline thioureas (positions 14 - 23).

Compound	R	R'	H14	H15, H16	H18	H19	H21	H22	H23
R-L10 A = CH ₃ , B = H			1.80 – 1.82 m 1H	0.98, d (8), 3H 0.89, d (8), 3H	7.36 – 7.39 m 4H			2.44 s 3H	
S-L10 A = H, B = CH ₃			1.78 – 1.83 m 1H	1.05, d (7), 3H 0.89, d (7), 3H	7.36 – 7.40 m 1H			2.44 s 3H	
L9 (B1 fraction)			1.71 – 1.76 m 1H	0.90, d (7), 3H 0.83, d (7), 3H	Aromatic protons; 8.18, s, 1H; 8.09, d (8), 1H; 7.99, d (8), 1H; 7.92, d (8), 1H; 7.86, d (8), 1H; 7.73 – 7.77, m, 4H; 7.34 – 7.40, m, 3H; 7.31, t (8), 1H				
L9 (C1 fraction)			1.65 – 1.70 m 1H	0.95, d (7), 3H 0.81, d (7), 3H	Aromatic protons; 8.18, s, 1H; 8.08, d (8), 1H; 8.00, d (8), 1H; 7.92, d (8), 1H; 7.86, d (8), 1H; 7.72 – 7.77, m, 4H; 7.35 – 7.40, m, 3H; 7.31, t (8), 1H				

From Tables 5 – 9, the ^1H NMR of the protons in the parent structure, positions 1 – 14, of the bidentate S,N-oxazoline thiourea ligands shows similar chemical shifts. However, the H4 resonance of **L3** (Ph), 5.21 ppm, is significantly shifted from **L6** (iPr), 3.39 ppm. The methyl H1 and H2 signals, which normally appear at *ca.* 2.2 ppm, are shifted considerably to higher field, *ca.* 1.7 and 1.9 ppm, when the substituent –R' is ortho-9-anthryl (**L11up**, **L11down** and **L13**). The H1 resonances of the β -monomethyl and β -dimethyl substituents are significantly shifted. For example, H1 of **L7** (β -dimethyl) appears at δ 2.2 ppm, but for **S-L10** and **R-L10** (β -monomethyl), it appears at δ 1.83 ppm. This can be attributed to the effect of the substituent at the β -position in the oxazoline thiourea ligands. Surprisingly, one proton in the aromatic region of **L8** shows broad signals in the ^1H NMR spectrum obtained at room temperature but gives a sharp signal at $-30\text{ }^\circ\text{C}$, (see Figures A15 and A16 in Appendix B for the ^1H and $^{13}\text{C}\{^1\text{H}\}$ spectra at room temperature and $-30\text{ }^\circ\text{C}$, respectively). We have no explanation for this broad signal.

Interestingly, the ^1H and $^{13}\text{C}\{^1\text{H}\}$ NMR spectra of the two atropoisomers **L2up** vs **L2down**, **R-L10** vs **S-L10**, **R-L9up** vs **S-L9down** and **L11up** vs **L11down** are very similar (see Figures 22 and 23 for ^1H and $^{13}\text{C}\{^1\text{H}\}$ of **L2up** vs **L2down**, respectively; for spectra of other atropoisomers, see Appendix B). The main differences in the $^{13}\text{C}\{^1\text{H}\}$ NMR spectra between **L2up** and **L2down** are the Me carbon signals at positions 1 and 2. They appear at 29.2 and 26.5 ppm in **L2up** and 28.2 and 27.9 ppm in **L2down**, respectively. Moreover, the NOESY NMR spectrum of **L2up** and **L2down**, as well as for other atropoisomers, also show similar signals. However, the structures of both isomers are confirmed from single-crystal X-ray diffraction.

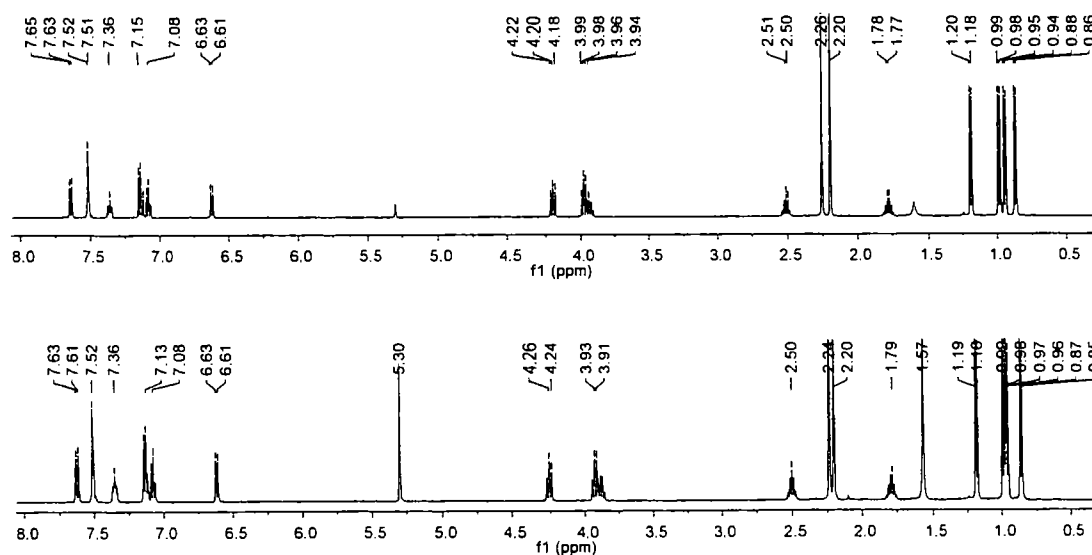


Figure 21. The ^1H NMR (500 MHz, CD_2Cl_2) spectra of **L2up** (top) and **L2down** (bottom).

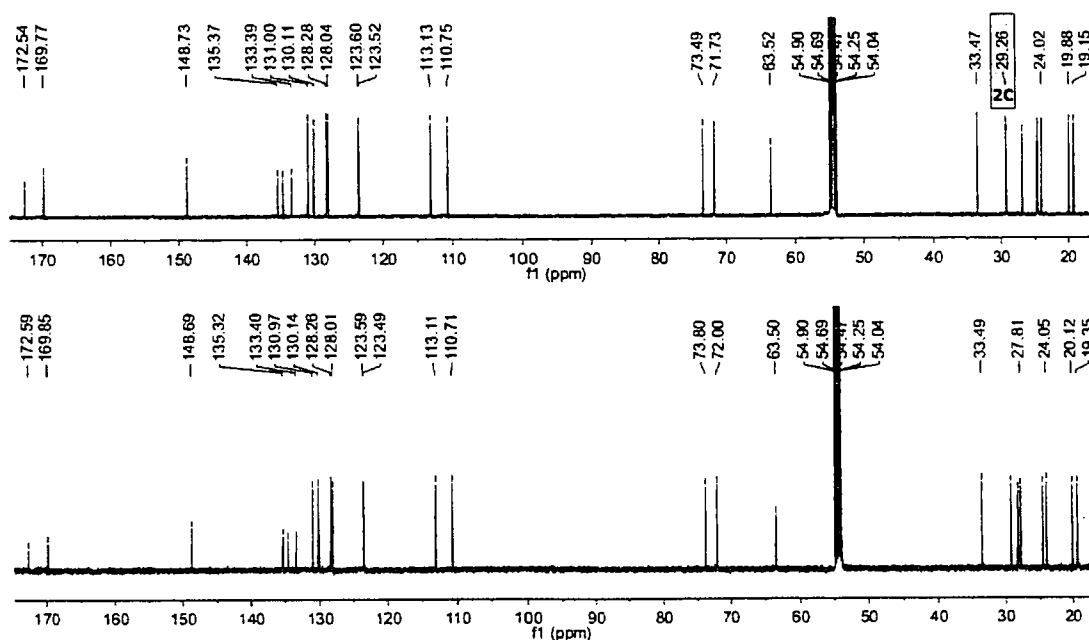


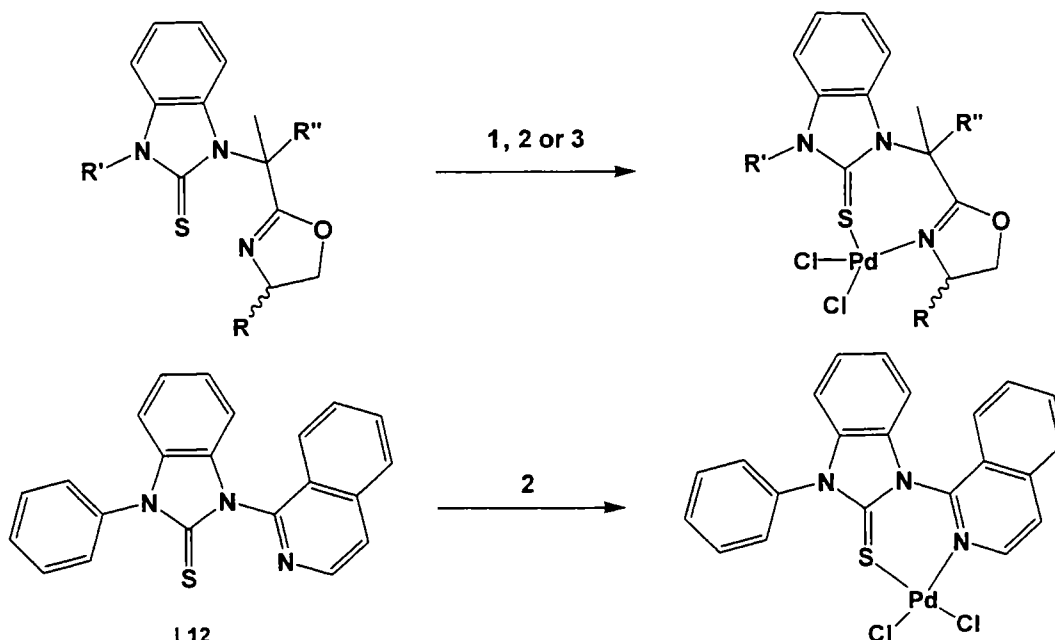
Figure 22. The $^{13}\text{C}\{^1\text{H}\}$ (125 MHz, CD_2Cl_2) spectra of **L2up** (top) and **L2down** (bottom).

The inter-conversion barriers between the ‘up’ and ‘down’ isomers *via* rotation around the $\text{C}_{\text{phenyl}}\text{-N}$ [(C(21)-N(3))] bond were obtained by DFT (B3LYP, 6-31G) calculations both in CH_3OH solution and in the gas phase.²⁸ For an unsubstituted phenyl ring, **L6**, the $\text{C}_{\text{phenyl}}\text{-N}$ bond rotation barrier is calculated to be *ca.* 12 kcal $\cdot\text{mol}^{-1}$. The *ortho*-*i*Pr substituent analogue, **L2up** and **L2down**, gave an

energy barrier of 37 kcal·mol⁻¹. The high energy barrier between **L2up** and **L2down** was consistent with experiment, as an identical ¹H NMR spectrum was observed after **L2up** was heated to 125 °C for 6 h, thereby proving that it had not been converted to **L2down**.

II.2 Synthesis of S,N-bidentate oxazoline thiourea palladium complexes

The bidentate S,N-oxazoline thiourea palladium complexes PdCl₂-L2up **PdL2up**, PdCl₂-L2down **PdL2down**, PdCl₂-L3 **PdL3**, PdCl₂-L4 **PdL4**, PdCl₂-L5 **PdL5**, PdCl₂-L6 **PdL6**, PdCl₂-L7 **PdL7**, PdCl₂-L8 **PdL8**, PdCl₂-L9 **PdL9** (using **B1** and **C1** **L9** fractions), PdCl₂-R-L10 **Pd-R-L10**, PdCl₂-S-L10 **Pd-S-L10**, PdCl₂-L11 **PdL11** (two fractions), PdCl₂-L12 **PdL12** and PdCl₂-L13 **PdL13** were synthesized by reaction of one equivalent of PdCl₂ or PdCl₂(PhCN)₂ with one equivalent of the appropriate ligand under conditions outlined in Scheme 5. It should be noted that by using PdCl₂(CH₃CN)₂ with the 1st fraction of **L11**, the reaction does not go to completion as evidence from the *in situ* ¹H NMR. The complexes are shown as monomers, but it is possible that they may exist as cyclic dimers, trimers or even higher order oligomers.



1. PdCl₂, CH₃OH, 50 °C, 48 h for **L2up**, **L2down**, **L3**, **L4** and **L5**
2. PdCl₂(PhCN)₂, CH₂Cl₂, room temperature for 30 min for **L6**, **L7**, **L8**, **L9** (both **B1** and **C1** fractions), **R-L10**, **S-L10**, **L11** (first fraction), **L12** and **L13**
3. PdCl₂(CH₃CN)₂, CH₂Cl₂, room temperature for 30 min for the second **L11** fractions

Scheme 5. The preparation of oxazoline thiourea palladium complexes.

II.3 Characterization of S,N-oxazoline thiourea palladium complexes

The complexes were characterized by solution ^1H , $^{13}\text{C}\{^1\text{H}\}$, COSY, NOESY, HSQC and HMBC NMR spectroscopy, elemental analysis and single-crystal X-ray diffraction. Full details of the X-ray and NMR analyses are provided (*vide infra*).

II.3.1 The crystal structures of bidentate S,N-thiourea palladium complexes

A) Crystal structures of the β -dimethyl oxazoline thiourea complexes

A.1 Monopalladium β -dimethyl oxazoline thiourea complexes.

Single crystals of **PdL2up**, **PdL2down** and **PdL3** were obtained from slow evaporation of $\text{CH}_2\text{Cl}_2:\text{Et}_2\text{O}$ solutions and **PdL6** likewise from $\text{CD}_2\text{Cl}_2:\text{Et}_2\text{O}$. Similarly, single crystals of **PdL4** were obtained from three different solvent mixtures; CH_2Cl_2 , $\text{CH}_2\text{Cl}_2:\text{Et}_2\text{O}$ and $\text{CH}_2\text{Cl}_2:\text{CH}_3\text{OH}$. Single crystals of **PdL7** were obtained from slow evaporation of a solution in $\text{CH}_2\text{Cl}_2:\text{DMF}$. Finally, single crystals of **PdL11** (from the second **L11** fraction) were obtained from an NMR solution in CDCl_3 . They were found to crystallize in the following space groups: **PdL2up** (tetragonal $P4_1$); **PdL2down**, **PdL3**, **PdL6**, **PdL7** and **PdL11** (orthorhombic $P2_12_12_1$); **PdL4** (from three different solvents as described previously, but all are monoclinic $P2_1$). The structures contain one full molecule in the asymmetric unit, apart from **PdL7** and **PdL4** (from CH_2Cl_2) which contain two independent molecules. The structures of **PdL3**, **PdL6**, **PdL4** (CH_2Cl_2) and **PdL4** ($\text{CH}_2\text{Cl}_2:\text{CH}_3\text{OH}$) also contain one molecule of CH_2Cl_2 , CD_2Cl_2 , CH_2Cl_2 and CH_3OH solvate, respectively, in the asymmetric unit. The atomic displacement parameters of **PdL2up** are on average 1.7 times larger than in **PdL2down**, and in some cases are large enough to suspect static disorder. The structure of **PdL4** (from CH_2Cl_2), contains one independent molecule which has the isopropyl group at C14' disordered between two orientations C18'-C19'-C20' and C18''-C19''-C20'' with equal occupancies, and the methyl group at position C29' is disordered over two positions with equal occupancies. The molecular structures of all of the complexes are shown in Figure 24. All crystallographic data are summarized in Table 9 and selected bond lengths, angles and dihedral angles are given in Tables 10 and 11, respectively.

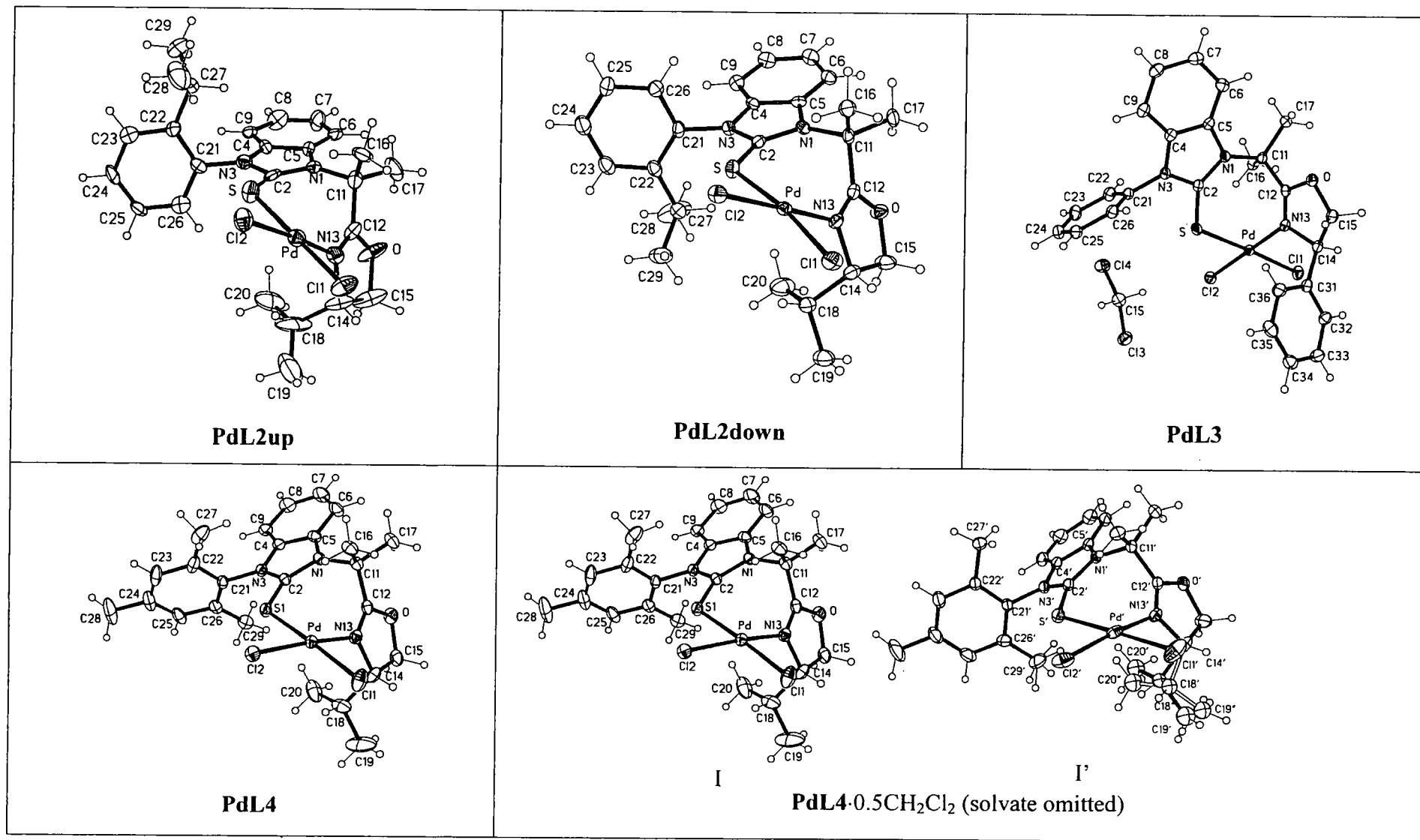


Figure 23. The molecular structures of the β -dimethyl oxazoline thiourea mono-palladium complexes.

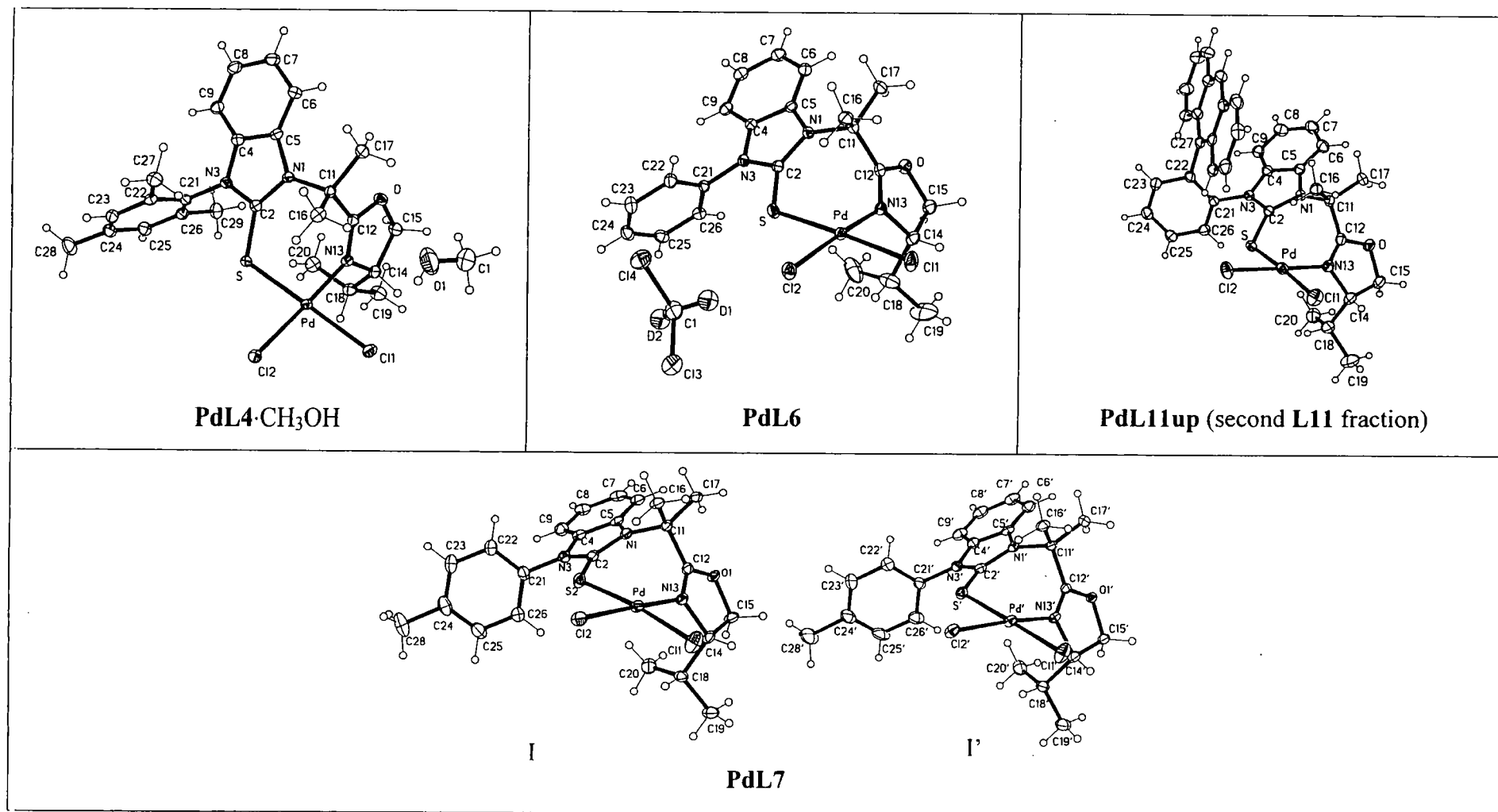


Figure 23 (continued)

Table 9. Crystallographic data for PdL2up, PdL2down, PdL3 and PdL6.

	PdL2up	PdL2down	PdL3	PdL6	PdL11up
Empirical formula	C ₂₅ H ₃₁ N ₃ OPdS	C ₂₅ H ₃₁ Cl ₂ N ₃ OPdS	C ₂₆ H ₂₅ C ₁₄ N ₃ OPdS	C ₂₂ H ₂₅ Cl ₂ N ₃ OPdS, CD ₂ Cl ₂	C ₃₆ H ₃₃ Cl ₂ N ₃ OPdS, 4CDCl ₃
Formula weight	598.89	598.89	675.75	643.75	1214.51
Temperature (K)	120(2)	120(2)	120(2)	120(2)	120(2)
Crystal system	Tetragonal	Orthorhombic	Orthorhombic	Orthorhombic	Orthorhombic
Space group	<i>P</i> 4 ₁	<i>P</i> 2 ₁ 2 ₁ 2 ₁	<i>P</i> 2 ₁ 2 ₁ 2 ₁	<i>P</i> 2 ₁ 2 ₁ 2 ₁	<i>P</i> 2 ₁ 2 ₁ 2 ₁
a (Å)	9.2008(4)	9.7352(9)	8.8287(4)	8.7002(4)	10.6901(8)
b (Å)	9.0028(4)	12.5655(11)	16.038(1)	16.4004(7)	16.9534(13)
c (Å)	31.3481(1)	21.1503(19)	18.728(1)	18.4949(8)	13.9363(10)
α (°)	90.00	90.00	90.00	90.00	90.00
β (°)	90.00	90.00	90.00	90.00	100.58(1)
γ (°)	90.00	90.00	90.00	90.00	90.00
Volume (Å ³)	2653.8(2)	2587.3(4)	2651.8(2)	2639.02(2)	2474.3(3)
Z	4	4	4	4	2
Density (calculated) (Mg/m ³)	1.499	1.537	1.693	1.620	1.630
Absorption coefficient (mm ⁻¹)	1.002	1.027	1.208	1.209	1.290
Crystal size (mm ³)	0.16 x 0.03 x 0.02	0.42 x 0.13 x 0.01	0.44 x 0.10 x 0.05	0.30 x 0.20 x 0.07	0.23 x 0.19 x 0.09
Theta range for data collection (°)	2.21 to 27.49	1.89 to 29.00	1.67 to 29.99	2.20 to 34.97	2.29 to 30.00
Reflections collected	22405	13750	36495	46575	45106
Independent reflections	6077 [R(int)=0.1516]	6345 [R(int)=0.0383]	7734 [R(int)=0.0329]	11231 [R(int)=0.0226]	14411 [R(int)=0.0275]
Data / restraints / parameters	6077 / 1 / 304	6345 / 0 / 310	7734 / 0 / 329	11231 / 0 / 306	14411 / 23 / 635
Final R indices I > 2σ	R1=0.0676, wR2=0.0955	R1=0.0389, wR2=0.0615	R1=0.0228, wR2=0.0516	R1=0.0206, wR2=0.0467	R1=0.0273, wR2=0.0605
R indices (all data)	R1=0.1545, wR2=0.1143	R1=0.0518, wR2=0.0646	R1=0.0257, wR2=0.0530	R1=0.0228, wR2=0.0475	R1=0.0326, wR2=0.0630

Table 9 (continued)

	PdL7	PdL4	PdL4·0.5CH₂Cl₂	PdL4·CH₃OH
Empirical formula	C ₂₆ H _{30.5} Cl ₂ N _{3.5} O _{1.50} PdS	C ₂₅ H ₃₁ C ₁₂ N ₃ OPdS	C ₂₅ H ₃₁ Cl ₂ N ₃ OPdS, 0.5(CH ₂ Cl ₂)	C ₂₅ H ₃₁ Cl ₂ N ₃ OPdS, CH ₃ OH
Formula weight	625.40	598.89	641.35	630.93
Temperature (K)	120(0)	120(2)	120(2)	120(2)
Crystal system	Orthorhombic	Monoclinic	Monoclinic	Monoclinic
Space group	<i>P</i> 2 ₁ 2 ₁ 2 ₁	<i>P</i> 2 ₁	<i>P</i> 2 ₁	<i>P</i> 2 ₁
a (Å)	10.3512(5)	8.7588(7)	8.8412(6)	8.6727(11)
b (Å)	12.6007(7)	17.1200(17)	15.3859(14)	15.598(2)
c (Å)	44.087(2)	9.0371(10)	20.422(2)	10.2831(13)
α (°)	90.00	90.00	90.00	90.00
β (°)	90.00	93.23	94.86(1)	94.95(1)
γ (°)	90.00	90.00	90.00	90.00
Volume (Å ³)	5750.3(5)	1353.0(2)	2768.0(4)	1385.9(3)
Z	8	2	4	2
Density (calculated) (Mg/m ³)	1.445	1.470	1.539	1.512
Absorption coefficient (mm ⁻¹)	0.930	0.982	1.059	0.966
Crystal size (mm ³)	-	0.16 x 0.13 x 0.03	0.37 x 0.22 x 0.11	0.48 x 0.21 x 0.15
Theta range for data collection (°)	1.68 to 29.99	2.26 to 30.01	2.00 to 35.00	1.99 to 30.02
Reflections collected	110085	20560	48486	17097
Independent reflections	16499 [R(int)=0.0385]	7886 [R(int)=0.0358]	22630 [R(int)=0.0255]	7670 [R(int)=0.0186]
Data/restraints/parameters	16499 / 0 / 665	7886 / 1 / 312	22630 / 6 / 643	7670 / 1 / 336
Final R indices I > 2σ	R1=0.0401, wR2=0.1108	R1=0.0260, wR2=0.0487	R1=0.0323, wR2=0.0742	R1=0.0173, wR2=0.0427
R indices (all data)	R1=0.0446, wR2=0.1121	R1=0.0319, wR2=0.0500	R1=0.0360, wR2=0.0756	R1=0.0179, wR2=0.0430

Table 10. Selected bond lengths and angles of the mono-palladium β -dimethyl oxazoline thiourea complexes.

Selected bond lengths (Å)	PdL2up	PdL2down	PdL11up	PdL7	
Pd-Cl(1)	2.312(2)	2.318(1)	2.3090(6)	2.3022(10)	2.3210(10)
Pd-Cl(2)	2.299(2)	2.275(1)	2.3039(6)	2.2976(8)	2.3079(8)
Pd-S	2.271(3)	2.268(1)	2.2833(6)	2.2755(9)	2.2714(9)
Pd-N(13)	2.021(7)	2.001(3)	2.0069(18)	2.027(3)	2.011(3)
S=C(2)	1.678(10)	1.708(4)	1.716(2)	1.714(4)	1.706(4)
N(1)-C(2)	1.398(11)	1.364(4)	1.373(2)	1.370(4)	1.384(4)
N(3)-C(2)	1.374(10)	1.357(4)	1.362(3)	1.350(5)	1.356(4)
Selected bond angles (deg)					
S-C(2)-N(1)	137.0(7)	135.2(3)	134.40(15)	134.2(3)	135.3(3)
S-C(2)-N(3)	117.4(7)	116.3(3)	117.50(14)	117.3(3)	117.3(3)
S-Pd-N(13)	93.2(2)	94.18(8)	90.98(5)	95.49(8)	93.43(8)
Pd-S-C(2)	116.6(3)	118.17(13)	116.65(7)	117.64(12)	116.18(12)
Cl(1)-Pd-Cl(2)	91.61(9)	90.83(4)	90.86(2)	90.39(4)	92.62(3)
Selected dihedral angles (deg)					
S-C(2)-N(3)-C(21)	-8.0	5.8	10.0	4.0	-2.7
C(2)-N(3)-C(21)-C(22)	100.0	-91.8	106.5	-79.2	-95.7
C(2)-N(1)-C(11)-C(12)	60.4	60.6	62.7	68.6	60.4
N(1)-C(11)-C(21)-N(13)	-85	-88.2	-87.7	-85.9	-83.2

Table 10 (continued)

Selected bond lengths (Å)	PdL3	PdL6	PdL4	PdL4·0.5CH ₂ Cl ₂		PdL4·CH ₃ OH
Pd-Cl(1)	2.3074(5)	2.3066(3)	2.3255(6)	2.3337(6)	2.3162(7)	2.3358(4)
Pd-Cl(2)	2.3010(5)	2.3003(3)	2.2976(6)	2.2978(5)	2.3040(7)	2.3017(5)
Pd-S	2.2852(5)	2.2803(3)	2.2898(6)	2.2728(6)	2.2968(6)	2.2897(4)
Pd-N(13)	2.0084(17)	2.0032(10)	2.0195(19)	2.0093(19)	2.019(2)	2.0026(13)
S=C(2)	1.713(2)	1.7148(13)	1.717(2)	1.721(2)	1.711(2)	1.7222(16)
N(1)-C(2)	1.371(3)	1.3750(16)	1.364(3)	1.379(3)	1.371(3)	1.3707(19)
N(3)-C(2)	1.359(2)	1.3577(16)	1.348(3)	1.353(3)	1.356(3)	1.358(2)
Selected bond angles (deg)						
S-C(2)-N(1)	135.10(15)	135.23(10)	134.17(17)	135.07(17)	134.73(16)	134.83(12)
S-C(2)-N(3)	116.86(15)	116.99(9)	117.38(16)	116.72(15)	117.19(15)	117.19(11)
S-Pd-N(13)	93.32(5)	93.80(3)	95.86(5)	92.40(6)	94.44(5)	92.60(4)
Pd-S-C(2)	118.10(7)	117.57(4)	117.17(8)	117.51(7)	116.04(7)	115.53(5)
Cl(1)-Pd-Cl(2)	91.656(19)	91.625(12)	91.71(2)	92.47(2)	92.95(3)	93.117(17)
Selected dihedral angles (deg)						
S-C(2)-N(3)-C(21)	-7.9	1.7	9.5	1	14.8	8.6
C(2)-N(3)-C(21)-C(22)	-71.0	73.0	87.6	73.7	83.8	82.6
C(2)-N(1)-C(11)-C(12)	-65.9	63.4	70.1	57.1	68.2	65.4
N(1)-C(11)-C(21)-N(13)	88.7	-88.0	-85.7	-88.4	-84.6	-84.4

In the palladium complexes of **L2**, the ⁱPr groups of both complexes are on opposite sides of the phenyl ring *iii*, namely in an *anti* position with respect to PdCl₂ for **PdL2up** but in a *syn* orientation for **PdL2down**. The structure of **PdL11** (from the second **L11** fraction) reveals the 9-anthryl to be in the 'up' conformation, which means that in the second fraction of **L11** it is in an 'up' conformation as well, so this ligand is referred to as **L11up**. Therefore, in the first fraction it must be in the 'down' conformation, so this is referred to as **L11down**. The bond lengths and angles of **PdL11up** are not significantly different to those in those **PdL2up** in which the 9-anthryl group is replaced by the ⁱPr substituent.

The crystal structure of **PdL6** and its analogue **PdL3** confirm that the carbons bearing the ⁱPr and the Ph substituents on the oxazoline ring have opposite configurations. However, the very similar Pd–S (2.2852(5) vs 2.2803(7) Å) and Pd–N (2.0084(17) vs 2.0032(10) Å) bond lengths suggest that both the substituent and its configuration on the oxazoline unit have little influence on the structures.

The structures show slightly distorted square planar coordination at the Pd atom with the chelating ligand bound through the S atom of the thiourea and the N atom of oxazoline ring. **PdL3** and **PdL4-CH₃OH** show the Pd, S, N(13), Cl(2) and Cl(1) atoms to be almost coplanar. **PdL2up** shows that Cl(2) deviates by 0.18 Å from the Pd-coordination plane, whereas **PdL2down**, **PdL4** (no solvate), **PdL6** and **PdL11** show almost coplanar Pd, S, N(13) and Cl(2) atoms, whereas Cl(1) deviates by 0.26, 0.22, 0.18 and 0.16 Å, respectively. One of the two independent molecules in **PdL4-0.5CH₂Cl₂** and **PdL7**, shows the Pd, S, N(13), and Cl(1) atoms to be almost coplanar but Cl(2) to deviate by 0.24 and 0.22 Å respectively, whereas in the other molecules, Cl(1) and Cl(2) deviate by 0.16 and 0.25 Å (for **PdL4-0.5CH₂Cl₂**) and 0.16 and 0.12 Å (for **PdL7**), respectively, from the Pd, S and N(13) plane. All of the complexes have slight tetrahedral distortions at the Pd centers with the largest dihedral angles between the Pd–S–N(13) and Cl(1)–Pd–Cl(2) planes being 6.7° for **PdL2down**. A summary of the distances of Cl(1) and Cl(2) from the Pd–S–N(13) and the angle between Pd–S–N(13) and Cl(1)–Pd–Cl(2) plane are given in Table B1 in Appendix B.

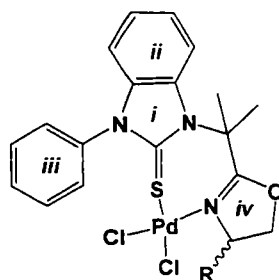
It is clear that the S atom exerts a slightly stronger *trans* influence than the N atom as the Pd–Cl bond lengths *trans* to S are slightly lengthened compared with those *trans* to N. The Pd–S bonds in all complexes are in the range 2.26 – 2.32 Å,

which are in the range of other thiourea palladium complexes in the literature (2.21 – 2.36 Å). The Pd–S bond lengths are 0.27 Å longer than the Pd–N (2.00 – 2.07 Å) bond lengths. Upon coordination to Pd, the C=S bond lengthens noticeably with concomitant shortening of the two adjacent C–N bonds, reflecting a redistribution of electrons in the N₂CS unit of the thiourea ligands. Interestingly, all of the complexes show longer C(2)–N(1) than C(2)–N(3) bond lengths which may be due to the steric bulk of the β -dimethyl moiety. The S–Pd–N(13) bond angles are in the range 93 – 96° whereas the Pd–S–C(2) angles are in the range 115 – 118° which are similar to the analogous angles in related seven-membered palladacycle involving chelating thiourea ligands. It is noteworthy that the complexes show significant differences in the S–C(2)–N(1) and S–C(2)–N(3) angles (134 – 137° vs 116 – 117°, respectively) whereas, smaller differences in the analogous angles were found in the free ligands (129 – 131° vs 122 – 125°).

The two independent molecules in the asymmetric unit of **PdL7** have slightly different bond lengths and angles. In molecule I, the C=S bond is longer consistent with the shortening of the C(2)–N(1) and C(2)–N(3) bonds (1.370(4) and 1.350(5) Å, respectively vs 1.38 Å in the free ligand). On the other hand, molecule I' shows a similar C(2)–N(1) bond length to that in the free ligand (1.384(4) Å), whereas the C(2)–N(3) bond length is shortened to 1.356(4) Å. The dihedral angle C(2)–N(3)–C(21)–C(22) in molecule I is 79° whereas it is 95° in molecule I'.

The angles between planes *i* and *iii* vary in the range 71 – 89° which is similar to that observed in the free ligands. This implies that there is no electron delocalization between rings *i* and *iii* in the palladium complexes as well as in the free ligands. In general, the structures with an *ortho*- substituent on phenyl ring *iii* show larger dihedral *i/iii* angles than those in the structures without *ortho*- groups. However, one of the largest *i/iii* angles occurs for one of the **PdL7** molecules (86.3°) and, surprisingly, the smallest *i/iii* angles occurs for **PdL11up** which has the bulky 9-anthryl group. This must be due to crystal packing. A summary of the angles between planes is given in Table 11.

Table 11. The angles between planes in the mono-palladium β -dimethyl oxazoline thiourea complexes.^a



Selected angles between planes (deg)	<i>i/ii</i>	<i>i/iii</i>	<i>i/iv</i>	<i>i/v</i>	<i>iv/v</i>
PdL2up	4.1	86.8	77.1	37.7	53.6
PdL2down	9.2	86.9	73.1	34.8	53.6
PdL3	1.3	74.7	67.5	34.8	52.7
PdL4	1.8	87.7	74.9	35.2	45.8
PdL4·0.5CH₂Cl₂	3.5	77.8	80.5	38.2	55.7
	2.9	88.9	81.5	35.2	53.5
PdL4·CH₃OH	2.3	88.0	78.5	40.3	59.2
PdL6	1.4	75.6	70.5	35.2	51.3
PdL7	0.9	74.7	75.0	35.5	49.0
	1.9	86.3	78.9	41.2	54.5
PdL11up	2.1	70.5	55.8	40.9	56.5

^a Plane *v* is Pd–S–N–Cl.

The molecular packing of the mono-palladium complexes of the β -dimethyl oxazoline thioureas features several close intermolecular Cl...H(D) and H...Cl(solvate) contacts which are less than the sum of the van der Waals radii, 2.88 Å.²⁹ This may be due to weak hydrogen bonds, or merely a by product of other crystal packing forces. A summary of these intermolecular contact distances and angles is given in Table 12.

Table 12. Intermolecular Cl...H(D) contact distances in the mono-palladium complexes of the β -dimethyl oxazoline thioureas.^a

Complex	X.....H	X.....H (Å)	X-H-Y (deg)
PdL2up	Cl(2).....H(25)	2.693	137.1
	Cl(2).....H(17)	2.745	164.7
	Pd.....H(25)	2.898	139.7
PdL2down	Cl(2).....H(6)	2.733	135.8
	Cl(2).....H(17)	2.816	145.6
PdL3	Cl(2).....H(17)	2.669	163.0
	Cl(2).....H(1S) ^b	2.796	136.5
PdL4	Cl(1).....H(29)	2.879	149.3
	Cl(2).....H(25)	2.817	168.8
	Cl(2).....H(17)	2.618	130.5
PdL4·0.5CH₂Cl₂	Cl(2).....H(16)	2.771	161.5
	Cl(2).....H(25)	2.801	129.1
PdL4·CH₃OH	Cl(2).....H(15)	2.744	142.4
	Cl(2).....H(29)	2.848	170.3
PdL6	Cl(2).....H(17)	2.781	161.8
	Cl(2).....D(1) ^b	2.755	135.6
PdL7	Cl(2).....H(6)	2.851	153.3
	H(23).....Cl(3) ^b	2.500	153.9
PdL11up	Cl(2).....H(15)	2.700	152.4

^a Cl(1) is the Cl atom *trans*- to the S of the thiourea and Cl(2) is the Cl atom *trans*- to the N atom of the oxazoline, ^b H, D or Cl atoms from the solvate molecules.

Close intermolecular Cl...H contacts with protons of the β -dimethyl groups are found in **PdL2up**, **PdL2down**, **PdL3**, **PdL4** and **PdL6**, ones involving the CH₂ protons next to the oxygen in the oxazoline moiety are found in **PdL4·CH₃OH** and **PdL11up**, and those involving the solvent in the lattice in **PdL3**, **PdL6** and **PdL7**.

In **PdL2up** (Figure 25), the proton at the *meta*-position in ring *iii* is involved in a very close Cl...H contact of 2.693 Å. Interestingly, a close intermolecular contact

of Pd.....H (2.898 Å) was also observed. The packing in **PdL2down** shows a Cl....H contact involving the proton at the *ortho*-position of the phenyl ring *ii* (Figure 26). **PdL4**, **PdL4·0.5CH₂Cl₂** and **PdL4·CH₃OH** show close Cl....H contacts involving the protons of the phenyl ring *iii*. Figures 27, 28, 29, 30, 31, 32 and 33 depict the close intermolecular contacts in **PdL3**, **PdL4**, **PdL4·0.5CH₂Cl₂**, **PdL4·CH₃OH**, **PdL6**, **PdL7** and **PdL11up**, respectively.

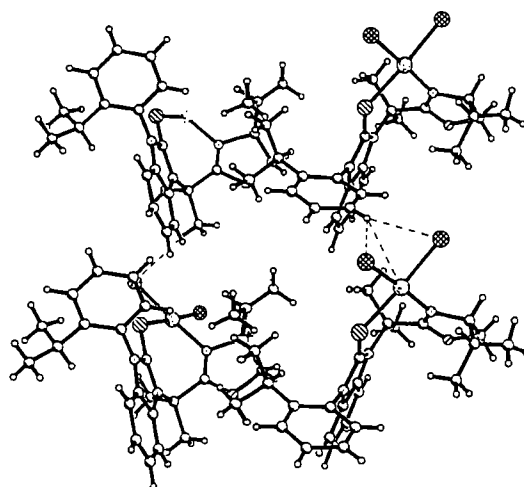


Figure 24. The crystal packing of **PdL2up** showing the close intermolecular contacts.

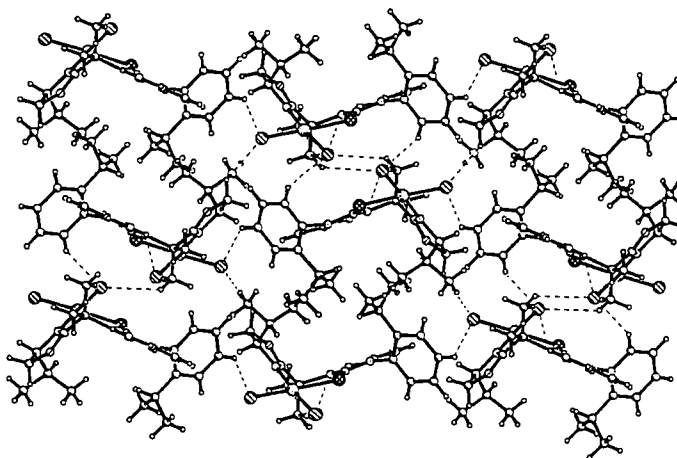


Figure 25. The crystal packing of **PdL2down** showing the close intermolecular contacts.

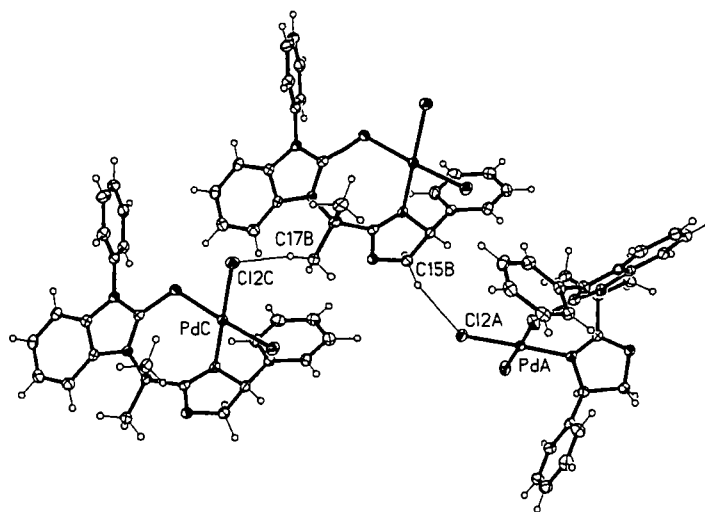


Figure 26. The crystal packing of **PdL3** showing the close intermolecular contacts.

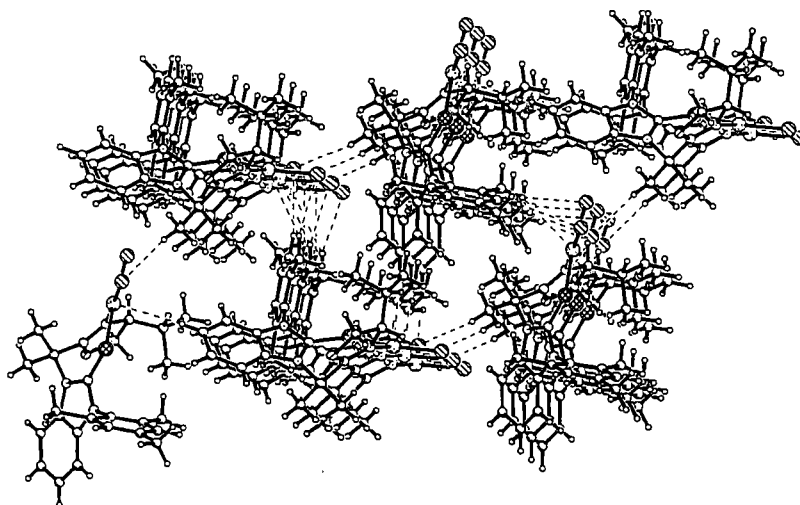


Figure 27. The crystal packing of **PdL4** showing the close intermolecular contacts.

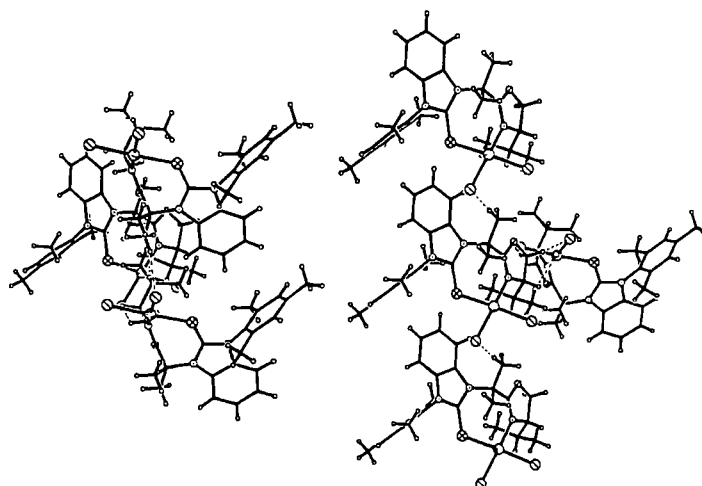


Figure 28. The crystal packing of **PdL4·0.5CH₂Cl₂** showing the close intermolecular contacts.

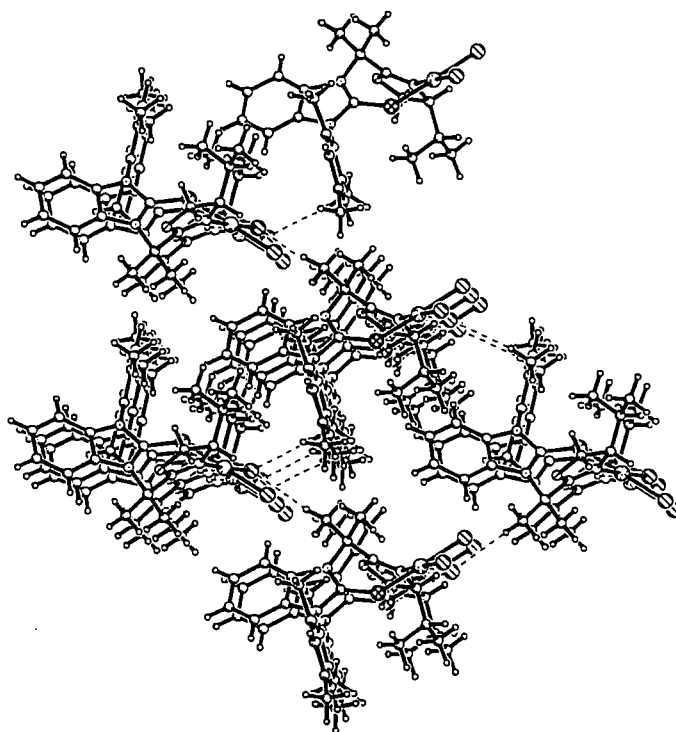


Figure 29. The crystal packing of **PdL4-CH₃OH** showing the close intermolecular contacts.

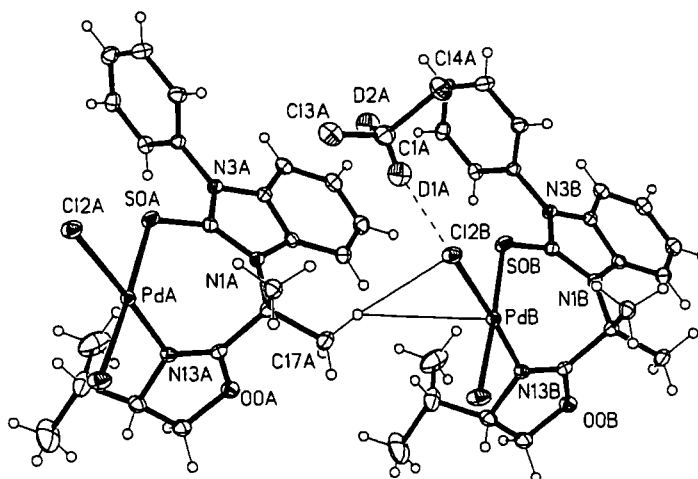


Figure 30. The crystal packing of **PdL6** showing the close intermolecular contacts.

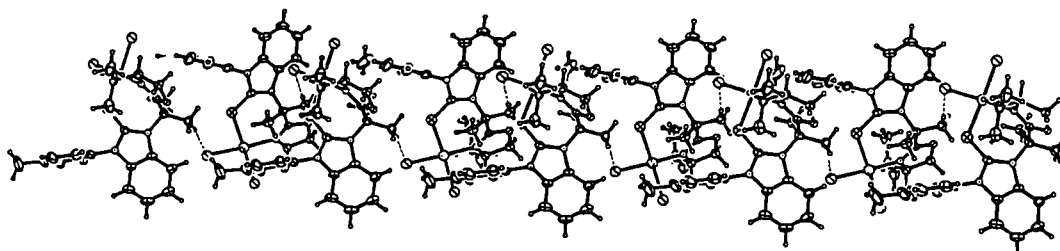


Figure 31. The crystal packing of **PdL7** showing the close intermolecular contacts.

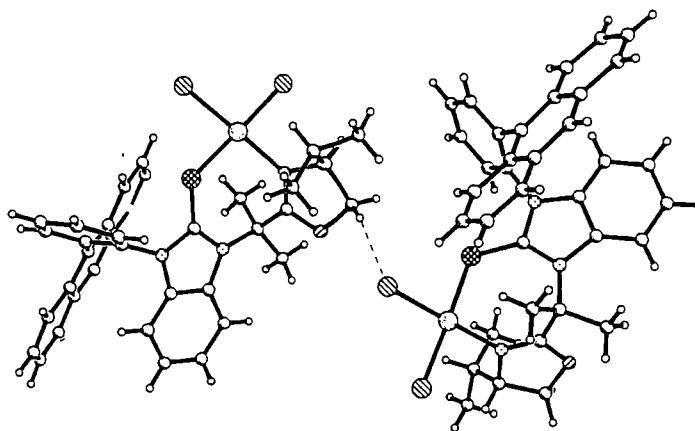


Figure 32. The crystal packing of **PdL11up** showing the close intermolecular contacts.

A.2 A dipalladium complex of the β -dimethyl oxazoline thiourea **L5**

The molecular structure of the complexes with **L5** were solved by X-ray diffraction on single crystals grown from the slow evaporation of solutions in $\text{CH}_2\text{Cl}_2:\text{Et}_2\text{O}$, $\text{CH}_2\text{Cl}_2:\text{hexane}$, $\text{CH}_2\text{Cl}_2:\text{toluene}$, $\text{CHCl}_3:\text{CH}_3\text{COCH}_3$ and $\text{CH}_2\text{Cl}_2:\text{CH}_3\text{OH}$. The crystals were found to crystallize in tetragonal $P4_12_12$ (from $\text{CH}_2\text{Cl}_2:\text{Et}_2\text{O}$), monoclinic $P2_1$ (from $\text{CH}_2\text{Cl}_2:\text{hexane}$ and $\text{CH}_2\text{Cl}_2:\text{CH}_3\text{OH}$) and orthorhombic $P2_12_12_1$ (from $\text{CH}_2\text{Cl}_2:\text{toluene}$ and $\text{CHCl}_3:\text{CH}_3\text{COCH}_3$) space groups. All of the structures have one full molecule in the asymmetric unit, which were revealed to be the dimer $\text{Pd}_2\text{Cl}_4(\text{L5})_2$ **Pd₂L5**, except for the structure obtained from $\text{CH}_2\text{Cl}_2:\text{Et}_2\text{O}$ which has 0.5 **Pd₂L5** molecules in the asymmetric unit with the center of the molecule shown lying on a crystallographic inversion centers. The molecular structures of the dimers are shown in Figure 34.

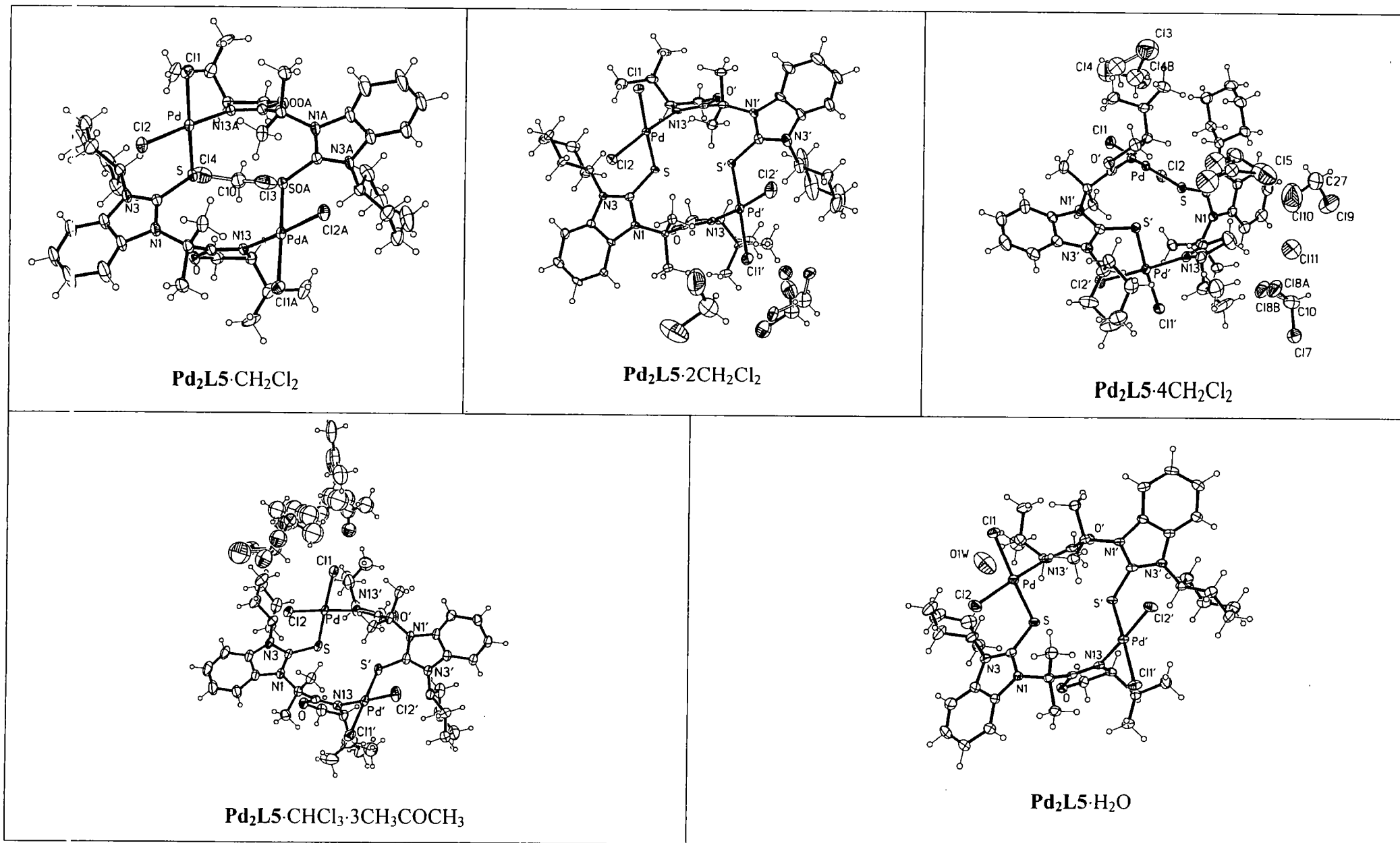


Figure 33. The molecular structures of five different solvates of **Pd₂L₅**.

The asymmetric units of the crystals obtained from $\text{CH}_2\text{Cl}_2\cdot\text{Et}_2\text{O}$, $\text{CH}_2\text{Cl}_2\cdot\text{hexane}$ and $\text{CH}_2\text{Cl}_2\cdot\text{toluene}$ also contain one, two and four molecules of CH_2Cl_2 solvate respectively, whereas the one obtained from $\text{CHCl}_3\cdot\text{CH}_3\text{COCH}_3$ also contains one of CHCl_3 and three of CH_3COCH_3 . The structure obtained from $\text{CH}_2\text{Cl}_2\cdot\text{CH}_3\text{OH}$ unexpectedly contains one H_2O molecule in the asymmetric unit, which is believed to originate from the presence of water in the methanol.

The CH_2Cl_2 molecule in $\text{Pd}_2\text{L5}\cdot\text{CH}_2\text{Cl}_2$ is disordered over two positions of equal occupancies related by a two-fold axis. One of the isopropyl groups in $\text{Pd}_2\text{L5}\cdot 2\text{CH}_2\text{Cl}_2$ is disordered over two positions with an occupancy ratio of 0.8:0.2, and one the CH_2Cl_2 molecules is disordered over four positions, the major position has an occupancy of 0.7, and the three minor positions share a common C atom and alternate over three Cl positions with equal occupancies of 0.2. The CH_2Cl_2 molecules in $\text{Pd}_2\text{L5}\cdot 4\text{CH}_2\text{Cl}_2$ show intense disorder, which was imperfectly rationalized. One of the isopropyl groups in $\text{Pd}_2\text{L5}\cdot\text{CHCl}_3\cdot 3\text{CH}_3\text{COCH}_3$ is disordered over two positions with a 0.75:0.25 occupancy ratio. The CHCl_3 solvate molecule is also disordered over two positions with a 0.93:0.07 occupancy ratio, and one of the CH_3COCH_3 solvate molecules is also disordered between two positions with an occupancy ratio of 0.6:0.4.

Generally, all of the $\text{Pd}_2\text{L5}$ molecular structures show that each Pd center is bound through S and N atoms (from two different ligands) and two chlorides which give square planar coordination at Pd. Interestingly, the dimers have a *cis*-configuration at the Pd centers (Figure 35) with all chloride ligands on the same side of the molecule creating a significant cavity.

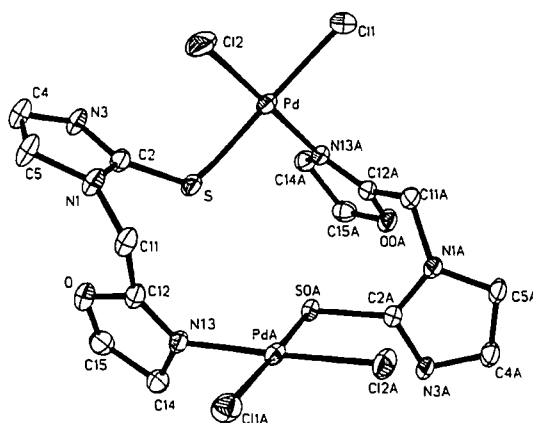


Figure 34. The molecular structure of the palladacycle of $\text{Pd}_2\text{L5}\cdot 0.5\text{CH}_2\text{Cl}_2$ (most of atoms are omitted for clarity).

The planes in the palladium complex of **L5** are defined in Figure 36. The crystallographic data are given in Table 13 and selected bond lengths and angles are given in Table 14.

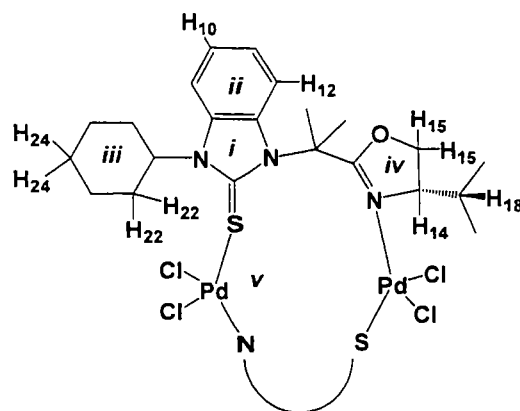


Figure 35. Definition of the planes in the palladium complex of **L5** (plane *v* is Pd–S–N–Cl).

Table 13. Crystal structure of palladium complexes of L5.

	Pd₂L5·CH₂Cl₂	Pd₂L5·2CH₂Cl₂	Pd₂L5·4(CH₂Cl₂)	Pd₂L5·CHCl₃· 3(CH₃COCH₃)	Pd₂L5·H₂O
Empirical formula	C ₄₄ H ₆₂ Cl ₄ N ₆ O ₂ Pd ₂ S ₂ · CH ₂ Cl ₂	C ₄₄ H ₆₂ Cl ₄ N ₆ O ₂ Pd ₂ S ₂ · 2CH ₂ Cl ₂	C ₄₈ H ₇₀ Cl ₁₄ N ₆ O ₂ Pd ₂ S ₂ · 4(CH ₂ Cl ₂)	C ₄₄ H ₆₂ Cl ₄ N ₆ O ₂ Pd ₂ S ₂ · CHCl ₃ ·3(CH ₃ COCH ₃)	C ₄₄ H ₆₂ Cl ₄ N ₆ O ₂ Pd ₂ S ₂ · H ₂ O
Formula weight	1210.64	1295.57	1465.42	1417.30	1143.73
Temperature (K)	120(2)	120(2)	120(2)	120(2)	120(2)
Crystal system	Tetragonal	Monoclinic	Orthorhombic	Orthorhombic	Monoclinic
Space group	<i>P</i> 4 ₁ 2 ₁ 2	<i>P</i> 2 ₁	<i>P</i> 2 ₁ 2 ₁ 2 ₁	<i>P</i> 2 ₁ 2 ₁ 2 ₁	<i>P</i> 2 ₁
a (Å)	10.7443(12)	12.0429(12)	13.410(1)	13.203(1)	11.841(1)
b (Å)	10.7443(12)	13.3538(12)	17.742(1)	18.439(1)	14.574(1)
c (Å)	45.840(5)	17.0295(15)	26.096(2)	26.019(2)	16.186(1)
α (°)	90.00	90.00	90.00	90.00	90.00
β (°)	90.00	96.59(2)	90.00	90.00	106.30(1)
γ (°)	90.00	90.00	90.00	90.00	90.00
Volume (Å ³)	5291.8(10)	2720.6(4)	6208.8(8)	6334.3(8)	2681(3)
Z	4	2	4	4	2
Density (calculated) (Mg/m ³)	1.520	1.582	1.568	1.486	1.417
Absorption coefficient (mm ⁻¹)	1.103	1.173	1.205	0.978	0.989
Crystal size (mm ³)	0.48 x 0.26 x 0.22	0.18 x 0.15 x 0.05	0.24 x 0.14 x 0.07	0.27 x 0.13 x 0.07	0.25 x 0.15 x 0.04
Theta range for data collection (°)	1.78 to 28.07	2.29 to 28.99	1.39 to 30.00	1.35 to 29.99	1.31 to 29.00
Reflections collected	59830	20134	80395	87565	40366
Independent reflections	6151 [R(int)=0.0349]	11363 [R(int)=0.0475]	18079 [R(int)=0.0572]	18450 [R(int)=0.0646]	14209 [R(int)=0.0440]
Data/restraints/parameters	6151 / 1 / 297	11363 / 2 / 641	18079 / 0 / 678	18450 / 0 / 707	14209 / 1 / 558
Final R indices I > 2σ	R1=0.0445, wR2=0.0941	R1=0.0690, wR2=0.1556	R1=0.0451, wR2=0.1169	R1=0.0437, wR2=0.0980	R1=0.0343, wR2=0.0681
R indices (all data)	R1=0.0482, wR2=0.0951	R1=0.0837, wR2=0.1629	R1=0.0607, wR2=0.1244	R1=0.0584, wR2=0.1032	R1=0.0453, wR2=0.0717

Table 14. Selected bond lengths, angles and dihedral angles of di-palladium β -dimethyl oxazoline thiourea complexes.^a

Selected bond lengths (Å)	Pd ₂ L5 ·CH ₂ Cl ₂ ^b	Pd ₂ L5·2CH ₂ Cl ₂		Pd ₂ L5·CHCl ₃ ·3CH ₃ COCH ₃		Pd ₂ L5·4CH ₂ Cl ₂		Pd ₂ L5·H ₂ O	
		part a	part a'	part a	part a'	part a	part a'	part a	part a'
Pd-Cl(1)	2.3280(13)	2.348(2)	2.339(2)	2.3243(11)	2.3162(10)	2.3250(11)	2.3235(11)	2.3282(9)	2.3374(8)
Pd-Cl(2)	2.2818(13)	2.286(3)	2.296(2)	2.2890(9)	2.2759(10)	2.2896(10)	2.2797(11)	2.2754(9)	2.2938(8)
Pd-S	2.3240(13)	2.313(2)	2.303(2)	2.3138(10)	2.3276(10)	2.3145(11)	2.3235(11)	2.3091(8)	2.3160(8)
Pd-N(13)	2.049(4)	2.050(8)	2.032(7)	2.030(3)	2.045(3)	2.031(3)	2.038(14)	2.034(3)	2.030(3)
S=C(2)	1.730(4)	1.733(8)	1.726(8)	1.718(3)	1.737(4)	1.726(4)	1.722(4)	1.730(3)	1.731(3)
N(1)-C(2)	1.345(6)	1.378(11)	1.349(11)	1.344(5)	1.346(5)	1.351(5)	1.362(5)	1.346(4)	1.358(4)
N(3)-C(2)	1.338(6)	1.332(10)	1.338(10)	1.358(4)	1.341(4)	1.345(5)	1.360(5)	1.344(4)	1.342(4)
Selected bond angles (deg)									
S-C(2)-N(1)	125.1(3)	123.2(6)	124.7(6)	125.3(3)	124.8(3)	124.9(3)	124.8(3)	125.0(2)	125.1(2)
S-C(2)-N(3)	125.0(4)	126.6(7)	125.5(6)	125.0(3)	124.9(3)	125.6(3)	125.7(3)	124.6(3)	125.3(2)
S-Pd-N(13)	85.65(11)	83.6(2)	82.1(2)	83.99(10)	85.81(9)	83.52(9)	84.78(10)	83.99(7)	85.10(7)
Pd-S-C2	105.81(18)	111.1(3)	109.3(3)	106.48(12)	107.06(12)	106.32(15)	107.92(14)	107.80(11)	108.01(10)
Cl-Pd-Cl	88.87(5)	92.19(9)	91.72(11)	90.39(4)	89.55(4)	90.47(4)	90.18(4)	90.87(3)	91.64(3)
Selected dihedral angles (deg)									
S-C(2)-N(3)-C(21)	1.3	-10.8	-10.6	-7.7	-1.8	-1.9	-2.8	-9.3	-4.0
C(2)-N(3)-C(21)-C(22)	107.6	113.1	103.3	106.0	104.7	113.0	103.8	101.1	105.0
C(2)-N(1)-C(11)-C(12)	-50.7	-58.5	-57.9	-55.5	-51.5	-50.9	-54.7	-54.3	-54.2
N(1)-C(11)-C(21)-N(13)	149.2	155.0	151.6	149.1	152.4	145.8	150.2	153.4	152.6
Selected angles between planes (deg) ^c									
<i>i/ii</i>	3.3	1.9	2.5	1.8	2.8	3.0	1.6	2.8	2.5
<i>i/iii</i>	84.5	84.5	87.0	82.0	82.9	85.9	87.5	82.9	89.5
<i>i/iv</i>	66.4	72.0	74.5	74.5	69.4	72.2	73.3	69.7	70.7
<i>i/v</i>	85.3	79.9	74.5	76.4	78.1	76.1	73.4	77.4	77.4
<i>iv/v</i>	53.6	61.9	65.4	54.9	55.8	55.6	56.6	58.1	57.2

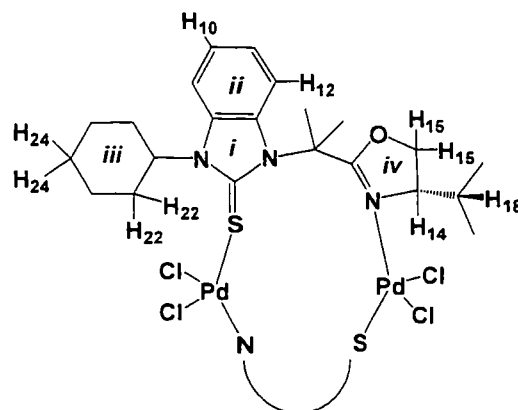
^a Two independent molecules halves of the molecules: part a = labelled with normal numbers, part a' = labelled with ' numbers,

^b The molecule lies on an inversion center, ^c see Figure 37 for plane definitions.

Most of the dimers show the Pd, S, N(13), Cl(2) and Cl(1) atoms to be almost coplanar. The maximum deviations of Cl(1) and Cl(2) are 0.13 and 0.14 Å respectively, from the Pd, S and N(13) plane which was observed in **Pd₂L5**·2CH₂Cl₂. All of the complexes show slight tetrahedral distortions with the largest dihedral angles between the Pd–S–N(13) and Cl(1)–Pd–Cl(2) planes being 4.7° for **Pd₂L5**·2CH₂Cl₂. A summary of the distances of Cl(1) and Cl(2) from the Pd–S–N(13) plane and the angle between planes Pd–S–N(13) to Cl(1)–Pd–Cl(2) of the dimer complexes is given in Table B2 in Appendix B. All of the complexes show similar bond lengths and angles to those of the mono-palladium complexes.

The S atom of the thiourea exerts a stronger *trans* influence than the N atom similar to that observed in the monomeric palladium complexes. However, the average Pd–S and Pd–N bond lengths of two ligands of **Pd₂L5** (2.31 and 2.04 Å, respectively) are slightly longer than those in the corresponding mono-palladium complexes (Pd–S and Pd–N 2.28 and 2.01 Å, respectively). This implies slightly weaker Pd–S and Pd–N bonding in the palladium dimer complexes. Moreover, both the Pd–S–C(2) angles are in the range 106 – 111°, which is smaller than in the monomers (116 – 117°). The S–Pd–N(13) angles in the dimers are in the range 82 – 85°, significantly smaller than in the mono-palladium complexes (93 – 96°).

The crystal packing of all the **Pd₂L5** structures show close intermolecular Cl...H contacts which are less than the sum of the van der Waals radii, 2.88 Å.²⁹ These contacts involve the protons of the cyclohexyl ring, the CH and CH₂ protons of the oxazoline moiety, the CH of the ⁱPr group and the protons at both *ortho*- and *meta*-positions of the phenyl ring *ii* (see Table 15). Surprisingly, no close contacts between the solvate molecules and the complexes were observed.

Table 15. Close intermolecular contact distances and angles in $\text{Pd}_2\text{L5}$.^a

Compounds	Cl.....H	Cl.....H (Å)	C-H-Cl (deg)
$\text{Pd}_2\text{L5}\cdot\text{CH}_2\text{Cl}_2$	Cl(2).....H(22)	2.723	147.4
$\text{Pd}_2\text{L5}\cdot 2\text{CH}_2\text{Cl}_2$	Cl(2).....H(14)	2.735	148.0
	Cl(2).....H(15)	2.794	162.6
$\text{Pd}_2\text{L5}\cdot 4\text{CH}_2\text{Cl}_2$	Cl(1).....H(6')	2.734	133.4
	Cl(2).....H(8')	2.719	144.3
$\text{Pd}_2\text{L5}\cdot\text{CHCl}_3\cdot 3\text{CH}_3\text{COCH}_3$	Cl(1).....H(15)	2.843	149.8
	Cl(2).....H(8)	2.876	135.8
$\text{Pd}_2\text{L5}\cdot\text{H}_2\text{O}$	Cl(1).....H(18)	2.842	130.9
	Cl(2).....H(15)	2.695	168.4
	Cl(2).....H(24)	2.878	132.3

^a Cl(1) is the Cl atom *trans*- to the S of the thiourea and Cl(2) is the Cl atom *trans*- to the N atom of the oxazoline.

The close intermolecular contacts of $\text{Pd}_2\text{L5}\cdot\text{CH}_2\text{Cl}_2$, $\text{Pd}_2\text{L5}\cdot 2\text{CH}_2\text{Cl}_2$, $\text{Pd}_2\text{L5}\cdot 4\text{CH}_2\text{Cl}_2$, $\text{Pd}_2\text{L5}\cdot\text{CHCl}_3\cdot 3\text{CH}_3\text{COCH}_3$ and $\text{Pd}_2\text{L5}\cdot\text{H}_2\text{O}$ are depicted in Figures 37, 38, 39, 40 and 41, respectively.

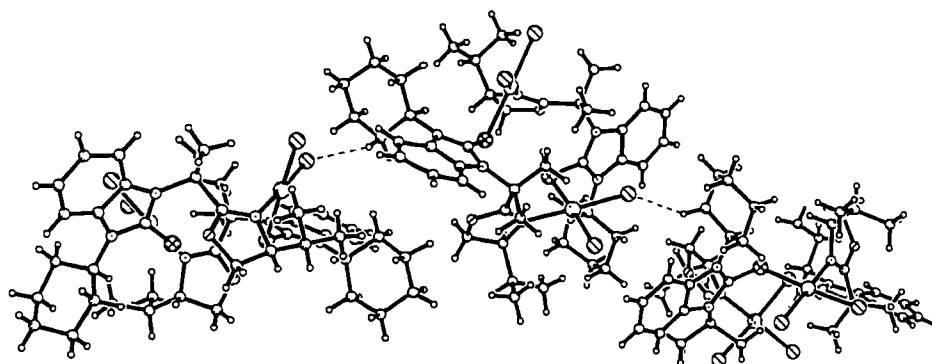


Figure 36. The crystal packing of **Pd₂L₅·CH₂Cl₂** showing the close intermolecular contacts.

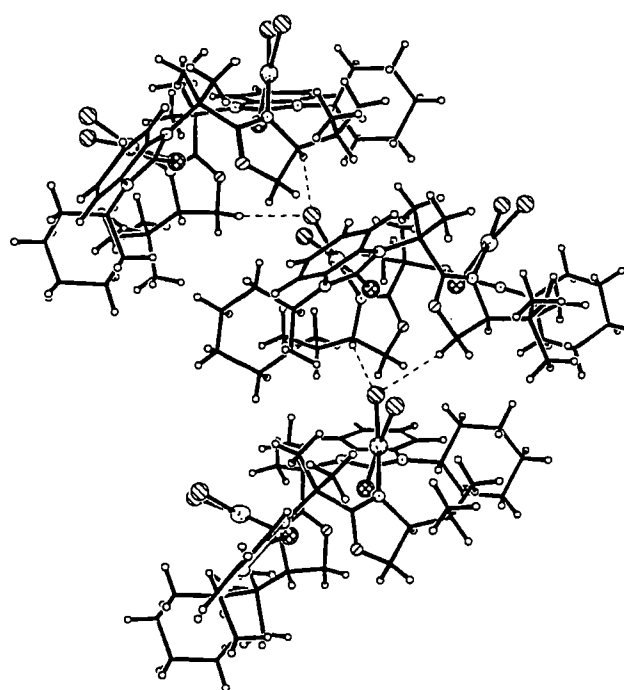


Figure 37. The crystal packing of **Pd₂L₅·2CH₂Cl₂** showing the close intermolecular contacts.

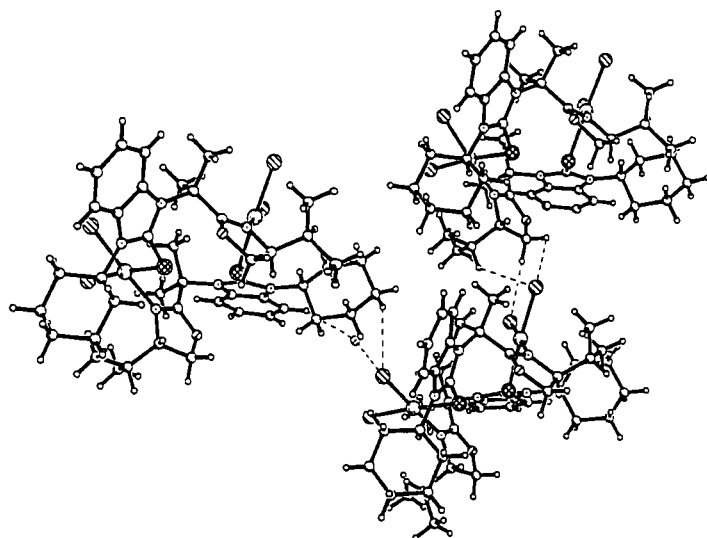


Figure 38. The crystal packing of $\text{Pd}_2\text{L}_5 \cdot 4\text{CH}_2\text{Cl}_2$ showing the close intermolecular contacts.

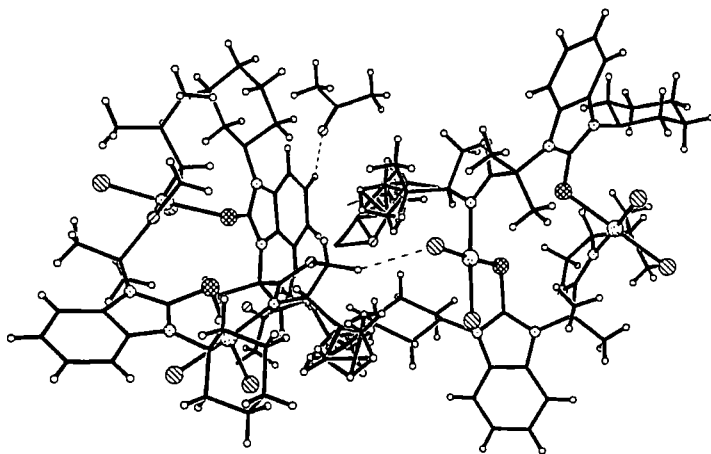


Figure 39. The crystal packing of $\text{Pd}_2\text{L}_5 \cdot \text{CHCl}_3 \cdot 3\text{CH}_3\text{COCH}_3$ showing the close intermolecular contacts.

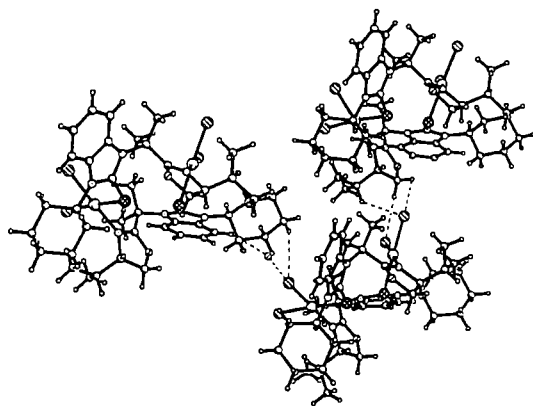


Figure 40. The crystal packing of $\text{Pd}_2\text{L}_5 \cdot \text{H}_2\text{O}$ showing the close intermolecular contacts.

A.3 A tripalladium complex of the β -dimethyl oxazoline thiourea ligand **L7**

Another single crystal of the palladium complex of **L7** was obtained from the slow evaporation of a solution in $\text{CH}_2\text{Cl}_2:\text{Et}_2\text{O}$. Interestingly, the molecular structure shows it to be the trimer $\text{Pd}_3\text{Cl}_6(\text{L7})_3$ **Pd₃L7** which crystallizes in the monoclinic space group $I2$ with one molecule each of **Pd₃L7** and CH_2Cl_2 in the asymmetric unit. The tolyl substituent at N(3)'' is disordered between two orientations with occupancies 45% and 55%, whereas the CH_2Cl_2 solvates are chaotically disordered in continuous channels parallel to the y axis. Unlike the other complexes, the Pd-centers have *trans* configurations. This is the first example of a trimer for palladium thiourea complexes. Three ligands are bridged through Pd–S and Pd–N bonds (Figure 42) and the complex adopts a 3D cage-like structure with a 21-membered ring. The crystallographic data are given in Table 16 whereas selected bond lengths and angles are summarized in Table 17.

In comparison with mono-palladium complex **PdL7**, the Pd–Cl bond lengths are fairly similar. The three Pd–N bond lengths are very close to one another (2.062(4), 2.067(4) and 2.065(4) Å), but significantly longer than Pd–N(13) in **PdL7** whereas two of the Pd–S are almost identical (2.2980(12) and 2.2990(14) Å) but the other is significantly shorter (2.2778(11) Å) all being longer than Pd–S in **PdL7**. Thus, it would appear that the *trans*- influence of both oxazoline nitrogen and thioureas sulfur exceed that of a chloride ligand. Therefore, the dimer and trimer complexes may have slightly weaker Pd–S and Pd–N bonds than the mono-palladium complexes. The Pd–S–C bond angles (103 – 110°) of **Pd₃L7** are smaller than in the mono-palladium complexes (116 – 118 °).

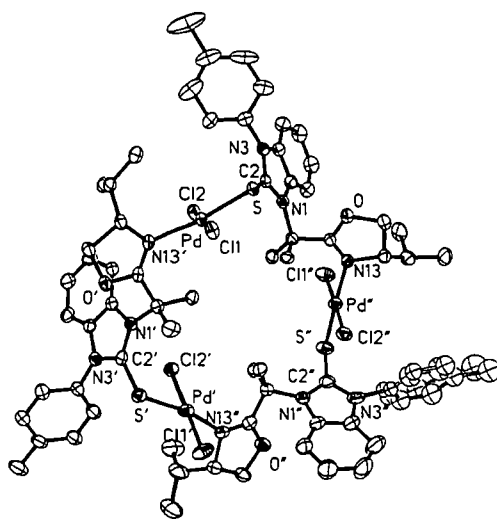


Figure 41. The molecular structure of **Pd₃L7** (disorder is shown with open bonds, and hydrogen atoms and solvents molecules are omitted for clarity).

Table 16. Crystallographic data for **Pd₃L7**.

	Pd₃L7
Empirical formula	C ₆₉ H ₈₁ N ₉ O ₃ S ₃ Pd ₃ Cl ₆ ·4CH ₂ Cl ₂
Formula weight	2052.21
Temperature (K)	120(2)
Crystal system	Monoclinic
Space group	<i>I</i> 2
a (Å)	15.997(2)
b (Å)	12.6668(18)
c (Å)	43.0533(6)
α (°)	90.00
β (°)	92.787(13)
γ (°)	90.00
Volume (Å ³)	8714(2)
Z	4
Density (calculated) (Mg/m ³)	1.564
Absorption coefficient (mm ⁻¹)	1.163
Crystal size (mm ³)	0.40 x 0.25 x 0.12
Theta range for data collection (°)	2.15 to 29.81
Reflections collected	79092
Independent reflections	25307
Data/restraints/parameters	25307/1/934
Final R indices I > 2σ	R1=0.0486, wR2=0.1266
R indices (all data)	R1=0.0588, wR2=0.1345

Table 17. The selected bonds, angles and dihedral angles of Pd₃L7.

Pd ₃ L7					
Selected bond lengths (Å)		Selected bond lengths (Å)		Selected bond lengths (Å)	
Pd-Cl(1)	2.2939(11)	Pd'-Cl(1)'	2.2939(13)	Pd''-Cl(1)''	2.3104(13)
Pd-Cl(2)	2.3089(11)	Pd'-Cl(2)'	2.3132(11)	Pd''-Cl(2)''	2.3099(12)
Pd-S	2.2778(11)	Pd'-S'	2.2980(12)	Pd''-S''	2.2990(14)
Pd-N(13)'	2.062(4)	Pd'-N(13)''	2.067(4)	Pd''-N(13)	2.065(4)
S=C(2)	1.728(4)	S'=C(2)'	1.723(5)	S''=C(2)''	1.722(6)
N(1)-C(2)	1.366(5)	N(1)'-C(2)'	1.348(6)	N(1)''-C(2)''	1.369(7)
N(3)-C(2)	1.352(5)	N(3)'-C(2)'	1.369(6)	N(3)''-C(2)''	1.352(8)
Selected bond angles (deg)					
S-C(2)-N(1)	130.4(3)	S'-C(2)'-N(1)'	129.2(4)	S''-C(2)''-N(1)''	130.2(4)
S-C(2)-N(3)	121.3(3)	S'-C(2)'-N(3)'	122.8(3)	S''-C(2)''-N(3)''	122.8(4)
Pd-S-C(2)	110.65(15)	Pd'-S'-C(2)'	104.74(15)	Pd''-S''-C(2)''	103.2(2)
S-Pd-N(13)'	169.38(10)	S'-Pd'-N(13)''	169.73(11)	S''-Pd''-N(13)	175.58(11)
Cl(1)-Pd-Cl(2)	176.15(4)	Cl(1)'-Pd'-Cl(2)'	176.85(6)	Cl(1)''-Pd''-Cl(2)''	177.60(6)
Selected dihedral angles (deg)					
S-C(2)-N(3)-C(21)	-13.22	S'-C(2)'-N(3)'-C(21)'	2.69	S''-C(2)''-N(3)''-C(21)''	1.56
C(2)-N(3)-C(21)-C(26)	-61.31	C(2)'-N(3)'-C(21)'-C(26)'	-72.21	C(2)''-N(3)''-C(21)''-C(26)''	103.15
C(2)-N(1)-C(11)-C(12)	-122.98	C(2)'-N(1)'-C(11)'-C(12)'	-131.14	C(2)''-N(1)''-C(11)''-C(12)''	139.30
Selected angles between planes (deg)					
<i>i/ii</i>	1.06	<i>i/ii</i>	0.82	<i>i/ii</i>	2.55
<i>i/iii</i>	62.28	<i>i/iii</i>	70.04	<i>i/iii</i>	69.45
<i>i/iv</i>	80.55	<i>i/iv</i>	71.82	<i>i/iv</i>	66.78

B) Crystal structures of the β -monomethyl oxazoline thiourea complexes

B.1 Mono-palladium complexes of the β -monomethyl oxazoline thiourea.

The palladium complex from the **B1** fraction of **L9** was found to crystallize from $\text{CD}_2\text{Cl}_2:\text{Et}_2\text{O}$ in the orthorhombic $P2_12_12_1$ space group. The molecular structure reveals that C11 has an R-configuration and that the 9-anthryl group is in the 'up' position. Therefore, this complex is referred to as **Pd-R-L9up**. The structure of **Pd-R-L9up** contains one molecule in the asymmetric unit. Single crystals of **Pd-R-L10** were obtained from slow evaporation of a solution in $\text{CH}_2\text{Cl}_2:\text{Et}_2\text{O}$. It crystallizes in the orthorhombic $P2_12_12_1$ space group. The structure of **Pd-R-L10** contains one molecule in the asymmetric unit. The molecular structures of **Pd-R-L9up** and **Pd-R-L10** are shown Figures 43 and 44, respectively. The crystallographic data are given in Table 18 and the selected bond lengths and angles are given in Table 19.

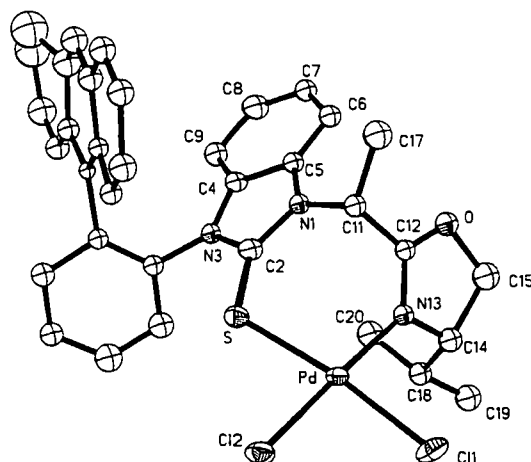


Figure 42. The molecular structure of **Pd-R-L9up**.

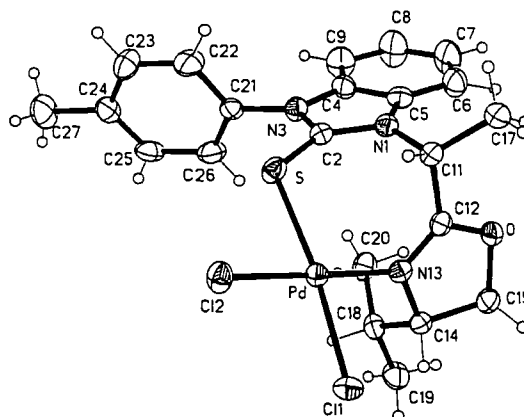


Figure 43. The molecular structure of **Pd-R-L10**.

Table 18. Crystallographic data for **Pd-R-L9up** and **Pd-R-L10**.

	Pd-R-L9up	Pd-R-L10
Empirical formula	C ₃₆ H ₃₂ Cl ₅ N ₃ OPdS	C ₂₂ H ₂₅ Cl ₂ N ₃ OPdS, CH ₂ Cl ₂
Formula weight	836.36	641.74
Temperature (K)	120(2)	120(2)
Crystal system	Orthorhombic	Orthorhombic
Space group	<i>P</i> 2 ₁ 2 ₁ 2 ₁	<i>P</i> 2 ₁ 2 ₁ 2 ₁
a (Å)	17.7318(8)	10.1551(3)
b (Å)	8.9055	12.1994(4)
c (Å)	25.4835(11)	21.7391(6)
α (°)	90.00	90.00
β (°)	90.00	90.00
γ (°)	90.00	90.00
Volume (Å ³)	4024.1(3)	2693.17(14)
Z	4	4
Density (calculated) (Mg/m ³)	1.384	1.583
Absorption coefficient (mm ⁻¹)	0.875	1.185
Crystal size (mm ³)	0.27 x 0.17 x 0.09	0.15 x 0.10 x 0.08
Theta range for data collection (°)	1.40 to 30.00	2.21 to 29.95
Reflections collected	55369	37393
Independent reflections	11736 [R(int)=0.0597]	7856 [R(int)=0.0469]
Data/restraints/parameters	11736 / 0 / 444	7856 / 7 / 318
Final R indices I > 2σ	R1=0.1253, wR2=0.3795	R1=0.0249, wR2=0.0529
R indices (all data)	R1=0.1295, wR2=0.3809	R1=0.0301, wR2=0.0544

The molecular structure of **Pd-R-L9up** shows the Pd, S, N(13), Cl(2) and Cl(1) atoms to be almost coplanar. The complex shows no tetrahedral distortion with the dihedral angle between the Pd–S–N(13) and Cl(1)–Pd–Cl(2) planes being 0.72°. The Pd–Cl(1) and Pd–Cl(2) bond lengths in **Pd-R-L9up** are 2.314(3) and 2.276(3) Å, respectively. The thiourea moiety reflects the stronger *trans* influence of the thiourea than the oxazoline moiety more clearly in other cases, as the two Pd–Cl bonds differ by *ca.* 0.038 Å (*ca.* 0.005 Å difference in its analogue, **PdL11up**). The Pd–S and Pd–N bond lengths (2.307(3) and 2.028(9) Å) are longer than those in **PdL11up** (2.2833(6) and 2.0069(18) Å). Furthermore, the C=S (1.708(10) Å) and C(2)–N(1) and C(2)–N(3) (1.362(12) and 1.342(13) Å) bond lengths in **Pd-R-L9up** are slightly shorter than those in **PdL11up** (C=S 1.716(2) Å, C–N(1) 1.373(2) Å and C–N(3) 1.362(3) Å). The S–C(2)–N(1) and S–C(2)–N(3) bond angles are very similar

(127.8(8)^o and 124.8(8)^o, respectively). The angles between planes (see Table 20) in both structures are similar except for the angle between planes *i* and *iv*; in **Pd-R-L9up** this angle is 80.6^o, whereas it is only 55.8^o in **PdL11up**. Clearly, the substituent at the β -position has a significant effect on the bond lengths and angles.

In **Pd-R-L10**, the C=S bond length is 1.711(2) Å, which is 0.05 Å longer than that in the free ligand **R-L10** (1.658(2) Å). **Pd-R-L10** shows similar C(2)–N(1) and C(2)–N(3) bond lengths (1.35 Å) which are different from those in the β -dimethyl oxazoline thiourea analogue **PdL7** (1.37 and 1.35 Å for C(2)–N(1) and C(2)–N(3), respectively). Moreover, **Pd-R-L10** shows a longer Pd–S (2.3036(6) Å) bond than the β -dimethyl complexes (2.268 – 2.297 Å). As discussed previously, in the free ligand **R-L10**, we believe that the β -monomethyl oxazoline thiourea complex is more flexible than the β -dimethyl oxazoline thiourea analogues. This is also confirmed by the C(2)–N(1)–C(11)–C(12) (83.5^o) torsion angle in **Pd-R-L10**, which is *ca.* 20^o larger than in its corresponding analogue, **PdL7**. This reflects the large *i/iv* interplanar angle, which is 85^o, nearly 10^o greater than that in **PdL7**. The flexibility of the β -monomethyl oxazoline thioureas may be the reason why many of their complexes exist in equilibria, which will be discussed later along with the NMR studies of their palladium complexes.

Table 19. Selected bonds and angles of **Pd-R-L9up** and **Pd-R-L10**.

Selected bond lengths (Å)	Pd-R-L9up	Pd-R-L10
Pd-Cl(1)	2.314(3)	2.3299(5)
Pd-Cl(2)	2.276(3)	2.2941(5)
Pd-S	2.307(3)	2.3036(6)
Pd-N(13)	2.028(9)	2.0353(16)
S=C(2)	1.708(10)	1.711(2)
N(1)-C(2)	1.362(12)	1.358(3)
N(3)-C(2)	1.342(13)	1.351(3)
Selected bond angles (deg)		
S-C(2)-N(1)	127.8(8)	128.28(16)
S-C(2)-N(3)	124.8(8)	123.20(16)
S-Pd-N(13)	99.1(2)	99.26(5)
Pd-S-C(2)	114.6(4)	111.84(7)
Cl(1)-Pd-Cl(2)	90.94(12)	91.359(19)
Selected dihedral angles (deg)		
S-C(2)-N(3)-C(21)	5.5	-2.1
C(2)-N(3)-C(21)-C(22)	-68.8	82.0
C(2)-N(1)-C(11)-C(12)	86.6	83.5
N(1)-C(11)-C(21)-N(13)	-85.0	-79.1
Selected angles between planes (deg)		
<i>i/ii</i>	2.2	2.0
<i>i/iii</i>	68.1	79.2
<i>i/iv</i>	80.6	85.0
<i>i/v</i>	40.3	46.1
<i>iv/v</i>	43.1	46.7

B.2 A dipalladium complex of the β -monomethyl oxazoline thiourea ligand **L9**.

Good quality crystals of the palladium complex of the **C1 L9** fraction suitable for single-crystal X-ray diffraction were obtained from slow evaporation of a solution in $\text{CH}_2\text{Cl}_2:\text{Et}_2\text{O}$. It crystallizes in the tetragonal space group $P4_22_12$ and the asymmetric unit contains one molecule of the $\text{Pd}_2\text{Cl}_4(\text{L9})_2$ palladium dimer, as well as one molecule of Et_2O and one CH_2Cl_2 , the latter is disordered around a two-fold axis. The C(11) centers have *S* configurations, and the 9-anthryl groups are in the 'down' conformation. Therefore, we refer to the dimer as **Pd₂-S-L9down**. The crystallographic data are given in Table 20 and selected bond lengths and angles are listed in Table 21.

Pd₂-S-L9down contains a 14-membered ring structure linked by two Pd atoms bound to the S atom of the thiourea and the N atom of the oxazoline moiety (Figure 45). The center of the dimer lies on a crystallographic inversion center. The Pd centers have *trans*- configurations, similar to **Pd₃L7**, but opposite to all of the monomer and **Pd₂L5** dimers, which have *cis*-configurations. The Pd centers have slight tetrahedral distortions with dihedral angles between the S–Pd–Cl(1) and N–Pd–Cl(2) planes of 6.5° . N and Cl(2) deviate by 0.10 and 0.24 Å from the S–Pd–Cl(1) plane. The angle between the two palladium planes, N(13A)–Pd–S–Cl(1)–Cl(2) and N(13)–Pd(A)–S(0A)–Cl(1A)–Cl(2A), is 19.82° . Another view of the cross-section of the molecule is shown in Figure 46.

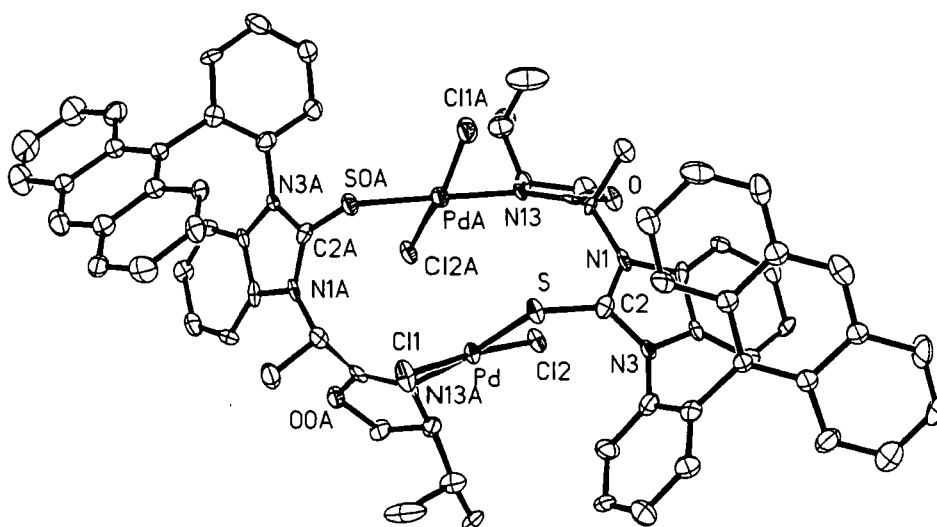


Figure 44. The molecular structure of **Pd₂-S-L9down** (hydrogen atoms and solvent molecules omitted for clarity).

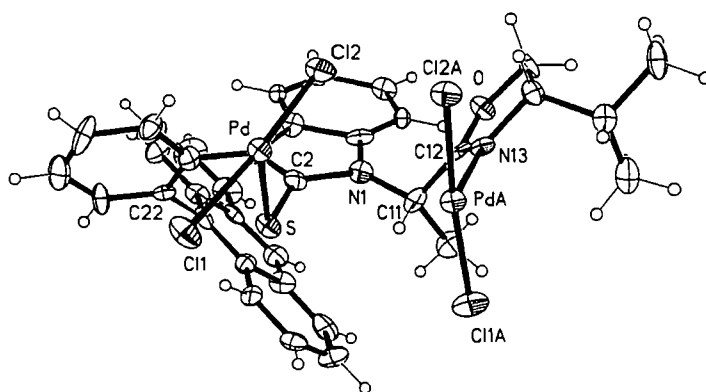


Figure 45. The cross-section of the **Pd₂-S-L9down** structure (half of the atoms omitted for clarity).

The Pd–S bond length of **Pd₂-S-L9down** (2.294(2) Å) is similar to that in **Pd-R-L10** (2.3036(6) Å). This result suggests that the dimers and monomers of the β -monomethyl oxazoline thioureas have the similar Pd–S bond lengths. However, the Pd–N bond length of **Pd₂-S-L9down** (2.070(7) Å) is slightly longer than that of **Pd-R-L10** (2.0353(16) Å). This result suggests that the dipalladium complex has a weaker Pd–N bond than in the monopalladium complex which may be a result of the *trans* influence of the thiourea moiety.

The Pd–S–C(2) angle of **Pd₂-S-L9down** is 105.6°, which is in the same range as the equivalent angles in the **Pd₂L5** structure, but small compared to the monomeric palladium complexes (115 – 118°). The S–C(2)–N(1) and S–C(2)–N(3) angles of **Pd₂-S-L9down** are similar to one another (126.4(7) and 124.7(7)°, respectively) and also similar to the S–C–N angles found in **Pd-R-L10** (128.3(2) and 123.2(2)°). Moreover, the N(1)–C(2) and N(3)–C(2) bond lengths in **Pd₂-S-L9down** (1.365(11) and 1.355(11) Å) are also similar to those in **Pd-R-L10** (1.358(3) and 1.351(3) Å).

The molecular packing of **Pd₂-S-L9down** shows close intermolecular Cl...H contacts involving protons of the CH₂ and CH groups on the oxazoline ring, *i.e.*, Cl...H(13) (2.788 Å) and Cl...H(55) (2.769 Å). The close contacts in the molecular sections are shown in Figure 47, and the crystal packing is depicted in Figure 48.

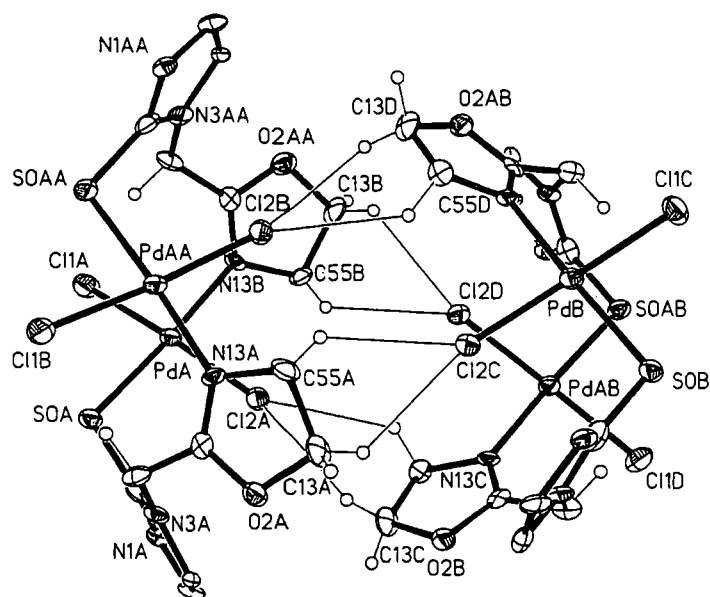


Figure 46. The molecular cross-section shows close intermolecular Cl....H contact of **Pd₂-S-L9down** (most of the atoms are omitted for clarity).

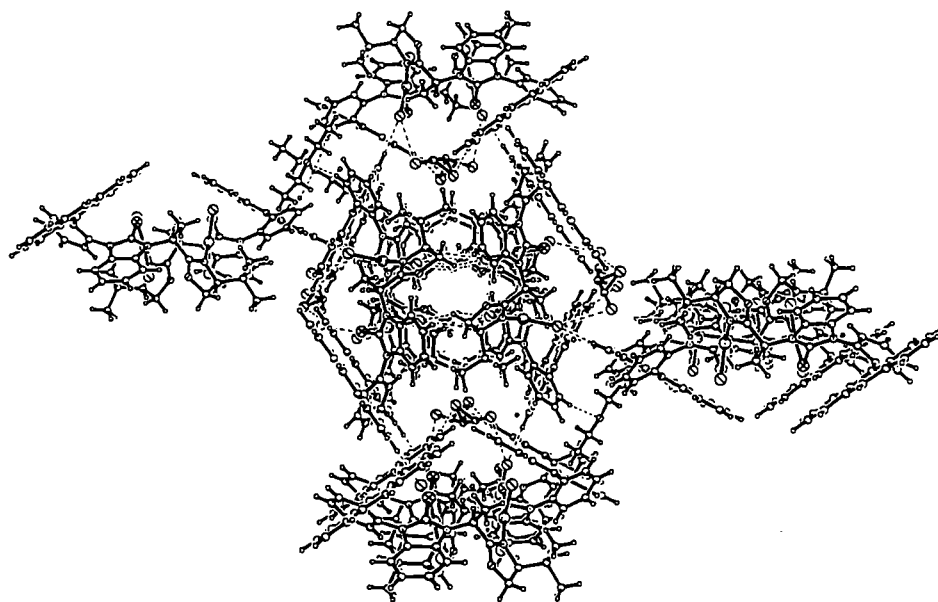


Figure 47. The crystal packing of **Pd₂-S-L9down**.

Table 20. Crystallographic data for **Pd₂-S-L9down**.

Pd₂-S-L9down	
Empirical formula	C ₇₀ H ₆₂ Cl ₄ N ₆ O ₂ Pd ₂ S ₂ ·C ₄ H ₁₀ O·1.5(CH ₂ Cl ₂)
Formula weight	1639.49
Temperature (K)	120(2)
Crystal system	Tetragonal
Space group	<i>P</i> 4 ₂ 2 ₁ 2
a (Å)	22.781(2)
b (Å)	22.781(14)
c (Å)	14.1327(14)
α (°)	90.00
β (°)	90.00
γ (°)	90.00
Volume (Å ³)	7334.2(12)
Z	4
Density (calculated) (Mg/m ³)	1.485
Absorption coefficient (mm ⁻¹)	0.854
Theta range for data collection (°)	2.30 to 23.00
Reflections collected	39838
Independent reflections	6466 [R(int)=0.2414]
Data/restraints/parameters	6466 / 2 / 444
Final R indices I > 2σ	R1=0.0684, wR2=0.1016
R indices (all data)	R1=0.1377, wR2=0.1212

Table 21. Selected bond lengths and angles of **Pd₂-S-L9down**.

Pd₂-S-L9down			
Selected bond lengths (Å)		Selected dihedral angles (deg)	
Pd-Cl(1)	2.304(3)	S-C(2)-N(3)-C(21)	-5.4
Pd-Cl(2)	2.300(2)	C(2)-N(3)-C(21)-C(22)	-107.9
Pd-S	2.294(2)	C(2)-N(1)-C(11)-C(12)	-114.6
Pd-N(13)	2.070(7)	N(1)-C(11)-C(21)-N(13)	124.5
S=C(2)	1.730(9)	Selected angles between planes (deg)	
N(1)-C(2)	1.365(11)	<i>i/ii</i>	1.8
N(3)-C(2)	1.355(11)	<i>i/iii</i>	68.0
Selected bond angles (deg)		<i>i/iv</i>	53.1
S-C(2)-N(1)	126.4(7)	<i>i/v</i>	85.5
S-C(2)-N(3)	124.7(7)	<i>iv/v</i>	36.1
S-Pd-N(13)	176.6(2)		
Pd-S-C(2)	105.6(3)		
Cl-Pd-Cl	173.87(10)		

C) The crystal structures of the α -isoquinoline thiourea complex: **PdL12**

Single crystals of **PdL12** were obtained from slow evaporation of a solution in $\text{CH}_2\text{Cl}_2:\text{Et}_2\text{O}$. It crystallizes in the monoclinic space group $P2_1/n$ ($Z = 4$) with one **PdL12** molecule and one CH_2Cl_2 solvent molecule in the asymmetric unit (Figure 49). The crystallographic data are given in Table 22 and selected bond lengths and angles are given in Table 23.

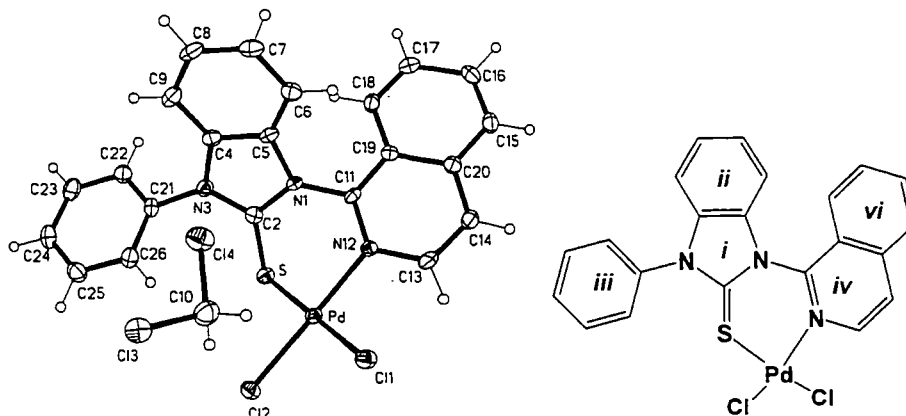


Figure 48. The molecular structure of **PdL12**.

The structure shows a *cis*-configuration at the square planar Pd center, involving coordination through the S atom of the thiourea and the N atom of the isoquinoline. The Pd center has a tetrahedral distortion with a dihedral angle between the Cl(1)–Pd–Cl(2) and S–Pd–N(12) planes of 2.6° . The Cl(1) and Cl(2) atoms deviate from the S–Pd–N plane by 0.09 and 0.05 Å, respectively. The Pd–S and Pd–N bond lengths are 2.3062(11) Å and 2.050(2) Å, respectively. The Pd–Cl(1) and Pd–Cl(2) bond lengths are 2.337(1) and 2.2932(8) Å, respectively, which shows the stronger *trans* influence of the thiourea compared with that of the isoquinoline. Furthermore, **PdL12** shows similar S–C(2)–N(1) and S–C(2)–N(3) bond angles ($124.5(2)^\circ$ vs $127.6(2)^\circ$). The Pd–S and Pd–N bond lengths and S–C(2)–N(1) and S–C(2)–N(3) angles are similar to those in the β -monomethyl palladium complexes. It is possible to conclude that the α -isoquinoline thiourea complex has slightly weaker Pd–S and Pd–N bonds than the β -dimethyl oxazoline thiourea complexes. The Pd–S–C(2) bond angle ($92.89(10)^\circ$) is quite small compared to the equivalent angles in the seven-membered rings of the β -mono and dimethyl oxazoline thiourea

complexes (av. 107°), which is due to the fact that it is only involved in a six-membered ring. The bite angle (S–Pd–N13), is $89.34(7)^\circ$, *i.e.* very close to 90° .

The molecular packing of **PdL12** involves a close Cl...H contact involving a proton in the isoquinoline group (Cl(2)...H(17), 2.835 Å). Furthermore, there is a close intermolecular S...H contact of 2.821 Å, which is less than the sum of the van der Waals radii (2.91 Å),²⁹ involving a hydrogen atom from the solvent. The crystal packing of **PdL12** is depicted in Figure 50.

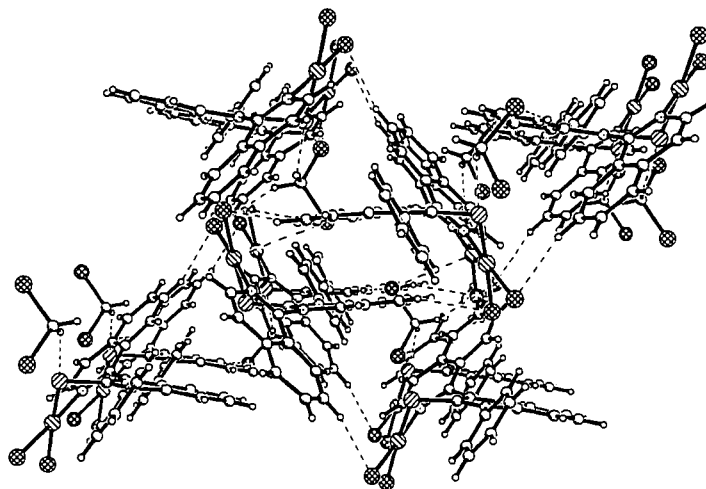


Figure 49. The crystal packing of **PdL12** showing the close intermolecular contacts.

Table 22. Crystallographic data for PdL12.

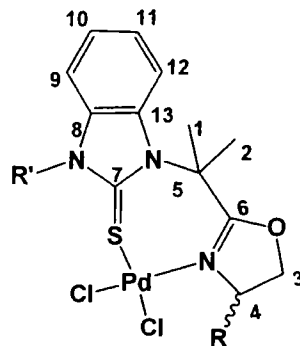
PdL12	
Empirical formula	C ₂₂ H ₁₅ Cl ₂ N ₃ PdS, CH ₂ Cl ₂
Formula weight	615.66
Temperature (K)	120(2)
Crystal system	Monoclinic
Space group	<i>P</i> 2 ₁ / <i>n</i>
a (Å)	12.9498(5)
b (Å)	12.9427(5)
c (Å)	15.1881(5)
α (°)	90.00
β (°)	114.26(3)
γ (°)	90.00
Volume (Å ³)	2320.86(15)
Z	4
Density (calculated) (Mg/m ³)	1.762
Absorption coefficient (mm ⁻¹)	1.368
Crystal size (mm ³)	0.10 x 0.06 x 0.02
Theta range for data collection (°)	2.33 to 29.97
Reflections collected	28136
Independent reflections	5891 [R(int)=0.0862]
Data/restraints/parameters	5891 / 0 / 289
Final R indices I > 2σ	R1=0.0356, wR2=0.0543
R indices (all data)	R1=0.0690, wR2=0.0601

Table 23. Selected bond lengths and angles of PdL12.

Selected bond lengths (Å)		Selected dihedral angles (deg)	
Pd-Cl(1)	2.337(1)	S-C(2)-N(3)-C(21)	2.7
Pd-Cl(2)	2.2932(8)	C(2)-N(3)-C(21)-C(22)	-126.8
Pd-S	2.3062(11)	C(2)-N(1)-C(11)-C(19)	131.1
Pd-N(12)	2.050(2)	C(2)-N(1)-C(11)-N(12)	-49.9
S=C(2)	1.698(3)	Selected angles between planes (deg)	
N(1)-C(2)	1.368(4)	<i>i/ii</i>	5.9
N(3)-C(2)	1.351(4)	<i>i/iii</i>	60.9
Selected bond angles (deg)		<i>i/iv</i>	49.2
S-C(2)-N(1)	124.5(2)	<i>i/v</i>	71.4
S-C(2)-N(3)	127.6(2)	<i>v/iv</i>	40.5
S-Pd-N(13)	89.34(7)		
Pd-S-C(2)	92.89(10)		
Cl(1)-Pd-Cl(2)	92.19(3)		

II.3.2 NMR characterization of *S,N*-oxazoline thiourea complexes

The *S,N*-oxazoline thiourea complexes β -monomethyl oxazoline thiourea, β -dimethyl oxazoline thiourea and α -isoquinoline thiourea were characterized by NMR (1D and 2D) spectroscopy. By comparison with assignments for the free ligands, the ^1H and $^{13}\text{C}\{^1\text{H}\}$ of all palladium complexes can be assigned. Summaries of the ^1H NMR assignments are given in Tables 24 – 30, whereas the $^{13}\text{C}\{^1\text{H}\}$ NMR data are given in the experimental section, except for **PdL12**, for which both ^1H and $^{13}\text{C}\{^1\text{H}\}$ NMR data are provided in the experimental section. Complete ^1H and $^{13}\text{C}\{^1\text{H}\}$ NMR spectra are provided in Appendix B.

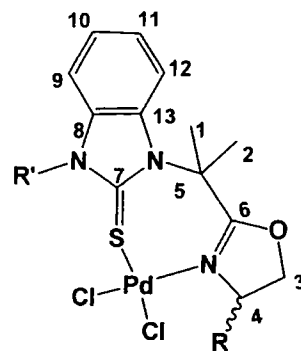
Table 24. ^1H NMR assignments for the β -dimethyl oxazoline thiourea monopalladium complexes (positions 1-12)

Compound	R	R'	H1 and H2	H3	H4	H9	H10	H11	H12
PdL3			3.42, s, 3H 2.61, s, 3H	4.90, t (9), 1H 4.52, t (9), 1H	5.89 – 5.93 m 1H	6.98 d (8) 1H	7.39 – 7.44 m 2H		8.04 d (7) 1H
PdL2up			3.38, s, 3H 2.55, s, 3H	4.46, t (9), 1H 4.24, t (9), 1H	4.85 – 4.88 m 1H	6.83 d (8) 1H	7.31 t (8) 1H	7.34 t (8) 1H	7.99 d (8) 1H
PdL2down			3.37, s, 3H 2.54, s, 3H	4.50, t (9), 1H 4.28, t (9), 1H	4.88 m 1H	6.81 d (9) 1H	7.29 t (9) 1H	7.35 t (9) 1H	7.99 d (9) H

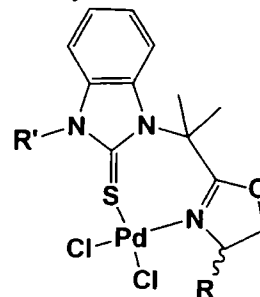
Table 25 (continued)

Compound	R	R'	H1 and H2	H3	H4	H9	H10	H11	H12
PdL4			3.36, s, 3H 2.55, s, 3H	4.50, dd (10, 9), 1H 4.27, dd (10, 9), 1H	4.88 – 4.92 m 1H	6.83 d (8) 1H	7.32 t (8) 1H	7.38 t (8) 1H	7.97 d (8) 1H
PdL5			3.33, s, 3H 2.47, s, 3H	4.42, dd (8, 1.2), 1H 4.17, dd (8, 2.1), 1H	4.82 – 4.87 m 1H	7.76 d (8) 1H	7.31 – 7.39 m 2H		7.98 d (8) 1H
PdL6			3.47, s, 3H 2.55, s, 3H	4.46, t (8), 1H 4.23, t (8), 1H	4.92 – 4.95 m 1H	6.91 d (8) 1H	7.30 t (8) 1H		7.96 d (8) 1H
PdL7			3.46, s, 3H 2.54, s, 3H	4.45, t (9), 1H 4.22, t (9), 1H	4.88 – 4.91 m 1H	6.95 d (8) 1H	7.28 t (8) 1H	7.35 t (8) 1H	7.96 d (8) 1H
PdL8			3.53, s, 3H 2.64, s, 3H	4.54, t (9), 1H 4.42, t (9), 1H	4.91 – 4.95 m 1H	7.70 dd (8, 3) 1H	7.77 – 7.79 m 2H		7.95 dd (8, 3) 1H

Table 24 (continued)

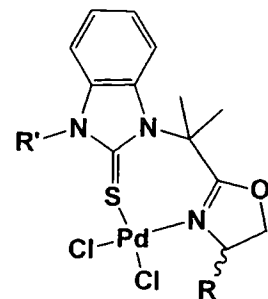


Compound	R	R'	H1 and H2	H3	H4	H9	H10	H11	H12
PdL11up			2.67, s, 3H 2.18, s, 3H	4.25, t (8), 1H 4.14, t (8), 1H	4.71 – 4.74 m 1H	6.72 d (7) 1H	6.59 t (7) 1H	6.83 t (7) 1H	7.33 – 7.34 m 1H
PdL11down			2.36, s, 3H 1.44, s, 3H	4.22, t (8), 1H 4.15, t (8), 1H	4.69 – 4.71 m 1H	7.14 d (8) 1H	7.00 t (8) 1H	7.06 t (8) 1H	7.41 d (8) 1H
PdL13	H		2.80, s, 3H 2.16, s, 3H	4.29 – 4.33, m, 1H 3.80, q (9), 1H	4.20 – 4.25, m, 1H 3.64 – 3.68, m, 1H	7.00 d (8) 1H	6.87 t (8) 1H	6.97 t (8) 1H	7.43 d (8) 1H

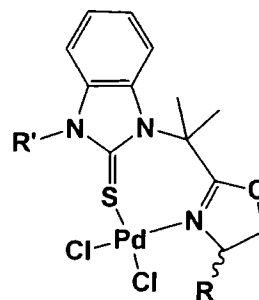
Table 25. ^1H NMR assignments for R-substituents of the β -dimethyl oxazoline thiourea monopalladium complexes.

Compound	R	R'	Aromatic protons (R)						
PdL3			7.69 – 7.15 m 5H						
Compound	R	R'	H14	H15 and H16	Compound	R	R'	H14	H15 and H16
PdL2up			3.07 – 3.12 m 1H	0.87, d (7), 3H 0.75, d (7), 3H	PdL8			3.17 – 3.23 m 1H	0.96, d (7), 3H 0.88, d (7), 3H
PdL2down			3.00 – 3.06 m 1H	0.92, d (7), 3H 0.85, d (7), 3H	PdL11up			3.19 – 3.24 m 1H	0.91, d (8), 3H 0.81, d (8), 3H
PdL4			3.06 – 3.13 m 1H	0.93, d (7), 3H 0.84, d (7), 3H	PdL11down			3.02 – 3.05 m 1H	0.83, d (7), 3H 0.42, d (7), 3H

Table 26 (continued)



Compound	R	R'	H14	H15 and H16	Compound	R	R'	H14	H15 and H16
PdL5			3.07 – 3.15 m 1H	0.84, d (7), 3H 0.64, d (7), 3H	PdL7			3.13 – 3.16 m 1H	0.86, d (7), 3H 0.76, d (7), 3H
PdL6			3.17 – 3.21 m 1H	0.88, d (7), 3H 0.78, d (7), 3H					

Table 26. ^1H NMR assignment for R' -substituents of the β -dimethyl oxazoline thiourea monopalladium complexes.

Compound	R	R'	Aromatic protons (R')
PdL3			7.69 – 7.15 m 5H

Table 26 (continued)

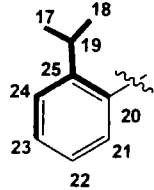
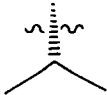
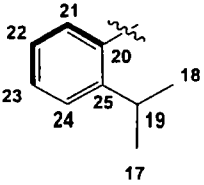
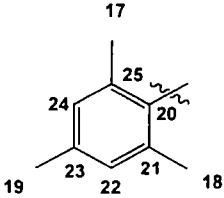
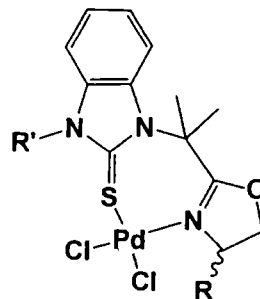
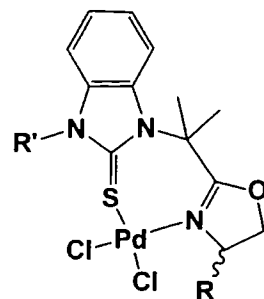
Compound	R	R'	H17 and H18	H19	H21	H22	H23	H24
PdL2up			1.27, d (7), 3H 1.00, d (7), 3H	2.31 – 2.35 m 1H	6.93 d (8) 1H	7.45 t (8) 1H	7.65 t (8) 1H	7.61 d (8) 1H
PdL2down			1.24, d (7), 3H 0.98, d (7), 3H	2.26 – 2.31 m 1H	7.17 d (9) 1H	7.45 t (9) 1H	7.60 – 7.66 m 2H	
PdL4			1.87, s, 3H 1.85, s, 3H	2.41 s 3H	-	7.13 s 1H	-	7.13 s 1H

Table 26 (continued)

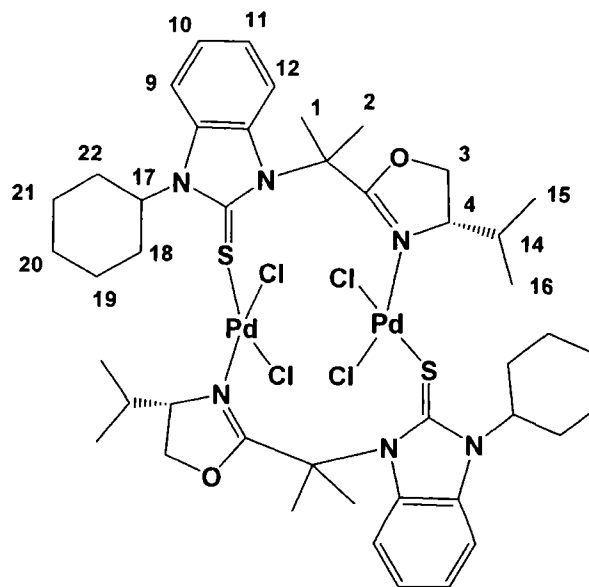


Compound	R	R'	H17	H18	H19	H20	H21	H22	H23
PdL5			3.15 – 3.20 m 1H	1.24 – 2.24 , m, 10H					-
PdL6			7.10 d (7) 1H	7.60 – 7.61 m 3H			7.38 d (7) 1H	-	
PdL7			6.92 d (8) 1H	7.36 – 7.40 m 1H	-	7.36 – 7.40 m 1H	7.23 d (8) 1H	2.45 s 3H	

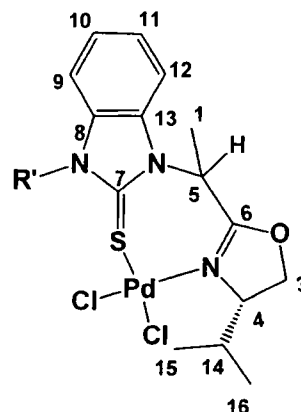
Table 26 (continued)



Compound	R	R'	Aromatic protons (R')
PdL8			8.63, s, 1H; 8.13 – 8.16, m, 2H; 7.77 – 7.79, m, 1H; 7.67, d (9), 1H; 7.53 – 7.59, m, 3H; 7.45 – 7.49, m, 4H; 7.21, dd (10, 3), 1H
PdL11up			8.21, s, 1H; 8.10, d (8), 1H; 7.87, t (8), 1H; 7.77 – 7.83, m, 4H; 7.68 – 7.73, m, 2H; 7.57, d (8), 1H; 7.46, t (8), 1H; 7.33 – 7.34, m, 2H
PdL11down			8.26, s, 1H; 8.09, t (5), 1H; 8.02, d (9), 1H; 7.86, d (9), 1H; 7.79 – 7.81, m, 3H; 7.66, t (5), 1H; 7.60, d (9), 1H; 7.55, t (9), 1H; 7.41, d (8), 1H; 7.28, d (9), 1H, 7.18, t (9), 1H
PdL13			8.26, s, 1H; 8.10, d (9), 1H; 7.90, d (8), 1H; 7.84, t (8), 1H; 7.71 – 7.79, m, 5H; 7.52 – 7.53, m, 2H; 7.23, t (8), 1H; 7.15, t (8), 1H

Table 27. ^1H NMR assignment for $\text{Pd}_2\text{L5}$.

Part	H1 and H2	H3	H4	H9	H10 and H11	H12
parent	3.93, s, 3H 2.26, s, 3H	4.12 – 4.19, m, 2H	4.51 – 4.55, m, 1H	7.81, d (9), 1H	7.35 – 7.41, m, 2H	7.93, d (8), 1H
	H14	H15 and H16		H17	H18 – H22	-
	3.37 – 3.42, m, 1H	1.16, d (7), 3H 1.10, d (7), 3H		2.93 – 3.00, m, 1H	1.40 – 2.17, m, 10H	

Table 28. ^1H NMR assignment for the β -monomethyl oxazoline thiourea monopalladium complexes (positions 1 - 16).

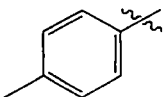
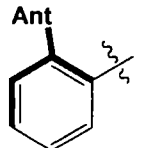
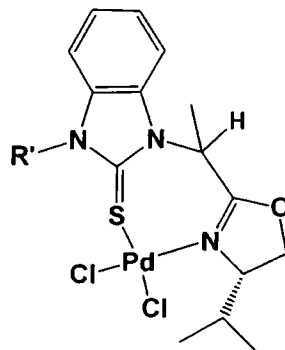
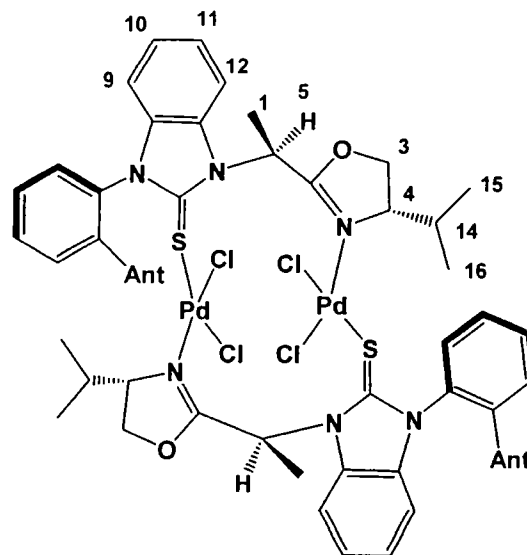
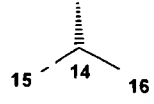
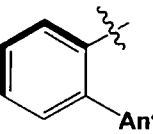
Compound	R'	H1	H5	H3	H4	H9	H10	H11	H12	H14	H15 and H16
Pd-R-L10		2.21 d (7) 3H	6.75 q (7) 1H	4.57, t (9), 1H 4.25, t (9), 1H	4.87 – 4.91 m 1H	7.12 d (8) 1H	7.36 t (8) 1H	7.38 – 7.43 m 1H	7.71 d (8) 1H	2.60 – 2.63 m 1H	1.05, d (8), 3H 0.50, d (8), 3H
Pd-R-L9up		1.70 d (7) 3H	6.28 q (7) 1H	4.43, t (9), 1H 4.12, t (9), 1H	4.83 – 4.86 m 1H	6.79 d (8) 1H	6.70 t (8) 1H	6.97 t (8) 1H	7.18 d (8) 1H	2.59 – 2.60 m 1H	0.64, d (7), 3H 0.37, d (7), 3H

Table 29. ^1H NMR assignment for the R' -substituent of the β -monomethyl oxazoline thiourea mono-palladium complexes.

Compound	R'	Aromatic protons (R')	H_{23}
Pd-R-L10		7.38 – 7.43, m, 2H 7.38 – 7.43, m, 2H	2.48, s, 3H
Pd-R-L9up		8.23, s, 1H; 7.93, d (8), 1H; 7.75 – 7.88, m, 4H; 7.64 – 7.65, m, 1H; 7.58 – 7.60, m, 1H; 7.45 – 7.49, m, 2H; 7.39, t (8), 1H; 7.34 – 7.35, m, 2H	-

Table 30. ^1H NMR assignment for **Pd₂-S-L9down**.

Part	H1	H3	H4	H5	H9	H10	H11	H12
parent	1.52, d (7), 3H	4.14 – 4.21, m, 1H 4.70 – 4.78, m, 1H	3.99, t (9), 1H	8.01 – 8.12, m, 1H	6.52, d (8), 1H	6.32, t (8), 1H	6.89, t (8), 1H	7.41 – 7.55, m, 1H
	H14	H15 and H16		Aromatic protons 9.09, d (7), 1H; 8.15, s, 1H; 7.86 – 7.94, m, 4H; 7.65 – 7.75, m, 2H; 7.41 – 7.55, m, 4H; 7.31 – 7.35, m, 1H				
2.90 – 3.10, m, 1H	1.35, d (7), 3H 1.14, d (7), 3H							

II.4 NMR study of S,N-oxazoline thiourea palladium complexes

A) Synthesis of the β -dimethyl oxazoline thiourea palladium complexes

The ^1H NMR spectra of the products obtained from the *in situ* reactions of the palladium sources with the β -dimethyl oxazoline thiourea ligands **L2up**, **L2down**, **L3**, **L4**, **L5**, **L6**, **L7** and **L11up**, were found to be identical to the ^1H NMR spectra of solutions of the single crystals of their respective complexes grown for X-ray diffraction, except for the complex with **L5**. The fact that this complex was only found to crystallize as the dimer, whereas all of the others crystallized as the monomers, leads us to assume that the original products are the mono-palladium complexes. The $^{13}\text{C}\{^1\text{H}\}$ NMR spectra of the isolated palladium complexes **PdL2up**, **PdL2down**, **PdL3**, **PdL4**, **PdL5** and **PdL6** were recorded in CD_2Cl_2 and those of **PdL7**, **PdL8**, **PdL11up**, **PdL11down** and **PdL13** were measured in CDCl_3 . The $^{13}\text{C}\{^1\text{H}\}$ NMR spectrum of a solution of the single crystals of **Pd₂L5** was also obtained in CDCl_3 . The $^{13}\text{C}\{^1\text{H}\}$ NMR signals of the C=S and C=N carbons are given in Table 31.

Table 31. The $^{13}\text{C}\{^1\text{H}\}$ NMR shifts (ppm) for the C=S and C=N carbons of the β -dimethyl oxazoline thiourea palladium complexes in CD_2Cl_2 unless other noted.

Complex	C=S	C=N
PdL2up	164.8	168.4
PdL2down	164.9	168.7
PdL3	164.6	168.8
PdL4	163.8	168.6
PdL5	161.7	167.5
PdL6	164.2	167.4
PdL7^a	164.1	167.5
PdL8^a	164.8	168.6
PdL11up^a	164.3	167.5
PdL11down^a	163.7	166.9
PdL13^a	163.4	168.2
Pd₂L5^a	161.8	173.2

^a measured in CDCl_3 .

Table 32 further confirms that the original complexes are monomers as they show one signal for the C=S carbon are in the range of δ 161.7 – 164.9 ppm and one C=N signal in the range of δ 166.9 – 168.8 ppm. The palladium dimer, **Pd₂L5**, only has one C=S and one C=N signal at δ 161.8 ppm and 173.2 ppm, respectively; therefore, the dimer must contain a center of symmetry. Using this $^{13}\text{C}\{^1\text{H}\}$ NMR information, we can speculate that the palladium complexes for which we were unable to obtain crystal structures (**PdL5**, **PdL8**, **PdL11down** and **PdL13**), are also monomers, as their C=N signals are in the range of δ 166.9 – 168.8 ppm.

The ^1H NMR spectrum of the *in situ* reaction of $\text{Pd}(\text{PhCN})_2\text{Cl}_2$ and **L5** in a 1:1 molar ratio in CDCl_3 after 15 minutes was shown to be identical to the spectrum of the initial isolated product obtained from this reaction. A comparison of the spectrum of the *in situ* reaction and that of the crystals of **Pd₂L5** is shown in Figure 51. Thus, it would appear that the dimer is formed during the growth of the single crystals by slow evaporation of solvent. The conversion of **PdL5** to **Pd₂L5** is depicted in Scheme 6. However, we have no explanation as to exactly how the monomer is transformed to the dimer. Clearly, **Pd₂L5** must be thermodynamically more stable and/or less soluble than **PdL5**. In any case, their interconversion must be relatively slow as neither spectrum shown in Figure 51 displays even traces of the other species.

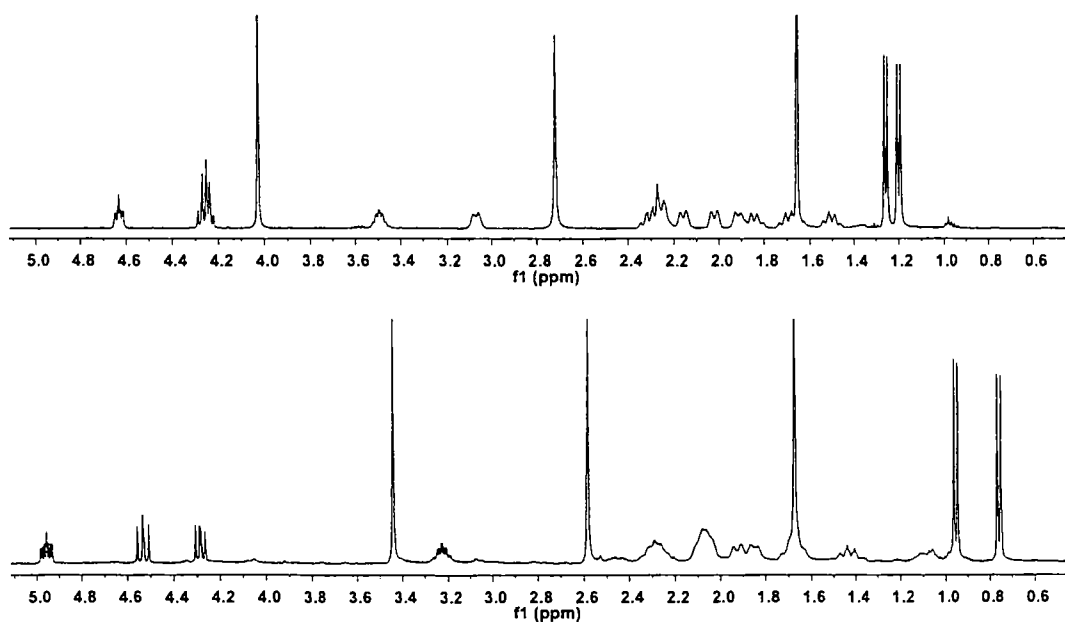
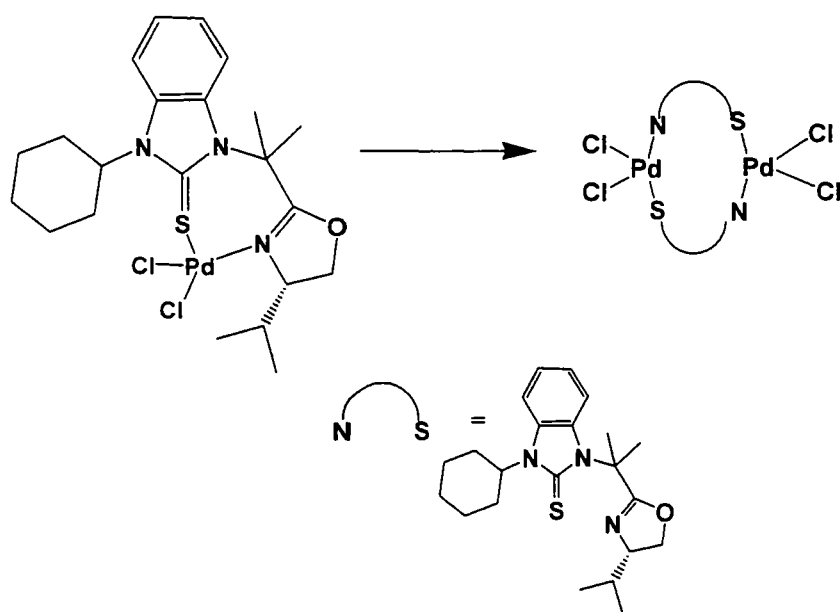


Figure 50. The ^1H NMR (500 MHz, CDCl_3) spectra of the *in situ* reaction of 1:1 $\text{PdCl}_2(\text{PhCN})_2$ and **L5** (bottom) and **Pd₂L5** crystals (top).



Scheme 6. The conversion of **PdL5** to **Pd₂L5**.

The ^1H NMR spectra after 24 h in CDCl_3 of the single crystals of **PdL7** grown from $\text{CH}_2\text{Cl}_2:\text{DMF}$, shown by X-ray diffraction to be a monomer, and those grown from $\text{CH}_2\text{Cl}_2:\text{Et}_2\text{O}$, shown to be a trimer (Figure 42), are displayed in Figure 51. Surprisingly, the ^1H NMR spectrum of the latter, shows additional signals, some of which can be attributed to the monomer. The integrals of the monomer signals increase over time, whereas those of the trimer decrease (Figure 53). We believe that the trimer is in dynamic equilibrium with the monomer at room temperature. Close inspection of the ^1H NMR spectrum of the trimer reveals other signals which could not be identified. They are believed to belong to an intermediate and are marked by asterisks. It is noteworthy that the $^{13}\text{C}\{^1\text{H}\}$ NMR spectrum of the C=N trimer shows three signals at δ 171.3, 171.5 and 171.6 ppm. The C=S signals could not be observed. The conversion between **PdL7** and **Pd₃L7** is depicted in Scheme 7.

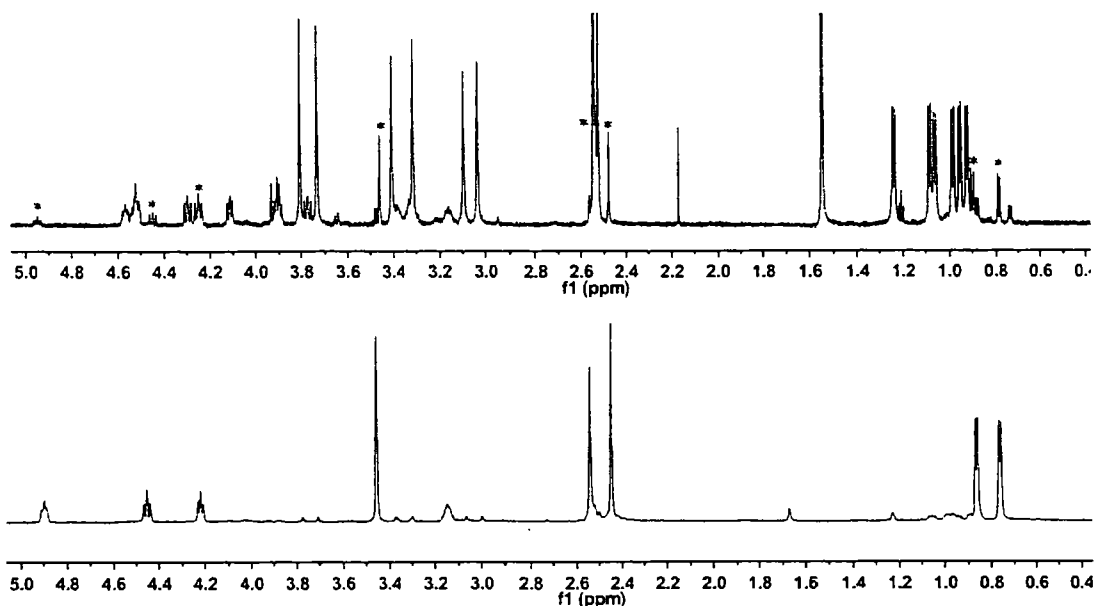


Figure 51. The ^1H NMR (700 MHz, CDCl_3) spectra of the aliphatic region of **PdL7** (bottom) and the **Pd₃L7** crystals after 24 h at room temperature (top): * = **PdL7**.

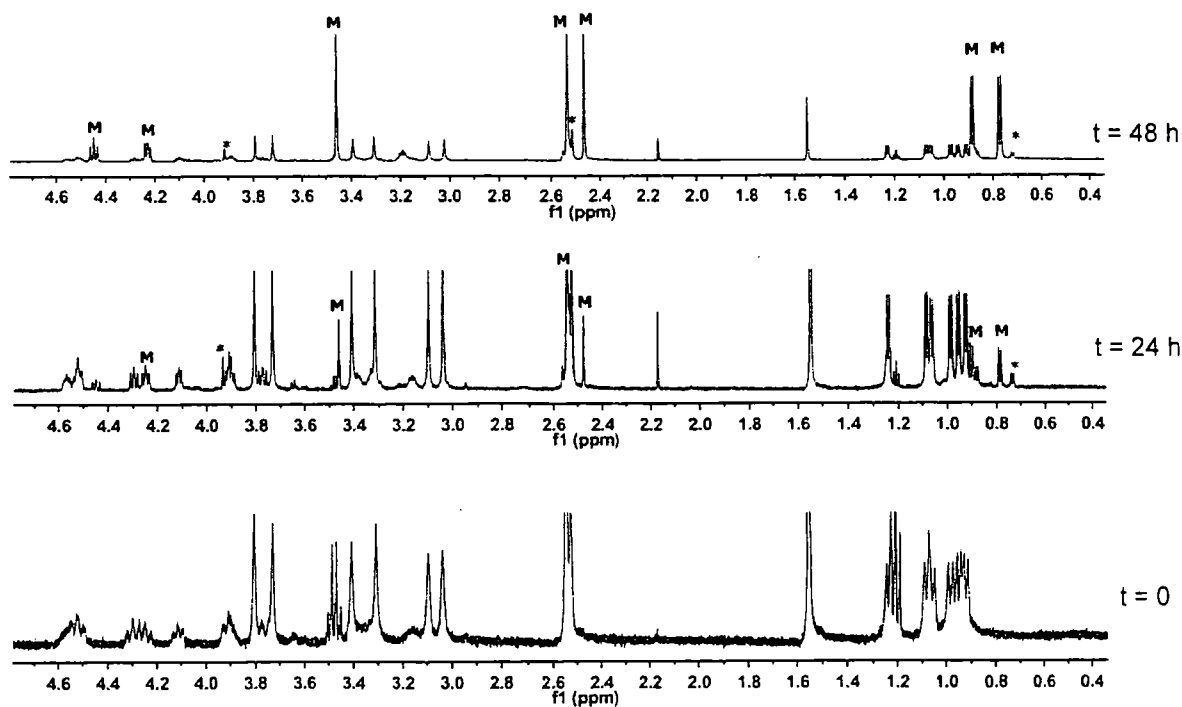
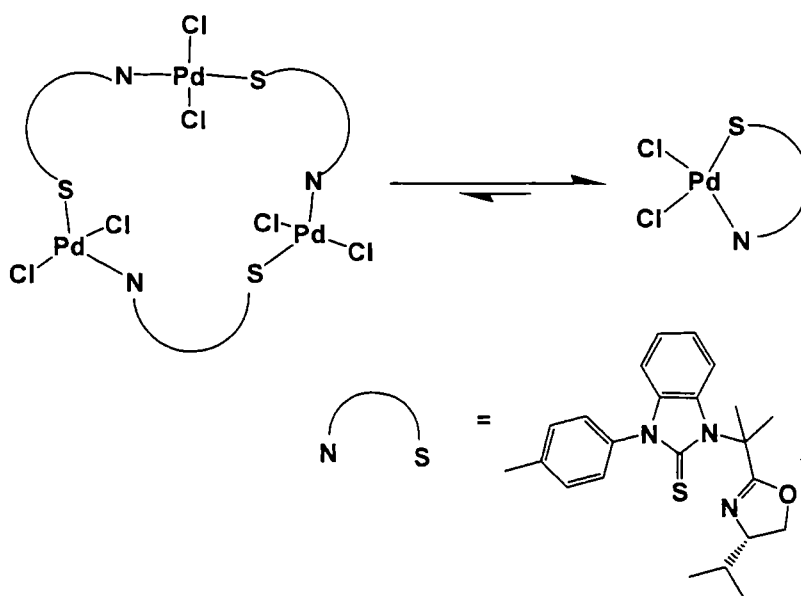


Figure 52. The ^1H NMR (CDCl_3) spectra of the aliphatic region of the **Pd₃L7** crystals at various times; bottom (400 MHz immediately after the solution was prepared), middle (700 MHz, after 24 h at room temperature) and top (700 MHz, after 48 h at room temperature); **M** = monomer, * = intermediates.



Scheme 7. The interconversion of **PdL7** and **Pd₃L7** in solution at room temperature.

B) Synthesis of the β -monomethyl oxazoline thiourea palladium complexes

The ^1H and $^{13}\text{C}\{^1\text{H}\}$ NMR spectra of the products of the reactions of the palladium sources with the β -monomethyl oxazoline thiourea ligands **R-L9up**, **S-L9down**, **R-L10** and **S-L10** were obtained in CDCl_3 . In addition, *in situ* ^1H NMR spectra for all of the above reactions were obtained shortly after mixing of the reagents. Finally, ^1H NMR spectra of the single crystals grown for X-ray diffraction of **Pd-R-L9up**, **Pd₂-S-L9down**, **Pd-R-L10** were recorded in CDCl_3 .

All of the ^1H spectra involving **R-L9up** are identical, appearing as a single species, which we believe to be the mono-palladium complex **Pd-R-L9up**, as found by X-ray analysis. The ^1H spectra of the product of the reaction of **S-L9down** and its *in situ* reaction, are also identical, and appear to show two species. The ^1H spectrum of the **Pd₂-S-L9down** crystals obtained soon after the solution was prepared shows only one species, which is present in the other two spectra. Since this species is likely to be the dimer, we can identify the dimer peaks in the other two spectra. The other signals are likely to originate from the monomer, which we believe to exist in equilibrium with the dimer. Further evidence for this equilibrium comes from the spectrum of a solution of the **Pd₂-S-L9down** crystals after being left to stand at room temperature overnight. The spectrum was identical to those obtained for the product and *in situ* reaction, which would appear to indicate that the dimer is now in equilibrium with the monomer. The ^1H NMR spectrum of the **Pd₂-S-L9down** crystals

shortly after preparation is shown in Figure 54, and that obtained on the same sample after standing overnight is shown in Figure 55.

The $^{13}\text{C}\{^1\text{H}\}$ NMR spectrum of the product of the reaction with **S-L9down**, shows two signals for the C=S carbon and two for the C=N carbon (see Table 32), which would only arise if the dimer contained a center of symmetry. The C=N signals were assigned to the monomer and dimer using HMBC, and the C=S signals on the basis of their intensities. The equilibrium between the **Pd-S-L9down** and **Pd₂-S-L9down** is shown in Scheme 8.

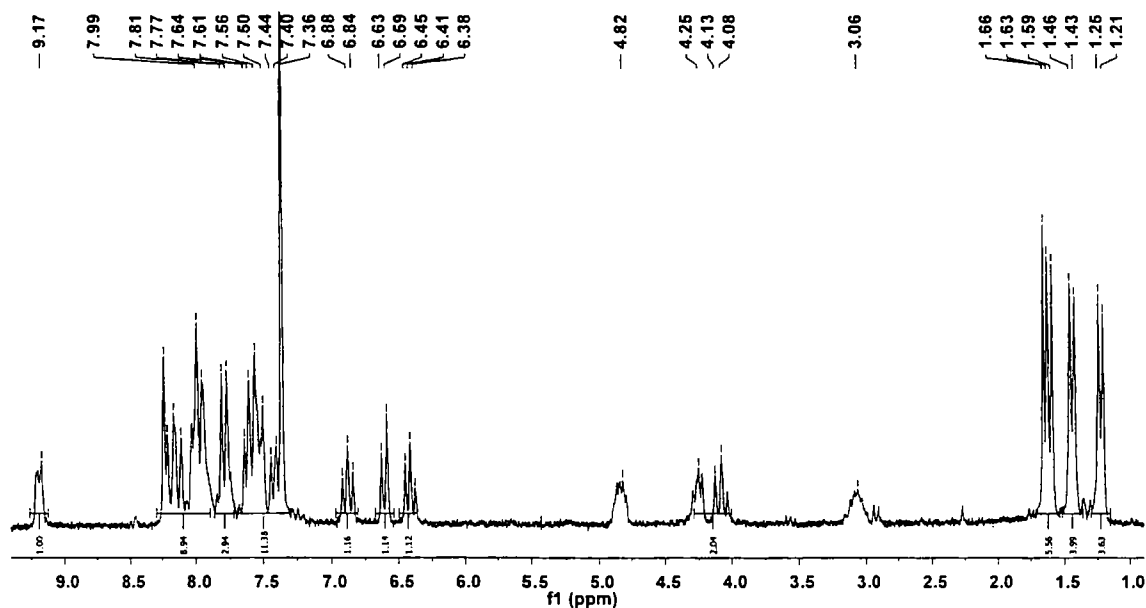


Figure 53. The ^1H NMR (200 MHz, CDCl_3) spectrum of a solution of the **Pd₂-S-L9down** crystals shortly after preparation.

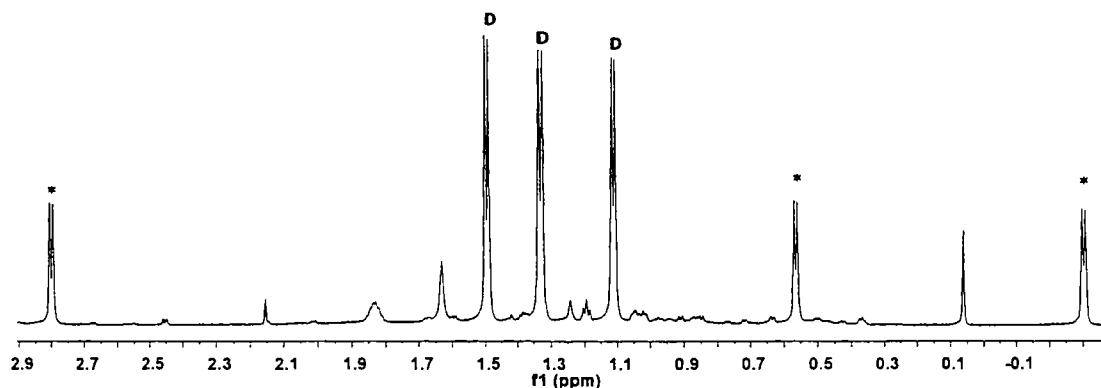
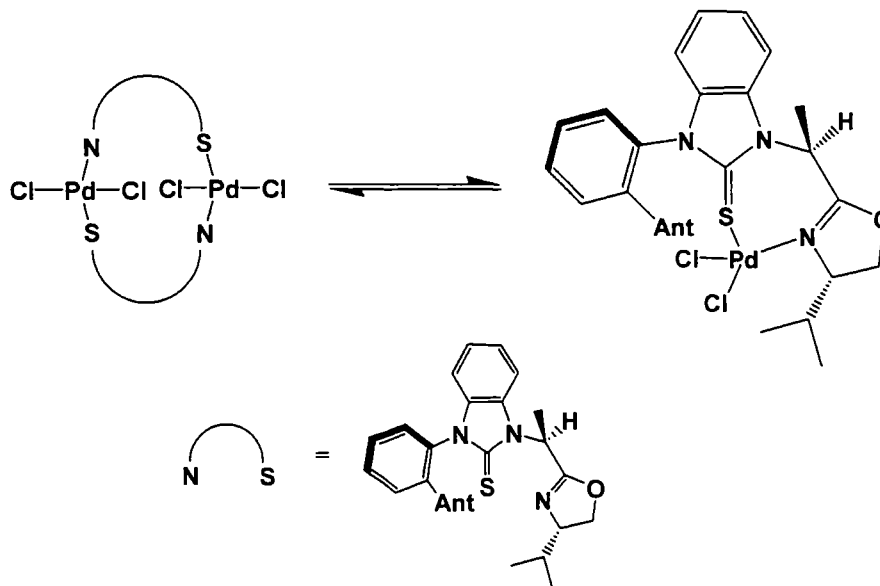


Figure 54. The ^1H NMR (700 MHz, CDCl_3) of the aliphatic region of **Pd₂-S-L9down** (D) after standing overnight (**Pd-S-L9down** signals marked with *).

Table 32. The C=S and C=N $^{13}\text{C}\{^1\text{H}\}$ signals of the β -monomethyl oxazoline thiourea palladium complexes in CDCl_3 (ppm).

Compound	Complex	
	C=S	C=N
Pd-S-L9down	164.1	165.4
Pd₂-S-L9down	166.3	167.5



Scheme 8. The interconversion between dimeric **Pd₂-S-L9down** and monomeric **Pd-S-L9down**.

All of the ^1H NMR spectra involving **R-L10** are identical; they initially appear to show one species, which is believed to be the monomer **Pd-R-L10**, as found by X-ray diffraction analysis. This is confirmed by the $^{13}\text{C}\{^1\text{H}\}$ NMR spectrum of the product which shows single signals for C=S and C=N. However, traces of other signals are present in all of the ^1H spectra, which increase in intensity until 3 days, when they have integrals equal to 0.4 of the original peaks. We believe that these peaks originate from a single species which exists in a slowly established equilibrium with the monomer. ^1H NMR spectra of the aliphatic region of the **Pd-R-L10** crystals after 0, 1, 2 and 3 days are shown in Figure 56. A ^1H NMR spectrum of the *in situ* reaction of $\text{PdCl}_2(\text{PhCN})_2$ and **R-L10** in a 1:2 molar ratio in CDCl_3 after 3 days only showed signals for the **Pd-R-L10** monomer and the **R-L10** free ligand, which indicates that the excess of free ligand is impeding the equilibrium. This observation

is related to the catalytic activity of this ligand which will be discussed later. ^1H NMR spectra of the aliphatic region of the 1:2 *in situ* reaction after 3 days is shown in Figure 57, along with those of the free ligand and the 1:1 *in situ* reaction, soon after preparation, for comparison.

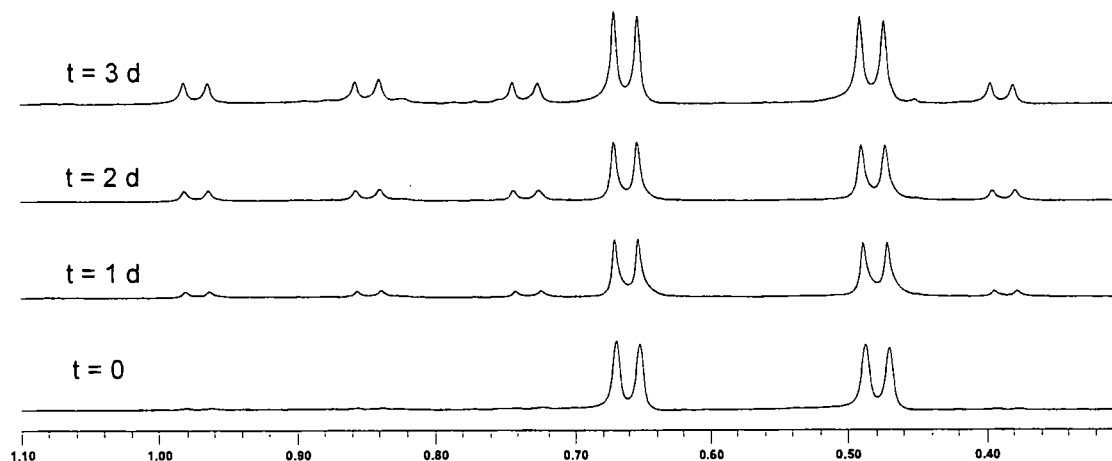


Figure 55. ^1H NMR (400 MHz, CDCl_3) spectra of the aliphatic region of **Pd-R-L10** at various times.

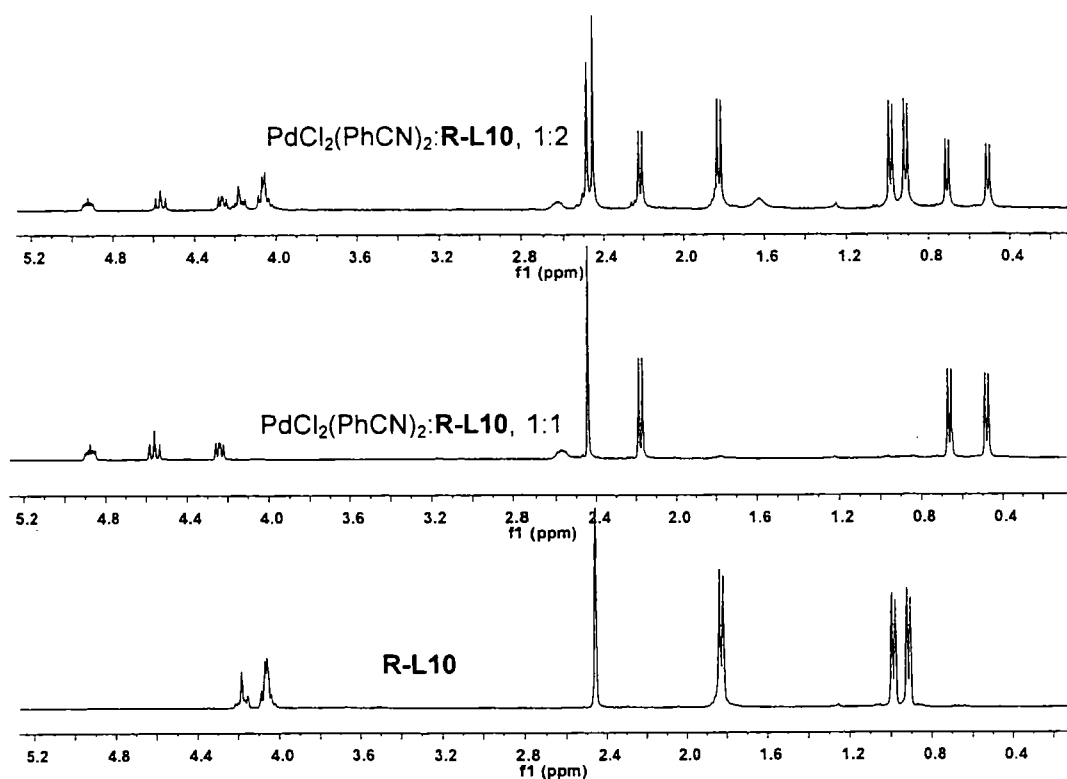


Figure 56. ^1H NMR (400 MHz, CDCl_3) spectra of the aliphatic region of **R-L10** (bottom), the *in situ* reaction of $\text{PdCl}_2(\text{PhCN})_2$ with **R-L10** at 1:1 molar ratio soon after preparation (middle) and the *in situ* reaction of $\text{PdCl}_2(\text{PhCN})_2$ with **R-L10** at 1:2 molar ratio after 3 days (top).

The ^1H NMR spectra of the product of the reaction of $\text{PdCl}_2(\text{PhCN})_2$ and **S-L10**, and the *in situ* reaction soon after preparation are identical. Analysis of the aliphatic region which contains the isopropyl signals, reveals three species to be present in differing amounts. This is confirmed by their respective $^{13}\text{C}\{^1\text{H}\}$ NMR spectra which show three signals for both $\text{C}=\text{S}$ and $\text{C}=\text{N}$. Their relative integrals of the ^1H NMR signals change over a period of 3 days, after which there was no further change, leading us to conclude that the species have attained equilibrium, with a 1.8:1.8:1 ratio. The ^1H NMR spectra of the aliphatic region of the *in situ* reaction after 0, 1, 2 and 3 days are shown in Figure 58. A ^1H NMR spectrum of the *in situ* reaction of $\text{PdCl}_2(\text{PhCN})_2$ with **S-L10** in a 1:2 molar ratio in CDCl_3 , obtained soon after preparation, shows signals from the same three species, but with different integrals to those of the analogous 1:1 *in situ* reaction, and also signals from the free ligand, which indicates that the excess of free ligand has an effect on the equilibrium. The ^1H NMR spectrum of the aliphatic region of the 1:2 *in situ* reaction soon after preparation is shown in Figure 59, along with those of the free ligand and the 1:1 *in situ* reaction, soon after preparation, for comparison.

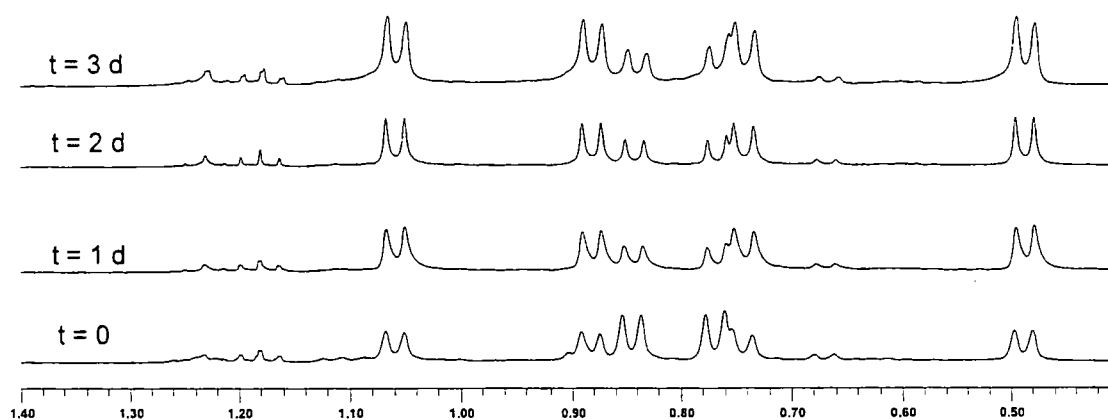


Figure 57. ^1H NMR (400 MHz, CDCl_3) spectra of the aliphatic region of the *in situ* reaction of 1:1 $\text{PdCl}_2(\text{PhCN})_2$:**S-L10** at various times.

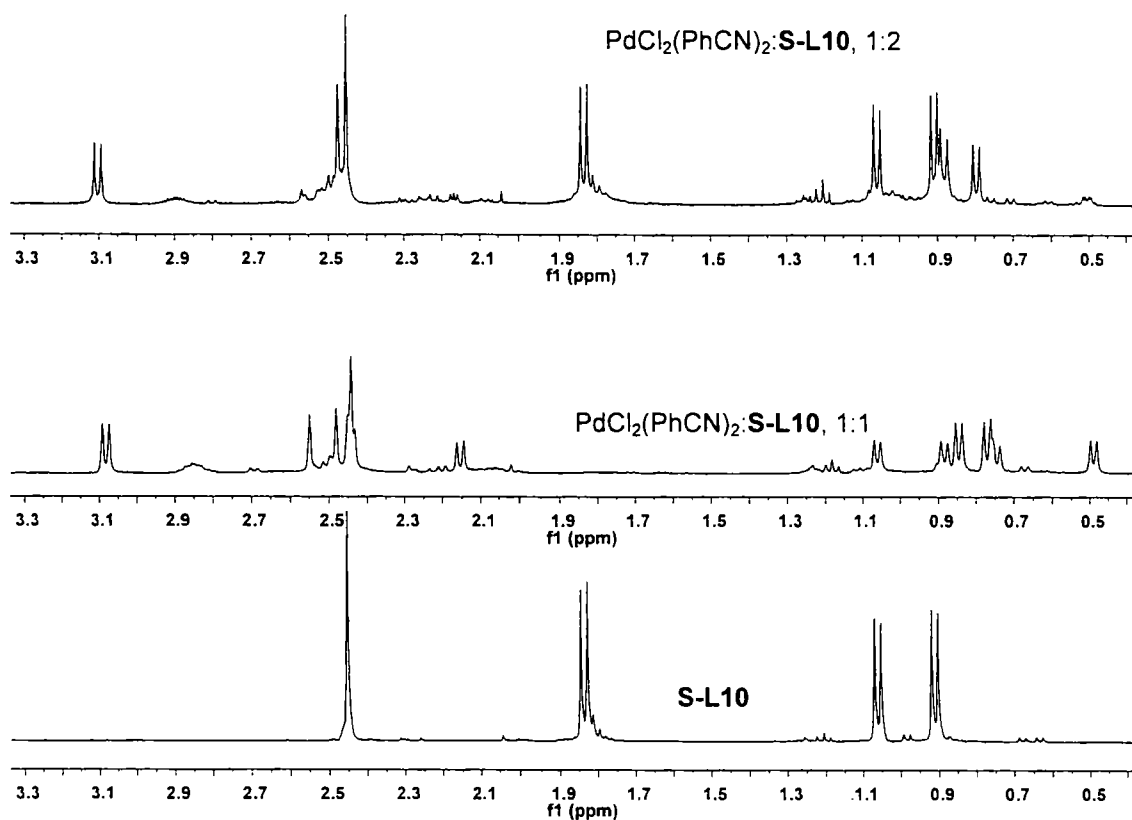


Figure 58. ^1H NMR (400 MHz, CDCl_3) spectra of the aliphatic region of **S-L10** (bottom) and the *in situ* reaction soon after preparation of $\text{PdCl}_2(\text{PhCN})_2$ with **S-L10** at 1:1 (middle) and 1:2 (top) molar ratios.

C) Preliminary studies on the synthesis of the **L6** and **L7** thiourea palladium complexes using $[(\eta^3\text{-allyl})\text{Pd}(\mu\text{-Cl})]_2$

In situ NMR reactions of $[(\eta^3\text{-allyl})\text{Pd}(\mu\text{-Cl})]_2$ and **L6** at the following molar ratios; 1:1.50, 1:2.0 and 1:3 in CDCl_3 at room temperature were carried out. The ^1H NMR spectra are shown in Figure 60. Broad ^1H signals were observed in all cases. However, we observed ^1H NMR signals of the free ligand when a 1:3.0 $[(\eta^3\text{-allyl})\text{Pd}(\mu\text{-Cl})]_2$:**L6** molar ratio was used. Interestingly, the signals from the free ligand itself are also broad. The precipitated allyl palladium complexes from *in situ* NMR reactions of $[(\eta^3\text{-allyl})\text{Pd}(\mu\text{-Cl})]_2$ to **L6** at 1:1 and 1:2 molar ratios were obtained as orange solids by adding Et_2O . The elemental analyses confirm the stoichiometric product from the reaction of $[(\eta^3\text{-allyl})\text{Pd}(\mu\text{-Cl})]_2$ with **L6** at a 1:1 molar ratio (Anal. Calcd. for $\text{C}_{28}\text{H}_{35}\text{Cl}_2\text{N}_3\text{OPd}_2\text{S}$: C 45.12, H 4.73; Found C 45.24, H

4.92) but not for the 1:2 molar ratio (Anal. Calcd. for $C_{25}H_{30}ClN_3OPdS$: C 53.38, H 5.38 ; Found C 52.40, H 5.32).

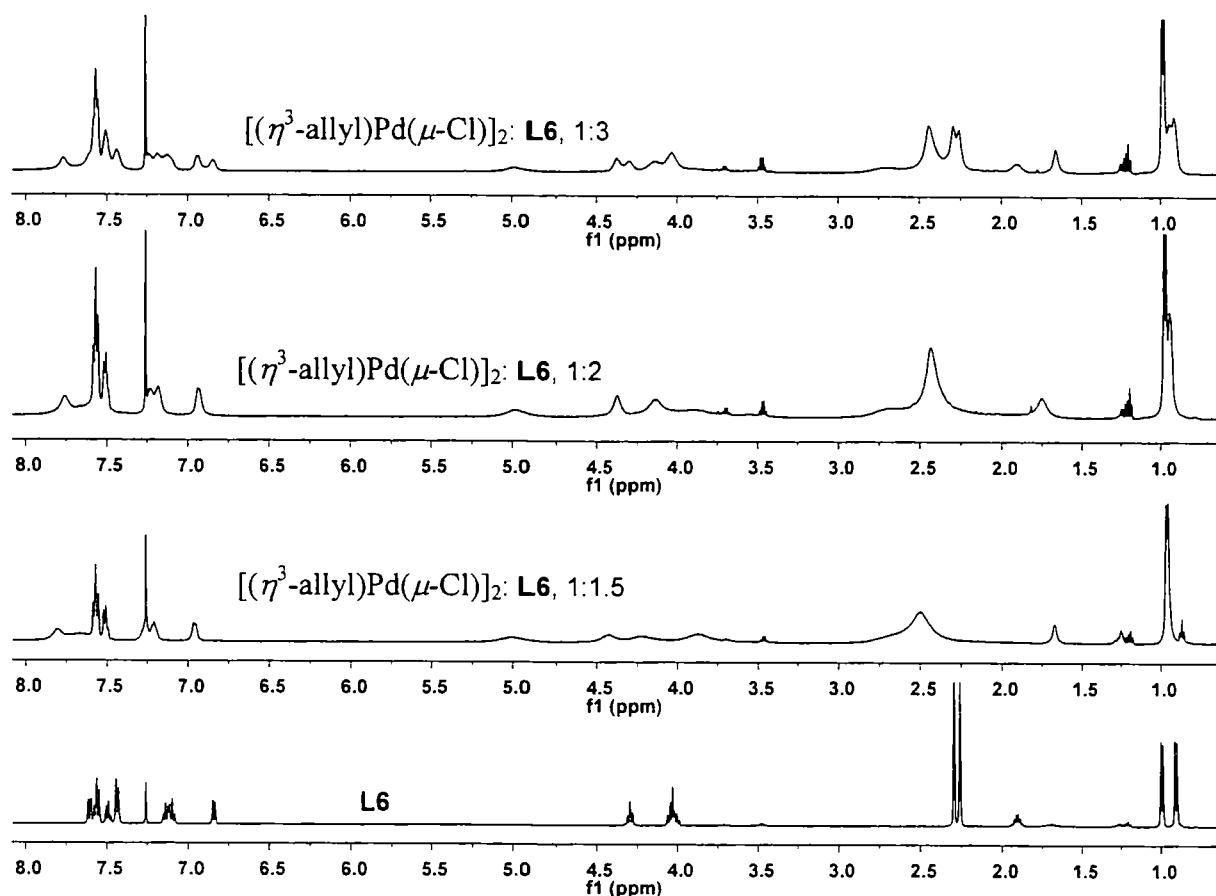


Figure 59. 1H NMR (400 MHz, $CDCl_3$) spectra of **L6** (bottom) and the *in situ* reaction of $[(\eta^3\text{-allyl})Pd(\mu\text{-Cl})]_2$ with **L6** in different molar ratios.

Similar reactions of $[(\eta^3\text{-allyl})Pd(\mu\text{-Cl})]_2$ and **L7** were carried out (1:1.5, 1:2, 1:3 and 1:6 molar ratios in $CDCl_3$) and were followed by *in situ* NMR spectroscopy. The 1H NMR spectra are shown in Figure 61. We observed similar results to those of the reaction with **L6**. They all show broad 1H signals but we can observe signals of the free ligand in 1:3.0 and 1:6 $[(\eta^3\text{-allyl})Pd(\mu\text{-Cl})]_2$:**L7** molar ratio spectra. The signals from the free ligand itself are also broad. Clearly, this suggests some dynamic equilibria in these systems.

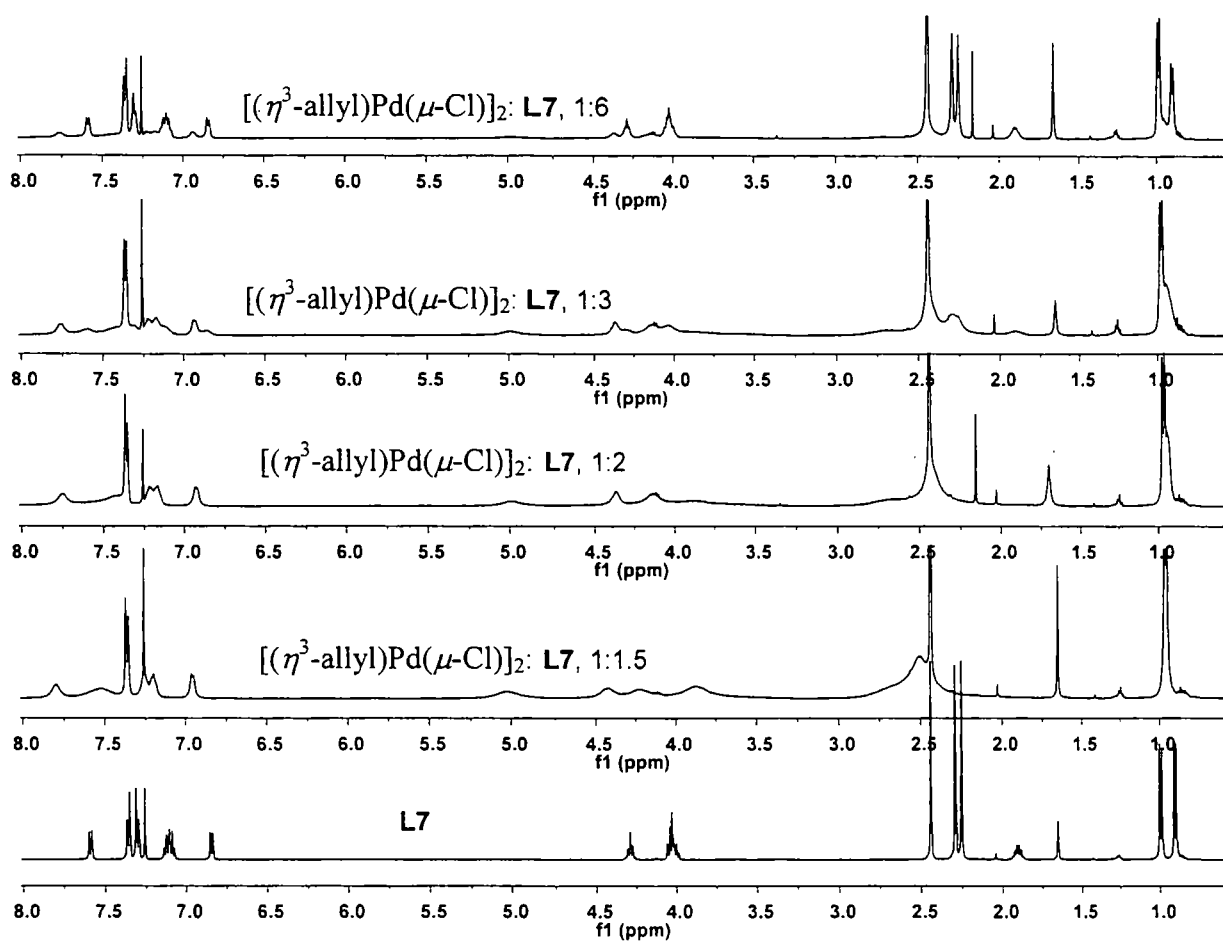
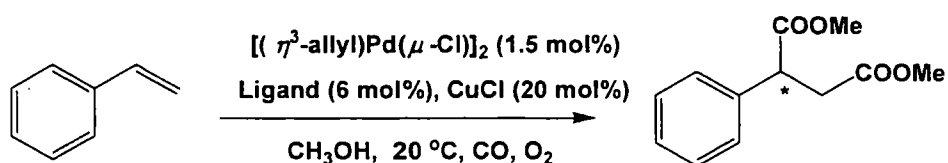


Figure 60. ^1H NMR (400 MHz, CDCl_3) spectra of L7 (bottom) and the *in situ* reaction of $[(\eta^3\text{-allyl})\text{Pd}(\mu\text{-Cl})]_2$ with L7 in different molar ratios.

II.5 Testing of the oxazoline thioureas as ligands for Pd/Cu catalyzed bis(methoxycarbonylation) of styrene

The oxazoline thiourea ligands in this study were tested in the bis(methoxycarbonylation) reaction of styrene both as *in situ* mixtures of palladium source and ligands and, in some cases, using our pure **PdL2up**, **PdL2down**, **PdL11up** and **Pd-R-L10** complexes, by Mr. B. Liang and Ms. Y. -X. Gao in the group of Prof. Z. Yang at Peking University. A summary of the results and reaction conditions is given in Table 33.

Table 33. Pd-catalyzed bis(methoxycarbonylation) of styrene using oxazoline thioureas.^a



β -dimethyl oxazoline thioureas				β -monomethyl oxazoline thioureas			
Entry	Ligand	Yield (%) ^b	<i>ee</i> (%) ^c	Entry	Ligand	Yield (%) ^b	<i>ee</i> (%) ^c
1	L2up	96 [98] ^d	65 [58] ^d	1	R-L9up	75	18
2	L2down	96 [94] ^d	-57 [-51] ^d	2	S-L9down	95	-21
3	L3	-	48	3	R-L10	57 [30] ^d	31 [9] ^d
4	L5	-	18	4	S-L10	59	-9
5	L6	98	-51				
6	L7	98	45				
7	L11up	98 [95] ^d	76 [69] ^d				
8	L11down	95	-69				
9	L13down	88	-65				

^a Reaction conditions: styrene (1.0 mmol), $[(\eta^3\text{-allyl})\text{Pd}(\mu\text{-Cl})_2]$ (0.015 mmol), ligand (0.06 mmol), and CuCl (0.2 mmol) in CH₃OH (4.0 mL) at 20 °C for 3 days under balloon pressure of CO and O₂ (*ca.* 4:1); ^b Isolated yield after silica gel chromatography; ^c The enantiomeric excess (*ee*) was determined by chiral HPLC analysis (Daicel Chiralcel OJ-H); the minus sign refers to the opposite enantiomer; ^d Yields and *ee*'s in brackets were obtained from the reactions using pure palladium complexes: **PdL2up**, **PdL2down**, **PdL11up** and **Pd-R-L10**.

From the results in Table 33, we can make the following observations:

β -Dimethyl oxazoline thioureas

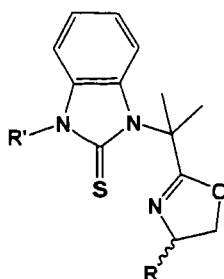


Figure 61. The general structure of the β -dimethyl oxazoline thioureas.

(i) For both catalysts generated *in situ* or using isolated palladium complexes, high *ee*'s were obtained when using **L2up**, **L2down**, **L11up**, **L11down** and **L13**. The best *ee*'s were obtained with **L11** (both **L11up**, **L11down** gave similar magnitudes but opposite signs of the *ee*) whereas **L5** gave the lowest *ee*. These results suggest that the R' substituent on the thiourea plays an important role in determining the enantioselectivity of the reactions. Furthermore, the particular atropoisomer (resulting from the *ortho*-substitution on the phenyl ring **ii**, Figure 63, *vide infra*) is crucially important to the sign of the *ee* ('up' ligands give positive *ee*'s whereas the 'down' ligands lead to negative *ee*'s). The *ee* was also improved when the bulky 9-anthryl group was introduced (69% *ee* with isolated **PdL11up**) compared to the less sterically demanding isopropyl group (58% *ee* with isolated **PdL2up**).

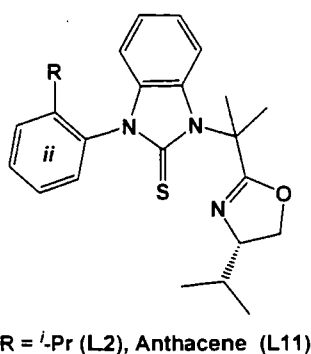


Figure 62. The atropoisomer oxazoline thioureas.

(ii) When **L13** (which also has a 9-anthryl in the 'down' conformation) was employed in the reaction, it gave a slightly reduced (65% *ee* for **L13** vs 69% for **L11down** (cf. 76% *ee* for **L11up**)). This implies that the R substituent on the oxazoline moiety plays a small role in the asymmetric induction. In addition, opposite *ee*'s were observed for the reactions carried out using **L3** and its analogue **L6** (48% *ee*

in **L3** and -51% *ee* in **L6**, see Table 33), reflecting the opposite chiralities of the respective phenyl and isopropyl groups on the oxazoline. The structures of **L3**, **L6**, **L11up** and **L13** are shown in Figure 64.

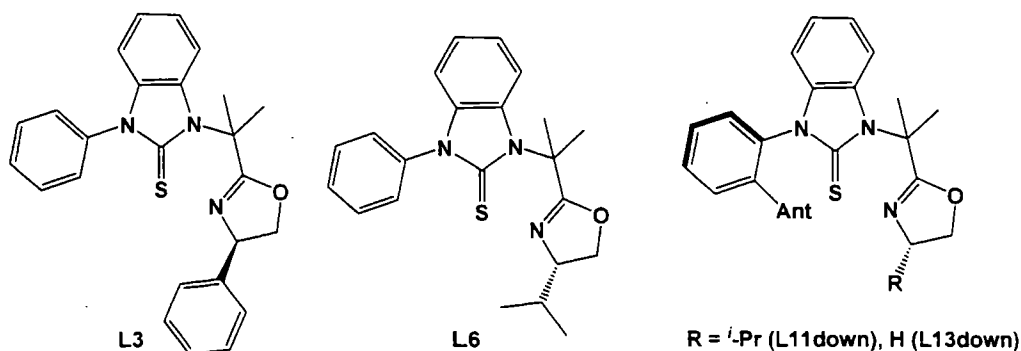


Figure 63. The structures of **L3**, **L6**, **L11up** and **L13**.

(iii) Interestingly, the *ee*'s obtained from reactions using isolated palladium thiourea complexes were slightly lower than for the catalysts formed *in situ* (see entries 1, 2 and 7 in Table 33).

(iv) A low *ee* was obtained when **L5** was employed in the reactions (18%). This is probably related to the fact that, in solution, palladium complexes of **L5** show dynamic equilibria, as we were able to obtain crystals of the dimer. It is reasonable to speculate that this may be the reason for the low *ee*.

(v) It should be noted that the allyl palladium chloride dimer, $[(\eta^3\text{-allyl})\text{Pd}(\mu\text{-Cl})_2]$, was used for the testing of bis(methoxycarbonylation) reaction of styrenes. It was found that both yield and *ee*'s are slightly better when two equivalents of thiourea ligands are employed.² Our preliminary studies of the reaction of $[(\eta^3\text{-allyl})\text{Pd}(\mu\text{-Cl})_2]$ with both **L6** and **L7** suggest some dynamic equilibria in these system. This implies that the catalytic system using $[(\eta^3\text{-allyl})\text{Pd}(\mu\text{-Cl})_2]$ may be even more complicated than with PdCl_2 .

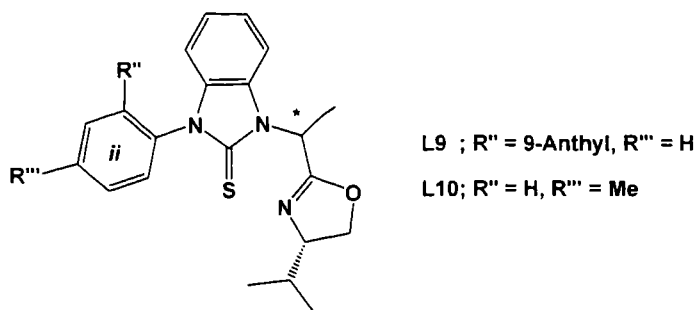
β -monomethyl oxazoline thioureas

Figure 64. The general structures of the β -monomethyl oxazoline thioureas.

(i) The best yields were obtained from **R-L9up** and **S-L9down** (75 and 95 %, respectively). However, yields for the β -monomethyl oxazoline thioureas are generally lower than for the β -dimethyl oxazoline thioureas.

(ii) Lower *ee*'s were obtained compared to the β -dimethyl oxazoline thioureas. These results are probably related to the NMR experiments in which we observed mixtures of palladium complexes for most of the β -monomethyl oxazoline thioureas. Therefore, less selectivity could reasonably be expected using these ligands.

(iii) Interestingly, a low *ee* was also observed in the case of **R-L9up**. However, the solution NMR studies in CDCl_3 indicate that only the monomer **Pd-R-L9up** is present even after 3 days. This may not be the case in CH_3OH , in which the reaction was performed. It would be useful to monitor the reaction of a Pd source with **R-L9up** by NMR spectroscopy in CD_3OD .

(iv) The highest *ee* was obtained from **R-L10** via the *in situ* generated catalyst (31% *ee*, entry 3), whereas a much lower *ee* was obtained using its isolated palladium complex. The low *ee* in the latter case is probably related to its instability. In the NMR spectroscopic study of **Pd-R-L10**, we initially obtained a mono-palladium complex, which in solution converted to other palladium complexes over a period of days (see Figure 56). The high *ee* for the *in situ* mixing can be explained from the 1:2 Pd:L ratio. Our NMR study of the 1:2 Pd:L *in situ* reaction showed that the monomer complex does not decompose after several days with free ligand also being observed (see Figure 57). It is therefore likely that the monomer remains completely intact during the reaction, and is therefore better able to perform enantioselective catalysis.

III. Conclusions

Several chiral β -dimethyl and β -monomethyl oxazoline thiourea ligands and an α -isoquinoline thiourea ligand have been fully characterized by solution NMR spectroscopy, elemental analysis and single-crystal X-ray diffraction (in some cases). Moreover, we succeeded in the synthesis of their palladium complexes, which were characterized by solution NMR spectroscopy, elemental analysis and single-crystal X-ray diffraction (in some cases). The single-crystal X-ray diffraction analyses (both of the ligands and the complexes) allows us to distinguish between the atropoisomers and diastereomers. Most Pd complexes were shown to be monomers, although one ligand with a cyclohexyl group formed exclusively dimers, and one formed a trimer, as well as a monomer, depending on the solvent mixtures that the crystals were grown from. The X-ray diffraction studies show that the ligands are bidentate through their S and N atoms. All of the mono-palladium complexes and most of the dimers have *cis*-configurations at the Pd centers; however, we also found a *trans*-configuration in the trimer and the dimer of one of the palladium complex of the β -monomethyl ligands. The structures show that the β -monomethyl oxazoline and α -isoquinoline thiourea complexes have longer Pd–S and Pd–N bonds than the β -dimethyl ones. The increased flexibility of the mono-methyl thioureas may be responsible for this.

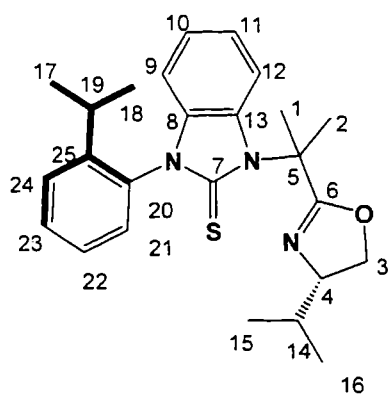
The complexes for which we were unable to obtain crystal structures were deduced to be monomeric from their $^{13}\text{C}\{^1\text{H}\}$ NMR spectra. This also showed that the β -dimethyl ligand which forms dimers does so only on slow evaporation from solvent mixtures. The trimeric complex and the dimeric β -monomethyl complex were shown by ^1H NMR to be unstable in solution forming equilibrium mixtures with their monomer complexes over 3 days. One of the β -monomethyl complexes was shown to be stable in the presence of excess ligand. The structure of the ligands (in particular the 'up' or 'down' conformation of the atropoisomers) was shown to be intimately related to their enantioselectivities in bis(methoxycarbonylation) reactions of styrene. The β -dimethyl ligands were, in generally, found to be more selective than the β -monomethyl ones, and the complexes with the β -monomethyl ligands were generally found to be less stable.

IV. Experimental

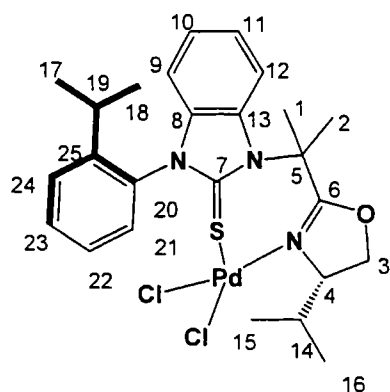
Synthesis

The thiourea ligands were prepared by the group of Prof. Z. Yang. PdCl₂ was purchased from Precious Metals Online and used without further purification. The PdCl₂(CH₃CN)₂ and PdCl₂(PhCN)₂ were prepared *via* literature procedures.³⁰ The 1D (¹H and ¹³C{¹H}) and 2D (COSY, NOESY, HSQC and HMBC) NMR spectra were obtained using Varian Inova 500 and 700 VNMRS spectrometers at the following frequencies: ¹H-500, 700 MHz, ¹³C{¹H}-125, 175 MHz in CDCl₃ or CD₂Cl₂. The chemical shifts are reported in ppm and referenced to the external standard SiMe₄. Assignments of the NMR spectroscopic data for the free ligands and their palladium complexes were based on a series of 2D NMR studies. MS analyses were performed using a Thermo LTQFT mass spectrometer (for ESI/HRMS-ESI). Elemental analyses were performed using an Exeter Analytical CE-440 analyzer. Melting points were obtained using a Sanyo Gallenkamp apparatus, and are uncorrected. All palladium complexes (except that with L3) were initially prepared in NMR tubes and the reactions were followed *in situ*.

L2up



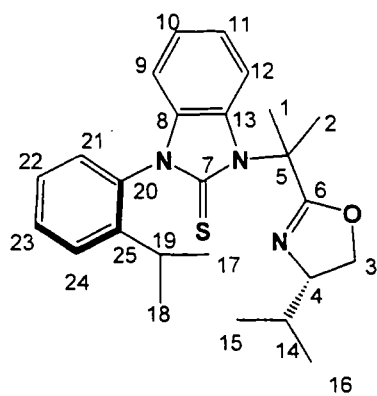
¹H NMR (500 MHz, CD₂Cl₂): δ 7.63 (d, $J_{H-H} = 9$ Hz, H12), 7.57 – 7.59 (m, 2H, H23,24), 7.39 – 7.42 (m, H22), 7.18 – 7.21 (m, 2H, H11,21), 7.08 (t, $J_{H-H} = 8$ Hz, H10), 6.62 (d, $J_{H-H} = 8$ Hz, H9), 4.18 – 4.22 (m, H3), 3.95 – 3.99 (m, H3'), 3.90 – 3.94 (m, H4), 2.46 – 2.51 (m, H19), 2.26, 2.19 (s, 2CH₃, 6H, H1,2), 1.74 – 1.81 (m, H14), 1.19, 0.98 (d, $J_{H-H} = 7$ Hz, 2CH₃, 6H, H17,18), 0.94, 0.87 (d, $J_{H-H} = 7$ Hz, 2CH₃, 6H, H15,16). ¹³C{¹H} NMR (100 MHz): δ 172.5 (C7), 169.8 (C6), 148.7 (C25), 135.4 (C8), 134.7 (C20), 133.4 (C13), 131.0 (C24), 130.1 (C11), 128.3 (C23), 128.0 (C22), 123.6 (C10), 123.5 (C21), 113.1 (C12), 110.6 (C9), 73.5 (C4), 71.7 (C3), 63.5 (C5), 33.5 (C14), 29.3 (C19), 29.2, 26.9 (C1,2), 24.7, 24.0 (C17,18), 19.9, 19.2 (C15,16). m.p. 125.4-126.0 °C. HRMS (EI): calcd for C₂₅H₃₁N₃OS (M⁺) 422.2221, found 422.2262.

PdL2up

To a solution of **L2up** (213 mg, 0.05 mmol) in CH_3OH (4 mL) was added PdCl_2 (197 mg, 0.05 mmol). The reaction mixture was heated to reflux at $50\text{ }^\circ\text{C}$ for 4 h. The solvent was removed on a rotary evaporator. The residue was dissolved in CH_2Cl_2 and then Et_2O was added to precipitate the product as an orange solid which was collected by filtration, washed with Et_2O (x3) and then dried *in vacuo*. The

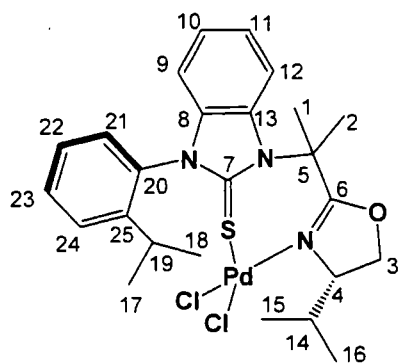
single crystal for X-ray diffraction was grown *via* slow evaporation of a solution in $\text{CH}_2\text{Cl}_2:\text{CH}_3\text{OH}$ (50:50). Yield: 274 mg, 92 %. ^1H NMR (700 MHz, CD_2Cl_2): δ 8.00 (d, $J_{\text{H-H}} = 8\text{ Hz}$, H12), 7.65 (t, $J_{\text{H-H}} = 8\text{ Hz}$, H23), 7.61 (t, $J_{\text{H-H}} = 8\text{ Hz}$, H24), 7.45 (t, $J_{\text{H-H}} = 8\text{ Hz}$, H22), 7.37 (t, $J_{\text{H-H}} = 8\text{ Hz}$, H11), 7.31 (t, $J_{\text{H-H}} = 8\text{ Hz}$, H10), 6.93 (d, $J_{\text{H-H}} = 8\text{ Hz}$, H21), 6.83 (d, $J_{\text{H-H}} = 8\text{ Hz}$, H9), 4.85 – 4.88 (m, H4), 4.47 (t, $J_{\text{H-H}} = 9\text{ Hz}$, H3), 4.25 (t, $J_{\text{H-H}} = 9\text{ Hz}$, H3'), 3.07 – 3.12 (m, H14), 3.38, 2.55 (s, 6H, 2 CH_3 , H1,2), 2.31 – 2.35 (m, H19), 1.27, 1.00 (d, $J_{\text{H-H}} = 7\text{ Hz}$, 2 CH_3 , 6H, H17,18), 0.87, 0.75 (d, $J_{\text{H-H}} = 7\text{ Hz}$, 2 CH_3 , 6H, H15,16). $^{13}\text{C}\{^1\text{H}\}$ NMR (175 MHz): δ 168.4 (C6), 164.8 (C7), 148.4 (C25), 135.1 (C8), 133.2 (C23), 132.7 (C13), 132.1 (C20), 129.2 (C24), 129.1 (C22), 128.6 (C21), 126.5 (C11), 126.3 (C10), 115.8 (C12), 112.6 (C9), 72.1 (C4), 70.2 (C3), 63.2 (C5), 31.5 (C14), 29.7 (C19), 29.6, 29.3 (C1,2), 24.9, 24.2 (C17,18), 19.4, 15.7 (C15,16).

Alternative synthesis of **PdL2up**: To a solution of **L2up** (10.7 mg, 0.026 mmol) in CD_2Cl_2 (1 mL) was added $\text{PdCl}_2(\text{PhCN})_2$ (10.3 mg, 0.026 mmol). The solution was transferred to an NMR tube and the reaction was shown to complete and quantitative within 2 min at room temperature, as evidenced by ^1H NMR spectroscopy. The sample was transferred to a small round bottom flask using CH_2Cl_2 and the combined solution was evaporated to dryness on a rotary evaporator. The solid sample was then dried *in vacuo* for 3 h and was shown to contain 1 eq. of benzonitrile of crystallization by elemental analysis. Anal. Calcd. for $\text{C}_{25}\text{H}_{31}\text{Cl}_2\text{N}_3\text{OPdS}\cdot\text{C}_6\text{H}_5\text{CN}$: C 54.75, H 5.17, N 7.98; Found C 54.47, H 5.12, N 7.94 %.

L2down

^1H NMR (500 MHz, CD_2Cl_2): δ 7.62 (d, $J_{\text{H-H}} = 8$ Hz, H12), 7.52 (m, 2H, H23,24), 7.35 (m, H22), 7.13 (m, 2H, H11,21), 7.08 (t, $J_{\text{H-H}} = 7$ Hz, H10), 6.62 (d, $J_{\text{H-H}} = 7$ Hz, H9), 4.23 (t, $J_{\text{H-H}} = 9$ Hz, H3), 3.90 (m, H3,4), 2.50 (m, H19), 2.24, 2.20 (s, 2 CH_3 , 6H, H1,2), 1.78 (m, H14), 1.18, 0.99 (d, $J_{\text{H-H}} = 7$ Hz, 2 CH_3 , 6H, H17,18), 0.96, 0.86 (d, $J_{\text{H-H}} = 7$ Hz, 2 CH_3 , 6H, H15,16). $^{13}\text{C}\{^1\text{H}\}$ NMR (125 MHz): δ 172.6 (C7),

169.9 (C6), 148.7 (C25), 135.4 (C8), 134.7 (C20), 133.4 (C13), 131.0 (C24), 130.2 (C11), 128.3 (C23), 128.0 (C22), 123.6 (C10), 123.5 (C21), 113.1 (C12), 110.7 (C9), 73.8 (C4), 72.0 (C3), 63.5 (C5), 33.5 (C14), 29.3 (C19), 28.2, 27.9 (C1,2), 24.6, 24.1 (C17,18), 20.1, 19.4 (C15,16). m.p. 110.0-110.7 $^\circ\text{C}$. HRMS (EI): calcd for $\text{C}_{25}\text{H}_{31}\text{N}_3\text{OS}$ (M^+) 422.2221, found 422.2263.

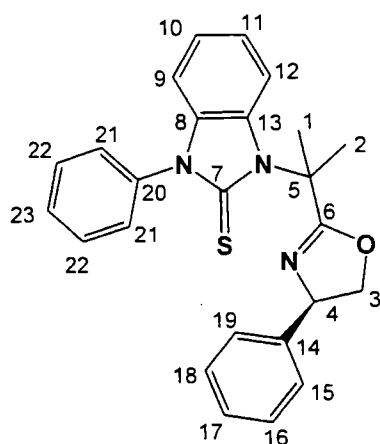
PdL2down

Compound **PdL2down** was synthesized by the same procedure as was employed to synthesize **PdL2up** using PdCl_2 (197 mg, 0.05 mmol) and **L2down** (217 mg, 0.05 mmol). The single crystal was obtained from evaporation of a solution in $\text{CH}_2\text{Cl}_2:\text{CH}_3\text{OH}$ (50:50). Yield: 270 mg, 90 %. ^1H NMR (500 MHz, CD_2Cl_2): δ 7.99 (d, $J_{\text{H-H}} = 9$ Hz, H12), 7.60 – 7.66

(m, 2H, H23,24), 7.45 (t, $J_{\text{H-H}} = 9$ Hz, H22), 7.35 (t, $J_{\text{H-H}} = 9$ Hz, H11), 7.29 (t, $J_{\text{H-H}} = 9$ Hz, H10), 7.17 (d, $J_{\text{H-H}} = 9$ Hz, H21) 6.81 (d, $J_{\text{H-H}} = 9$ Hz, H9), 4.86 – 4.91 (m, H4), 4.50 (t, $J_{\text{H-H}} = 9$ Hz, H3), 4.28 (t, $J_{\text{H-H}} = 9$ Hz, H3'), 3.00 – 3.06 (m, H14), 3.37, 2.54 (s, 2 CH_3 , 6H, H1,2), 2.26 – 2.31 (m, H19), 1.24, 0.98 (d, $J_{\text{H-H}} = 7$ Hz, 2 CH_3 , 6H, H17,18), 0.92, 0.85 (d, $J_{\text{H-H}} = 7$ Hz, 2 CH_3 , 6H, H15,16). $^{13}\text{C}\{^1\text{H}\}$ NMR (125 MHz): δ 168.7 (C6), 164.9 (C7), 147.4 (C25), 135.1 (C8), 133.2 (C13), 132.8 (C24), 131.8 (C20), 129.6 (C21), 129.2 (C22), 129.1 (C23), 126.4 (C10), 126.1 (C11), 115.9 (C12), 112.4 (C9), 72.1 (C4), 70.2 (C3), 63.0 (C5), 31.3 (C14), 30.2, 29.48 (C1,2), 29.45 (C19), 25.1, 24.5 (C17,18), 19.6, 16.0 (C15,16). Anal. Calcd. for $\text{C}_{25}\text{H}_{31}\text{Cl}_2\text{N}_3\text{OPdS}$: C 50.13, H 5.22, N 7.02; Found C 49.83, H 5.13, N 6.50 %.

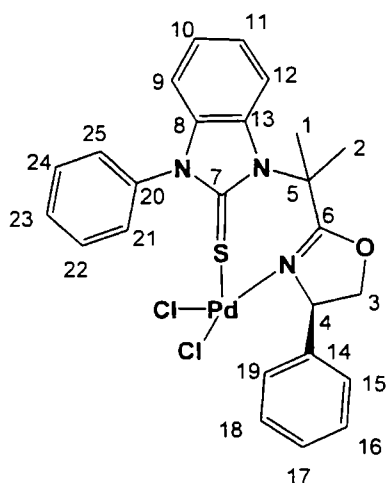
Alternative synthesis of **PdL2down**: Compound **PdL2down** was synthesized by the same procedure as for **PdL2up**. To a solution of **L2down** (11.0 mg, 0.026 mmol) in CD_2Cl_2 (1 mL) was added $\text{PdCl}_2(\text{PhCN})_2$ (10.4 mg, 0.026 mmol). The reaction was completed and conversion quantitative within 2 min at room temperature, as evidenced by ^1H NMR spectroscopy.

L3



^1H NMR (500 MHz, CD_2Cl_2): δ 7.68 (d, $J_{\text{H-H}} = 7$ Hz, H12), 7.58 (t, $J_{\text{H-H}} = 8$ Hz, 2H, H22), 7.50 – 7.53 (m, H23), 7.42 (t, $J_{\text{H-H}} = 7$ Hz, 2H, H21), 7.31 – 7.36 (m, 4H, H15, 16, 18, 19), 7.24 – 7.27 (m, H17), 7.16 (d, $J_{\text{H-H}} = 7$ Hz, H11), 7.12 (d, $J_{\text{H-H}} = 7$ Hz, H10), 6.84 (d, $J_{\text{H-H}} = 7$ Hz, H9), 5.21 (t, $J_{\text{H-H}} = 10$ Hz, H4), 4.66 (t, $J_{\text{H-H}} = 7$ Hz, H3'), 4.12 (t, $J_{\text{H-H}} = 7$ Hz, H3), 2.30, 2.27 (s, 2 CH_3 , 6H, H1,2). $^{13}\text{C}\{^1\text{H}\}$ NMR (125 MHz): δ 172.0 (C7), 171.5 (C6), 143.6 (C14), 137.1 (C20), 135.1 (C8), 133.3 (C13), 130.6 (2C, C22), 130.1 (C23), 129.7 (2C, C21), 129.6 (2C, C16,18), 128.5 (C17), 128.8 (2C, C15,19), 128.4 (C11), 128.2 (C10), 113.1 (C12), 110.9 (C9), 76.6 (C3), 71.2 (C4), 63.6 (C5), 28.1 (C1,2). MS (ESI) m/z : 414.2 ($\text{M}+\text{H}$) $^+$. HRMS (EI): calcd for $\text{C}_{25}\text{H}_{23}\text{N}_3\text{OS}$ ($\text{M}+\text{H}$) $^+$ 414.1635, found 414.1631.

PdL3

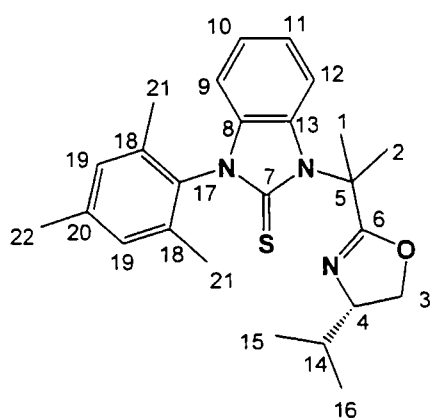


Compound **PdL3** was synthesized by the same procedure as was employed to synthesize **PdL2up** using PdCl_2 (22.6 mg, 0.059 mmol) and **L3** (24.3 mg, 0.059 mmol). The single crystal was obtained *via* evaporation of a solution in $\text{CH}_2\text{Cl}_2:\text{CH}_3\text{OH}$ (50:50). Yield: 33.8 mg, 97 %. m.p. 253.7–254.2 °C. ^1H NMR (500 MHz, CD_2Cl_2): δ 8.04 (d, $J_{\text{H-H}} = 7$ Hz, H12), 7.69 – 7.15 (m, 10H, H15,16,17,18,19,21,22,23,24,25), 7.39 – 7.44 (m, 2H, H10,11), 6.98 (d, $J_{\text{H-H}} = 8$ Hz, H9), 5.89 – 5.92 (m, H4), 4.90 (t, $J_{\text{H-H}} = 9$ Hz, H3'), 4.52 (t, $J_{\text{H-H}} = 9$ Hz, H3), 3.42, 2.61 (s, 2 CH_3 , 6H, H1,2). $^{13}\text{C}\{^1\text{H}\}$ NMR (125 MHz): δ 168.8 (C6), 164.6 (C7), 140.0 (C14), 135.0 (C20), 134.5

(C8), 133.3 (C13), 131.9, 131.58, 131.33, 130.3, 130.2 (2CH), 129.3, 129.0 (2CH), 128.6, 126.5, 126.4 (C10,11,15,16,17,18,19,21,22,23,24,25), 115.7 (C12), 112.6 (C9), 76.6 (C3), 70.9 (C4), 63.4 (C5), 29.5, 28.3 (C1,2). Anal. Calcd. for $[\text{C}_{25}\text{H}_{23}\text{Cl}_2\text{N}_3\text{OPdS}]_2 \cdot \text{CH}_2\text{Cl}_2$: C 48.36, H 3.82, N 6.63; Found C 48.23, H 4.54, N 4.90 %.

Alternative synthesis of **PdL3**: Compound **PdL3** was synthesized by the same procedure as for **PdL2up** using L3 (3.1 mg, 8.22 μmol) in CD_2Cl_2 (0.5 mL) and $\text{PdCl}_2(\text{PhCN})_2$ (3.4 mg, 8.22 μmol). The reaction was complete and conversion quantitative within 2 min at room temperature, as evidenced by ^1H NMR spectroscopy.

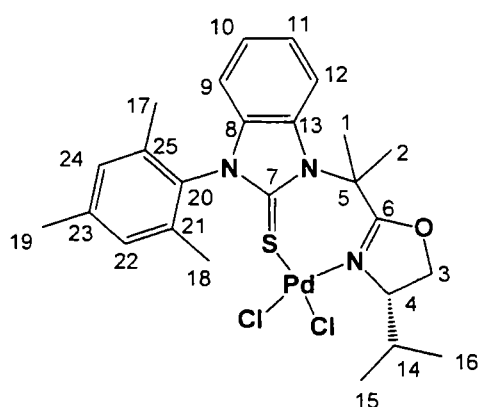
L4



^1H NMR (500 MHz, CD_2Cl_2): δ 7.64 (d, $J_{\text{H-H}} = 8$ Hz, H12), 7.14 (d, $J_{\text{H-H}} = 8$ Hz, H11), 7.08 (d, $J_{\text{H-H}} = 8$ Hz, H10), 7.03 (s, 2H, H19), 6.58 (d, $J_{\text{H-H}} = 7$ Hz, H9), 4.23 (t, $J_{\text{H-H}} = 8$ Hz, H3), 3.95 (t, $J_{\text{H-H}} = 8$ Hz, H3'), 3.93 – 3.98 (m, H4), 2.35 (s, 3H, H22), 2.25, 2.20 (s, 2CH₃, 6H, H1,2), 1.87 (s, 2CH₃, 6H, H21), 1.80 – 1.87 (m, H14), 0.95, 0.86 (d, $J_{\text{H-H}} = 7$ Hz, 2CH₃, 6H, H15,16). $^{13}\text{C}\{^1\text{H}\}$ NMR (125

MHz): δ 171.1 (C7), 169.8 (C6), 140.3 (2C, C18), 137.58 (C20), 133.66 (C8), 133.59 (C13), 132.1 (C17), 130.3 (2C, C19), 123.7 (C10), 123.6 (C11), 113.3 (C12), 110.4 (C9), 73.7 (C4), 71.9 (C3), 63.5 (C5), 33.5 (C14), 28.7, 27.5 (C1,2), 22.0 (C22), 20.0, 19.3 (C15,16), 18.4 (2C, C21). MS (EI) m/z : 421 (M^+).

PdL4

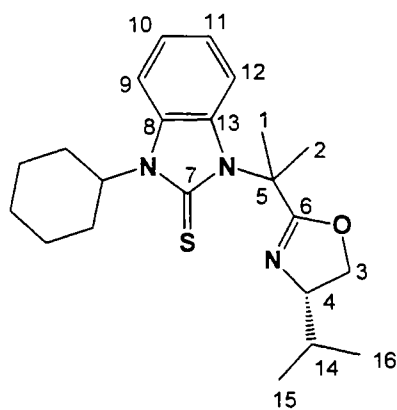


The **PdL4** complex was synthesized by the same procedure as for **PdL2up** using PdCl_2 (19.7 mg, 0.05 mmol) and L4 (21.7 mg, 0.05 mmol). The single crystal was obtained from evaporation of a solution in $\text{CH}_2\text{Cl}_2:\text{CH}_3\text{OH}$ (50:50). Yield: 27.5 mg, 92 %. m.p. 273.0–273.4 $^\circ\text{C}$. ^1H NMR (500 MHz, CD_2Cl_2): δ

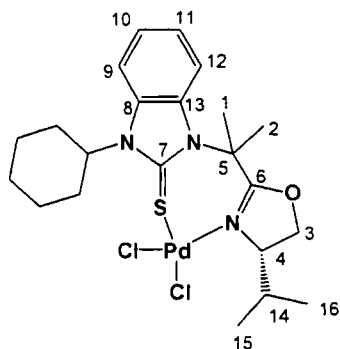
7.97 (d, $J_{H-H} = 8$ Hz, H12), 7.38 (d, $J_{H-H} = 8$ Hz, H11), 7.32 (d, $J_{H-H} = 8$ Hz, H10), 7.13 (s, 2H, H22,24), 6.83 (d, $J_{H-H} = 8$ Hz, H9), 4.88 – 4.92 (m, H4), 4.50 (dd, $J_{H-H} = 10$ Hz, $J_{H-H} = 9$ Hz, H3), 4.27 (dd, $J_{H-H} = 10$ Hz, $J_{H-H} = 9$ Hz, H3'), 3.06 – 3.13 (m, H14), 3.36, 2.55 (s, 2CH₃, 6H, H1,2), 2.41 (s, CH₃, 3H, H19), 1.87, 1.85 (s, 2CH₃, 6H, H17,18), 0.93, 0.84 (d, $J_{H-H} = 7$ Hz, 2CH₃, 6H, H15,16). ¹³C{¹H} NMR (125 MHz): δ 168.6 (C6), 163.8 (C7), 142.4, 137.1, 136.2, 133.4, 133.2 (C8,13,21,23,25), 131.6 (C22), 131.1 (C24), 129.5 (C20), 126.6 (C10), 126.2 (C11), 115.9 (C12), 112.0 (C9), 72.2 (C4), 70.1 (C3), 62.8 (C5), 31.3 (C14), 29.8, 29.3 (C1,2), 22.0 (C19), 18.35, 18.28 (C17,18), 19.60,16.20 (C15,16). Anal. Calcd. for C₂₅H₃₁Cl₂N₃OPdS: C 50.13, H 5.22, N 7.02; Found C 50.08, H 5.21, N 6.94 %.

Alternative synthesis of **PdL4**: Compound **PdL4** was synthesized by the same procedure as for **PdL2up** using L4 (6.0 mg, 14.23 μ mol) in CD₂Cl₂ (0.5 mL) to which was added Pd(PhCN)₂Cl₂ (5.5 mg, 14.23 μ mol). The reaction was complete and conversion quantitative within 2 min at room temperature, as evidenced by ¹H NMR spectroscopy.

L5



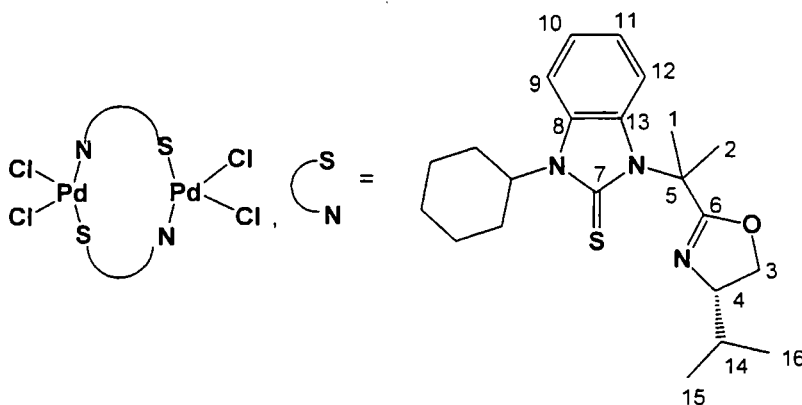
¹H NMR (500 MHz, CD₂Cl₂): δ 7.57 (d, $J_{H-H} = 8$ Hz, H12), 7.49 (d, $J_{H-H} = 8$ Hz, H9), 7.14 (d, $J_{H-H} = 8$ Hz, H11), 7.08 (d, $J_{H-H} = 8$ Hz, H10), 4.22 (t, $J_{H-H} = 8$ Hz, H3), 3.94 (t, $J_{H-H} = 8$ Hz, H3'), 3.93 – 3.96 (m, H4), 2.17, 2.12 (s, 2CH₃, 6H, H1,2), 2.08 – 2.02 (m, 2H, H_{cyclo}), 1.94 – 1.97 (m, 2H, H_{cyclo}), 1.82 – 1.87 (m, 5H, H14&4H_{cyclo}), 1.49 – 1.59 (m, 2H, H_{cyclo}), 1.29 – 1.38 (m, 1H, H_{cyclo}). 0.95, 0.87 (d, $J_{H-H} = 7$ Hz, 2CH₃, 6H, H15,16). ¹³C{¹H} NMR (125 MHz): δ 170.5 (C7), 170.1 (C6), 133.3 (C8), 132.4 (C13), 122.8 (C11), 122.6 (C10), 113.0 (C9), 111.9 (C12), 73.5 (C4), 71.9 (C3), 63.5 (C5), 56.8 (C17), 33.5 (C14), 30.3 (CH_{cyclo}), 28.6, 27.6 (C1,2), 27.15 (3C, CH_{cyclo}), 26.6 (CH_{cyclo}), 20.0, 19.3 (C15,16). MS (EI) m/z : 385 (M⁺).

PdL5

The **PdL5** complex was synthesized by similar procedure as for **PdL2up** using **L5** (35.1 mg, 0.09 mmol) and PdCl₂ (34.9 mg, 0.09 mmol). Yield: 23.2 mg, 45 %. ¹H NMR (500 MHz, CDCl₃): δ 7.98 (d, *J*_{H-H} = 8 Hz, H12), 7.76 (d, *J*_{H-H} = 8 Hz, H9), 7.31 – 7.39 (m, 2H, H10,11), 4.82 – 4.87 (m, H4), 4.42 (dd, *J*_{H-H} = 8 Hz, *J*_{H-H} = 1.2 Hz, H3), 4.17 (dd, *J*_{H-H} = 8 Hz, *J*_{H-H} = 2.1 Hz, H3), 3.33, 2.47 (s, 2CH₃, 6H, H1,2), 3.07 – 3.15 (m, H14), 1.24 – 2.24 (m,

11H, H_{cyclo}), 0.64 (d, *J*_{H-H} = 7 Hz, 2CH₃, 6H, H15,16). ¹³C{¹H} NMR (125 MHz, CD₂Cl₂): δ 167.5 (C6), 161.6 (C7), 124.8, 124.6, 115.0, 112.6 (C9,10,11,12), 71.2, 69.2 (C3,4), 62.8, 59.1 (C5, C17), 30.7, 29.6, 29.1, 28.8, 25.8, 25.3, 18.6, 14.6 (5C_{cyclo}, C1,2,15,16).

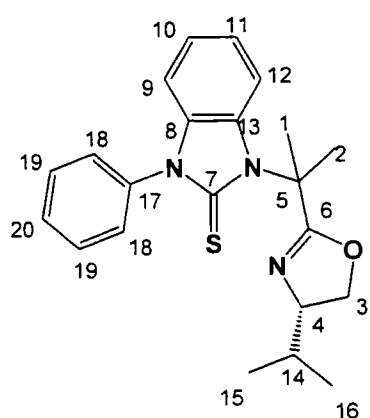
Alternative synthesis of **PdL5**: Compound **PdL5** was synthesized by the same procedure as for **PdL2up** using **L5** (5.0 mg, 12.97 μmol) in CD₂Cl₂ (0.5 mL) to which was added Pd(PhCN)₂Cl₂ (4.9 mg, 12.97 μmol). The reaction was complete and conversion quantitative within 2 min at room temperature, as evidenced by ¹H NMR spectroscopy.

Pd₂L5

Pd₂L5 was obtained from **PdL5**. m.p. 243.0-243.5 °C. ¹H NMR (500 MHz, CD₂Cl₂): δ 7.93 (d, *J*_{H-H} = 8 Hz, H12), 7.81 (d, *J*_{H-H} = 8 Hz, H9), 7.35 – 7.41 (m, 2H, H10,11), 4.51 – 4.55 (m, H4), 4.12 – 4.19 (m, 2H, H3,3'), 3.37 – 3.42 (m, H14), 2.93 – 3.00 (m, H17), 3.93, 2.62 (s, 2CH₃, 6H, H1,2), 1.40 – 2.17 (m, 10H, H_{cyclo}), 1.16, 1.10 (d, *J*_{H-H} = 7 Hz, 2CH₃, 6H, H15,16). ¹³C{¹H} NMR (125 MHz): δ 173.2 (C6), 161.8

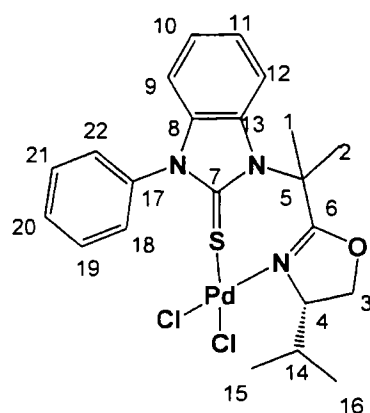
(C7), 132.6, 131.6 (C8,13), 125.3, 124.8, 115.0, 114.1 (C9,10,11,12), 74.2 (C4), 68.7 (C3), 68.1 (C5), 61.4 (C17), 31.6, 29.9, 27.2, 26.0 (5C_{cyclo}, C18,19,20,21,22), 31.4 (C14), 29.5, 27.8 (C1,2), 19.7, 15.8 (C15,16). Anal. Calcd. for C₄₄H₆₂Cl₄N₆O₃Pd₃S₃·H₂O: C 45.49, H 5.73, N 7.23; Found C 45.67, H 5.69, N 7.27 %.

L6



¹H NMR (500 MHz, CD₂Cl₂): δ 7.66 (d, *J*_{H-H} = 8 Hz, H12), 7.62 (t, *J*_{H-H} = 8 Hz, 2H, H19), 7.55 (t, *J*_{H-H} = 8 Hz, H20), 7.44 (d, *J*_{H-H} = 8 Hz, 2H, H18), 7.19 (t, *J*_{H-H} = 8 Hz, H11), 7.15 (t, *J*_{H-H} = 8 Hz, H10), 6.86 (d, *J*_{H-H} = 8 Hz, H9), 4.31 (t, *J*_{H-H} = 8 Hz, H3'), 4.03 (t, *J*_{H-H} = 8 Hz, H3'), 3.39 (t, *J*_{H-H} = 8 Hz, H4), 2.28, 2.23 (s, 2CH₃, 6H, H1,2), 1.81 – 1.88 (m, H14), 1.02, 0.93 (d, *J*_{H-H} = 8 Hz, 2CH₃, 6H, H15,16). ¹³C{¹H} NMR (125 MHz): δ 171.9 (C7), 169.8 (C6), 137.1 (C17), 135.0 (C8), 133.3 (C3), 130.5 (2CH_{arom}, C19), 130.0 (C20), 129.7 (2CH_{arom}, C18), 122.9 (C10,11), 112.9 (C9), 110.8 (C12), 73.5 (C4), 72.0 (C3), 63.5 (C5), 33.5 (C14), 28.4, 27.5 (C1,2), 19.9, 19.26 (C15,16). m.p. 94.6-95.2 °C. MS (EI) *m/z*: 380.3 (M⁺). HRMS (EI): calcd for C₂₂H₂₅N₃OS (M+H)⁺ 380.1791, found 380.1791.

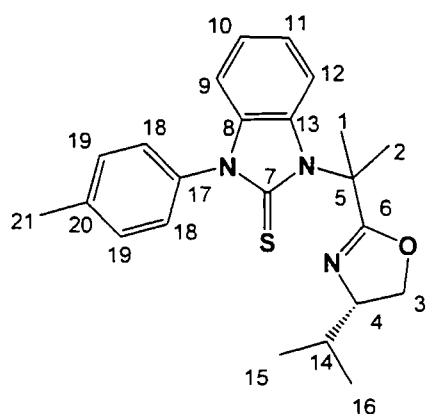
PdL6



To a solution of L6 (100.0 mg, 0.264 mmol) in CHCl₃ (4 mL) was added PdCl₂(PhCN)₂ (101.2 mg, 0.264 mmol). The reaction mixture was left to stir overnight at room temperature. The solvent was removed on a rotary evaporator. The residue was dissolved in CH₂Cl₂ and then Et₂O was added to precipitate the product as an orange solid which was collected by filtration, washed with Et₂O (x3) and then dried *in vacuo*. Yield: 132.2 mg, 90 %. m.p. 221.0-221.4 °C. The single crystal was obtained from evaporation of a solution in CD₂Cl₂. ¹H NMR (700 MHz, CD₂Cl₂): δ 7.96 (d, *J*_{H-H} = 8 Hz, H12), 7.60 – 7.61 (m, 3H, H19,20,21), 7.38 (d, *J*_{H-H} = 7 Hz, H22), 7.35 (t, *J*_{H-H} = 8 Hz, H11), 7.30 (t, *J*_{H-H} = 8 Hz, H10), 7.10 (d, *J*_{H-H} = 7 Hz, H18), 6.91 (d, *J*_{H-H}

= 8 Hz, H9), 4.92 – 4.95 (m, H4), 4.46 (t, $J_{H-H} = 8$ Hz, H3'), 4.23 (t, $J_{H-H} = 8$ Hz, H3), 3.17 – 3.21 (m, H14), 3.47, 2.55 (s, 2CH₃, 6H, H1,2), 0.88, 0.78 (d, $J_{H-H} = 8$ Hz, 2CH₃, 6H, H15,16). ¹³C{¹H} NMR (125 MHz): δ 167.4 (C6), 164.2 (C7), 134.2 (C8), 133.7 (C17), 132.4 (C13), 131.1 (C20), 130.88, 130.86 (C19,21), 128.8 (C22), 127.5 (C18), 125.63, 125.57 (C10,11), 114.8 (C12), 111.8 (C9), 71.3 (C4), 69.3 (C3), 62.5 (C5), 30.6 (C14), 29.2, 28.8 (C1,2), 18.9, 15.0 (C15,16). Anal. Calcd. for C₂₂H₂₅Cl₂N₃OSPd·CH₂Cl₂: C 43.04, H 4.24, N 6.55; Found C 42.57, H 4.24, N 6.38 %.

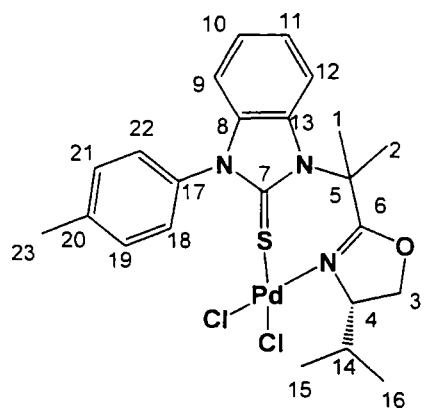
L7



¹H NMR (700 MHz, CDCl₃): δ 7.58 (d, $J_{H-H} = 8$ Hz, H12), 7.34 (d, $J_{H-H} = 8$ Hz, 2H, H19), 7.29 (d, $J_{H-H} = 8$ Hz, 2H, H18), 7.12 (t, $J_{H-H} = 8$ Hz, H11), 7.08 (t, $J_{H-H} = 8$ Hz, H10), 6.83 (d, $J_{H-H} = 8$ Hz, H9), 4.28 (t, $J_{H-H} = 8$ Hz, H3), 4.00 – 4.05 (m, 2H, H3',4), 2.43 (s, 3H, CH₃, H21), 2.28, 2.24 (s, 2CH₃, 6H, H1,2), 1.88 – 1.93 (m, H14), 0.98, 0.89 (d, $J_{H-H} = 7$ Hz, 2CH₃, 6H, H15,16). ¹³C{¹H}

NMR (175 MHz): δ 171.3 (C7), 169.4 (C6), 139.3 (C20), 134.4 (C8), 133.5 (C13), 132.5 (C17), 130.5 (2C, C19), 128.5 (2C, C18), 122.9 (C12,9), 112.1 (C10), 110.2 (C11), 72.5 (C3), 70.9 (C4), 62.7 (C5), 32.5 (C14), 27.9, 26.9 (C1,2), 21.6 (C21), 19.5, 18.5 (C15,16). m.p. 145.5-147.0 °C. MS (EI) m/z : 394.3 (M⁺). HRMS (EI): calcd for C₂₃H₂₇N₃OS (M+H)⁺ 394.1948, found 394.1947.

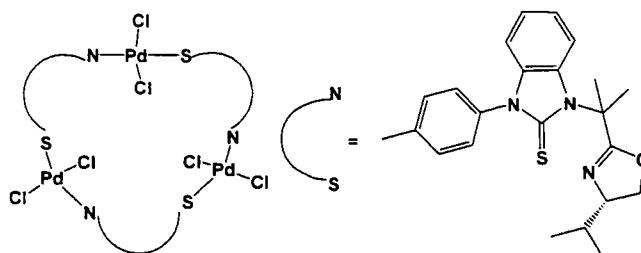
PdL7



Compound **PdL7** was synthesized by the same procedure as for **PdL6** using **L7** (100.0 mg, 0.254 mmol) and PdCl₂(PhCN)₂ (97.1 mg, 0.254 mmol). Yield: 106.3 mg, 73 %. The single crystal was obtained from slow evaporation of a solution in DMF:Et₂O. ¹H NMR (700 MHz, CDCl₃): δ 7.95 (d, $J_{H-H} = 8$ Hz, H12), 7.36 – 7.38 (m, 2H, H19,21), 7.35 (t, $J_{H-H} = 8$ Hz, H11), 7.28 (t, $J_{H-H} = 8$ Hz,

H10), 7.23 (d, $J_{H-H} = 8$ Hz, 2H, H21,19), 6.95 (d, $J_{H-H} = 8$ Hz, H9), 6.92 (d, $J_{H-H} = 8$ Hz, 2H, H18,22), 4.88 – 4.91 (m, H4), 4.45, 4.22 (t, $J_{H-H} = 9$ Hz, 2H, H3), 3.13 – 3.16 (m, CH), 3.46, 2.54 (s, 2CH₃, 6H, H1,2), 2.45 (s, CH₃, 3H, H23), 0.86, 0.76 (d, $J_{H-H} = 7$ Hz, 2CH₃, 6H, H15,16). ¹³C{¹H} NMR (175 MHz): δ 167.5 (C6), 164.1 (C7), 141.5 (C17), 134.2 (C8), 132.3 (C13), 131.4 (C19,21), 131.0 (C20), 128.5 (C22), 127.1 (C18), 125.6 (C10,11), 114.8 (C12), 111.8 (C9), 71.3 (C4), 69.3 (C3), 62.4 (C5), 30.6 (C14), 29.1, 28.8 (C1,2), 21.6 (C23), 18.6, 15.0 (C15,16).

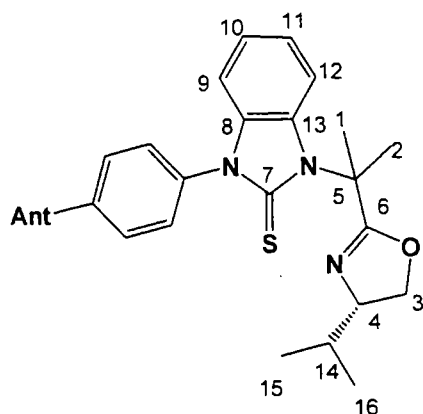
Pd₃L7



Compound **Pd₃L7** was obtained from **PdL7** complexes *via* slow evaporation of a solution in CH₂Cl₂:Et₂O. ¹H NMR (700 MHz, CDCl₃):^a δ 8.03 – 8.08 (m, 4H, CH_{arom}), 7.96 – 7.97 (m, 2H, CH_{arom}), 7.46 (t, $J_{H-H} = 8$ Hz, 2H, CH_{arom}), 7.36 – 7.42 (m, 6H, CH_{arom}), 7.26 – 7.32 (m, 3H, CH_{arom}), 7.21 – 7.26 (m, 4H, CH_{arom}), 7.07 (d, $J_{H-H} = 8$ Hz, CH_{arom}), 7.01 – 7.03 (m, 2H, CH_{arom}), 4.54 – 4.58 (m, 1H, CH₂), 4.48 – 4.54 (m, 2H, CH₂), 4.29 (t, $J_{H-H} = 9$ Hz, 1H, CH₂), 4.24 (t, $J_{H-H} = 9$ Hz, 1H, CH₂), 4.08 – 4.12 (m, 1H, CH₂), 3.89 – 3.90 (m, 1H, CH₂), 3.80 (s, 3H, CH₃), 3.74 – 3.78 (m, 1H, CH), 3.72 (s, 3H, CH₃), 3.40 (s, 3H, CH₃), 3.36 – 3.38 (m, 1H, CH₂), 3.30 – 3.38 (m, H, CH₂), 3.30 (s, 3H, CH₃), 3.12 – 3.18 (m, 1H, CH₂), 3.09 (s, 3H, CH₃), 3.02 (s, 3H, CH₃), 2.53–2.51 (m, 9H, 3CH₃), 1.23 (t, $J_{H-H} = 7$ Hz, 3H, CH₃), 1.07 (t, $J_{H-H} = 7$ Hz, 3H, CH₃), 1.05 (t, $J_{H-H} = 7$ Hz, 3H, CH₃), 0.97 (t, $J_{H-H} = 7$ Hz, 3H, CH₃), 0.94 (t, $J_{H-H} = 7$ Hz, 3H, CH₃), 0.91 (t, $J_{H-H} = 7$ Hz, 3H, CH₃). ¹³C{¹H} NMR (175 MHz):^b δ 171.6, 171.5, 171.3 (C=N).

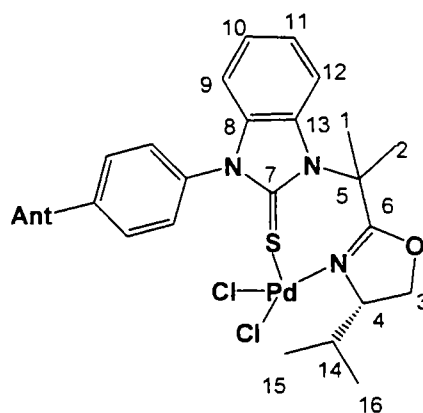
^a ¹H NMR from **Pd₃L7** minus **PdL7**. ^b Spectrum of a mixture containing **PdL7** and **Pd₃L7**; the remainder of the spectrum was too complicated to be assigned. The C=S signals were not observed because the signals were too weak.

L8



^1H NMR (500 MHz, CDCl_3 , $-30\text{ }^\circ\text{C}$): δ 8.58 (s, 1H, CH_{arom}), 8.11 (t, $J_{\text{H-H}} = 9\text{ Hz}$, 2H, CH_{arom}), 7.85 (d, $J_{\text{H-H}} = 8\text{ Hz}$, 1H, CH_{arom}), 7.75 (d, $J_{\text{H-H}} = 9\text{ Hz}$, 1H, CH_{arom}), 7.65 – 7.77 (m, 6H, H12&5 CH_{arom}), 7.53 (d, $J_{\text{H-H}} = 7\text{ Hz}$, 2H, CH_{arom}), 7.41 – 7.47 (m, 2H, CH_{arom}), 7.26 (t, $J_{\text{H-H}} = 7\text{ Hz}$, 2H, H10,11), 7.14 (d, $J_{\text{H-H}} = 8\text{ Hz}$, H9), 4.39 (t, $J_{\text{H-H}} = 8\text{ Hz}$, H3), 4.08 – 4.15 (m, 2H, H3',4), 2.36, 2.34 (s, 2 CH_3 , 6H, H1,2), 1.95 – 1.99 (m, H14), 1.02, 0.92 (d, $J_{\text{H-H}} = 7\text{ Hz}$, 2 CH_3 , 6H, H15,16). $^{13}\text{C}\{^1\text{H}\}$ NMR (125 MHz, CDCl_3 , $-30\text{ }^\circ\text{C}$): δ 170.6 (C7), 169.5 (C6), 139.7 (C), 135.8 (C), 135.1 (C), 134.2 (C), 132.83 (CH_{arom}), 132.80 (CH_{arom}), 132.3 (C), 131.4 (C), 131.3 (C), 130.2 (C), 130.0 (C), 128.81 (CH_{arom}), 128.75 (CH_{arom}), 128.66 (CH_{arom}), 128.5 (CH_{arom}), 127.3 (2 CH_{arom}), 126.6 (CH_{arom}), 126.0 (CH_{arom}), 125.8 (CH_{arom}), 125.7 (CH_{arom}), 125.4 (CH_{arom}), 123.3 (C10), 123.2 (C11), 112.4 (C12), 110.6 (C9), 72.2 (C4), 70.9 (C3), 62.8 (C5), 32.4 (C14), 28.1, 26.9 (C1,2), 19.6, 18.3 (C15,16). m.p. 177.4–179.0 $^\circ\text{C}$. MS (EI) m/z : 556.4 (M $^+$). HRMS (EI): calcd for $\text{C}_{36}\text{H}_{31}\text{N}_3\text{OS}$ (M+H) $^+$ 556.24171, found 556.24218.

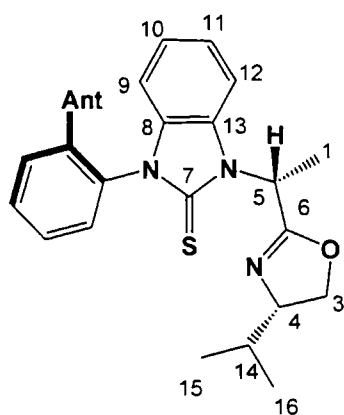
PdL8



Compound **PdL8** was synthesized by the same procedure as for **PdL6** using **L8** (40.0 mg, 0.072 mmol) and $\text{PdCl}_2(\text{PhCN})_2$ (27.6 mg, 0.072 mmol). Yield: 50.8 mg, 96 %. ^1H NMR (500 MHz, CDCl_3): δ 8.63 (s, CH_{arom}), 8.13 – 8.16 (m, 2H, CH_{arom}), 7.95 (dd, $J_{\text{H-H}} = 8\text{ Hz}$, $J_{\text{H-H}} = 3\text{ Hz}$, H12), 7.85 (d, $J_{\text{H-H}} = 8\text{ Hz}$, CH_{arom}), 7.77 – 7.79 (m, 3H, H10&H11& CH_{arom}), 7.70 (dd, $J_{\text{H-H}} = 8\text{ Hz}$, $J_{\text{H-H}} = 3\text{ Hz}$, H9), 7.67 (d, $J_{\text{H-H}} = 9\text{ Hz}$, CH_{arom}), 7.53 – 7.59 (m, 3H, CH_{arom}), 7.45 – 7.49 (m, 4H, CH_{arom}), 7.21 (dd, $J_{\text{H-H}} = 10\text{ Hz}$, $J_{\text{H-H}} = 3\text{ Hz}$, CH_{arom}), 4.91 – 4.95 (m, H4), 4.54 (t, $J_{\text{H-H}} = 9\text{ Hz}$, 1H, H3), 4.32 (t, $J_{\text{H-H}} = 9\text{ Hz}$, H3'), 3.17 – 3.23 (m, H14), 3.53, 2.64 (s, 2 CH_3 , 6H, H1,2), 0.96, 0.88 (d, $J_{\text{H-H}} = 9\text{ Hz}$, 2 CH_3 , 6H, H15,16). $^{13}\text{C}\{^1\text{H}\}$ NMR (125 MHz): δ 168.6 (C6), 164.8 (C7), 143.1 (C), 136.0 (C), 135.4 (C), 134.83

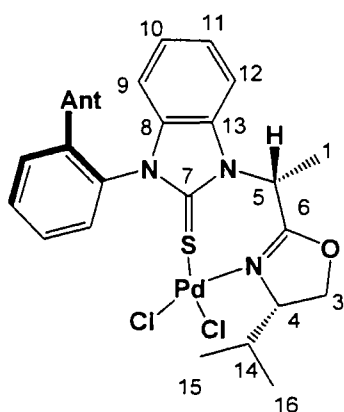
(CH_{arom}), 134.79 (CH_{arom}), 134.1 (C), 133.6 (C), 132.6 (C), 132.5 (C), 131.24 (C), 131.18 (C), 129.84 (CH_{arom}), 129.79 (CH_{arom}), 129.5 (CH_{arom}), 128.9 (CH_{arom}), 128.6 (CH_{arom}), 127.7 (CH_{arom}), 127.6 (CH_{arom}), 127.2 (CH_{arom}), 126.97 (CH_{arom}), 126.79 (CH_{arom}), 126.74 (CH_{arom}), 126.67 (CH_{arom}), 126.4 (CH_{arom}), 116.0 (C12), 112.9 (C9), 72.3 (C3), 70.4 (C5), 63.6 (C4), 31.6 (C14), 29.9, 29.7 (C1,2), 19.7, 15.9 (C15,16).

R-L9up



¹H NMR (700 MHz, CDCl₃): δ 8.18 (s, CH_{arom}), 8.09 (d, J_{H-H} = 8 Hz, CH_{arom}), 7.99 (d, J_{H-H} = 8 Hz, CH_{arom}), 7.92 (d, J_{H-H} = 8 Hz, CH_{arom}), 7.86 (d, J_{H-H} = 8 Hz, CH_{arom}), 7.73 – 7.77 (m, 4H, CH_{arom}), 7.34 – 7.40 (m, 3H, CH_{arom}), 7.31 (t, J_{H-H} = 8 Hz, CH_{arom}), 6.77 (d, J_{H-H} = 8 Hz, H12), 6.62 (t, J_{H-H} = 8 Hz, H11), 6.40 (d, J_{H-H} = 8 Hz, H9), 6.27 (t, J_{H-H} = 8 Hz, H10), 6.16 (q, J_{H-H} = 7 Hz, H5), 4.04 (t, J_{H-H} = 8 Hz, H3), 3.97 (t, J_{H-H} = 8 Hz, H3'), 3.88 – 3.91 (m, H4), 1.71 – 1.76 (m, H14), 1.14 (d, J_{H-H} = 7 Hz, 3H, H1), 0.90, 0.83 (d, J_{H-H} = 7 Hz, 2CH₃, 6H, H15,16). ¹³C {¹H} NMR (175 MHz): δ 170.8 (C7), 164.6 (C6), 136.4 (C), 135.9 (C), 134.3 (CH_{arom}), 131.9 (CH_{arom}), 131.8 (C), 131.6 (C), 131.4 (2C), 130.8 (C), 130.2 (2C), 129.4 (CH_{arom}), 129.00 (CH_{arom}), 128.99 (CH_{arom}), 128.4 (CH_{arom}), 127.8 (CH_{arom}), 127.7 (CH_{arom}), 126.2 (CH_{arom}), 125.8 (CH_{arom}), 125.7 (CH_{arom}), 125.4 (CH_{arom}), 124.8 (CH_{arom}), 122.4 (C11), 121.4 (C10), 111.3 (C9), 109.3 (C12), 72.3 (C4), 70.7 (C3), 49.5 (C5), 32.6 (C14), 18.9, 18.1 (C15,16), 15.0 (C1). m.p. 107.7-109.1 °C. MS (EI) m/z : 542.4 (M⁺). HRMS (EI): calcd for C₃₅H₃₁N₃OS (M+H)⁺ 542.2261, found 542.2268.

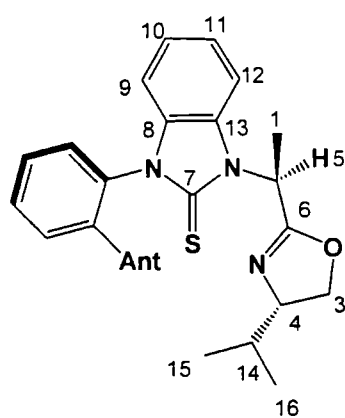
Pd-R-L9up



Compound **Pd-R-L9up** was synthesized by the same procedure as for **PdL6** using **R-L9up** (33.4 mg, 0.062 mmol) and PdCl₂(PhCN)₂ (23.5 mg, 0.062 mmol). The single crystal was obtained from slow evaporation of a solution in CDCl₃. Yield: 32.5 mg, 73 %. m.p. 314.3-314.8 °C. ¹H NMR (700 MHz, CDCl₃): δ 8.23 (s, 1H, CH_{arom}), 7.93 (d, J_{H-H} = 8 Hz, 1H, CH_{arom}), 7.75 – 7.88

(m, 4H, CH_{arom}), 7.64 – 7.65 (m, 1H, CH_{arom}), 7.58 – 7.60 (m, 1H, CH_{arom}), 7.45 – 7.49 (m, 2H, CH_{arom}), 7.39 (t, $J_{H-H} = 8$ Hz, 1H, CH_{arom}), 7.34 – 7.35 (m, 2H, CH_{arom}), 7.18 (d, $J_{H-H} = 8$ Hz, H12), 6.97 (t, $J_{H-H} = 8$ Hz, H11), 6.79 (d, $J_{H-H} = 8$ Hz, H9), 6.70 (t, $J_{H-H} = 8$ Hz, H10), 6.27 – 6.30 (m, H5), 4.83 – 4.86 (m, H4), 4.43 (t, $J_{H-H} = 9$ Hz, H3), 4.12 (t, $J_{H-H} = 9$ Hz, H3'), 2.59 – 2.60 (m, H14), 1.70 (d, $J_{H-H} = 7$ Hz, 3H, H1), 0.64, 0.37 (d, $J_{H-H} = 7$ Hz, 2CH₃, 6H, H15,16). ¹³C{¹H} NMR (175 MHz): δ 165.9 (C7), 164.2 (C6), 137.5 (C), 134.9 (CH_{arom}), 134.1 (C), 133.0 (CH_{arom}), 132.6 (C), 132.4 (CH_{arom}), 131.2 (CH_{arom}), 131.0 (C), 130.5 (CH_{arom}), 130.2 (C), 130.0 (C), 129.8 (C), 129.7 (C), 129.3 (CH_{arom}), 129.2 (C), 129.1 (CH_{arom}), 128.3 (CH_{arom}), 128.0 (CH_{arom}), 127.6 (CH_{arom}), 127.1 (CH_{arom}), 126.2 (CH_{arom}), 126.0 (C11), 125.0 (C10), 124.3 (C9), 112.8 (C12), 111.6 (CH_{arom}), 71.6 (C3), 68.3 (C4), 52.7 (C5), 29.9 (C14), 17.9, 14.9 (C15,16), 13.2 (C1).

S-L9down

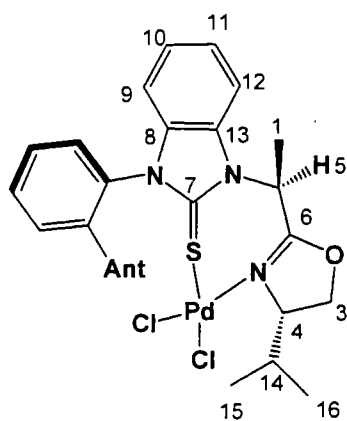


¹H NMR (700 MHz, CDCl₃): δ 8.18 (s, 1H, CH_{arom}), 8.08 (d, $J_{H-H} = 8$ Hz, 1H, CH_{arom}), 8.00 (d, $J_{H-H} = 8$ Hz, 1H, CH_{arom}), 7.92 (d, $J_{H-H} = 8$ Hz, 1H, CH_{arom}), 7.86 (d, $J_{H-H} = 8$ Hz, 1H, CH_{arom}), 7.72 – 7.77 (m, 4H, CH_{arom}), 7.35 – 7.40 (m, 3H, CH_{arom}), 7.31 (t, $J_{H-H} = 8$ Hz, 1H, CH_{arom}), 6.82 (d, $J_{H-H} = 8$ Hz, H12), 6.62 (t, $J_{H-H} = 8$ Hz, H11), 6.40 (d, $J_{H-H} = 8$ Hz, H9), 6.27 (t, $J_{H-H} = 8$ Hz, H10), 6.15 (q, $J_{H-H} = 7$ Hz, H5), 4.22 (t, $J_{H-H} = 8$ Hz, H3), 3.87 (q, $J_{H-H} = 8$ Hz, H4), 3.73 (t, $J_{H-H} = 8$ Hz, H3'), 1.65 – 1.70 (m, H14), 1.17 (d, $J_{H-H} = 7$ Hz, 3H, H1), 0.95, 0.81 (d, $J_{H-H} = 7$ Hz, 2CH₃, 6H, H15,16). ¹³C{¹H} NMR (175 MHz): δ 170.9 (C7), 164.7 (C6), 136.4 (C), 135.9 (C), 134.3 (CH_{arom}), 131.9 (CH_{arom}), 131.8 (C), 131.6 (C), 131.4 (C), 130.8 (C), 130.2 (C), 129.5 (C), 129.4 (C), 129.0 (3CH_{arom}), 128.4 (CH_{arom}), 127.8 (CH_{arom}), 127.7 (CH_{arom}), 126.2 (CH_{arom}), 125.8 (CH_{arom}), 125.7 (CH_{arom}), 125.4 (CH_{arom}), 124.8 (CH_{arom}), 122.2 (C11), 121.4 (C10), 111.3 (C9), 109.2 (C12), 72.7 (C4), 70.9 (C3), 49.3 (C5), 32.8 (C14), 19.5, 18.6 (C15,16), 15.1 (C1). m.p. 103.5-105.0 °C. MS (EI) m/z : 542.4 (M⁺). HRMS (EI): calcd for C₃₅H₃₁N₃OS (M⁺) 542.2261, found 542.2268.

Palladium complexes of **S-L9down**

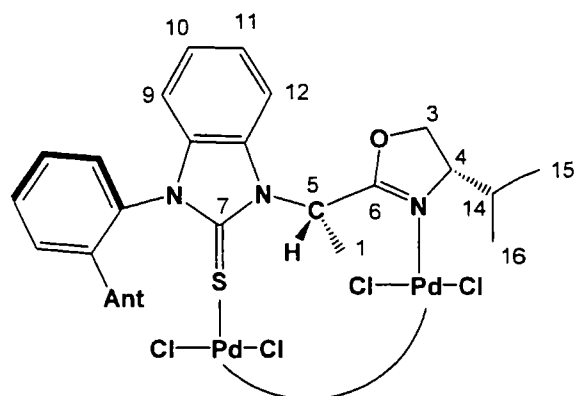
Palladium complexes of **S-L9down** were synthesized by the same procedure as for **PdL6** using **S-L9down** (50.0 mg, 0.09 mmol) and $\text{PdCl}_2(\text{PhCN})_2$ (35 mg, 0.09 mmol). The single crystals of palladium complexes were obtained from evaporation of a solution in $\text{CH}_2\text{Cl}_2:\text{Et}_2\text{O}$ (50:50). Yield: 51.9 mg (mixture). The product is a mixture of **Pd-S-L9down** and **Pd₂-S-L9down**. The single crystals of **Pd₂-S-L9down** were obtained from slow evaporation from $\text{CH}_2\text{Cl}_2:\text{hexane}$. **Pd₂-S-L9down** is in equilibrium with **Pd-S-L9down**. ^1H and $^{13}\text{C}\{^1\text{H}\}$ NMR spectra show a mixture of products and it is difficult to assign each product. The $^{13}\text{C}\{^1\text{H}\}$ NMR spectrum in CDCl_3 at 175 MHz of the mixture appeared as follows: δ 167.89, 166.69, 165.75, 164.41, 138.54, 135.86, 135.69, 135.41, 134.51, 134.21, 133.20, 132.41, 131.88, 131.79, 131.70, 131.52, 131.49, 131.14, 131.09, 130.96, 130.90, 130.70, 130.59, 130.48, 129.95, 129.42, 129.38, 129.30, 128.92, 128.67, 128.27, 128.11, 128.05, 127.94, 127.77, 127.05, 126.99, 126.49, 126.45, 126.35, 125.98, 125.83, 125.66, 125.41, 125.21, 125.18, 124.93, 123.98, 123.25, 114.96, 113.30, 112.74, 110.35, 109.61, 70.86, 70.07, 69.55, 69.37, 53.33, 48.80, 31.80, 30.71, 19.24, 18.74, 18.45, 18.04, 16.77, 14.86, 1.35.

Pd-S-L9down



^1H NMR (700 MHz, CDCl_3):^a δ 8.34 (s, 1H, CH_{arom}), 5.29 (q, $J_{\text{H-H}} = 7$ Hz, H5), 4.69 – 4.75 (m, H4), 4.22 (t, $J_{\text{H-H}} = 8$ Hz, H3), 3.88 (t, $J_{\text{H-H}} = 8$ Hz, H3'), 2.80 (d, $J_{\text{H-H}} = 7$ Hz, CH_3 , H1), 1.79 – 1.86 (m, H14), 0.56, -0.31 (d, $J_{\text{H-H}} = 7$ Hz, 2CH_3 , 6H, H15,16). $^{13}\text{C}\{^1\text{H}\}$ NMR (175 MHz):^a δ 165.4 (C6), 164.1 (C7), 48.8 (C5), 30.7 (C14), 18.4, 14.8 (C15,16), 18.0 (C1).

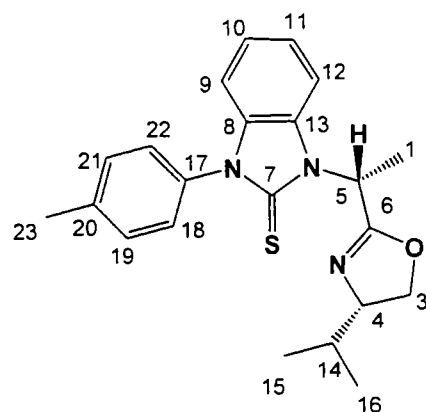
^a Aromatic protons and carbons cannot be assigned due to the overlap of signals of **Pd-S-L9down** and **Pd₂-S-L9down**.

Pd₂-S-L9down

¹H NMR (200 MHz, CDCl₃):^a δ 9.09 (d, $J_{H-H} = 7$ Hz, 1H, CH_{arom}), 8.15 (s, 1H, CH_{arom}), 8.01 – 8.12, m, H5), 7.86 – 7.94 (m, 4H, CH_{arom}), 7.65 – 7.75 (m, 2H, CH_{arom}), 7.41 – 7.55 (m, 4H, 3CH_{arom}&H12), 7.31 – 7.35, m, 1H, CH_{arom}), 6.89 (t, $J_{H-H} = 8$ Hz, H11), 6.52 (d, $J_{H-H} = 8$ Hz,

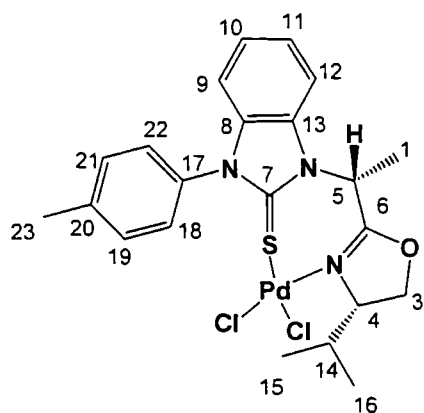
H9), 6.32 (t, $J_{H-H} = 8$ Hz, H10), 4.75 (m, H3), 4.16 (m, H3'), 3.99 (t, $J_{H-H} = 9$ Hz, H4), 2.90 – 3.10 (m, H14), 1.52 (d, $J_{H-H} = 7$ Hz, 3H, H1), 1.35, 1.14 (d, $J_{H-H} = 7$ Hz, 6H, H15,16). ¹³C{¹H} NMR (175 MHz):^b δ 167.5 (C6), 166.3 (C7), 124.0 (C11), 123.3 (C10), 115.0 (C12), 113.3 (C9), 69.5 (C4), 69.4 (C3), 53.3 (C5), 31.8 (C14), 19.2 (C1), 18.7, 16.8 (C15,16).

^a The ¹H NMR spectrum was obtained soon after **Pd₂-S-L9down** crystals were dissolved in CDCl₃. ^b The ¹³C{¹H} NMR spectrum was obtained after 24 h from the same solution employed for ¹H NMR. Aromatic and quaternary carbons cannot be assigned due to overlap of signals of **Pd-S-L9down** and **Pd₂-S-L9down**.

R-L10

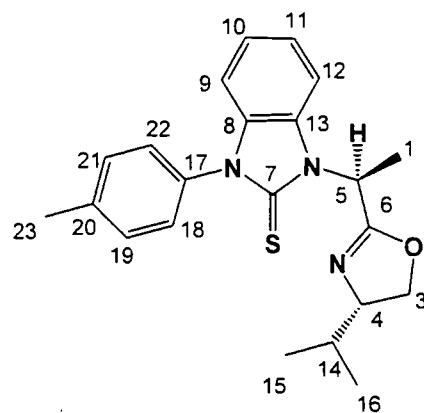
¹H NMR (700 MHz, CDCl₃): δ 7.36 – 7.39 (m, 4H, H18,19,21,22), 7.37 (d, $J_{H-H} = 8$ Hz, H12), 7.17 (t, $J_{H-H} = 8$ Hz, H11), 7.13 (t, $J_{H-H} = 8$ Hz, H10), 6.96 (d, $J_{H-H} = 8$ Hz, H9), 6.43 (q, $J_{H-H} = 7$ Hz, H5), 4.15 – 4.18 (m, H3), 4.02 – 4.07 (m, 2H, H3',4), 2.44 (s, 3H, H23), 1.81 (d, $J_{H-H} = 7$ Hz, 3H, H1), 1.80 – 1.82 (m, H14), 0.98, 0.89 (d, $J_{H-H} = 8$ Hz, 2CH₃, 6H, H15,16). ¹³C{¹H} NMR (175

MHz): δ 170.8 (C7), 164.7 (C6), 139.4 (C8), 133.7 (C17), 133.6 (C20), 130.8 (C13), 130.5 (C18,22), 128.0 (C19,21), 123.3 (C10), 123.2 (C11), 110.6, 110.3 (C9,12), 77.2 (C4), 70.9 (C3), 49.9 (C5), 32.8 (C14), 21.5 (C23), 19.0, 18.2 (C15,16), 15.8 (C1). m.p. 135.9-137.2 °C. MS (EI) m/z : 380.4 (M⁺). HRMS (EI): calcd for C₂₂H₂₅N₃OS (M+H)⁺ 380.1791, found 380.1792.

Pd-R-L10

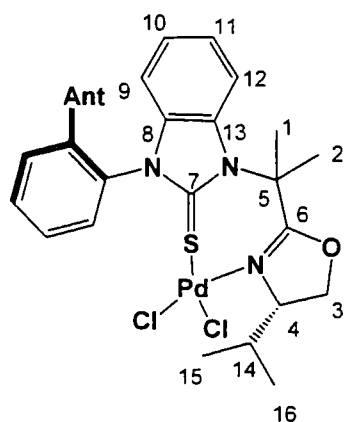
Compound **R-PdL10** was synthesized by the same procedure as for **PdL6** using **R-L10** (100 mg, 0.264 mmol) and $\text{PdCl}_2(\text{PhCN})_2$ (100 mg, 0.264 mmol). The single crystal was obtained from evaporation of a solution in $\text{CH}_2\text{Cl}_2:\text{Et}_2\text{O}$ (50:50). Yield : 140 mg, 96 %. m.p. 257.0-258.2 °C. ^1H NMR (700 MHz, CDCl_3): δ 7.71 (d, $J_{\text{H-H}} = 8$ Hz, H12), 7.38 – 7.43 (m, 5H, H11,18,19,21,22), 7.36 (t, $J_{\text{H-H}} = 8$ Hz, H11), 7.12 (d, $J_{\text{H-H}} = 8$ Hz, H9),

6.71 – 6.79 (m, H5), 4.87 – 4.91 (m, H4), 4.57 (t, $J_{\text{H-H}} = 9$ Hz, H3), 4.25 (t, $J_{\text{H-H}} = 9$ Hz, H3'), 2.60 – 2.63 (m, H14), 2.48 (s, 3H, H23), 2.21 (d, $J_{\text{H-H}} = 7$ Hz, 3H, H1), 1.05, 0.50 (d, $J_{\text{H-H}} = 8$ Hz, 2 CH_3 , 6H, H15,16). $^{13}\text{C}\{^1\text{H}\}$ NMR (175 MHz): δ 165.0 (C6), 164.8 (C7), 141.6 (C20), 133.9 (C8), 131.4 (C18,22), 131.2 (C17), 130.4 (C13), 126.0 (C19,21), 125.9 (C10,11), 112.6 (C12), 112.1 (C9), 71.9 (C3), 68.5 (C4), 53.5 (C5), 30.4 (C14), 21.6 (C23), 17.9, 15.0 (C15,16), 13.8 (C1). Anal. Calcd. for $\text{C}_{22}\text{H}_{25}\text{Cl}_2\text{N}_3\text{OPdS}$: C 47.45, H 4.53, N 7.55; Found C 47.23, H 4.50, N 7.40 %.

S-L10

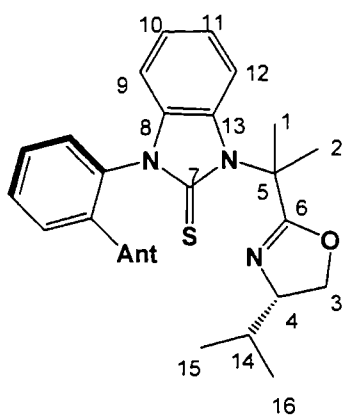
^1H NMR (700 MHz, CDCl_3): δ 7.41 (d, $J_{\text{H-H}} = 8$ Hz, H12), 7.36 – 7.40 (m, 4H, H18,19,21,22), 7.17 (t, $J_{\text{H-H}} = 8$ Hz, H11), 7.13 (t, $J_{\text{H-H}} = 8$ Hz, H10), 6.95 (d, $J_{\text{H-H}} = 8$ Hz, H9), 6.44 (q, $J_{\text{H-H}} = 8$ Hz, H5), 4.31 (t, $J_{\text{H-H}} = 9$ Hz, H3), 3.98 (t, $J_{\text{H-H}} = 9$ Hz, H4), 3.87 (t, $J_{\text{H-H}} = 9$ Hz, H3'), 2.44 (s, 3H, H23), 1.83 (d, $J_{\text{H-H}} = 8$ Hz, 3H, H1), 1.78 – 1.83 (m, H14), 1.05, 0.89 (d, $J_{\text{H-H}} = 7$ Hz, 2 CH_3 , 6H,

H15,16). $^{13}\text{C}\{^1\text{H}\}$ NMR (175 MHz): δ 171.0 (C7), 164.9 (C6), 139.5 (C8), 133.8 (C17), 133.7 (C20), 130.8 (C13), 130.6 (C18,22), 128.1 (C19,21), 123.4 (C10), 123.3 (C11), 110.6 (C12), 110.4 (C9), 73.0 (C4), 71.2 (C3), 49.9 (C5), 33.0 (C14), 21.6 (C23), 19.7, 18.8 (C15,16), 15.7 (C1). m.p. 69.7-70.1 °C. MS (EI) m/z : 380.4 (M⁺). HRMS (EI): calcd for $\text{C}_{22}\text{H}_{25}\text{N}_3\text{OS}$ (M+H)⁺ 380.1791, found 380.1792.

PdL11up

Compound **PdL11up** was synthesized by a similar procedure as for **PdL6**, using **L11up** (150 mg, 0.270 mmol) and $\text{PdCl}_2(\text{CH}_3\text{CN})_2$ (69 mg, 0.270 mmol) in CHCl_3 (10 mL). Yield: 158 mg, 80 % (crystals). m.p. 305.0-306.4 °C. ^1H NMR (700 MHz, CDCl_3): δ 8.21 (s, 1H, CH_{arom}), 8.10 (d, $J_{\text{H-H}} = 8$ Hz, 1H, CH_{arom}), 7.87 (t, $J_{\text{H-H}} = 8$ Hz, 1H, CH_{arom}), 7.77 – 7.83 (m, 4H, CH_{arom}), 7.68 – 7.73 (m, 2H, CH_{arom}), 7.57 (d, $J_{\text{H-H}} = 8$ Hz, 1H, CH_{arom}), 7.46 (t, $J_{\text{H-H}} = 8$ Hz, 1H, CH_{arom}), 7.33 – 7.34

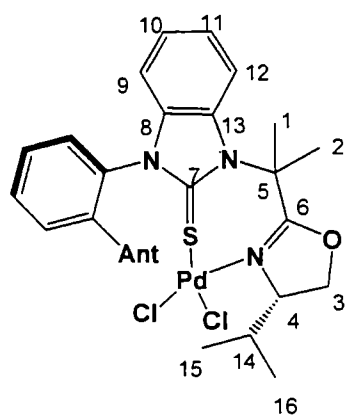
(m, 3H, H12&2 CH_{arom}), 6.83 (t, $J_{\text{H-H}} = 7$ Hz, H11), 6.72 (d, $J_{\text{H-H}} = 7$ Hz, H9), 6.59 (d, $J_{\text{H-H}} = 7$ Hz, H10), 4.71 – 4.74 (m, H4), 4.25 (t, $J_{\text{H-H}} = 8$ Hz, H3), 4.14 (t, $J_{\text{H-H}} = 8$ Hz, H3'), 3.19 – 3.24 (m, H14), 2.67, 2.18 (s, 2 CH_3 , 6H, H1,2), 0.91, 0.81 (d, $J_{\text{H-H}} = 7$ Hz, 2 CH_3 , 6H, C15,16). $^{13}\text{C}\{^1\text{H}\}$ NMR (175 MHz): δ 167.5 (C6), 164.3 (C7), 137.7 (C), 134.9 (CH_{arom}), 133.6 (C), 130.98 (C), 130.93 (C), 130.8 (C), 130.15 (C), 130.01 (C), 129.8 (C), 132.3 (C), 131.2 (CH_{arom}), 130.8 (C), 130.1 (CH_{arom}), 128.9 (CH_{arom}), 128.4 (CH_{arom}), 127.9 (CH_{arom}), 127.6 (CH_{arom}), 127.4 (CH_{arom}), 126.3 (CH_{arom}), 125.9 (CH_{arom}), 125.8 (CH_{arom}), 124.8 (CH_{arom}), 124.3 (C11), 123.6 (C10), 113.3 (C12), 112.7 (C9), 71.3 (C4), 69.1 (C3), 61.3 (C5), 30.2 (C14), 29.1, 28.2 (C1,2), 19.0, 15.1 (C15,16). Anal. Calcd. for $\text{C}_{36}\text{H}_{33}\text{Cl}_2\text{N}_3\text{OPdS}\cdot 3\text{CHCl}_3$: C 54.63, H 4.21, N 5.73; Found C 54.45, H 4.21, N 5.21 %.

L11down

^1H NMR (700 MHz, CDCl_3): δ 8.21 (s, 1H, CH_{arom}), 8.15 – 8.17 (m, 1H, CH_{arom}), 7.84 (d, $J_{\text{H-H}} = 8$ Hz, 1H, CH_{arom}), 7.78 – 7.82 (m, 3H, CH_{arom}), 7.72 – 7.74 (m, 2H, CH_{arom}), 7.68 – 7.70 (m, 1H, CH_{arom}), 7.31 – 7.32 (m, 3H, CH_{arom}), 7.27 (d, $J_{\text{H-H}} = 7$ Hz, 1H, CH_{arom}), 7.08 (d, $J_{\text{H-H}} = 8$ Hz, H12), 6.64 (t, $J_{\text{H-H}} = 7$ Hz, H11), 6.57 (d, $J_{\text{H-H}} = 7$ Hz, H9), 6.41 (t, $J_{\text{H-H}} = 7$ Hz, H10), 4.06 (t, $J_{\text{H-H}} = 8$ Hz, H3), 3.87 (t, $J_{\text{H-H}} = 8$ Hz, H4), 3.70 (t, $J_{\text{H-H}} = 8$ Hz, H3'), 1.76 – 1.81 (m, H14), 1.94, 1.68 (s, 2 CH_3 , 6H, H1,2), 0.91, 0.83 (d, $J_{\text{H-H}} = 7$ Hz, 2 CH_3 , 6H, H15,16). $^{13}\text{C}\{^1\text{H}\}$ NMR (175 MHz): δ 171.1 (C7), 169.5 (C6), 137.4

(C), 136.1 (C), 134.6 (CH_{arom}), 132.7 (C), 132.2 (CH_{arom}), 131.7 (C), 131.4 (C), 131.2 (C), 130.2 (C), 130.1 (C), 129.5 (CH_{arom}), 129.05 (CH_{arom}), 128.91 (CH_{arom}), 128.9 (CH_{arom}), 127.8 (CH_{arom}), 127.6 (CH_{arom}), 126.6 (CH_{arom}), 125.8 (CH_{arom}), 125.6 (CH_{arom}), 125.5 (CH_{arom}), 124.8 (CH_{arom}), 122.1 (C11), 121.3 (C10), 110.4 (C9), 111.2 (C12), 72.4 (C4), 70.8 (C3), 62.4 (C5), 32.5 (C14), 28.3, 25.8 (C1,2), 19.5, 18.6 (C15,16). m.p. 102.5-103.3 °C. HRMS(ESI⁺): m/z cal for C₃₆H₃₃ON₃S (M+H)⁺ 556.2417, found 556.2420.

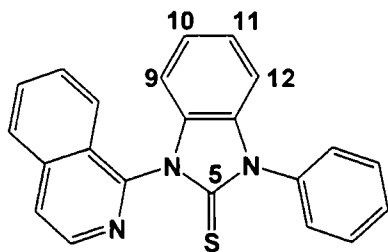
PdL11down



Compound **PdL11down** was synthesized by the same procedure as for **PdL6** using **L11down** (150 mg, 0.270 mmol) and PdCl₂(PhCN)₂ (103 mg, 0.270 mmol). Yield: 155.9 mg, 79 %. ¹H NMR (700 MHz, CDCl₃): δ 8.26 (s, 1H, CH_{arom}), 8.09 (t, *J*_{H-H} = 5 Hz, 1H, CH_{arom}), 8.02 (d, *J*_{H-H} = 9 Hz, 1H, CH_{arom}), 7.86 (d, *J*_{H-H} = 9 Hz, 1H, CH_{arom}), 7.79 – 7.81 (m, 3H, CH_{arom}), 7.66 (t, *J*_{H-H} = 5 Hz, 1H, CH_{arom}), 7.60 (d, *J*_{H-H} = 9 Hz, 1H, CH_{arom}), 7.55

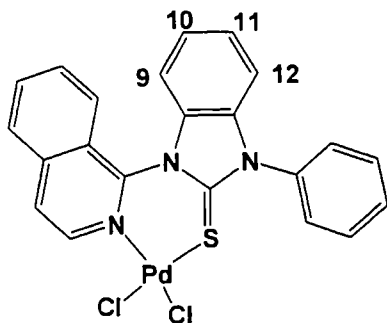
(t, *J*_{H-H} = 9 Hz, 1H, CH_{arom}), 7.44 (t, *J*_{H-H} = 9 Hz, 1H, CH_{arom}), 7.41 (d, *J*_{H-H} = 8 Hz, H12), 7.28 (d, *J*_{H-H} = 9 Hz, 1H, CH_{arom}), 7.18 (t, *J*_{H-H} = 9 Hz, 1H, CH_{arom}), 7.14 (d, *J*_{H-H} = 8 Hz, H9), 7.06 (t, *J*_{H-H} = 8 Hz, H11), 7.00 (t, *J*_{H-H} = 8 Hz, H10), 4.69 – 4.71 (m, H4), 4.22 (t, *J*_{H-H} = 8 Hz, H3), 4.15 (t, *J*_{H-H} = 8 Hz, H3'), 3.02 – 3.05 (m, H14), 2.36, 1.44 (s, 2CH₃, 6H, H1,2), 0.83, 0.42 (d, *J*_{H-H} = 7 Hz, 2CH₃, 6H, H15,16). ¹³C{¹H} NMR (175 MHz): δ 166.9 (C6), 163.7 (C7), 134.2 (CH_{arom}), 134.0 (C), 132.2 (CH_{arom}), 133.6 (C), 131.7 (C), 131.3 (C), 131.2 (CH_{arom}), 130.9, 130.8 (C), 130.3 (C), 130.2 (CH_{arom}), 129.8 (C), 128.6 (CH_{arom}), 128.4 (CH_{arom}), 127.9 (CH_{arom}), 127.8 (CH_{arom}), 126.8 (CH_{arom}), 126.3 (CH_{arom}), 126.1 (CH_{arom}), 125.6 (CH_{arom}), 125.3 (C11), 125.2 (CH_{arom}), 124.7 (C10), 115.0 (C12), 113.7 (C9), 72.2 (C4), 69.0 (C3), 63.7 (C5), 30.5 (C14), 29.1, 28.7 (C1,2), 19.1, 14.3 (C15,16).

L12

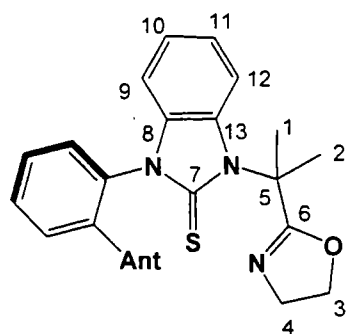


^1H NMR (700 MHz, CD_2Cl_2): δ 8.68 (d, $J_{\text{H-H}} = 6$ Hz, CH_{arom}), 8.00 (d, $J_{\text{H-H}} = 8$ Hz, 1H, CH_{arom}), 7.91 (d, $J_{\text{H-H}} = 6$ Hz, 1H, CH_{arom}), 7.84 (d, $J_{\text{H-H}} = 8$ Hz, 1H, CH_{arom}), 7.77 (t, $J_{\text{H-H}} = 8$ Hz, 1H, CH_{arom}), 7.68 (d, $J_{\text{H-H}} = 8$ Hz, 2H, CH_{arom}), 7.14 (d, $J_{\text{H-H}} = 8$ Hz, 2H, CH_{arom}), 7.62 (d, $J_{\text{H-H}} = 8$ Hz, 1H, CH_{arom}), 7.54 (t, $J_{\text{H-H}} = 8$ Hz, 1H, CH_{arom}), 7.21 (t, $J_{\text{H-H}} = 8$ Hz, 1H, CH_{arom}), 7.15 (t, $J_{\text{H-H}} = 8$ Hz, H10), 7.09 (d, $J_{\text{H-H}} = 8$ Hz, H12), 6.79 (d, $J_{\text{H-H}} = 8$ Hz, H9). $^{13}\text{C}\{^1\text{H}\}$ NMR (175 MHz): δ 171.4 (C5), 148.5 (C), 142.5 (CH_{arom}), 138.8 (2C), 135.8 (C), 134.0 (C13), 133.6 (C2), 131.5 (CH_{arom}), 130.0 (2 CH_{arom}), 129.4 (CH_{arom}), 128.8 (CH_{arom}), 128.4 (2 CH_{arom}), 127.5 (CH_{arom}), 125.6 (CH_{arom}), 124.02 (C10), 123.95 (C11), 123.6 (CH_{arom}), 110.3 (C9), 110.2 (C12). MS (EI) m/z : 354.3 (M^+).

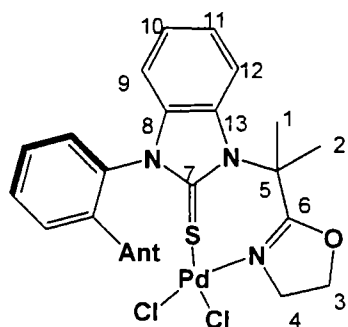
PdL12



Compound **PdL12** was synthesized by the same procedure as for **PdL6**, using **L12** (20 mg, 0.056 mmol) and $\text{PdCl}_2(\text{PhCN})_2$ (21.7 mg, 0.056 mmol) in CDCl_3 (ca. 0.7 mL) in an NMR tube. The red crystals were obtained from slow evaporation of CDCl_3 . Yield: 20 mg, 66 %. m.p. 247.0-247.5 °C. ^1H NMR (700 MHz, CD_2Cl_2): δ 9.44 (d, $J_{\text{H-H}} = 7$ Hz, 1H, CH_{arom}), 8.15 (d, $J_{\text{H-H}} = 9$ Hz, 1H, CH_{arom}), 8.11 (d, $J_{\text{H-H}} = 7$ Hz, 1H, CH_{arom}), 7.97 (t, $J_{\text{H-H}} = 8$ Hz, 1H, CH_{arom}), 7.73 – 7.81 (m, 4H, CH_{arom}), 7.67 (t, $J_{\text{H-H}} = 9$ Hz, 1H, CH_{arom}), 7.66 (d, $J_{\text{H-H}} = 8$ Hz, 1H, CH_{arom}), 7.62 (d, $J_{\text{H-H}} = 9$ Hz, 1H, CH_{arom}), 7.56 (t, $J_{\text{H-H}} = 9$ Hz, H11), 7.47 (d, $J_{\text{H-H}} = 9$ Hz, H10), 7.43 (d, $J_{\text{H-H}} = 7$ Hz, H12), 6.90 (d, $J_{\text{H-H}} = 9$ Hz, H9). $^{13}\text{C}\{^1\text{H}\}$ NMR (125 MHz): δ 164.9 (C), 146.6 (CH_{arom}), 145.7 (C), 140.2 (C), 134.9 (CH_{arom}), 134.6 (C), 133.9 (C), 132.2 (C), 131.0 (CH_{arom}), 132.1 (2 CH_{arom}), 131.0 (CH_{arom}), 130.1 (CH_{arom}), 128.28 (C11), 128.25 (2 CH_{arom}), 127.5 (C10), 126.0 (CH_{arom}), 125.7 (CH_{arom}), 122.4 (C), 114.3 (C9), 113.9 (C12). Anal. Calcd. for $6(\text{C}_{22}\text{H}_{15}\text{Cl}_2\text{N}_3\text{PdS}) \cdot 8(\text{CDCl}_3)$: C 40.54, H 2.58, N 6.08; Found C 40.63, H 2.48, N 6.27 %.

L13down

^1H NMR (700 MHz, CDCl_3): δ 8.21 (s, 1H, CH_{arom}), 8.15 – 8.17 (m, 1H, CH_{arom}), 7.81 – 7.84 (m, 2H, CH_{arom}), 7.77 – 7.80 (m, 2H, CH_{arom}), 7.72 – 7.75 (m, 2H, CH_{arom}), 7.68 – 7.69 (m, 1H, CH_{arom}), 7.31 – 7.33 (m, 3H, CH_{arom}), 7.27 (t, $J_{\text{H-H}} = 7$ Hz, 1H, CH_{arom}), 7.09 (d, $J_{\text{H-H}} = 8$ Hz, H12), 6.65 (t, $J_{\text{H-H}} = 8$ Hz, H11), 6.59 (d, $J_{\text{H-H}} = 8$ Hz, H9), 6.42 (t, $J_{\text{H-H}} = 8$ Hz, H10), 4.09 (q, $J_{\text{H-H}} = 9$ Hz, H3), 3.98 (q, $J_{\text{H-H}} = 9$ Hz, H3'), 3.76 – 3.84 (m, 2H, H4), 1.93, 1.68 (s, 2 CH_3 , 6H, H1,2). $^{13}\text{C}\{^1\text{H}\}$ NMR (175 MHz): δ 170.9 (C7), 170.7 (C6), 137.3 (C), 136.0 (C), 134.5 (CH_{arom}), 132.6 (C), 132.1 (CH_{arom}), 131.5 (C), 131.2 (2C), 131.0 (C), 130.1 (C), 130.0 (C), 129.4 (CH_{arom}), 129.0 (CH_{arom}), 128.9 (CH_{arom}), 128.8 (CH_{arom}), 127.6 (CH_{arom}), 127.5 (CH_{arom}), 126.4 (CH_{arom}), 125.6 (CH_{arom}), 125.42 (CH_{arom}), 125.38 (CH_{arom}), 124.7 (CH_{arom}), 122.1 (C11), 121.2 (C10), 111.4 (C9), 111.1 (C12), 68.4 (C4), 62.0 (C5), 54.6 (C3), 27.7, 25.8 (C1,2). m.p. 89.7-91.3 °C. HRMS(ESI⁺): m/z cal for $\text{C}_{33}\text{H}_{27}\text{ON}_3\text{S}$ ($\text{M}+\text{H}$)⁺ 514.1948, found 514.1946.

PdL13down

Compound **PdL13down** was synthesized by the same procedure as for **PdL6**, using **L13down** (40.2 mg, 0.078 mmol) and $\text{PdCl}_2(\text{PhCN})_2$ (30.0 mg, 0.078 mmol). Yield: 48 mg, 90 %. m.p. 327.0-327.5 °C. ^1H NMR (700 MHz, CDCl_3): δ 8.26 (s, 1H, CH_{arom}), 8.10 (d, $J_{\text{H-H}} = 9$ Hz, 1H, CH_{arom}), 7.90 (d, $J_{\text{H-H}} = 8$ Hz, 1H, CH_{arom}), 7.84 (t, $J_{\text{H-H}} = 8$ Hz, 1H, CH_{arom}), 7.71 – 7.79 (m, 5H, CH_{arom}), 7.52 – 7.54 (m, 2H, CH_{arom}), 7.43 (d, $J_{\text{H-H}} = 8$ Hz, H12), 7.23 (t, $J_{\text{H-H}} = 8$ Hz, 1H, CH_{arom}), 7.15 (t, $J_{\text{H-H}} = 8$ Hz, 1H, CH_{arom}), 7.00 (d, $J_{\text{H-H}} = 8$ Hz, H9), 6.97 (t, $J_{\text{H-H}} = 8$ Hz, H11), 6.87 (t, $J_{\text{H-H}} = 8$ Hz, H10), 4.29 – 4.33 (m, H3), 4.20 – 4.25 (m, H4), 3.80 (q, $J_{\text{H-H}} = 9$ Hz, H3'), 3.64 – 3.68 (m, H4'), 2.80, 2.16 (s, 2 CH_3 , 6H, H1,2). $^{13}\text{C}\{^1\text{H}\}$ NMR (175 MHz): δ 168.2 (C6), 163.4 (C7), 137.6 (C), 134.9 (CH_{arom}), 133.8 (C), 132.8 (C), 131.4 (C), 131.3 (CH_{arom}), 131.1 (C), 131.0 (CH_{arom}), 130.87 (C), 130.6 (2C), 130.3 (CH_{arom}), 130.1 (C), 129.8 (CH_{arom}), 128.9 (CH_{arom}), 128.6 (CH_{arom}), 127.8 (CH_{arom}), 127.7 (CH_{arom}), 126.8 (CH_{arom}), 126.4 (CH_{arom}), 125.6 (CH_{arom}), 125.2 (CH_{arom}), 124.9

(C11), 124.1 (C10), 113.8 (C12), 113.0 (C9), 69.3 (C3), 61.5 (C5), 55.3 (C4), 28.3, 27.9 (C1,2).

V. References

1. Dai, M.; Wang, C.; Dong, G.; Xiang, J.; Luo, T.; Liang, B.; Chen, J.; Yang, Z., *Eur. J. Org. Chem.* **2003**, 4346.
2. Liang, B.; Liu, J.; Gao, Y.-X.; Wongkhan, K.; Shu, D.-X.; Lan, Y.; Li, A.; Batsanov, A. S.; Howard, J. A. H.; Marder, T. B.; Chen, J.-H.; Yang, Z., *Organometallics* **2007**, *26*, 4756.
3. Kovala-Demertzi, D.; Yadav, P. N.; Demertzis, M. A.; Jasiski, J. P.; Andreadaki, F. J.; Kostas, I. D., *Tetrahedron Lett.* **2004**, *45*, 2923.
4. Chen, W.; Li, R.; Han, B.; Li, B.-J.; Chen, Y.-C.; Wu, Y.; Ding, L.-S.; Yang, D., *Eur. J. Org. Chem.* **2006**, 1177.
5. Kostas, I. D.; Heropoulos, G. A.; Kovala-Demertzi, D.; Yadav, P. N.; Jasinski, J. P.; Demertzis, M. A.; Andreadaki, F. J.; Vo-Thanh, G.; Petit, A.; Loupy, A., *Tetrahedron Lett.* **2006**, *47*, 4403.
6. Dai, M.; Wang, C.; Liang, B.; Chen, J.; Yang, Z., *Org. Lett.* **2004**, *6*, 221.
7. Yang, D.; Chen, Y.-C.; Zhu, N.-Y., *Org. Lett.* **2004**, *6*, 1577.
8. Dai, M.; Liang, B.; Wang, C.; You, Z.; Xiang, J.; Dong, G.; Chen, J.; Yang, Z., *Adv. Synth. Catal.* **2004**, 1669.
9. Tang, Y.; Deng, L.; Zhang, Y.; Dong, G.; Chen, J.; Yang, Z., *Org. Lett.* **2005**, *7*, 1657.
10. Li, Z.; Gao, Y.; Tang, Y.; Dai, M.-j.; Wang, G.; Wang, Z.; Yang, Z., *Org. Lett.* **2008**, *10*, 3017.
11. Liu, J.; Liang, B.; Shu, D.; Hu, Y.; Yang, Z.; Lei, A., *Tetrahedron* **2008**, *64*, 9581.
12. Matt, P. V.; Pfaltz, A., *Angew. Chem., Int. Ed.* **1993**, *32*, 566.
13. Sprinz, J.; Helmchen, G., *Tetrahedron Lett.* **1993**, *34*, 1769.
14. Dawson, G. J.; Frost, C. G.; Williams, J. M. J.; Coote, S. J., *Tetrahedron Lett.* **1993**, *34*, 3149.
15. Lloyd-Jones, G.; Pfaltz, A., *Angew. Chem., Int. Ed.* **1995**, *34*, 462.
16. Glorius, F.; Pfaltz, A., *Org. Lett.* **1999**, *1*, 141.
17. Lowenthal, R. E.; Abiko, A.; Masamune, S., *Tetrahedron Lett.* **1990**, *31*, 6005.
18. Evans, D. A.; Woerpel, K. A.; Hinman, M. M.; Faul, M. M., *J. Am. Chem. Soc.* **1991**, *113*, 726.
19. Corey, E. J.; Imai, N.; Zhang, H.-Y., *J. Am. Chem. Soc.* **1991**, *113*, 728.
20. Muller, D.; Umbrecht, G.; Weber, B.; Pfaltz, A., *Helv. Chim. Acta* **1991**, *74*, 232.
21. Ghosh, A. K.; Mathivanan, P.; Cappiello, J., *Tetrahedron: Asymmetry* **1998**, *9*, 1.
22. James, D. E.; Hines, L. F.; Stille, J. K., *J. Am. Chem. Soc.* **1976**, *98*, 1806.
23. Pisano, C.; Nefkens, S. C. A.; Consiglio, G., *Organometallics* **1992**, *11*, 1975.
24. Lloyd, W. G.; Rowe, D. R., *Environ. Sci. Technol.* **1971**, *5*, 1133.
25. Fenton, D. M.; Steinwand, P. J., *J. Org. Chem.* **1974**, *39*, 701.
26. Tamaru, Y.; Yamada, Y.; Yamamoto, Y.; Yoshida, Z.-I., *Tetrahedron Lett.* **1979**, *16*, 1401.

27. Choudary, B. M.; Prabhabar, N. R.; Lakshmi, M. K., *Tetrahedron Lett.* **1985**, *26*, 6257.
28. Yu, L., *Private Communication* **2007**.
29. Rowland, R. S.; Taylor, R., *J. Phys. Chem.* **1996**, *100*, 7384.
30. Heck, R. F., *Palladium reagents in organic syntheses*, Academic Press: London, 1990; p 461.

Chapter 5

Phosphine Sulfides and Their Palladium Complexes

Abbreviations

AIM	Atoms in Molecules
dmpmS	1,1-Bis(dimethylphosphino)methane monosulfide
dppmS	1,1-Bis(diphenylphosphino)methane monosulfide
dppmS ₂	1,1-Bis(diphenylphosphino)methane disulfide
dpeS	1,2-Bis(diphenylphosphino)ethane monosulfide
dpeS ₂	1,2-Bis(diphenylphosphino)ethane disulfide
dppbS	1,4-Bis(diphenylphosphino)butane monosulfide
dppbS ₂	1,4-Bis(diphenylphosphino)butane disulfide
dcpeS	1,2-Bis(dicyclohexylphosphino)ethane monosulfide
dcpeS ₂	1,2-Bis(dicyclohexylphosphino)ethane disulfide
dppttS ₂	3,5-Bis(diphenylphosphinothioyl)toluene
dppfS	1,1'-Bis(diphenylphosphino)ferrocene monosulfide
dppfS ₂	1,1'-Bis(diphenylphosphino)ferrocene disulfide
dppp	1,4-Bis(diphenylphosphino)propane
^t Bu	<i>tert</i> -Butyl
Cy	Cyclohexyl
Et	Ethyl
Fc	Ferrocenyl
Me	Methyl
Cp*	Pentamethylcyclopentadienyl
Ph	Phenyl
ⁱ Pr	<i>iso</i> -Propyl
tol	Tolyl
OTf	Trifluoromethanesulfonyl

I. Literature Review

I.1 Introduction

Phosphine compounds are well known organic ligands for homogenous catalysis in organometallic reaction. Other phosphine derivatives are also used (*e.g.* phosphine oxides).¹ Much less attention has been paid to phosphine sulfides compared to phosphines, as there are less than 200 hits for complexes of phosphine sulfides in the CSD (2007).² Part of this lack of attention on phosphine sulfides may be the lack of quantitative information on the PS bond and how it is perturbed upon coordination. However, the high stability of phosphine sulfides to oxidation and their easy preparation make them potentially attractive ligands for a wide range of processes, for example, as ligands in metal catalyzed processes, *vide infra*. To the best of our knowledge, there is no review concerning the properties of coordinated phosphine sulfides. This review will concentrate on the coordination of phosphine sulfides to a variety of metals; the structures and dimensions derived from the X-ray crystallographic study of a large number of phosphine sulfide complexes will be emphasized in order to understand the bonding in such complexes. The synthesis of phosphine sulfides, their complexes and their applications in catalysis will also be discussed.

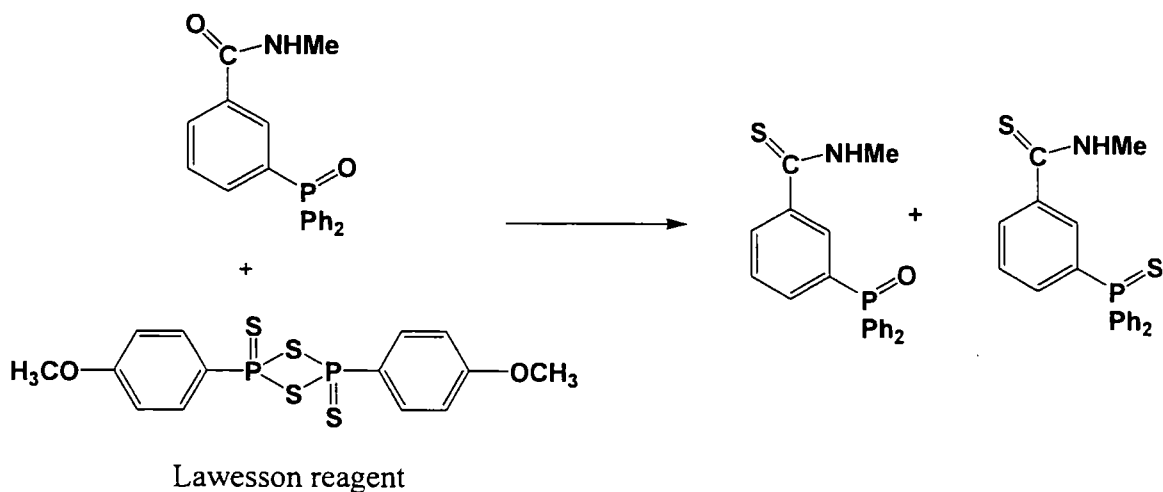
I.2 Synthesis of phosphine sulfides ligands

The simplest route to phosphine sulfides is the reaction of sulfur with a phosphine in a suitable solvent (*e.g.*, CH₂Cl₂). One equivalent of elemental sulfur will lead to the oxidation of the phosphorus (Scheme 1).³ For bis(phosphine) compounds, mixtures of bis(phosphine) monosulfides and disulfides are usually obtained even if one equivalent of elemental sulfur is used. However, the mixtures can be separated using column chromatography. Phosphine sulfides can be converted back to phosphines by treatment with lithium aluminium hydride in refluxing THF.⁴



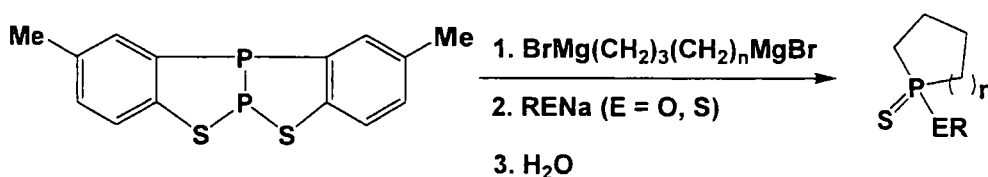
Scheme 1. The synthesis of phosphine sulfides from the reaction of phosphines with sulfur.

The other efficient method for phosphine sulfides is the conversion of phosphine oxide using the Lawesson reagent (Scheme 2).⁵



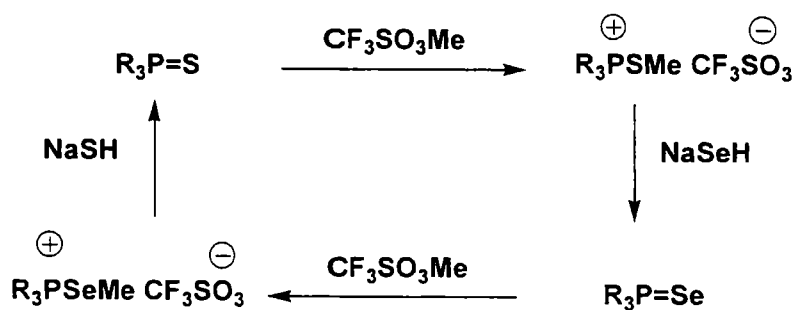
Scheme 2. The synthesis of phosphine sulfides using the Lawesson reagent.

Recently, acyclic phosphine sulfides were prepared from the reaction of a cyclic phosphine with a Grignard reagent, followed by the addition of nucleophilic reagents, such as sodium alkoxide or thiolate (Scheme 3).⁶

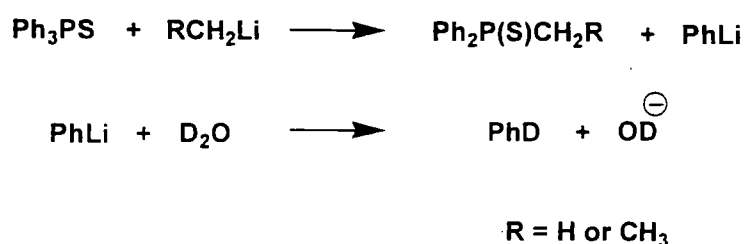


Scheme 3. Synthesis of acyclic phosphine sulfides.⁶

The interconversion of phosphine sulfide and phosphine selenide can be achieved (Scheme 4).⁷ These conversions are stereoselective and proceed with retention >90 % of configuration at the phosphorus center.

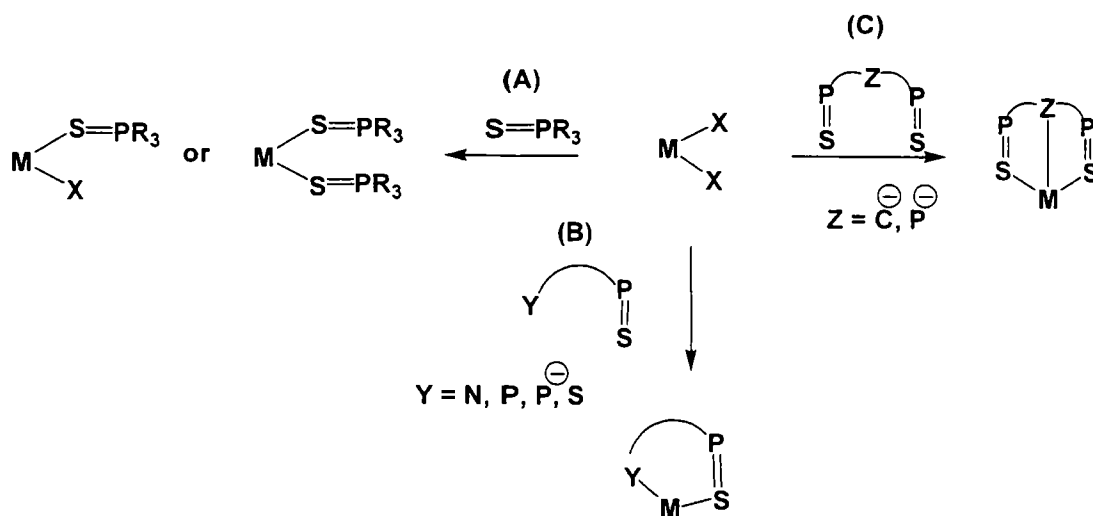
Scheme 4. Interconversion of SPR_3 and SePR_3 .⁷

Unsymmetric phosphine sulfides were first reported by Seyferth and Welch as shown in Scheme 5.^{8, 9} Triphenylphosphine sulfide was reacted with an alkyllithium reagent to form a diphenyl-alkyl phosphine sulfide. The reaction proceeded by the exchange-metalation mechanism which can be proved by quenching of phenyl lithium with D_2O which yields Ph-D.

Scheme 5. The synthesis of unsymmetric phosphine sulfides developed by Seyferth.^{8, 9}

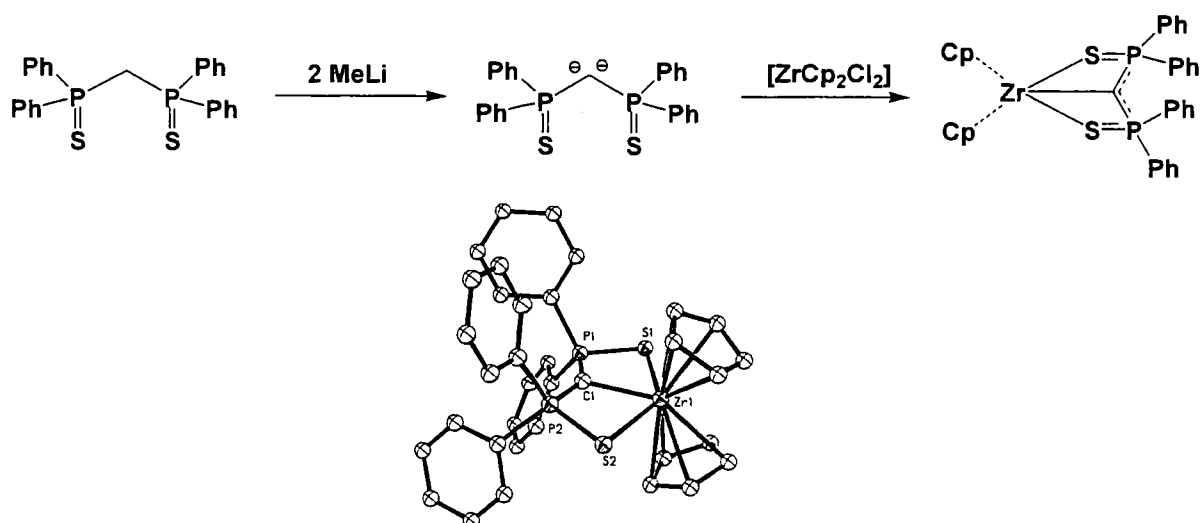
I.3 Synthesis of metal-phosphine sulfide complexes

Ligand substitution (exchange) reactions are common processes for the synthesis of organometallic and coordination compounds. The ligand exchange process is important as it may be necessary to replace a ligand in a metal complex to adjust the reactivity of a coordinated substrate.¹⁰ Metal-phosphine sulfide complexes can be synthesized by this procedure (Scheme 6).

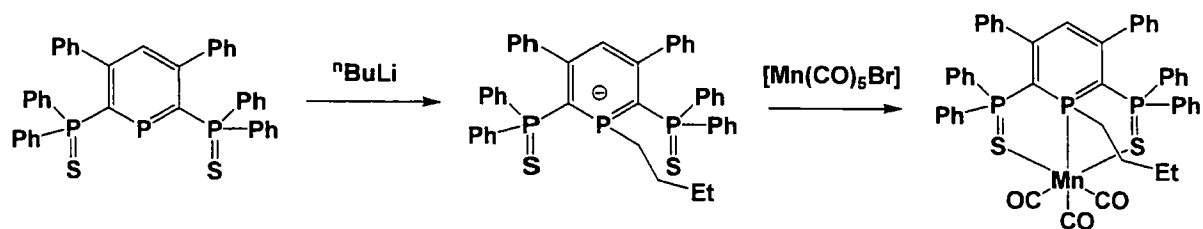


Scheme 6. Preparation of phosphine sulfide complexes.

In route **A**, the innocent neutral or anionic monodentate ligands can be simply exchanged with phosphine sulfide to form the metal-phosphine sulfide complexes. The ratio of metal to phosphine sulfide ligand can be varied to obtain the desired product. Route **B** involves the bidentate phosphine sulfides κ^2 -S, Y (Y = N, S, P, P⁻), whereas route **C** employs the tridentate phosphine sulfides κ^3 -S, Z, S (Z = S, C⁻, P⁻). In routes **B** and **C**, anionic phosphine sulfides can be prepared by treatment of neutral ligands with strong base (*e.g.*, methyl lithium or butyl lithium). Examples of metal-phosphine sulfide κ^3 -S, C⁻, S and κ^3 -S, P⁻, S complexes are shown in Schemes 7 and 8, respectively.

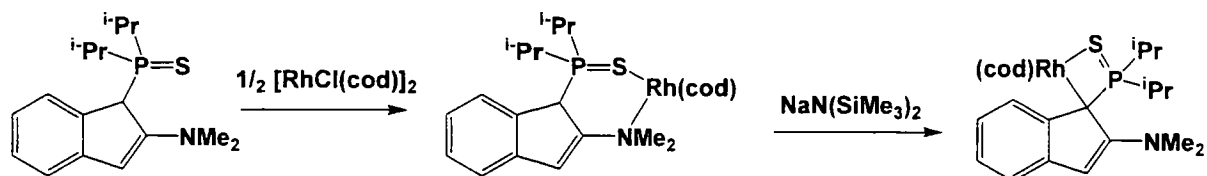


Scheme 7. A bis(diphenyl phosphino)zirconium(IV) carbene disulfide complex and its molecular structure.¹¹



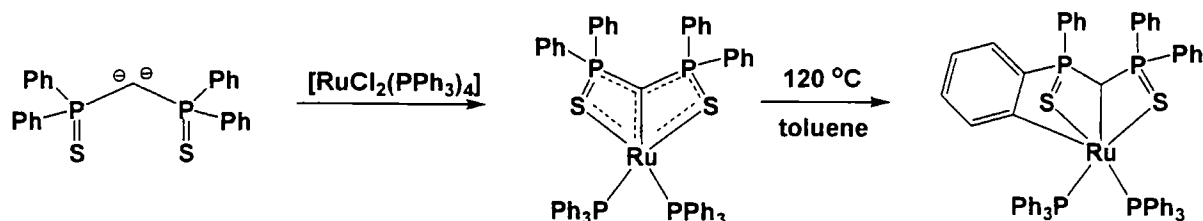
Scheme 8. The synthesis of a $\kappa^3\text{-S, P}^-, \text{S}$ -(diphenylphosphine)phosphinine disulfide manganese tricarbonyl complex.¹²

Cyclometallated metal–phosphine sulfide complexes can be achieved *via* the ligand exchange process which is shown in Scheme 9. The carbon next to the phosphorus atom in a rhodium–phosphine sulfide complex can be deprotonated by $\text{NaN}(\text{SiMe}_3)_2$. After that, the carbanion exchanged with the amine ligand to afford the cyclometallated product (Scheme 9).¹³



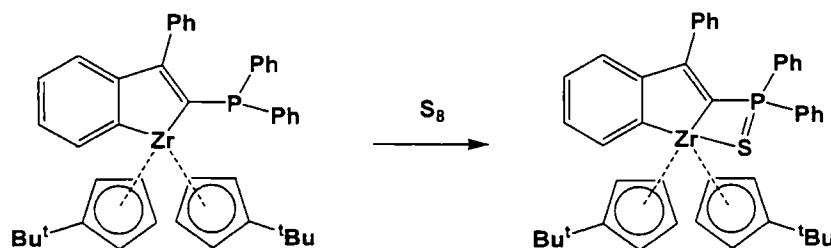
Scheme 9. Synthesis of cyclometallation rhodium phosphine sulfide.¹³

Cyclometallated $\kappa^3\text{-S, C}^-, \text{S}$ ruthenium phosphine sulfide complexes (Scheme 10) were prepared by the reaction of the dppmS_2 dianion with one equivalent of $[\text{RuCl}_2(\text{PPh}_3)_4]$ at room temperature. Subsequent heating in toluene at $120\text{ }^\circ\text{C}$ for 15 h results in metallation of one phenyl group and formal protonation at the carbene carbon (Scheme 10).¹⁴

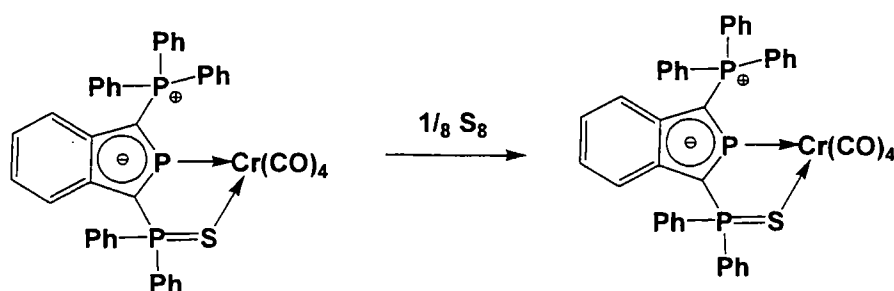


Scheme 10. A cyclometallated phosphine sulfide ruthenium complex.¹⁴

Metal phosphine sulfide complexes can also be synthesized from phosphine complexes by reaction with elemental sulfur. A zirconaindene phosphine sulfide (Scheme 11)¹⁵ and a tetracarbonyl chromium phosphine sulfide (Scheme 12)¹⁶ are examples of complexes which were prepared by this procedure.



Scheme 11. The synthesis of a zirconaindene phosphine sulfide complex.



Scheme 12. The synthesis of a tetracarbonyl chromium phosphine sulfide complex.¹⁶

Cis- and *trans*- isomeric phosphine sulfide metal complexes are known. Thus reaction of PtCl₂(cod) or PdCl₂(cod) with the monoxidized sulfur or selenium derivative of bis(diphenylphosphino)amine, Ph₂P(E)NPh₂ (E = S, Se), gave a mixture of *cis*- and *trans*- products (Figure 1).¹⁷ Due to their different solubilities, *cis*-/*trans*- [Pt{Ph₂P(E)NPh₂}]Cl₂ and *cis*-/*trans*- [Pd{Ph₂P(E)NPh₂}]Cl₂ were successfully separated and characterized by single-crystal X-ray diffraction. The ³¹P{¹H} NMR spectrum showed the ratio of *cis*-/*trans*-[Pt{Ph₂P(E)NPh₂}]Cl₂ to be 2:1 whereas for *cis*-/*trans*- [Pd{Ph₂P(E)NPh₂}]Cl₂ the ratio was 1:5. No further investigations regarding dynamic equilibrium of these complexes were reported.

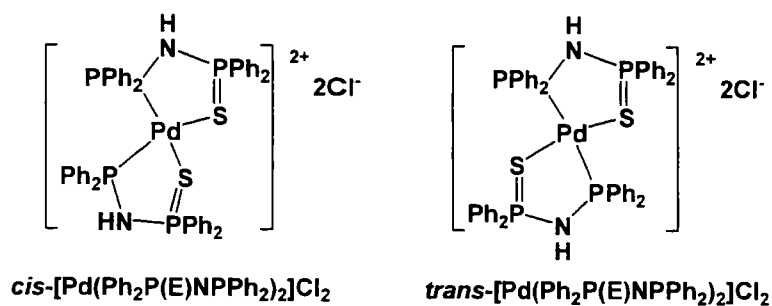
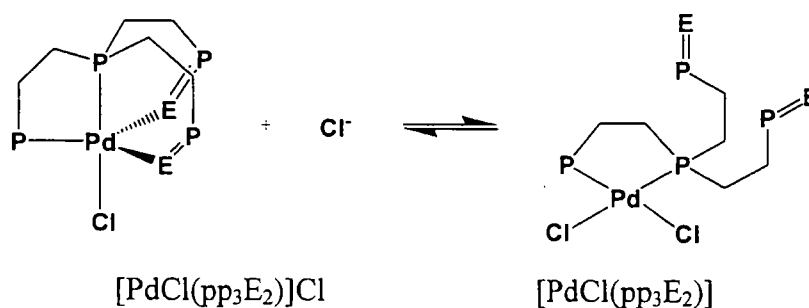


Figure 1. *Cis*- and *trans*- $[Pd\{Ph_2P(E)NPPh_2\}]Cl_2$.¹⁷

Examples of dynamic equilibria were observed for the palladium complexes of tris[2-(diphenylphosphino)ethyl]phosphine disulfides and diselenides. They both showed rapid geometrical equilibria between the five coordinate $[PdCl(pp_3E_2)]Cl$ ($E = S, Se$) species with two bound phosphine chalcogenide group and four-coordinate $[PdCl(pp_3E_2)]$ species with two pendant $P=E$ arms (Scheme 13).¹⁸ The equilibrium constant obtained from $^{31}P\{^1H\}$ NMR studies at 298 K of the sulfide and selenide derivatives are 3.7×10^3 and $5.4 \times 10^2 \text{ mol}^{-1}$, respectively.



Scheme 13. The dynamic equilibrium of $[PdCl(\kappa^4-pp_3E_2)]Cl$ ($X = S, Se$) with $[PdCl_2(\kappa^2-pp_3E_2)]$.

From the observation of the dynamic equilibrium in Scheme 13, we can conclude that phosphine sulfide ligands are labile.

I.4 Properties of phosphine sulfides and their metal complexes

I.4.1 Bond properties

Phosphine oxides are well known derivatives of phosphines. The structure can be written as **A**, **B**, **C** or **D** in Figure 2. **A** indicates only σ donor bond and three lone pairs on the oxygen atom. **B** and **C** show the structures where the d orbitals on the phosphorus atom form double and triple bonds, respectively with the oxygen atom. Another structure, **D** recognizes the polarity of the P–O bond. The multiple P–O bond structures indicate oxygen-phosphorus p-d overlap, leading to donation of the oxygen lone pairs back to the phosphorus d levels. This concept has been discussed by Gilheany¹⁹ via, one σ bond and two π back-bonds (negative hyperconjugation); **E**, one σ bond and three π back-bonds; or **F**, three Ω bonds (banana bonds); **G**.

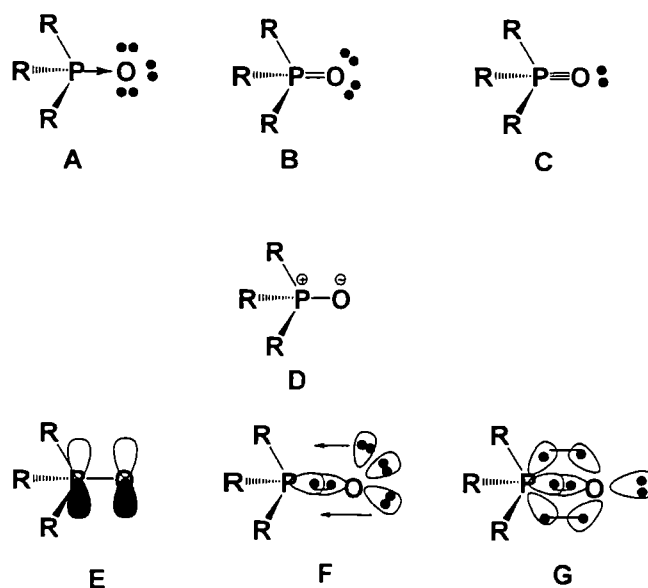
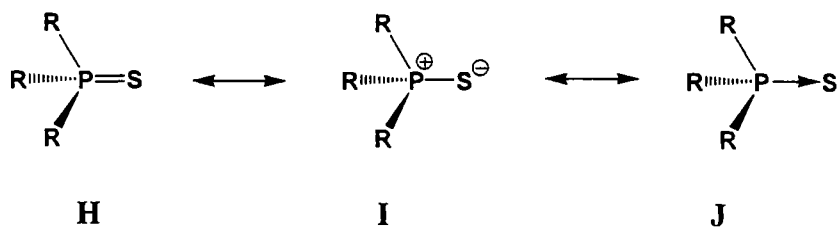


Figure 2. The resonance structures of phosphine oxide.

With respect to phosphine oxides, three models of bonding in phosphine sulfides are shown in Scheme 14. Analysis of the chemical bonding of SPR_3 ($\text{R} = \text{H}, \text{Me}$) was undertaken by using the *Atoms in Molecules Theory* (AIM). The results showed that the model **I** with a polarized σ bond, is the most appropriate description.²⁰



Scheme 14. The resonance structures of phosphine sulfide.

DFT calculations on the Ag(I) and Cu(I) tetramethyldiphosphine disulfide ($S_2P_2Me_4$) complexes were carried out and compared with X-ray structural data.²¹ The free ligands show P=S π bonding, in contrast to the previous interpretation for SPR_3 . Clearly, this issue remains unresolved. Experimental and calculated results agree that the length of the P=S bond is barely affected by coordination, indicating that π bonding is not important in binding to Cu or Ag. This result contrasts with the studies of the palladium complexes of phosphine sulfides reported by Aizawa *et al.*²² Those authors suggested that the P=S π bonding orbital is not very stabilized and consequently, the unoccupied π^* orbital is moderately low in energy and can accept electrons from Pd^0 to stabilize the low oxidation state.

I.4.2 Spectroscopic studies: IR and $^{31}P\{^1H\}$ NMR spectroscopy

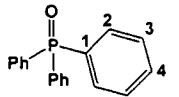
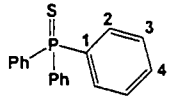
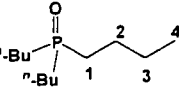
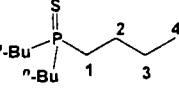
In IR spectroscopy, certain groups of atoms give rise to bands which permit the chemist to obtain useful structural information. This technique has been used to characterize phosphine sulfides and their complexes. The P=S bond stretches in free phosphine sulfides are in the range of 565 – 675 cm^{-1} (Table 1). When phenyl groups are present in the phosphine sulfides, P=S bonds absorb at higher frequencies (stronger bonds). However, the P=S bond in $SPhP_3$ is much weaker than the P=O bond in $OPPh_3$ (*i.e.*, 1200 cm^{-1}).²³ The P=S bonds in $SPhP_3$ complexes of Cr,²⁴ W,²⁴ Au,²⁵ Hg,²⁵ show absorptions in the range of 585 – 628 cm^{-1} . This suggests that the P=S bonds are slightly weaker upon coordination.

Table 1. P=S stretching of phosphine sulfides.

Compound	$SPMe_3$ ²⁴	$SPMe_2Ph$ ²⁴	$SPhP_3$ ²⁴	$SP(p\text{-tol})_3$ ²⁶	$SP(Mes)_3$ ²⁶	$dppmS_2$ ²⁷	$dppmS_2$ ²⁸
$\nu(P=S) / cm^{-1}$	565	590	637	675	626	597	628, 616

The $^{13}\text{C}\{^1\text{H}\}$ and $^{31}\text{P}\{^1\text{H}\}$ NMR resonances of phosphine oxides, phosphine sulfides and related compounds were also studied.²⁹ The $^{13}\text{C}\{^1\text{H}\}$, $^{31}\text{P}\{^1\text{H}\}$ NMR shifts and $^{13}\text{C}-^{31}\text{P}$ coupling constants of OPPh_3 , SPPPh_3 , $\text{OP}(\text{}^n\text{Bu})_3$ and $\text{SP}(\text{}^n\text{Bu})_3$ are given in Table 2. The $^{31}\text{P}\{^1\text{H}\}$ signals for SPPPh_3 (43.2 ppm) is shifted 13.9 ppm downfield compared to OPPh_3 (29.3 ppm).²³ The $^{31}\text{P}\{^1\text{H}\}$ signal of $\text{SP}(\text{}^n\text{Bu})_3$ (46.9 ppm) is shifted only 1.2 ppm downfield compared to that in $\text{OP}(\text{}^n\text{Bu})_3$ (48.1 ppm). When the substituent at the phosphorus atom was changed from Ph to ${}^n\text{Bu}$, the $^{31}\text{P}\{^1\text{H}\}$ signals of $\text{OP}(\text{}^n\text{Bu})_3$ and $\text{SP}(\text{}^n\text{Bu})_3$ are shifted by 17.6 and 4.9 ppm downfield from OPPh_3 and SPPPh_3 respectively. This effect was attributed to the phosphorus center becoming more positively charged or more electronegative when alkyl groups are replaced by phenyl moieties.³⁰ From Table 2, it can be seen that the $^{13}\text{C}\{^1\text{H}\}$ signal of the carbon in position 1 (C_{ipso}), in OPPh_3 and SPPPh_3 , appears at higher field than the carbon in position 2 (*ortho*-) and becomes more shielded in positions 3 (*meta*-) and 4 (*para*-). A similar trend was also observed in both $\text{OP}(\text{}^n\text{Bu})_3$ and $\text{SP}(\text{}^n\text{Bu})_3$. The highest coupling constant is $^1J_{P-C}$ (103.5 Hz, 85.0 Hz, 65.1 Hz and 50.5 Hz for OPPh_3 , SPPPh_3 , $\text{OP}(\text{}^n\text{Bu})_3$ and $\text{SP}(\text{}^n\text{Bu})_3$, respectively). Interestingly, $^3J_{P-C}$ is larger than $^2J_{P-C}$; for example, $^3J_{P-C} = 17.7$ Hz and $^2J_{P-C} = 9.8$ Hz on OPPh_3 .

Table 2. The $^{13}\text{C}\{^1\text{H}\}$ and $^{31}\text{P}\{^1\text{H}\}$ NMR shifts and $^{13}\text{C}-^{31}\text{P}$ coupling constants of EPR_3 (E = O, S; R = Ph, ${}^n\text{Bu}_3$).

Compound	$^{31}\text{P}\{^1\text{H}\}$ (ppm)	$^{13}\text{C}\{^1\text{H}\}$ (ppm)			
		1	2	3	4
	29.3	132.8 (d, $J = 103.5$ Hz)	132.1 (d, $J = 9.8$ Hz)	128.5 (d, $J = 17.7$ Hz)	131.8 (d, $J = 2.4$ Hz)
	43.2	133.0 (d, $J = 85.0$ Hz)	132.2 (d, $J = 10.6$ Hz)	128.5 (d, $J = 12.7$ Hz)	131.5 (d, $J = 2.8$ Hz)
	46.9	27.9 (d, $J = 65.1$ Hz)	23.9 (d, $J = 3.9$ Hz)	24.3 (d, $J = 13.9$ Hz)	13.7 (s)
	48.1	30.8 (d, $J = 50.5$ Hz)	24.5 (d, $J = 3.8$ Hz)	23.9 (d, $J = 15.4$ Hz)	13.6 (s)

The "J" alternation has been noted for phosphorus as well and was discussed in terms of a "W" relationship.³¹

1.4.3 Crystal structure studies

Before understanding the coordination of phosphine sulfides, it is useful to discuss the properties of the phosphine sulfide free ligand. The P=S bond lengths, from single X-ray diffraction studies of phosphine sulfides with variation of the substituent at the para-position at the phenyl (-F, -Cl, -Br, -CH₃) and tricyclohexylphosphine sulfides are given in Table 3. The mean P=S bond length of the phosphine sulfides from the X-ray structures in Table 3 are 1.95 Å which is significantly longer than the P-O bonds in triphenyl phosphine oxide (1.483(2) Å).³² The average P=S (1.955 Å (av) from CSD 2007)² bond length shows more single bond character than P-O; the P-O bond order was deemed to be greater than 2 and the P=S bond order somewhat less than 2.³² However, the P=S bond lengths of phosphine sulfide ligands are dependent on the nature of the substituents on the P atom. Cyclohexyl substituents on the P atom lengthen the P=S bond (1.966(2) Å in SPCy₃ vs. 1.950(3) Å in SPPH₃). Interestingly, increasing the electronegativity of the atom at the para-position (-Br, -Cl, -F) on the phenyl groups does not change the P=S bond length.

Table 3. P=S bond lengths of phosphine sulfides.

	SPPH ₃	SP(<i>p</i> -FC ₆ H ₄) ₃	SP(<i>p</i> -ClC ₆ H ₄) ₃	SP(<i>p</i> -BrC ₆ H ₄) ₃	SP(<i>o</i> -CH ₃ C ₆ H ₄) ₃	SPCy ₃ ³³
P=S (Å)	1.950(3) ³⁴	1.9540(9) ³⁵	1.949(2) ³⁶	1.950(3) ³⁶	1.947(4) ³⁷	1.966(2)

P=S bond lengths and the M-S-P bond angle upon coordination should reveal important information about bonding. If a lone pair on the S atom was used to form a bond, a bent geometry at the S atom (angle <109°) in the phosphine sulfide would be expected. However, if the π electrons are used for bonding, a lengthening of the P=S bond should be observed.

With this information in mind, the X-ray crystal structures of all phosphine sulfide complexes reported in the CSD (2007)² were investigated. The P=S bond lengths and M-S-P bond angles are listed in Table C3 in Appendix C. Summaries of the M-S, P=S bond lengths and M-S-P bond angles in mono-, bi-, and tridentate complexes are given in Tables 4 – 11.

Table 4. Bond lengths and angles of monodentate metal-phosphine sulfide complexes.

Metal	M-S (Å)	P=S (Å)	M-S-P (deg)	Metal	M-S (Å)	P=S (Å)	M-S-P (deg)
Nb ³⁸	2.577(3)	2.028(5)	116.6(2)	Au ³⁹	2.286	2.016	105.62
Nb ⁴⁰	2.573(4)	2.026(6)	115.5(2)	Au ⁴¹	2.277(2)	2.023(3)	103.27(12)
Cr ⁴²	2.510(2)	1.990(3)	112.5(1)	I ⁴³	2.753(2)	1.998(2)	108.78(7)
Mo ⁴⁴	2.460(1)	2.041(1)	111.31(4)	I ⁴⁵	2.656(1)	2.007(1)	107.63(5)
W ⁴⁶	2.6009(7)	2.004(1)	113.24(4)	I ⁴⁵	2.705(3)	2.014(4)	103.63
Fe ⁴⁷	2.361	2.005	109.5	I ⁴⁸	2.809(2)	1.990(3)	98.44(10)
Fe ⁴⁹	2.316	2.014	108.0	I ³⁵	2.787(5)	1.984(5)	100.4(3)
	2.321	2.017			2.792(6)	1.997(6)	102.9(2)
Ru ²³	2.414(3)	1.998	115.7	I ⁵⁰	2.7670(12)	2.0015(14)	109.71(5)
	2.426(3)	2.012	116.1				
Rh ⁵¹	2.307(5)	2.036(9)	104.19(5)	Al ⁵²	2.797(2)	2.028(2)	109.62(8)
	2.036(9)						
Pd ⁵³	2.453(1)	2.009	105.39	Al ⁵⁴	2.506(3)	1.989(2)	108.4(1)
Pd ⁵⁵	2.334	2.014	112.04	In ⁵⁶	2.630(3)	2.003(2)	109.2(1)
					2.663(3)	2.014(3)	117.7(1)
Pd ⁵⁷	2.326(1)	2.013(13)	103.7(1)	In ⁵⁶	2.643(3)	1.998(2)	110.6(1)
					2.653(3)	2.010(3)	113.2(1)
Pt ⁵⁸	2.300(4)	2.026(6)	105.7(2)	Te ⁵⁹	2.6910(12)	1.9994(16)	105.69(6)
					2.7560(6)	2.0062(17)	111.69(6)
Pt ⁵⁸	2.305(3)	2.018(4)	104.05(13)	Te ⁶⁰	2.752(1)	2.008(1)	102.78(4)
*Cu ⁶¹	2.253(5)	1.96667(7)	104.3(3)	Te ⁶⁰	2.772(2)	2.012(2)	110.27(9)
	2.264(5)	2.009(7)	110.3(3)				
Cu ⁶²	2.290	1.975	109.9	Te ⁶⁰	2.787	2.058	101.1
	2.290	1.992	115.6				
Cu ⁶³	2.3444(13)	1.9880(1)	111.28(6)	Te ⁶⁰	2.785(2)	1.999(2)	103.16(17)
*Cu ⁶⁴	2.264(1)	2.024(2)	103.88(6)	Te ⁶⁰	2.753(1)	2.008(1)	105.29
	2.267(2)	2.026(1)	104.72(5)				

* Only the lowest and highest values are presented for disordered structures and/or cases in which there are more than one independent molecule in the asymmetric unit.

Table 5. Bond lengths and angles of κ^2 -C,S bidentate metal-phosphine sulfide complexes.

Metal	M-S (Å)	P=S (Å)	M-S-P (deg)	Metal	M-S (Å)	P=S (Å)	M-S-P (deg)
Zr ¹⁵	2.797(1)	2.005(1)	85.4(4) ^a	Ni ⁶⁵	2.284(2)	1.999(3)	80.0 ^a
Mn ⁶⁶	2.404	1.993	100.0 ^b	Ni ⁶⁷	2.194	2.004	99.0 ^b
Mn ⁶⁸	2.410(1)	1.996(1)	99.64(3) ^b	Pd ⁶⁹	2.284(3)	2.012(4)	106.7(1) ^b
Mn ⁶⁸	2.412(1)	1.993(2)	99.59(6) ^b	Au ⁷⁰	2.361(13) 2.361(13)	1.972(13) 2.031(11)	81.67(5) ^a
Rh ¹³	2.3811(7)	2.01127(8)	81.41(3) ^a	Sn ⁷¹	2.872	1.976	91.89 ^b
Ir ⁷²	2.3653(8)	2.019(1)	82.63(4) ^a				

^a four-membered ring complexes, ^b five-membered ring complexes.

Table 6. Bond lengths and angles of κ^2 -N,S bidentate metal-phosphine sulfide complexes.^a

Metal	M-S (Å)	P=S (Å)	M-S-P (deg)
Pd ⁷³	2.3796(14)	2.0084(18)	94.04
Pd ⁷³	2.3159(13)	2.0306(17)	100.26
	2.3228(13)	2.0187(18)	101.06
Pd ⁷⁴	2.3070(8)	2.026(1)	104.43
Pd ⁷⁴	2.3877(5)	2.0090(6)	98.99
Pd ⁷⁵	2.307(2)	1.991(2)	94.23(8)
In ⁷⁶	2.780(1)	1.986(1)	96.7(4)

^a All complex contain five-membered rings.

Table 7. Bond lengths and angles of κ^2 -P,S bidentate metal-phosphine sulfide complexes.

Metal	M-S (Å)	P=S (Å)	M-S-P (deg)	Metal	M-S (Å)	P=S (Å)	M-S-P (deg)
Cr ¹⁶	2.5056(10)	2.0184(12)	108.45(4)	Pd ⁷⁷	2.3112(9)	2.0220(12)	116.26(4)
W ⁴⁸	2.566(3)	1.990(4)	102.9(2)	Pd ⁷⁸	2.412(2)	2.001(3)	101.49(9)
W ¹⁶	2.602(3)	2.015(2)	104.97(10)	Pd ⁷⁹	2.314(2)	1.991(3)	105.49(11)
W ⁸⁰	2.483(2)	2.019(3)	106.9(1)	Pd ⁷⁹	2.388(2)	1.994(3)	104.64(9)
	2.451(2)	2.027(3)	108.3(1)				
Ru ⁸¹	2.4615(13)	2.0130(17)	105.0	Pd ⁷⁸	2.388(2)	2.003(2)	106.17(8)
Ru ⁸²	2.421	2.016	105.4	Pd ⁷⁸	2.3904(12)	1.995(2)	104.74(6)
Ru ⁸³	2.387	1.973	103.9	Pd ⁸⁴	2.299(1)	2.002(1)	116.8(1)
	2.451	1.977	104.9				
Ru ⁸⁵	2.4239(5)	2.0283(7)	101.4	Pd ⁸⁴	2.266(3)	1.984(5)	97.4(1) ^a
					2.468(3)		
Rh ⁸⁶	2.403(2)	2.005(3)	98.6(1) ^a	Pd ⁸⁴	2.308(3)	1.999(5)	96.9(1) ^a
					2.445(3)		
Rh ⁸⁷	2.402(3)	2.008(3)	117.1	Pd ⁸⁸	2.324(1)	2.017(1)	93.1(5)
Rh ⁸⁹	2.357(2)	2.027(2)	106.5	Pd ⁸⁸	2.481(1)	1.987(2)	92.4(1)
Rh ⁹⁰	2.349(2)	2.026(3)	105.2(4)	Pd ⁸⁵	2.3371(6)	2.0288(8)	105.04
Ir ⁸⁹	2.4194(9)	2.0126(13)	105.4	Pd ⁹¹	2.3187(10)	2.0092(12)	101.85(5)
					2.3530(10)	2.0077(13)	104.43(4)
Ir ⁸⁹	2.4182(13)	2.0138	102.25	Pd ⁹²	2.3432(4)	2.027(2)	108.19(7)
Ir ⁹³	2.416(2)	2.009(3)	105.7	Pd ⁹⁴	2.286	2.018	103.65
Ir ⁹⁰	2.324(3)	2.034(5)	107.2(2)	Cu ⁹⁵	2.392(3)	1.975(3)	98.96
					2.398(3)	1.981(3)	99.62
Pd ⁹⁶	2.331(2)	2.007(3)	101.3(1)	Ag ⁹⁷	2.4574(9)	1.9920(10)	99.03(4)
Pd ⁹⁸	2.350	2.013	107.6	Hg ⁹⁹	2.760(4)	1.968(6)	99.3(2)

^a five-membered ring complexes.

Table 8. Bond lengths and angles of κ^2 -S,S bidentate metal-phosphine sulfide complexes.

Metal	M-S (Å)	P=S (Å)	M-S-P (deg)	Metal	M-S (Å)	P=S (Å)	M-S-P (deg)
Li ¹⁰⁰	2.440	1.995(1)	106.23	Cu ¹⁰¹	2.140(5)	1.985(5)	100.8(2)
	2.461	1.987(1)	106.97		2.144(5)	2.001(4)	105.5(2)
Mn ¹⁰²	2.410	1.996	99.2	Cu ¹⁰³	2.231(4)	1.990(3)	117.5(2)
					2.235(2)	1.995(4)	117.8(1)
Rh ¹⁰⁴	2.397(2)	1.996(2)	101.06(9)	Cu ¹⁰⁵	2.287(4)	1.976(5)	73.7(1)
	2.402(3)	1.999(2)	105.10(8)		2.376(4)	1.991(5)	106.8(2)
					2.459(4)		110.1(2)
Rh ¹⁰⁴	2.403(5)	2.001(6)	102.4(2)	Cu ¹⁰⁶	2.296(2)	1.971(2)	99.56(10)
	2.417(5)	1.994(6)	106.6(2)			1.972(3)	100.1(1)
Ir ¹⁰⁷	2.389(2)	1.998(2)	112.3(1)	Cu ¹⁰⁸	2.307(1)	1.999(1)	102.47(5)
	2.408(2)	2.003(2)	117.3(1)				
Ni ¹⁰⁹	2.197(2)	2.001(3)	105.4(1)	Ag ¹¹⁰	2.583	1.960	96.06
					2.635	1.977	101.16
Pd ⁷⁴	2.364(1)	2.005(1)	99.6	*Ag ¹¹¹	2.501	1.677	90.13
					2.770	1.975	100.77
							105.57
Pd ¹¹²	2.3858(14)	2.0026(18)	100.2	Ag ¹¹³	2.5919(12)	1.967	99.94
	2.4069(13)	2.0064(17)	105.8		2.6012(11)	1.971	106.36

Table 8 (continued)

Metal	M-S (Å)	P=S (Å)	M-S-P (deg)	Metal	M-S (Å)	P=S (Å)	M-S-P (deg)
Pd ¹¹²	2.3878(10)	1.9994(14)	108.3	*Ag ¹¹⁴	2.530(2)	1.972(2)	103.95(9)
	2.3960(10)	1.9966(14)	109.5		2.801(2)	1.997(2)	106.01(9) 107.74
Pd ¹¹⁵	2.490(2)	1.996(2)	108.6(1)	Hg ⁹⁹	2.760(4)	1.968(6)	99.3(2)
Pd ¹¹⁶	2.314	2.017	102.50	Hg ¹¹⁷	2.552(2)	1.990(4)	104.79(11)
					2.678(2)	1.999(3)	108.96(11)
Cu ⁶²	2.294	1.946	108.04	In ¹¹⁸	2.532	2.011	111.11
		1.957	106.77				
Cu ¹¹⁹	2.5263(13)	1.9630(13)	103.52	Pb ¹²⁰	2.885(12)	1.973(13)	117.44
					3.151(9)		118.05
Cu ¹²¹	2.259(2)	1.970(2)	91.52(8)	Te ¹²²	2.633(4)	1.984(4)	109.3(2)
	2.321(2)	1.974(3)	95.68(8)		2.891(3)	1.950(4)	111.7(2)
Cu ¹²³	2.247	1.980	102.15	*Te ⁵⁹	2.5311(8)	1.9719(10)	94.19(4)
	2.259	1.985	106.37		2.9372(12)	2.0604(10)	111.7(2)
*Cu ¹²⁴	2.304	1.969	98.75	Te ⁵⁹	2.6759(16)	2.0134(16)	97.85(6)
	2.426	1.968	104.27		2.6851(12)	2.0061(16)	97.03(6)
Cu ¹²⁵	2.303(3)	1.985(3)	106.57(11)				
	2.305(3)		109.88(10)				

* Only the lowest and highest values are presented for disordered structures and/or cases in which there are more than one independent molecule in the asymmetric unit.

Table 9. Bond lengths and angles of κ^3 -S,P,S tridentate metal-phosphine sulfide complexes.

Metal	M-S (Å)	P=S (Å)	M-S-P (deg)	Metal	M-S (Å)	P=S (Å)	M-S-P (deg)
Rh ¹²⁶	2.3197(6)	2.0219(7)	101.34(3)	Pd ¹²⁷	2.3250(8)	2.029(1)	101.81
	2.3213(6)	2.0235(8)	107.73(3)		2.3275(8)	2.033(1)	104.62
Rh ¹²⁶	2.5040(8)	2.0135(8)	101.33(3)	Pd ¹²⁷	2.313(1)	2.033(2)	101.89
	2.4193(7)	2.025(1)	106.94(3)		2.328(1)		102.93
Rh ¹²⁸	2.374(2)	2.041(3)	103.1(1)	Pd ¹²⁹	2.317(1)	2.036(1)	104.64
	2.442(2)	2.016(3)	107.9(1)		2.3277(8)		106.51
Rh ¹²⁸	2.3641(8)	2.017(1)	108.26(4)	Pd ¹³⁰	2.317(2)	2.031(4)	101.82
	2.4462(8)	2.041(1)			2.321(2)	2.0337(7)	104.84
Ir ⁹⁰	2.438(3)	2.001(4)	100.2(1)	*Cu ⁷¹	2.355	2.003	100.56
	2.574(3)	1.977(4)	105.0(1)		2.388		102.43
Ir ¹³¹	2.4717(6)	2.0127(8)	112.3	Cu ⁷¹	2.3621(6)	2.0072(8)	94.31
	2.4514(5)	2.0140(8)	117.3				
Ir ¹³²	2.397(4)	2.030(6)	97.6	Cu ⁷¹	2.4119(9)	1.9987(9)	99.77(4)
	2.405(5)	2.033(6)	103.9		2.4280(13)	2.0052(11)	102.09(3)
Ni ¹²⁷	2.185(1)	2.039(2)	104.3	Cu ⁷¹	2.3694(5)	2.0021(6)	102.03
	2.194(1)	2.045(2)	106.7		2.4321(6)		103.87
Pd ¹²⁷	2.310(1)	2.1018(2)	94.24	Au ⁷¹	2.5919(12)	1.967	99.94
	2.353(1)	2.039(2)	108.19		2.6012(11)	1.971	106.36

Table 10. Bond lengths and angles of κ^3 -S,C,S tridentate metal-phosphine sulfide complexes.

Metal	M-S (Å)	P=S (Å)	M-S-P (deg)	Metal	M-S (Å)	P=S (Å)	M-S-P (deg)
Zr ¹¹	2.7499(6)	2.019(1)	81	^a Pt ¹³³	2.299(5)	1.996(7)	97.5(3)
		2.010(8)			2.307(5)	2.002(7)	99.3(3)
Zr ¹¹	2.6813(8)	2.025(1)	82	*Sm ¹³⁴	2.2816(2)	2.034	79.34
	2.6912(8)	2.020(1)			2.851(2)	2.042	81.66
Zr ¹¹	2.6813(8)	2.025(1)	81	*Sm ¹³⁴	2.891(1)	2.019	80.38
	2.6912(8)	2.020(1)			2.922(11)	2.020	81.60
Ru ¹³⁵	2.4739(5)	2.0269(7)	79.0	Tm ¹³⁶	2.788(2)	2.028	79.12
	2.4843(5)	2.0206(6)			2.747(2)	2.037	80.30
*Ru ¹³⁵	2.620	1.986	72.3	Tm ¹³⁶	2.777(1)	2.024(2)	80.16
	2.504	1.996	90.0		2.822(1)	2.030(2)	80.62
Pd ¹³⁷	2.3741(6)	2.0424(8)	78.58				
	2.3677(6)	2.0451(7)	79.10				
^a Pd ¹³³	2.312(4)	1.955(5)	97.9(2)				
	2.321(4)	2.007(5)	98.8(2)				

* Only the lowest and highest values are presented for disordered structures and/or cases in which there are more than one independent molecule in the asymmetric unit.; ^a [5,5] bicyclic complexes whereas others are [4,4].

Table 11. Bond lengths and angles of other tridentate metal-phosphine sulfide complexes.

Chelate type	Metal	M-S (Å)	P=S (Å)	M-S-P (deg)
κ^3 -N,S,N	Mo ¹³⁸	2.6242(14)	1.973(2)	85.43(5)
κ^3 -C,C,S	Co ¹³⁹	2.350	1.980	93.0
κ^3 -O,C,S	Sn ^{140, 141}	2.6295(9)	2.006(1)	96.38
κ^3 -S,N,S	Ni ¹⁴²	2.402(1)	1.980(2)	103.3
		2.481(1)	1.981(2)	101.6
	Sn ¹⁴³	2.514(1)	1.989(2)	98.72
		2.503(1)	1.992(2)	99.20

Pd-S bond lengths and Pd-S-P bond angles in phosphine sulfide complexes of palladium are given in Table 12.

Table 12. Pd-S bond lengths and Pd-S-P bond angles in phosphine sulfide palladium complexes.

Chelate types	Pd-S (Å)	Pd-S-P (deg)
κ^1 -S	2.33 – 2.45	103.7 – 112.0
κ^2 -C,S	2.28	106.7
κ^2 -N,S	2.31 – 2.39	94.0 – 104.4
κ^2 -P,S	2.26 – 2.48 *	92.4 – 116.8
κ^2 -S,S	2.31 – 2.36	99.6 – 105.8
κ^3 -S,P,S	2.31 – 2.32	94.2 – 108.2
κ^3 -S,C,S	2.30 – 2.37	78.6 – 98.8

* Long bond length in a disordered structure.

From Tables 4 – 12, we can make following general observations, with exceptions in some cases which will be discussed later:

i. Surprisingly, the P=S bond lengths in all phosphine sulfide complexes (monodentate, bidentate and tridentate) are in the narrow range of 1.97 – 2.05 Å (in free ligands 1.95 Å (av)), which means that the P=S bond order is slightly smaller in the complexes than in the free ligands and is also relatively independent of the metal center.

ii. If restricted to the palladium complexes, the Pd–S bond lengths in the phosphine sulfide complexes fall in a relatively narrow range of 2.30 – 2.39 Å. The monocarbonyl phosphine sulfide palladium complex shown in Figure 3 has a significantly longer Pd–S bond (2.45 Å) than in other complexes, but this may be caused by the *trans*-influence of the σ -carbon ligand *trans*- to the S=P bond.

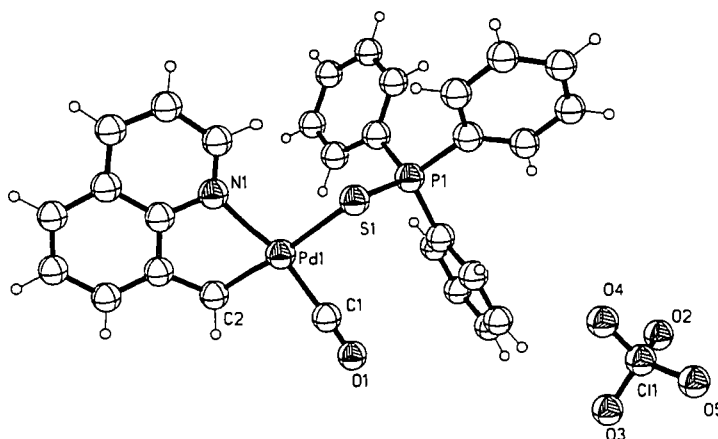


Figure 3. A phosphine sulfide monocarbonyl palladium complex.⁵³

iii. The M–S–P bond angles vary from 72.3 – 117.2° (120.5° including lanthanides). These suggest that the geometries of the sulfur atoms are flexible. The complexes which show a small M–S–P bond angle are normally found in the cyclometalated metal phosphine sulfides with small ring sizes (four membered rings 72.3 – 85.4°). The smallest M–S–P angle for a transition metal complex was found in the four membered ring of the cyclometallated bis(thiophosphinoyl)methylene ruthenium complex (Figure 4)¹³⁴ and the widest was found in the seven membered ring complex [RhCl(Cp*)(*o*-Ph₂PNHC₆H₄P(S)Ph₂-P,S)]ClO₄ (Figure 4).⁸⁷ For the phosphine sulfide complexes of lanthanides, the widest M–S–P bond angles was observed in cerium complexes of bis(diphenylphosphinine sulfide), being 120.5°

(Figure 5).¹⁴⁴ Small ring [4,4] and [5,5] bicyclic products of the η^3 -S,C,S phosphine sulfide type show small M–S–P angles of 72.3 – 99.3°.

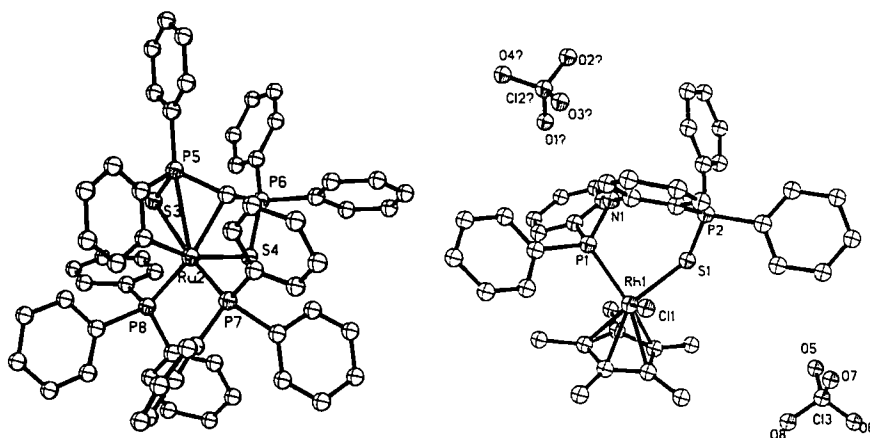


Figure 4. Bis(thiophosphinoyl)methylene ruthenium (left),¹³⁴ and $[\text{RhCl}(\text{Cp}^*)(o\text{Ph}_2\text{PNHC}_6\text{H}_4\text{P}(\text{S})\text{Ph}_2\text{-P,S})]\text{ClO}_4$ (right).⁸⁷

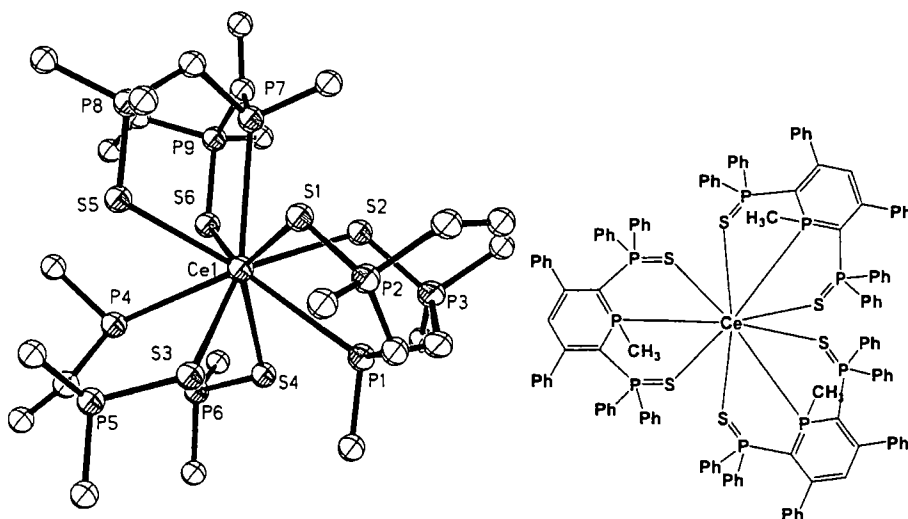


Figure 5. Tris(1-methyl-3,5-diphenyl-2,6-bis(diphenylphosphine sulfide)-14-phosphinine)-cerium(III). Phenyl rings are omitted for clarity.¹⁴⁴

In monodentate phosphine sulfide complexes, the smallest M–S–P angle was found to be 98.44(10)° in the 1,3-diphosphapropene sulfide iodine adduct (Figure 6)⁴⁸ but, in general, the angles are not far from the tetrahedral angle of *ca.* 109°.

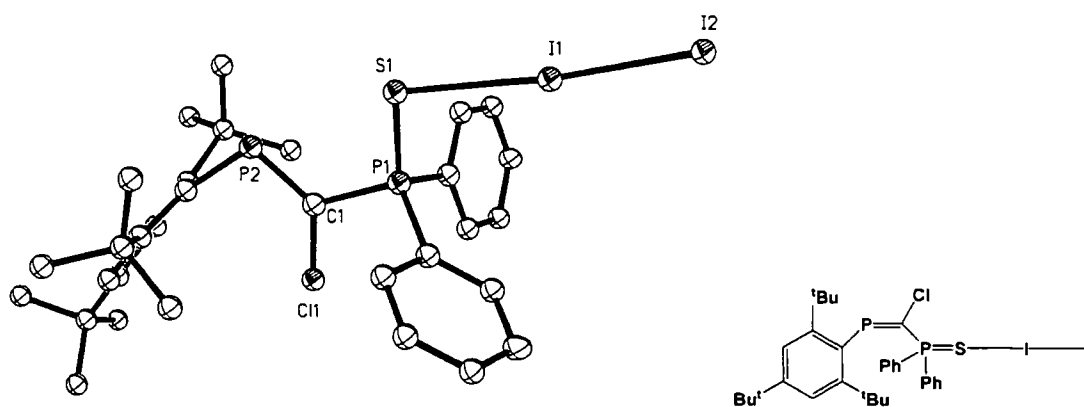


Figure 6. 1,3-Diphosphapropene sulfide iodine adduct.⁴⁸

Small M–S–P angles were observed in the complexes of κ^2 -C,S bidentate phosphine sulfides (81 – 106.7°) and κ^2 -N,S bidentate phosphine sulfides (94 – 105°). However, these small angles no doubt result from the small ring size in these complexes (four- or five-membered rings). In five-membered ring complexes, the M–S–P angles were found to range from 85.43(5)° to 117.3°. The smallest angles observed were in the five-membered ring in $\text{Mo}(\text{CO})_4(\text{SPPh}(\text{py})_2-\kappa^3\text{-N,S,N})$ ¹³⁸ (Figure 7). In this molecule, the Mo–N bond lengths are 2.274 and 2.281 Å. They may increase ring strain which then causes the Mo–S–P angle to be as small as in four-membered ring complexes.

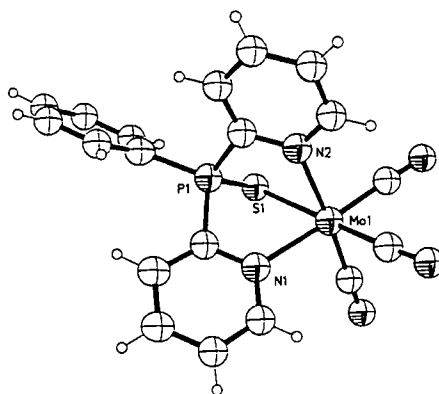


Figure 7. Molecular structure of $[\text{Mo}(\text{CO})_4(\text{SPPH}(\text{py})_2-\kappa^3\text{-N,S,N})]$.¹³⁸

The palladium complexes of 4,5-bis(diphenylthiophosphinoyl)-1,2,3-triazole in the (κ^3 -methallyl)-palladium complex⁷³ and the related bis(chelate) complex show a significant difference in M–S–P angles (94.04° in the (κ^3 -methallyl)-palladium complex, and 100.26° and 101.06° in the bis(chelate) (Figure 8).

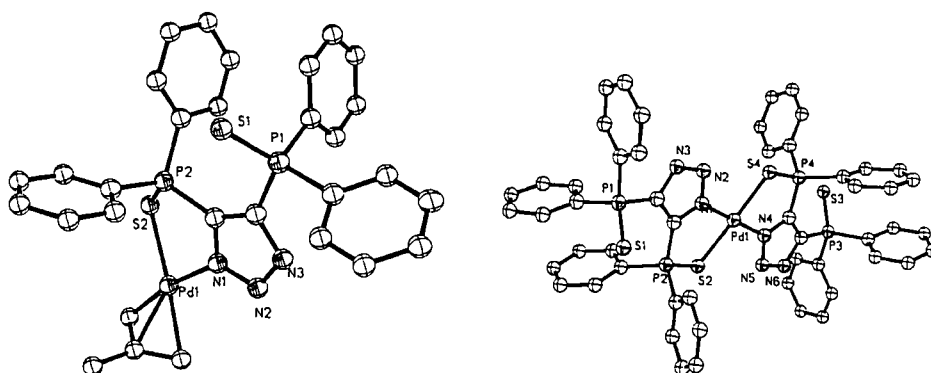


Figure 8. 4,5-Bis(diphenylthiophosphinoyl)-1,2,3-triazole(κ^3 -methallyl)-palladium (left)⁷³ and bis(4,5-bis(diphenylthiophosphinoyl)-1,2,3-triazole)-palladium (right).⁷³

In six-membered ring complexes, it was surprising that some show small M–S–P angles. For example, the M–S–P angle in the palladium chloride complex of 3,4-dimethyl-1-phenylphosphole is only $93.1(5)^\circ$ (Figure 9).⁸⁸

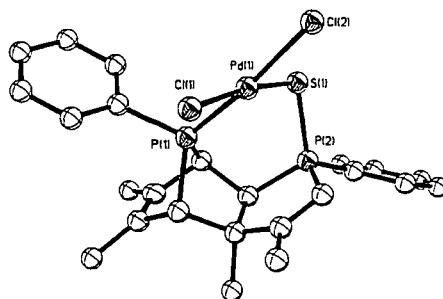


Figure 9. (3,4-Dimethyl-1-phenylphosphole)palladium dichloride.⁸⁸

The M–S–P angle can also be influenced by the nature of halogen atoms in the complexes. For example, the Cu–S–P angles in the six membered rings of $\text{CuCl}(\text{dppmS}_2)$ ¹²¹ are $91.52(8)^\circ$ and $95.68(8)^\circ$, whereas in $\text{CuI}(\text{dppmS}_2)$, the angles are 102.15° and 106.37° .¹²³ The structures of $\text{CuCl}(\text{dppmS}_2)$ and $\text{CuI}(\text{dppmS}_2)$ are shown in Figure 10.

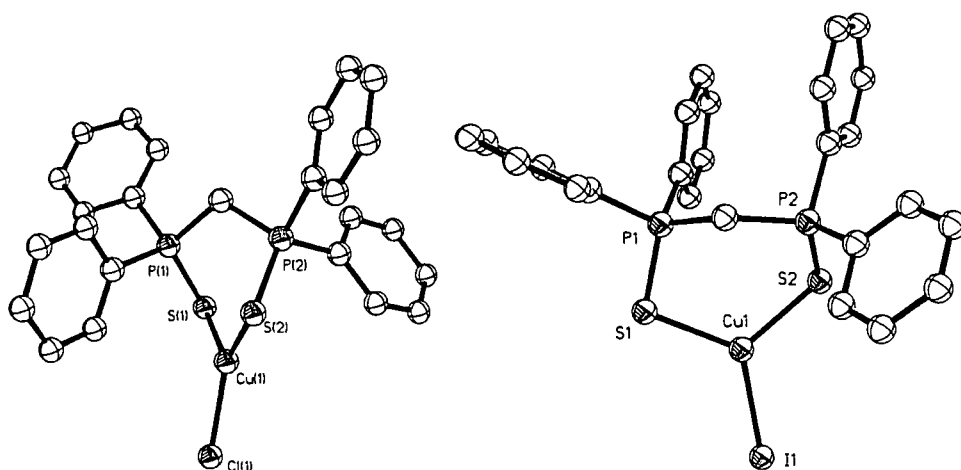


Figure 10. $\text{CuCl}(\text{dppmS}_2)^{121}$ (left) and $\text{CuI}(\text{dppmS}_2)$ (right).¹²³

iv. Metal complexes of phosphinine and bis(diphenylphosphinine sulfide) ($\kappa^3\text{-S,P,S}$) ligands (Figure 11) show slightly longer P–S bond lengths (2.00 – 2.05 Å). The delocalization of electrons may be responsible for the lengthening of the P–S bonds without affecting the M–S–P bond angles. These types of ligands are reported to be highly flexible as they allow any potential geometry at the metal centers to be stabilized (square planar, octahedral, *etc.*).¹² However, there are two complexes which show significantly smaller M–S–P angles than observed for other ligands in this type (see Figure 12).

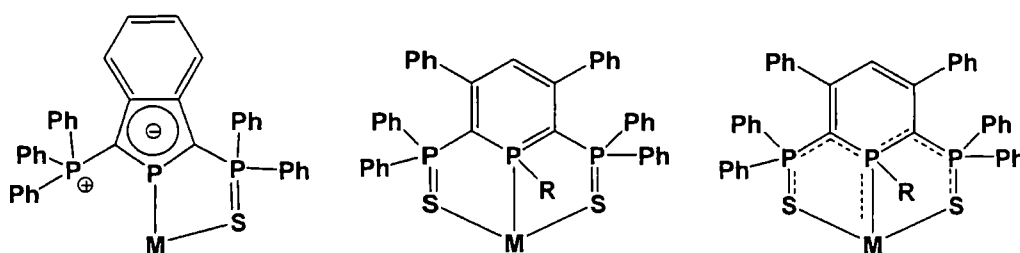
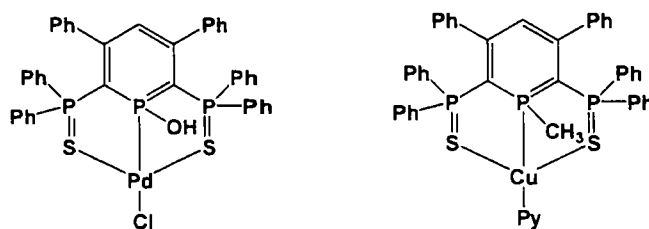


Figure 11. Phosphinine (left), bis(diphenylphosphinine sulfide) (middle) and resonance structure (right).

M-S-P ($^{\circ}$)

94.24, 108.19

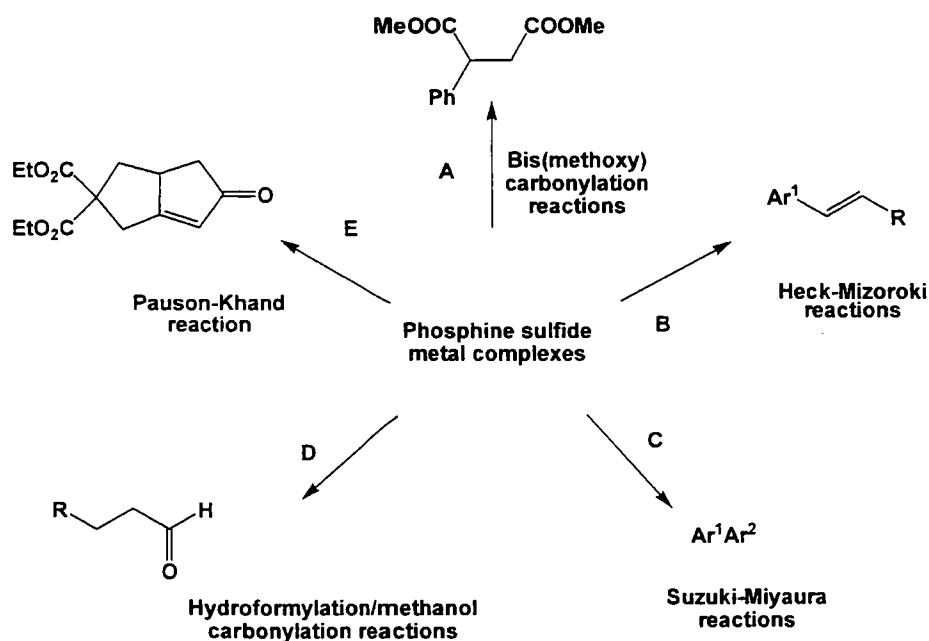
94.31

Figure 12. Bis(diphenylphosphinine sulfide) palladium¹²⁷ and copper complexes.⁷¹

In order to classify the properties of phosphine sulfides by using the M-S-P bond angle, it may be worth comparing them with M-O-P bond angles. Phosphine oxide complexes show a wide range of M-O-P bond angles (*ca.* 140-180 $^{\circ}$), with only two exceptions (134 and 123 $^{\circ}$).⁵² This range is in complete contrast to the range of M-S-P bond angles in phosphine sulfides, which are substantially smaller (72.3 – 117 $^{\circ}$). Furthermore, the P=S bond lengths in phosphine sulfide complexes are only slightly lengthened on coordination, suggesting little change in P=S bonding.

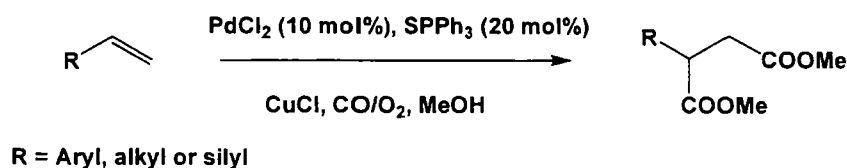
I.5 Applications of phosphine sulfide complexes

Phosphine sulfides are used as ligands for catalysis in organic synthesis as summarized in Scheme 15.



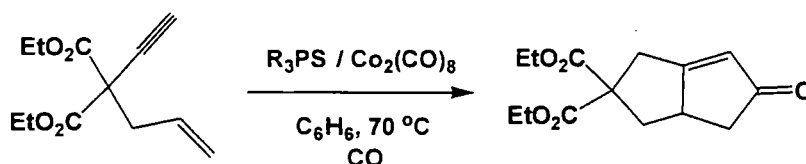
Scheme 15. Applications of phosphine sulfide metal complexes.

Hashimoto *et al.* demonstrated that using PdCl₂ with SPPH₃ for the palladium-catalyzed bis-(methoxycarbonylation) of olefins gave the products in yields as high as 90 %. (Scheme 16).¹⁴⁵ They found that no reaction occurred when PPh₃ was used as the ligand, but 16, 80 and 36 % yields were obtained using SePPh₃, OPPh₃ or no ligand, respectively.



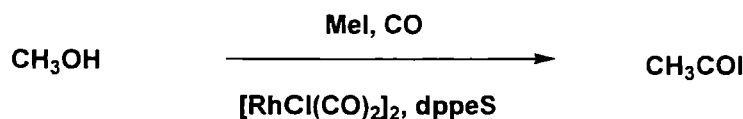
Scheme 16. Bis(methoxycarbonylation) reaction using SPPH₃ ligand as ligand.¹⁴⁵

Various phosphine sulfides were also used as additives in the cobalt-catalyzed Pauson-Khand reaction (Scheme 17).¹⁴⁶ Yields obtained were 48, 55, 72 and 79% using a 1:4 ratio of Co₂(CO)₈ to ligand where ligands are OPPh₃, SPPH₃, SPBu₃ and SP(NMe)₃, respectively. Furthermore, up to 90% yield was obtained using a 1:6 ratio of Co₂(CO)₈ to SPBu₃.



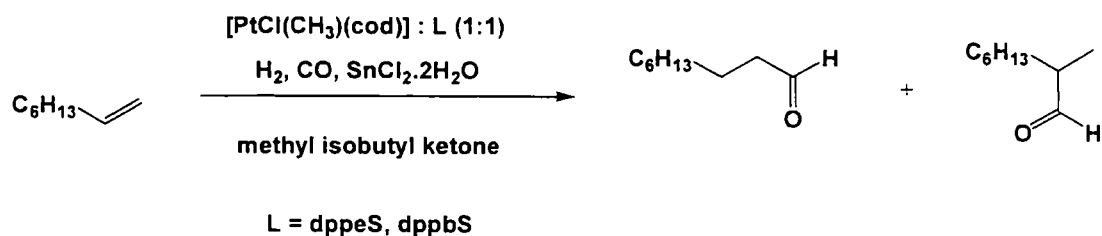
Scheme 17. Cobalt-catalyzed Pauson-Khand reaction using a phosphine sulfide as ligand.¹⁴⁶

Backer and co-workers found that the methanol carbonylation reaction is eight times faster than the classic Monsanto catalyst when the reaction was catalyzed by complexes of phosphine sulfides with rhodium.⁹³ The reaction also works well when the iridium complex was used (Scheme 18).



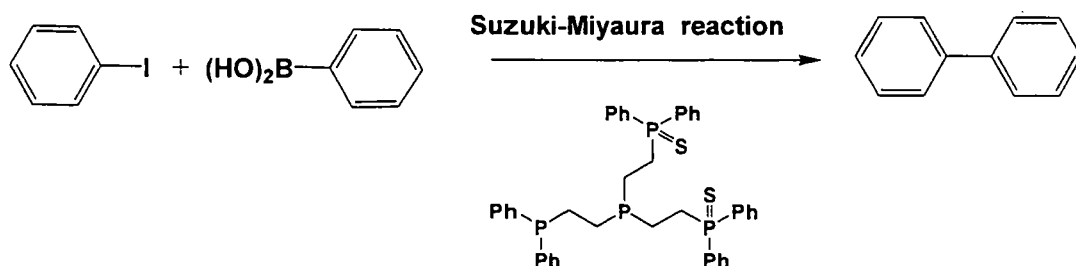
Scheme 18. Methanol carbonylation catalyzed by a dppeS rhodium complex.⁹³

Platinum phosphine sulfide complexes, for example, dppmS, dppeS and dpppS were used as catalyst precursors for the hydroformylation of 1-octene (Scheme 19) in the presence of five equivalents of $\text{SnCl}_2 \cdot 2\text{H}_2\text{O}$ as co-catalyst, in methyl isobutyl ketone as solvent. The best selectivity (n-nonanal/total aldehyde) is 89% at 52% conversion.¹⁴⁷



Scheme 19. The hydroformylation of 1-octene with platinum phosphine sulfide complexes.¹⁴⁷

The Suzuki-Miyaura reaction of iodobenzene and phenyl boronic acid in DMF and K_2CO_3 with a palladium tris(phosphine) disulfide dichloride complex to give the cross-coupling product was demonstrated by Aizawa and co-workers (Scheme 20).¹⁸



Scheme 20. The Suzuki-Miyaura reaction with a palladium tris(phosphine) disulfide complex as catalyst.

Recently, palladacyclic complexes containing phosphine sulfides (Figure 13) were shown to give quantitative yields of cross-coupled products in the Suzuki-Miyaura reaction of aryl bromides with phenylboronic acid in the presence of K_3PO_4 and Bu_4NBr in DMF, using catalyst loadings of 0.1 – 3 mol %.⁵

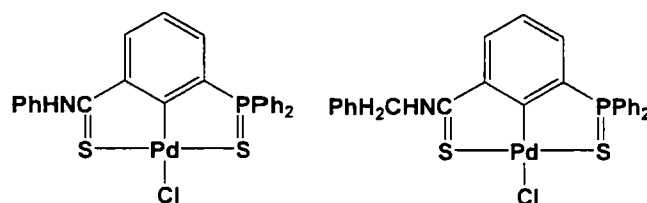
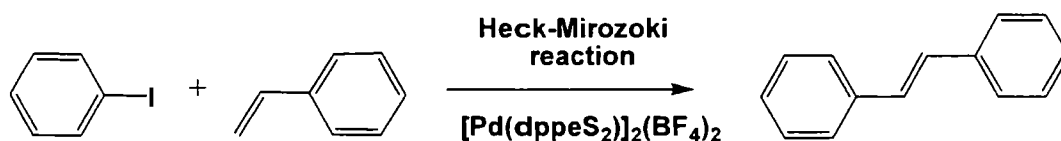


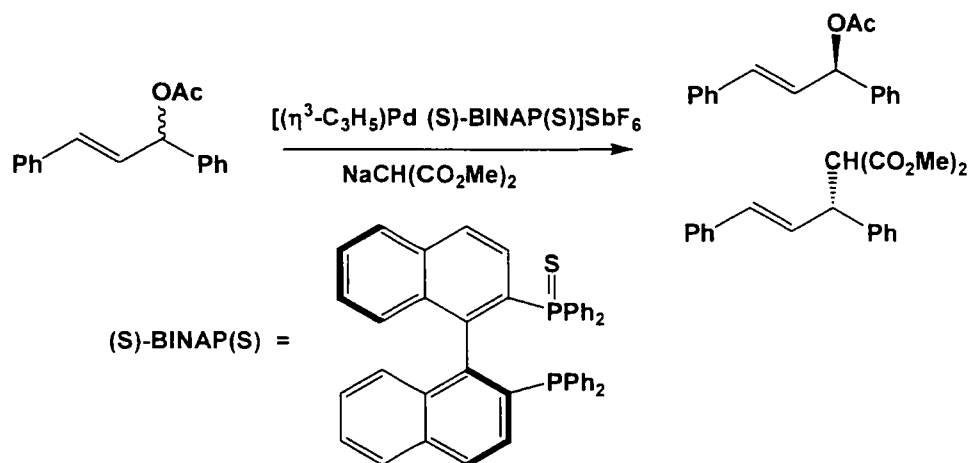
Figure 13. Palladacyclic pincer complexes of phosphine sulfides used in the Suzuki-Miyaura reactions.⁵

In a Heck-Mizoroki reaction (Scheme 21),¹⁴⁸ iodobenzene and styrene reacted in DMF and NEt_3 in the presence of $[\text{Pd}(\text{dppeS}_2)](\text{BF}_4)_2$ to give the stilbene coupling product which was identified by the proton signal in the *ortho*-position.



Scheme 21. The Heck-Mizoroki reaction with palladium catalysts and dppeS_2 as ligand.

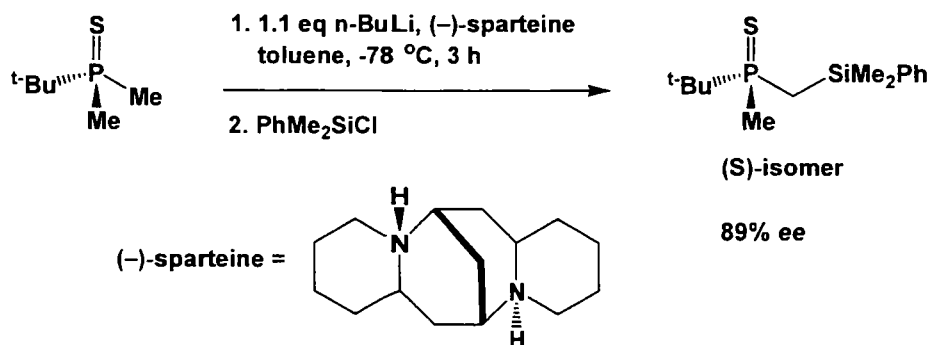
Asymmetric synthesis using chiral phosphine sulfide ligands has also been reported. Thus, palladium complexes of the mono-sulfide of the chiral BINAP ligand show a high degree of selectivity for the branched regioisomer in allylic alkylations giving 80% *ee* (Scheme 22).¹⁴⁹



Scheme 22. Allylic alkylations using a chiral P,S ligand.¹⁴⁹

Moreover, palladium complexes of phosphine sulfides also reported good catalytic activity in the copolymerization of ethylene and carbon monoxide.¹⁵⁰

Recently, a phosphine sulfide underwent asymmetric deprotonation using BuLi and a catalytic amount of (-)-sparteine to give, after treatment with PhMe₂SiCl, the P-stereogenic product. Yields of asymmetric product up to 90% and 89% ee with 1.1 equivalent of *n*-BuLi and 0.05 equivalent of (-)-sparteine in toluene were obtained (Scheme 23).¹⁵¹



Scheme 23. The asymmetric lithiation-silylation of a phosphine sulfide.¹⁵¹

Triisobutyl phosphine sulfides, as functional side chains in polymers (Figure 14), were found to bind Au(III) and Pd(II) selectively which may be developed to aid the recovery of precious metals.¹⁵²

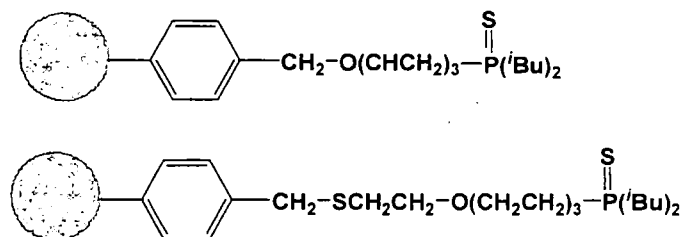


Figure 14. Polymer supported with phosphine sulfide side chain.¹⁵²

Recently, new fluorescent molecular sensors for Hg²⁺ based on phosphine sulfide derivatives, which exhibit high sensitivity and selectivity have been reported (Figure 15).¹⁵³

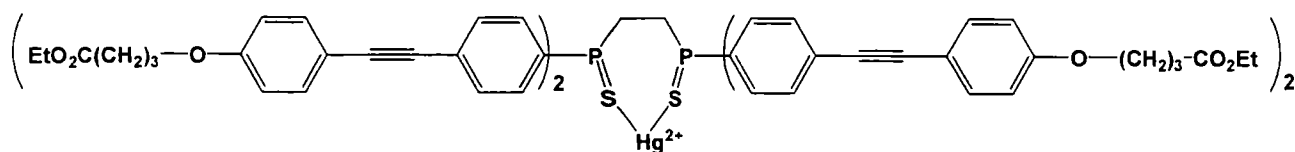


Figure 15. Fluorescent molecular sensor for Hg^{2+} .¹⁵³

To date, several complexes of phosphine mono- and disulfides have been synthesized, but there are only a limited number of studies in the literature related to palladium complexes. Due to their high stability to oxidation, easy preparation, as well as a potentially wide range of applications, it became apparent to us that the coordination chemistry of phosphine sulfides would be a fruitful investigation.

In this study, we will restrict ourselves to the case of bis(phosphines). The ligands are based on bis(diphenylphosphino)methane (dppm), 1,2-bis(diphenylphosphino)ethane (dppe), 1,2-bis(cyclohexylphosphino)ethane (dcpe), 1,4-bis(diphenylphosphino)butane (dppb) and 1,1'-bis(diphenylphosphino)ferrocene (dppf). We chose these ligands as they show; (i) variation in the alkyl chain length: $\text{PPh}_2(\text{CH}_2)_n\text{PPh}_2$ ($n = 1, 2, 4$ for dppm, dppe and dppb, respectively) and dppf (contains a ferrocene backbone); (ii) variation in the substituents on the phosphorus atoms: cyclohexyl (Cy) moieties in dcpe and phenyl (Ph) ones in the other bis(phosphine).

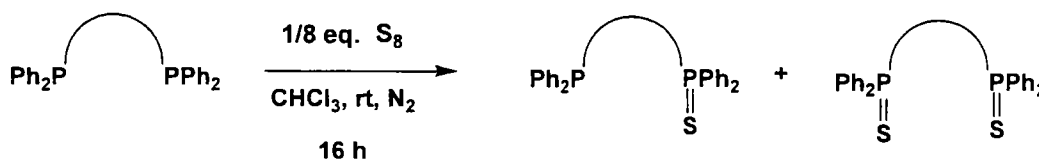
The objectives of this study are:

1. synthesis of the bis(phosphine) monosulfide and disulfide ligands including full characterization;
2. synthesis of the palladium complexes of bis(phosphine) monosulfides and disulfides, both neutral and cationic, with full characterization and investigation of their properties;
3. investigation of their catalytic activity in the oxidative homo-coupling of phenylacetylene.

II. Results and Discussion

II.1 Synthesis and characterization of ligands

The bis(diphenylphosphino) monosulfide ligands bis(diphenylphosphino)methane monosulfide **dppmS**, 1,2-bis(diphenylphosphino)ethane monosulfide **dppeS**, 1,4-bis(diphenylphosphino)butane monosulfide **dppbS** and 1,1'-bis(diphenylphosphino)ferrocene monosulfide **dppfS** were prepared from the reaction of one equivalent of the respective bis(phosphine) ligand with one equivalent of elemental sulfur in CHCl_3 under an inert atmosphere at room temperature (Scheme 24). This resulted in mixtures of the appropriate bis(phosphine) monosulfides, bis(phosphine) disulfides and bis(phosphine) starting materials, which were separated by column chromatography to yield the monosulfides as pure products, along with the other components. The ratio of bis(phosphine) to bis(phosphine) monosulfide to bis(phosphine) disulfide was 1:2:1 in all cases.



Scheme 24. The synthesis of the bis(phosphine) monosulfides and disulfides.

The $^{31}\text{P}\{^1\text{H}\}$ NMR signal of the P(S) atoms in the bis(phosphine) monosulfides are shifted to significantly lower fields than the P atoms in the bis(phosphines) (Figure 16). The signals for **dppmS** and **dppeS** appeared as AB spin systems with shifts of $\delta_{\text{P}} = -27.07$ and $\delta_{\text{PS}} = 41.29$ ppm for **dppmS** and $\delta_{\text{P}} = -11.89$ and $\delta_{\text{PS}} = 45.36$ ppm for **dppeS** and $J_{\text{P-P}}$ coupling constants of 76 Hz for **dppmS** and 50 Hz for **dppeS**. The $J_{\text{P-P}}$ coupling constants are strongly related to the distance between the two phosphorus nuclei. No coupling was observed in **dppbS** and **dppfS**, which have well-separated P atoms.

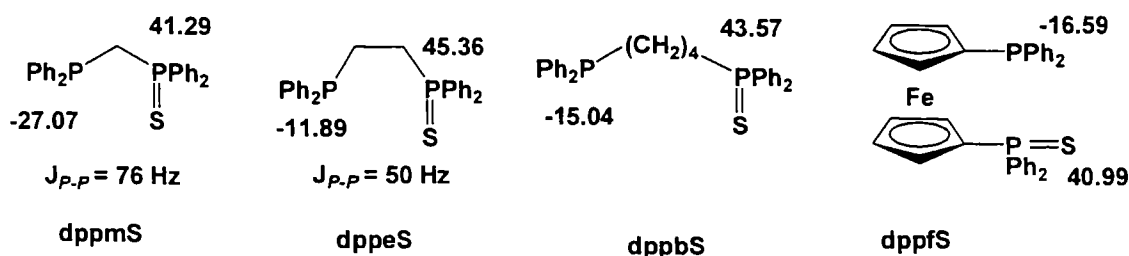
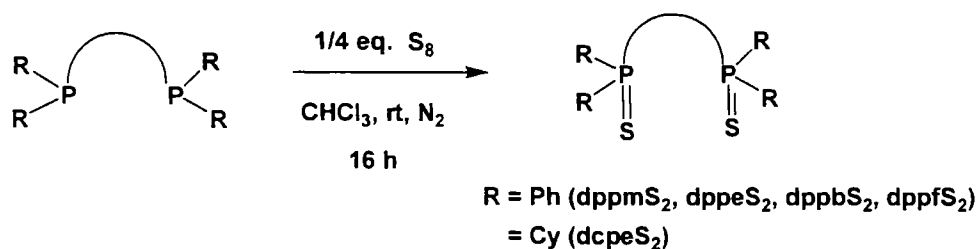


Figure 16. The $^{31}\text{P}\{^1\text{H}\}$ NMR chemical shifts of the bis(phosphine) monosulfides.

The bis(diphenylphosphino) disulfide ligands bis(diphenyl(phosphino)methane) disulfide **dppmS₂**, 1,2-bis(diphenylphosphino)ethane disulfide **dppeS₂**, 1,4-bis(diphenylphosphino)butane disulfide **dppbS₂**, 1,2-bis(dicyclohexylphosphino)ethane **dcpeS₂** and 1,1'-bis(diphenylphosphino)ferrocene disulfide **dppfS₂** were also prepared from the reaction of the appropriate bis(phosphine) with two equivalents of elemental sulfur at room temperature in CHCl_3 under an inert atmosphere. The air-stable bis(phosphine) disulfides were obtained in quantitative yields (Scheme 25).



Scheme 25. The synthesis of the bis(phosphine) disulfides.

The effect of different backbone lengths on the $^{31}\text{P}\{^1\text{H}\}$ chemical shifts is very similar to that of the bis(phosphine) monosulfides (Figure 17). The P(S) signal of **dppmS₂** ($\delta_{\text{PS}} = 36.41$ ppm) occurs at a higher field than that of **dppeS₂** ($\delta_{\text{PS}} = 45.42$ ppm). The chemical shifts of the P(S) atoms in **dppbS₂** ($\delta_{\text{PS}} = 43.47$) and **dppfS₂** ($\delta_{\text{PS}} = 41.08$ ppm) are only slightly different than those in the monosulfides, whereas the $^{31}\text{P}\{^1\text{H}\}$ signals of **dcpeS₂** ($\delta_{\text{PS}} = 62.52$ ppm) appeared at 17 ppm lower field than for the other disulfides. The influence on the $^{31}\text{P}\{^1\text{H}\}$ shifts of the substituents on the P atom is apparent in comparing them to those of SPPH_3 ($\delta 43.2$ ppm)²⁹ and $\text{SP}(\text{tBu})_3$ ($\delta 48.1$ ppm).²⁹ Other examples of the influence of the substituents occur in OPPh_3 and $\text{OP}(\text{tBu})_3$, which show $^{31}\text{P}\{^1\text{H}\}$ signals at $\delta 29.3$ ppm

and δ 46.9 ppm, respectively.²⁹ Various studies¹⁵⁴ have revealed that P becomes more positively charged, hence, more electronegative when alkyl substituents are replaced by phenyl ones. However, explanations of the factors influencing $^{31}\text{P}\{^1\text{H}\}$ and $^{13}\text{C}\{^1\text{H}\}$ shifts and the J_{P-C} couplings are likely to be quite complex.²⁹

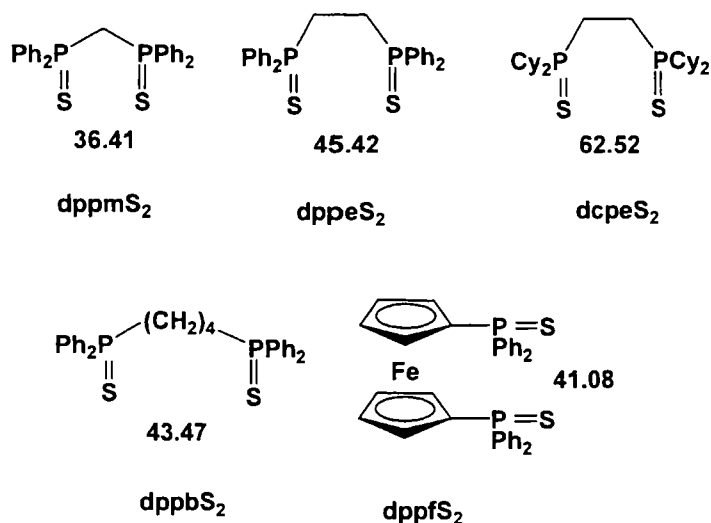


Figure 17. The $^{31}\text{P}\{^1\text{H}\}$ NMR chemical shifts of the bis(phosphine) disulfides.

X-ray structures of ligands

Single crystals of **dppmS**, **dppeS**, **dppfS**, **dcpeS₂** and **dppbS₂** suitable for X-ray diffraction were grown from slow evaporation of solutions in $\text{CH}_2\text{Cl}_2:\text{EtOH}$ mixtures. **dppmS**, **dcpeS₂** and **dppbS₂** were found to crystallize in the triclinic space group *P*-1 (with two independent molecules in the asymmetric unit for **dppmS** but only one for both **dcpeS₂** and **dppbS₂**). **dppeS** crystallizes in the triclinic space group *P*1 with *Z* = 2 and two independent molecules in the asymmetric unit and **dppfS** crystallizes in the monoclinic space group *I*2/*a* with *Z* = 4 with 0.5 molecules in the asymmetric unit. The molecular structures of **dppmS**, **dppeS**, **dppfS**, **dppbS₂** and **dcpeS₂** are depicted in Figures 18, 19, 20, 21 and 22, respectively. The structures of **dppmS₂**,¹⁴⁷ **dppeS₂**^{86, 93, 155} and **dppfS₂**¹⁵⁰ are known in the literature. The two independent molecules in **dppmS** and **dppeS** are labeled I and I' (Figures 18 and 19) with all differences in bond lengths and angles within experimental error. Molecule I' of **dppmS** is disordered between two positions which differ only in the positions of the S atoms. The minor position has an occupancy of only 3%. The diphenylphosphino unit of molecule I' in **dppeS** is disordered between two positions with a 2:1 occupancy ratio. In **dppfS**, the S atom is disordered between two positions

related *via* a crystallographic inversion center with necessarily equal occupancies. Crystallographic data for all of the structures are given in Table 13 and selected bond lengths and angles of **dppmS**, **dppsS** and **dppfS** are listed in Table 14. Table 15 lists selected bond lengths and angles of **dppbS₂** and **dcpsS₂** as well as **dppmS₂**, **dppsS₂** and **dppfS₂**, for comparison.

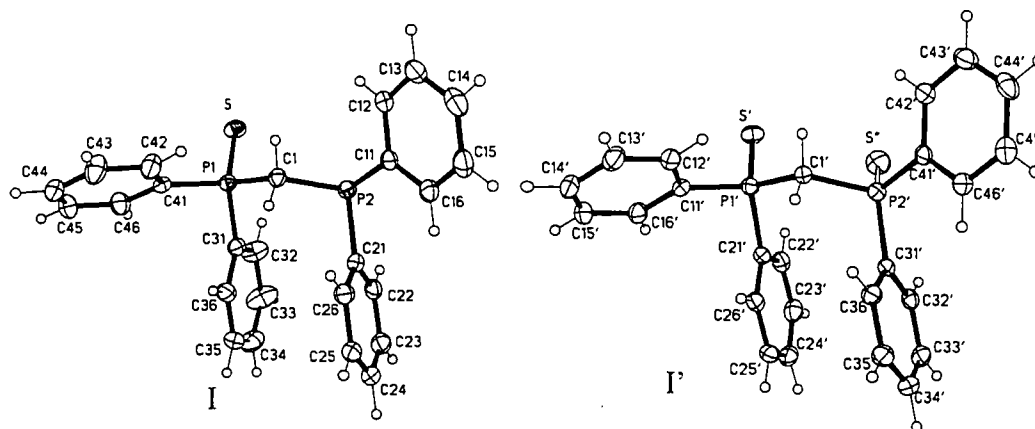


Figure 18. The molecular structure of **dppmS** (minor disordered position shown with open bonds).

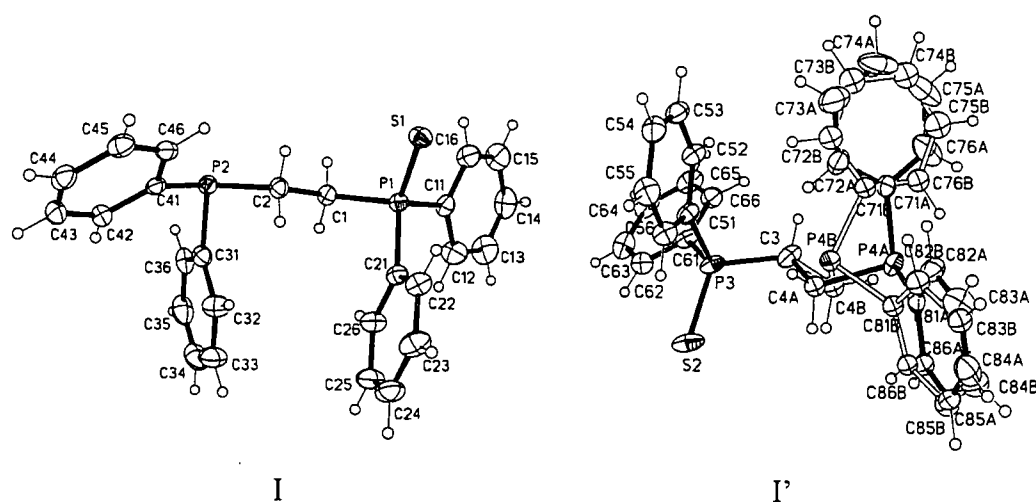


Figure 19. The molecular structure of **dppsS** (minor disordered position shown with open bonds).

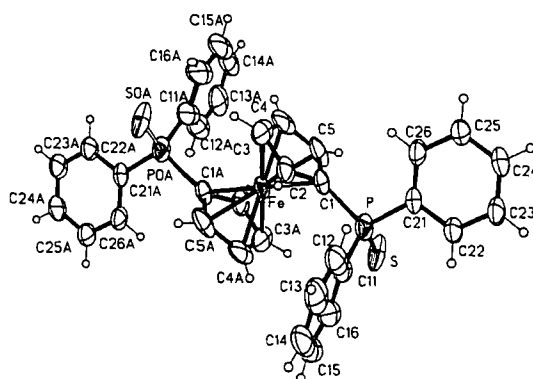


Figure 20. The molecular structure of **dppfS** (one disordered position shown with open bonds).

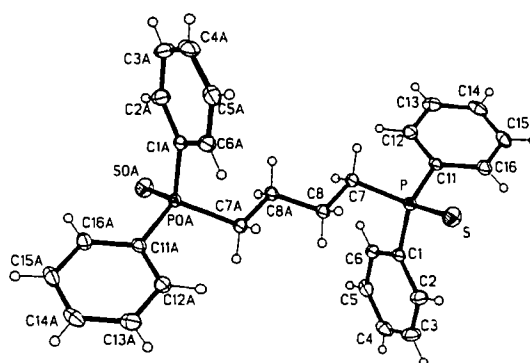


Figure 21. The molecular structure of **dppbS₂**.

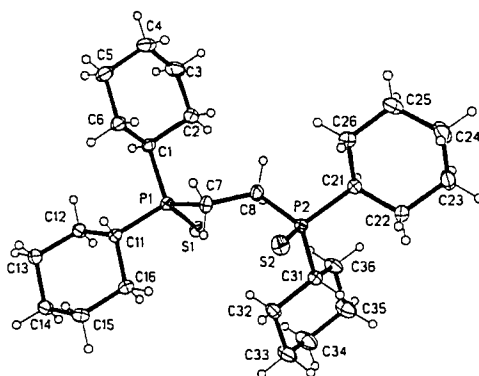


Figure 22. The molecular structure of **dcpeS₂**.

Table 13. Crystallographic data for **dppmS**, **dppeS**, **dppfS**, **dcpeS₂** and **dppbS₂**.

Compound	dppmS	dppeS	dppfS	dcpeS₂	dppbS₂
Formula	C ₂₅ H ₂₂ P ₂ S	C ₂₆ H ₂₄ P ₂ S	C ₃₄ H ₂₈ FeP ₂ S	C ₂₆ H ₄₈ P ₂ S ₂	C ₂₈ H ₂₈ P ₂ S ₂
FW	416.43	430.45	586.41	486.70	490.56
<i>T</i> (K)	120(2)	120(2)	120(2)	120(2)	120(2)
Crystal system	Triclinic	Triclinic	Monoclinic	Triclinic	Triclinic
Space group	<i>P</i> -1	<i>P</i> 1	<i>I</i> 2/ <i>a</i>	<i>P</i> -1	<i>P</i> -1
<i>a</i> (Å)	9.7045(11)	9.2241(14)	11.714(3)	9.7968(12)	6.5090(7)
<i>b</i> (Å)	12.1870(15)	10.0841(16)	10.779(2)	12.1426(16)	8.6599(10)
<i>c</i> (Å)	20.009(2)	12.4364(19)	22.448(5)	13.2461(17)	12.4248(14)
α (°)	105.37(2)	88.07(1)	90.00	108.77(2)	72.17(2)
β (°)	91.30(2)	76.19(1)	99.30(1)	95.44(2)	76.13(2)
γ (°)	108.22(2)	78.53(1)	90.00	111.51(2)	73.36(2)
<i>U</i> (Å ³)	2152.9(4)	1121.1(3)	2797(1)	1346.9(3)	629.86(12)
<i>Z</i>	4	2	4	2	1
<i>D_x</i> (Mg cm ⁻³)	1.285	1.275	1.393	1.200	1.293
μ (mm ⁻¹)	0.307	0.297	0.751	0.329	0.353
Refls measured	25544	13414	17629	11287	8722
Independent reflections	11287	10488	3911	7101	3316
Data/restraints/parameters	11287/0/509	10488/3/527	3911/0/178	7101/0/463	3316/0/201
Final R indices <i>I</i> > 2 σ	R1=0.0431, WR2=0.0923	R1=0.0326, WR2=0.0832	R1=0.0530, WR2=0.1193	R1=0.0287, WR2=0.0739	R1=0.0460, WR2=0.1261
R indices (all data)	R1=0.0668, WR2=0.1009	R1=0.0332, WR2=0.0838	R1=0.0816, WR2=0.1334	R1=0.0337, WR2=0.0771	R1=0.0531, WR2=0.1303

Table 14. Selected bond lengths and angles of **dppmS**, **dppeS** and **dppfS**.

Bond (Å)	dppmS		dppeS		dppfS
P=S	1.9515(7)	1.9517(8)	1.9541(6)	1.9548(8)	1.8241(7) ^c
P(S)-CH ₂ ^a	1.8116(19)	1.8134(19)	1.8209(17)	1.817(2)	1.793(3)
P-CH ₂ ^a	1.8632(18)	1.8591(18)	1.8504(17)	1.855(3)	1.793(3)
P(S)-C _{ipso}	1.8105(19)	1.8142(18)	1.8209(18)	1.8128(18)	1.817(3)
	1.8171(19)	1.8192(19)	1.8194(18)	1.8227(18)	1.821(2)
P-C _{ipso}	1.8307(19)	1.8326(18)	1.8276(19)	1.838(2)	1.817(3)
	1.833(2)	1.837(2)	1.8329(18)	1.8522(19)	1.821(2)
Angle (deg)					
S-P-CH ₂ ^a	113.56(7)	113.96(7)	113.27(6)	113.41(7)	116.32(10)
S-P-C _{ipso}	112.90(7)	112.71(7)	113.48(6)	112.80(7)	111.88(13)
	114.44(6)	113.31(6)	112.42(6)	112.95(7)	115.73(10)
CH ₂ -P(S)-C _{ipso} ^b	105.40(9)	105.09(9)	103.62(8)	104.50(8)	104.37(13)
	104.94(9)	105.09(8)	104.58(8)	106.25(9)	103.84(12)
CH ₂ -P-C _{ipso} ^b	101.73(8)	102.47(8)	101.71(8)	101.01(12)	103.84(12)
	97.75(8)	99.09(8)	99.93(8)	99.28(12)	104.37(13)

^a P-C(sp²) for **dppfS**, ^b C(sp²)-P-C_{ipso} for **dppfS**, ^c S atom is disordered between two positions.

Table 15. Selected bond lengths and angles of the bis(phosphine) disulfides.

Bond (Å)	dppmS₂ ¹⁵⁶	dppeS₂ ¹⁵⁵	dcpeS₂	dppbS₂	dppfS₂ ¹⁵⁷
P=S	1.948(1) 1.941(1)	1.9526(5)	1.9682(7) 1.9521(6)	1.9333(8)	1.938(2)
P-CH ₂ ^a	1.827(3) 1.831(3)	1.8135(12)	1.8303(13) 1.8302(12)	1.823(2)	1.796(3)
P-C _{ipso} ^b	1.808(3)		1.8348(11)		
	1.819(3)	1.8159(12)	1.8357(11)	1.823(2)	1.815(4)
	1.814(3)	1.8245(13)	1.8341(12)	1.817(2)	1.818(3)
	1.806(3)		1.8354(12)		
Angle (deg)					
S-P-CH ₂ ^a	113.9(1)		113.08(5)		
	115.3(1)	112.91(4)	113.62(5)	113.89(7)	113.4(1)
S-P-C _{ipso} ^b	111.22(9)		111.01(4)		
	113.7(1)	114.00(4)	113.47(5)	112.83(7)	114.3(2)
	115.3(1)	111.98(4)	112.39(4)	112.79(7)	112.2(1)
	113.3(1)		113.38(4)		
CH ₂ -P-C _{ipso} ^c	104.8(1)		106.67(6)		
	103.5(1)	106.23(5)	104.23(5)	105.53(9)	105.3(2)
	103.4(1)	106.15(6)	107.50(6)	106.42(9)	106.1(2)
	106.5(1)		103.58(5)		

^a P-C(sp²) **dppfS₂**, ^b P-CH for **dcpeS₂**, ^c C(sp²)-P-C_{ipso} for **dppfS₂**.

Single-crystal X-ray structures of the monosulfides show the geometries of the P(S) atoms in all of the ligands to be distorted tetrahedra with S–P–C bond angles larger than the C–P–C ones. The P=S bond lengths and S–P–C bond angles of the monosulfides and disulfides (except **dppfS**) are comparable to those reported in the literature for SPh₃ and its related phosphine sulfides (1.947(4)³⁷ – 1.966(2)³³ Å see Table 3 in the introduction and 1.955 Å (av) from CSD 2007).² A very short P=S bond length (1.8241(17) Å) was observed in **dppfS**. However, this is probably related to the disorder, as it is remarkably shorter than that observed in **dppfS**₂ (1.938(2) Å), in which the other bond lengths and angles are similar. In the monosulfide structures, the P(S)–CH₂ bond lengths are *ca.* 0.02 – 0.05 Å shorter than the P–CH₂ ones. In **dcpeS**₂, the cyclohexyl rings adopt chair conformations. The P=S bond lengths in **dcpeS**₂ are slightly longer (1.9521(6) and 1.9682(7) Å), compared to the other ligands.

The molecular packing of the monosulfides and disulfides show several close intermolecular S...H contacts which are less than the sum of the van der Waals radii (S...H, 2.91 Å).¹⁵⁸ In the case of **dppfS**, a short intermolecular S...S contact is observed (3.133 Å); (this may be a function of the disorder of the S atom) which is shorter than the sum of the van der Waals radii (3.60 Å).¹⁵⁸ Furthermore, close intermolecular P...H contacts are also observed in the case of **dppmS** and **dppeS** (2.968 and 2.911 Å, respectively). A summary of the close intermolecular contact distances and angles for all of the structures is given in Table 16.

Table 16. Intermolecular contact distances in the monosulfides and disulfides.

Compound	X.....Y	X.....Y (Å)	W–H.....Y (deg)
dppmS	S''.....H(25)	2.754	122.2
	P(2).....H(36)	2.968	131.5
dppeS	S(2).....H(24)	2.765	154.2
	S(2).....H(23)	2.911	171.4
	P(4).....H(65)	2.873	172.9
dppfS	S.....H(3)	2.836	151.1
	S.....S	3.133	-
dppbS ₂	S.....H(72)	2.677	171.6
dcpeS ₂	S(2).....H(33)	2.889	144.5

The close intermolecular contacts of **dppmS**, **dppfS**, **dppbS₂** and **dcpeS₂** are depicted with dashed lines in Figures 23, 24, 25 and 26, respectively.

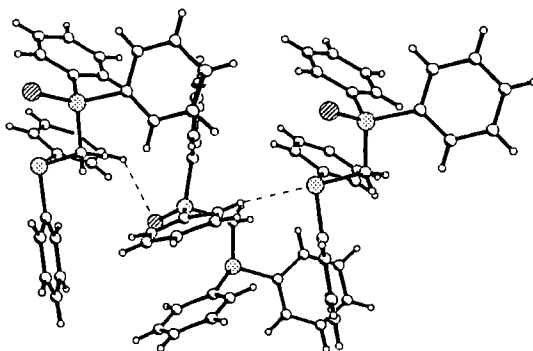


Figure 23. Close intermolecular contacts in **dppmS**.

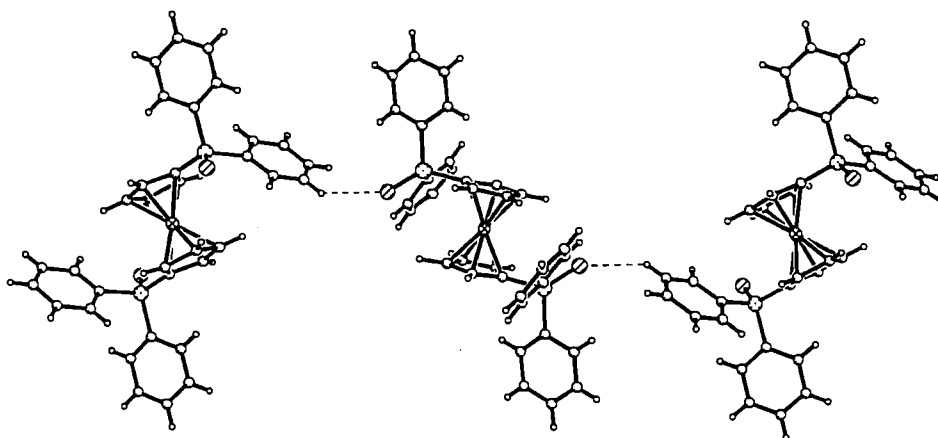


Figure 24. Close intermolecular contacts in **dppfS** (both disordered position of S atom are shown).

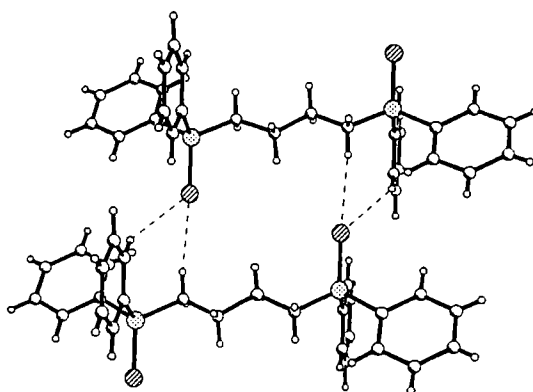


Figure 25. Close intermolecular contacts in **dppbS₂**.

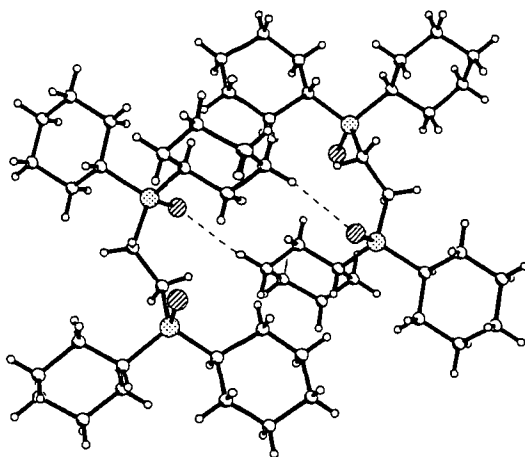


Figure 26. Close intermolecular contact in **dpeS₂**.

Close inspection of the molecular packing of the two independent molecules in the asymmetric unit of **dppsS** reveals different close S...H contacts found in molecules I and I'. In molecule I, a close S...H contact between the S atoms and the H atom in the *para*-position of the phenyl ring is observed (Figure 27). In molecule I', the same intermolecular contact is observed, as well as a close contact between the P atom and the *meta*-H (Figure 28). This may be the reason for the disorder in molecule I'.

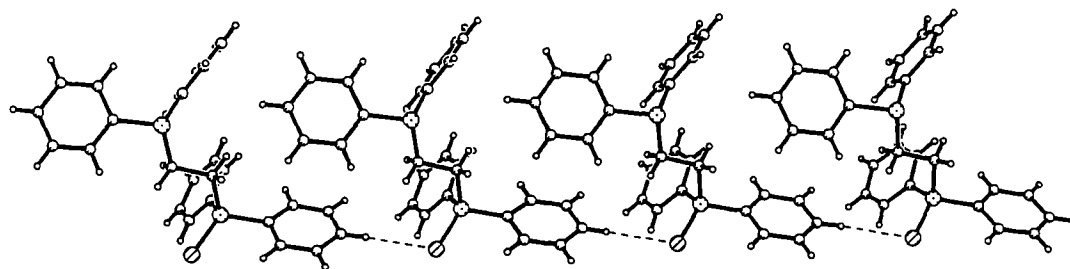


Figure 27. Close intermolecular contacts in molecule I of **dppsS**.

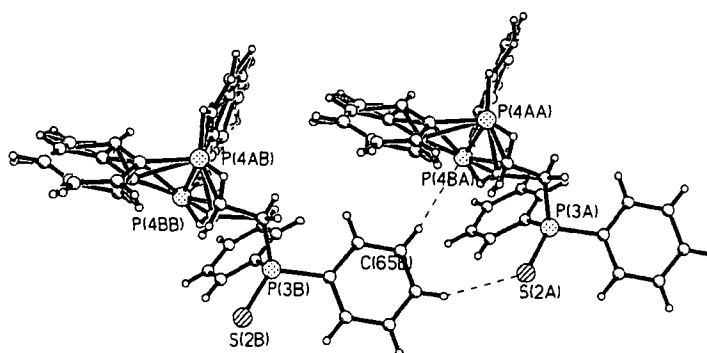


Figure 28. Close intermolecular contacts in molecule I' of **dppsS**.

Attempts to grow single crystals of **dppbS** by slow evaporation from a solution in $\text{CH}_2\text{Cl}_2:\text{EtOH}$ in an inert atmosphere glovebox failed. After a considerable amount of time, single crystals were obtained in the solution. Two different molecular structures were obtained from different crystals, which both have the same space group $P-1$ but with different cell parameters. Both structures have one molecule in the asymmetric unit, which was revealed to contain 67 % of $\text{PPh}_2\text{P}(\text{S})(\text{CH}_2)_4\text{P}(\text{O})\text{PPh}_2$ **dppbSO**, which was disordered over two positions with equal occupancies, differing only in the positions of the S and O atoms. The remaining **dppbS** is disordered in a similar way. The other structure was found to contain 25% of **dppbSO**. Crystallographic data are given in Table C1 and selected bond lengths and angles are listed in Table C2 in the Appendix). Monitoring of the $^{31}\text{P}\{^1\text{H}\}$ NMR signals of **dppbS** in CDCl_3 solution in air was carried out by Mr. T. Turner¹⁵⁵ in our group. The amount of the P(O) signal at 2 d, 6 d, 6 weeks and 10 weeks was 3%, 10%, 23% and 33%, respectively, which suggests that the oxidation of **dppbS** in air is very slow. We have no explanation of how oxidation occurred under an inert atmosphere.

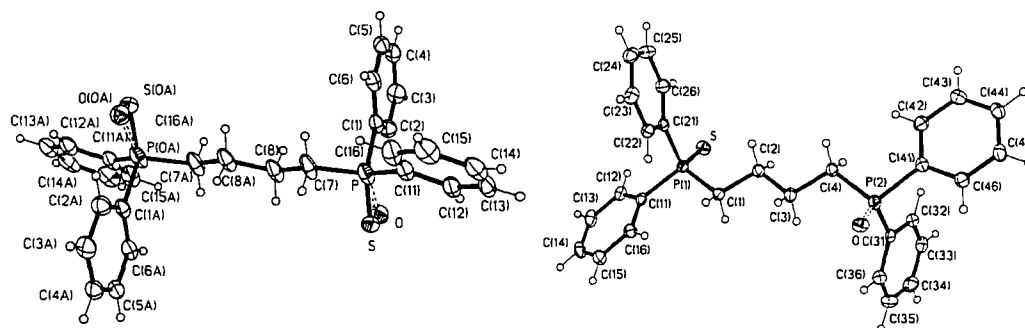


Figure 29. The molecular structures of **dppbS:dppbSO** (0.33:0.67) (left) **dppbS:dppbSO** (0.75:0.25) (right) (**dppbSO** is shown with dashed bonds).

II.2 Synthesis and characterization of palladium complexes

II.2.1 Palladium complexes obtained from reaction of Pd with L in a 1:1 molar ratio

The 1:1 reactions of $\text{PdCl}_2(\text{PhCN})_2$ with bis(phosphine) monosulfides

The monomeric palladium complexes $\text{PdCl}_2\text{-dppmS}$ **Pd(dppmS)**, $\text{PdCl}_2\text{-dppeS}$ **Pd(dppeS)** and $\text{PdCl}_2\text{-dppfS}$ **Pd(dppfS)**, were prepared from the reaction of one equivalent of the appropriate monosulfide ligand with one equivalent of $\text{PdCl}_2(\text{PhCN})_2$ in an inert atmosphere at room temperature to obtain the products

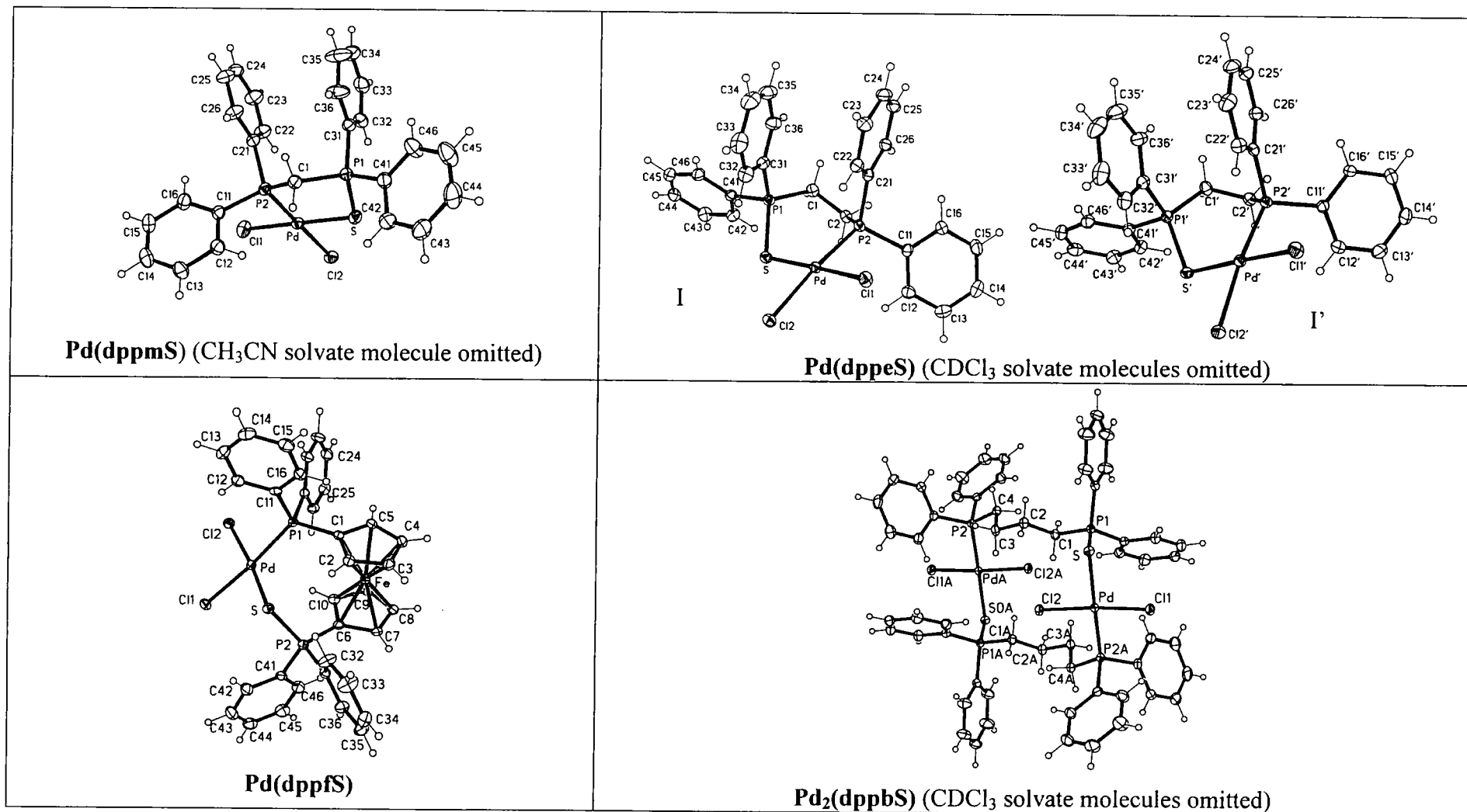


Figure 31. The molecular structures of the bis(phosphine) monosulfide palladium complexes.

Table 17. Crystallographic data for **Pd(dppmS)**, **Pd(dppeS)**, **Pd(dppfS)** and **Pd(dppbS)**.

Compound	Pd(dppmS) ·CH ₃ CN	Pd(dppeS) ·2CDCl ₃	Pd(dppfS) ·3CHCl ₃	Pd₂(dppbS) ·6CHCl ₃
Formula	C ₂₅ H ₂₂ Cl ₂ P ₂ PdS·C ₂ H ₃ N	C ₂₆ H ₂₄ Cl ₂ P ₂ PdS·2(CDCl ₃)	C ₃₄ H ₂₈ Cl ₂ FeP ₂ PdS·3(CHCl ₃)	C ₅₆ H ₅₆ Cl ₄ P ₄ Pd ₂ S ₂ ·6(CHCl ₃)
FW	634.78	848.50	1121.82	1987.82
<i>T</i> , K	120(2)	120(2)	120(2)	120(2)
Crystal system	Monoclinic	Monoclinic	Triclinic	Triclinic
Space group	<i>P</i> 2 ₁ / <i>n</i>	<i>P</i> 2 ₁ / <i>n</i>	<i>P</i> -1	<i>P</i> -1
<i>a</i> (Å)	8.9419(4)	18.7177(16)	11.5912(10)	11.6534(14)
<i>b</i> (Å)	16.1765(8)	14.2401(12)	13.6942(12)	12.5742(16)
<i>c</i> (Å)	19.1835(9)	25.718(2)	16.1661(1)	14.7937(19)
α (°)	90.00	90.00	109.90(1)	111.865(10)
β (°)	95.27(2)	95.63(2)	90.73(1)	93.532(11)
γ (°)	90.00	90.00	114.06(1)	99.035(11)
<i>U</i> (Å ³)	2763.1(2)	6821.9(10)	2168.6(3)	1969.7(4)
<i>Z</i>	4	8	2	1
<i>D</i> _x (Mg cm ⁻³)	1.526	1.652	1.718	1.676
μ (mm ⁻¹)	1.073	1.346	1.577	1.375
Refls measured	64823	89068	25623	18024
Independent reflections	11815	19529	11391	10690
Data/restraints/parameters	11815 / 0 / 307	19529 / 0 / 721	11391 / 15 / 496	10690 / 0 / 415
Final R indices <i>I</i> > 2σ	R1=0.0300, WR2=0.0768	R1=0.0387, R2=0.0749	R1=0.0477, WR2=0.0841	R1=0.0271, WR2=0.0631
R indices (all data)	R1=0.0373, WR2=0.0824	R1=0.0743, WR2=0.0850	R1=0.0877, WR2=0.0946	R1=0.0336, WR2=0.0665

Table 18. Bond lengths and angles of the bis(phosphine) monosulfide palladium complexes.

	Pd(dppmS)	Pd(dppeS) (Z'=2)		Pd(dppfS)	Pd₂(dppbS)
Pd-Cl(<i>trans</i> -S)	2.3188(4)	2.3173(7)	2.3291(7)	2.3035(10)	2.3086(5) ^a
Pd-Cl(<i>trans</i> -P)	2.3713(4)	2.3790(8)	2.3755(7)	2.3596(9)	2.3043(5) ^a
Pd-S	2.2874(4)	2.3053(7)	2.3088(7)	2.3267(10)	2.4253(6)
Pd-P	2.2282(4)	2.2315(8)	2.2232(8)	2.2701(10)	2.2486(6)
S-P	2.0150(5)	2.0083(9)	2.0100(9)	2.0151(13)	2.0005(6)
P(S)-CH ₂ ^b	1.8097(14)	1.818(3)	1.814(4)	1.774(4)	1.8087(17)
P-CH ₂ ^b	1.8444(14)	1.828(3)	1.829(3)	1.805(3)	1.8291(18)
P(S)-C _{ipso}	1.7886(14)	1.799(3)	1.799(3)	1.802(4)	1.8069(18)
	1.7937(15)	1.805(3)	1.803(3)	1.808(4)	1.8102(18)
P-C _{ipso}	1.8073(14)	1.814(3)	1.807(3)	1.818(4)	1.8115(18)
	1.8094(14)	1.824(3)	1.816(3)	1.822(4)	1.8161(18)
S-Pd-P	93.052(14)	96.07(3)	95.59(3)	95.88(4)	178.609(17)
P(S)-S-Pd	104.099(19)	107.03(3)	108.21(3)	110.59(5)	97.29(2)
S-Pd-Cl	85.059(15)	85.39(3)	86.39(3)	87.97(4)	90.566(19)
	178.253(14)	175.10(3)	176.14(3)	172.04(3)	91.09(2)
P-Pd-Cl	88.536(15)	88.14(3)	87.85(3)	86.44(4)	88.76(2)
	177.959(14)	173.86(3)	172.90(3)	174.88(3)	89.72(2)
Cl-Pd-Cl	93.363(15)	90.69(3)	90.40(3)	89.31(4)	173.483(18)
S-P(S)-CH ₂ ^b	106.56(5)	112.11(9)	112.76(10)	115.65(12)	114.12(6)
S-P(S)-C _{ipso}	108.64(6)	105.34(9)	106.10(9)	107.39(12)	109.88(6)
	113.36(5)	112.76(10)	112.97(10)	113.44(12)	113.75(6)
C-P(S)-C _{ipso}	107.44(6)	108.47(13)	107.26(13)	106.13(16)	105.35(8)
	111.12(7)	109.04(13)	109.23(13)	106.12(16)	107.13(8)
C-P-C _{ipso}	105.34(6)	100.60(12)	99.20(12)	99.84(16)	101.95(8)
	105.89(6)	106.27(12)	106.34(12)	99.84(16)	104.53(8)
Pd-P-C _{ipso}	113.52(5)	111.90(9)	111.29(9)	110.30(12)	112.03(6)
	114.63(5)	115.01(9)	114.52(9)	115.13(12)	115.55(6)

^a Pd-Cl *trans* to Cl, ^b P-C(sp²) for Pd(dppfS).

The structures show slightly distorted square planar coordination at the Pd centres with the chelating ligand bound through the P and S atoms. **Pd(dppmS)**, **Pd(dppeS)** and **Pd(dppfS)** have *cis*-configurations whereas **Pd₂(dppbS)** is a *trans*-dimeric complex. All of the complexes have slight tetrahedral distortions at the Pd centres with the largest dihedral angle between the S–Pd–P and Cl(1)–Pd–Cl(2) planes being 8.3° in **Pd(dppfS)**. In **Pd(dppmS)**, the Pd, S, P, Cl(1) and Cl(2) atoms are almost coplanar. The two independent molecules of **Pd(dppeS)** show the Cl (*trans*-S) to deviate by +0.102 and +0.072 Å from the S–Pd–P plane, whereas the other Cl (*trans*-P) deviates by -0.248 and -0.283 Å. The Cl (*trans*-S) and Cl (*trans*-P) atoms of **Pd(dppfS)** deviate from the S–Pd–P plane by +0.306 and +0.139 Å. Finally, the Cl(2) atom in **Pd₂(dppbS)** deviates from the Pd–S–P–Cl(1) plane by 0.254 Å.

In **Pd(dppmS)**, the **dppmS** ligand forms a five-membered chelating ring, which has a twisted conformation, so that the P(S) atom lies out of the coordination plane S–Pd–P by 0.41 Å. The **Pd(dppmS)** structure in this study is similar to that reported for PdI₂-dppmS.⁹⁶ **Pd(dppeS)** forms a six-membered ring with a twisted boat conformation. The two independent molecules in the asymmetric unit show almost the same bond lengths and angles. The **Pd(dppfS)** bond lengths and angles are almost the same as reported in PdCl₂{Fe(η^5 -C₅Me₄(S)PPh₂(η^5 -C₅Me₄PPh₂))}.¹⁵⁹ Interestingly, the S–Pd–P bite angle and Cl–Pd–Cl angles (95.88(4)° and 89.31(4)°, respectively) of **Pd(dppfS)** are significantly larger than the analogous angles in PdCl₂{Fe(η^5 -C₅Me₄P(S)(η^5 -PPh₂))} (89.41(3)° and 85.75(2)°). The Cp rings in **Pd(dppfS)** are twisted from the eclipsed conformation by 7.1° (cf. 4.6° in PdCl₂{Fe(η^5 -C₅Me₄P(S)(η^5 -PPh₂))}). The bond lengths and bond angles of all these structures will be discussed in detail later.

The molecular packings of the monosulfide complexes show close intermolecular S...H, Cl...H, Cl...D, S...S and Cl...Cl contacts which are less than the sum of the van der Waals radii (2.91, 2.88, 2.88, 3.60 and 3.50 Å, respectively).¹⁵⁸ A summary of the intermolecular contact distances and angles is given in Table 19.

Table 19. Intermolecular contact distances in monosulfide complexes.

Compounds	X.....Y	X.....Y (Å)	W-H(D).....Y (deg)
Pd(dppmS)	H3.....Cl(1)	2.776	156.3
Pd(dppeS)	H1..... Cl(1)	2.807	154.2
	D.....Cl(1) ^a	2.810	143.3
	D.....Cl(2) ^a	2.429	164.0
	D.....Cl(2) ^a	2.698	138.8
Pd(dppfS)	H.....Cl ^a	2.733	131.0
	H.....Cl ^a	2.716	118.9
	H(33).....S	2.755	171.7
Pd₂(dppbS)	Cl.....Cl ^a	3.311	-

^a H, D or Cl atoms of the solvate.

The formation of palladium complexes can also be identified by $^{31}\text{P}\{^1\text{H}\}$ NMR spectroscopy. A summary of $^{31}\text{P}\{^1\text{H}\}$ NMR signals of the bis(phosphine) monosulfide palladium complexes and the free ligands is given in Table 20. Upon coordination, the $^{31}\text{P}\{^1\text{H}\}$ NMR signals of the phosphine are significantly shifted to lower field, whereas the P(S) signals are only slightly changed. The largest changes in the chemical shifts are observed in **Pd(dppmS)** ($\Delta\delta(\text{P}) = 58.70$ ppm and $\Delta\delta(\text{P(S)}) = 15.08$ ppm). The $\Delta\delta(\text{P})$ and $\Delta\delta(\text{P(S)})$ values in the other palladium complexes (**Pd(dppeS)**, **Pd(dppfS)** and **Pd₂(dppbS)**) are very similar (33.11 – 40.19 ppm and 3.11 – 4.42 ppm for $\Delta\delta(\text{P})$ and $\Delta\delta(\text{P(S)})$, respectively). Furthermore, the $J_{\text{P-P}}$ couplings of **Pd(dppmS)** ($J_{\text{P-P}} = 37$ Hz) and **Pd(dppeS)** ($J_{\text{P-P}} = 15$ Hz) are much less than those in the free ligands, for which $J_{\text{P-P}} = 76$ Hz and $J_{\text{P-P}} = 50$ Hz, respectively. The $^{31}\text{P}\{^1\text{H}\}$ chemical shift observed for the phosphino P atom in **Pd(dppmS)** ($\delta_{\text{P}} = 31.63$ ppm) can be explained *via* the chelate ring size effect.¹⁶⁰

Table 20. The $^{31}\text{P}\{^1\text{H}\}$ (202 MHz) NMR chemical shifts and J_{P-C} couplings of bis(phosphine) monosulfide palladium complexes and the free ligands.^a

	$\delta(\text{P})$ ppm	$\delta(\text{PS})$ ppm	J_{P-P} Hz ^b
Pd(dppmS)	31.63 [-27.07, $\Delta = 58.70$]	56.37 [41.29, $\Delta = 15.08$]	d, 37 Hz [d, 76 Hz]
Pd(dppeS)	23.22 [-11.89, $\Delta = 35.11$]	42.25 [45.36, $\Delta = 3.11$]	d, 15 Hz [d, 50 Hz]
Pd(dppfS)	22.88 [-16.59, $\Delta = 39.47$]	45.41 [40.99, $\Delta = 4.42$]	-
Pd₂(dppbS)	25.15 [-15.04, $\Delta = 40.19$]	47.45 [43.57, $\Delta = 3.88$]	-

^a [X, $\Delta = Y$] where X = $^{31}\text{P}\{^1\text{H}\}$ resonance of the free ligand, and Y the difference in the chemical shifts between the palladium complex and the free ligand, ^b Values in square brackets are for the free ligands.

Reactions of PdCl₂ with bis(phosphine) disulfides in 1:1 molar ratios

Using the palladium source, PdCl₂(PhCN)₂, and the bis(phosphine) disulfides, we attempted to synthesize palladium complexes. However, we were unable to characterize the products. The *in situ* reactions of one equivalent of PdCl₂(PhCN)₂ with one equivalent of the bis(phosphine) disulfides **dppmS₂**, **dppeS₂**, **dcpeS₂** and **dppbS₂** in CDCl₃ was followed by $^{31}\text{P}\{^1\text{H}\}$ NMR spectroscopy. Orange precipitates were immediately observed, as well as the disappearance of the ligand signals in the $^{31}\text{P}\{^1\text{H}\}$ NMR spectra, indicating that all the ligands had been consumed. The precipitated products had limited solubility. They were soluble in dmsd-d₆ but showed the $^{31}\text{P}\{^1\text{H}\}$ signals only from the ligands. Furthermore, the elemental analyses are not correct for a 1:1 ratio of Pd to ligand. The solid state $^{31}\text{P}\{^1\text{H}\}$ NMR spectra of the complexes obtained from **dppmS₂** and **dppbS₂** showed the signals at δ 31.43, 33.98, 36.24, 38.95 ppm and δ 43.93, 46.04 ppm respectively (see Figures C1 and C2 in the Appendix for the solid state $^{31}\text{P}\{^1\text{H}\}$ NMR spectra of the complexes obtained from **dppmS₂** and **dppbS₂**, respectively).

Use of a different palladium source, PdCl₂, enabled the bis(phosphine) disulfide palladium complexes PdCl₂(dppmS₂) **Pd(dppmS₂)**, PdCl₂(dppeS₂) **Pd(dppeS₂)** and PdCl₂(dcpeS₂) **Pd(dcpeS₂)** (Figure 32) to be prepared by refluxing in acetonitrile for 3 h, giving moderate yields (35 – 40%) of deep red crystals from acetonitrile, except for **Pd(dcpeS₂)** which was obtained in 83% yield as an orange

solid by adding Et₂O. **Pd(dppeS₂)** has been prepared using this method, but no ³¹P{¹H} NMR data were reported.¹¹⁷ The ³¹P{¹H} signals of the palladium complexes are only slightly shifted compared to those of the free ligands and are summarized in Table 21.

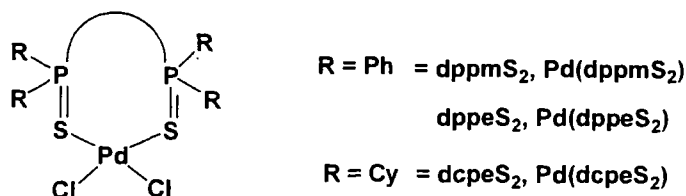


Figure 32. The bis(phosphine) disulfide palladium complexes.

Table 21. The ³¹P{¹H} chemical shifts of the bis(phosphine) disulfide palladium complexes.^a

	Pd(dppmS₂)	Pd(dppeS₂)	Pd(dcpeS₂)
$\delta(\text{PS})$	37.87 [36.41, $\Delta = 1.46$]	45.77 [45.42, $\Delta = 0.35$]	70.29 [62.52, $\Delta = 7.77$]

^a [X, $\Delta = Y$] where X = ³¹P{¹H} resonances of the free ligand, and Y is the difference in chemical shift between the ³¹P{¹H} signals of the palladium complex and the appropriate free ligand.

Single crystals of **Pd(dppmS₂)** and **Pd(dcpeS₂)** suitable for diffraction analysis were obtained by crystallization from acetonitrile and by the slow evaporation of a solution in CH₂Cl₂:Et₂O, respectively. Both **Pd(dppmS₂)** and **Pd(dcpeS₂)** were subjected to X-ray structure analysis. They were found to crystallize in the orthorhombic space group *Fdd2* with Z = 8, and the monoclinic space group *P2₁/c* with Z = 4, respectively. **Pd(dppmS₂)** contains 0.5 molecules in the asymmetric unit whereas **Pd(dcpeS₂)** has one molecule. The latter also contains three molecules of CH₂Cl₂ solvate. The molecular structures of **Pd(dppmS₂)** and **Pd(dcpeS₂)** are depicted in Figures 33 and 34, respectively, whereas the molecular structure of **Pd(dppeS₂)** is known in the literature and the molecular structure is depicted in Figure 35 for comparison.¹¹⁷ Their crystallographic data are given in Table 22 and their selected bond lengths and angles are summarized in Table 23.

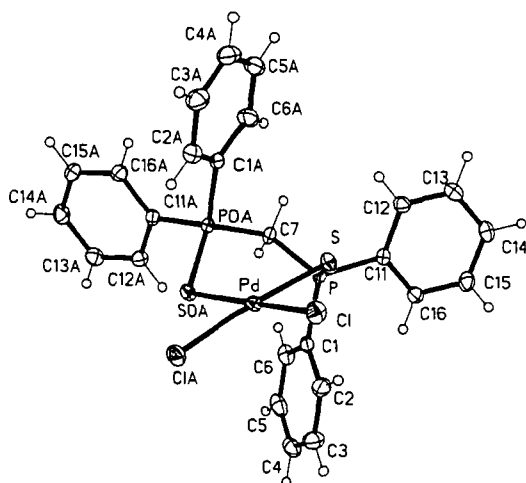


Figure 33. The molecular structure of **Pd(dppmS₂)**.

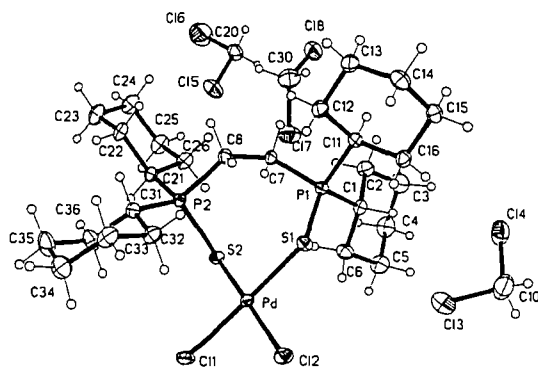


Figure 34. The molecular structure of **Pd(dcpes₂)**.

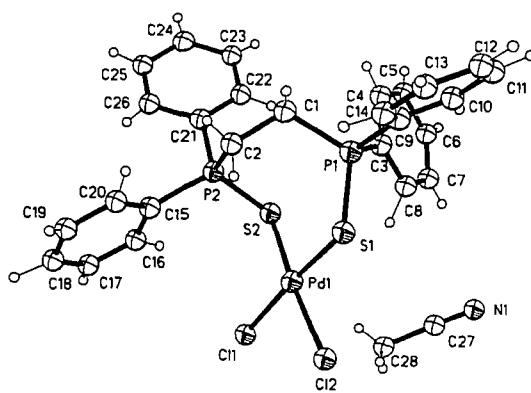


Figure 35. The molecular structure of **Pd(dppeS₂)**.¹¹⁷

Table 22. Crystallographic data for **Pd(dppmS₂)** and **Pd(dcpeS₂)·2CH₂Cl₂**.

Compound	Pd(dppmS₂)	Pd(dcpeS₂)·2CH₂Cl₂
Formula	C ₂₃ H ₂₂ Cl ₂ P ₂ PdS ₂	C ₂₆ H ₄₈ Cl ₂ P ₂ PdS ₂ ·3(CH ₂ Cl ₂)
FW	625.79	918.78
<i>T</i> (K)	120(2)	120(2)
Crystal system	Orthorhombic	Monoclinic
Space group	<i>Fdd2</i>	<i>P2₁/n</i>
<i>a</i> (Å)	18.4575(10)	25.255(11)
<i>b</i> (Å)	28.5897(16)	9.4707(4)
<i>c</i> (Å)	9.1394(5)	17.4385(8)
α (°)	90.00	90.00
β (°)	90.00	107.53(2)
γ (°)	90.00	90.00
<i>U</i> (Å ³)	4822.8(5)	3977.3(3)
<i>Z</i>	8	4
<i>D_x</i> (g cm ⁻³)	1.724	1.534
μ (mm ⁻¹)	1.311	1.201
Refls measured	16264	48576
Independent reflections	3515	10534
Data/restraints/parameters	3515/1/146	10534/0/376
Final R indices <i>I</i> > 2σ	R1=0.0189, WR2=0.0401	R1=0.0465, WR2=0.1310
R indices (all data)	R1=0.0220, WR2=0.0412	R1=0.0534, WR2=0.1373

Table 23. Bond lengths and angles of **Pd(dppmS₂)**, **Pd(dppeS₂)** and **Pd(dcpeS₂)**.

	Pd(dppmS₂)	Pd(dppeS₂)¹¹⁷	Pd(dcpeS₂)
Pd-Cl(1)	2.3216(5)	2.3161(15)	2.3292(8)
Pd-Cl(2)		2.3347(14)	2.3330(7)
Pd-S(1)	2.2961(5)	2.3005(14)	2.3214(7)
Pd-S(1)		2.3018(13)	2.3119(7)
P=S(1)	2.0151(7)	2.0181(18)	2.0214(9)
P=S(2)		2.0089(18)	2.0103(9)
P-CH ₂	1.8242(15)	1.808(5)	1.814(3)
		1.832(5)	1.820(2)
P-C _{ipso}	1.8001(19)	1.803(5)	1.817(2)
	1.8011(19)	1.804(5)	1.810(2)
		1.799(6)	1.834(2)
		1.802(5)	1.821(3)
S-Pd-S	97.28(2)	97.76(5)	100.93(2)
P=S-Pd	109.86(2)	113.54(7)	117.99(3)
		105.11(7)	106.57(4)
S-Pd-Cl	86.551(16)	88.06(5)	83.32(2)
	86.547(16)	83.19(5)	86.22(2)
Cl-Pd-Cl	89.92(3)	91.17(5)	90.36(2)
S-P-CH ₂ ^a	113.43(6)	114.34(19)	115.58(9)
		112.00(19)	110.54(8)

^a P-CH for **Pd(dcpeS₂)**.

The palladium centers are bonded to the two S atoms of the chelating ligands forming a six-membered ring in **Pd(dppmS₂)**, and seven-membered rings in both **Pd(dppeS₂)** and **Pd(dcpeS₂)**. The cyclohexyl rings in **Pd(dcpeS₂)** adopt chair conformations. The structures show slightly distorted square planar coordinations at the Pd atoms, which all have *cis*-configurations. All of the complexes have slight tetrahedral distortions at the Pd centers with the dihedral angles between the S-Pd-P and Cl(1)-Pd-Cl(2) planes being 5.7°, 7.2° and 9.6° for **Pd(dppmS₂)**, **Pd(dppeS₂)** and **Pd(dcpeS₂)**, respectively.

The structure of **Pd(dppmS₂)** shows the S, Pd, S and Cl(2) atoms to be almost coplanar whereas Cl(1) deviates from them by 0.289 Å. The **Pd(dppeS₂)** structure shows the Cl(1) and Cl(2) atoms to deviate by +0.162 and -0.162 Å from the S-Pd-S plane, whereas that of **Pd(dcpeS₂)** shows Cl(1) and Cl(2) to deviate by +0.224 and -0.322 Å, respectively. The bond lengths and bond angles of these three complexes will be discussed in detail later.

The crystal packing of **Pd(dppmS₂)** shows short intermolecular Cl.....H contacts (2.906 Å) involving protons on the phenyl rings. Unlike the packing of **Pd(dppmS₂)**, the close intermolecular contacts in **Pd(dcpeS₂)** (Cl.....H7, 2.711 Å and Cl.....H8, 2.734 Å) involve protons in the ethylene backbone. Interestingly, no close intermolecular contacts were observed in **Pd(dppeS₂)**. The close intermolecular contacts in the structures of **Pd(dppmS₂)** and **Pd(dcpeS₂)** are shown in Figures 36 and 37 as dashed lines, respectively.

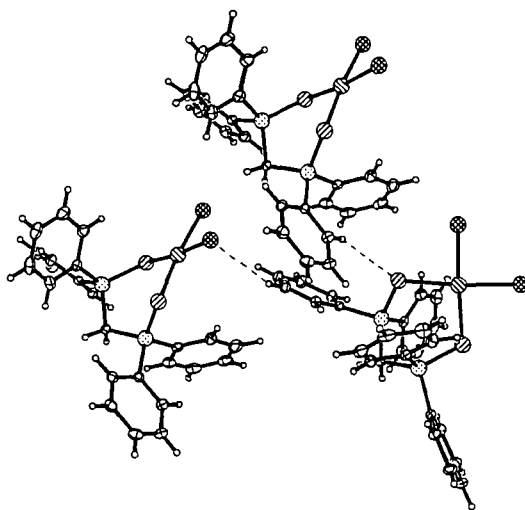


Figure 36. Close intermolecular contacts in the structure of **Pd(dppmS₂)**.

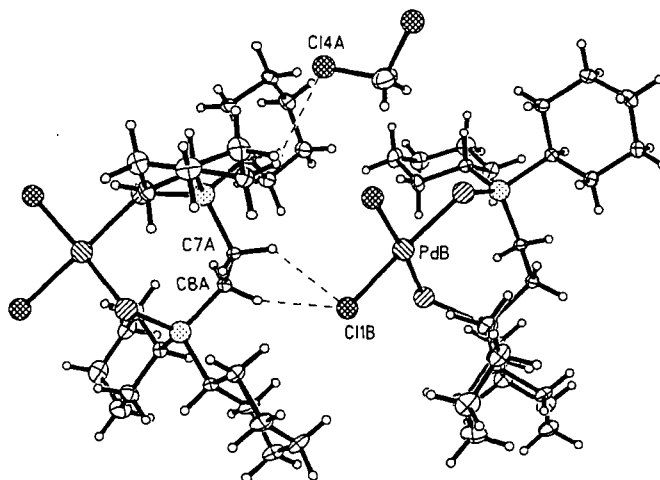


Figure 37. Close intermolecular contacts in the structure of **Pd(dcpeS₂)**.

II.2.2 Palladium complexes obtained from reactions of Pd with L in a 1:2 molar ratio

Reactions of $\text{PdCl}_2(\text{PhCN})_2$ with bis(phosphine) monosulfides in 1:2 molar ratios

The reactions of the bis(phosphine) monosulfides **dppmS**, **dppeS**, **dppbS** and **dppfS**, with 0.5 equivalents of $\text{PdCl}_2(\text{PhCN})_2$ in CH_2Cl_2 at room temperature gave different forms of products. The product from the reaction of **dppfS** gave $\text{PdCl}_2(\text{dppfS})_2$ **Pd(dppfS)₂**. It shows $^{31}\text{P}\{^1\text{H}\}$ NMR signals for P and P(S) of δ 15.65 and 41.92 ppm, respectively. Suitable single crystals for X-ray diffraction of **Pd(dppfS)₂** were obtained from slow evaporation of a solution in $\text{CH}_2\text{Cl}_2:\text{Et}_2\text{O}$. It crystallizes in the orthorhombic space group $Pna2_1$ with one molecule in the asymmetric unit. The molecular structure reveals a *trans* geometry at the Pd center and coordination only from the phosphines and not the phosphine sulfides (selected bond lengths and angles in Figure 38).

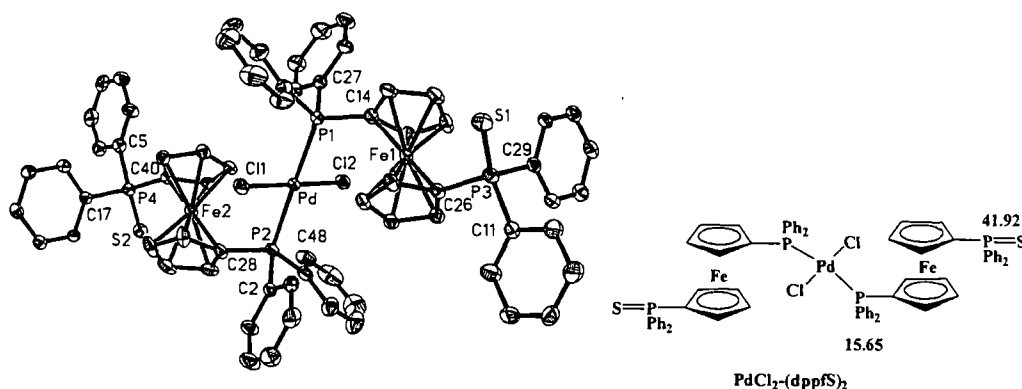


Figure 38. The molecular structure of **Pd(dppfS)₂**; selected bond lengths (Å) and angles (deg); Pd–Cl(1) 2.2980(7), Pd–Cl(2) 2.2993(7), Pd–P(1) 2.3383(8), Pd–P(2) 2.3462(8), P(3)–S(1) 1.953(11), P(4)–S(2) 1.9527(11), P(1)–CH 1.808(3), P(2)–CH 1.793(3), P(1)–Pd–P(2) 179.02(3)°, Cl(1)–Pd–Cl(2) 179.22(3)°.

The $^{31}\text{P}\{^1\text{H}\}$ NMR spectrum of the product from the reaction of a 1:2 molar ratio of $\text{PdCl}_2(\text{PhCN})$ and **dppeS** shows signals which we believe to originate from *cis*- $\text{PdCl}_2(\text{dppeS})_2$ *cis*-**Pd(dppeS)₂** and *trans*- $\text{PdCl}_2(\text{dppeS})_2$ *trans*-**Pd(dppeS)₂**, which coordinate to the Pd center only through the phosphorus atoms **Pd(dppfS)₂** (Figure 39). The doublets at $\delta = 28.2$ and 44.1 ppm [$J_{\text{P-P}} = 56$ Hz] were assigned to the P and P(S) atoms of the *cis*-isomer, whereas the triplet signals at $\delta = 18.8$ and 44.5 ppm [$J_{\text{P-P}} = 28$ Hz] were assigned to the P and P(S) atoms of the *trans*-isomer.

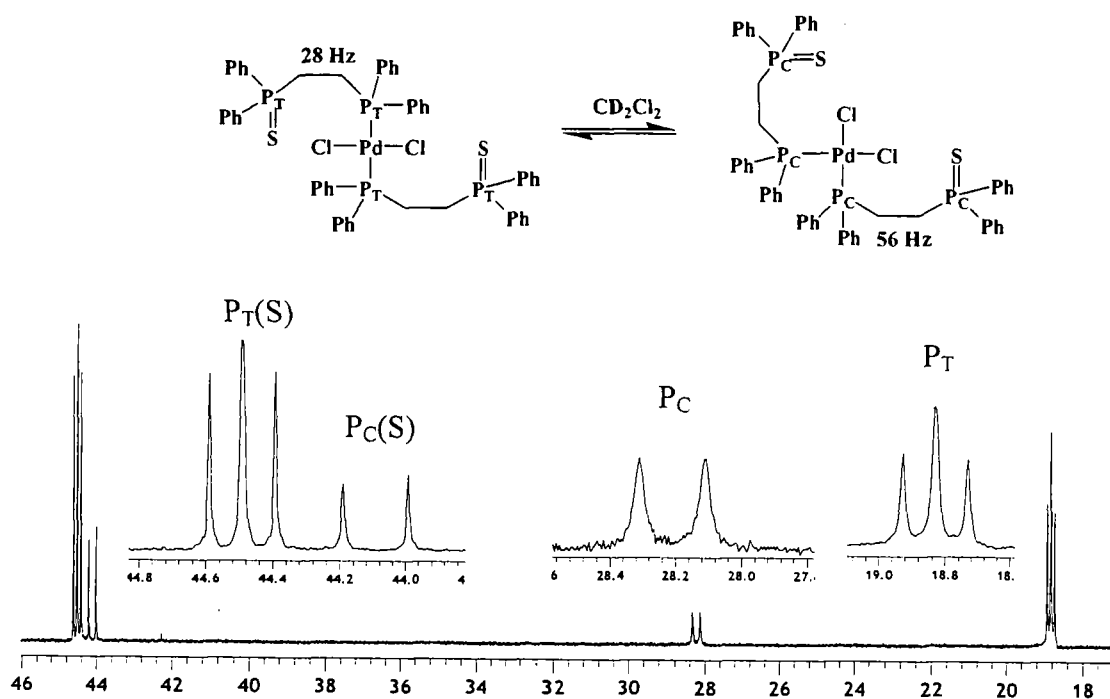


Figure 39. The $^{31}\text{P}\{^1\text{H}\}$ NMR spectrum (202 MHz) in CD_2Cl_2 of the products of the 1:2 molar ratio reaction of $\text{PdCl}_2(\text{PhCN})_2$ with **dppeS**.

A solution NMR study of *cis*- $\text{Pd}(\text{dppeS})_2$ and *trans*- $\text{Pd}(\text{dppeS})_2$ in a range of solvents was undertaken by Mr. T. Turner.¹⁵⁵ It was found that the ratio between these species is dependent on solvent polarity. The *cis*- form, which has a dipole moment, is favoured in strongly polar solvents (*e.g.* CD_3OD) whereas the *trans*- form is favoured in less polar solvents (*e.g.* C_6D_6). The rate of isomerization was found to be $0.13 (\pm 0.005) \text{ s}^{-1}$, at 25°C in CD_2Cl_2 .¹⁵⁵ Single crystals suitable for X-ray diffraction were obtained from a solution of the mixture in CDCl_3 . The *trans*- isomer was found to crystallize selectively in the monoclinic space group $P2_1/n$ with $Z = 2$ and 0.5 molecules of the complex and two molecules of CDCl_3 solvate in the asymmetric unit. The molecular structure of $\text{Pd}(\text{dppeS})_2$ and selected bond lengths and angles are given in Figure 40, whereas the crystallographic data are given in Table 24. The structure was revealed to be that of the *trans*- isomer. The Pd–P bond length is $2.3182(4) \text{ \AA}$ which is significantly longer than the Pd–P bond lengths ($2.23 - 2.25 \text{ \AA}$) observed in the chelating palladium bis(phosphine) monosulfide complexes (see Table 18).

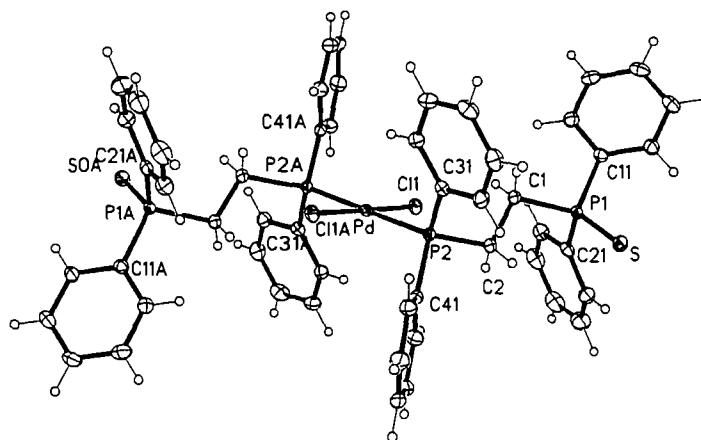


Figure 40. The molecular structure of **Pd(dppeS)₂** (solvate molecules are omitted for clarity); Pd–Cl 2.3079(5), Pd–P(2) 2.3182(4), P(1)–S 1.9605(6), P(1)–C(1) 1.8188(14), P(1)–C(11) 1.8124(15), P(1)–C(21) 1.8133(15), P(2)–C(2) 1.8383(14), P(2)–C(31) 1.8166(15), P(2)–C(41) 1.8165(14). P(2A)–Pd–P(2) 180.000(1)^o, Cl(1)–Pd–Cl(1A) 179.998(13)^o, P(2A)–Pd–Cl(1) 86.068(18)^o.

Interestingly, a ³¹P{¹H} NMR spectrum of the single crystals of the *trans*-isomer in CD₂Cl₂ showed mixed signals from both the *cis*- and *trans*- isomers, consistent with the equilibrium discussed above.

Unlike the other 1:2 molar ratio reactions of PdCl₂(PhCN)₂:L, the reaction with **dppmS** gave the cationic palladium complex salt [Pd(dppmS)₂]Cl₂ **Pd(dppmS)₂**. Suitable single crystals of **Pd(dppmS)₂** were obtained from slow evaporation of a solution in CHCl₃:Et₂O and CD₂Cl₂:Et₂O. **Pd(dppmS)₂** was found to crystallize in two different polymorphs, both in the triclinic space group *P*-1 with 0.5 molecules and two half molecules, respectively, in the asymmetric unit. The first polymorph also contains one CD₂Cl₂ solvate molecule, and the second two CHCl₃ molecules in their asymmetric units. The CD₂Cl₂ molecule is slightly disordered: one of the Cl atoms is disordered among three positions with occupancies of 0.9, 0.06 and 0.04, and the other over two positions with occupancies of 0.9 and 0.1. The disorder of the CHCl₃ molecules could not be satisfactorily rationalized, so they were given occupancies of 0.9, and the remaining electron density was approximated by arbitrary atomic positions with occupancies of 0.07 – 0.10. Another polymorph of *trans*-**Pd(dppmS)₂** has been reported in the literature, and was also found to crystallize in the triclinic

space group $P-1$ with $Z = 1$ and to contain one CH_2Cl_2 molecule and 0.5 molecules in the asymmetric unit.⁹⁶ The molecular structures of $\text{Pd}(\text{dppmS})_2\cdot\text{CD}_2\text{Cl}_2$ and $\text{Pd}(\text{dppmS})_2\cdot 4\text{CHCl}_3$ are shown in Figures 41 and 42, respectively. Crystallographic data are given in Table 24 and selected bond lengths and bond angles are given in Table 25.

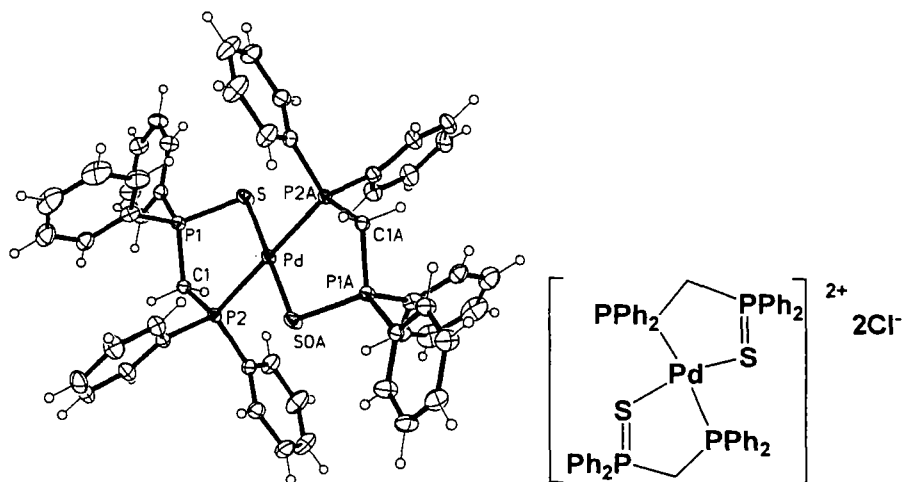


Figure 41. The molecular structure of $\text{Pd}(\text{dppmS})_2\cdot 2\text{CD}_2\text{Cl}_2$ (Cl counter anions and solvate molecules omitted for clarity).

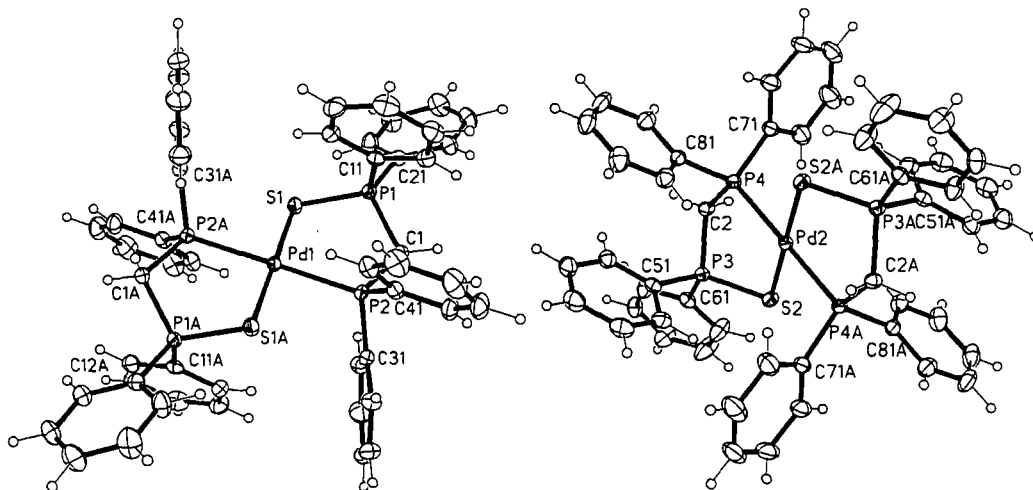


Figure 42. The molecular structure of $\text{Pd}(\text{dppmS})_2\cdot 4\text{CHCl}_3$ (solvate molecules and Cl counter anions omitted for clarity).

Table 24. Crystallographic data for **Pd(dppmS)₂** and **Pd(dppeS)₂**.

Compound	Pd(dppmS)₂·2CD₂Cl₂	Pd(dppmS)₂·4CHCl₃	Pd(dppeS)₂·4CD₂Cl₂
Formula	C ₅₀ H ₄₄ Cl ₂ P ₄ PdS ₂ ·2(CCl ₂ D ₂)	C ₅₀ H ₄₄ Cl ₂ P ₄ PdS ₂ ·4(CCl ₃ H)	C ₅₂ H ₄₈ Cl ₂ P ₄ PdS ₂ ·4(CCl ₂ D ₂)
FW	1184.03	1487.62	1519.70
<i>T</i> (K)	129(2)	120(2)	129(2)
Crystal system	Triclinic	Triclinic	Monoclinic
Space group	<i>P</i> -1	<i>P</i> -1	<i>P</i> 2 ₁ / <i>n</i>
<i>a</i> (Å)	10.241(1)	11.1225(16)	9.2057(9)
<i>b</i> (Å)	11.498(1)	14.199(2)	21.475(2)
<i>c</i> (Å)	11.783(1)	20.830(3)	16.1111(16)
α (°)	80.61(1)	85.69(3)	90.00
β (°)	82.58(1)	87.44(2)	92.85(1)
γ (°)	83.40(1)	89.99(3)	90.00
<i>U</i> (Å ³)	1351.1(2)	3277.0(8)	3181.1(6)
<i>Z</i>	1	2	2
<i>D</i> _x (Mg cm ⁻³)	1.455	1.508	1.587
μ (mm ⁻¹)	0.870	1.050	1.083
Refls measured	18368	39092	38892
Independent reflections	7831	17257	9101
Data/restraints/parameters	7831/4/307	17257/0/691	9101/0/361
Final R indices <i>I</i> > 2σ	R1=0.0266, WR2=0.0661	R1=0.0370, WR2=0.0877	R1=0.0259, WR2=0.0610
R indices (all data)	R1=0.0309, WR2=0.0688	R1=0.0666, WR2=0.1013	R1=0.0315, WR2=0.0634

Table 25. Selected bond lengths and angles of **Pd(dppmS)₂·2CD₂Cl₂** and **Pd(dppmS)₂·4CHCl₃**.

Bond (Å)	Pd(dppmS)₂·2CD₂Cl₂	Pd(dppmS)₂·4CHCl₃	
Pd-S	2.3277(4)	2.3361(8)	2.3305(8)
Pd-P	2.3195(4)	2.3174(7)	2.3197(7) 2.3198(7)
P=S	2.0209(6)	2.0197(10)	2.0216(10)
P(S)-CH ₂	1.7914(14)	1.804(2)	1.805(2)
P-CH ₂	1.8349(14)	1.843(2)	1.838(2)
P(S)-C _{ipso}	1.7917(14)	1.797(2)	1.791(2)
	1.8001(16)	1.800(2)	1.800(2)
P-C _{ipso}	1.8108(15)	1.808(2)	1.807(3)
	1.8113(14)	1.809(3)	1.812(3)
Angle (deg)			
S-Pd-P	91.536(15)	88.13(3)	88.00(3)
		91.87(3)	92.00(3)
P(S)-S-Pd	99.527(19)	97.96(4)	98.68(4)
S-P(S)-CH ₂	107.85(5)	107.52(9)	107.53(9)
Pd-P-CH ₂	110.51(5)	109.99(8)	109.94(8)
Pd-P-C _{ipso}	111.48(5)	111.01(8)	111.45(9)
	115.34(5)	116.74(9)	115.84(9)
S-P(S)-C _{ipso}	107.67(5)	109.93(9)	110.11(9)
	112.50(6)	111.79(9)	111.76(9)

The Pd centers have *trans*-square planar structures which are slightly distorted from perfect square planarity (S–Pd–S 92.0° (av), see Table 25) but with no tetrahedral distortions (angle between S(1)–Pd–P(1) and S(0A)–Pd–P(1A) planes for both structures are 0°). The bond lengths and angles will be discussed in detail later.

The crystal packing of **Pd(dppmS)₂·2CD₂Cl₂** features close Cl.....H intermolecular contacts between the chloride counter anions and the aromatic protons (2.837 Å), whereas no close intermolecular contacts were observed in **Pd(dppmS)₂·4CHCl₃**. The crystal packing of **Pd(dppmS)₂·CD₂Cl₂**, with close intermolecular contacts shown as dashed lines, is depicted in Figure 43.

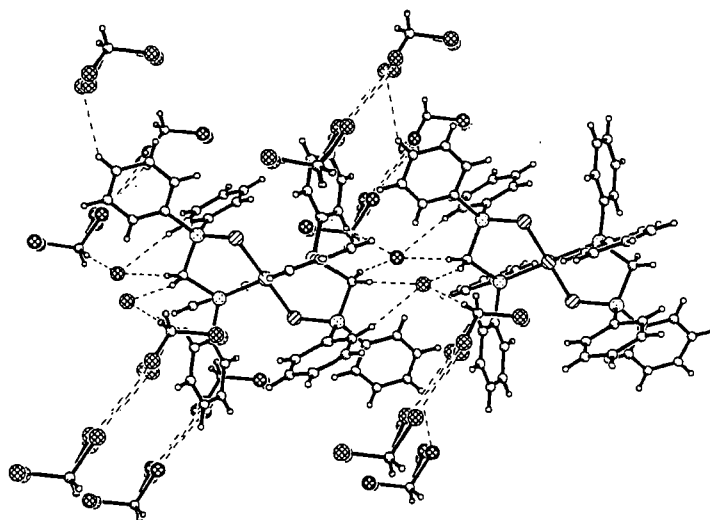


Figure 43. Close intermolecular contacts in the structure of **Pd(dppmS)₂·2CD₂Cl₂**.

Pd(dppmS)₂ has limited solubility; however, a $^{31}\text{P}\{^1\text{H}\}$ NMR spectrum was obtained from a saturated solution in CD_2Cl_2 (Figure 44) which consists of three sets of peaks: doublets at $\delta = -28.42$ and 39.94 ppm [$^2J_{\text{P-P}} = 78$ Hz] which correspond to the signals from P and P(S) of the free ligand (see Figure 16); doublets at $\delta = 33.64$ and 55.55 ppm [$^2J_{\text{P-P}} = 36$ Hz] which are the P and P(S) signals of **Pd(dppmS)** (see Table 20); and broad signals at $\delta = 27.55$, 35.28 , 47.02 and 54.26 ppm, assigned to the two P and two P(S) atoms bound to the Pd center of **Pd(dppmS)₂**. As *cis*- and *trans*- isomers of very similar complexes of both palladium¹⁷ and platinum¹⁶¹ are known in the literature, it is likely that **Pd(dppmS)₂** exists as *cis*- and *trans*- isomers in solution which would explain the four $^{31}\text{P}\{^1\text{H}\}$ NMR signals. The spectrum suggests that **Pd(dppmS)₂** is partially dissociated in solution, as evidenced by signals from the free ligand and **Pd(dppmS)**. Due to the limited solubility of **Pd(dppmS)₂**, no dynamic NMR studies have been carried out. The $^{31}\text{P}\{^1\text{H}\}$ NMR signals of **Pd(dppmS)₂** in dmsO-d_6 were reported to be 37.6 ppm for P and 49.6 ppm for P(S) [$^2J_{\text{P-P}} = 23$ Hz].⁹⁶ Interestingly, there is no report of any dissociation. We then obtained a $^{31}\text{P}\{^1\text{H}\}$ NMR spectrum of **Pd(dppmS)₂** from a freshly prepared solution in dmsO-d_6 and another spectrum after 18 h. At $t = 15$ min (Figure 45), we observed two doublets at 38.12 ppm and 50.00 ppm [$^2J_{\text{P-P}} = 26$ Hz] as well as the signal for free ligand and **Pd(dppmS)**. Furthermore, we also observed broad signals at 28.93 and 57.44 ppm. We believe that the signal at 38.12 ppm and 50.00 ppm [$^2J_{\text{P-P}} = 26$ Hz] are those of P and P(S) of *cis*-**Pd(dppmS)₂**, respectively, and that the broad signals at 28.93 and

57.44 ppm are P and P(S) of *trans*-Pd(dppmS)₂. At t = 18 h, the integration of all peaks are almost the same as that observed at t = 15 min. It would appear that, in dmsO-d₆, Pd(dppmS)₂ dissociates to give free ligand and Pd(dppmS) and isomerizes to *trans*-Pd(dppmS)₂, but at a slow rate. We conclude that the Pd(dppmS)₂ solution ³¹P{¹H} NMR spectrum in CD₂Cl₂ (Figure 44) already represents the system at equilibrium. A summary of the dissociation equilibria of Pd(dppmS)₂ is shown in Scheme 26.

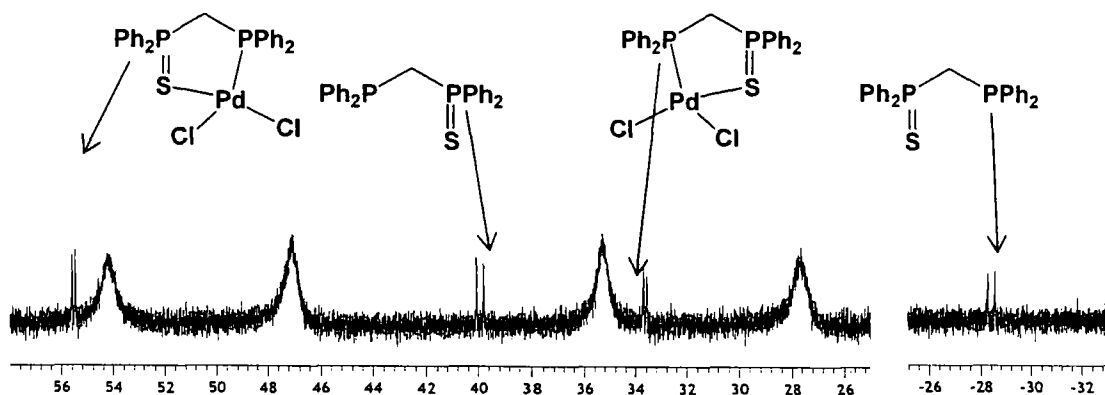


Figure 44. The ³¹P{¹H} NMR spectrum (202 MHz) of Pd(dppmS)₂ in CD₂Cl₂.

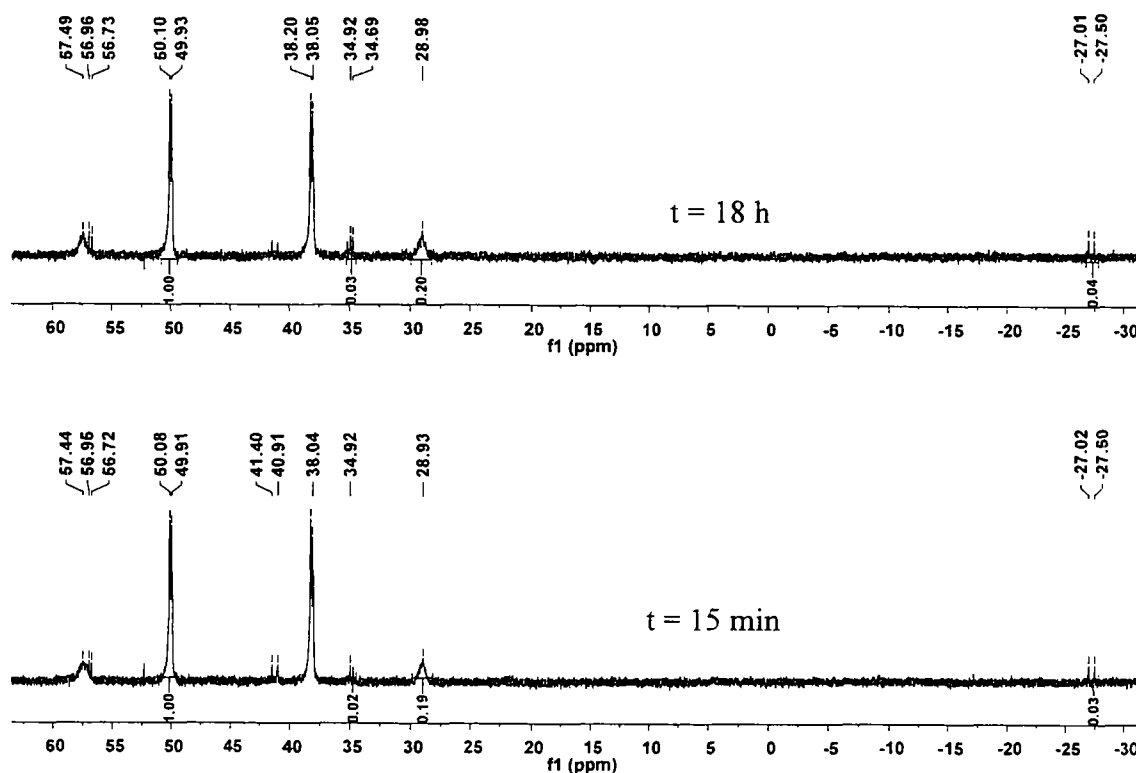
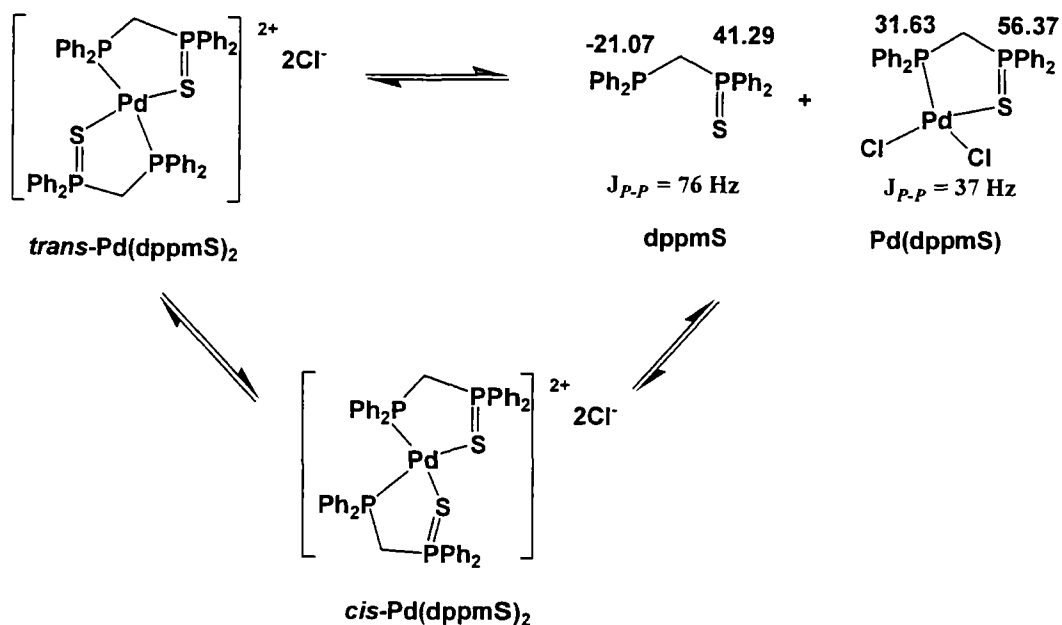


Figure 45. The ³¹P{¹H} NMR spectrum (161 MHz) of Pd(dppmS)₂ in dmsO-d₆ at t = 15 min and 18 h.



Scheme 26. The equilibria of $\text{Pd}(\text{dppmS})_2$ in CD_2Cl_2 solution.

Reaction of $[\text{Pd}(\text{CH}_3\text{CN})_4](\text{BF}_4)_2$ with bis(phosphine) disulfides in a 1:2 molar ratio

The cationic palladium salts $[\text{Pd}(\text{dppmS}_2)_2](\text{BF}_4)_2$ **Pd(dppmS₂)₂**, $[\text{Pd}(\text{dppeS}_2)_2](\text{BF}_4)_2$ **Pd(dppeS₂)₂** and $[\text{Pd}(\text{dppfS}_2)_2](\text{BF}_4)_2$ **Pd(dppfS₂)₂** (Figure 46) were prepared *via* reaction of the appropriate bis(phosphine) disulfide ligand with 0.5 equivalents of $[\text{Pd}(\text{CH}_3\text{CN})_4](\text{BF}_4)_2$ ¹⁴⁸ in CH_2Cl_2 at room temperature. The products were obtained in quantitative yields. The $^{31}\text{P}\{^1\text{H}\}$ NMR resonances of the palladium complexes differ only slightly from those of the free ligands. An *in situ* NMR reaction of two equivalents of **dppbS₂** with one equivalent of $[\text{Pd}(\text{CH}_3\text{CN})_4](\text{BF}_4)_2$ showed a mixture of palladium complexes as well as the signals of **dppbS₂** (see Figure C3 in Appendix C for the $^{31}\text{P}\{^1\text{H}\}$ NMR spectrum).

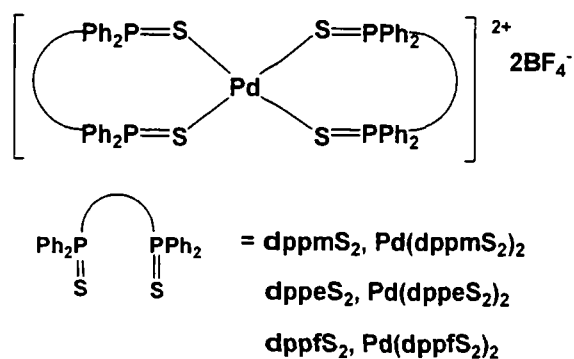


Figure 46. The palladium complex products from the 1:2 molar ratio reaction of $[\text{Pd}(\text{CH}_3\text{CN})_4](\text{BF}_4)_2 \cdot \text{L}$ (L = bis(phosphine) disulfides).

Suitable single crystals for X-ray diffraction of **Pd(dppmS₂)₂** and **Pd(dppfS₂)₂** were obtained from slow evaporation of solutions in $\text{CH}_2\text{Cl}_2:\text{Et}_2\text{O}$ and **Pd(dppeS₂)₂** from a solution in CHCl_3 :hexane. They were found to crystallize in the following space groups: **Pd(dppmS₂)₂** in the monoclinic space group $P2_1/n$ with $Z = 2$, **Pd(dppeS₂)₂** and **Pd(dppfS₂)₂** in the triclinic space group $P-1$ with $Z = 1$ and $Z = 2$, respectively. **Pd(dppmS₂)₂** and **Pd(dppeS₂)₂** contain 0.5 molecules in the asymmetric unit, whereas **Pd(dppfS₂)₂** has one molecule. Another polymorph of **Pd(dppeS₂)₂** has been reported in the literature,¹⁴⁸ in the monoclinic space group $P2_1/n$ with $Z = 4$, but it shows similar bond lengths and angles to those in our structure. The molecular structures of **Pd(dppmS₂)₂**, **Pd(dppeS₂)₂** and **Pd(dppfS₂)₂** are shown in Figures 47, 48 and 49, respectively. Crystallographic data for these complexes are given in Table 26 and selected bond lengths and angles are given in Table 27.

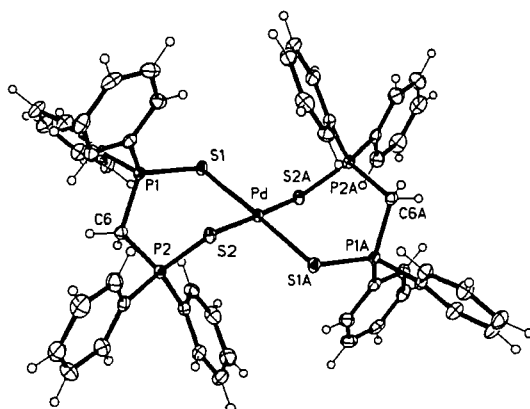


Figure 47. The molecular structure of **Pd(dppmS₂)₂** (BF_4^- counter anions omitted for clarity).

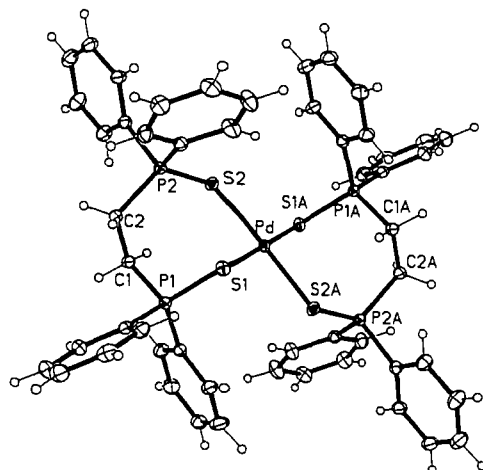


Figure 48. The molecular structure of **Pd(dppeS₂)₂** (BF₄⁻ counter anions omitted for clarity).

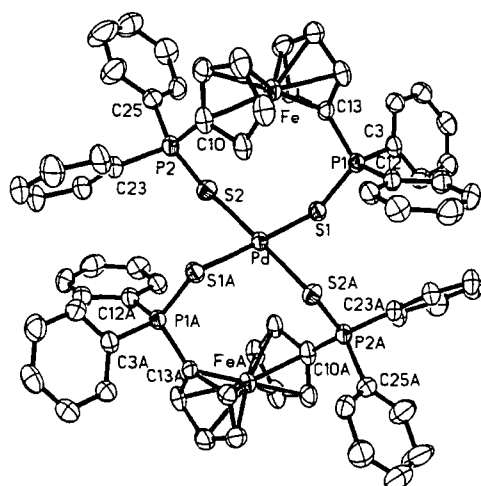


Figure 49. The molecular structure of **Pd(dppfS₂)₂** (BF₄⁻ counter anions omitted for clarity).

Table 26. Crystallographic data for **Pd(dppmS₂)₂**, **Pd(dppeS₂)₂** and **Pd(dppfS₂)₂**.

Compound	Pd(dppmS₂)₂	Pd(dppeS₂)₂·2CHCl₃	Pd(dppfS₂)₂
Formula	C ₅₀ H ₄₄ P ₄ PdS ₄ ²⁺ , 2(BF ₄ ¹⁻)	C ₅₄ H ₄₈ P ₄ PdS ₄ ²⁺ , 2(BF ₄ ¹⁻)·2(CHCl ₃)	C ₆₈ H ₅₆ P ₄ PdS ₄ ²⁺ , 2(BF ₄ ¹⁻)·4(CHCl ₃)
FW	1176.99	1443.78	1994.44
<i>T</i> (K)	120(2)	120(2)	230(2)
Crystal system	Monoclinic	Triclinic	Triclinic
Space group	<i>P</i> 2 ₁ / <i>n</i>	<i>P</i> -1	<i>P</i> -1
<i>a</i> (Å)	10.8321(12)	10.3040(12)	12.5884(17)
<i>b</i> (Å)	14.9990(17)	12.1295(12)	13.3026(11)
<i>c</i> (Å)	15.4466(18)	13.3630(13)	13.7109(19)
α (°)	90.00	86.110	84.571(6)
β (°)	91.097(20)	74.106(12)	76.625(4)
γ (°)	90.00	70.059(12)	68.449(6)
<i>U</i> (Å ³)	2509.2(5)	1509.4(3)	2077.4(6)
<i>Z</i>	2	1	1
<i>D_x</i> (Mg cm ⁻³)	1.558	1.588	1.594
μ (mm ⁻¹)	0.730	0.879	1.181
Refls measured	25461	35263	14855
Independent reflections	5746	12659	9167
Data/restraints/parameters	5746 / 0 / 313	12659 / 3 / 370	9167 / 0 / 479
Final R indices <i>I</i> > 2σ	R1=0.0351, WR2=0.0644	R1=0.0344, WR2=0.0861	R1=0.0711, WR2=0.1802
R indices (all data)	R1=0.0547, WR2=0.0697	R1=0.0416, WR2=0.0901	R1=0.1127, WR2=0.0205

Table 27. Bond lengths and angles of **Pd(dppmS₂)₂**, **Pd(dppeS₂)₂** and **Pd(dppfS₂)₂**.

Bond (Å)	Pd(dppmS₂)₂	Pd(dppeS₂)₂	Pd(dppfS₂)₂
Pd-S	2.3256(6)	2.3339(4)	2.3484(13)
	2.3357(7)	2.3403(5)	2.3597(13)
P-S	2.0107(9)	2.0177(6)	2.0161(19)
	2.0145(8)	2.0216(5)	2.013(2)
P-CH ₂ ^a	1.814(2)	1.7972(13)	1.774(5)
	1.829(2)	1.8339(13)	1.773(6)
P-C _{ipso}	1.798(2)	1.7946(13)	1.803(5)
	1.802(2)	1.7993(13)	1.807(5)
	1.798(2)	1.7893(14)	1.809(5)
	1.800(2)	1.8084(14)	1.800(6)
Angle (deg)			
S-Pd-S	82.57(2)	82.584(14)	87.85(5)
	97.43(2)	97.417(14)	92.15(15)
P-S-Pd	98.60(3)	100.33(2)	112.23(7)
	110.60(3)	113.642(19)	112.56(7)
S-P-CH ₂ ^a	111.37(8)	110.56(5)	114.70(17)
	113.40(8)	114.93(5)	114.6(2)
S-P-C _{ipso}	106.54(8)	115.84(5)	116.87(19)
	114.41(9)	107.77(5)	104.18(19)
	106.75(9)	114.22(5)	117.1(2)
	112.84(8)	105.14(5)	107.5(2)

^a P-C(sp²) for **Pd(dppfS₂)₂**.

The palladium (II) centers are bound to four S atoms from two ligands to form six-membered rings in **Pd(dppmS₂)₂** and seven-membered ones in **Pd(dppeS₂)₂**. The Pd centers have no tetrahedral distortion but are slightly distorted from square planar (S-Pd-S 95.7° (av)).

The close S...H and F...H intermolecular contacts of 2.803 Å and 2.488 Å, respectively, which are shorter than the sum of van der Waals radii¹⁵⁸ (2.91 and 2.54 Å, respectively) were observed in **Pd(dppeS₂)₂** and **Pd(dppfS₂)₂**, respectively, but no close contacts were observed in **Pd(dppmS₂)₂**. The close intermolecular contacts are shown as dashed lines in Figures 50 and 51.

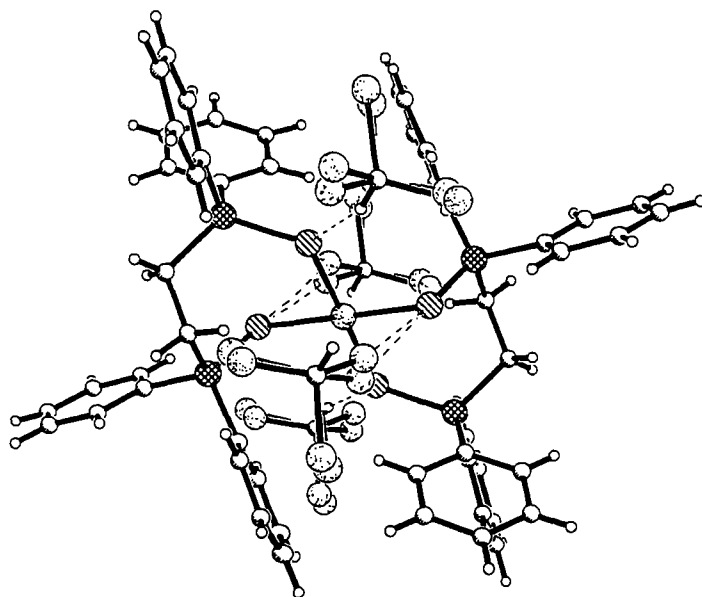


Figure 50. Close intermolecular contacts in the structure of **Pd(dppeS₂)₂**.

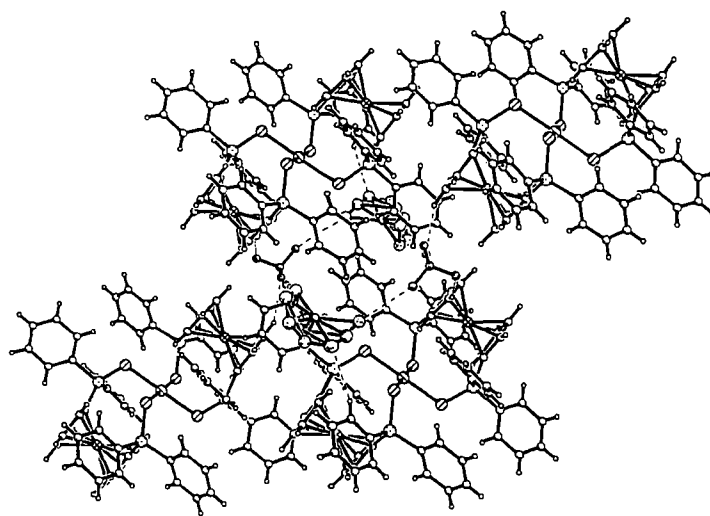


Figure 51. Close intermolecular contacts in the structure of **Pd(dppfS₂)₂**.

II.3 Discussion of the crystal structures of the palladium complexes

Pertinent bond lengths and angles for all of the chelate complexes in this study are presented in Figure 52. Both bond lengths and angles for **Pd(dppeS)** and **Pd(dppmS)₂** are the average values (from the two independent molecules in the asymmetric unit and three molecules (from two polymorphs) for **Pd(dppeS)** and **Pd(dppmS)₂**, respectively). To investigate the influence of the addition of sulfur atoms to the ligands on the structures of the resulting Pd complexes, comparisons of the bond lengths and bond angles in the palladium complexes with dppm, dppe, dppp, dppf and dcpe will be made, with the reference to the reported structures of PdCl₂(dppm) **Pd(dppm)**, PdCl₂(dppe) **Pd(dppe)**,¹⁶² PdCl₂(dppp) **Pd(dppp)**,¹⁶² PdCl₂(dcpe) **Pd(dcpe)**,¹⁶³ PdCl₂(dppf)·CHCl₃ **Pd(dppf)·CHCl₃**,¹⁶⁴ PdCl₂(dppf)·CH₂Cl₂ **Pd(dppf)·CH₂Cl₂**¹⁶⁵ and [Pd(dppe)₂]Cl₂ **Pd(dppe)₂**.¹⁶⁶ Selected bond lengths and angles for all of these reported structures are given in Table 28.

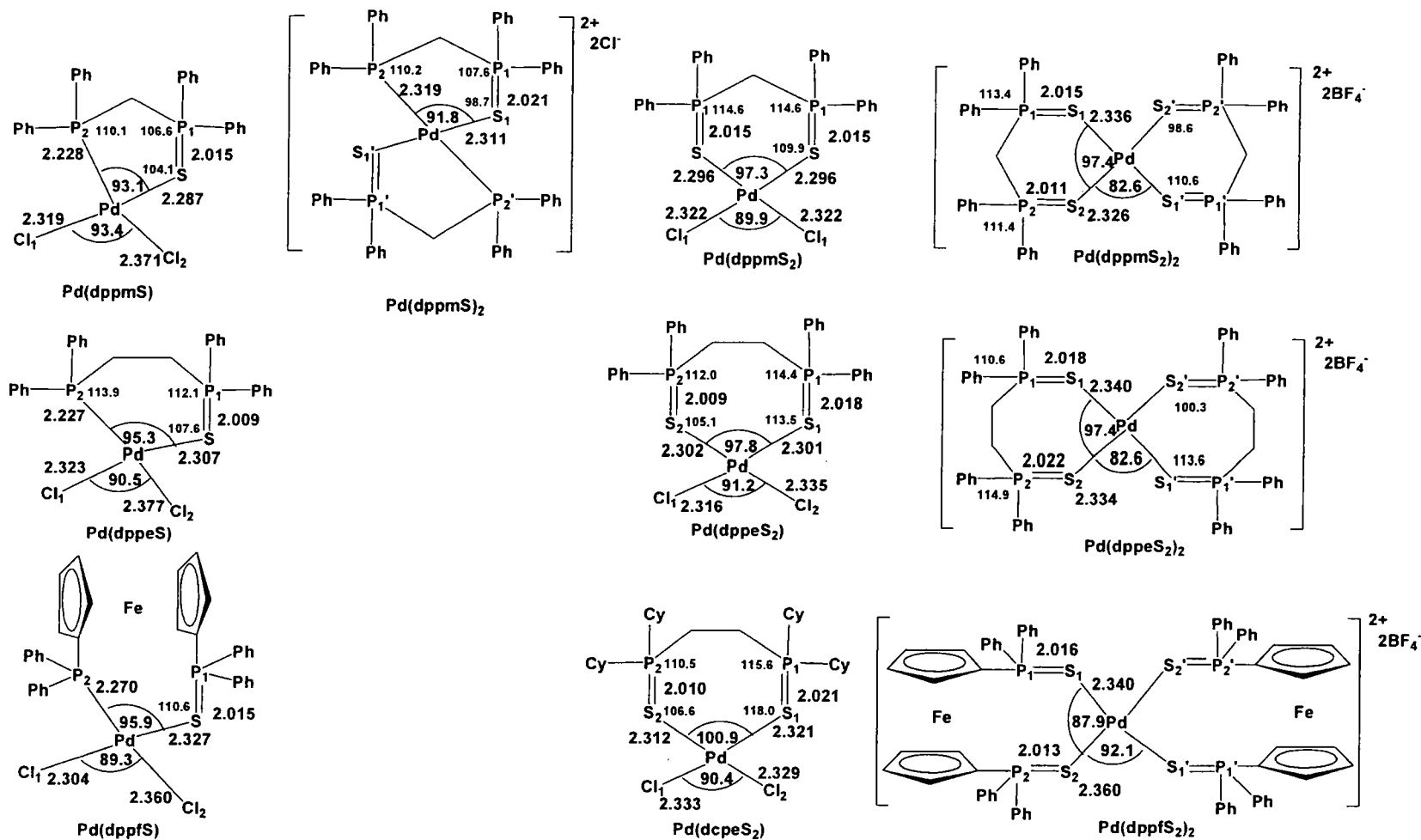


Figure 52. Comparison of the geometries about the Pd atoms in the related palladium complexes.

Table 28. Bond lengths and angles of the structures of **Pd(dppm)**, **Pd(dppe)**, **Pd(dppp)**, **Pd(dcpe)**, **Pd(dppf)·CHCl₃**, **Pd(dppf)·CH₂Cl₂** and **[Pd(dppe)₂]Cl₂**.

Bond (Å)	Pd(dppm) ¹⁶²	Pd(dppe) ¹⁶²	Pd(dppp) ¹⁶²	Pd(dcpe) ¹⁶³	Pd(dppf)·CHCl₃ ¹⁶⁴	Pd(dppf)·CH₂Cl₂ ¹⁶⁵	[Pd(dppe)₂]Cl₂ ¹⁶⁶
Pd-Cl(1)	2.236(1)	2.361(2)	2.351(1)	2.369(1)	2.347(1)	2.340(1)	-
Pd-Cl(2)	2.352(1)	2.357(2)	2.358(2)	2.376(1)	2.348(1)	2.358(1)	-
Pd-P(1)	2.234(1)	2.233(2)	2.244(1)	2.232(1)	2.283(1)	2.289(1)	2.3469(10)
Pd-P(2)	2.250(1)	2.226(2)	2.249(2)	2.233(1)	2.301(1)	2.278(1)	2.3348(10)
Angle (deg)							
Cl(1)-Pd-Cl(2)	93.63(3)	94.19(7)	90.78(5)	94.85(5)	87.8(1)	89.97(4)	-
P(1)-Pd-P(2)	72.68(3)	85.82(7)	90.58(5)	87.05(5)	99.07(5)	97.98(4)	82.66(4)
Pd-P(1)-CH ₂	94.7(1)	108.5(7)	115.9(2)	109.30	115.97	113.49	105.0
Pd-P(2)-CH ₂	94.3(1)	107.9(2)	115.5(2)	109.10	124.10	123.07	109.4

From analysis of all of the structures we can make the following observations:

1. Upon coordination, the S–P–C bond angles become wider and the C–P–C angles become smaller than in the free ligands which suggest that the geometries at P and P(S) become more tetrahedral on coordination.

2. The Pd–Cl (*trans*-S) bond lengths range from 2.3035(10) Å in **Pd(dppfS)** to 2.3291(7) Å in one of the molecules in **Pd(dppeS)**, whereas those of the Pd–Cl (*trans*-P) range from 2.3596(9) Å in **Pd(dppfS)** to 2.3790(8) Å in **Pd(dppeS)**. This implies that phosphorus has a stronger *trans*-influence and is apparently a stronger σ -donor than sulfur as the Pd–Cl bond lengths *trans* to phosphorus are slightly lengthened compared with those *trans* to sulfur.

3. The bis(phosphine) monosulfides are more likely to form P-bound complexes than S-bound complexes, (**Pd(dppeS)**₂ and **Pd(dppfS)**₂). This suggests that the phosphine sulfide groups are more labile than the phosphine groups.

4. The P=S bond lengths in all of the palladium complexes in which S is coordinated to Pd are in the range 2.00 – 2.03 Å, which is in the range reported in the literature for phosphine sulfide complexes (1.97 – 2.05 Å) and are longer than the P=S bond lengths (1.955 Å (av)) for the free phosphine sulfides reported in the CSD (2007).²

5. **Pd(dppmS)**, **Pd(dppeS)** and **Pd(dppfS)** which have increasingly longer backbones, show essentially no difference in the Pd–P bond lengths from **Pd(dppmS)**, to **Pd(dppeS)** (2.2282(4) and 2.227 (av) Å, respectively), but Pd–P is slightly longer in **Pd(dppfS)** (2.270 Å), whereas the Pd–S bonds become longer (2.2874(4), 2.307 (av), 2.3267(10) Å, respectively. The bite angles are found to be 93.1°, 95.3° (av) and 95.9° in **Pd(dppmS)**, **Pd(dppeS)** and **Pd(dppfS)**, respectively.

6. In **Pd₂(dppbS)**, the Pd–P bond length is 2.2486(6) Å, similar to the other bis(phosphine) monosulfide complexes discussed previously, but the Pd–S bond length (2.4253(6) Å) is significantly longer than those in the other complexes. This can be attributed to the greater *trans*- influence of the P atom compared to that of Cl.

7. When comparing the five-membered ring complexes **Pd(dppmS)** and **Pd(dppmS)**₂ (Figure 53), the palladium bite angle is slightly smaller (91.8° (av) vs 93.1°) in **Pd(dppmS)**₂, whereas both Pd–P and Pd–S bond lengths are longer in **Pd(dppmS)**₂.

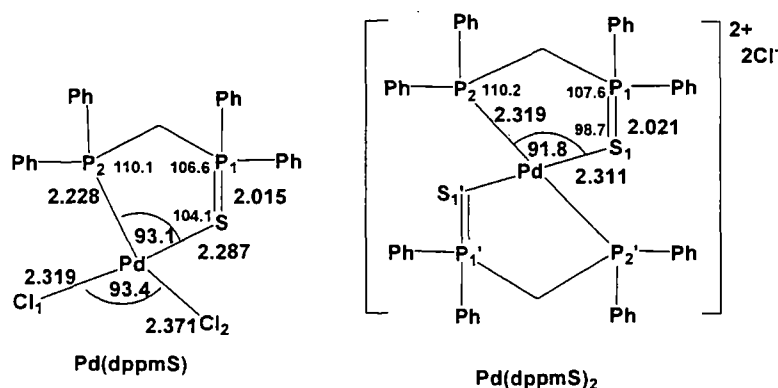


Figure 53. Comparison of the geometries of the **Pd(dppmS)** and **Pd(dppmS)₂** structures.

8. As expected, the bite angles become larger when the ring size is increased. The following structures have the following bite angles; **Pd(dppm)**, **Pd(dppmS)** and **Pd(dppmS₂)** (72.7° , 93.1° and 97.3° , respectively) (see Figure 54); **Pd(dppe)**, **Pd(dppeS)** and **Pd(dppeS₂)** (85.8° , 95.3° and 97.8° , respectively) (see Figure 55); and **Pd(dcpe)** and **Pd(dcpeS₂)** (87.1° and 100.9° , respectively) (see Figure 56). It should be noted that the bite angles are markedly increased in going from the bis(phosphine) to the bis(phosphine) monosulfide complexes, but only slightly increased from the bis(phosphine) monosulfide to the bis(phosphine) disulfide complexes. However, this trend was not observed in the case of **Pd(dppf)** and **Pd(dppfS)**. The bite angle in **Pd(dppfS)** is 95.9° , substantially smaller than that in **Pd(dppf)** (99.6° (av)). The Cl–Pd–Cl bond angles generally decrease going from the bis(phosphine) to the bis(phosphine) monosulfide and bis(phosphine) disulfide complexes.

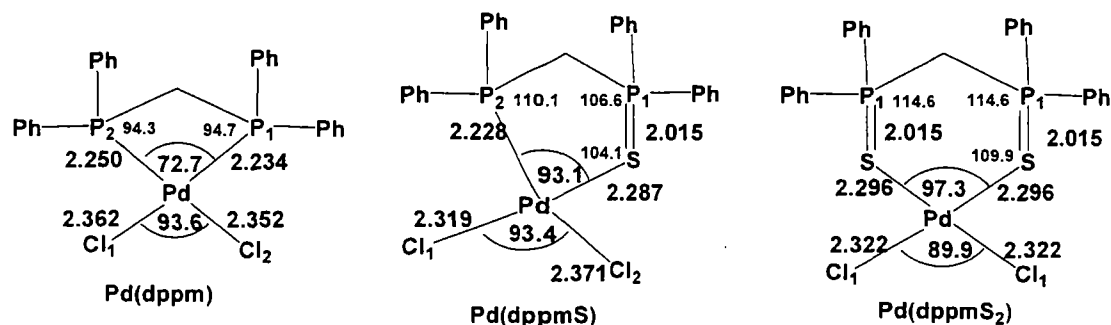


Figure 54. Comparison of the geometries of the **Pd(dppm)**, **Pd(dppmS)** and **Pd(dppmS₂)** structures.

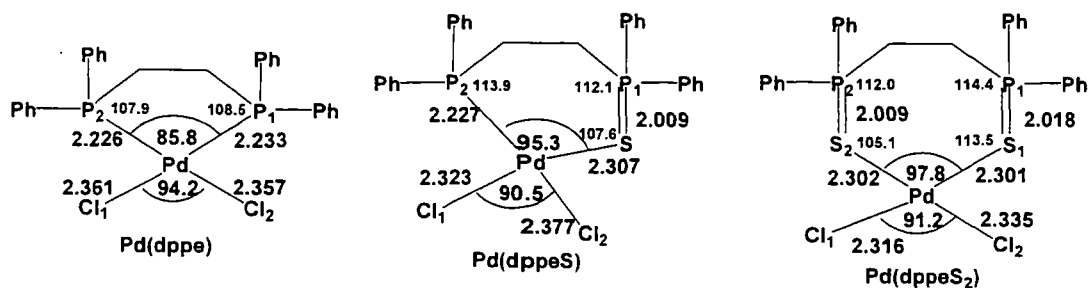


Figure 55. Comparison of the geometries of the **Pd(dppe)**, **Pd(dppeS)** and **Pd(dppeS₂)** structures.

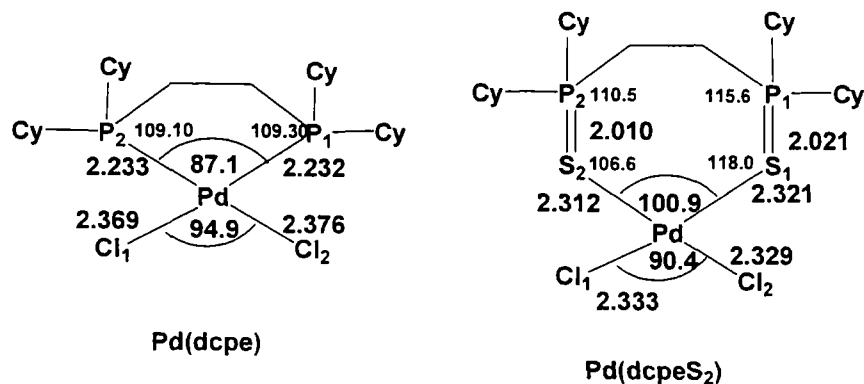


Figure 56. Comparison of the geometries of the **Pd(dcpe)** and **Pd(dcpeS₂)** structures.

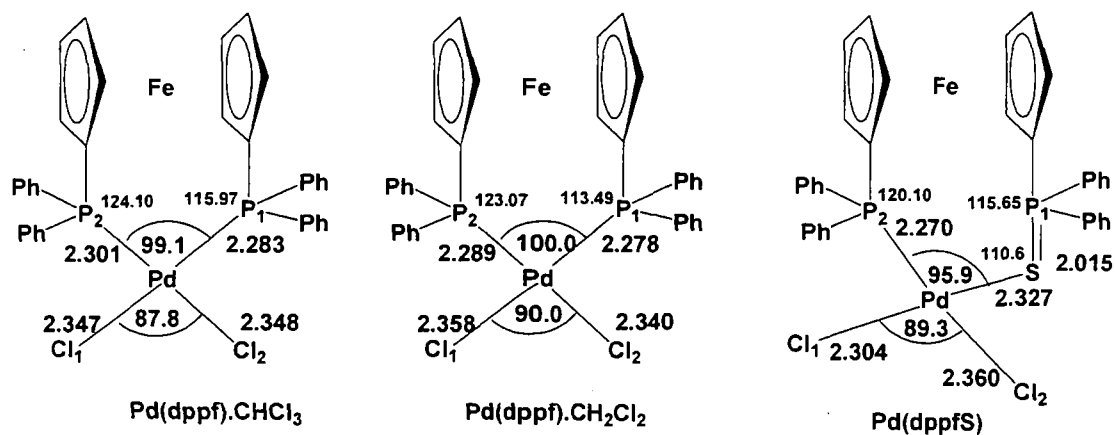


Figure 57. Comparison of the geometries of the **Pd(dppf)·CHCl₃**, **Pd(dppf)·CH₂Cl₂** and **Pd(dppfS)** structures.

9. The Pd-S-P angles vary from *ca.* 97° in **Pd₂(dppbS)** to 118° in **Pd(dcpeS₂)**. The latter is larger than in any of the palladium complexes of phosphine sulfides reported previously (78.6° – 116.8°). **Pd₂(dppbS)**, with its 16-membered ring, has small Pd-S-P angles (97°), comparable to those observed in the five-membered ring

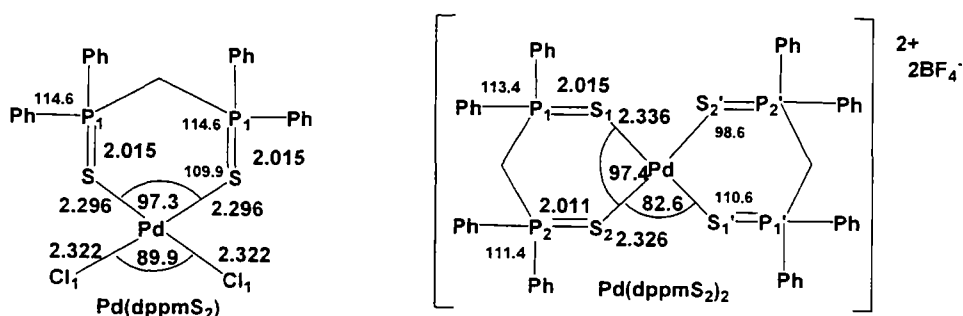
palladium phosphine sulfide complexes ($78.6 - 98.8^\circ$). This implies that the geometries at the S atoms are flexible and depend on the nature of the complexes.

10. Interestingly, the internal X–P–CH₂ (X = Pd or S) bond angles increase from the bis(phosphine) complexes to bis(phosphine) monosulfide complexes (94.5° (av) vs 110.1° in **Pd(dppm)** and **Pd(dppmS)** and 108.2° vs 113.9° in **Pd(dppe)** and **Pd(dppeS)**, respectively). One of the internal S–P–CH₂ bond angles in **Pd(dcpeS₂)** is larger (115.6°) and one smaller (110.5°) than the equivalent angles in **Pd(dppmS₂)** and **Pd(dppeS₂)** ($112.0 - 114.6^\circ$).

11. **Pd(dppeS₂)** and **Pd(dcpeS₂)** have P atoms which deviate from the Cl(1)–Pd–Cl(2) planes by $+1.07$ and -1.07 Å vs $+1.52$ and -0.22 Å, respectively.

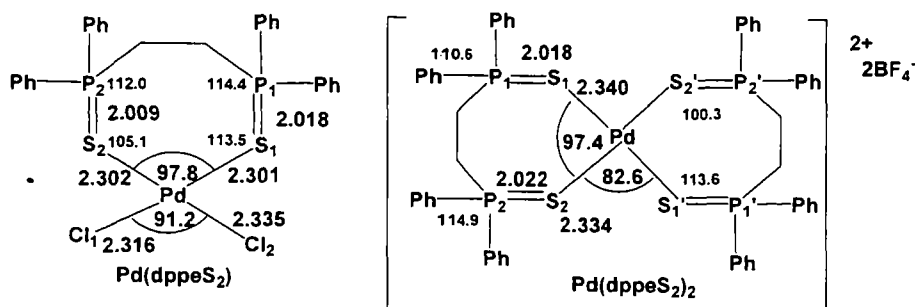
When comparing the mono- and bicyclic palladium complexes, we can make the following observations:

Pd(dppmS₂) and **Pd(dppmS₂)₂**



1. The bite angles in both complexes are almost the same ($97.28(2)^\circ$ vs $97.43(2)^\circ$).
2. The Pd–S bond lengths in **Pd(dppmS₂)** are shorter than in **Pd(dppmS₂)₂** (2.296 Å vs 2.331 Å (av)).
3. One of Pd–S–P angles in **Pd(dppmS₂)₂** is wider than the equivalent angle in **Pd(dppmS₂)**, whereas the other angle is smaller, 98.6° and 113.5° in **Pd(dppmS₂)₂** and 109.9° in **Pd(dppmS₂)**.
4. The S–P–CH₂ bond angles in both complexes are quite similar ($111.4 - 114.6^\circ$).

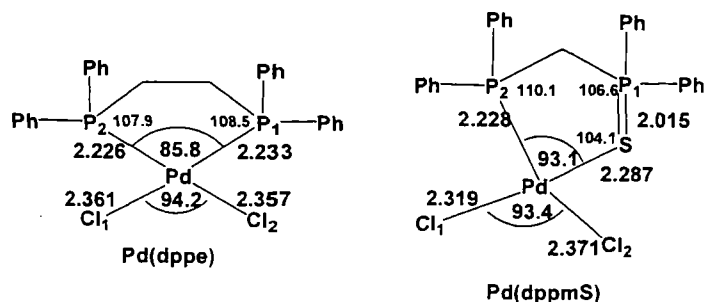
Pd(dppeS₂) and Pd(dppeS₂)₂



1. The bite angles in both complexes are quite similar ($97.76(5)^\circ$ vs $97.417(14)^\circ$ in Pd(dppeS₂) and Pd(dppeS₂)₂, respectively).
2. The Pd-S bond lengths in Pd(dppeS₂) are shorter compared to those in Pd(dppeS₂)₂ (2.302 Å vs 2.337 Å (av)). This suggests that the S has a slightly stronger *trans*-influence than the Cl atom.
3. Two Pd-S-P bond angles in Pd(dppeS₂) are significantly different (105.1° and 113.5°). The difference between these angles is even more pronounced in Pd(dppeS₂)₂ (100.3° and 113.6°).
4. The S-P-CH₂ bond angles in both complexes are quite similar ($110.6 - 114.9^\circ$).

When considering the palladium complexes with the same ring sizes, we can make the following observations:

Five-membered rings: Pd(dppe) and Pd(dppmS)

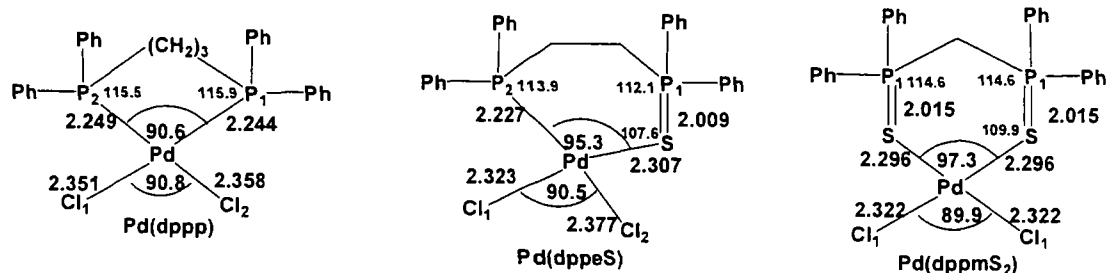


1. The bite angle is larger for Pd(dppmS) ($93.052(14)^\circ$) than for Pd(dppe) ($85.82(7)^\circ$).

2. The Pd–P bond lengths are very similar (2.230 Å (av) in **Pd(dppe)** vs 2.2282(4) Å in **Pd(dppmS)**), but the Pd–Cl (*trans*-P) bond length is longer in **Pd(dppmS)** than **Pd(dppe)** (2.359 Å (av)).

3. The structure of **Pd(dppmS)** is less planar than **Pd(dppe)**. In **Pd(dppmS)**, P(1) is coplanar with the Cl(1)–Pd–Cl(2) plane but P(2) deviates by 0.42 Å, whereas the two P atoms in **Pd(dppe)** deviate only slightly from Cl(1)–Pd–Cl(2) (+0.09 and -0.07 Å).

Six-membered rings: **Pd(dppp)**, **Pd(dppeS)** and **Pd(dppmS₂)**



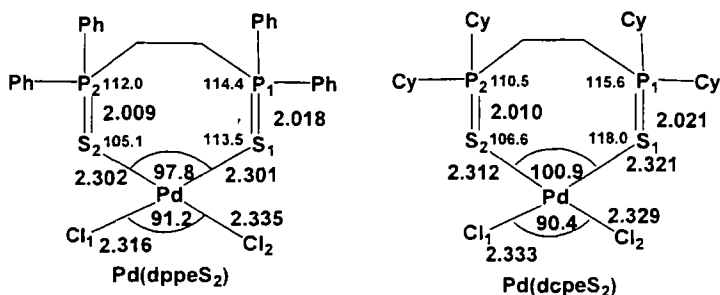
1. The bite angle becomes successively larger in the series **Pd(dppp)**, **Pd(dppeS)**, **Pd(dppmS₂)** (90.6°, 95.3° and 97.3°, respectively).

2. The X–P–CH₂ (X = S or Pd) angles in three complexes are quite similar.

3. By comparing **Pd(dppp)** with **Pd(dppeS)**, the Pd–P bond length becomes shorter (2.247 Å (av) vs 2.227 Å) whereas Pd–Cl (*trans*-P) becomes longer (2.355 Å (av) vs 2.377 Å).

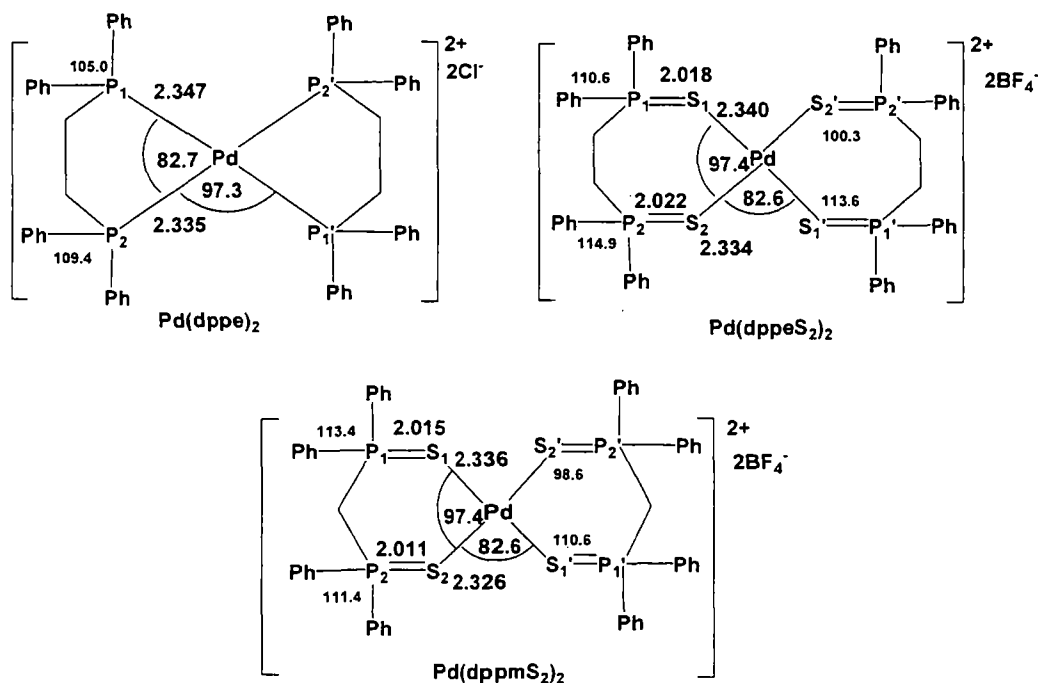
4. In **Pd(dppeS)** and **Pd(dppmS₂)**, both Pd–S and Pd–Cl (*trans*-S) bond lengths are very similar. The Pd–S bond lengths are 2.307 Å vs 2.296 Å and the Pd–Cl (*trans*-S) bond lengths are almost identical (2.323 Å (av) vs 2.322 Å for **Pd(dppeS)** and **Pd(dppmS₂)**, respectively). The P=S bond lengths and P–S–Pd angles are slightly decreased in **Pd(dppeS)**.

Seven-membered rings: **Pd(dppeS₂)** and **Pd(dcpeS₂)**



1. The bite angle in **Pd(dcpeS₂)** is 100.9°, which is wider than in **Pd(dppeS₂)** (97.8°).
2. The average bond lengths of Pd–S and Pd–Cl in **Pd(dcpeS₂)** are longer than in **Pd(dppeS₂)** (Pd–S; 2.317 (av) vs 2.301 (av) Å and Pd–Cl; 2.331 (av) vs 2.326 (av) Å).
3. The two Pd–S–P angles in **Pd(dcpeS₂)** (106.6° and 118.0°) are wider than the equivalent ones in **Pd(dppeS₂)** (105.1° and 113.5°).

Bicyclic complexes: **Pd(dppe)₂**, **Pd(dppeS₂)₂** and **Pd(dppmS₂)₂**



1. The bite angle of **Pd(dppeS₂)₂** is wider than in **Pd(dppe)₂** (97.4° vs 82.7°).
2. Two X–P–CH₂ (X = Pd or S) bond angles in **Pd(dppe)₂** (105.0° and 109.4°) are significantly smaller than in **Pd(dppeS₂)₂** (110.6° and 114.94°).

3. Interestingly, the bite angle in **Pd(dppeS₂)₂** is the same as in **Pd(dppmS₂)₂** (97.4°). Furthermore, the Pd–S and P=S bond lengths and S–P–CH₂ bond angles are quite similar (Pd–S 2.337 (av) Å vs 2.331 (av) Å, S–P–CH₂ 112.8° vs 112.4° (av) in **Pd(dppeS₂)₂** and **Pd(dppmS₂)₂**, respectively).

Torsion angles in palladium complexes

1. The S–P(1)–C–P(2) torsion angles in **Pd(dppmS)** and **Pd(dppmS₂)** are -46.6° and -36.5° respectively, whereas the P(1)–C(1)–C(2)–P(2) angles in **Pd(dppeS)** and **Pd(dppeS₂)** are -46.8° (av) and -78.0°, respectively. The largest P(1)–C(1)–C(2)–P(2) torsion angle was observed in **Pd(dcpeS₂)** (-102.3°). Views along the central bonds in the torsion angles discussed above are shown in Figure 58.

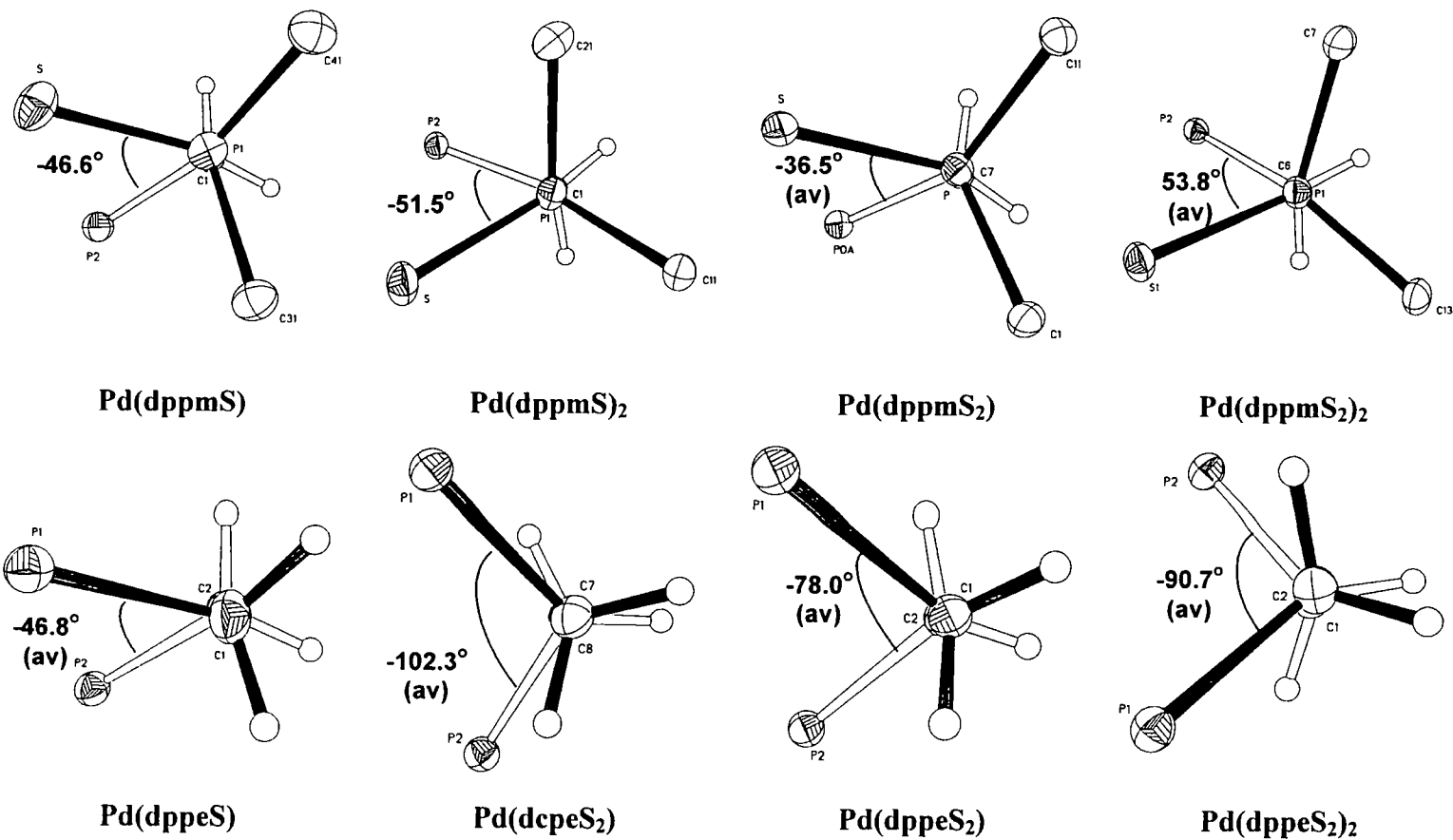


Figure 58. Views along the central bonds in the torsion angles in the palladium complexes (the atoms at the rear are shown with open bonds).

2. Views perpendicular to the Cp rings in **Pd(dppf)** and **Pd(dppfS)** showing the twist in the ferrocene units are given in Figure 59. It can be seen that the Cp rings in **Pd(dppf)** are twisted from the eclipsed conformation by an average of *ca.* 35° , whereas the twist in **Pd(dppfS)** 64.5° .

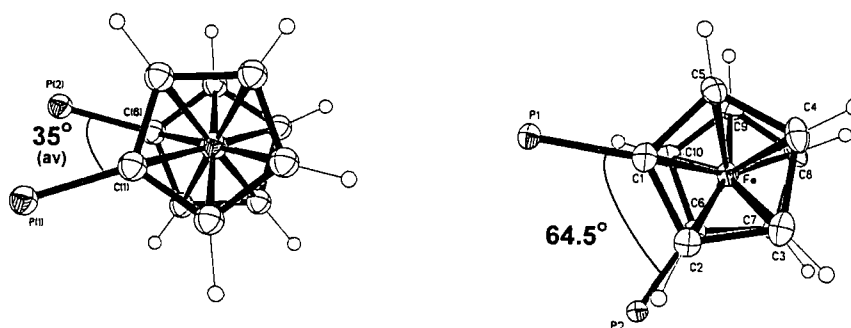
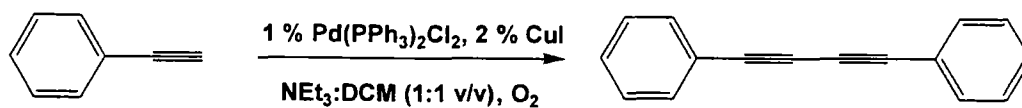


Figure 59. Views perpendicular to the Cp rings in **Pd(dppf)** (left) and **Pd(dppfS)** (right).

II.4 Activity of palladium complexes in homo-coupling reaction

The catalytic activity of the bis(phosphine) mono- and disulfide palladium complexes were tested in the oxidative homo-coupling reaction of phenylacetylene. Reactions were conducted in $\text{NEt}_3:\text{CH}_2\text{Cl}_2$ (1:1 v/v) using 1 mol% of the palladium complexes and 2 mol% of CuI with an oxygen balloon. The initially orange solutions turned brown when phenylacetylene was added. The reaction was followed to completion by GC-MS. At the end, brown solutions with black precipitates were observed. It is worth noting that a pale yellow solution was observed when $\text{PdCl}_2(\text{PPh}_3)_2$ was used as a catalyst. Surprisingly, this suggests that the PPh_3 may remain bound to the palladium without being oxidised. Palladium mirrors were not observed under any conditions. The results are summarized in Table 29. As can be seen, the conversions are good, although longer reaction times are needed to achieve complete conversion with **Pd(dppeS₂)₂** and **Pd(dcpes₂)** (entries 7 and 10). Palladium complexes of both monosulfides and disulfides seem to work well for the reaction. So far, no efforts have been made to optimise these reactions.

Table 29. Isolated yields for the homo-coupling of phenylacetylene using palladium complexes of bis(phosphine) monosulfides and disulfides.



Entry	Catalysts	Time [d]	Isolated yield [%]
1	PdCl ₂	1	86
2	PdCl ₂ (PPh ₃) ₂	1	90
3	Pd(dppmS)	1	87
4	Pd(dppmS₂)	1	90
5	Pd(dppmS₂)₂	1	90
6	Pd(dppeS₂)	1	95
7	Pd(dppeS₂)₂	2	90
8	Pd(dppfS)	1	93
9	Pd(dppeS₂)₂	1	92
10	Pd(dcpeS₂)	2	92

III. Conclusions

Several bis(phosphine) monosulfides and disulfide ligands have been synthesized and fully characterized by NMR spectroscopy, mass spectrometry, elemental analysis and single-crystal X-ray diffraction. The palladium complexes of the bis(phosphine) monosulfides and disulfides have also been obtained and fully characterized by NMR, elemental analysis and X-ray diffraction. The reaction with 1:1 molar ratios of Pd source to ligand were found to produce monomeric palladium complexes with chelating ligands, apart from the reaction with bis(diphenylphosphino)butane **dppbS** which was found to result in a dimer being formed. The reactions with 1:2 molar ratio of Pd source to monosulfide ligands gave complexes which were bound only through the phosphine groups, except for bis(diphenylphosphino)methane **dppmS** which formed cationic palladium complexes with two chelating ligands. Analogous reactions with the disulfide ligands and the Pd source $[\text{Pd}(\text{CH}_3\text{CN})_4](\text{BF}_4)_2$ also resulted in cationic Pd complexes incorporating two chelating ligands. In some cases, in solution, the complexes showed dynamic equilibria between *cis*- and *trans*- isomers.

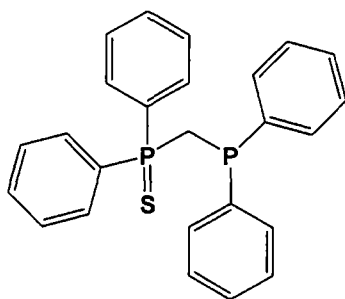
Comparison of the structures with those of analogous bis(phosphine) complexes reveals that the bite angles are substantially increased for the monosulfide complexes, except for the complexes of bis(diphenylphosphino)ferrocene **dppfS**. From the palladium complexes of bis(phosphine) monosulfides and disulfides and their related bis(phosphine) complexes, it is interesting that the Pd-S-P angles are variable whereas the P=S bond lengths are all in a narrow range. However, since there are no Pd-S-P angles less than 90° , it is unlikely that there is any η^2 - π bonding involving the P=S bond.

Preliminary results show that the activities of phosphine sulfide palladium complexes in the homo-coupling of phenylacetylene are comparable to that of the commonly used catalyst, $\text{PdCl}_2(\text{PPh}_3)_2$.

IV. Experimental

Tetrakis(acetonitrile)palladium(II) tetrafluoroborate $[\text{Pd}(\text{CH}_3\text{CN})_4][\text{BF}_4]_2$, from Aldrich, whereas $[\text{PdCl}_2(\text{PhCN})_2]$ and $[\text{PdCl}_2(\text{CH}_3\text{CN})_2]$ were prepared *via* literature procedure.¹⁶⁷ All the bis(phosphine) ligands were purchased from commercial suppliers and used without further purification except dppf which was synthesized *via* the literature procedure.¹⁶⁸ The ^1H , $^{13}\text{C}\{^1\text{H}\}$ and $^{31}\text{P}\{^1\text{H}\}$ NMR spectra were obtained in CDCl_3 unless otherwise indicated using Varian Mercury 400, Inova 500 and 700 VNMR spectrometers at the following frequencies: ^1H -500, 700 MHz, $^{13}\text{C}\{^1\text{H}\}$ -125, 175 MHz, $^{31}\text{P}\{^1\text{H}\}$ -161, 202, 283 MHz. Elemental analyses were performed using an Exeter Analytical CE-440 analyzer. Melting points were obtained using a Sanyo Gallenkamp apparatus, and are uncorrected. The chemical shifts are reported in ppm and are referenced to the internal standard SiMe_4 (for ^1H , $^{13}\text{C}\{^1\text{H}\}$), and external H_3PO_4 (for ^{31}P). MS analyses were performed using Thermo LTQFT (for ESI/HRMS-ESI) and Applied Biosystems Voyager-DE STR (for MALDI) instruments. All palladium complexes were initially prepared in NMR tubes in air and the reactions were followed by *in situ* $^{31}\text{P}\{^1\text{H}\}$ NMR spectroscopy. A nitrogen atmosphere was employed when the reactions were scaled up. The compounds **dppmS**,^{161, 169-171} **dppeS**,^{83, 161, 169, 170} **dppmS₂**,^{112, 172-174} **dppeS₂**^{117, 148, 175} and **dppfS₂**^{103, 157, 176} have been reported previously.

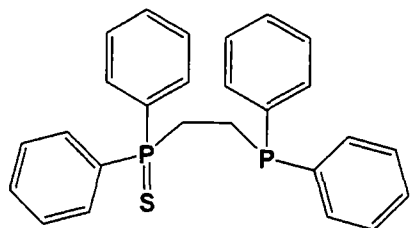
Bis(diphenylphosphino)methane monosulfide: **dppmS**



Dppm (1.740 g, 4.53 mmol) was dissolved in 10 mL of CHCl_3 and S_8 (0.145 g, 0.56 mmol) was added at room temperature and the mixture left over night in a glove box. After removing the solvent *in vacuo*, the crude product was purified by column chromatography in air on silica using CHCl_3 as eluent. The ratio of recovered **dppm**:**dppmS**:**dppmS₂** was approximately 1:2:1 (0.354 g : 1.072 g : 0.444 g). Yield: 1.072 g, 57 %. The single-crystal suitable for X-ray diffraction was grown *via* slow evaporation of a solution in CHCl_3 : CH_3OH . m.p. 87.7 - 88.5 °C. ^1H NMR (500 MHz): δ 7.79 (m, 4H, CH_{arom}), 7.44 (m, 2H, CH_{arom}), 7.36 (m, 8H, CH_{arom}), 7.26 (m, 6H, CH_{arom}), 3.34 (dd, $J_{\text{P-H}} = 10, 1$ Hz, 2H, CH_2). $^{13}\text{C}\{^1\text{H}\}$ NMR (125 MHz): δ 138.3 (dd, $J_{\text{P-C}} = 15, 9$ Hz, 2C_{arom}), 133.4 (d, $J_{\text{P-C}} = 81$ Hz,

$2C_{\text{arom}}$), 133.2 (d, $J_{P-C} = 20$ Hz, $4CH_{\text{arom}}$), 131.7 (d, $J_{P-C} = 3$ Hz, $2CH_{\text{arom}}$), 131.6 ($2CH_{\text{arom}}$), 131.5 (d, $J_{P-C} = 2$ Hz, $2CH_{\text{arom}}$), 129.1 ($2CH_{\text{arom}}$), 128.7 (d, $J_{P-C} = 7$ Hz, $4CH_{\text{arom}}$), 128.7 (d, $J_{P-C} = 12$ Hz, $4CH_{\text{arom}}$), 35.3 (dd, $J_{P-C} = 54, 32$ Hz, CH_2). $^{31}P\{^1H\}$ NMR (162 MHz): δ 41.29 (d, $J_{P(S)-P} = 76$ Hz, P(S)), -27.07 (d, $J_{P-P(S)} = 76$ Hz, P). MS (ES+) m/z : 417 (m^+). Anal. Calcd. for $C_{25}H_{22}P_2S$: C 72.10, H 5.32; Found C 72.06, H 5.32 %.

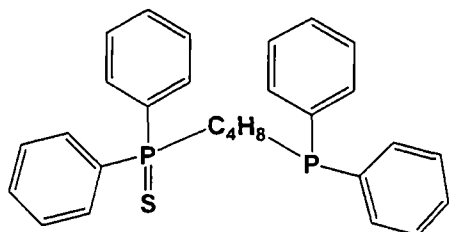
Bis(diphenylphosphino)ethane monosulfide: **dppeS**



DppeS was synthesized by the same procedure as was employed to synthesize **dppmS**, but using dppe (1.000 g, 1.76 mmol) and S_8 (0.081 g, 0.31 mmol). After removing the solvent *in vacuo*, the crude product was purified by column chromatography on

silica using chloroform as eluent. The ratio of recovered dppe:**dppeS**:**dppeS₂** was approximately 1:2:1 (0.238 g : 0.519 g : 0.32 g). Yield: 0.519 g, 48 %. The single-crystal suitable for X-ray diffraction was grown *via* slow evaporation of a solution in $CHCl_3$:MeOH. 1H NMR (500 MHz): δ 7.71 (m, 4H, CH_{arom}), 7.48 (m, 2H, CH_{arom}), 7.42 (m, 4H, CH_{arom}), 7.35 (m, 4H, CH_{arom}), 7.32 (m, 6H, CH_{arom}), 2.47 (m, 2H, CH_2), 2.28 (m, 2H, CH_2). $^{13}C\{^1H\}$ NMR (175 MHz): δ 137.5 (d, $J_{P-C} = 13$ Hz, $2C_{\text{arom}}$), 133.0 (d, $J_{P-C} = 18$ Hz, $4CH_{\text{arom}}$), 132.6 (d, $J_{P-C} = 80$ Hz, 2C), 131.7 (d, $J_{P-C} = 3$ Hz, $2CH_{\text{arom}}$), 131.3 (d, $J_{P-C} = 10$ Hz, $4CH_{\text{arom}}$), 129.1 ($2CH_{\text{arom}}$), 128.9 (d, $J_{P-C} = 21$ Hz, $4CH_{\text{arom}}$), 128.8 (d, $J_{P-C} = 2$ Hz, $4CH_{\text{arom}}$), 29.0 (dd, $^1J_{P-C} = 54$ Hz, $^3J_{P-C} = 18$ Hz, CH_2), 20.3 (dd, $^1J_{P-C} = 18$ Hz, $^3J_{P-C} = 3$ Hz, CH_2). $^{31}P\{^1H\}$ NMR (283 MHz): δ 44.17 (d, $J_{P(S)-P} = 50$ Hz, P(S)), -12.96 (d, $J_{P-P(S)} = 50$ Hz, P). MS (ES+) m/z : 431 (M^+). Anal. Calcd. for $C_{26}H_{24}P_2S$: C 67.54, H 5.62; Found C 67.60, H 5.18 %.

Bis(diphenylphosphino)butane monosulfide: **dppbS**

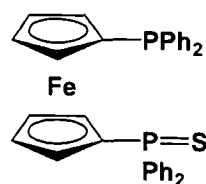


DppbS was synthesized by the same procedure as was employed to synthesize **dppmS**, but using dppb (1.061 g, 2.49 mmol) and S_8 (0.080 g, 0.31 mmol). After removing the solvent *in vacuo*, the crude product was

purified by column chromatography on silica using CH_2Cl_2 as eluent. The ratio of recovered dppb:**dppbS**:**dppbS₂** was approximately 1:2:1 (0.242 g : 0.499 g : 0.367 g).

Yield: 0.499 g, 44 %. ^1H NMR (500 MHz): δ 7.79 (m, 4H, CH_{arom}), 7.46 (m, 6H, CH_{arom}), 7.37 (m, 4H, CH_{arom}), 7.31 (m, 6H, CH_{arom}), 2.41 (m, 2H), 2.02 (m, 2H), 1.73 (m, 2H), 1.52 (m, 2H). $^{13}\text{C}\{^1\text{H}\}$ NMR (125 MHz): δ 138.5 (d, $J_{P-C} = 12$ Hz, 2C_{arom}), 133.0 (d, $J_{P-C} = 80$ Hz, 2C_{arom}), 132.9 (d, $J_{P-C} = 18$ Hz, 4CH_{arom}), 131.7 (d, $J_{P-C} = 3$ Hz, 2CH_{arom}), 131.3 (d, $J_{P-C} = 11$ Hz, 4CH_{arom}), 128.9 (d, $J_{P-C} = 2$ Hz, 2CH_{arom}), 128.2 (d, $J_{P-C} = 13$ Hz, 4CH_{arom}), 128.7 (d, $J_{P-C} = 7$ Hz, 4CH_{arom}), 32.6 (d, $J_{P-C} = 57$ Hz, CH_2), 27.8 (d, $J_{P-C} = 12$ Hz, CH_2), 27.3 (d, $J_{P-C} = 17$ Hz, CH_2), 24.1 (d, $J_{P-C} = 13$ Hz, CH_2). $^{31}\text{P}\{^1\text{H}\}$ NMR (283 MHz): δ 43.57 (P(S)), -15.04 (P). MS (ES+) m/z : 459 (M^+). Anal. Calcd. for $\text{C}_{28}\text{H}_{28}\text{P}_2\text{S}$: C 73.34, H 6.15; Found C 73.01, H 6.12 %.

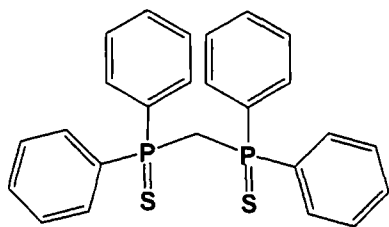
Bis(diphenylphosphino)ferrocene monosulfide: **dppfS**



DppfS was synthesized by the same procedure as was employed to synthesize **dppmS**, but using **dppf** (2.000 g, 3.61 mmol), S_8 (0.116 g, 0.45 mmol) and CHCl_3 25 mL. After removing the solvent *in vacuo*, the crude product was purified by column chromatography

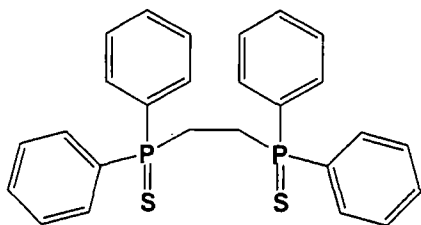
on silica using CH_2Cl_2 as eluent. The ratio of recovered **dppf**:**dppfS**:**dppfS₂** was approximately 1:2:1 (0.552 g: 0.988 g: 0.439 g). Yield: 0.987 g, 47 %. The single-crystal suitable for X-ray diffraction was grown *via* slow evaporation of a solution in CH_2Cl_2 :MeOH. m.p. 194.2 - 195.0 °C. ^1H NMR (500 MHz): δ 7.65 (m, 4H, CH_{arom}), 7.45 (m, 2H, CH_{arom}), 7.38 (m, 4H, CH_{arom}), 7.27 (m, 10H), 4.48 (s, 2H, CH), 4.37 (s, 2H, CH), 4.31 (s, 2H, CH), 3.99 (s, 2H, CH). $^{13}\text{C}\{^1\text{H}\}$ NMR (125 MHz): δ 138.8 (d, $J_{P-C} = 10$ Hz, 2C_{arom}), 134.6 (d, $J_{P-C} = 87$ Hz, 2C_{arom}), 133.6 (d, $J_{P-C} = 20$ Hz, 4CH_{arom}), 131.8 (d, $J_{P-C} = 11$ Hz, 4CH_{arom}), 131.4 (d, $J_{P-C} = 3$ Hz, 2CH_{arom}), 128.8 (2CH_{arom}), 128.5 (d, $J_{P-C} = 8$ Hz, 4CH_{arom}), 128.4 (d, $J_{P-C} = 3$ Hz, 4CH_{arom}), 77.9 (d, $J_{P-C} = 9$ Hz, C), 75.7 (d, $J_{P-C} = 97$ Hz, C), 74.5 (d, $J_{P-C} = 14$ Hz, 2CH), 74.0 (d, $J_{P-C} = 3$ Hz, 2CH), 73.8 (m, 4CH). $^{31}\text{P}\{^1\text{H}\}$ NMR (283 MHz): δ 42.27 (P(S)), -16.59 (P). MS (ES+) m/z : 641 ($\text{M}+\text{Fe}$)⁺. Anal. Calcd. for $\text{C}_{34}\text{H}_{28}\text{FeP}_2\text{S}$: C 69.63, H 4.81; Found C 68.82, H 4.93 %.

* Relative proton integrals quoted according to proton environment.

Bis(diphenylphosphino)methane disulfide: **dppmS₂**

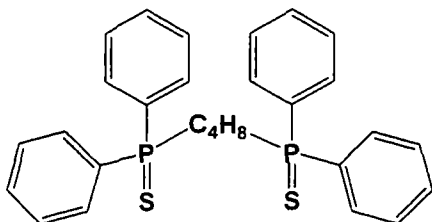
Dppm (0.500 g, 1.30 mmol) was dissolved in 4 mL of CHCl₃ and then S₈ (0.083 g, 0.33 mmol) was added at room temperature and the mixture was left overnight in a glove box. The crude product was filtered through a 5 cm silica pad with additional CH₂Cl₂. After removing the solvent *in vacuo*, the white, solid product was obtained. Yield: 0.572 g, 98 %. m.p. 178.8 - 180.0 °C. ¹H NMR (500 MHz): δ 7.81 (m, 4H, CH_{arom}), 7.42 (t, *J*_{H-H} = 7 Hz, 2H, CH_{arom}), 7.33 (m, 4H, CH_{arom}), 3.98 (t, *J*_{P-H} = 13 Hz, 1H, CH₂). ¹³C{¹H} NMR (125 MHz): δ 134.4 (2CH_{arom}), 132.1 (vt, *J*_{P-C} = 6 Hz, 4CH_{arom}), 129.9 (vt, *J*_{P-C} = 7 Hz, 4CH_{arom}), 125.8 (d, *J*_{P-C} = 87 Hz, 2C), 33.5 (vt, *J*_{P-C} = 48 Hz, CH₂). ³¹P{¹H} NMR (162 MHz): δ 36.41. MS (ES+) *m/z*: 471 (M+Na)⁺. Anal. Calcd. for C₂₅H₂₂P₂S₂: C 66.95, H 4.94; Found C 66.89, H 4.89 %.

* Relative proton integrals quoted according to proton environment.

Bis(diphenylphosphino)ethane disulfide: **dppeS₂**

DPpeS₂ was synthesized by the same procedure as was employed to synthesize **dppmS₂**, but using dppe (0.700 g, 1.76 mmol) and S₈ (0.113 g, 0.44 mmol). Yield: 0.798 g, 98 %. m.p. 237.0 - 238.4 °C. ¹H NMR (500 MHz): δ 7.80 (m, 4H, CH_{arom}), 7.49 (m, 2H, CH_{arom}), 7.44 (m, 4H, CH_{arom}), 2.72 (d, *J*_{P-H} = 3 Hz, 2H, CH₂). ¹³C{¹H} NMR (125 MHz): δ 132.1 (2CH_{arom}), 131.9 (vt, *J*_{P-C} = 42 Hz, 2C), 131.4 (vt, *J*_{P-C} = 5 Hz, 4CH_{arom}), 129.1 (vt, *J*_{P-C} = 6 Hz, 4CH_{arom}), 25.9 (m, ABX, CH₂). ³¹P{¹H} NMR (161 MHz): δ 45.42. MS (ES+) *m/z*: 485 (M+Na)⁺. Anal. Calcd. for C₂₆H₂₄P₂S₂: C 67.51, H 5.23; Found C 67.60, H 5.18 %.

* Relative proton integrals quoted according to proton environment.

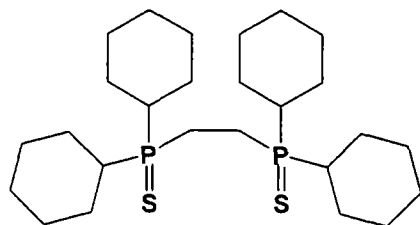
Bis(diphenylphosphino)buthane disulfide: **dppbS₂**

DppbS₂ was synthesized by the same procedure as was employed to synthesize **dppmS₂**, but using dppb (0.500 g, 1.17 mmol) and S₈ (0.075 g, 0.293 mmol). Yield: 0.566 g, 98 %. m.p. 229.8-231.2

°C. The single-crystal suitable for X-ray diffraction was grown *via* slow evaporation of a solution in CH₂Cl₂:MeOH. ¹H NMR (500 MHz): δ 7.77 (m, 4H, CH_{arom}), 7.49 (m, 2H, CH_{arom}), 7.44 (m, 4H, CH_{arom}), 2.42 (m, 2H, CH₂), 1.72 (m, 2H, CH₂). ¹³C{¹H} NMR (125 MHz): δ 132.8 (d, *J*_{P-C} = 80 Hz, 2C_{arom}), 131.7 (d, *J*_{P-C} = 3 Hz, 2CH_{arom}), 131.2 (d, *J*_{P-C} = 11 Hz, 4CH_{arom}), 128.9 (d, *J*_{P-C} = 13 Hz, 4CH_{arom}), 32.5 (d, *J*_{P-C} = 58 Hz, CH₂), 23.6 (dd, ²*J*_{P-C} = 18 Hz, ³*J*_{P-C} = 3 Hz, CH₂). ³¹P{¹H} NMR (161 MHz): δ 43.37. MS (ES+) *m/z*: 513 (M+Na)⁺. Anal. Calcd. for C₂₈H₂₈P₂S₂: C 68.55, H 5.75; Found C 68.15, H 5.68 %.

* Relative proton integrals quoted according to proton environment.

Bis(dicyclophosphino)ethane disulfide: **dcpeS₂**



DcpeS₂ was synthesized by the same procedure as was employed to synthesize **dppmS₂**, but using **dcpe** (0.146 g, 0.35 mmol) and S₈ (0.022 g, 0.09 mmol). Yield: 0.164 g, 97 %. The single-crystal suitable for X-ray diffraction was grown *via* slow

evaporation of a solution in CH₂Cl₂:CH₃OH. m.p. 146.7 - 147.0 °C. ¹H NMR (500 MHz): δ 1.99 (d, *J*_{H-P} = 13 Hz, 4H, CH_{cyclo}), 1.85 (m, 8H, CH_{cyclo}), 1.72 (d, *J*_{H-P} = 9 Hz, 2H, CH₂), 1.32 (m, 10H, CH_{cyclo}). ¹³C{¹H} NMR (125 MHz): δ 38.1 (m, 2CH), 26.8 (vt, *J*_{P-C} = 6 Hz, 4CH₂), 26.4 (d, *J*_{P-C} = 14 Hz, 4CH₂), 26.0 (2CH₂), 19.0 (m, CH₂). ³¹P{¹H} NMR (161 MHz): δ 62.52. MS (ES+) *m/z*: 509 (M+Na)⁺. Anal. Calcd. for C₂₆H₄₈P₂S₂: C 64.16, H 9.94; Found C 63.89, H 9.96 %.

* Relative proton integrals quoted according to proton environment.

Bis(diphenylphosphino)ferrocene disulfide: **dppfS₂**



DppfS₂ was synthesized by the same procedure as was employed to synthesize **dppmS₂**, but using **dppf** (1.000 g, 1.80 mmol) and S₈



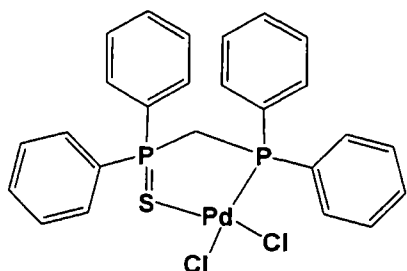
(1.115 g, 0.45 mmol). Yield: 1.083 g, 98 %. m.p. 248.7 - 250.1 °C.

¹H NMR (500 MHz): δ 7.61 (m, 4H, CH_{arom}), 7.46 (m, 2H, CH_{arom}), 7.38 (m, 4H, CH_{arom}), 4.64 (app. q, *J*_{H-H} = 2 Hz, 2H, CH), 4.28 (app. q, *J*_{H-H} = 2 Hz, 2H, CH). ¹³C{¹H} NMR (125 MHz): δ 138.8 (d, *J*_{P-C} = 10 Hz, 2C_{arom}), 134.3 (d, *J*_{P-C} = 86 Hz, 2C_{arom}), 131.7 (d, *J*_{P-C} = 11 Hz, 4CH_{arom}), 131.6 (d, *J*_{P-C} = 3 Hz, 2CH_{arom}), 128.5 (d, *J*_{P-C} = 12 Hz, 4CH_{arom}), 75.3 (d, *J*_{P-C} = 10 Hz, 2CH), 74.3 (d, *J*_{P-C} = 13 Hz,

2CH). $^{31}\text{P}\{^1\text{H}\}$ NMR (283 MHz): δ 41.08. MS (ES+) m/z : 620 (m^+). Anal. Calcd. for $\text{C}_{34}\text{H}_{28}\text{FeP}_2\text{S}_2$: C 66.02, H 4.56; Found C 65.44, H 4.49 %.

* Relative proton integrals quoted according to proton environment.

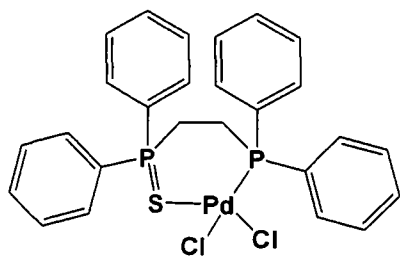
Bis(diphenylphosphino)methane palladium(II) dichloride: **Pd(dppmS)**



To **dppmS** (0.210 g, 0.51 mmol) in CHCl_3 (2 mL) was added $\text{PdCl}_2(\text{PhCN})_2$ (0.200 g, 0.50 mmol) in CHCl_3 (2 mL) to give a yellow solution which was stirred over night at room temperature. The solvent was concentrated on a rotary evaporator and then Et_2O was added giving an orange precipitate. The

precipitate was collected by filtration and washed with Et_2O (x3). Yield: 0.209 g, 70%. The single-crystal suitable for X-ray diffraction was grown *via* slow evaporation of a solution in CDCl_3 (crystals deposit in the NMR tube). m.p. 250.3 - 252.0 °C. The product has limited solubility. ^1H NMR (500 MHz, CD_2Cl_2): δ 7.74 (m, 8H, CH_{arom}), 7.62 (m, 2H, CH_{arom}), 7.48 (m, 6H, CH_{arom}), 7.39 (m, 4H, CH_{arom}), 3.93 (vt, $J_{\text{H-H}} = 11$ Hz, 2H, CH_2). $^{13}\text{C}\{^1\text{H}\}$ NMR (175 MHz): δ 134.5 (d, $J_{\text{P-C}} = 14$ Hz, 4CH_{arom}), 134.3 (2CH_{arom}), 132.5 (d, $J_{\text{P-C}} = 11$ Hz, 4CH_{arom}), 132.4 (2CH_{arom}), 129.9 (d, $J_{\text{P-C}} = 13$ Hz, 4CH_{arom}), 129.0 (d, $J_{\text{P-C}} = 11$ Hz, 4CH_{arom}), 125.7 (m, 2C), 125.3 (m, 2C), 31.2 (d, $J_{\text{P-C}} = 18$ Hz, CH_2). $^{31}\text{P}\{^1\text{H}\}$ NMR (161 MHz, CD_2Cl_2): δ 56.37 (d, $J_{\text{P(S)-P}} = 37$ Hz, P(S)), 31.63 (d, $J_{\text{P-P(S)}} = 37$ Hz, P). Anal. Calcd. for $\text{C}_{25}\text{H}_{22}\text{Cl}_2\text{P}_2\text{PdS}$: C 50.57, H 3.73; Found C 50.45, H 3.78 %.

Bis(diphenylphosphino)ethane monosulfide palladium(II) dichloride: **Pd(dppeS)**

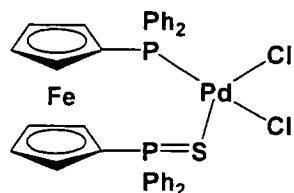


Pd(dppeS) was synthesized by the same procedure as was employed to synthesize **Pd(dppmS)**, but using $\text{PdCl}_2(\text{PhCN})_2$ (0.089 g, 0.23 mmol) and **dppeS** (0.100 g, 0.23 mmol). Yield: 0.114 g, 79 %.

The single-crystal suitable for X-ray diffraction was grown *via* slow evaporation of a solution in CDCl_3 (crystals deposit in the NMR tube). m.p. 175.8 - 176.0 °C. ^1H NMR (700 MHz): δ 7.90 (m, 4H, CH_{arom}), 7.73 (m, 6H, CH_{arom}), 7.61 (m, 4H, CH_{arom}), 7.54 (vt, $J_{\text{H-H}} = 8$ Hz, 2H, CH_{arom}), 7.42 (m, 4H, CH_{arom}), 2.80 (m, 4H, CH_2). $^{13}\text{C}\{^1\text{H}\}$ NMR (175 MHz): δ 133.9 (d, $J_{\text{P-C}} = 13$ Hz,

4CH_{arom}), 133.9 (2CH_{arom}), 131.9 (d, $J_{P-C} = 10$ Hz, 4CH_{arom}), 131.9 (2CH_{arom}), 129.9 (d, $J_{P-C} = 13$ Hz, 4CH_{arom}), 128.9 (d, $J_{P-C} = 11$ Hz, 4CH_{arom}), 128.3 (d, $J_{P-C} = 58$ Hz, 2C), 128.1 (d, $J_{P-C} = 81$ Hz, 2C), 24.2 (d, $J_{P-C} = 50$ Hz, CH₂), 22.6 (dd, $^1J_{P-C} = 35$ Hz, $^2J_{P-C} = 5$ Hz, CH₂). $^{31}\text{P}\{^1\text{H}\}$ NMR (283 MHz): δ 41.11 (d, $J_{P(S)-P} = 15$ Hz, P(S)), 22.05 (d, $J_{P-P(S)} = 15$ Hz, P). Anal. Calcd. for C₂₆H₂₄Cl₂P₂PdS·CHCl₃: C 44.60, H 3.47; Found C 44.15, H 3.41 %.

Bis-(diphenylphosphino)ferrocene monosulfide palladium(II) dichloride: **Pd(dppfS)**

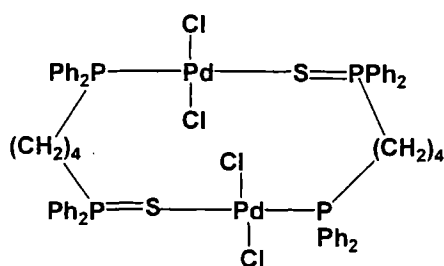


Pd(dppfS) was synthesized by the same procedure as was employed to synthesize **Pd(dppmS)**, but using PdCl₂(PhCN)₂ (0.196 g, 0.51 mmol) and **dppfS** (0.300 g, 0.510 mmol). Yield: 0.260 g, 88 %. The single-crystal for X-ray diffraction

was grown *via* slow evaporation of a solution in CHCl₃:hexane. ^1H NMR (500 MHz): δ 7.76 (m, 6H, CH_{arom}), 7.60 (m, 2H, CH_{arom}), 7.47 (m, 8H, CH_{arom}), 7.41 (m, 4H, CH_{arom}), 5.23 (s, 2H, CH), 4.69 (s, 2H, CH), 4.62 (s, 2H, CH), 4.44 (s, 2H, CH). $^{13}\text{C}\{^1\text{H}\}$ NMR (125 MHz): δ 134.2 (d, $J_{P-C} = 11$ Hz, 4CH_{arom}), 133.5 (2CH_{arom}), 133.3 (d, $J_{P-C} = 11$ Hz, 4CH_{arom}), 131.4 (2CH_{arom}), 130.7 (d, $J_{P-C} = 56$ Hz, 2C_{arom}), 129.1 (d, $J_{P-C} = 13$ Hz, 4CH_{arom}), 128.5 (d, $J_{P-C} = 11$ Hz, 4CH_{arom}), 127.9 (d, $J_{P-C} = 90$ Hz, 2C_{arom}), 79.6 (d, $J_{P-C} = 3$ Hz, 2CH), 78.2 (d, $J_{P-C} = 6$ Hz, 2CH), 74.3 (d, $J_{P-C} = 57$ Hz, C), 73.6 (2CH), 73.1 (2CH), 72.4 (d, $J_{P-C} = 87$ Hz, C). $^{31}\text{P}\{^1\text{H}\}$ NMR (283 MHz): δ 4.33 (P(S)), 21.80 (P). Anal. Calcd. for C₃₄H₂₈Cl₂FeP₂PdS: C 53.47, H 3.70; Found C 53.08, H 3.71 %.

Bis(diphenylphosphino)buthane monosulfide palladium(II) dichloride dimer:

Pd₂(dppbS)



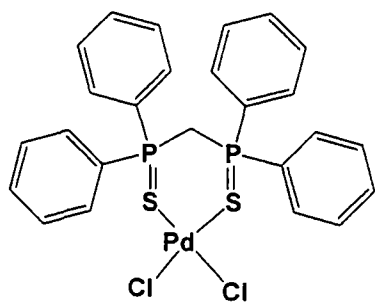
Pd₂(dppbS) was synthesized by a similar procedure as was employed to synthesize PdCl₂-**dppmS**, but using PdCl₂(PhCN)₂ (0.095 g, 0.25 mmol) in CH₂Cl₂ (5 mL) and **dppbS** (0.113 g, 0.25 mmol) in CH₂Cl₂ (5 mL). Yield: 0.220 g, 70 %.

The single-crystal suitable for X-ray diffraction was grown *via* slow evaporation of a solution in CDCl₃ (crystals deposit in the NMR tube). m.p. 260.0 - 260.6 °C. The compound has limited solubility. ^1H NMR

(700 MHz, dms -d_6): δ 7.83 (dd, $J_{\text{P-H}} = 14$ Hz, $J_{\text{H-H}} = 7$ Hz, 4H, CH_{arom}), 7.67 (dd, $J_{\text{P-H}} = 14$ Hz, $J_{\text{H-H}} = 8$ Hz, 4H, CH_{arom}), 7.50 (m, 12H, CH_{arom}), 3.31 (m, 2H, CH_2), 2.56 (m, 2H, CH_2), 2.37 (m, 2H, CH_2), 1.48 (m, 2H, CH_2). $^{13}\text{C}\{^1\text{H}\}$ NMR (175 MHz, dms -d_6): δ 133.7 (m, 4 CH_{arom}), 133.5 (d, $J_{\text{P-C}} = 77$ Hz, 2 C_{arom}), 132.1 (2 CH_{arom}), 131.9 (2 CH_{arom}), 131.4 (d, $J_{\text{P-C}} = 10$ Hz, 4 CH_{arom}), 129.8 (d, $J_{\text{P-C}} = 10$ Hz, 2 C_{arom}), 129.3 (m, 4 CH_{arom}), 129.1 (m, 4 CH_{arom}), 30.7 (d, $J_{\text{P-C}} = 55$ Hz, CH_2), 27.5 (d, $J_{\text{P-C}} = 37$ Hz, CH_2), 25.2 (d, $J_{\text{P-C}} = 18$ Hz, CH_2), 23.8 (d, $J_{\text{P-C}} = 15$ Hz, CH_2). $^{31}\text{P}\{^1\text{H}\}$ NMR (162 MHz): 47.45 (P(S)), 25.15 (P). Anal. Calcd. for $\text{C}_{57}\text{H}_{58}\text{Cl}_4\text{P}_4\text{Pd}_2\text{S}_2$: C 49.58, H 4.23; Found C 49.88, H 4.18 %.

* Relative proton integrals quoted according to proton environment.

Bis(diphenylphosphino)methane disulfide palladium(II) dichloride: **Pd(dppmS $_2$)**

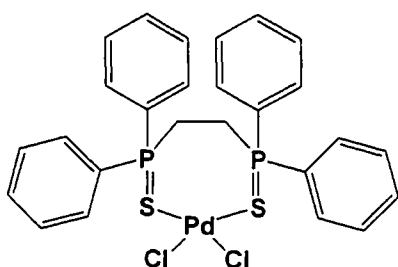


A solution of PdCl_2 (0.050 g, 0.28 mmol) in hot CH_3CN (10 mL) was added to a solution of the ligand, **dppmS $_2$** (0.127 g, 0.28 mmol) in CH_3CN (10 mL), and the reaction was heated to reflux for 3 h. The solution was filtered and allowed to crystallize. Light red coloured single crystals were formed. Yield: 0.074

g, 42 %. m.p. 252.5-253.8 $^\circ\text{C}$. The compound has limited solubility in any solvent. $^{31}\text{P}\{^1\text{H}\}$ NMR spectroscopy in dms -d_6 showed peaks due to the free ligand, indicating dissociation from the complex. ^1H and $^{13}\text{C}\{^1\text{H}\}$ show complicated patterns arising from the free ligand and the complex. $^{31}\text{P}\{^1\text{H}\}$ NMR (161 MHz, dms -d_6): δ 37.87. Anal. Calcd. for $\text{C}_{34}\text{H}_{22}\text{P}_2\text{PdS}_2$: C 47.98, H 3.54; Found C 47.86, H 3.55 %.

* Relative proton integrals quoted according to proton environment.

Bis-(diphenylphosphino)ethane disulfide palladium(II) dichloride: **Pd(dppeS $_2$)**



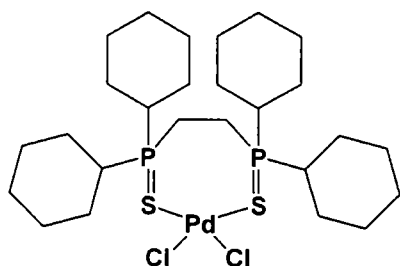
Pd(dppeS $_2$) was synthesized by the same procedure as was employed to synthesize **Pd(dppmS $_2$)**, but using PdCl_2 (0.050 g, 0.28 mmol) in hot CH_3CN (10 mL) and **dppeS $_2$** (0.130 g, 0.28 mmol) in CH_3CN (10 mL). Light red coloured crystals were formed.

Yield: 0.087 g, 48 %. m.p. 269.4 - 271.5 $^\circ\text{C}$. ^1H NMR (500 MHz, dms -d_6): δ 7.84 (m, 4H, CH_{arom}), 7.54 (m, 6H, CH_{arom}), 2.70 (m,

2H, CH₂). ¹³C{¹H} NMR (125 MHz, dms_o-d₆): δ 132.7 (2CH_{arom}), 131.7 (d, *J*_{P-C} = 41 Hz, 2C_{arom}), 131.5 (4CH_{arom}), 129.6 (4CH_{arom}), 25.8 (vt, *J*_{P-C} = 25 Hz, 2C). ³¹P{¹H} NMR (202 MHz, dms_o-d₆): δ 45.77. Anal. Calcd. for C₂₆H₂₄Cl₂P₂PdS₂·CH₃CN: C 49.39, H 4.60; Found C 49.43, H 4.01 %.

* Relative proton integrals quoted according to proton environment.

Bis(dicyclohexylphosphino)ethane disulfide palladium(II) dichloride; **Pd(dcpes₂)**



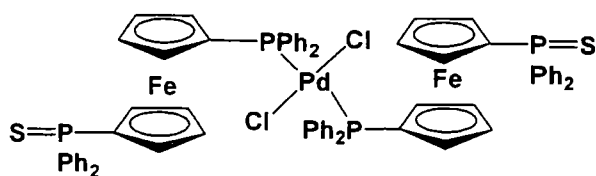
Pd(dcpes₂) was synthesized by the same procedure as was employed to synthesize **Pd(dppmS₂)**, but using PdCl₂ (0.017 g, 0.10 mmol) in CH₃CN (5 mL) and **dcpes₂** (0.093 g, 0.19 mmol) in CH₃CN (5 mL). To collect the product, the solution was filtered and concentrated and Et₂O was added giving an orange precipitate. Yield: 0.053 g, 83%. The single-crystal for X-ray diffraction was grown

via slow evaporation of a solution in CH₂Cl₂:Et₂O. m.p. 257.2 - 257.6 °C. ¹H NMR (500 MHz): δ 2.37 (m, 2H), 2.16 (m, 1H), 2.01 (m, 1H), 1.86 (m, 2H), 1.70 (d, *J*_{H-H} = 12 Hz, 1H), 1.53 (m, 2H), 1.28 (m, 4H). ¹³C{¹H} NMR (125 MHz): δ 38.10 (m, 4CH), 26.78 (dd, *J*_{P-C} = 7, 3 Hz, 8CH₂), 26.4 (d, *J*_{P-C} = 14 Hz, 8CH₂), 26.04 (4CH₂), 19.0 (m, 2CH₂). ³¹P{¹H} NMR (283 MHz): δ 68.16. Anal. Calcd. for C₂₆H₄₈Cl₂P₂PdS₂: C 47.03, H 7.29; Found C 46.90, H 7.22 %.

* Relative proton integrals quoted according to proton environment.

Di-bis(diphenylphosphino)ferrocene monosulfide palladium(II) dichloride:

Pd(dppfS)₂

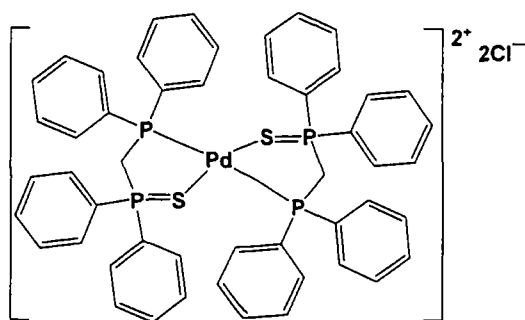


To **dppfS** (0.600 g, 1.020 mmol) in CHCl₃ (10 mL) was added PdCl₂(PhCN)₂ (0.196 g, 0.510 mmol) in CHCl₃ (5 mL) to give yellow

solution which was stirred over night at room temperature. The solvent was concentrated on a rotary evaporator and then Et₂O was added giving an orange precipitate. The precipitate was collected by filtration and washed with Et₂O (x3). Yield: 0.719 g, 72 %. The single-crystal suitable for X-ray diffraction was grown *via* slow evaporation of a solution in CHCl₃:Et₂O. m.p. 199.3 - 200.0 °C. ¹H NMR (500

Di-(bis(diphenylphosphino)methane monosulfide) palladium(II) dichloride:

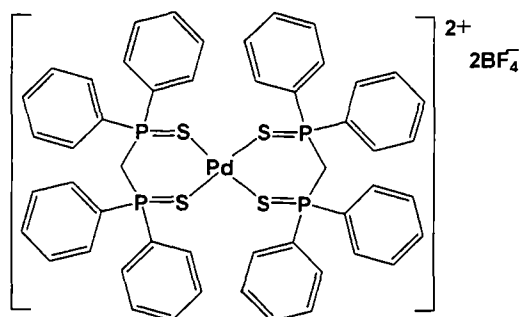
Pd(dppmS)₂



Pd(dppmS)₂ was synthesized by a similar procedure as was used to synthesize **Pd(dppfS)₂**, but using PdCl₂(PhCN)₂ (0.092 g, 0.24 mmol) in CHCl₃ (2 mL) and **dppmS** (0.200 g, 0.48 mmol) in CHCl₃ (2 mL). Yield: 0.475 g, 98 %. The single-crystal suitable for X-ray diffraction was grown *via* slow evaporation of a solution in CHCl₃ and by slow evaporation of NMR solution in CD₂Cl₂ which gave two polymorphs, **Pd(dppmS)·CHCl₃** and **Pd(dppmS)·CD₂Cl₂**, respectively. m.p. 198.7-198.9 °C. ³¹P{¹H} NMR spectroscopy in CD₂Cl₂ showed peaks due to **dppmS**, **Pd(dppmS)** and *cis*-, *trans*- **Pd(dppmS)₂**, indicating dissociation from the complex. The compound has low solubility in CDCl₃ and CD₂Cl₂. The ¹H NMR spectrum from a concentrated solution in CD₂Cl₂ shows broad signals. The ¹³C{¹H} spectrum was obtained from the same solution but only the signals of **dppmS** and **Pd(dppmS)** were observed. ³¹P{¹H} NMR (283 MHz, CD₂Cl₂): δ 55.55 (d, J_{P(S)-P} = 36 Hz), 54.26 (broad), 47.02 (broad), 39.94 (d, J_{P(S)-P} = 78 Hz), 35.28 (broad), 33.64 (d, J_{P(S)-P} = 36 Hz), 27.55 (broad), -28.42 (d, J_{P(S)-P} = 78 Hz). Anal. Calcd. for C₅₀H₄₄Cl₂P₄PdS₂₂·1/6CHCl₃: C 58.49, H 4.32; Found C 58.47, H 4.49 % (the crystal structure indicated four molecules of CHCl₃ and CD₂Cl₂ for each polymorphs).

Di-(bis(diphenylphosphino)methane disulfide) palladium(II) di-tetrafluoroborate;

Pd(dppmS₂)₂

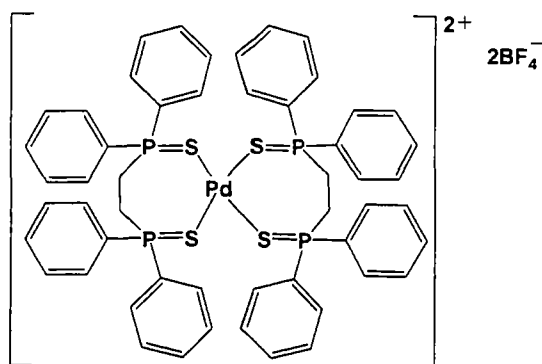


[Pd(CH₃CN)₄](BF₄)₂ (0.099 g, 0.22 mmol) and **dppmS₂** (0.200 g, 0.45 mmol) were added to 100 mL round bottom flask and CHCl₃ (10 mL) was added. The reaction was left to stir at room temperature overnight. The solution was concentrated on a rotary evaporator and then Et₂O was added giving an orange precipitate. The precipitate was collected by filtration and washed with Et₂O (x3). The suitable single-crystal for X-ray diffraction was grown *via* slow evaporation of a solution in CH₂Cl₂:Et₂O. Yield: 0.262 g, 96 %. m.p. 257.5-259.2 °C. ¹H NMR (500 MHz): δ 7.75 (m, 8H, CH_{arom}), 7.62 (vt, *J*_{H-H} = 7 Hz, 4H, CH_{arom}), 7.46 (m, 8H, CH_{arom}), 4.72 (vt, *J*_{H-H} = 13 Hz, 4H, CH₂). ¹³C{¹H} NMR (125 MHz): δ 134.4 (2CH_{arom}), 132.1 (vt, *J*_{P-C} = 6 Hz, 4CH_{arom}), 129.9 (vt, *J*_{P-C} = 7 Hz, 4CH_{arom}), 126.1 (d, *J*_{P-C} = 87 Hz, 2C_{arom}), 33.5 (m, CH₂). ³¹P{¹H} NMR (283 MHz): δ 35.74. MS (ES+) *m/z*: 1001 (M⁺). Anal. Calcd. for C₅₀H₄₄B₂F₈P₄PdS₄: C 51.02, H 3.77; Found C 50.53, H 3.74 %.

* Relative proton integrals quoted according to proton environment.

Di-bis(diphenylphosphino)ethane disulfide palladium(II) di-tetrafluoroborate;

Pd(dppeS₂)₂

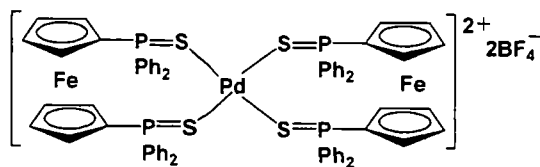


Pd(dppeS₂)₂ was synthesized by the same procedure as was employed to synthesize **Pd(dppmS₂)₂**, but using [Pd(CH₃CN)₄](BF₄)₂ (0.096 g, 0.22 mmol) and **dppeS₂** (0.200 g, 0.43 mmol). The single-crystal suitable for X-ray diffraction was grown *via* slow evaporation of a solution in CHCl₃:hexane. Yield: 0.260 g, 98 %. m.p. 179.2 - 179.6 °C. ¹H NMR (700 MHz): δ 7.64 (m, 6H, CH_{arom}), 7.53 (m, 4H, CH_{arom}), 3.55 (m, 2H, CH₂). ¹³C{¹H} NMR (175 MHz): δ 134.2 (2CH_{arom}), 132.0 (d, *J*_{P-C} = 11 Hz, 4CH_{arom}), 129.9 (d, *J*_{P-C} = 13 Hz, 4CH_{arom}), 126.4 (d, *J*_{P-C} = 83 Hz, 2C_{arom}), 23.0 (d, *J*_{P-C} = 57 Hz, CH₂). ³¹P{¹H} NMR (283 MHz): δ 46.43. Anal. Calcd. for C₅₂H₄₈B₂F₈P₄PdS₄: C 51.83, H 4.01; Found C 50.96, H 3.99 %.

* Relative proton integrals quoted according to proton environment.

Di-(bis(diphenylphosphino)ferrocene sulfide) palladium(II) di-hexafluoroborate;

Pd(dppfS₂)₂



Pd(dppfS₂)₂ was synthesized by the same procedure as was employed to synthesize **Pd(dppmS₂)₂**, but using [Pd(CH₃CN)₄](BF₄)₂ (0.144 g, 0.32 mmol) and **dppfS₂** (0.400 g, 0.65 mmol). Yield: 0.421 g, 97%. The single-crystal suitable for X-ray diffraction was grown *via* slow evaporation of a solution in CH₂Cl₂. m.p. 289.5-290.3 °C. ¹H NMR (700 MHz, CD₂Cl₂): δ 7.70 (m, 2H, CH_{arom}), 7.53 (m, 4H, CH_{arom}), 7.46 (m, 4H, CH_{arom}), 5.02 (s, 2H, CH), 4.67 (s, 2H, CH). ¹³C{¹H} NMR (175 MHz, CD₂Cl₂): δ 134.1 (d, *J*_{P-C} = 3 Hz, 2CH_{arom}), 132.6 (d, *J*_{P-C} = 11 Hz, 4CH_{arom}), 129.5 (d, *J*_{P-C} = 12 Hz, 4CH_{arom}), 127.3 (d, *J*_{P-C} = 88 Hz, 2C_{arom}), 77.1 (d, *J*_{P-C} = 13 Hz, 2CH), 75.4 (d, *J*_{P-C} = 11 Hz, 2CH), 71.8 (d, *J*_{P-C} = 93 Hz, 2C). ³¹P{¹H} NMR (283 MHz, CD₂Cl₂): δ 43.61. Anal. Calcd. for C₆₈H₅₆B₂F₈Fe₂P₄PdS₄: C 53.84, H 3.72; Found C 53.78, H 3.70 %.

* Relative proton integrals quoted according to proton environment.

Catalytic activity in homo-coupling of phenylacetylene

CuI (0.0370 g, 0.019 mmol) and **Pd(dppeS)** (0.0060 g, 9.8 μmol) was transferred to a Schlenk tube with a magnetic stirrer bar and then solvent (5 mL, 1:1 NEt₃:CH₂Cl₂) was added. To this phenylacetylene (0.1000 g, 0.97 mmol) was added. A balloon filled with oxygen was carefully attached to the side arm of the Schlenk tube. The reaction was left to stir and its progress was monitored by GC-MS. When the reaction was complete, the solvent was removed *in vacuo* and the residue was washed with hexane through a silica pad to obtain the colourless diphenyl butadiyne product. The same conditions as mentioned above were employed using different palladium complexes as catalysts (1 mol %, 9.8 μmol): **Pd(dppeS₂)** (0.0063 g), **Pd(dppeS₂)₂** (0.0118 g), **Pd(dppmS)** (0.0058 g), **Pd(dppmS₂)** (0.0061 g), **Pd(dppmS₂)₂** (0.0115 g), **Pd(dppfS)** (0.0075 g), **Pd(dcpes₂)** (0.0065 g), PdCl₂ (0.0017 g) and PdCl₂(PPh₃)₂ (0.0069 g).

V. References

1. Grushin, V. V., *Chem. Rev.* **2004**, *104*, 1629.
2. Allen, F., *Acta Crystallogr.* **1998**, *A54*, 758.
3. Bond, A.; Colton, R.; Panaglotidou, P., *Organometallics* **1988**, *7*, 1767.
4. Luckenbach, R., *Tetrahedron Lett.* **1971**, 2177.
5. Kozlov, V. A.; Aleksanyan, D. V.; Nelyubina, Y. V.; Lyssenko, K. A.; Gutsul, E. I.; Puntus, L. N.; Vasil'ev, A. A.; Petrovskii, P. V.; Odinets, I. L., *Organometallics* **2008**, *27*, 4062.
6. Baccolini, G.; Boga, C.; Mazzacurati, M., *J. Organomet. Chem.* **2005**, *70*, 4774.
7. Omelanczuk, J., *Tetrahedron* **1993**, *49*, 8887.
8. Seyferth, D.; Welch, D. E., *J. Organomet. Chem.* **1964**, *2*, 1.
9. Seyferth, D., *Chem. Abstr.* **1969**, *71*, 167.
10. Hegedus, L. S., *Transition Metals in the Synthesis of Complex Organic Molecules*, University Science Books: Mill Valley, California, 1994.
11. Cantat, T.; Ricard, L.; Mezailles, N.; Le Floch, P., *Organometallics* **2006**, *25*, 6030.
12. Doux, M.; Mezailles, N.; Ricard, L.; Le Floch, P.; Vaz, P. D.; Calhorda, M. J.; Mahabiersing, T.; Hartl, F., *Inorg. Chem.* **2005**, *44*, 9213.
13. Wechsler, D.; McDonald, R.; Ferguson, M. J.; Stradiotto, M., *Chem. Commun.* **2004**, 2446.
14. Cantat, T.; Jaroschik, F.; Nief, F.; Ricard, L.; Mezailles, N.; Le Floch, P., *Chemical Commun.* **2005**, 5178.
15. Miquel, Y.; Igau, A.; Donnadiou, B.; Majoral, J.-P.; Dupuis, L.; Pirio, N.; Meunier, P., *Chem. Commun.* **1997**, 279.
16. Bajko, Z.; Daniels, J.; Gudat, D.; Hap, S.; Nieger, M., *Organometallics* **2002**, *21*, 5182.
17. Bhattacharyya, P.; Slawin, A. M. Z.; Williams, D. J.; Woollins, J. D., *J. Chem. Soc., Dalton Trans* **1995**, 3189.
18. Aizawa, S.-I.; Hase, T.; Wada, T., *J. Organomet. Chem.* **2007**, *692*, 813.
19. Gilheany, D. G., *Chem. Rev.* **1994**, *94*, 1339.
20. Dobado, J. A.; Marítnez-García, H.; Molina, J. M.; Sundberg, M. R., *J. Am. Chem. Soc.* **1998**, *120*, 8461.
21. Liu, H.; Calhorda, M. J.; Drew, M. G. B.; Félix, V., *Inorg. Chim. Acta* **2003**, *347*, 175.
22. Aizawa, S.-i.; Tamai, M.; Sakuma, M.; Kubo, A., *Chem. Lett.* **2007**, *36*, 130.
23. Chutia, P.; Kumari, N.; Sharma, M.; Woollins, J. D.; Slawin, A. M. Z.; Dutta, D. K., *Polyhedron* **2004**, *23*, 1657.
24. Ainscough, E. W.; Brodie, A. M.; Furness, A. R., *J. Chem. Soc., Dalton Trans.* **1973**, 2360.
25. King, C.; McQuillan, G. P., *J. Chem. Soc. (A)* **1967**, 898.
26. Lobana, T. S.; Gupta, T. R.; Sandhu, M. K., *Polyhedron* **1982**, *1*, 781.
27. Bondy, C. R.; Gale, P. A.; Loeb, S. J., *J. Supramol. Chem.* **2003**, *2*, 93.
28. Ainscough, E. W.; Brodie, A. M.; Mentzer, E., *J. Chem. Soc., Dalton Trans.* **1973**, 2167.
29. Albright, T. A.; Freeman, W. J.; Schweizer, E. E., *J. Org. Chem.* **1975**, *40*, 3437.
30. Haake, P.; Miller, W. B.; Tyssee, D. A., *J. Am. Chem. Soc.* **1964**, *86*, 3577.

31. Silverstein, R. M.; Webster, F. X., *Spectrometric Identification of Organic Compounds*, Wiley: 1997; p 482.
32. Gilheany, D. G., *The Chemistry of Organophosphorus Compounds* Wiley-Interscience: Chichester: 1992; Vol. 2.
33. Kerr, K. A.; Boorman, P. M.; Misener, B. S.; van Roode, J. G. H., *Can. J. Chem.* **1977**, *55*, 3081.
34. Coddling, P. W.; Kerr, K. A., *Acta Crystallogr.* **1978**, *B34*, 3785.
35. Barnes, N. A.; Godfrey, S. M.; Halton, R. T. A.; Khan, R. Z.; Jackson, S. L.; Pritchard, R. G., *Polyhedron* **2007**, *26*, 4294.
36. Dreissig, W.; Plieth, K.; Zäske, P., *Acta Crystallogr.* **1972**, *B28*, 3473.
37. Cameron, T. S.; Howlett, K. D.; Shaw, R. A.; Woods, M., *Phosphorus* **1973**, *3*, 71.
38. Stumpf, K.; Blachnik, R.; Roth, G.; Kastner, G., *Z. Kristallogr.* **2000**, *215*, 589.
39. Hussain, M. S.; Isab, A. A.; Saeed, A.; Al-Arfaj, A. R., *Z. Kristallogr.* **2001**, *216*, 629.
40. Drew, M. G. B.; Hobson, R. J., *Inorg. Chim. Acta* **1983**, *72*, 233.
41. LeBlanc, D. J.; Britten, J. F.; Lock, C. J. L., *Acta Crystallogr.* **1997**, *C53*, 1204.
42. Baker, E. N.; Reay, B. R., *J. Chem. Soc., Dalton Trans.* **1973**, 2205.
43. Apperley, D. C.; Bricklebank, N.; Burns, S. L.; Hibbs, D. E.; Hursthouse, M. B.; Malik, K. M. A., *J. Chem. Soc., Dalton Trans.* **1998**, 1289.
44. Garner, C. D.; Howlander, N. C.; Mabbs, F. E.; Boorman, P. M.; King, T. J., *J. Chem. Soc., Dalton Trans.* **1978**, 1350.
45. Cross, W. I.; Godfrey, S. M.; Jackson, S. L.; McAuliffe, C. A.; Pritchard, R. G., *J. Chem. Soc., Dalton Trans.* **1999**, 2225.
46. Cook, J. B.; Nicholson, B. K.; Smith, D. W., *J. Organomet. Chem.* **2004**, *689*, 860.
47. Saak, W.; Haase, D.; Pohl, S., *Z. Naturforsch., B:* **1988**, *43*, 289.
48. Ito, S.; Liang, H.; Yoshifuji, M., *Chem. Commun.* **2003**, 398.
49. Saak, W.; Pohl, S., *Z. Naturforsch., B:* **1988**, *43*, 813.
50. Bricklebank, N.; Coles, S. J.; Forder, S. D.; Hursthouse, M. B.; Poulton, A.; Skabara, P. J., *J. Organomet. Chem.* **2005**, *690*, 328.
51. Grim, S. O.; Kettler, P. B.; Thoden, J. B., *Organometallics* **1991**, *10*, 2399.
52. Burford, N.; Royan, B. W.; Spence, R. E. H.; Rogers, R. D., *J. Chem. Soc., Dalton Trans.* **1990**, 2111.
53. Ara, I.; Fornis, J.; Navarro, R.; Sicilia, V.; Urriolabeitia, E. P., *Polyhedron* **1997**, *16*, 1963.
54. Self, M. F.; Lee, B.; Sangokoya, S. A.; Pennington, W. T.; Robinson, G. H., *Polyhedron* **1990**, *9*, 313.
55. Richadson, M. F., *Acta Crystallogr.* **1985**, *C41*, 27.
56. Robinson, W. T.; Wilkins, C. J.; Zeying, Z., *J. Chem. Soc., Dalton Trans.* **1988**, 2187.
57. Fornies, J.; Navarro, R.; Sicilia, V.; Tomas, M., *Inorg. Chim. Acta* **1990**, *168*, 201.
58. Skvortsov, A. N.; Reznikov, A. N.; de Vekki, D. A.; Stash, A. I.; Belsky, V. K.; Spevak, V. N.; Skvortsov, N. K., *Inorg. Chim. Acta* **2006**, *359*, 1031.
59. Necas, M.; Novosad, J.; Husebye, S., *J. Organomet. Chem.* **2001**, *623*, 124.
60. Matulova, V.; Man, S.; Necas, M., *Polyhedron* **2007**, *26*, 2569.
61. Eller, P. G.; Corfield, P. W. R., *J. Chem. Soc., Dalton Trans.* **1971**, 105.

62. Reigle, R. K.; Casadonte, D. J. J.; Bott, S. G., *J. Chem. Cryst.* **1994**, *24*, 769.
63. Lobana, T. S.; Mahajan, R.; Castineiras, A., *Transition Met. Chem.* **2001**, *26*, 440.
64. Tiethof, J. A.; Stalick, J. K.; Meek, D. W., *Inorg. Chem.* **1973**, *12*, 1170.
65. Mazany, A. M.; Jr. Fackler, J. P., *Organometallics* **1982**, *1*, 752.
66. Lindner, E.; Rau, A.; Hoehne, S., *Chem. Ber.* **1981**, *114*, 3281.
67. Lindner, E.; Bouachir, F.; Hoehne, S., *Chem. Ber.* **1983**, *116*, 46.
68. Depree, G. J.; Childerhouse, N. D.; Nicholson, B. K., *J. Organomet. Chem.* **1997**, *533*, 143.
69. Liang, H.; Ito, S.; Yoshifuji, M., *Org. Lett.* **2004**, *6*, 425.
70. Murray, H. H.; Garzon, G.; Raptis, R. G.; Mazany, A. M.; Porter, L. C.; Jr. Fackler, J. P., *Inorg. Chem.* **1988**, *27*, 836.
71. Doux, M.; Ricard, L.; Le Floch, P.; Mezailles, N., *J. Chem. Soc., Dalton Trans.* **2004**, 2593.
72. Wechsler, D.; Myers, A.; McDonald, R.; Ferguson, M. J.; Stradiotto, M., *Inorg. Chem.* **2006**, *45*, 4562.
73. Rheingold, A. L.; Liable-Sands, L. M.; Trofimenko, S., *Inorg. Chim. Acta* **2002**, *330*, 38.
74. Piechaczyk, O.; Doux, M.; Ricard, L.; Le Floch, P., *Organometallics* **2005**, *24*, 1204.
75. Casares, J. A.; Coco, S.; Espinet, P.; Lin, Y.-S., *Organometallics* **1995**, *14*, 3058.
76. Moya-Cabrera, M.; Jancik, V.; Castro, R. A.; Herbst-Irmer, R.; Roesky, H. W., *Inorg. Chem.* **2006**, *45*, 5167.
77. Thurner, C. L.; Barz, M.; Spiegler, M.; Thiel, W. R., *J. Organomet. Chem.* **1997**, *541*, 39.
78. Faller, J. W.; Wilt, J. C., *Organometallics* **2005**, *24*, 5076.
79. Faller, J. W.; Wilt, J. C., *Org. Lett.* **2005**, *7*, 633.
80. Cotton, F. A.; Llusar, R., *Acta Crystallogr.*, **1988**, *C44*, 952.
81. Dutta, D. K.; Chutia, P.; Woollins, J. D.; Slawin, A. M. Z., *Inorg. Chim. Acta* **2006**, *359*, 877.
82. Faller, J. W.; Fontaine, P. P., *J. Organomet. Chem.* **2007**, *692*, 976.
83. Chutia, P.; Sharma, M.; Das, P.; Kumari, N.; J. D. Woollins; Slawin, A. M. Z.; Dutta, D. K., *Polyhedron* **2003**, *22*, 2725.
84. Qin, Y.; Selvaratnam, S.; Vittal, J. J.; Leung, P.-H., *Organometallics* **2002**, *21*, 5301.
85. Dochnahl, M.; Doux, M.; Faillard, E.; Ricard, L.; Le Floch, P., *Eur. J. Inorg. Chem.* **2005**, 125.
86. Baker, M. J.; Giles, M. F.; Guy, A.; Taylor, M. J.; Watt, R. J., *J. Chem. Soc., Chem. Commun.* **1995**, 197.
87. Aucott, S. M.; Slawin, A. M. Z.; Woollins, J. D., *Polyhedron* **2003**, *22*, 361.
88. Pullarkat, S. A.; Tan, K.-W.; Ma, M.; Tan, G.-K.; Koh, L. L.; Vittal, J. J.; Leung, P.-H., *J. Organomet. Chem.* **2006**, *691*, 3083.
89. Gonsalvi, L.; Adams, H.; Sunley, G. J.; Ditzel, E.; Haynes, A., *J. Am. Chem. Soc.* **1999**, *121*, 11233.
90. Browning, J.; Bushnell, G. W.; Dixon, K. R.; Hilts, R. W., *J. Organomet. Chem.* **1993**, *452*, 205.
91. Stampfl, T.; Haid, R.; Langes, C.; Oberhauser, W.; Bachmann, C.; Kopacka, H.; Ongania, K.-H.; Brüggeller, P., *Inorg. Chem. Commun.* **2000**, *3*, 387.

92. Aucott, S. M.; Slawin, A. M. Z.; Woollins, J. D., *Eur. J. Inorg. Chem.* **2002**, 2002, 2408.
93. Gonsalvi, L.; Adams, H.; Sunley, G. J.; Ditzel, E.; Haynes, A., *J. Am. Chem. Soc.* **2002**, 124, 13597.
94. Karacar, A.; Freytag, M.; Thonnessen, H.; Omelanczuk, J.; Jones, P. G.; Bartsch, R.; Schmutzler, R., *Z. Anorg. Allg. Chem.* **2000**, 626, 2361.
95. Sivasankar, C.; Bera, J. K.; Nethaji, M.; Samuelson, A. G., *J. Organomet. Chem.* **2004**, 689, 2726.
96. Wong, T. Y. H.; Rettig, S. J.; James, B. R., *Inorg. Chem.* **1999**, 38, 2143.
97. Matrosov, E. I.; Starikova, Z. A.; Yanovsky, A. I.; Lobanov, D. I.; Aladzheva, I. M.; Bykhovskaya, O. V.; Struchkov, Y. T.; Mastryukova, T. A.; Kabachnik, M. I., *J. Organomet. Chem.* **1997**, 535, 121.
98. Satek, L. C.; Ammon, H. L.; Stewart, J. M., *Acta Crystallogr.* **1975**, B31, 2691.
99. Lobana, T. S.; Sandhu, M. K., *J. Chem. Soc., Dalton Trans.* **1990**, 691.
100. Cantat, T.; Jacques, X.; Xavier, L. R.; Le Goff, F.; Mezailles, N.; Le Floch, P., *Angew. Chem. Int. Ed.* **2007**, 46, 5947.
101. Pilloni, G.; Longato, B.; Bandoli, G.; Corain, B., *J. Chem. Soc., Dalton Trans.* **1997**, 819.
102. Antoniadis, A.; Hiller, W.; Kunze, U.; Schall, H.; Strahle, J., *Z. Naturforsch., B:* **1982**, 37, 1289.
103. Pilloni, G.; Longato, B.; Bandoli, G., *Inorg. Chim. Acta* **1998**, 277, 163.
104. Abbassioun, M. S.; Chaloner, P. A.; Claver, C.; Hitchcock, P. B.; Masdeu, A. M.; Ruiz, A.; Saballs, T., *J. Organomet. Chem.* **1991**, 403, 229.
105. Ainscough, E. W.; Brodie, A. M.; Brown, K. L., *J. Chem. Soc., Dalton Trans.* **1980**, 1042.
106. Genge, A. R. J.; Gibson, A. M.; Guymmer, N. K.; Reid, G., *J. Chem. Soc., Dalton Trans.* **1996**, 4099.
107. Valderrama, M.; Contreras, R., *J. Organomet. Chem.* **1996**, 513, 7.
108. Horn, E.; Kurosawa, K.; Tiekink, E. R. T., *Acta Crystallogr.* **2000**, C56, 1319.
109. Siasios, G.; Tiekink, E. R. T., *J. Chem. Soc., Dalton Trans.* **1996**, 2269.
110. Yatsimirskii, K. B.; Talanova, G. G.; E. A. Nazarova; Kabachnik, M. I.; Mastryukova, T. A.; Aladzheva, I. M.; I. V. Leont'eva; Antipin, M. Y.; Struchkov, Y. T., *Koord. Khim. (Russ.)* **1993**, 19, 469.
111. Pasechnik, M. P.; Starikova, Z. A.; Yanovsky, A. I.; Aladzheva, I. M.; Bykhovskaya, O. V.; Matrosov, E. I.; Mastryukova, T. A.; Kabachnik, M. I., *Izv. Akad. Nauk SSSR, Ser. Khim. (Russ.)* **1997**, 846.
112. Irisli, S.; Yanar, S., *Polyhedron* **2006**, 25, 1333.
113. Canales, S.; Crespo, O.; Gimeno, M. C.; Jones, P. G.; Laguna, A., *J. Organomet. Chem.* **2000**, 613, 50.
114. Gimeno, M. C.; Jones, P. G.; Laguna, A.; Sarroca, C., *J. Chem. Soc., Dalton Trans.* **1998**, 1277.
115. Romero, P.; Valderrama, M.; Contreras, R.; Boys, D., *J. Organomet. Chem.* **2003**, 673, 102.
116. Carr, S. W.; Colton, R.; Hoskins, B. F.; P. M. Piko; Dakternieks, D.; Tiekink, E. R. T., *Z. Kristallogr.* **1996**, 211, 759.
117. Lobana, T. S.; Verma, R.; Singh, A.; Shikha, M.; Castineiras, A., *Polyhedron* **2002**, 21, 205.
118. Sigl, M.; Schier, A.; Schmidbaur, H., *Z. Naturforsch., B:* **1999**, 54, 21.

119. Zhou, X.-P.; Li, D.; Wu, T.; Zhang, X., *J. Chem. Soc., Dalton Trans.* **2006**, 2435.
120. Pérez-Lourido, P.; Romero, J.; García-Vázquez, J. A.; Sousa, A.; Zheng, Y.; Dilworth, J. R.; Zubieta, J., *J. Chem. Soc., Dalton Trans.* **2000**, 769.
121. Ainscough, E. W.; Bergen, H. A.; Brodie, A. M.; Brown, K. A., *J. Chem. Soc., Dalton Trans.* **1976**, 1649.
122. Carmalt, C. J.; Norman, N. C.; Farrugia, L. J., *Polyhedron* **1995**, *14*, 1405.
123. Lobana, T. S.; Singh, G.; Nishioka, T., *J. Coord. Chem.* **2004**, *57*, 955.
124. Jones, P. G., *Private Communication* **2004**, to the CSD, XADYAD.
125. Brown, K. L., *Acta Crystallogr.* **1979**, *B35*, 462.
126. Doux, M.; Mezailles, N.; Ricard, L.; Le Floch, P., *Organometallics* **2003**, *22*, 4624.
127. Doux, M.; Mézailles, N.; Ricard, L.; Le Floch, P., *Eur. J. Inorg. Chem.* **2003**, *2003*, 3878.
128. Doux, M.; Mezailles, N.; Ricard, L.; Le Floch, P.; Adkine, P.; Berclaz, T.; Geoffroy, M., *Inorg. Chem.* **2005**, *44*, 1147.
129. Doux, M.; Bouet, C.; Mezailles, N.; Ricard, L.; Le Floch, P., *Organometallics* **2002**, *21*, 2785.
130. Doux, M.; Mezailles, N.; Melaimi, M.; Ricard, L.; Le Floch, P., *Chem. Commun.* **2002**, 1566.
131. Doux, M.; Ricard, L.; Le Floch, P.; Jean, Y., *Organometallics* **2006**, *25*, 1101.
132. Doux, M.; Ricard, L.; Le Floch, P.; Jean, Y., *Organometallics* **2005**, *24*, 1608.
133. Kanbara, T.; Yamamoto, T., *J. Organomet. Chem.* **2003**, *688*, 15.
134. Cantat, T.; Jaroschik, F.; Nief, F.; Ricard, L.; Mézailles, N.; Le Floch, P., *Chem. Commun.* **2005**, 5178.
135. Cantat, T.; Demange, M.; Mezailles, N.; Ricard, L.; Jean, Y.; Le Floch, P., *Organometallics* **2005**, *24*, 4838.
136. Cantat, T.; Jaroschik, F.; Ricard, L.; Le Floch, P.; Nief, F.; Mezailles, N., *Organometallics* **2006**, *25*, 1329.
137. Cantat, T.; Mezailles, N.; Ricard, L.; Jean, Y.; Le Floch, P., *Angew. Chem. Int. Ed.* **2004**, *43*, 6382.
138. Casares, J. A.; Espinet, P.; Hernando, R.; Iturbe, G.; Villafane, F.; Ellis, D. D.; Orpen, A. G., *Inorg. Chem.* **1997**, *36*, 44.
139. Lindner, E.; Schlenker, T.; Fawzi, R.; Steimann, M., *Chem. Ber.* **1993**, *126*, 2433.
140. Fischer, J.; Schurmann, M.; Mehring, M.; Zachwieja, U.; Jurkschat, K., *Organometallics* **2006**, *25*, 2886.
141. Preut, H.; Godry, B.; Mitchell, T. N., *Acta Crystallogr.* **1992**, *C48*, 1491.
142. Gan, X.; Duesler, E. N.; Parveen, S.; Paine, R. T., *J. Chem. Soc., Dalton Trans.* **2003**, 4704.
143. Sevcik, R.; Necas, M.; Novosad, J., *Polyhedron* **2003**, 1585.
144. Arliguie, T.; Doux, M.; Mezailles, N.; Thuery, P.; Le Floch, P.; Ephritikhine, M., *Inorg. Chem.* **2006**, *45*, 9907.
145. Hayashi, M.; Takezaki, H.; Hashimoto, Y.; Yamamoto, Y.; Takaoki, K.; Saigo, K., *Tetrahedron Lett.* **1998**, *39*, 7529.
146. Hayashi, M.; Hashimoto, Y.; Yamamoto, Y.; Usuki, J.; Saigo, K., *Angew. Chem. Int. Ed.* **2000**, *39*, 631.
147. Lofù, A.; Mastroilli, P.; Nobile, C. F.; Suranna, G. P.; Frediani, P.; Iggo, J., *Eur. J. Inorg. Chem.* **2006**, 2268.

148. Aizawa, S.-I.; Kondo, M.; Miyatake, R.; Tamai, M., *Inorg. Chim. Acta* **2007**, *360*, 2809.
149. Faller, J. W.; Wilt, J. C.; Parr, J., *Org. Lett.* **2004**, *6*, 1301.
150. Suranna, G. P.; Mastroilli, P.; Nobile, C. F.; Keim, W., *Inorg. Chim. Acta* **2000**, *305*, 151.
151. Gammon, J. J.; Canipa, S. J.; Kelly, P. O. B.; Taylor, S., *Chem. Commun.* **2008**, 3750.
152. Sánchez, J. M.; Hidalgo, M.; Salvadó, V., *React. Funct. Polym.* **2001**, *49*, 215.
153. Ha-Thi, M. H.; Penhoat, M.; Michelet, V.; Leray, I., *Org. Lett.* **2007**, *9*, 1133.
154. Haake, P.; Miller, W. B.; Tyssee, D. A., *J. Am. Chem. Soc.* **1964**, *86*, 3577.
155. Turner, T. P. W. *Fourth year report: The coordination chemistry of phosphine sulfides and thioureas and their applications*; Durham University: Durham, M. Sc. (Chemistry) 2008.
156. Camelt, C. J.; Cowley, A. H.; Decken, A.; Lawson, Y. G.; Norman, N. C., *Acta Cryst., Cryst. Struct. Commun.* **1996**, *C52*, 931.
157. Fang, Z.-G.; Hor, T. S. A.; Wen, Y.-S.; Liu, L.-K.; Mak, T. C. W., *Polyhedron* **1995**, *14*, 2403.
158. Rowland, R. S.; Taylor, R., *J. Phys. Chem.* **1996**, *100*, 7384.
159. Broussier, R.; Bentabet, E.; Laly, M.; Richard, P.; Kuz'mina, L. G.; Serp, P.; Wheatley, N.; Kalck, P.; Gautheron, B., *J. Organomet. Chem.* **2000**, *613*, 77.
160. Garrou, P. E., *Chem. Rev.* **1981**, *81*, 229.
161. Mastroilli, P.; Nobile, C. F.; Suranna, G. P.; Fanizzi, F. P.; Ciccarella, G.; Englert, U.; Li, Q., *Eur. J. Inorg. Chem.* **2004**, *6*, 1234.
162. Steffen, W. L.; Palenik, G. J., *Inorg. Chem.* **1976**, *15*, 2432.
163. Ganguly, S.; Mague, J. T.; Roundhill, D. M., *Acta Crystallogr.* **1994**, *C50*, 217.
164. Hayashi, T.; Konishi, M.; Kobori, Y.; Kumada, M.; Higuchi, T.; Hirotsu, K., *J. Am. Chem. Soc.* **1984**, *106*, 158.
165. Butler, I. R.; Cullen, W. R.; Kim, T. J.; Rettig, S. J.; Trotter, J., *Organometallics* **1985**, *4*, 972.
166. Stockland, R. A.; Levine, A. M.; Giovine, M. T.; Guzei, I. A.; Cannistra, J. C., *Organometallics* **2004**, *23*, 647.
167. Heck, R. F., *Palladium reagents in organic syntheses*, Academic Press: London, 1990; p 461.
168. Bishop, J. J.; Davison, A.; Katcher, M. L.; Lichtenberg, D. W.; Merrill, R. E.; Smart, J. C., *J. Organomet. Chem.* **1971**, *27*, 241.
169. Faller, J. W. M., Suzanna C.; Parr, Jonathan., *J. Organomet. Chem.* **2008** *693*, 1478.
170. Faller, J. W. F., Philip P., *J. Organomet. Chem.* **2007**, *692*, 976.
171. Bond, A. M.; Colton, R.; Panagiotidou, P., *Organometallics* **1988**, *7*, 1774.
172. Palaiseau, F., *Organometallics* **2006**, *25*, 4965.
173. Gimeno, M. C.; Laguna, A.; Laguna, M.; Sanmartin, F.; Jones, P. G., *Organometallics* **1993**, *12*, 3984.
174. Divisia, B., *Tetrahedron* **1979**, *35*, 181.
175. Schumann, H., *J. Organomet. Chem.* **1987**, *320*, 145.
176. Lu, X. L.; Vittal, J. J.; Tiekink, E. R. T.; Tan, G. K.; Kuan, S. L.; Oh, L. Y.; Hor, T. S. A., *J. Organomet. Chem.* **2004**, *689*, 1978.

